SYMMETRIC AND ASYMMETRIC NEAR WAKE OF A FLAT PLATE

by

JOHN ANDREOPOULOS
Dipl. Ing., M.Sc., D.I.C.

DEPARTMENT OF AERONAUTICS
IMPERIAL COLLEGE
LONDON UNIVERSITY

A thesis submitted for the degree of
Doctor of Philosophy of the University of London

July, 1978

ABSTRACT

Conditionally sampled measurements in the symmetric and asymmetric near wake of a thin flat plate (asymmetry by means of roughening one side of the plate), at a Reynolds number, based on trailing edge momentum thickness of 1.3×10^4, are presented.

One of the two boundary layers was slightly heated to tag the fluid. The fluctuating temperature signal was used to distinguish "cold" and "hot" fluid. Intensive fine scale mixing around the centre-line leads to the formation of "warm" regions mainly consisting of fluid coming from the wall region of the boundary layers.

"Hot" and "cold" contributions seem to be the result of strong eruptions across the centre-line which transport kinetic energy and shear stress towards the centre-line.

The interaction between the two boundary layers is confined to an inner wake whose width at various x positions was found to obey some simple laws while in the outer part of the wake, the structural changes which take place are very weak.

Turbulent kinetic energy production and shear stress generation are very high at the edges of the inner wake, and the corresponding terms advection and mean transport, diffusion and turbulent transport are also important.

Similar behaviour characterizes the temperature fluctuation production and dissipation with advection and diffusion of $\overline{\theta^2}$ being quite different.

The zone structural parameters indicate that "cold" and "hot" zones do not affect each other and that any communication between them seems to be through the mean velocity profile only.

Finally, a calculation method is proposed based on physical

arguments previously mentioned.

ACKNOWLEDGEMENTS

I would like to express my gratitude to my supervisor, Mr. P. Bradshaw, for his guidance and constructive criticism throughout the duration of this project.

Thanks are also due to the technical staff in the Workshop and Electronics Laboratory, in particular, Messrs. J. Coles and L. Eals.

Help from my colleagues is greatly acknowledged: Mr. D. Wood for the stimulating discussions, Dr. P. Hoffmann for criticising the thesis draft, Dr. A. Weir for assisting with the earlier experimental work and Messrs. A. Nakayama, R. D. Mehta , P. H. Hancock, I. M. M. Shabaka, H. M. Mahgoub and P. Inman for making life at College most bearable.

Mrs. H. Bastin deserves a special mention for her fast and efficient typing and Miss M. Hahn for helping with the tracing of the figures.

Finally, the financial support of the Greek State Scholarships Establishment (I.K.Y.) is greatly acknowledged.

LIST OF CONTENTS

LIST OF FIGURES

Page

LIST OF SYMBOLS

a_1	$= -\overline{uv}/\overline{q^2}$ Bradshaw's constant
B	Calibration slope
c_f	Skin friction coefficient
c_p	Specific heat at constant pressure
d_w	Wire diameter
E	Hot wire total voltage output
E_o^2	Hot wire calibration intercept
e	Fluctuating voltage
G	Diffucion function in Bradshaw's calculation method
H	$= \delta^*/\theta$ Shape factor
H_f	Rate of heat transfer from hot wire
k	Thermal conductivity
k_f	Thermal conductivity of fluid
L	$= (-uv)^{3/2}/\varepsilon$ Dissipation length scale
Nu	Nusselt number
Pr	$= \frac{\mu c_p}{k}$ Prandtl number
Pr_t	$= -(\overline{uv})(\partial T/\partial y) \,/\, -(\overline{v\theta})(\partial U/\partial y)$ Turbulent Prandtl number
p	Mean static pressure
p'	Fluctuating pressure
$\overline{q^2}$	$= \overline{u^2} + \overline{v^2} + \overline{w^2}$ Turbulent kinetic energy
Re	Reynolds number
R_f	Flux Richardson number
R_{uv}	$= \overline{uv}/\sqrt{\overline{u^2}}\,\sqrt{\overline{v^2}}$ u, v correlation coefficient
$R_{u\theta}$	$= \overline{u\theta}/\sqrt{\overline{u^2}}\,\sqrt{\overline{\theta^2}}$ u, θ correlation coefficient
$R_{v\theta}$	$= \overline{v\theta}/\sqrt{\overline{v^2}}\,\sqrt{\overline{\theta^2}}$ v, θ correlation coefficient
T	Mean temperature
T_f	Temperature of fluid

T_w	Temperature of wire
U, V, W	Mean velocities in x, y, z directions respectively
u, v, w	Fluctuating velocities in x, y, z directions respectively
u_τ	$= \sqrt{\tau_w/\rho}$ Friction velocity
V_θ	$= \overline{v\theta^2}/\overline{\theta^2}$ Transport velocity of $\overline{\theta^2}$
$V_{\theta v}$	$= \overline{v^2\theta}/\overline{v\theta}$ Transport velocity of $\overline{v\theta}$
V_τ	$= \overline{uv^2}/\overline{uv}$ Transport velocity of shear stress
V_q	$= \overline{q^2 v}/\overline{q^2}$ Transport velocity of turbulent kinetic energy

Greek Symbols

α	Temperature coefficient of resistivity or thermal diffusivity $k/\rho c_p$
γ	Intermittency factor
δ	Shear layer width or hot wire yaw angle
δ_i	Inner wake width
δ_γ	Inner wake width deduced from γ
δ_τ	Inner wake width deduced from shear stress
δ^*	Displacement thickness
ΔT	$= T - T_e$ Temperature difference
ε	Dissipation
ε_θ	Thermal dissipation
Θ	Momentum thickness or instantaneous temperature ($\equiv T + \theta$)
θ	Fluctuating temperature
μ	Viscosity
ν	Kinematic viscosity
ν_τ	Eddy viscosity
ρ	Density
τ	$= \rho\overline{uv}$ Turbulent shear stress

τ_w	Wall shear stress
ψ	Hot wire angle

Subscripts and Special Symbols

H	"Hot" fluid
C	"Cold" fluid
W	"Warm" fluid
0	Values at x = 0 mm
U	Upper side
L	Lower side
UBLH	Upper Boundary Layer Heated
LBLH	Lower Boundary Layer Heated
e	Free stream values
ℓ	Centre-line values

1. INTRODUCTION

1.1 General

Over the past few years, turbulence research has attracted more and more people to its fascinating problems, the main emphasis being on establishing the structural parameters which are determined by the statistics of eddy behaviour and which form the empirical input, as functions or constants, to turbulence models.

The development of turbulence models is of great importance for engineering applications. The number of attempts which have been made in modelling justifies the significance of the problem. The reliability of a calculation method and its ability to be extrapolated to conditions beyond those which have been tested increase with the reliability of the physical plausibility of the basic assumptions made to obtain closure of the governing equations. It is common for a very well documented method with all its constants very carefully adjusted to fail to give reliable answers when it is applied to new types of cases because the physical processes are not represented well enough by the calculation method.

The lack of general applicability of the various turbulence models makes the further experimental study inevitable. On the other hand, difficulties in measuring terms like the pressure strain term, appearing in the shear stress transport equation, make a good theoretical basis for the use of experimental data an absolute necessity. Both ways of approaching the turbulence mystery have been improved by the recent development of more sophisticated means of data processing.

Simple turbulent flows seem to be rather rare in the practical problems which an engineer faces. "Complex" turbulent flows, in the sense used by Bradshaw (1975), are more common in real life applications.

Typical examples of such flows are those which are formed by two merging shear layers of opposite shear stress sign (to form a jet, a duct flow or a wake) or those of the same sign as in the case of a shear layer growing inside another one (flow downstream a change of roughness). The problem of understanding the basic behaviour of such flows requires focussing of attention on some simplified cases of "complex" flows.

The present work is an attempt to understand experimentally the character of turbulent flow behind an aerofoil and provide, at the same time, data for test cases of calculation methods, especially those based on the shear stress transport equation. Despite the recent developments in numerical methods, little work has been done in modelling of a turbulent near wake. It is obvious that in order to calculate wakes, something better than the eddy viscosity closure is required since such a model encounters difficulties in dealing with an asymmetric wake where the point of zero shear stress does not necessarily coincide with the point of zero velocity gradient.

The problems of turbulent near wakes behind aerofoils, because of their practical applications to turbomachinery and aircraft, are of great importance. The reasons for being interested in the near wake is that only the near wake of an aerofoil has much effect on the pressure distribution over the aerofoil itself. What happens far downstream, in the self-preserving part of the wake, is not very important. In turbomachinery, the main reason for the primary excitation of aerodynamically induced vibrations is the wake of an upstream element, stator or rotor blade, impinging on the downstream blades. As a result, individual blades are subject to time-dependent forces which may become quite destructive during a possible resonance.

In the hope of gaining more information about the turbulence

structure of such flows the near wake of a flat plate has been extensively investigated. In order to see if the interaction mechanism between the two boundary layers merging at the trailing edge is the same in the asymmetric wake as in the symmetric, we also produced dissimilar boundary layers by roughening one side of the plate. This is a more sensible way of producing asymmetry between the two boundary layers than imposing an arbitrary pressure gradient: it is simpler to deal with two flat plate boundary layers with zero pressure gradient everywhere than with two miscellaneous boundary layers in an arbitrary pressure gradient. In both cases, we used heat to tag one of the boundary layers and thus we were able to use conditional sampling techniques to determine the turbulent characteristics.

1.2 Review of Previous Work

A considerable number of scientific workers have dealt with the important problems of turbulent wake flows. The near wake is composed of two boundary layers merging at their low-speed edges and by affecting the displacement surface near the trailing edge alters the pressure distribution around the aerofoil. Previous work gives little information about the way the two boundary layers interact to form the wake.

The various types of interacting shear layers can be classified in two categories. In the first belong those with opposed shear layers as in a duct, jet or wake and in the second, those with an internally growing layer inside another shear layer, like the case of a flow downstream of step-change of roughness. The basic difference between them is that the two layers in the first category have opposite shear stress signs while in the second, the same sign is everywhere, regardless the case of rough to smooth or smooth to rough change. In

the case of rough to smooth change, the surface shear stress decreases greatly and in the case of the wake from a non-zero value at the trailing edge decreases abruptly to zero on the central line. These two cases also correspond on one more point: the relaxation of the boundary condition U = 0. But the situation is quite different since in the wake, there is an interchange of fluid across the centre-line which does not take place in any sort of change-of-roughness flow.

The aim of most of the studies of the intermittent regions of turbulent shear flows is to determine the interface which separates two different regions of the flow, the "zones", and then to provide separate statistical information by means of choosing a time-resolved function with quite different behaviour in the two zones. The most common interface is the "viscous super-layer" type interface, which separates turbulent fluid from the irrotational external flow. The usual way of sorting out the characteristics of such an interface is by means of measuring velocity fluctuations. Bradshaw and Murlis (1974) introduced the concept of the "retail intermittency" in which the fine scale turbulent structure is retained, as distinct from the classical "wholesale". They also pointed out the major difficulties in determining a turbulent/non-turbulent interface.

The situation is quite complicated when the interface separates two different turbulent fields. A good example is the interface between a boundary layer and an external uniform shear flow or free stream turbulence. Masuda et al (1972) studied a similar flow and as far as the intermittency is concerned, they pointed out the difficulty in measuring it directly.

Whether or not it is easy to determine the irrotational-turbulent fluid interface by measuring velocity fluctuations, for the internal interface separating generally two turbulent zones it is

necessary to use some sort of passive scalar "tagging".

Dean and Bradshaw (1976) have made extensive investigations into the development of two dimensional flow in a rectangular duct of aspect ratio of 12 : 1 at a Reynolds number of 10^5 (based on the duct height) by "tagging" with heat the lower boundary layer. The object was to explore how the conditionally-sampled measurements of the "cold" or "hot" fluid differed from those of an isolated boundary layer, in particular to see how the dimensionless structural parameters of the turbulent flow changed. The results have suggested that the interaction of the two boundary layers merging at their higher-velocity side and with rather low turbulence intensity is confined near the centr line, and the large eddies from either side of the duct seem to time-share in such a way that they compose a continuously contorting interface between the two boundary layers without much structural change. This interface seems to persist indefinitely far downstream although fine scale mixing made the distinction between "hot" and "cold" rather vague at a distance about twice that which the boundary layers took to meet. The above results justified plausibly the idea of superposition and led to the practical use of it. Bradshaw, Dean and McEligot (1973) succeeded in predicting the fully developed duct flow very well by calculating both a "hot" shear stress and "cold" one. Although the Navier-Stokes equations are non-linear and, therefore, exact superposition is not valid, the weak or negligible changes in the turbulent structure of the flow allow superposition as a reasonable first approximation by interaction only through the mean velocity profile.

In a similar experiment o two mixing layers merging to form a jet, Weir, Wood and Bradshaw (1978) found that the turbulence properties of one shear layer are again not greatly affected by interaction with the other layer. If the alteration in the turbulent structure

was negligible, as in the duct, the flow could be calculated by the previously mentioned assumptions of superposition. But in fact, some structural changes occur especially in triple products which represent the y component of bulk convection by large eddies. Effort is being made to correlate these changes by means of a simple interaction parameter in order to calculate the flow.

Antonia and Luxton (1971, 1972, 1974) have in depth investigated the second type of interacting shear layer. In their experimental study of the structure and growth of the internal layer which is formed downstream of a sudden change in roughness in a boundary layer, they confirmed that, in the smooth-to-rough case, the outer part of the boundary layer is not affected by the presence of the internally growing layer, but the inner is strongly influenced by the roughness geometry, because of the large turbulent energy production near the rough wall. They also found that the shear stress is not constant but decreases in the region near the wall due probably to a greater small scale contribution. From the initially self-preserving state on smooth wall, the turbulent boundary layer approaches a second self-preserving state on the rough wall well downstream of the step. In the case of a rough to smooth change, the turbulent boundary layer adjusts rather slowly to the self-preserving state and the slow adjustment is a feature of both the inner and outer layer because the latter tries to compensate for the fall in the energy production near the wall.

Despite the recent progress in numerical methods dealing with turbulent boundary layers, only a few attempts have been reported in the modelling of turbulent near wakes.

Bradshaw (1969) was the first to use transport equations to calculate the near wake of a symmetric aerofoil. Simply, he extended his turbulence calculation model by assuming that the perturbations due

to the change in the boundary conditions are confined in the inner layer for a region close enough to the trailing edge and fitting the length scale to the experimental data.

Morel (1972), by using Bradshaw et al (1967) one equation model, predicted mixing layers and symmetric jet and wake flows by assuming the validity of the interaction hypothesis after the latter had been applied successfully to the duct flow. The rather good predictions gave indirect evidence of the appropriateness of the superposition idea.

A very promising method of turbulent flow prediction is that of Hanjalic and Launder (1972b). They used transport equations for all the Reynolds stresses and the turbulent energy dissipation rate. It was a forward step beyond the eddy viscosity closure; they were able to cover asymmetric flows, although six constants needed to be adjusted.

Launder, Reece and Rodi (1975) used the above model with a better approximation to the pressure-strain term to predict two-dimensional shear flows. Their results for the symmetric wake case are in very good agreement with Chevray and Kovasznay (1969) data, especially the normal stresses at the furthest station from the trailing edge.

Very recently, Ng and Huffman (1977) developed a numerical scheme based on the "interaction hypothesis" as suggested by Bradshaw, Dean and McEligot (1973) in conjunction with the duct flow case mentioned earlier. The near wake was treated as a shear flow consisting of two simple shear layers with distinct but overlapping shear stress profiles of opposite sign and by relating the shear stress to the local turbulence quantities as proposed by Bradshaw, Ferriss and Atwell (1967). Very satisfactory predictions were obtained. The model appeared to be

superior to other wake calculation models in its ability to match the existing experimental data. Unlike the eddy viscosity methods, it can deal satisfactorily with asymmetric wakes, where the point of zero shear stress does not coincide with the point of zero mean velocity gradient. However, they demonstrated that the accuracy of the empirical functions used to define the turbulence structure had a direct impact on the success of any calculation method and finally concluded that more experimental data are needed.

Wake measurements are rather rare. The only measurements that include shear and normal stress profiles are those of Chevray and Kovasznay (1969) on a two-dimensional symmetric plane wake of a thin flat plate at zero pressure gradient. They found that the wake development is strongly dependent on the initial boundary layers at the trailing edge. The difference between their work and the present is that the latter is interested in the initial part of the wake very close to the trailing edge and not in the self-preserving region far downstream. Although their experiment was at a rather low Reynolds number, only 1550 based on the trailing edge momentum thickness, which probably affected the Reynolds number dependence of the outer part of the boundary layer (the viscous superlayer) and caused also a thick viscous sublayer, the effects of which should be relaxed at some distance downstream, their results constitute a useful basic test case for wake calculation methods.

Toyoda and Hirayama (1975) have studied the effects of the initial boundary layer and compressibility in the near wake of a flat plate experimentally and theoretically by using Reichardt's (1943) inductive theory of free turbulence. Their results are limited to mean velocity profiles only, but there is good agreement between measurements and predictions.

A similar experimental and theoretical approach to the near

wake problem has been made by Agrawal, Pande and Prakash (1977).

At this point, it is worth mentioning the experimental study of plane wake flows at O.N.E.R.A. together with the theoretical attempt to predict such flows by Leuchter (1977). The measurements include mean velocity profiles of symmetric plane wakes with and without pressure gradient and asymmetric wake by dissimilar boundary layers due to different pressure gradients. The predictions by using the eddy viscosity concept in the Prandtl-Kolmogovov form, i.e. the square root of turbulent kinetic energy x a length scale, to achieve closure of the mean flow equations, together with two transport equations of turbulent kinetic energy and of length scale x turbulent kinetic energy, are in quite reasonable agreement with the measurements. Turbulence measurements are not reported at all. In an attempt to get more details of the turbulence rather than to predict separately the various components of the Reynolds stress tensor, their transport equations were used, passively - not coupled with the mean flow equations, together with the eddy viscosity in a rather incomprehensive way. The results agreed fairly well with those of Chevray and Kovasznay.

It must be pointed out here that only Ng and Huffman predicted satisfactorily the asymmetric near wake with one equation model and without using the eddy viscosity closure.

A very interesting experimental study has been done by Hanjalic and Launder (1972a) in a fully developed asymmetric flow in a plane duct. The asymmetry was produced by means of roughening only one side of the duct, the other remaining smooth. The region of greatest interaction is characterized by strong diffusion of turbulent shear stress and kinetic energy from the rough plane where the production is higher, towards the smooth wall region.

Various investigators of flows over rough surfaces disagree

on whether the effect of roughness is felt across the entire boundary layer in the form of increased turbulent energy or not. Coleman, Moffat, Kays (1977) and Pimenta (1975) found that the roughness altered the turbulent structure in the outer part of the boundary layer, hence contradicting the classical views of Corrsin and Kistler (1954). But it can be argued that this is due to the type of roughness they have used (1.27 mm. diameter spheres packed in the most dense array).

Pertinent works to the present investigation are those which examined the characteristics of passive thermal fluctuations and their transport by turbulence. Studies by Corrsin (1943), Corrsin and Uberoi (1949) and Corrsin (1952) are generally considered to be pioneering efforts in this area.

Freymuth and Uberoi produced detailed measurements in the wake of heated cylinder. Alexopoulos and Keffer (1968) studied the dynamics of two-dimensional turbulent wake of cylinder superimposed upon a linear, thermally stratified main stream.

La Rue (1973) investigated the intermittent region of a plane turbulent wake of a slightly heated rod. His measurements suggested departures from the Gaussian interface model.

Kovasznay and Ali (1974) studied experimentally the temperature and velocity fluctuations in a slightly heated flat plate wake. The flow develops appreciable asymmetry far downstream. The computations of this flow by Gibson and Launder (1976) including buoyant terms in the turbulence closure account fairly well for this asymmetry.

The two merging wakes of a mildly heated and a cold cylinder have been studied extensively by Fabris (1976) with a four wire probe. Conventional and conditionally sampled higher order temperature velocity correlations are presented.

Fulachier and Dumas (1976) reported measurements in the energy-

containing eddy wavenumber range, in an attempt to establish an analogy between the velocity and temperature fluctuations in a turbulent boundary layer.

Launder (1976) pointed out the turbulent Prandtl number should not be considered constant everywhere in a boundary layer because near the wall (due to pressure fluctuation effects), the momentum and thermal diffusivities are about equal but elsewhere, the ratio is less than unity.

Chevray and Tutu (1976) found, in an experiment with round heated jet, that the large scale motions were responsible for the bulk of momentum and heat transport and that the small scale are more efficient in transporting heat than momentum. This result is in agreement with data given by Lawn (1977) who has studied the temperature spectra in liquid metals. He found that the "$v\theta$" correlation coefficient maintains higher values than "uv" coefficient in the inertial subrange.

Antonia et al (1975) have pointed out earlier than the two previously mentioned works that the small scale structure in an intermittent flow is not locally isotropic and consequently, the overall statistics may be affected.

There are a great number of studies of thermal characteristics in turbulent flows, besides those mentioned here. Generally speaking, the task of all the investigators of turbulent phenomena (with or without the use of heat as a tracer) is to provide more evidence about the structure of those flows on one hand and data test cases for calculation methods on the other.

Summing up as a conclusion of the literature review, it is quite clear that more experimental investigation of complicated turbulent flows is needed.

1.3 The Present Work

The present experimental study is the third in a series of investigations in interacting shear layers. To escalate these studies in order of increasing difficulty, the duct flow was first examined and then the plane jet.

In these two cases, the boundary conditions do not change abruptly as the interaction of the two shear layers starts and so the interaction takes place between well established large-eddy structures. The interaction of two boundary layers in the near wake of an aerofoil is a rather different case from the above. Here, interaction starts with the release of the $u = 0$ constraint at the wall, allowing two layers with opposite wall shear stress to meet; release of the $v = 0$ constraint allows mixing and growth of very small eddies. Since these eddies are the former occupants of the inner layers of the boundary layers, their size is proportional to the sublayer thickness in the sublayer and to the distance y from the wall in the inner layer and, consequently, the eddy size in the mixed inner wake is proportional to the inner wake thickness which is considerably less than the total shear layer thickness. This point reveals the complete contrast to the large eddy interaction process in duct or jet.

The aim of the present experiment is to investigate the above-mentioned interaction in the near wake and to extract as much information as possible.

2. EXPERIMENTAL ARRANGEMENT

2.1 Wind Tunnel

The experimental program was carried out in the 3' x 3' closed circuit low speed wind tunnel of the Aeronautics Department. The working section has a cross section of 91 cm. x 91 cm. and is about 5 m. long. The maximum speed was 45 m/s with extremely low turbulence level (only 0.05%). For more details, see Fig. 2.1.

2.2 The Flat Plate Model

Among the first problems was the proper choice of the flat plate dimensions. The requirements were:-

(i) Sufficient length to give a fully developed turbulent boundary layer at the trailing edge with high Reynolds number (Re > 5000 to avoid low Re effects in the outer layer).

(ii) The two boundary layers should leave the trailing edge almost parallel which means that the plate should be as thin as possible.

(iii) A very sharp trailing edge to avoid early separation and thus probably recirculating flow with additional but undesirable mixing of the two shear layers (e.g. bluff body wake).

(iv) Sufficient thickness for thermal insulation between the upper and the lower boundary layers.

After preliminary calculations of the heat flux through the plate, as an optimisation of the second and fourth incompatible requirements, the dimensions shown in Fig. 2.2 were finally decided. The leading edge was based on a NACA 0009 profile. The plate consisted of four parts, for easier manipulation and installation in the tunnel, all made from plywood layers except for the trailing edge part which had a core of plywood covered with a thin aluminium sheet. The trailing edge became quite thin with the use of aluminium shims, of 0.05 mm. thickness taped to the upstream section. The final trailing edge thickness was of the order of 0.07 mm., much less than the expected viscous sublayer thickness.

Both boundary layers were tripped by means of sand paper strips of 5 cm. width, glued to the leading edge in the spanwise direction.

In the asymmetric wake experiment, for reasons explained earlier in the introduction, one side of the flat plate was covered completely with rough sand paper with a roughness height of about 1 mm. Thus, the trailing edge thickness was 1 mm.

The flat plate was installed horizontally on the mid-plane of the tunnel working section as is shown in Fig. 2.2. It lay on two long aluminium angles, permanently bolted to the tunnel walls.

The leading edge was located just downstream of the contraction exit and the plate was carefully aligned at zero angle of attack. The last section of the plate, 450 mm. long, was slightly adjustable in order to produce a zero circulation around the plate.

The contraction exit velocity was always monitored by a Betz manometer, measuring the difference between the settling chamber total pressure and the exit static pressure.

2.3 Traverse Gear Mechanism

The present experiment required traverse gear which involved movements in two main directions, x and y (for axis notation, see Fig. 2.2), since the flow is two-dimensional. A lead screw type traverse gear, with electrically driven movement in the y-direction, was chosen as the basic movable mechanism. It was mounted on a steel angle, 30 cm. length, with a bolt in the z-direction, around which the traverse gear could be rotated to certain specific positions for yaw (strictly, pitch) calibrations of cross-wire probes. This angle lay on the tunnel floor and was clamped to another angle bolted to the tunnel floor, along which it was slid to change the position of the traverse gear.

The probe position was read out by a linear potentiometer, whose output voltage was calibrated against the actual probe position variation, which had been measured accurately with slip gauges.

This configuration is believed to cause much less interference to the actual flow than the traverse gear normally used in the tunnel.

2.4.1 Pressure Probes and Manometers

Roundpitot tubes of 1 mm. diameter were used for total pressure measurements, mounted on the traverse system previously described.

Static tubes of 2 mm O.D. with 4 holes were used for measuring the static pressure.

Betz manometers were used for all the static and total pressure measurements.

2.4.2 Mean Temperature Probes and Thermometers

Chromel-Alumel thermocouples were used for measuring mean

temperature profiles throughout the present investigation. Measurements of absolute temperature were rather meaningless and, thus, the thermocouples were connected to a COMARK differential thermometer. The free stream temperature, serving as a reference, was always monitored with an absolute COMARK thermometer with a thermocouple placed at $x = 0$ and $y = 0.25$ of tunnel height. The reference pitot tube was at the same position.

2.5 Hot Wire Anemometry

The usual hot wire anemometry arrangement was used for measurements of turbulence quantities and mean velocity, the latter being used primarily for comparison with the pitot tube results as a check on the general reliability of the hot wire reading rather than as actual measurements.

Longitudinal turbulence intensity was measured by using a DISA U-probe with a 5 μm platinum wire. The standard static calibration procedures have been carried out (see Appendix A). In general, a DISA 55D01 anemometer, a low pass filter set at 20 kHz, a high pass at 1 Hz and a DATRON true r.m.s. meter were used. For the mean velocity measurements, a low pass filter set at 1 Hz was used with a SOLARTRON type 4020 digital voltmeter to measure the anemometer output voltage. Analogue check measurements were made without lineariser since the turbulence intensity was rather low.

All measurements of the various turbulence components were performed by a DISA miniature cross-wire probe type 55A38. The determination of the "effective" angles between the flow and the wires was obtained from the yaw calibration together with the static velocity calibration. The method, which is described in Appendix A, avoids the need to measure the geometrical angles of the wires and includes the

contributions to the effective cooling velocity by the velocity components parallel to the wires.

Dynamic calibrations have not been made since Chandrsuda's (1976) comparisons with static calibrations showed only very small differences.

Analogue measurements were made for check purposes and were confined to U-probe measurements.

Calibrations were usually performed before and after each run of measurements or even more frequently when it seemed desirable. If the drift in the calibration curves was large (4% variation in slope or intercept), the measurements were repeated.

2.6 Skin Friction

Because of self-induced pressure gradient, the skin friction will vary rapidly close to the trailing edge. The actual perturbation is confined to the viscous sublayer of the flow. Therefore, in order to deduce a nominal value of skin friction at the trailing edge, it was decided to use Clauser charts, with universal logarithmic law constants, $K = 0.41$, $A = 5.0$, as suggested by Coles (1968). The mean velocity profiles were measured just upstream the trailing edge. The so determined skin friction value was later compared with the wall shear stress measured with a cross wire probe.

For the case of a boundary layer on rough surfaces, the problem is more complicated and it is difficult to measure the skin friction even far from the trailing edge. Perry et al (1963) suggested that the effective origin of the wall or the slip velocity must be known. Antonia and Luxton (1971) proposed a method to obtain the effective position of the wall by trial and error, i.e. the best fitting of a straight line in the log law.

The first results using the last method were not very encouraging. Other methods, like the momentum method or the mean velocity gradient at the wall method, were not adopted, mainly due to their inherent uncertainties.

Since the extrapolation of the cross-wire measurements to the wall on the smooth side agreed quite well with the Clauser charts' values of skin friction, we obtained the wall shear stress on the rough side simply by the same process of extrapolating the cross-wire results, assuming their accuracy. Indeed, it was decided to repeat a few times the turbulence measurements on the rough boundary layer and then to rotate the cross-wire 180^{o} and repeat the measurements for comparison with the previous measurements.

2.7 Conditional Sampling Techniques

2.7.1 Introduction

Earlier in the introduction, the two main types of fluctuating interfaces encountered in the experiment were mentioned: one near the outer edge of the boundary layer, which separates turbulent flow from irrotational, and the other, near the centre line of the wake, which separates fluid which has passed above the plate from fluid which has passed below it.

The difficulty in discrimination is much greater in the case of an internal interface: clearly, only permanent marking or "tagging" could provide the additional variable with different characteristics in the turbulent zones either side of the interface. The addition of heat to one turbulent field is a usual way of tagging and the instantaneous temperature is the time-resolved function which forms the basis of a conditional sampling technique. Johnson (1959) was the first to report

the existence of intermittent temperature fluctuations at an internal interface in a boundary layer with a step change in surface heat flux. Statistics of the thermal layer interface and conditionally sampled measurement with respect to this interface, in a similar experiment, were reported recently by Antonia et al (1977).

A problem associated with the use of heat as a passive scalar or tracer in these techniques is the certainty of the coincidence of the temperature and velocity interfaces.

In an external interface, heat conduction by molecular conductivity may be different from momentum transport by viscosity leading to different positions of temperature and velocity interfaces. If the molecular Prandtl number $Pr = \mu c_p/k$ is near unity, this is not significant. If $Pr \gg 1$, i.e. small conductivity, this means that temperature interface is on the inside of the viscous superlayer, i.e. the start of the viscous region. If $Pr \ll 1$, it is possible that heat conduction will extend farther out than the outer edge of the viscous superlayer.

In an internal interface, the heat marks the fluid (mass). Here, any sort of conductivity is unwelcome. The jump of vorticity which exists in the external interface may or may not exist here too. What should be a sharp interface between top fluid and bottom fluid will gradually become uncertain. In fact, the thickness of the interface will be of the order of $\sqrt{\nu\tau}$ where τ is the time that is taken for the fluid to flow from the trailing edge to the point considered, i.e. $\sqrt{\nu x/U}$ which means that the uncertainty in thickness of the interface is going to be of the order of laminar boundary layer imagined to be on a solid surface starting at the trailing edge, i.e. about 0.44 mm. for $x = 400$ mm., fairly small compared to the general uncertainties. This is an inevitable error even for flows with $Pr \simeq 1$.

Fiedler and Head (1966), by comparing the signals of a hot wire anemometer and a photoelectric smoke detector, found identity of smoke and turbulence distribution in a boundary layer. Chevray and Tutu (1972), by studying a large number of simultaneous velocity and temperature traces, concluded that the two interfaces coincide. Since then, all the investigators who used heat as a tracer in airflows assumed coincidence of these interfaces.

2.7.2 Heat Supply

The present conditional sampling techniques required tagging by heating one of the boundary layers. The method chosen for heating one boundary layer was to use Nichrome wires stretched in the spanwise direction at the leading edge. Heating wires within the boundary layer were chosen in preference to a heating element on the plate surface, to minimize heat transfer to the plate.

After some preliminary investigations, three heating wires were used: one 26 S.W.G. (0.457 mm. in diameter) and two 22 S.W.G. (0.71 mm.). This combination was a result of two different requirements:-

(a) the amount of heat required for the "hot" - "cold" discrimination;

(b) the amount of current which the wires could withstand together with the maximum output voltage of the auto-transformer.

The tests started with three wires of 26 S.W.G. and then it was necessary for two of them to be replaced by thicker 22 S.W.G. Special care was taken to avoid one wire being inside the other's wake because

it could be burnt out as happened sometimes during the tests. The position was as close to the wall as possible.

The inevitable longitudinal thermal expansion of the wires was taken up by the displacement of coil springs which kept the wires tensioned.

The two similar wires were connected in series and then to a VARIAC autotransformer, with maximum load 8A, 260 V. Another VARIAC of the same type was used for the other thinner heating wire.

For the sake of aerodynamic symmetry, three similar wires, unheated, were placed at symmetric positions on the other side of the plate.

The electric power, which was finally supplied to the airflow, was about 2 kW measured at the input of the autotransformers and, at a free stream velocity of 33 m/s, gave a maximum temperature difference between the heated and the unheated boundary layers at the trailing edge of $2^{o}C$. This amount of heat was sufficient to provide the required discrimination between "hot" and "cold" fluid and small enough to prevent any buoyancy effects. Proper checks carried out during the experiments, and comparisons between digital turbulent measurements with and without heat in the flow, gave convincing evidence of the absence of any buoyancy effects.

Steady state thermal conditions in the wind tunnel were reached after three hours of running at the required speed, although it was not necessary to have thermal equilibrium for conditional sampling technique. This is due mainly to the large thermal capacity of the tunnel and its environment.

2.7.3 Temperature Fluctuations

Temperature fluctuation measurements carried out with a 1 μm

Wollaston platinum wire soldered to a "home-made" probe and etched using the departmental facilities. The probe was operated as a "cold" wire in the constant current mode and it was connected to a simple circuit as a resistance thermometer. The output signal was then amplified by a BROOKDEAL 431 nanovolt preamplifier of very low noise level with its internal filters set at 1 Hz lower frequency limit and 20 kHz upper frequency limit and working at a fixed gain of 60 dB. The block diagram of the system is shown in Fig. 2.3: for more details, see Appendix B.

The fluctuating output voltage was directly proportional to the temperature fluctuation and the constant of proportionality was determined by a very simple calibration or it could be estimated algebraically, as described in Appendix B.

The present circuit of the temperature wire was found to have two main advantages. Firstly, it was simple and easy to operate and, secondly, it had a noise level 6 - 10 times less than the DISA temperature bridge of the 55M series.

The probe current chosen was a result of two contradicting requirements: good temperature sensitivity and negligible velocity sensitivity. Finally, after measuring the velocity sensitivity of a typical temperature wire, it was decided that adequate heating currents were 1.6 mA and 1.0 mA for the symmetric and asymmetric wakes respectively. At the operating points, the temperature sensitivity was at least two orders of magnitude greater than the velocity sensitivity. Consequently, the velocity fluctuations sensed by the temperature wire were negligible. For more details, see Appendix B.

The application of heat to tag one shear layer causes some difficulties in the use of hot wires for velocity measurements. Since

the fluid temperature was varying with time and was generally different from that at which the velocity calibration of the probe was performed, it was strictly necessary to allow for (a) the spurious voltage fluctuation caused by the temperature fluctuations, and (b) the effect of temperature fluctuations on the instantaneous sensitivity to velocity fluctuations. However, if the temperature fluctuations are small as they are in the present experiment, the latter effect can be neglected provided that the sensitivity is evaluated at the local mean temperature.

Dean and Bradshaw (1976) derived a simple formula for instantaneous temperature corrections of the hot wire output. This method was used throughout the present data analysis and it is briefly described in Appendix C.

The complete temperature probe was mounted on the stem of a DISA miniature cross-wire probe and parallel to it. The wire axis was perpendicular to the flat plate surface and was separated about 1 mm from the cross-wire. This three-wire probe provided simultaneous signals of velocity and temperature through the circuit components of Fig. 2.3 to an analogue magnetic tape-recorder (Ampex type FR1300) at a speed of 60 i.p.s. and 20 kHz frequency response (at 30 ms^{-1}, wavelength = 1.5 mm - compatible with wire length of 1.0 mm. which limits spatial resolution). The analogue recordings were digitized by using the Departmental digitization system which is described in Appendix E.

2.7.4 Compensation

The frequency response of uncompensated 1 μm wires is inadequate for resolving the fine structure. The - 3 dB point varies between 500 and 800 Hz depending upon the etching conditions and the

resistance (length). Frequency compensation is thus necessary. For that purpose, the most suitable circuit is illustrated in Fig. D.1a of Appendix D together with more details. By varying the capacitor, C_1, the amount of compensation may be adjusted so as to get a very sharp fall or rise into the temperature trace. This technique provided compensation adequate for the present purposes of "hot - cold" discrimination, regardless whether it was exact or not, compensating for the time lag of the wire and also for any molecular conductivity of heat which will also tend to smooth out sharp temperature jumps. The time constant is a function of velocity, since the Nusselt number is a function of Reynolds number and, therefore, the compensator must be set at each operating point.

It was found that the time constant was deteriorating with time since sub-micron contamination in the air flow adhered to the 1 μm wire. Thus, it was necessary from time to time to re-adjust the compensation and ultimately to clean the wire with a methanol solution.

3' × 3' LOW SPEED WIND TUNNEL

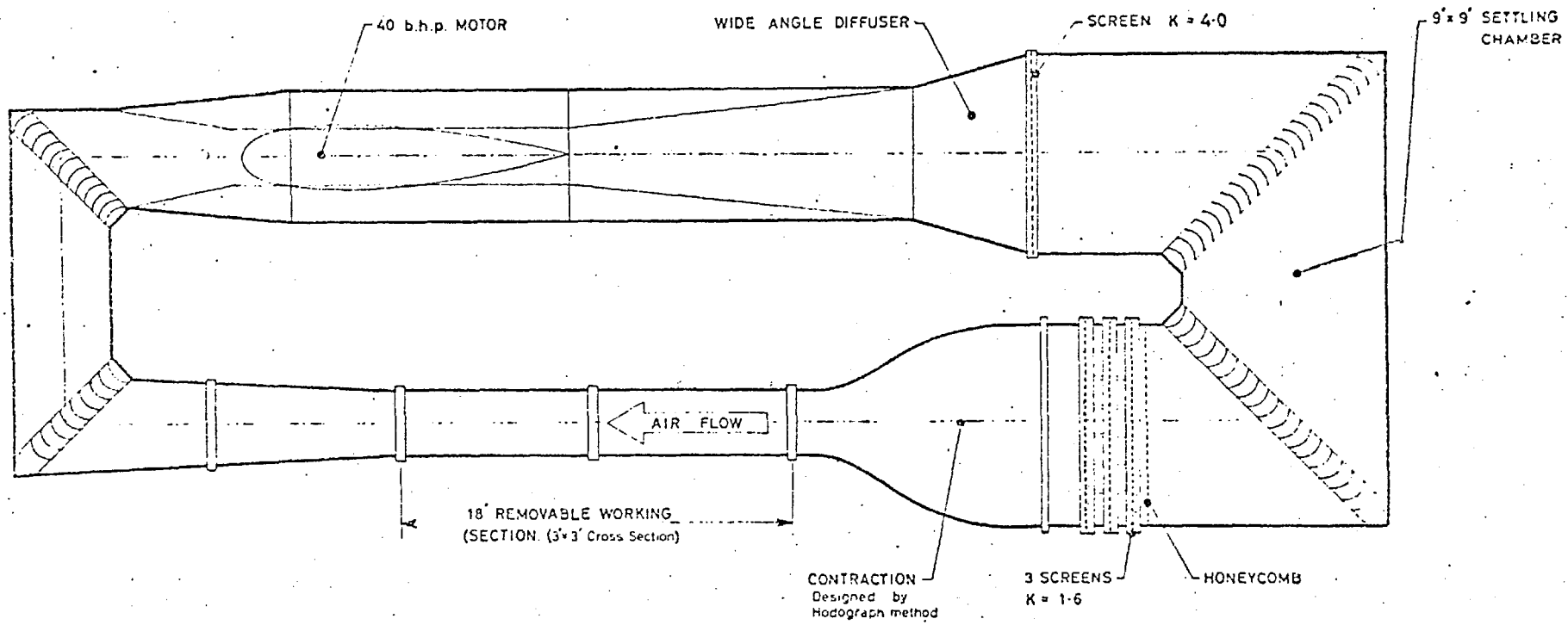

FIG. 2.1

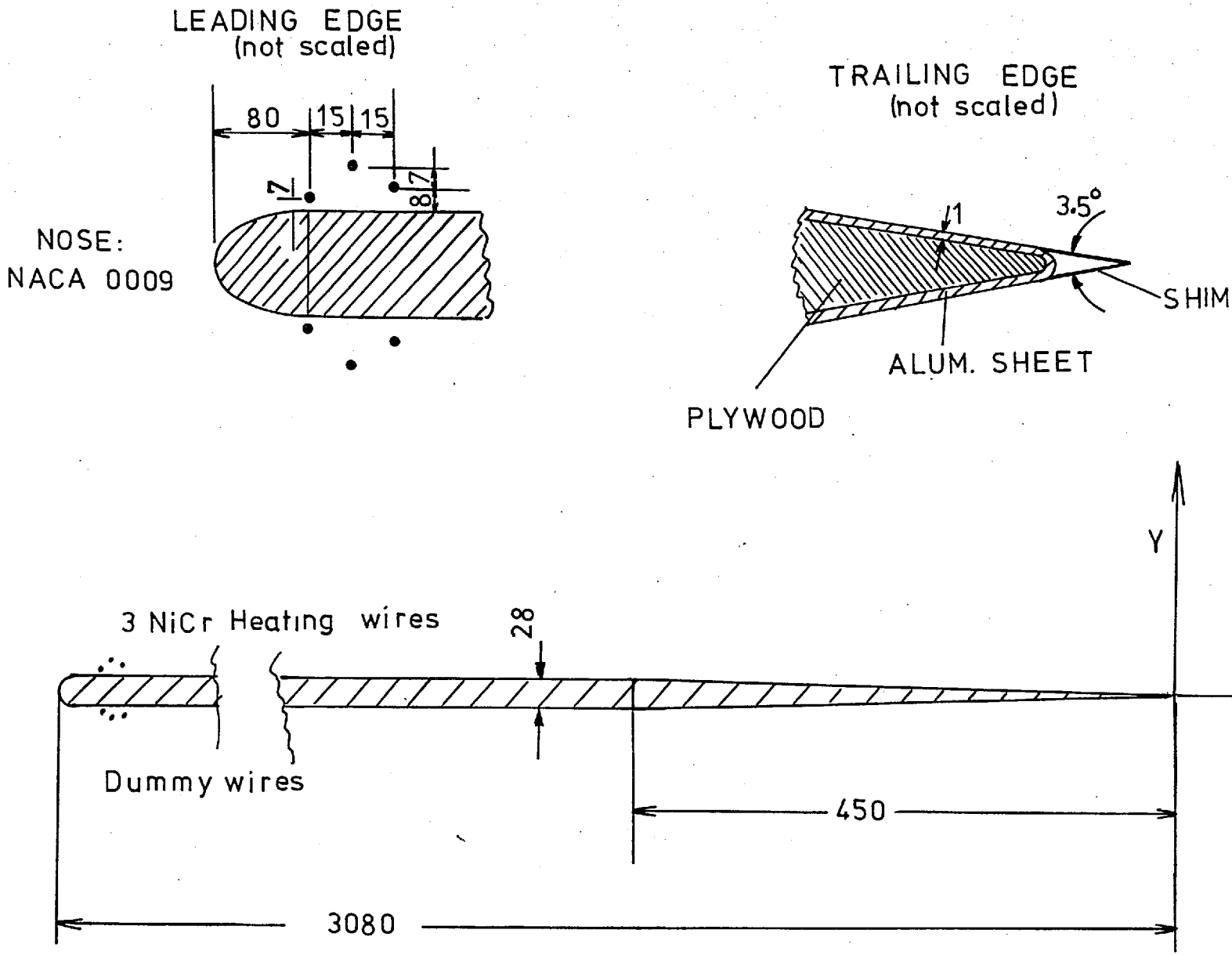

FIG. 2.2 FLAT PLATE

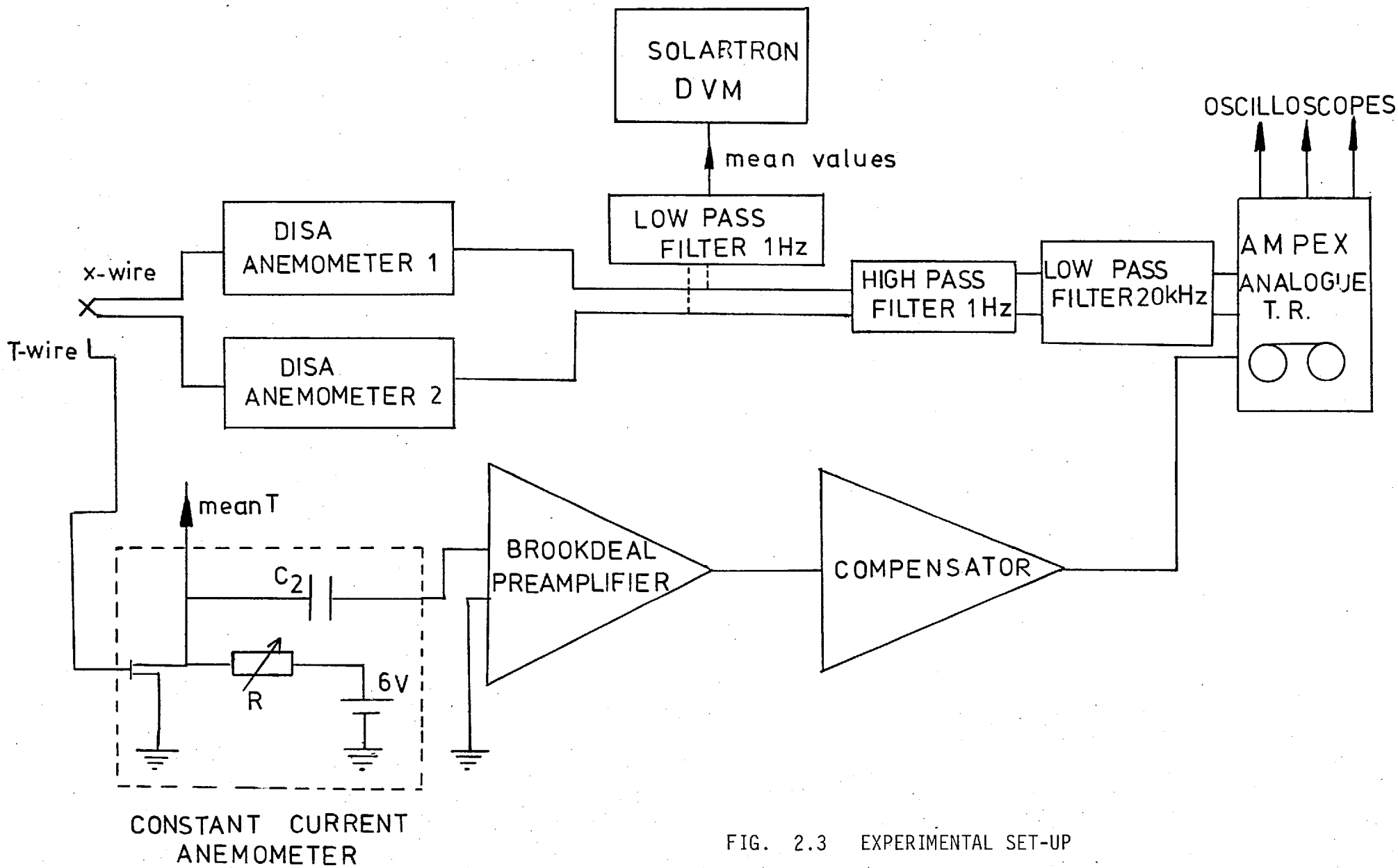

FIG. 2.3 EXPERIMENTAL SET-UP

3. INTERMITTENCY

3.1 Choice of Criteria and Thresholds

The right choice of intermittency criteria is very important in determining an interface. Usually they vary from flow to flow, however normalized. The present investigation involved determination of intermittency from a temperature signal, which is believed to involve less problems, difficulties and uncertainties than the determination from velocity signal.

There are generally two criteria which are in use, in various ways, by various investigators: the level criterion and the slope criterion. The choice mainly depends on the type of flow considered and on the special problems which are involved in each case, e.g. Dean and Bradshaw (1976) had the problem of a possible drift of the "cold" level and obviously they could not use an absolute level of temperature discrimination. Their signals consisted of slowly varying "cold" levels while in the "hot" regions, the slopes were fairly large compared with slopes in the slowly varying "cold" regions. Therefore, they used the slope criterion mainly, backed up with the level criterion. Other investigators like La Rue (1973), Antonia (1974) and Kovasznay and Ali (1974), had evidently had sufficiently small tunnel temperature variations and, consequently, they were able to use a simple level criterion. This is acceptable if the "cold" fluid is always the tunnel free stream fluid. However, if the "cold" fluid has actually been through a turbulent boundary layer, then its temperature is slightly disturbed and is liable to both compatibly low frequency temperature wanderings and a certain amount of temperature noise.

After careful study of many temperature traces in the present experiment using an interactive graphics program developed by Weir (1976)

and Calcomp plots with various combinations of different criteria, it was decided that a level criterion first and a slope as a back-up criterion was the most appropriate choice.

The algorithm based on this choice has two particular advantages. It can deal with a possible drift of the "cold" level and work easily with long bursts of "hot" fluid which, due to non-uniform heating of the heated boundary layer, has temperature fluctuations with temperature slope less than that of the "cold" fluid. The algorithm was incorporated into the main digital analysis program D3E as a subroutine called LAGTHR and it was developed by Weir (1976). The flow-chart of this algorithm is shown in Appendix F.

The slope $\partial T/\partial t$ was obtained from successive values of the digitized instantaneous temperature signals and was then compared with the value of the slope criterion Θ_3. The instantaneous $T_i - T_{cold}$ value was compared with the threshold level $\Theta_a = T_{cold} + \Theta_2$ where Θ_2 is the value of the level criterion. For the first data points, the T_{cold} was set temporarily to the mean temperature, T, and after the first "hot" burst was found, it was reset.

By adjusting the values of the various parameters involved in the program, apart from the main criterion, most of the difficulties arising at some areas of high or low intermittency, can be overcome easily, e.g. the longest expected length of a "cold" burst in a low intermittency area is not the same as in the medium or high intermittency area ("cold" region). Alternatively the longest expected length of a "hot" burst in a high intermittency area ("hot" side) is not the same as in a low intermittency area.

In the present case, the problem of drift of the "cold" level was not so important as in the jet experiment of Weir et al (1978) where the "cold" fluid was heated slightly after its passage through the

tunnel blower compared with the entrained fluid from the room at the ambient temperature and thus there resulted a significant variation of the "cold" level. There are some cases where a spike of "cold" fluid, say, happens inside a "hot" burst and its amplitude is higher than the level threshold. By the level criterion, it will be marked as "hot" but the slope criterion will detect it as "cold".

The proper values of the two criteria have been selected after inspecting a large number of Calcomp plots and they are tabulated in Appendix F.

By examining the response of the intermittency factor γ to the variation of the threshold level, it can be checked a posteriori that these values have been correctly chosen. In an "idealized" temperature signal, γ is independent of the threshold level. In the outer part of the wake where the interface of the turbulent - non-turbulent fluid is comparatively uncomplicated (see Figs. 3.1a, 3.1b), this argument is quite well justified over a wide range of threshold settings. In the case of an interface which separates two turbulent zones, the "true" value of the threshold is rather difficult to check, since a typical "hot" burst is like those in Figs. 3.2a, 3.2b, and must be as close to the T_{cold} as possible.

The values of the two criteria were kept constant throughout the same profile, with some very rare exceptions where it was necessary to increase, by not more than 10%, the threshold level to exceed the noise level in very-low-γ areas with a few "hot" bursts.

Inspection by eye of the Calcomp plots was always the key part of the operation of setting the proper values of the criteria. From profile to profile, the level criterion was not changed significantly. At the last downstream profile, at $x = 400$ mm , it was decreased by 8%. Decreased values for the slope criterion were also used for the

downstream profiles.

After the values of the criteria had been selected, the conditionally sampled turbulence quantities were calculated with respect to the conventional-average baseline. This enabled the addition law:-

$$\gamma \overline{Q}_{HOT} + (1 - \gamma) \overline{Q}_{COLD} = Q_{TOTAL} \qquad (3.1.1)$$

to be applied, with Q_{HOT} being the average inside the "hot" zone and $\gamma \overline{Q}_{HOT}$ the "hot-zone" contribution to the conventional average Q_{TOTAL}; similarly for the $(1 - \gamma) \overline{Q}_{COLD}$.

As in all previous work in the Department, the fluctuations were measured with respect to the overall mean velocity, not to the zone mean velocity, since in the latter, only the fine scale is taken into account and automatically the main eruption velocity of a burst is excluded.

3.2 Warm or Mixed Fluid Zone

Bradshaw and Murlis (1974) distinguished "retail" and "wholesale" intermittency measurements as those that do or do not resolve the fine-scale corrugations of the intermittency interface. Most of the previous measurements of velocity or temperature intermittency studies gave "wholesale" measurements which result whatever holding time is used because by definition dropouts or bursts shorter than the hold-time cannot be measured. In the present experiment and in both cases of the symmetric and asymmetric wakes, fine scale activities are quite intensive around the centre-line of the wake, since these small eddies were the former occupants of the inner layers of the boundary layers. Careful examinations of Calcomp plots of various temperature signals

revealed the existence of fine-grained mixing, starting immediately after the trailing edge and continuing downstream in the wake. which means that the interaction between the two shear layers takes place mainly by fine scale mixing (see a typical Calcomp plot in Figs. 3.2a and 3.2b).

Since the two layers, "cold" and "hot" interact strongly and mixed very rapidly to form a "mixed" or "warm" layer, it was desirable to distinguish the "hot", "cold" and "warm" regions (Fig. 3.4). This cannot be done directly, because the intermittency algorithm labels all as "hot" all regions that are not "cold". In the symmetrical case "warm" region statistics can be deduced by invoking symmetry, but in the asymmetric case it is necessary to do two experiments, one with the top side heated and another with the bottom side heated; the "hot", "cold" and "warm" regions can then be distinguished (see Figs. 3.3 and 3.4). The technique in detail is as follows.

In the case where the Upper Boundary Layer is heated (UBLH), a temperature signal of a typical eddy is as shown in Fig. 3.3a (fluctuations within the "hot" region have been underestimated for clarity). The temperature change from "cold" to "hot" is not quite abrupt because of fine scale mixing and this is the "warm" or "mixed" fluid. The "hot" fluid is purely the upper fluid (originating in the upper boundary layer) and the "cold" fluid is the lower fluid. The intermittency subroutine can detect the "cold" fluid and cannot discriminate the "warm" from the "hot". So if γ_{CU} is the fraction of time when "cold" fluid is detected in the case of the upper boundary layer being heated and γ_{HU} and γ_{WU}, the corresponding fractions for "hot" and "warm" fluid, we have:-

$$\gamma_{CU} + \gamma_{WU} + \gamma_{HU} = 1 \qquad (3.2.1)$$

with γ_{CU} being the only measurable quantity.

If the lower boundary layer is heated, the same typical eddy will give a temperature signal like in Fig. 3.3b. In this case, the upper fluid becoming now "cold" can be easily detected. An expression similar to (3.2.1) is valid but with suffix L for Lower:-

$$\gamma_{CL} + \gamma_{WL} + \gamma_{HL} = 1 \qquad (3.2.2)$$

In addition to (3.2.1) and (3.2.2):-

$$\gamma_{HL} = \gamma_{CL} \qquad \text{upper fluid intermittency} \qquad (3.2.3)$$

$$\gamma_{HL} = \gamma_{CU} \qquad \text{lower fluid intermittency} \qquad (3.2.4)$$

$$\gamma_{WL} = \gamma_{WU} \qquad \text{mixed fluid intermittency} \qquad (3.2.5)$$

Bearing in mind that γ_{CL}, γ_{CU} are directly measurable, from (3.2.1) and (3.2.3) we obtain:-

$$\gamma_{WL} = \gamma_{WU} = 1 - \gamma_{CU} - \gamma_{CL} \qquad (3.2.6)$$

or:-

$$\gamma_{WL} = \gamma_{WU} = \gamma'_{HU} - \gamma_{CL} = \gamma'_{HL} - \gamma_{CU} \qquad (3.2.7)$$

where $\gamma_H' = 1 - \gamma_C = \gamma_H + \gamma_W$, i.e. γ_H' is what is measured as "hot" by the algorithm. If Q is the contribution of each zone to the total conventional average, then:-

$$\overline{Q}_{CU} + \overline{Q}_{WU} + \overline{Q}_{HU} = Q_{TOTAL} \tag{3.2.8}$$

and similarly to (3.2.6) and (3.2.7) we get:-

$$\overline{Q}_{WU} = \overline{Q}_{HL}' - \overline{Q}_{CU} \tag{3.2.9}$$

and:-

$$\overline{Q}_{WL} = \overline{Q}_{HU}' - \overline{Q}_{CL} \tag{3.2.10}$$

where Q_{HU}' or Q_{HL}' are measured as "hot" and includes truly "hot" fluid plus "warm" as well.

Hereafter, because it is easier to deal with measurable quantities like $\overline{Q}_H'$ and $\overline{Q}_C$, $\overline{Q}_H'$ is replaced by $\overline{Q}_H$ and the original $\overline{Q}_H$ is going to be described when necessary, as "truly hot".

So:-

$$\overline{Q}_W = \overline{Q}_{HU} - \overline{Q}_{CL} = \overline{Q}_{HL} - \overline{Q}_{CU} \tag{3.2.11}$$

$$WARM = HOT_U - COLD_L = HOT_L - COLD_U$$

For large positive y, $\overline{Q}_{HU} = \overline{Q}_{TOTAL} = \overline{Q}_{CL}$ and $\overline{Q}_{HL} = \overline{Q}_{CU} = 0$ and for large negative y, $\overline{Q}_{HL} = \overline{Q}_{CU} = \overline{Q}_{TOTAL}$ and $\overline{Q}_{HU} = \overline{Q}_{CL} = 0$. For the case of the symmetric wake, the symmetry can, in principle, provide

the additional relation for determining the "mixed" or "warm" zone averages; a second experiment with the lower boundary layer heated is not needed.

$$Q(Y) = \overline{u^m v^n} \qquad \text{for } m, n = 0, 1, 2, 3$$

$$Q(Y) = +\,Q(-Y) \qquad \text{for } m = 0, 1, 2 \qquad n = 0, 2$$

or:-

$$Q(Y) = -\,Q(Y) \qquad \text{for } m = 0, 1, 2 \qquad n = 1$$

and consequently:-

$$\overline{Q}_{CL}(Y) = \pm\,\overline{Q}_{CU}(-Y)$$

$$\overline{Q}_{HL}(Y) = \pm\,\overline{Q}_{HU}(-Y)$$

and so:-

$$\overline{Q}_{W}(Y) = \overline{Q}_{HU}(Y) - (\pm)\,\overline{Q}_{CU}(-Y) \qquad (3.2.12)$$

Although the "warm" zone averages can be evaluated from (3.2.12), it was decided to make limited check measurements, heating the lower boundary layer as well. Such measurements were made for x = 100 mm and x = 400 mm downstream the trailing edge.

To summarise here, as a result of the early conclusion that the interaction takes place mainly by fine scale mixing of the two boundary layers after the removal of the wall constraint, i.e. the

trailing edge, the wake consists of three layers: the upper fluid layer, the lower fluid layer and the mixed layer of fine scale eddies (see Fig. 3.4). The purpose of the conditional sampling techniques employed was to distinguish the three.

FIG. 3.1a

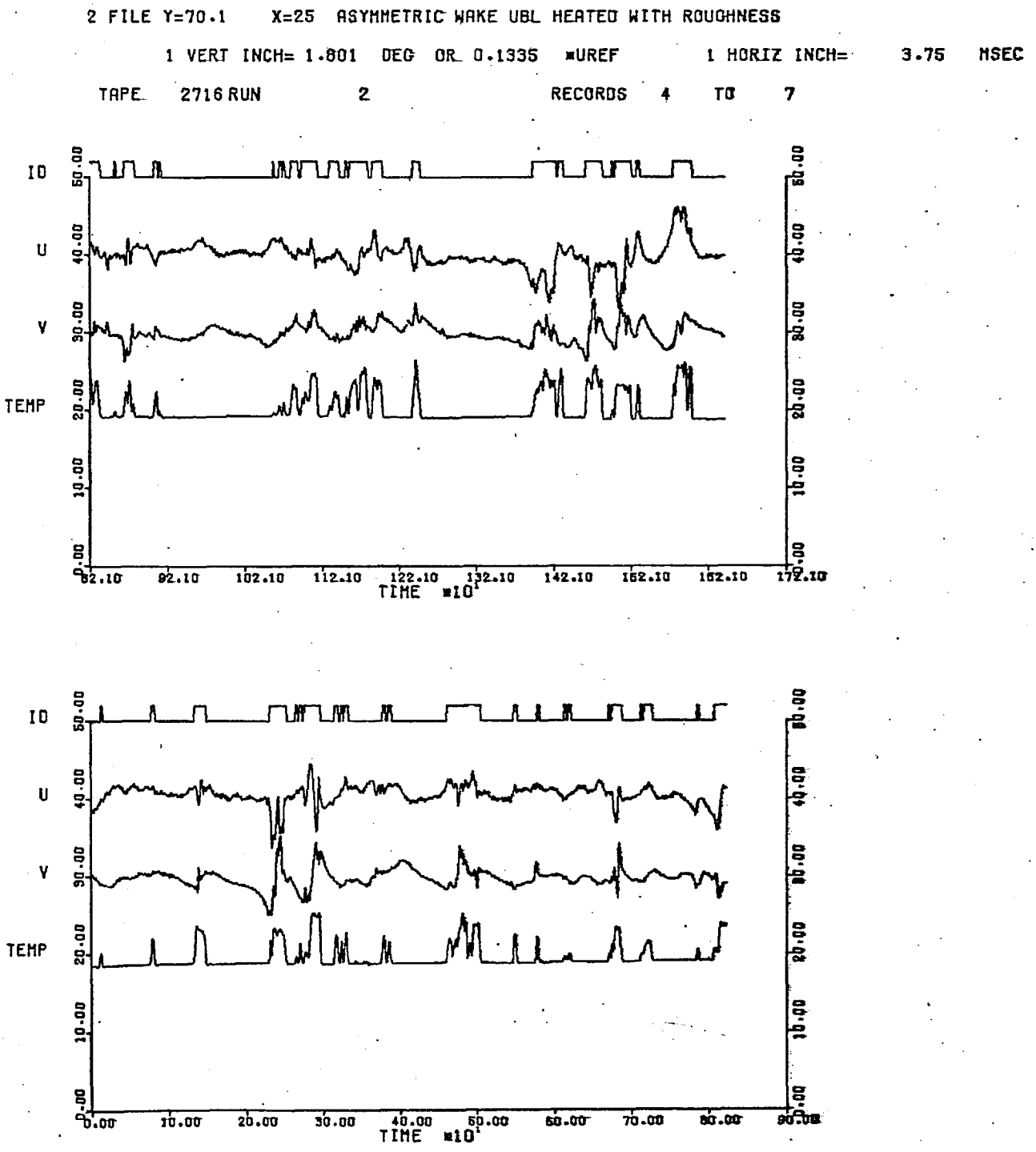
2 FILE Y=70.1 X=25 ASYMMETRIC WAKE UBL HEATED WITH ROUGHNESS
1 VERT INCH= 1.801 DEG OR 0.1335 *UREF
1 HORIZ INCH= 3.75 MSEC
TAPE 2716 RUN 2
RECORDS 4 TO 7
ID
U
V
TEMP
50.00
40.00
30.00
20.00
10.00
0.00
82.10
92.10
102.10
112.10
122.10
132.10
142.10
152.10
162.10
172.10
TIME *10
ID
U
V
TEMP
50.00
40.00
30.00
20.00
10.00
0.00
0.00
10.00
20.00
30.00
40.00
50.00
60.00
70.00
80.00
90.00
TIME *10

FIG. 3.1b

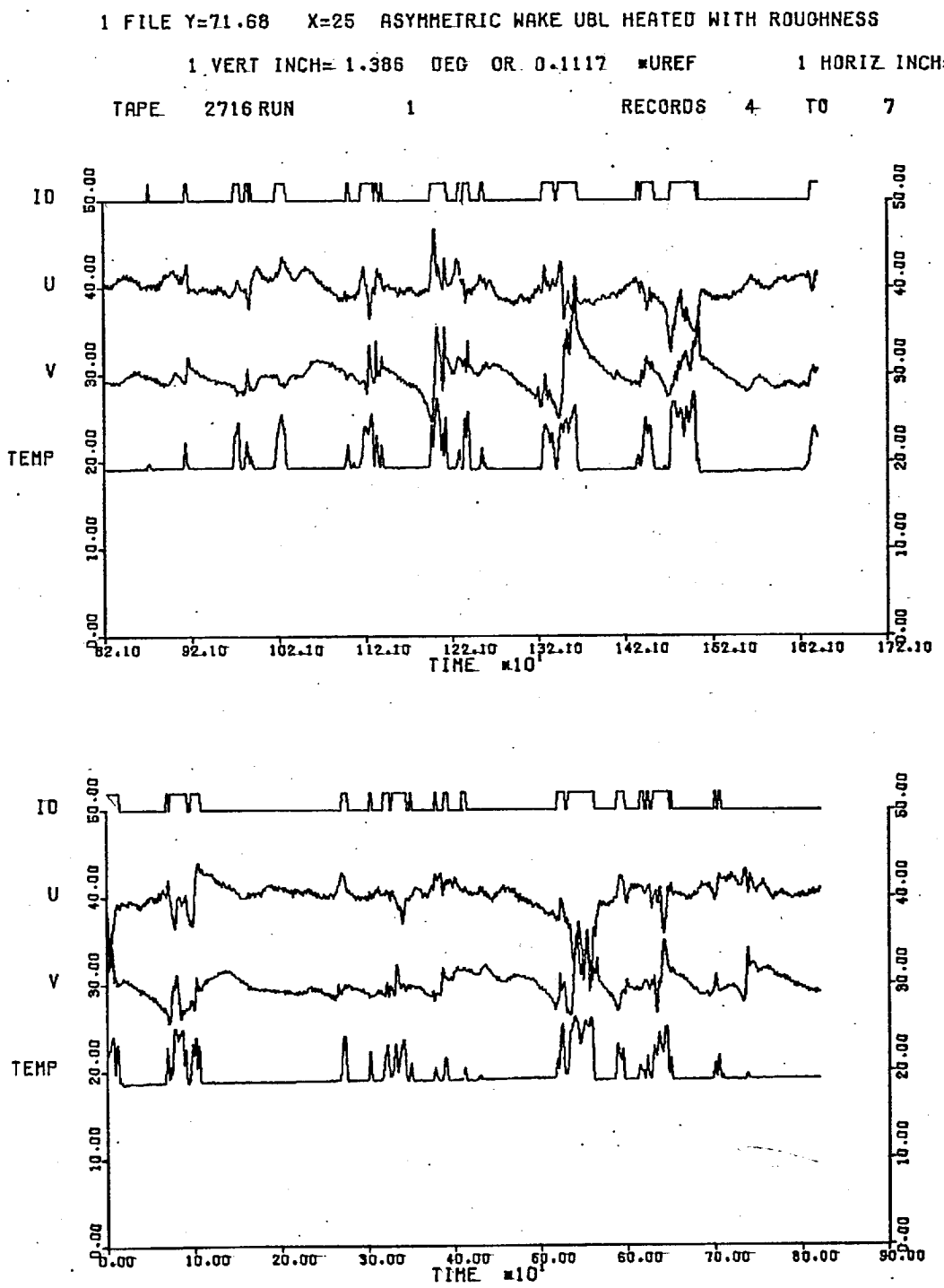
1 FILE Y=71.68 X=25 ASYMMETRIC WAKE UBL HEATED WITH ROUGHNESS
1 VERT INCH= 1.386 DEG OR 0.1117 *UREF
1 HORIZ INCH= 3.75 MSEC
TAPE 2716 RUN 1
RECORDS 4 TO 7
ID
U
V
TEMP
50.00
40.00
30.00
20.00
10.00
0.00
82.10
92.10
102.10
112.10
122.10
132.10
142.10
152.10
162.10
172.10
TIME *10¹
ID
U
V
TEMP
0.00
10.00
20.00
30.00
40.00
50.00
60.00
70.00
80.00
90.00
TIME *10¹

FIG. 3.2a

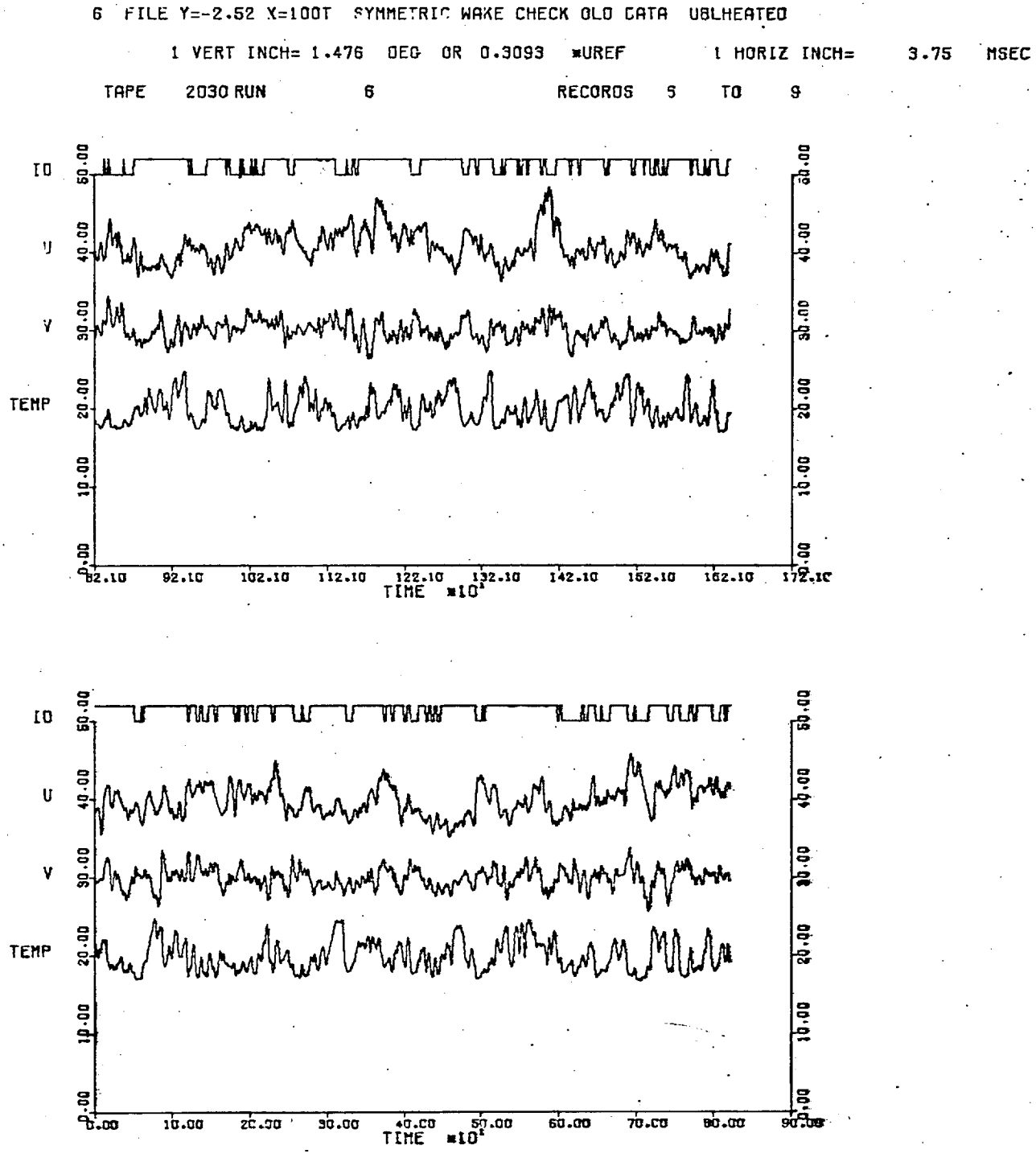
6 FILE Y=-2.52 X=100T SYMMETRIC WAKE CHECK OLD DATA UNLHEATED
1 VERT INCH= 1.476 DEG OR 0.3093 *UREF
1 HORIZ INCH= 3.75 MSEC
TAPE 2030 RUN 6
RECORDS 5 TO 9
IO
U
V
TEMP
60.00
40.00
30.00
20.00
10.00
0.00
82.10
92.10
102.10
112.10
122.10
132.10
142.10
152.10
162.10
172.10
TIME *10²
IO
U
V
TEMP
60.00
40.00
30.00
20.00
10.00
0.00
0.00
10.00
20.00
30.00
40.00
50.00
60.00
70.00
80.00
90.00
TIME *10²

FIG. 3.2b

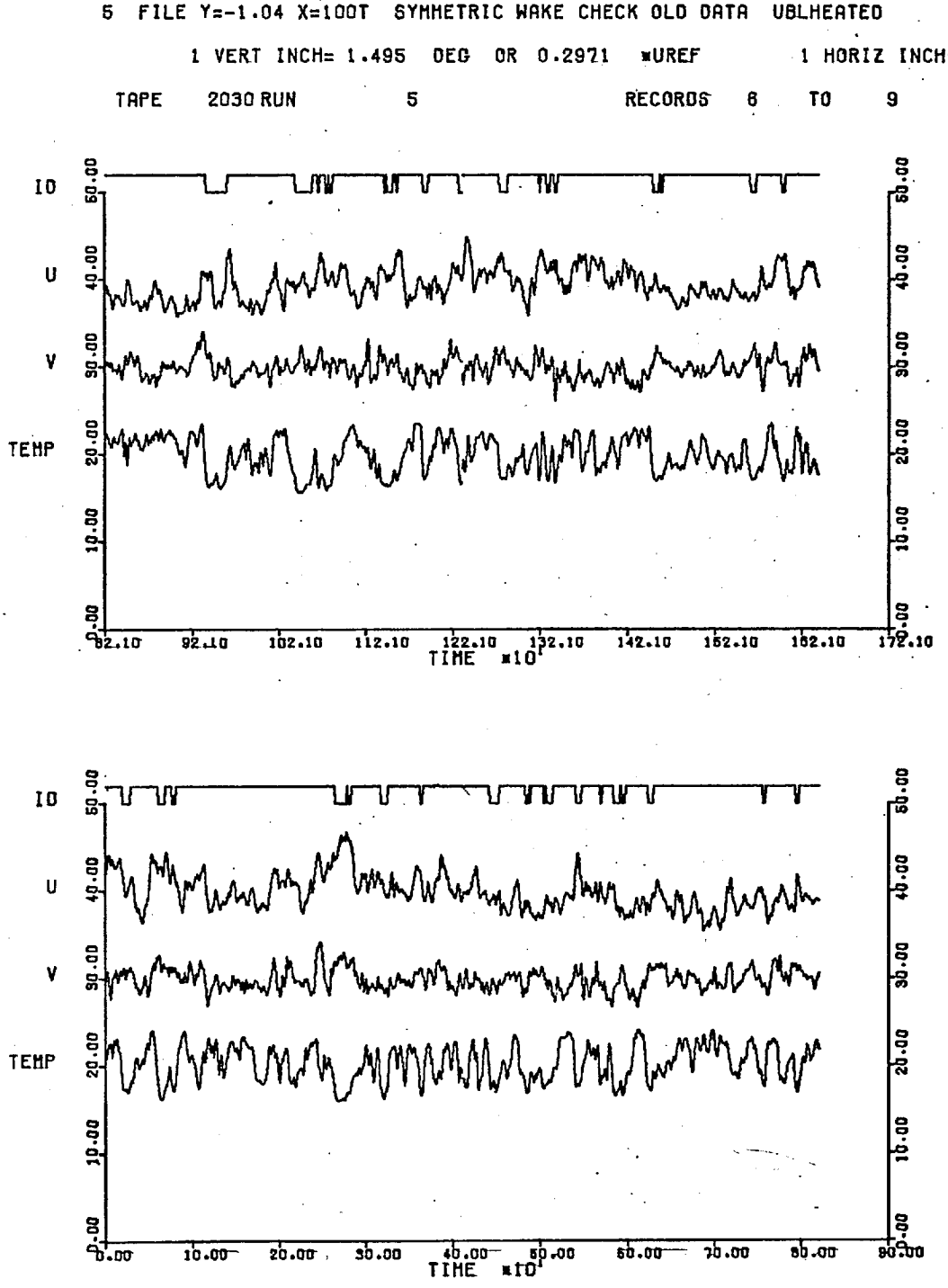
5 FILE Y=-1.04 X=100T SYMMETRIC WAKE CHECK OLD DATA UBLHEATED
1 VERT INCH= 1.495 DEG OR 0.2971 *UREF
1 HORIZ INCH= 3.75 MSEC
TAPE 2030 RUN 5
RECORDS 6 TO 9
IO
U
V
TEMP
60.00
40.00
30.00
20.00
10.00
0.00
82.10
92.10
102.10
112.10
122.10
132.10
142.10
152.10
162.10
172.10
TIME *10
IO
U
V
TEMP
60.00
40.00
30.00
20.00
10.00
0.00
0.00
10.00
20.00
30.00
40.00
50.00
60.00
70.00
80.00
90.00
TIME *10

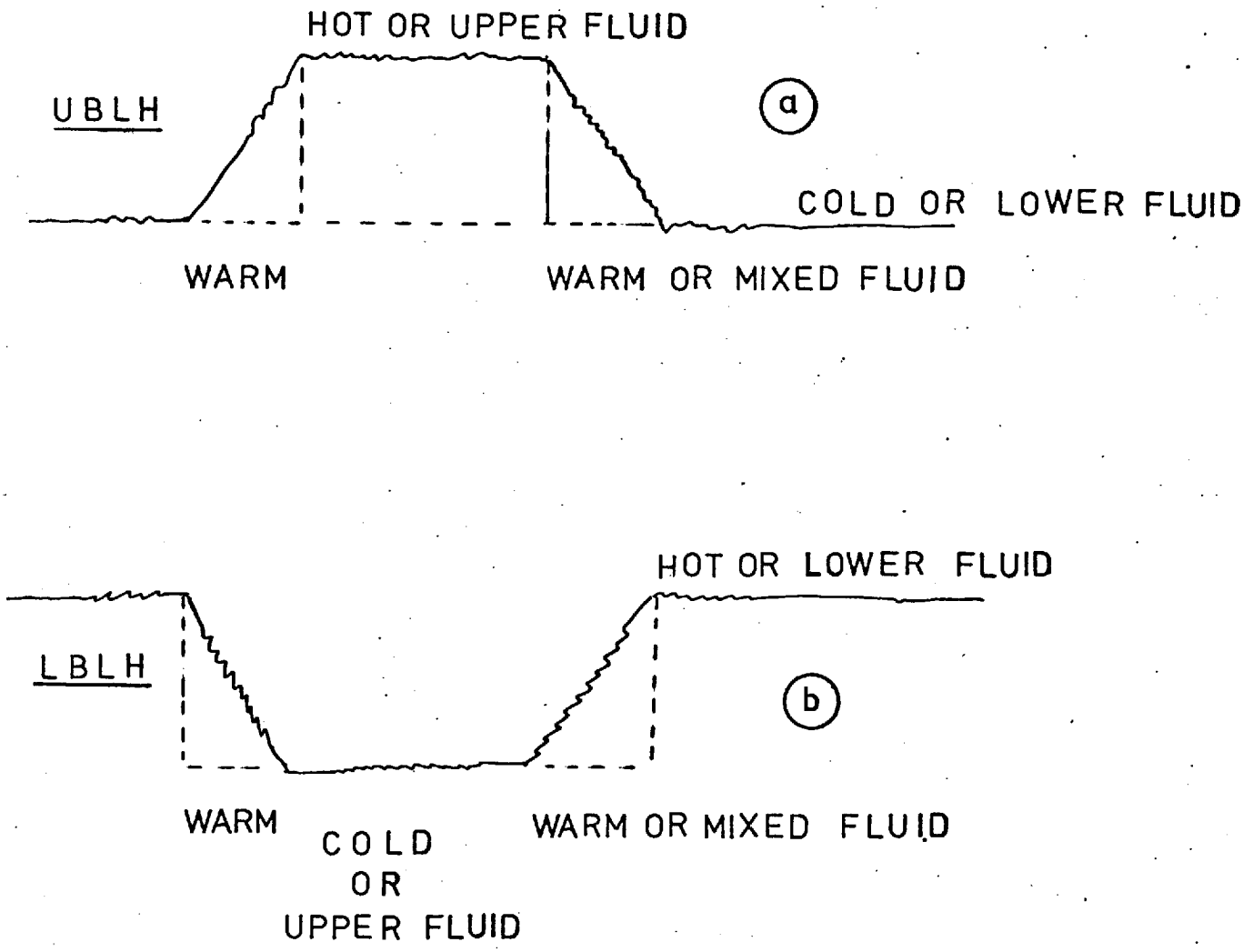

FIG. 3.3 TEMPERATURE SIGNAL OF A TYPICAL EDDY

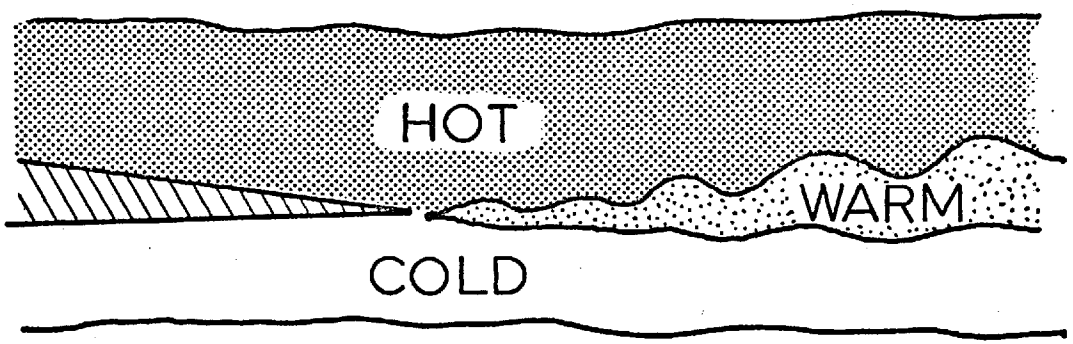

"HOT", "WARM" and "COLD" regions in wake

FIG. 3.4

4. SYMMETRIC WAKE RESULTS

4.1 Mean Velocities and Bulk Flow Parameters

4.1.1 General

The flow was investigated at a Reynolds number based on the momentum thickness at the trailing edge of 13600.

The first object of the experiment was to establish a two-dimensional flow. Checks were done at the trailing edge, $x = 0$ and at the furthest downstream station, $x = 500$ mm. Pitot tube traverses showed two-dimensionality in the mean flow to within 1 - 2% on mean velocity over 50% of the tunnel width at the tunnel centre-line, at $x = 500$ mm. To within the same limits, the flow at the trailing edge was uniform over 70% of the tunnel width. Clauser chart checks of the wall shear stress at the trailing edge and at $z = \pm 200$ mm gave results within about 5% of the centre-line value.

A static tube was used to check the zero circulation at the trailing edge (zero static pressure difference between upper or lower part). It was found that by slightly tilting the last part of the flat plate, it was possible to get better symmetry of the flow and near-zero circulation. The static pressure difference between $y = \pm 150$ mm was less than $0.008\ \rho U_e^2$.

The mean velocity profiles at the centre plane perpendicular to the plate, plotted as U/U_e versus y/Θ_0, are shown in Figs. 4.1 and 4.2, where Θ_0 is the momentum thickness at $x = 0$. The asymmetry which exists is of the order of $\left(1 - \frac{u_{\tau U}}{u_{\tau L}}\right)$, where $u_{\tau U}$ and $u_{\tau L}$ are the friction velocities for the upper and lower wall respectively at $x = 0$. In the region around the centre-line, $\partial U/\partial x > 0$ for $x > 0$ which means that for $y > 0$, V is negative, towards the centre-line (i.e. the wake growth is

TABLE I

BULK FLOW PARAMETERS

SYMMETRIC WAKE

x (mm.)	Wake Width $2 \times \delta_{0.995}$ (mm.)	δ^*/δ_0	Θ/δ_0	$H = \delta^*/\Theta$
0	107.0	0.164	0.1185	1.389
5	106.6	0.162	0.1186	1.369
10	106.0	0.162	0.1188	1.369
20	107.04	0.161	0.1192	1.354
30	107.0	0.158	0.1181	1.345
50	105.4	0.156	0.1175	1.327
100	105.0	0.149	0.1153	1.296
200	106.0	0.142	0.1121	1.273
300	106.0	0.137	0.1094	1.256
500	109.0	0.129	0.1061	1.224

δ_0 is $\delta_{0.995}$ at $x = 0$

Θ = momentum thickness

δ^* = displacement thickness

$U_e = 33.5$ m/s

From Clauser Charts

Upper Boundary Layer : $C_f = 0.0023$

Lower Boundary Layer : $C_f = 0.0024$

opposed by the mean V). In the outer part $\partial U/\partial x \simeq 0$ which means that V changes little across the outer part of the boundary layer.

The bulk flow parameters, as evaluated by the TURBWAK program developed to handle wake data, are given in Table I.

In Fig. 4.3, the mean velocity profiles are plotted in inner layer scaling. It is clear that even up to x = 100 mm there are points following the log law. All the curves asymptote to $U/u_\tau = U_\ell/u_\tau$ as y goes to zero ($\ln y \to -\infty$).

Since the experiment was carried out in nominally zero pressure gradient, the momentum thickness should be independent of x: the results confirm this. Fig. 4.4 shows the variation of Θ and δ^*, normalized by Θ at x = 0, along the wake compared with the results of Chevray and Kovasznay (1969).

4.1.2 The Inner Wake

The near wake is a "transitional" flow between two self-preserving flows, the boundary layer at the trailing edge and the far wake.

As can be seen in the mean velocity profiles (Figs. 4.1 and 4.2), the outer layer changes only very slowly as it travels downstream. Only the inner part of the wake (see Fig. 4.0) changes significantly, with a velocity scale u_τ at x = 0 and $\Delta U = U_e - U_\ell$ at $x \to \infty$, providing that it lies within the inner layer of the former boundary layer with y/δ_0 less than 0.2.

The inner part of a near wake should scale on the boundary layer inner layer parameters only. In fact, it is expected that:-

$$\frac{U}{u_\tau} = f_1\left[\frac{u_\tau x}{\nu}, \frac{u_\tau y}{\nu}\right] \qquad (4.1)$$

and for y = 0, i.e. on the centre-line:-

$$\frac{U_{\ell}}{u_{\tau}} = f_2\left[\frac{u_{\tau}x}{\nu}\right] \tag{4.2}$$

In Fig. 4.5a, the centre-line velocity is plotted as a function of x, in inner layer similarity parameters. A good fit to the present results is:-

$$\frac{U_{\ell}}{u_{\tau}} = A \ln \frac{u_{\tau}x}{\nu} + B \tag{4.3}$$

with A = 2.07 and B = 0.70, although an exactly logarithmic variation is not to be expected.

There is some difference between the present data and those of Chevray and Kovasznay (1969). For large x, the two curves should be expected to tend asymptotically to the same rate of variation, especially if the last point of Chevray and Kovasznay's results is discounted. For small x, the difference may be attributed to flat plate thickness of the present experiment.

In Fig. 4.5b, the $u_{\tau}\delta_i/\nu = f(u_{\tau}x/\nu)$ is plotted from the present experimental data. Here, δ_i is the semi-width of the inner wake deduced from the point of departure of the mean velocity profiles from the log law and is called δ_U in Fig. 4.5b. There are clearly two regions: the first region can be represented by:-

$$\frac{u_{\tau}\delta_i}{\nu} = C' \frac{u_{\tau}x}{\nu} \tag{4.4}$$

with $C' \simeq 0.09$ and it extends up to 200 viscous sublayer thicknesses. A sublayer thickness is about 0.4 mm for $y^+ = 30$. The above linear law is just an approximation and cannot be exact.

The second region should be free from any viscous sublayer effects and can be represented by the relation:-

$$\ln \frac{u_\tau \delta_i}{\nu} = A \ln \frac{u_\tau x}{\nu} + B \tag{4.5}$$

with $A \simeq 5.44$ and $B \simeq 0$.

Similarly these relations are an approximation and are not expected to be exact.

According to Bradshaw's hyperbolic turbulence model, a small disturbance at the wall surface propagates outwards with an angle $\sqrt{2a_1}\,\frac{u_\tau}{U}$. Thus:-

$$\frac{d\delta_i}{dx} = \sqrt{2a_1}\,\frac{u_\tau}{U_i} \tag{4.6}$$

where U_i is the mean velocity at $y = \delta_i$ or:-

$$\frac{d\delta_i}{dx} = \frac{\sqrt{2a_1}}{\frac{1}{k} \ln \frac{u_\tau \delta_i}{\nu} + C} \tag{4.7}$$

where the denominator is the logarithmic law for u/u_τ with $k = 0.41$ and $C \simeq 5.00$. So:-

$$x = \frac{1}{\sqrt{2a_1}} \int_0^{\delta_i} \left[\frac{1}{k} \ln \frac{u_\tau \delta_i'}{\nu} + C \right] d\delta_i'$$

and finally:-

$$\frac{u_\tau x}{\nu} = \frac{u_\tau \delta_i}{\nu} \frac{1}{\sqrt{2a_1}} \left[\frac{1}{k} \ln \frac{u_\tau \delta_i}{\nu} + C - \frac{1}{k} \right] \tag{4.8}$$

where $\sqrt{2a_1} = 0.55$.

Equation (4.6) represents a self-preserving inner wake law and it is plotted in Fig. 4.5b in log-log scales.

It is expected that further downstream the experimental curve $u_\tau \delta_i/\nu = f(u_\tau x/\nu)$ and that from equation (4.6) tend asymptotically to the same rate of growth. The rate of growth given by equation (4.6) assumes small disturbances with zero diffusion of kinetic energy and, of course, a_1 independent of x. For strong disturbances, as in the present case, constituted by the removal of the trailing edge, a_1 should have different values than the usual 0.15.

4.2 Conventional Turbulent Quantities

Extensive measurements of turbulent quantities have been made throughout the wake, specifically at x = 0 (the boundary layers), x = 25 mm , x = 50 mm , x = 100 mm , x = 200 mm and x = 400 mm. All the turbulent quantities presented here are non-dimensionalized by an appropriate power of U_e. In a plane symmetric flow like the present, the turbulent quantities containing an odd power of v, such as $\overline{uv}$, are expected to be antisymmetric. All the other quantities, such as $\overline{u^2}$ and $\overline{v^2}$, should be symmetric.

Figs. 4.6 to 4.11 show the longitudinal mean square intensity at various x positions; these profiles were obtained digitally from a cross-wire measurement at the same time as $\overline{v^2}$. "Digital results" implies later digital analysis as opposed to real time analogue analysis;

in both cases, hot wire equipment was the same. The analogue single wire measurements of $\overline{u^2}$, which are not presented, showed very good agreement with the "digital results", the maximum experimental scatter being of about 5%. It is clear that the maximum intensity moves away from the axis of symmetry, as x increases, while in each profile, there is a drop of $\overline{u^2}$ near the centre-line. The value of $\overline{u^2}$ on the centre-line remains constant for the first profiles and then starts to decrease with increasing x. The symmetry generally is quite good. The turbulence intensity in the outer part of the flow changes only slowly with x.

Figs. 4.12 to 4.17 display the distributions of $\overline{v^2}$ intensity. They show the same trend as the $\overline{u^2}$ profiles. For the first three stations in the wake, the results show a small scatter near the centre-line and no drop on the centre-line can be observed.

Shear stress measurements are presented in Figs. 4.18 to 4.23. The maximum shear stress at the trailing edge on both sides agrees quite well with the wall shear stress found from the mean velocity profile using Clauser charts. The antisymmetry at all stations is quite accurate and most of the profiles indicate an accurate zero value of shear stress on the centre-line. At the same point, $\partial U/\partial y$ is zero and, consequently, the energy production is zero. In the outer layer, the shear stress changes very slowly with x. Although the measurements extended over only about 8δ, the lack of any significant change in $\overline{uv}$ outside the inner wake suggests that the direct image effect of the solid wall on the pressure-rate-of-strain term in the shear stress transport equation $\overline{p'(\partial u/\partial y + \partial v/\partial x)}$ is small in the outer part of the shear layer.

Generally, the outer layer nearly remains unchanged on a given streamline; since the positive $\partial U/\partial x$ in the inner wake leads to

negative V which opposes the effect of the boundary layer growth, properties on given y may be more nearly constant than values on given streamlines.

Triple Products

The triple products $\overline{u_i u_j u_k}$ represent generally the transport of $u_i u_j$ by the action of the velocity u_k. They appear in the transport equation of the shear stress and turbulent kinetic energy (see Appendix G for detailed description of terms of these equations).

In Figs. 4.24 to 4.29, the $\overline{u^3}/U_e^3$ profiles are shown. $\overline{u^3}$ represents the transfer of u^2 by u. Close to the centre-line $\overline{u^3}$ has a high positive value meaning that in the flow there are short bursts of positive u and long interval of small negative u. This behaviour suggests that mixing near the centre-line takes place via short bursts and fine mixing. Here the short bursts go inwards towards the centre-line from regions of larger u.

$\overline{uv^2}$ is the transport of the shear stress (strictly of $\overline{uv}$) by v fluctuation. Such profiles are in Figs. 4.30 to 4.35. Close to the centre-line, positive values of $\overline{uv^2}$ for negative and positive values of y means that the transport velocity of shear stress $V_\tau = \overline{uv^2}/\overline{uv}$ is always directed towards the centre-line (for $y > 0$, $\overline{uv} < 0$ so V_τ is negative and for $y < 0$, $\overline{uv} > 0$, so V_τ is positive), i.e. there is an ingoing motion to transport shear stress towards the centre-line from both sides.

Figs. 4.36 to 4.41 show the variation of $\overline{u^2 v}$ across the wake. $\overline{u^2 v}$ is the transport of u^2 by v fluctuations and, together with $\overline{v^3}$ and $\overline{vw^2}$ which represent the transport of v^2 and w^2 by v, constitutes the diffusion term of the turbulent kinetic energy transport equation, $\partial\frac{1}{2}\overline{q^2 v}/\partial y$. $\overline{v^3}$ plots are in Figs. 4.42 to 4.47 and $\overline{vw^2}$ was not measured.

Both results indicate that there is a strong ingoing transport of turbulent kinetic energy. In particular, $\partial \overline{q^2 v}/\partial y$ is negative near the centre-line, i.e. a gain of kinetic energy by diffusion and $\partial \overline{q^2 v}/\partial y$ is positive near the edges of the inner wake, i.e. loss of kinetic energy.

4.3 Conditionally Sampled Results

4.3.1 "Cold" and "Hot" Fluid Averages

The temperature-intermittency factor of the outer part of the symmetric wake (outer layer) is plotted in Fig. 4.48. As was found earlier in Section 4.2, the outer part of the wake closely resembles the attached boundary layer. The present data agrees with the velocity-intermittency data of Klebanoff (1955) and temperature-intermittency data of Hancock (1978) both taken in the boundary layer on a flat plate in zero pressure gradient. In the same figure, the results from the asymmetric wake experiment are plotted and collapse well with the other results, showing that roughness does not affect the outer part of the layer provided that the roughness height is small compared to δ_o.

There is a significant difference between the present results and those of Dean and Bradshaw (1976) taken in a duct before the boundary layers merge. Their values are generally higher than the present and this may possibly be due to the uncompensated temperature signal which was used as the basis for conditional sampling or to the favourable pressure gradient in the duct.

In the next figure, Fig. 4.49, the intermittency factor γ in the inner part of the wake is presented for different downstream stations. If the large-eddy time sharing concept was applicable here as in the case of the duct, the intermittency on the centre-line $y = 0$

TABLE II

INNER WAKE WIDTHS - SYMMETRIC WAKE

I From Intermittency

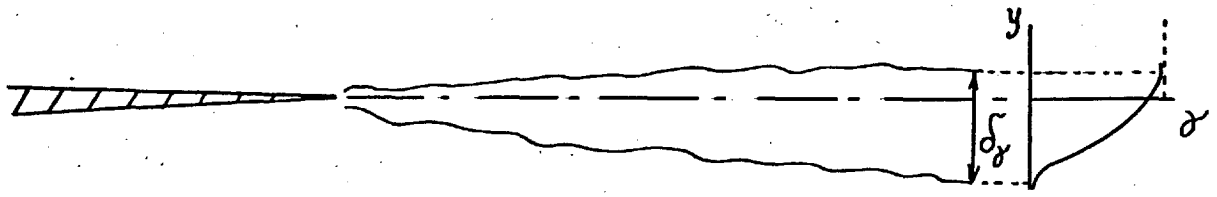

$\delta_\gamma/2$ (mm)	x (mm)
3.3	25
5.2	50
7.5	100
11.0	200
17.0	400

II From Shear Stress

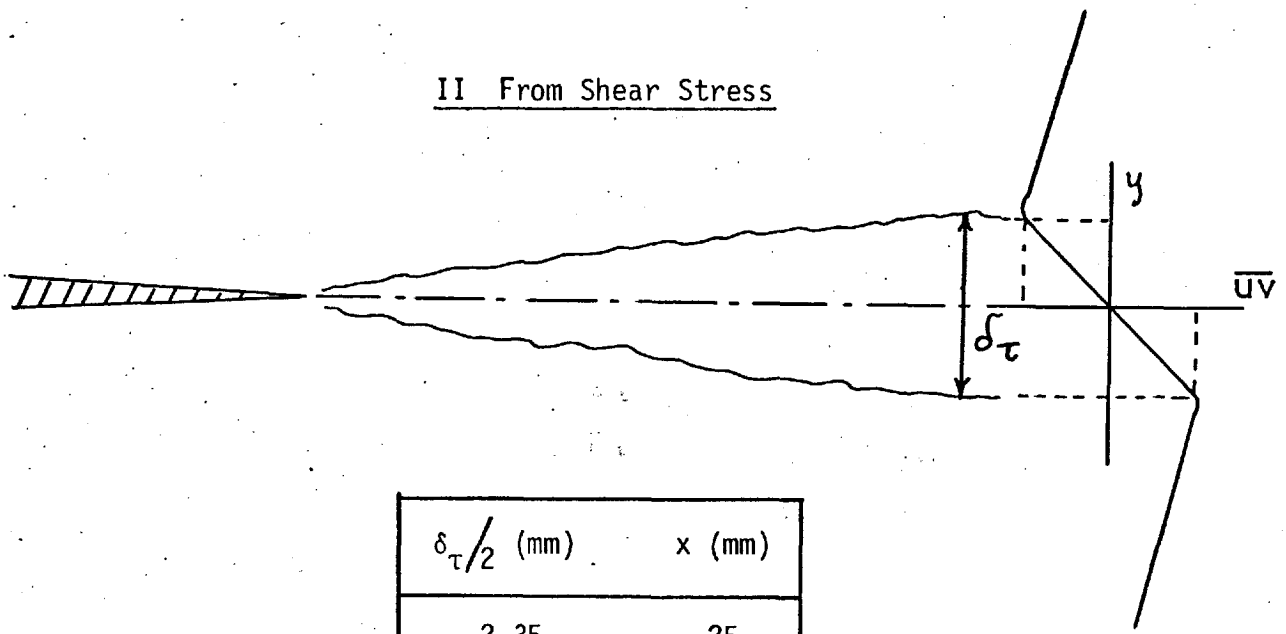

$\delta_\tau/2$ (mm)	x (mm)
2.35	25
3.65	50
5.2	100
9.6	200
14.1	400

should be 0.5 because of symmetry. In fact, the turbulence near the wake centre-line consists mainly of small eddies which have come from the inner layers of the boundary layers and they have smeared the interface into a "warm" region by fine grained mixing. So the fact that the intermittency is much higher than 0.5 is not surprising. Following the analysis of the previous chapter (Section 3.2 and Fig. 3.4), a value of $\gamma = 0.9$ at the centre-line of the symmetric wake means that 0.1 is the truly "cold" fluid intermittency, 0.1 is the truly "hot" fluid and 0.8, the "warm" fluid intermittency.

The symmetry between the intermittency results in the case where the upper boundary layer was heated and that with the lower boundary layer heated for x = 100 mm and x = 400 mm is quite good, indicating the absence of buoyancy.

For large positive y, the intermittency tends asymptotically to 1 (case of upper boundary layer heated) and for large negative y, it tends asymptotically to 0. If the width δ_i of an internal layer is defined as the distance between the points where $\gamma = 0.99$ and $\gamma = 0.01$, then the intermittency profiles are nicely scaled on δ_i as is shown in Fig. 4.50.

Now it is worthwhile to compare the inner wake widths which have been found from various definitions. In Section 4.1.2, δ_i has been defined from the mean velocity profiles and it was plotted in Fig. 4.5b as a semi-width δ_U against x. In the same figure, the variations of the inner wake semi-width $\delta_\gamma/2$ has been plotted as defined from the intermittency curves. Let $\delta_\tau/2$ be the inner wake semi-width deduced from the perturbation of the conventional shear stress profiles, i.e. δ_τ is the distance of points having shear stress $0.95\tau_{max}$ and $0.95\tau_{min}$. The variation of δ_τ with x is plotted again in Fig. 4.5b The values of δ_τ, δ_γ are given in Table II. From Fig. 4.5b, it seems the

rates of growth of δ_τ, δ_γ are closely the same and less than the growth rate of δ_U for small x but higher than δ_U for large x. Bradshaw's δ_i varies quicker than δ_U and δ_τ but it has been based on the assumption that diffusion is negligible. The main point of the comparison is that all δ_i show the same trends; therefore, the choice of definition is not critical.

In Figs. 4.51 to 4.55, $\overline{u^2}$ intensities are shown for the various downstream positions. They are plotted as "cold" and "hot" contributions to total (see equation (3.1.1)), i.e. as $\overline{\gamma u_H^2}$ and $\overline{(1 - \gamma)u_C^2}$. For symbols used hereafter, see Fig. 4.51; the mnemonic behind them is , a plume for "hot" (symbol ∇) and an iceberg for "cold" (symbol Δ). For better interpretation of the conditionally sampled results, the "cold" fluid-averages should be considered mainly since "cold" fluid is unmixed. "Cold" contributions in the "hot" region, i.e. for $y > 0$, are rather small since $(1 - \gamma)$ is small. The peak of the "hot" curve at $y < 0$ is due to the shape of the unconditional (conventional) curve and has nothing to do with any physical phenomenon. It decreases much more rapidly with x than the peak in the conventional averages. The level of the "hot" points on the centre-line is nearly constant for the first profiles but drops for x = 200 and 400 mm as do the conventional values. The "cold" contribution on the centre-line is nearly constant for all profiles.

$\overline{v^2}$ intensities are plotted in Figs. 4.56 to 4.60. There is more scatter of the conventional results than in $\overline{u^2}$ and, consequently, the symmetry looks rather poor. (Any scatter on the conventional results causes scatter in the conditional averages; scatter could be reduced by plotting $\overline{\gamma v_H^2}/\left[\overline{(1 - \gamma)v_C^2}\right]$ but this has not been done in this thesis). Generally, the behaviour of the conditional averages of $\overline{v^2}$ is similar to that of $\overline{u^2}$.

The shear stress profiles are given in Figs. 4.61 to 4.65. Some of the "hot" fluid crossing the centre-line soon changes its sign of shear stress by mixing with "cold" fluid to become less "hot" (i.e. "warm") but "cold" does not change its sign of $\overline{uv}$ because by definition it has not mixed significantly. Since "cold" fluid consists mainly of "large" eddies, the conclusion is that the shear stress of the "large" eddies do not change sign as they cross the centre-line, while the small eddies change their sign of τ rapidly, since smaller eddies have a shorter time scale. Here, the "cold" fluid shear stress, after its entrainment into the "hot" zone, $y > 0$, tends monotonically to zero for larger positive y, and it is rather difficult to argue the existence of any "negative loop" like that found by Dean and Bradshaw (1976). The height of the peak in the "hot" shear stress profile drops with x but generally less than in the case of $\overline{u^2}$. Generally, $\overline{u^2}$, $\overline{v^2}$ and $\overline{uv}$ present roughly the same behaviour.

In Figs. 4.66 and 4.67, the correlation coefficient, $\overline{uv}/\sqrt{\overline{u^2}}\ \sqrt{\overline{v^2}}$ is shown, for two downstream positions x = 100, 400 mm only. In the outer part, it reaches the value of $\pm$ 0.45. In the inner wake, it varies from - 0.45 to + 0.45 through the origin. The same behaviour characterizes the "cold" or "hot" fluid correlation coefficients defined as $\overline{uv}_C/\sqrt{\overline{u_C^2}}\ \sqrt{\overline{v_C^2}}$ and $\overline{uv}_H/\sqrt{\overline{u_H^2}}\ \sqrt{\overline{v_H^2}}$.

When plotted without factoring by $(1 - \gamma)$, values in "cold" fluid, i.e. the zone averages $(1 - \gamma)\overline{u_C^2}/(1 - \gamma)$, $(1 - \gamma)\overline{v_C^2}/(1 - \gamma)$ and $(1 - \gamma)\overline{uv_C}/(1 - \gamma)$ revealed the existence of the bursting phenomenon, similar to that appearing in the viscous sublayer near the wall, in the wake even up to x = 100 mm, near the centre-line. Despite the erratic behaviour of $(1 - \gamma)\overline{u_C^2}/(1 - \gamma)$ (because both the numerator and the denominator are very small) the evidence is rather strong. This bursting phenomenon will be discussed later.

The transport of uv is effected by the normal gradient of $\overline{uv^2}$ and the transport of turbulent kinetic energy by the gradient of $\frac{1}{2}(\overline{u^2v} + \overline{v^3} + \overline{w^2v})$. Therefore, a close study of the triple products is useful. The w component has not been measured in the present experiment but previous results indicated similar behaviour to u and v.

$\overline{u^3}$ does not affect any of the previous quantities significantly if the thin shear layer approximation is valid (even inside the inner wake, $\overline{\partial u^3/\partial x}$ is small), but it is helpful for interpretation of the flow. since it represents the transport of u^2 by u itself. Plots of $\overline{u^3}$ are in Figs. 4.68 to 4.72. Positive $\overline{u^3}$ means short bursts of positive u. In the "cold" zone, bursts of "cold" fluid are significant but they are reduced rapidly with x. These bursts are stronger closer to the centre-line . The same behaviour can be observed in the $\overline{v^3}$ profiles which are shown in Figs. 4.73 to 4.77. The "cold" fluid in the "cold" zone ($y < 0$) shows spikes of positive v, i.e. sweeps or "cold" bursts in the "hot" zone ($y > 0$)*.

The $\overline{u^2v}$ profiles in Figs. 4.78 to 4.82 indicate the same behaviour as $\overline{v^3}$. $\overline{u^2v_c}$ and $\overline{v_c^3}$ are positive in the "cold" region ($y < 0$). So "large" eddies transfer kinetic energy towards the centre-line.

The plots of $\overline{uv^2}$ are shown in Figs. 4.83 to 4.87. $\overline{uv^2}$ is the transport of uv by v. We concentrate on the "cold" fluid again since it is more meaningful for reasons explained earlier in Chapter 3. $(1 - \gamma)\overline{uv_c}$ in the "cold" zone ($y < 0$) is positive and since $(1 - \gamma)\overline{uv_c^2}$ is positive, this means that there is a transport velocity of shear stress inwards towards the centre-line.

To summarize the discussion of the triple-products, "large"

---

* Bursts are defined as high velocity fluid moving outwards the centre-line while sweeps are high velocity fluid moving inwards towards the centre-line.

eddies transport kinetic energy and shear stress towards the centre-line without immediately changing the sign of their shear stress when they cross the centre-line. Here, "large" eddy means large compared to the local length scale but still small with respect to outer layer eddies.

Generally, the triple-product measurements are more scattered than $\overline{u^2}$, $\overline{uv}$ and $\overline{v^2}$, $\overline{v^3}$ in particular shows a rather poor antisymmetry since the hot wire error is higher in $\overline{v^3}$.

4.3.2 "Warm" or Mixed-Fluid Averages

Following the analysis in the previous Chapter 3, the various parts of the flow can be discriminated as fully "hot", fully "cold" or "warm". The fully "cold" and fully "hot" fluid averages were discussed in the last section, Section 4.3.1. The "warm" averages can be deduced by the simple equations (3.2.11) earlier described. In the symmetric wake, the symmetry of the flow can provide the additional information which is needed for the determination of the "warm" averages, although for some profiles the experiment was repeated with the lower boundary layer heated. Here, the "warm" averages mainly for x = 25 mm and x = 100 mm are presented. All the other profiles have similar behaviour. The "warm" average of $\overline{u_W^2}$, $\overline{v_W^2}$, $\overline{uv_W}$, $\overline{u^2 v_W}$, $\overline{v_W^2}$ and $\overline{uv_W^2}$ are presented in Figs. 4.88 to 4.93.

The most striking result is that the "warm" fluid, or, better, the inner wake, appears to behave like an isolated shear layer. Indeed, after comparing the "warm" averages with the conventional averages, the shape is quite similar. Although the local behaviour of any conventional turbulence quantity is not expected to be the same as that of the "warm" layer, some basic differences should be mentioned. In particular, since $\partial \overline{v_W^3}/\partial y$ is positive near the centre-line, there is a loss of kinetic

energy there and a gain near the edges of the inner wake since $\partial\overline{v_W^3}/\partial y$ is negative. For the overall behaviour of the diffusion, the term $\overline{u^2 v_W}$ should be added to $\overline{v_W^3}$ while the $\overline{w^2 v_W}$ is approximated by $\frac{1}{2}(\overline{u^2 v_W} + \overline{v_W^3})$ and diffusion by pressure fluctuation is ignored. But still the term $\partial\,\frac{1}{2}\,\overline{q^2 v_W}/\partial y$ has a much smaller negative value than the conventional $\partial\,\frac{1}{2}\,\overline{q^2 v}/\partial y$, which means that the gain of energy by diffusion is very small in the "warm" fluid. This can be clearly seen in Fig. 4.94. Returning to $\overline{v_W^3}$, the positive values in the $y > 0$ and the negative values in $y < 0$ regions indicate "bursts" of "warm" fluid. In the same regions, the non-mixed fluid appears to have "sweeps" (see Fig. 4.75). So probably the "warm" fluid "bursts" are pushed by the upper and lower fluid sweeps and it seems that the u_W^2 profile, for example, is shaken bodily from side to side.

4.4 Conclusions to the Chapter

In this chapter, the results of an experiment in the symmetric near wake of a flat plate have been presented and discussed briefly.

Evidence was produced that only the "inner" wake changes with x, the outer part remaining undisturbed. The inner layer similarity scales evaluated at the trailing edge seem to apply quite well for the "inner" wake scaling. The flow behaves in an entirely different way from the large eddy time-sharing found in the case of the two merging boundary layers in the duct (Dean and Bradshaw (1976)), which has also been found by Weir and Bradshaw (1977) in mixing layers. Most of the fluid around the centre-line consists of small scale eddies since they are the former occupants of the inner layers of the boundary layers. These eddies have size proportional to their distance from the centre-line and grow as they travel downstream. The existence of small eddies and consequent rapid mixing is the reason why the intermittency is not

0.5 on the centre-line.

Non-mixed fluid eddies, as well as the mixed-fluid small eddies, transfer turbulent kinetic energy towards the centre-line.

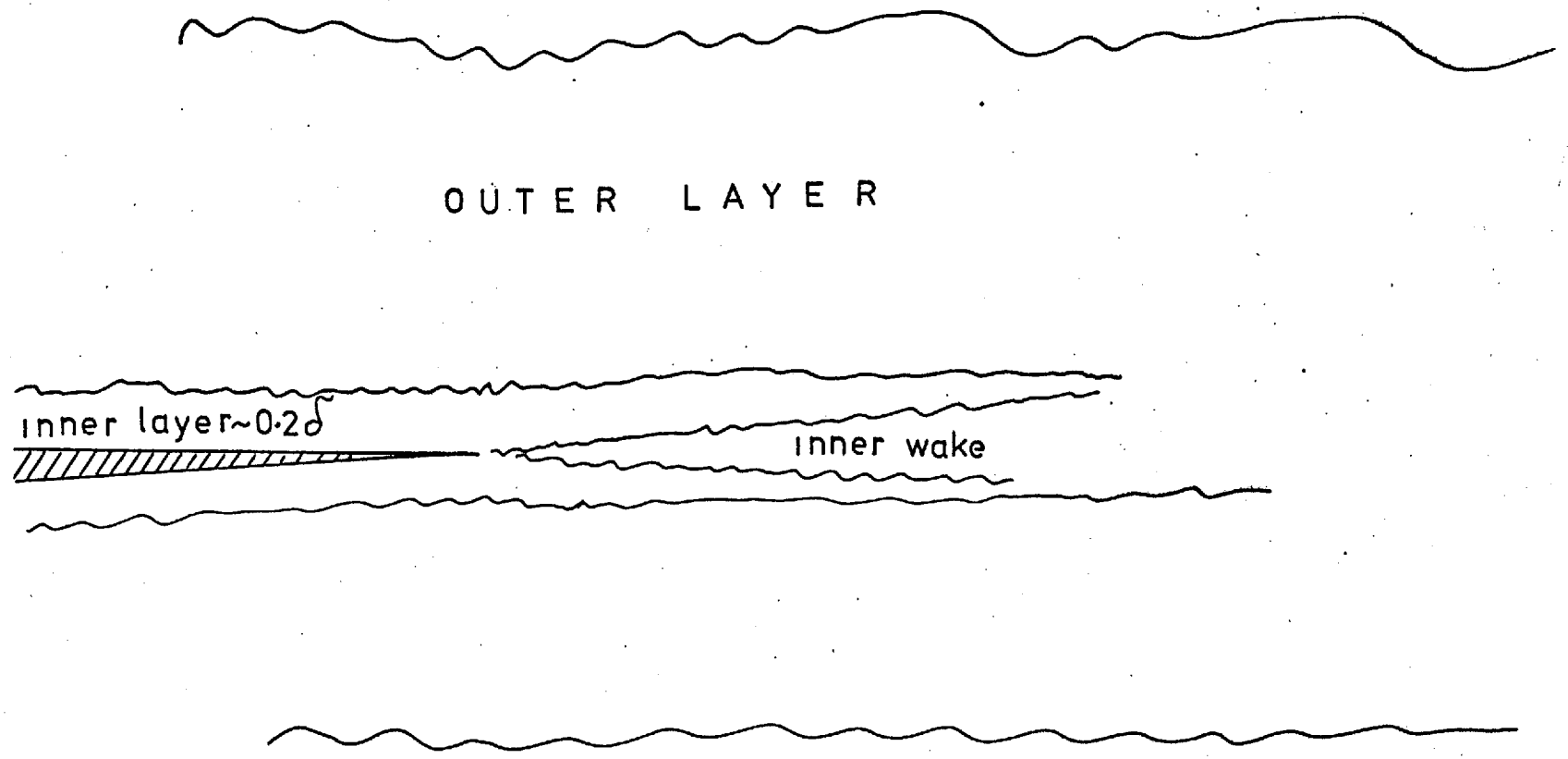

FIG. 4.0 INNER AND OUTER LAYER IN A WAKE

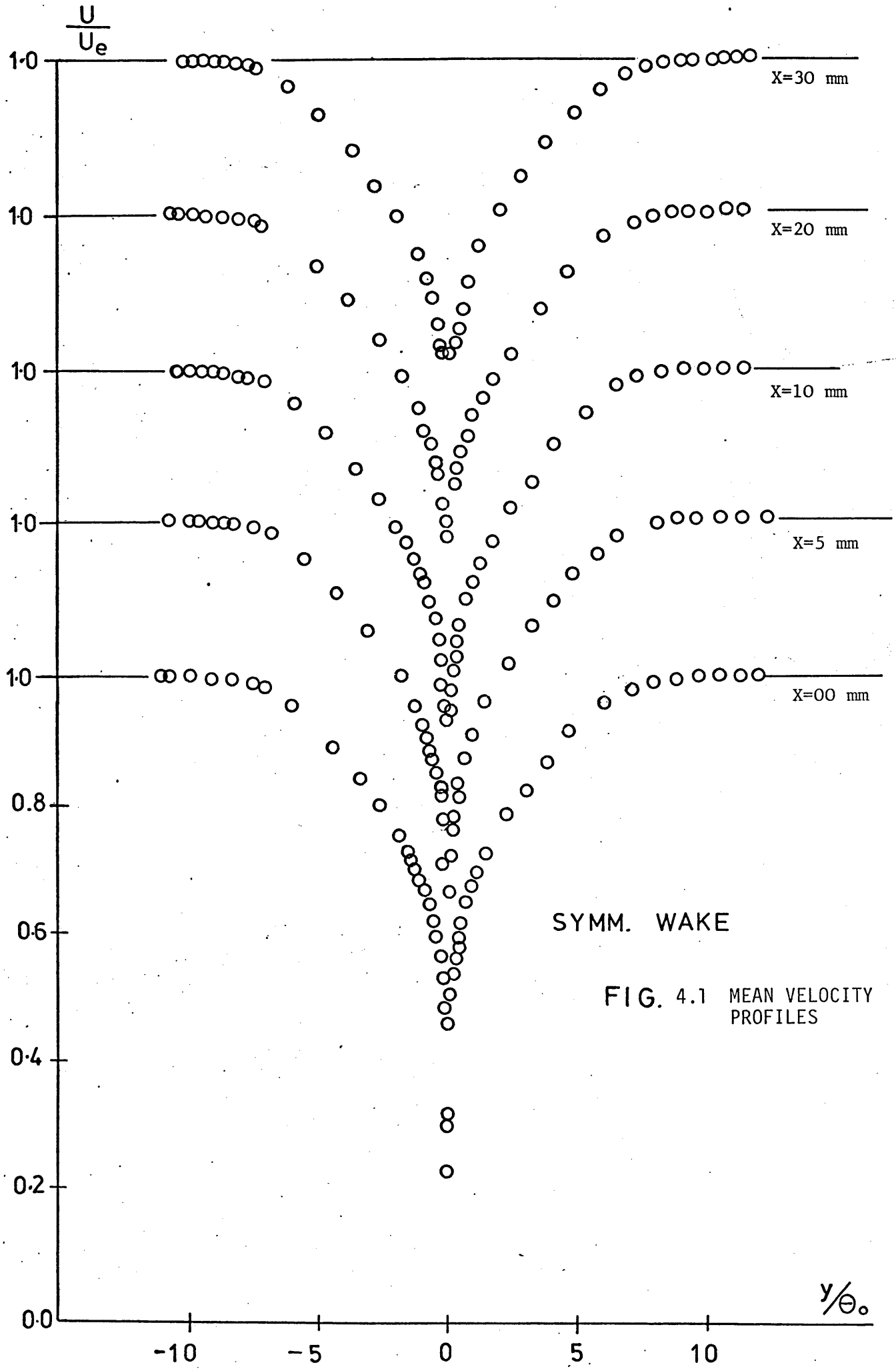

FIG. 4.1 MEAN VELOCITY PROFILES

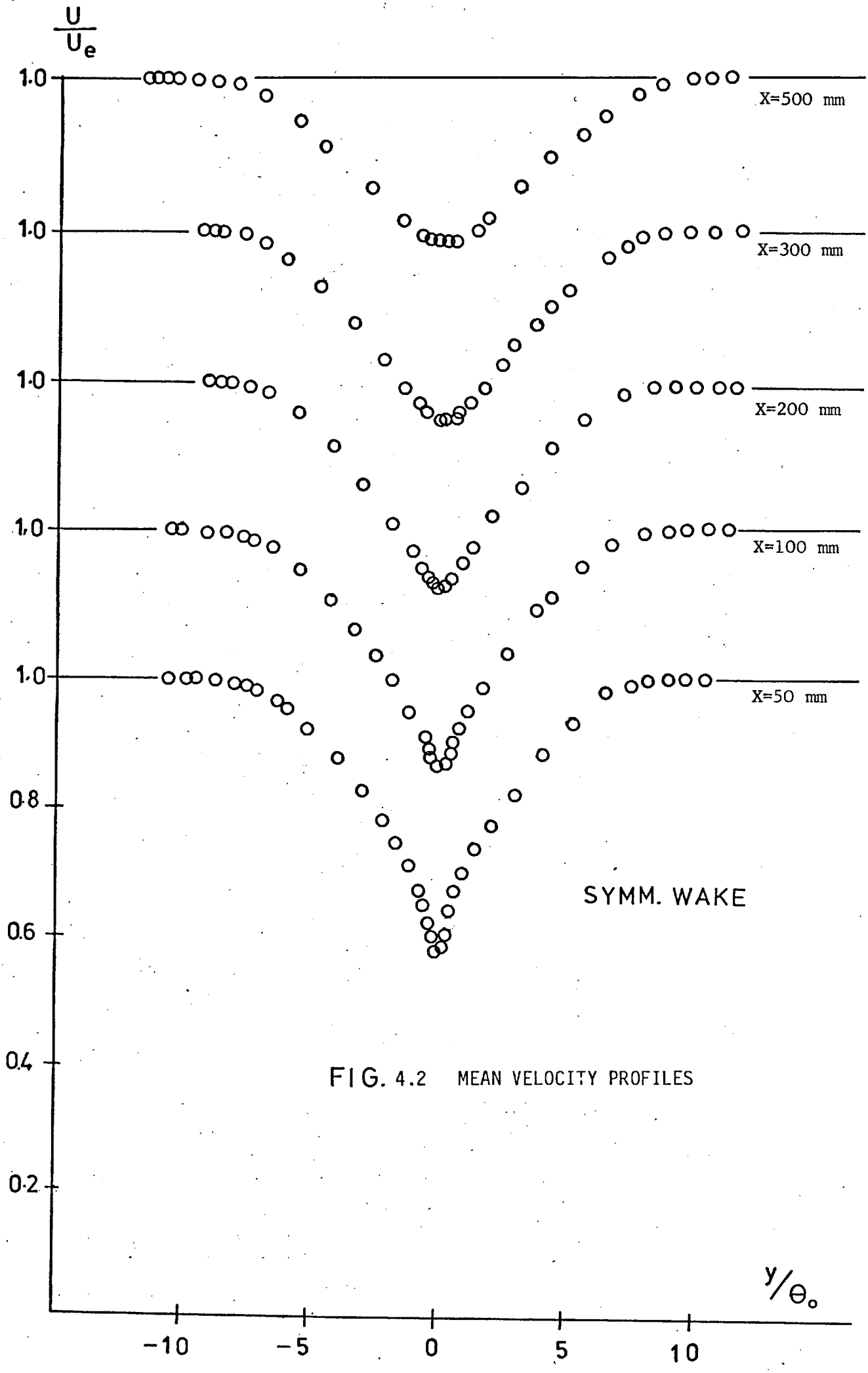

FIG. 4.2 MEAN VELOCITY PROFILES

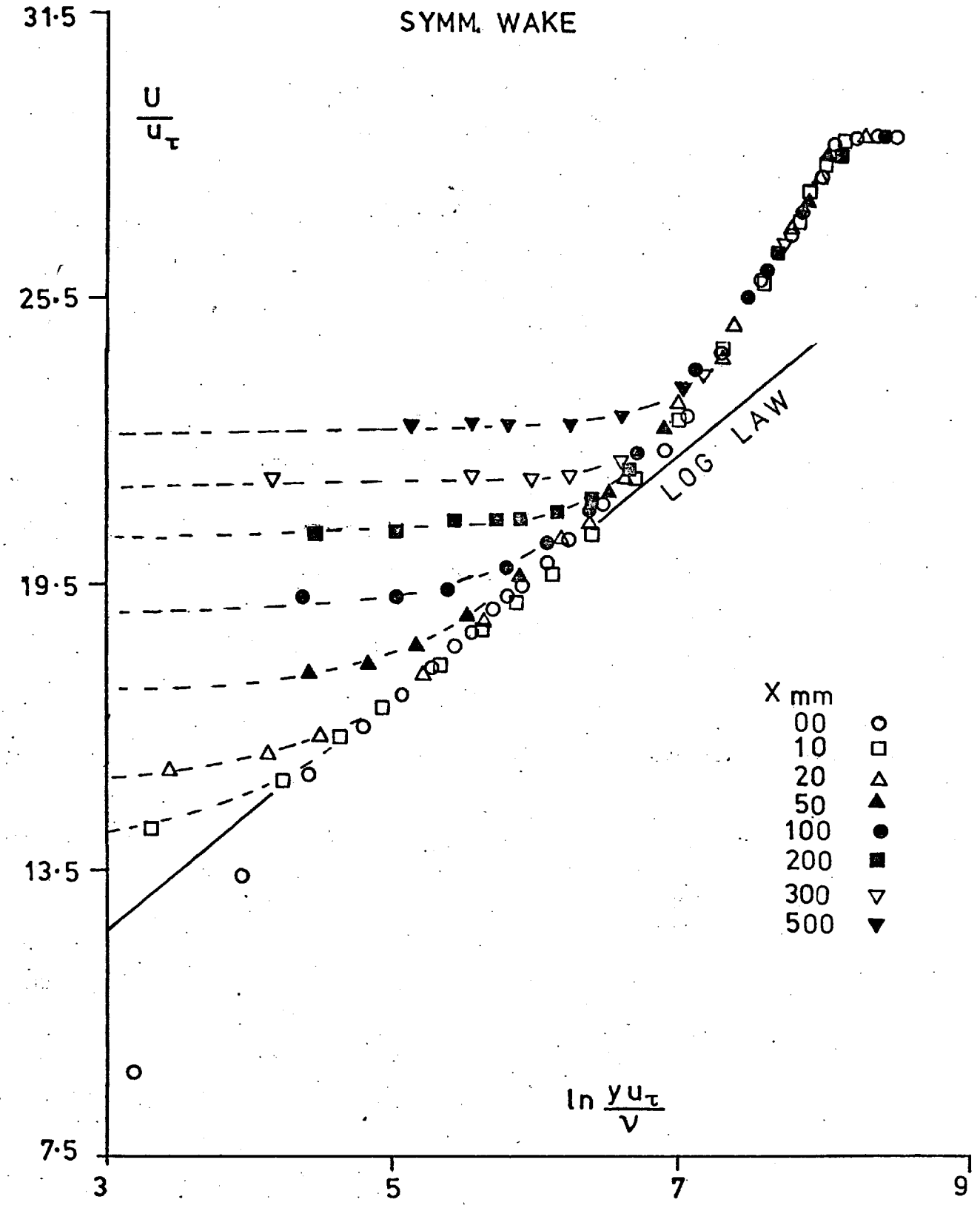

FIG. 4.3 SEMI-LOG VELOCITY PROFILES

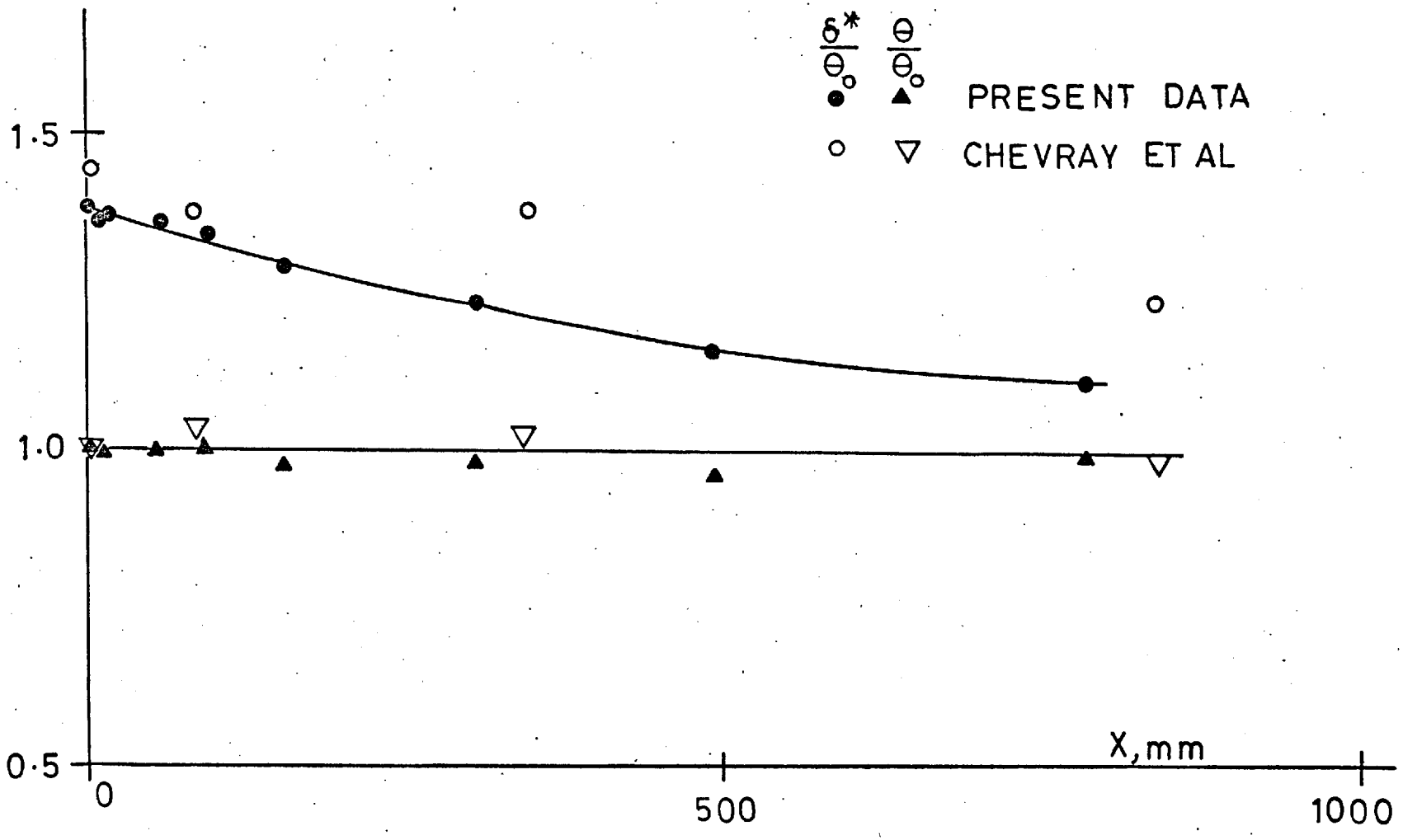

FIG. 4.4 STREAMWISE VARIATION OF δ^*, θ

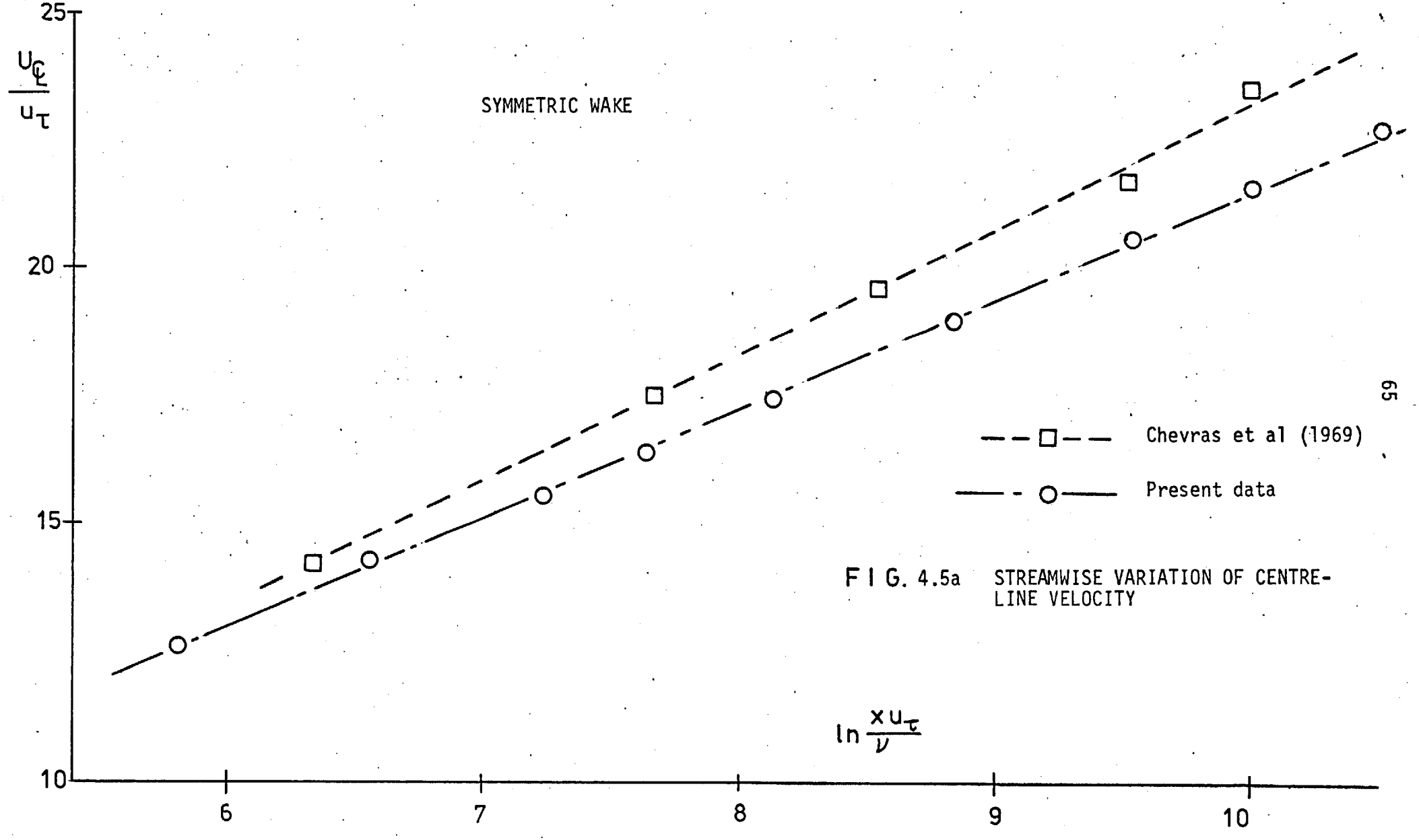

FIG. 4.5a STREAMWISE VARIATION OF CENTRE-LINE VELOCITY

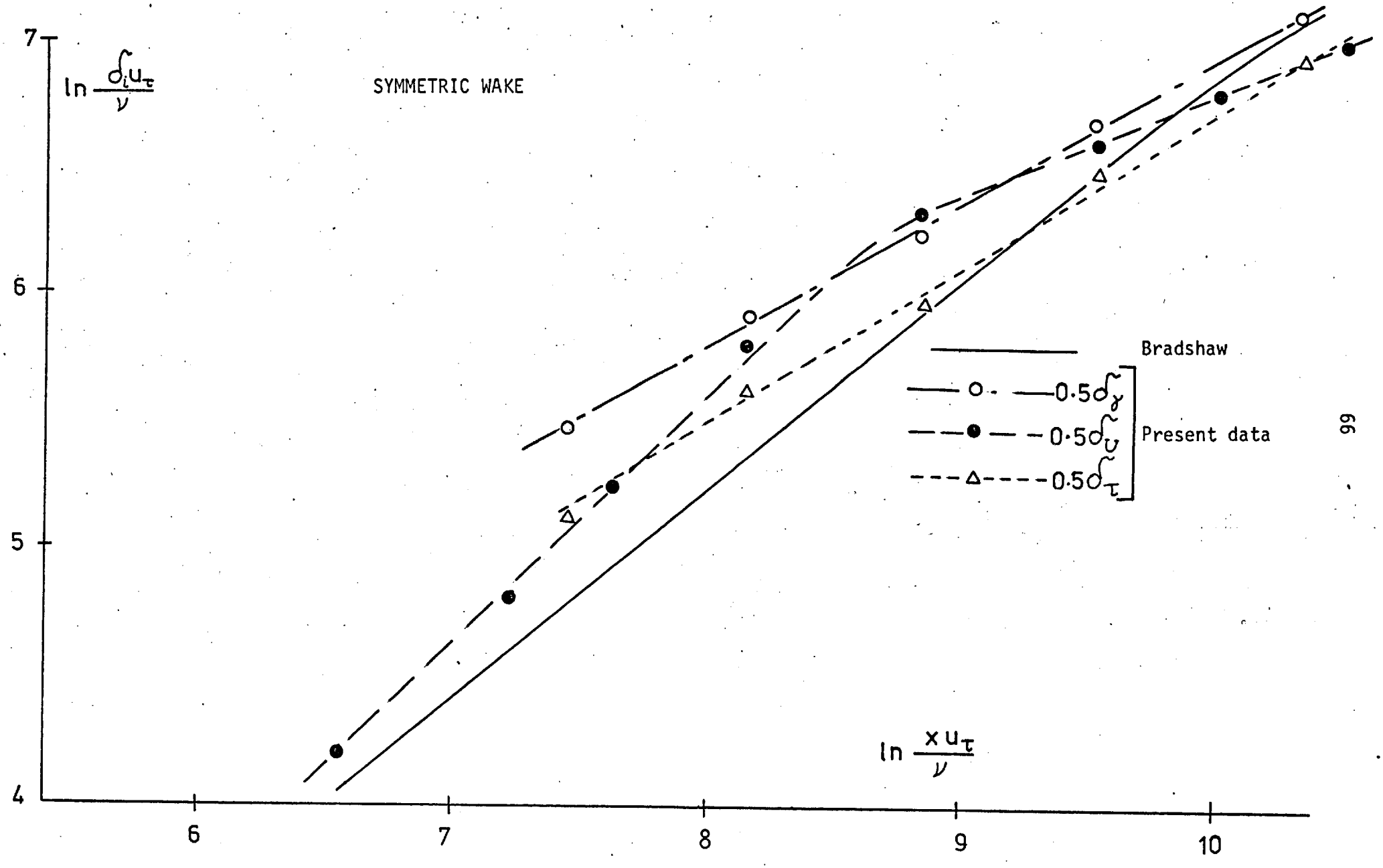

FIG. 4.5b STREAMWISE VARIATION OF INNER WAKE WIDTH

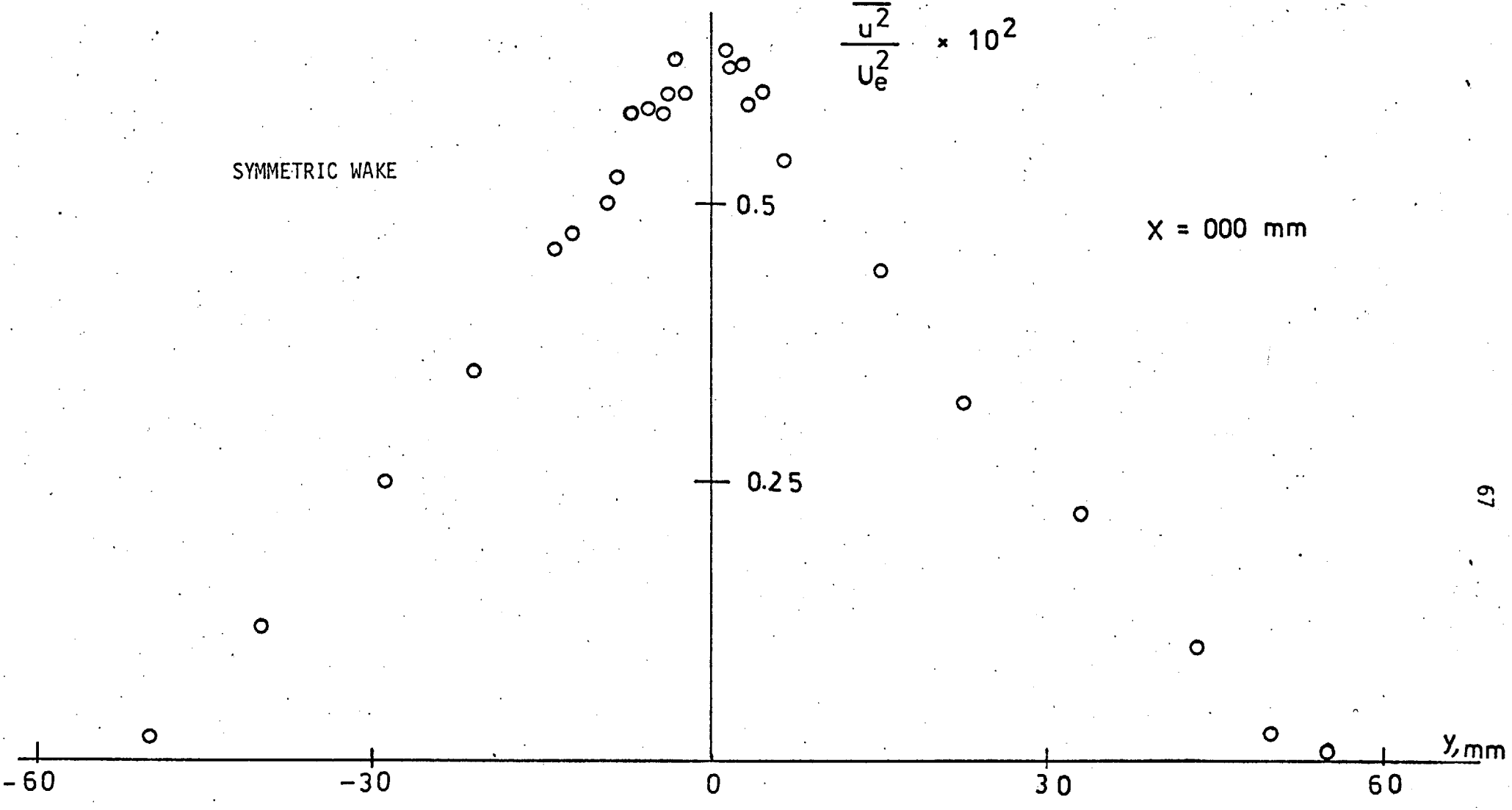

FIG. 4.6 $\overline{u^2}$ PROFILE AT x = 0 mm.

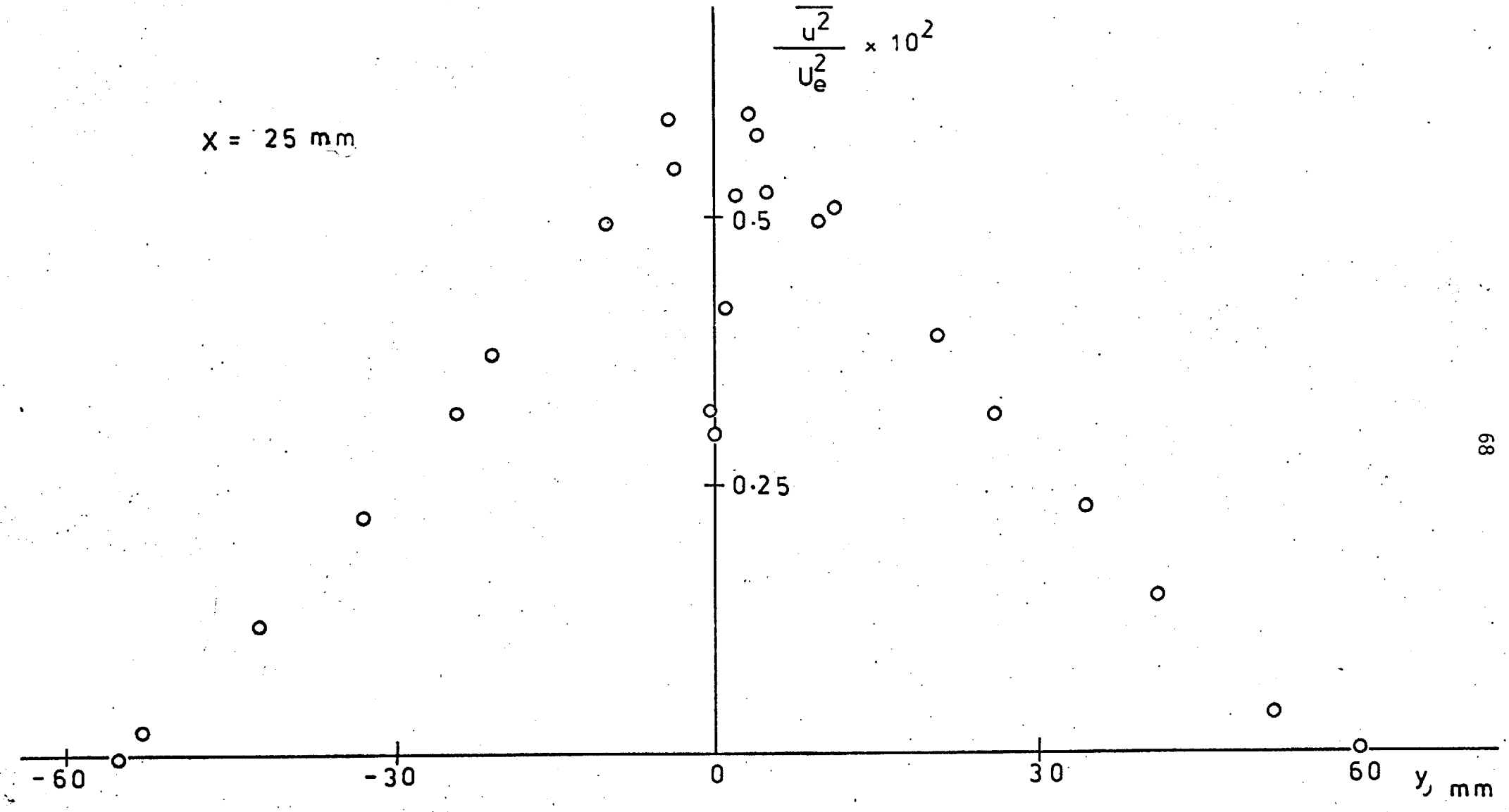

FIG. 4.7 $\overline{u^2}$ PROFILE AT x = 25 mm.

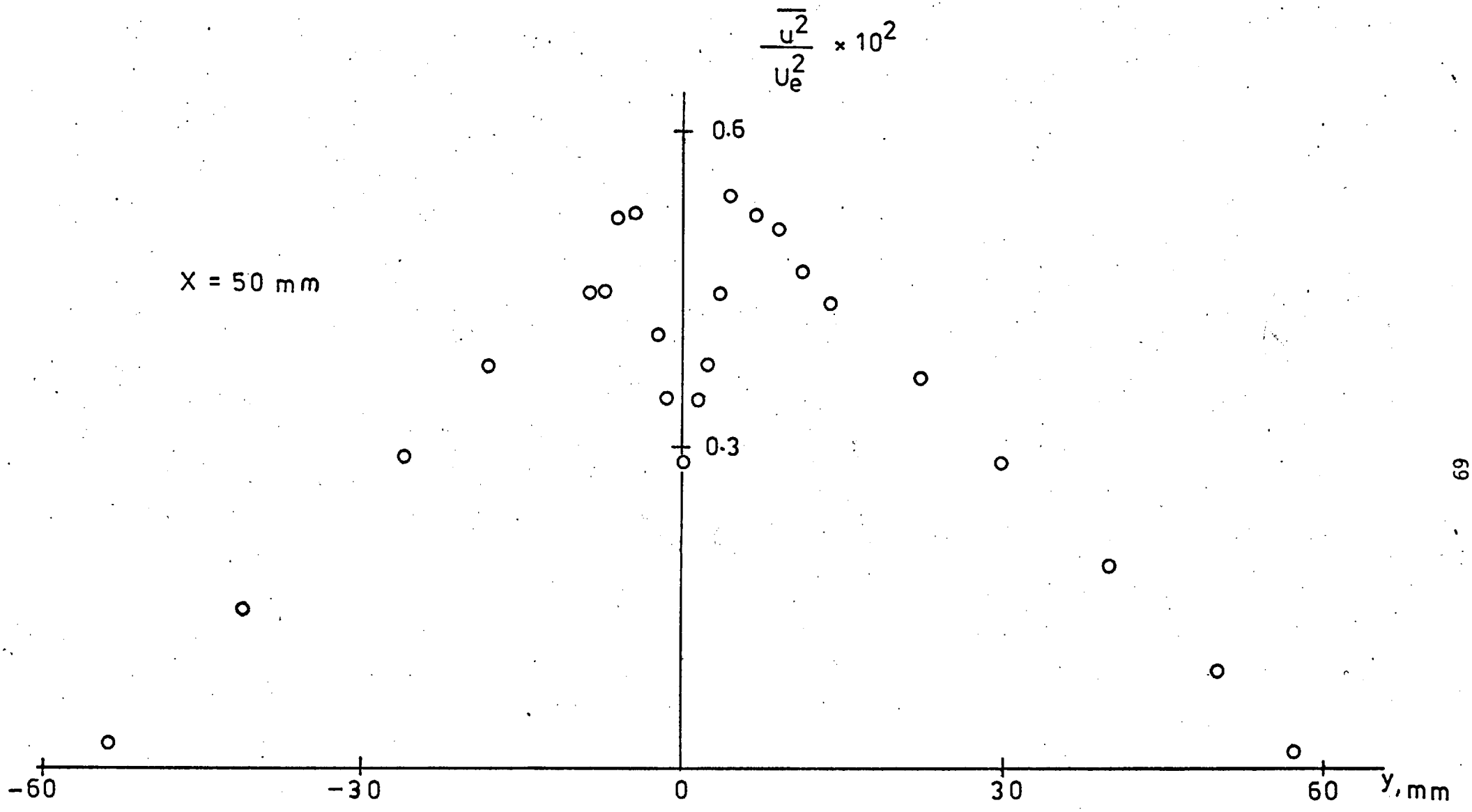

FIG. 4.8 $\overline{u^2}$ PROFILE AT x = 50 mm.

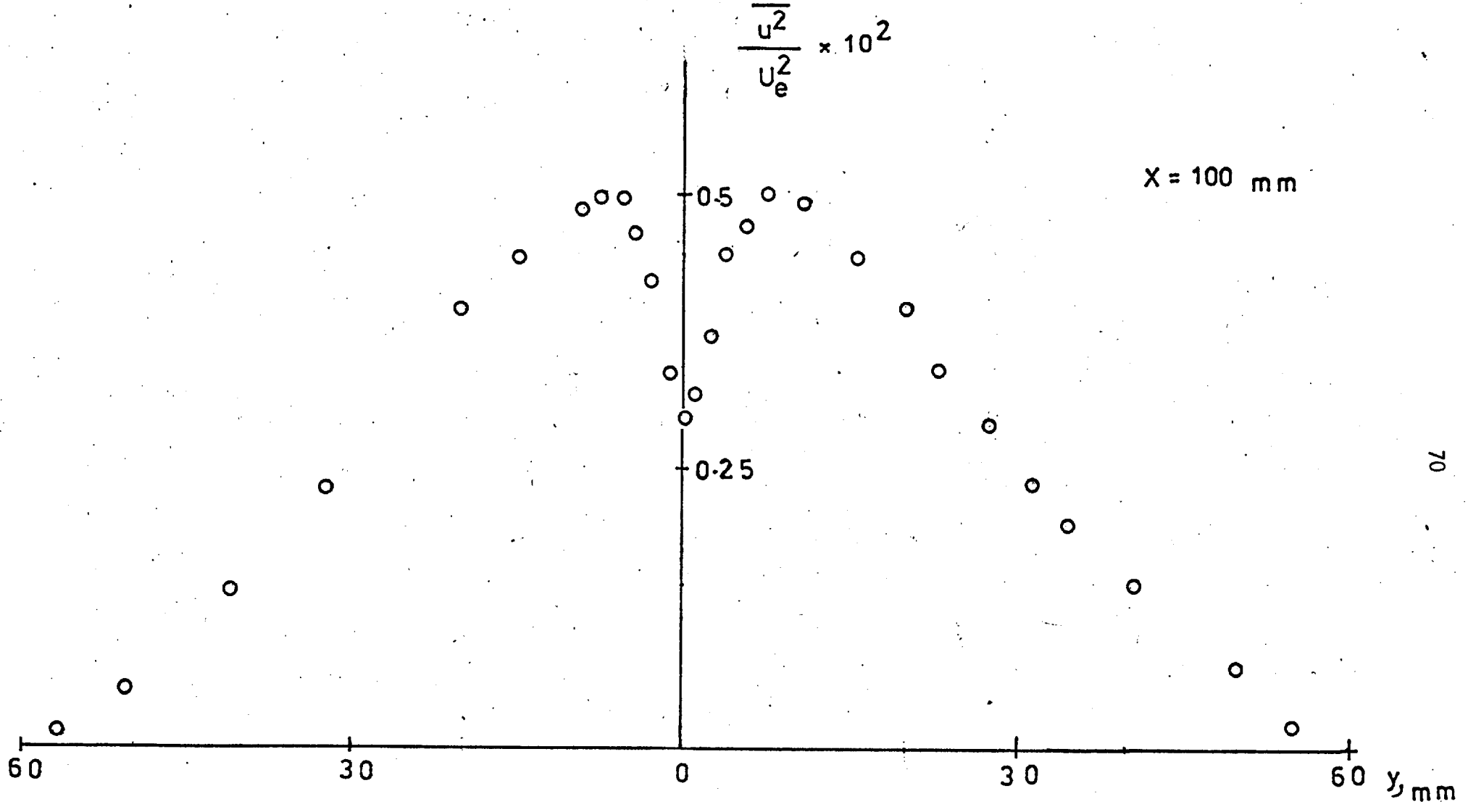

FIG. 4.9 $\overline{u^2}$ PROFILE AT x = 100 mm.

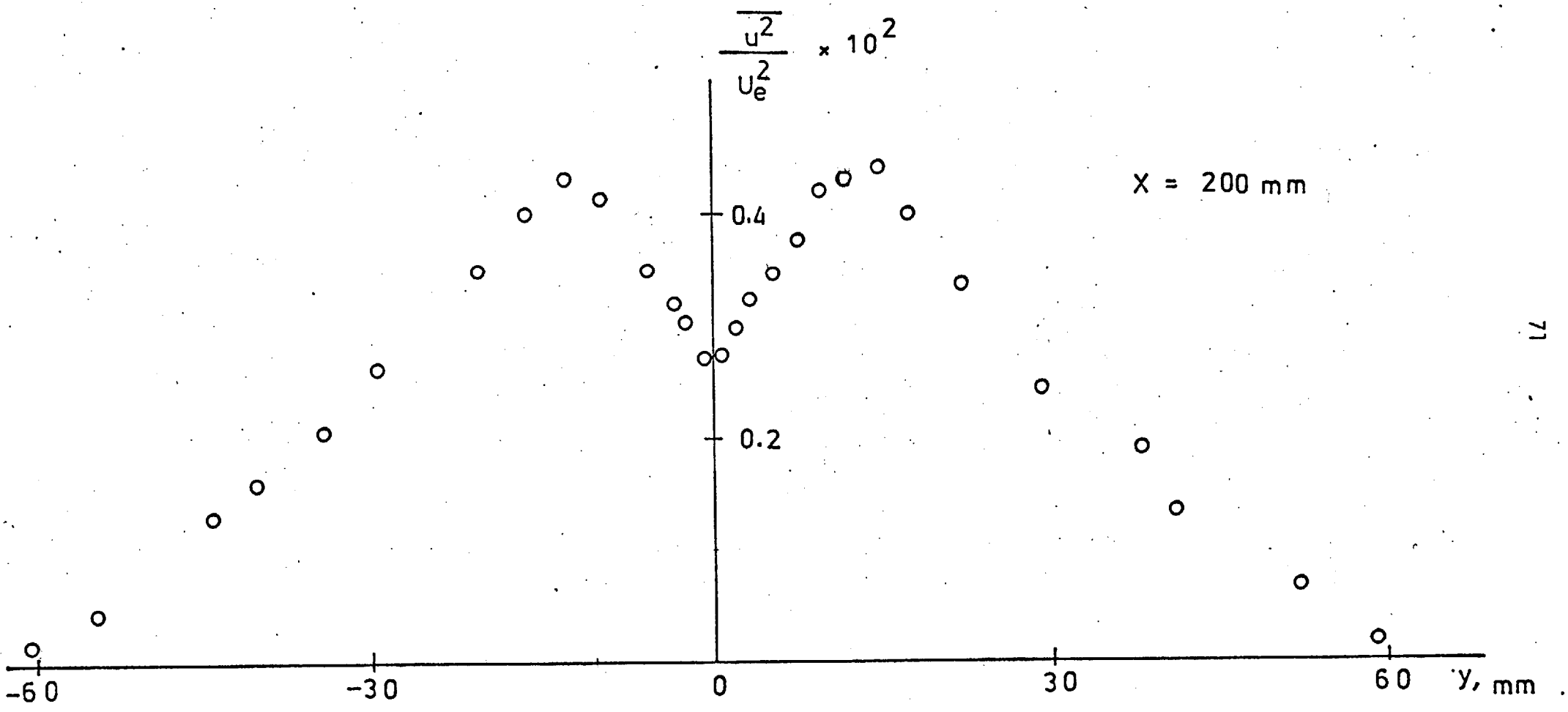

FIG. 4.10 $\overline{u^2}$ PROFILE AT x = 200 mm.

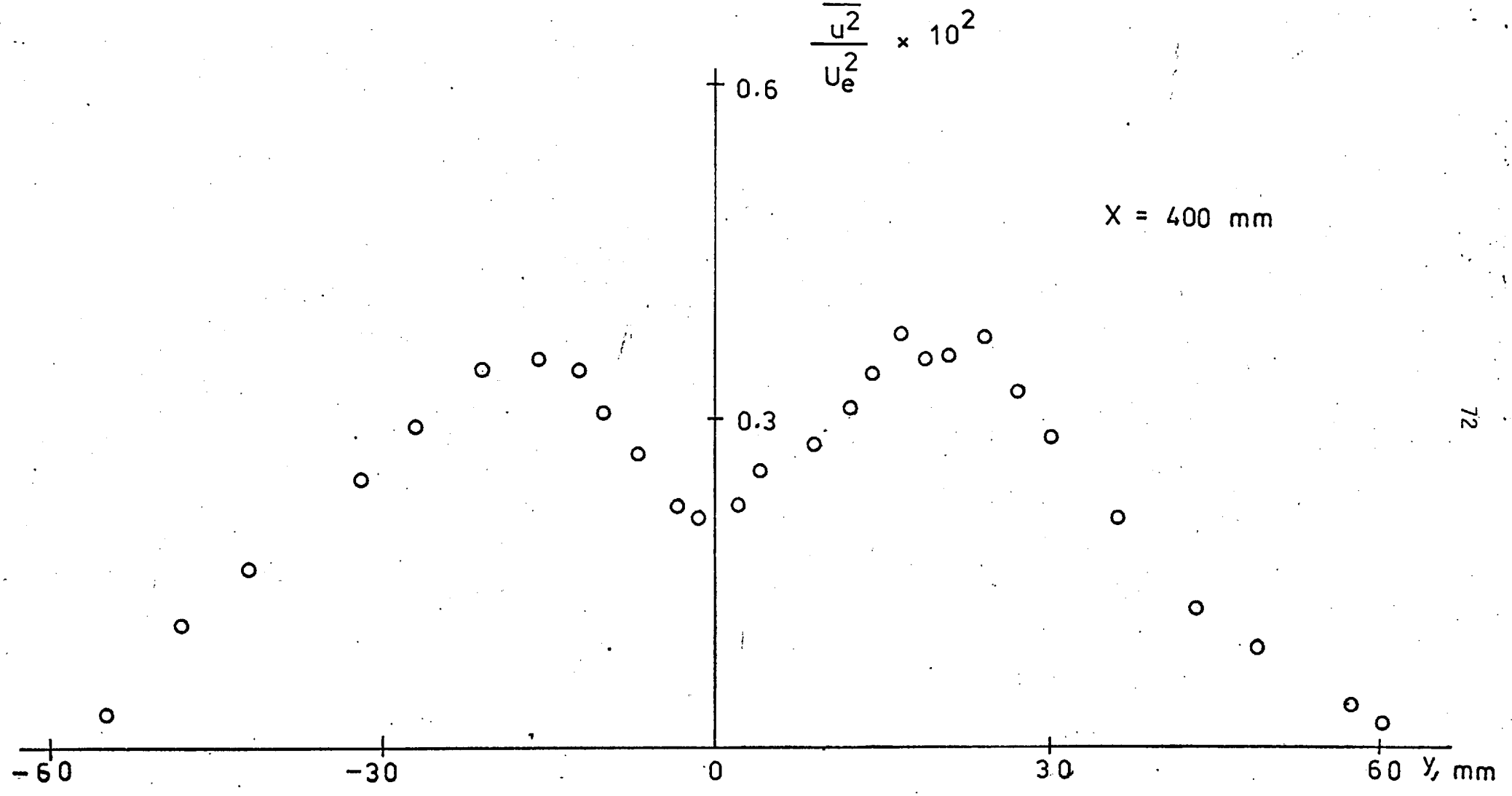

FIG. 4.11 $\overline{u^2}$ PROFILE AT x = 400 mm.

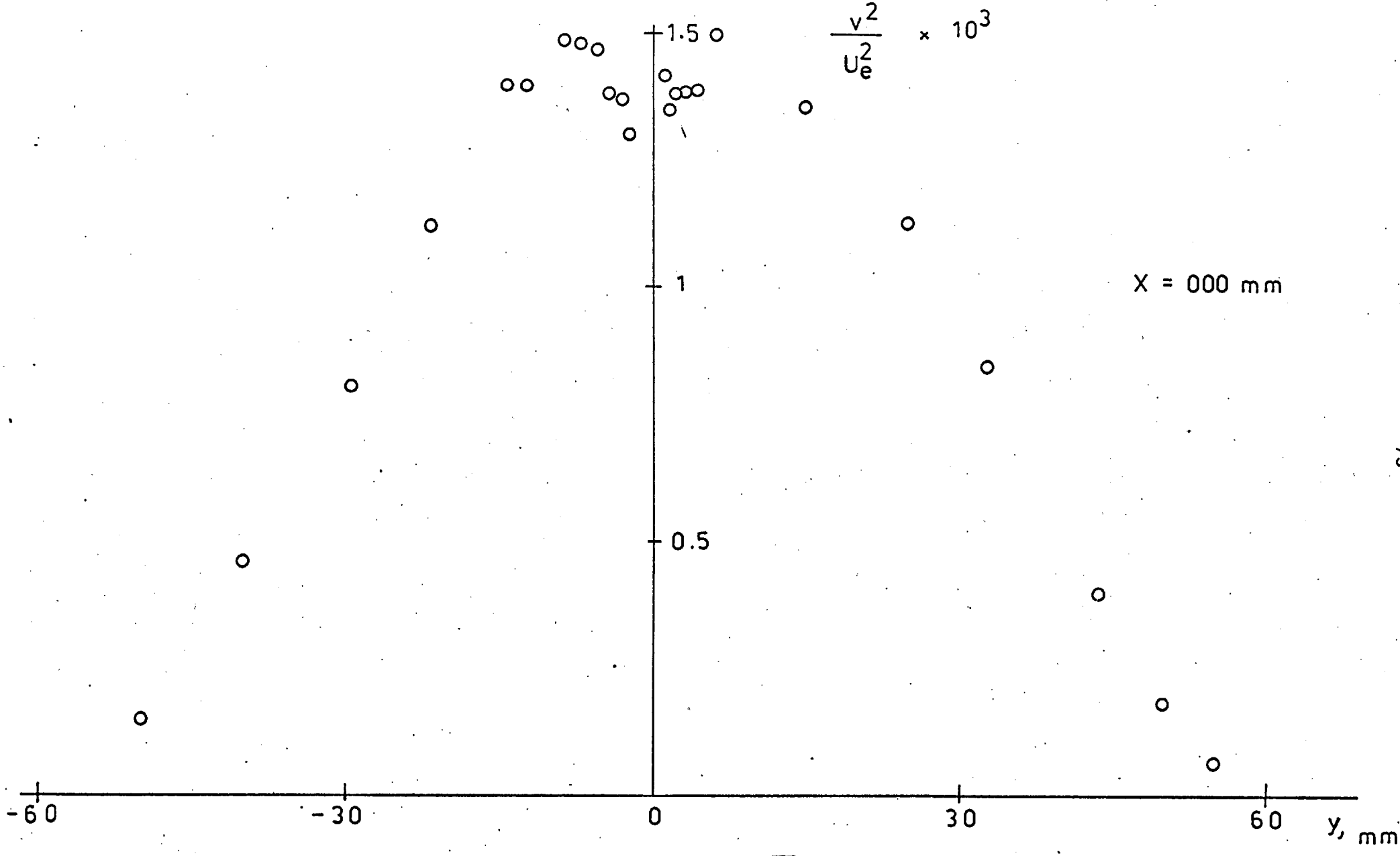

FIG. 4.12 $\overline{v^2}$ PROFILE AT x = 0 mm.

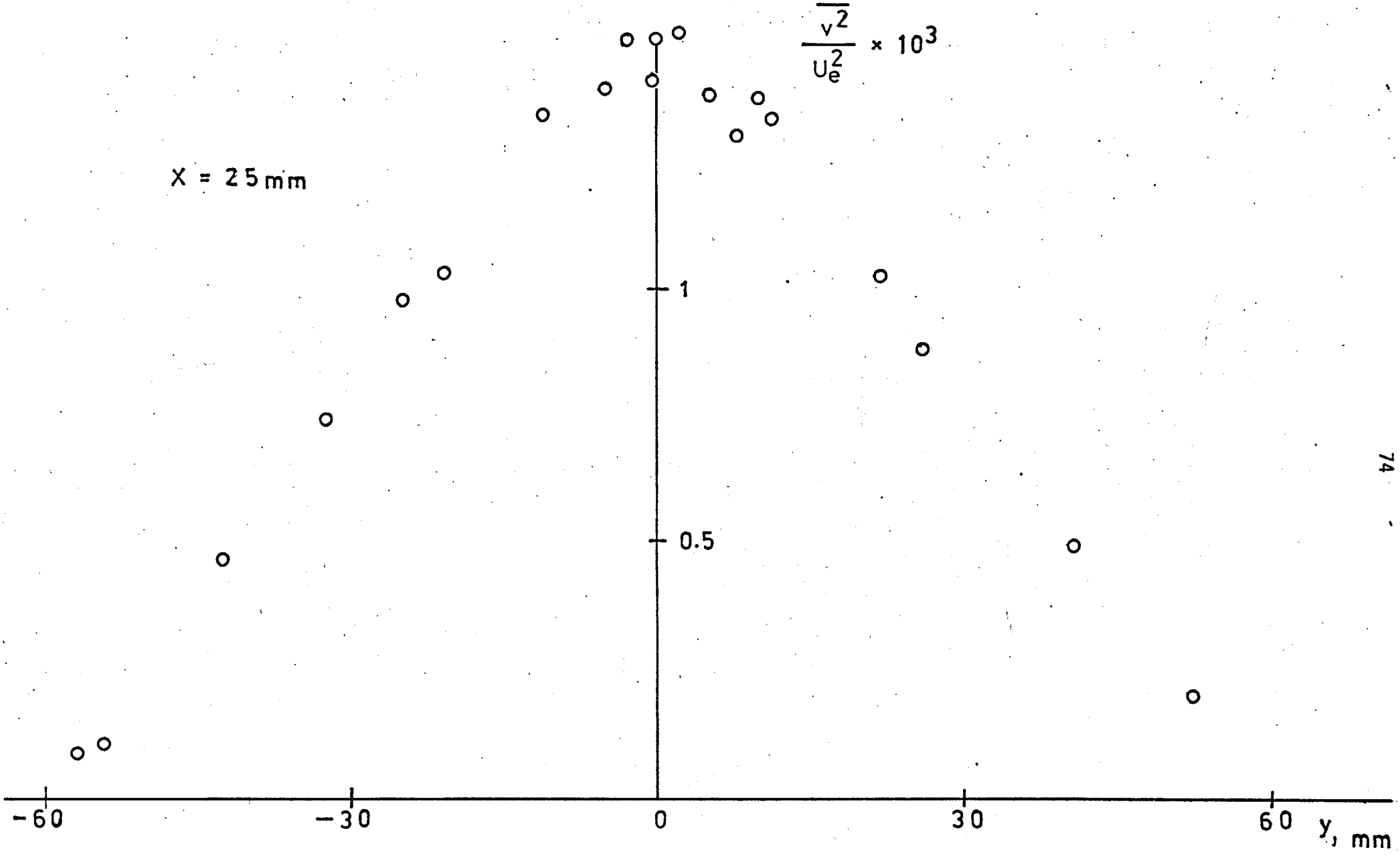

FIG. 4.13 $\overline{v^2}$ PROFILE AT x = 25 mm.

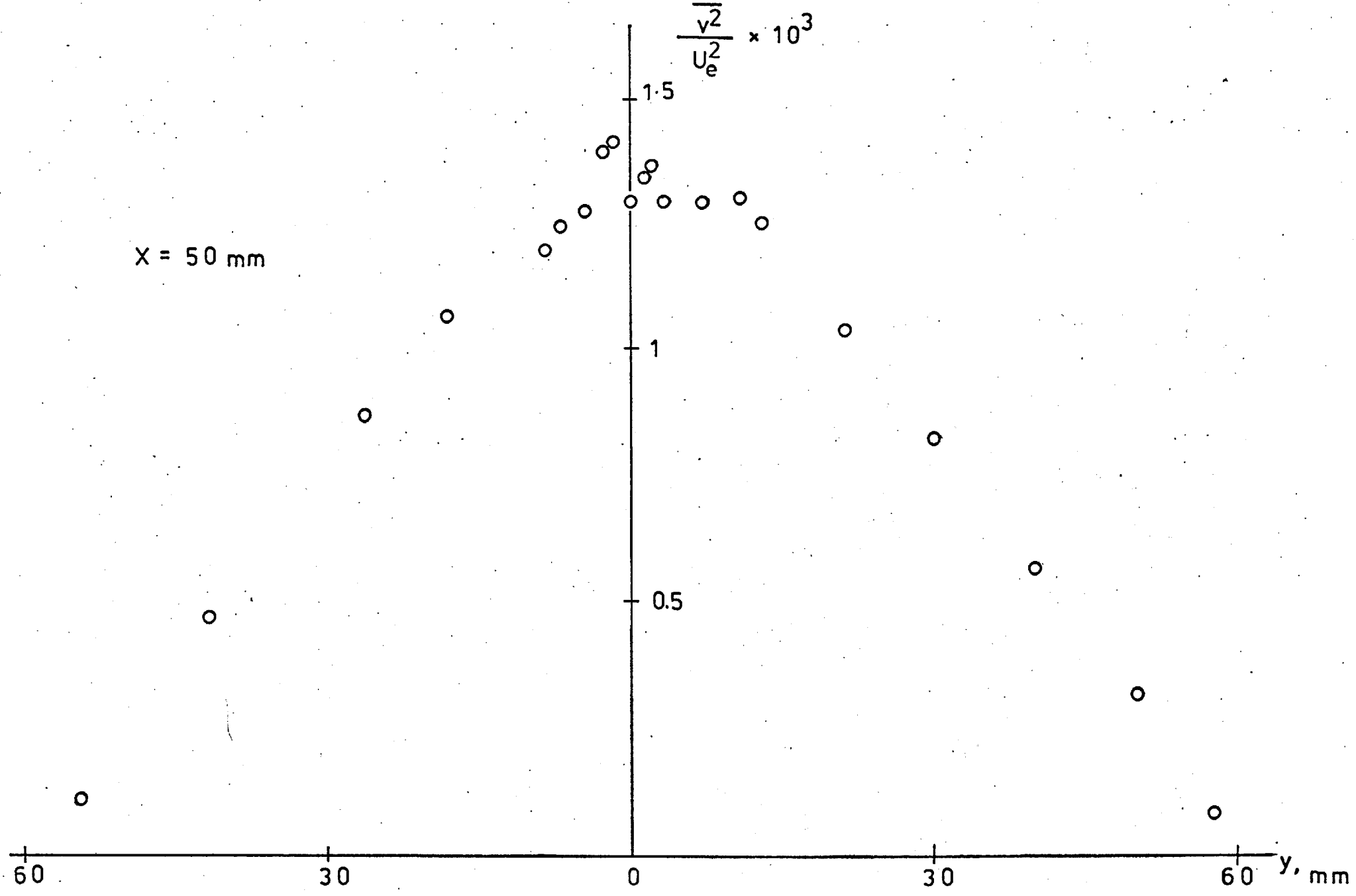

FIG. 4.14 $\overline{v^2}$ PROFILE AT x = 50 mm.

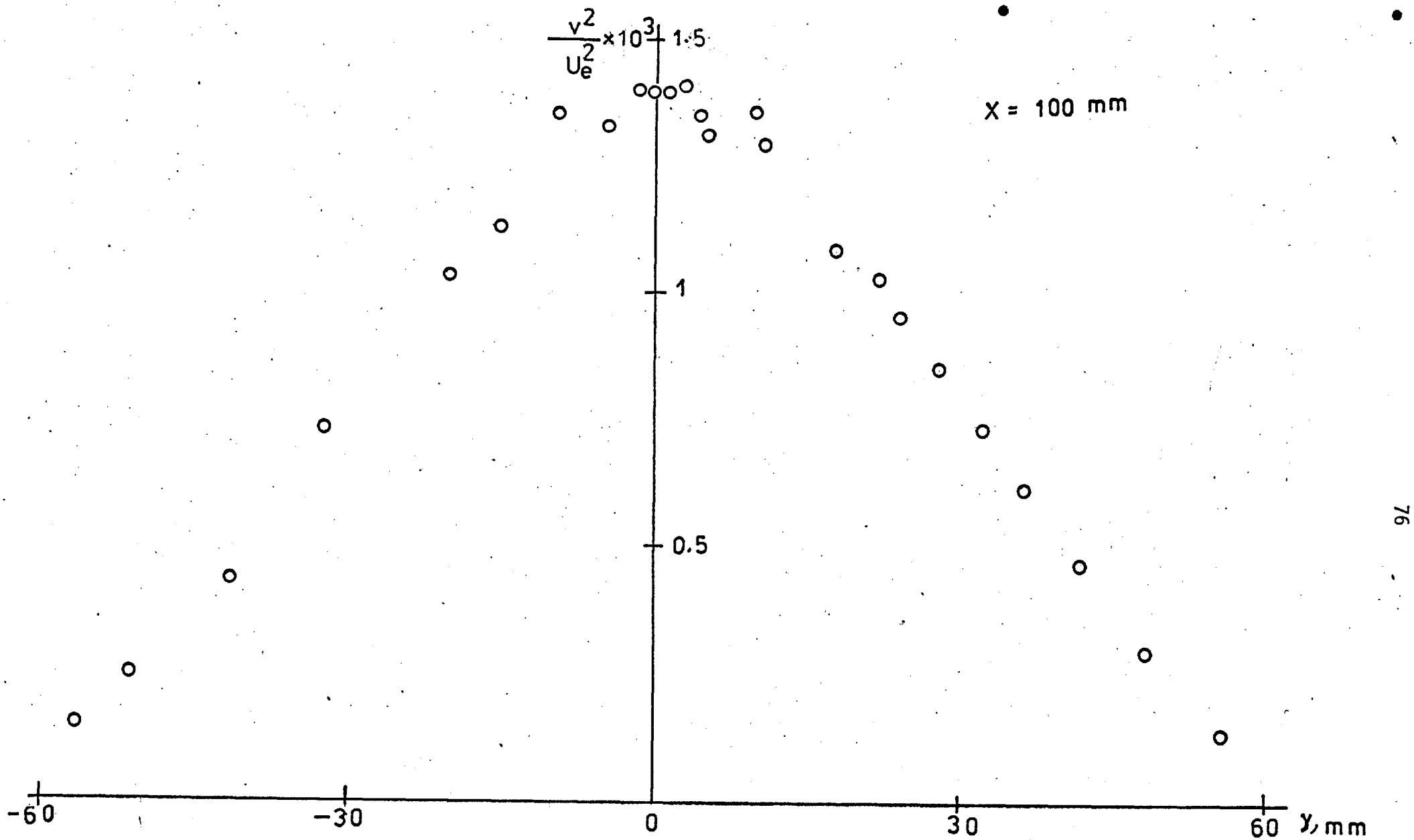

FIG. 4.15 $\overline{v^2}$ PROFILE AT x = 100 mm.

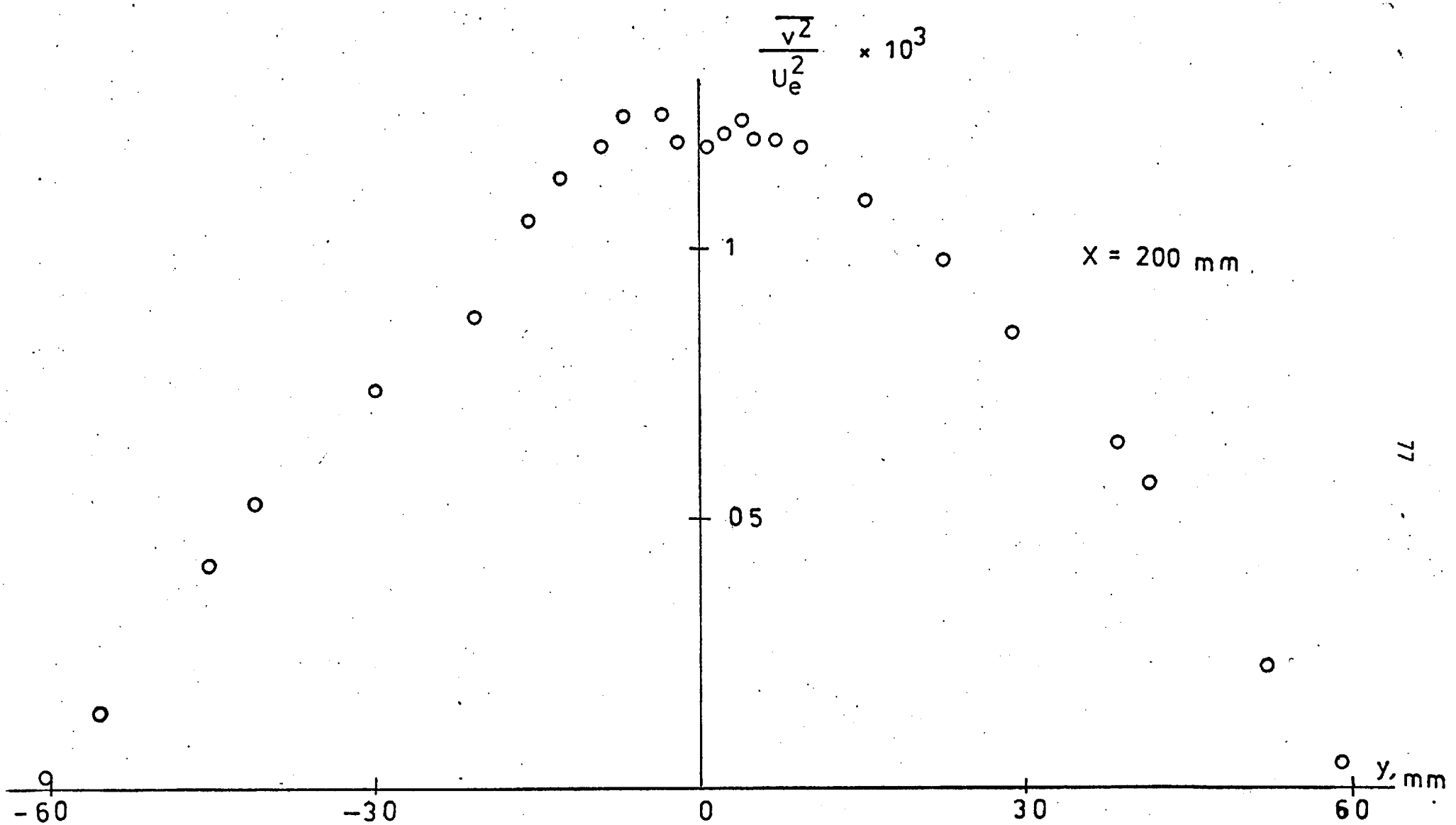

FIG. 4.16 $\overline{v^2}$ PROFILE AT x = 200 mm.

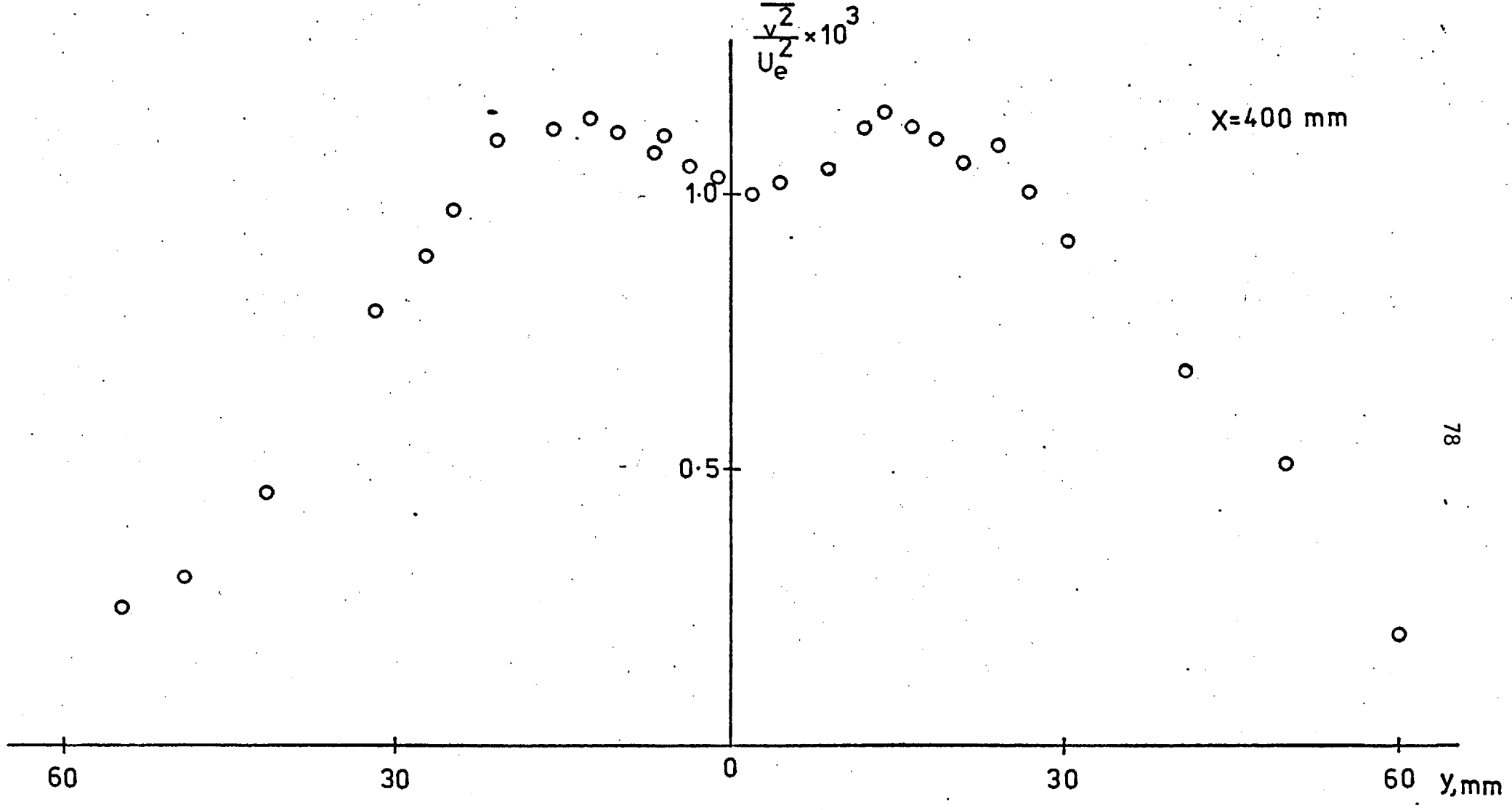

FIG. 4.17 $\overline{v^2}$ PROFILE AT x = 400 mm.

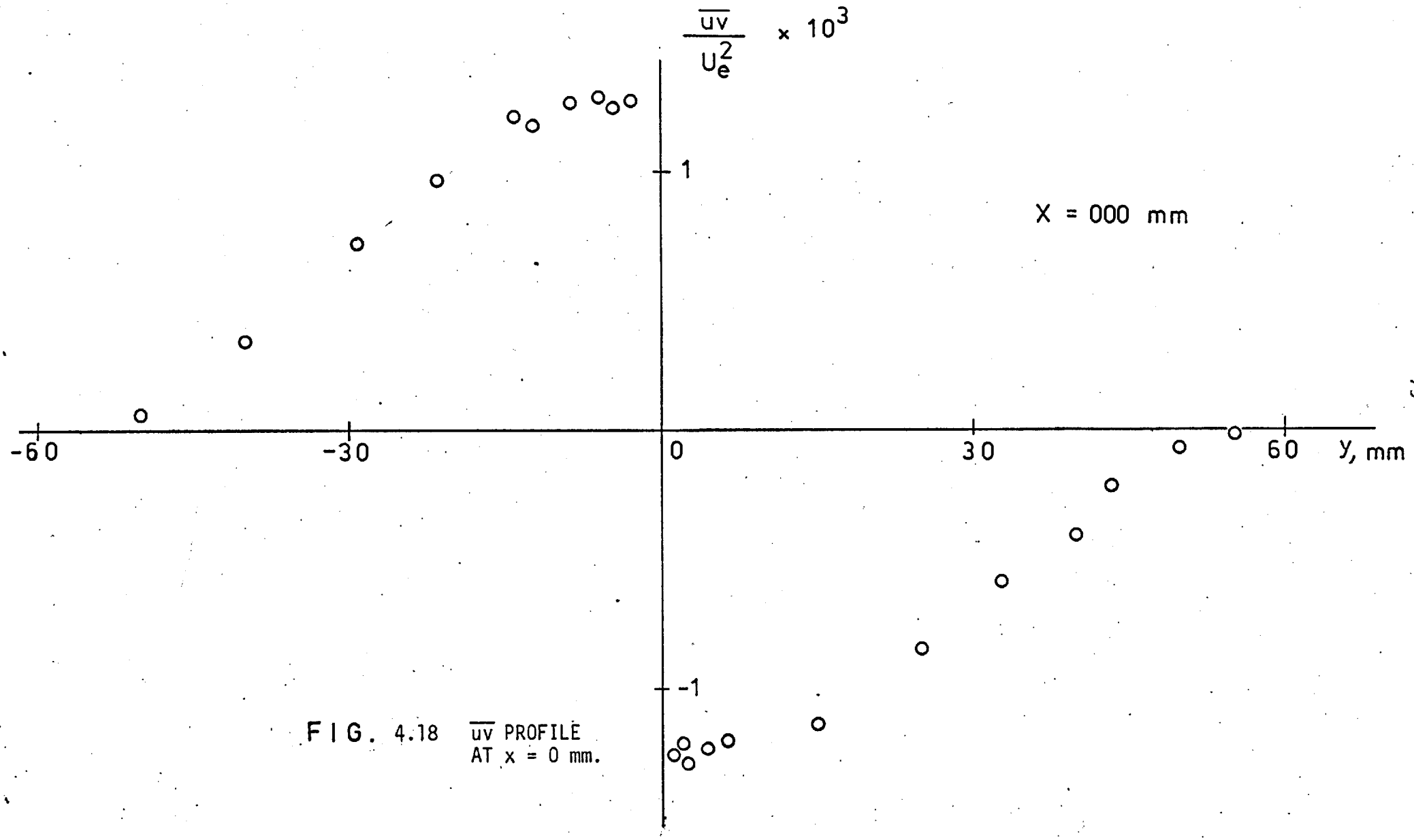

FIG. 4.18 $\overline{uv}$ PROFILE AT x = 0 mm.

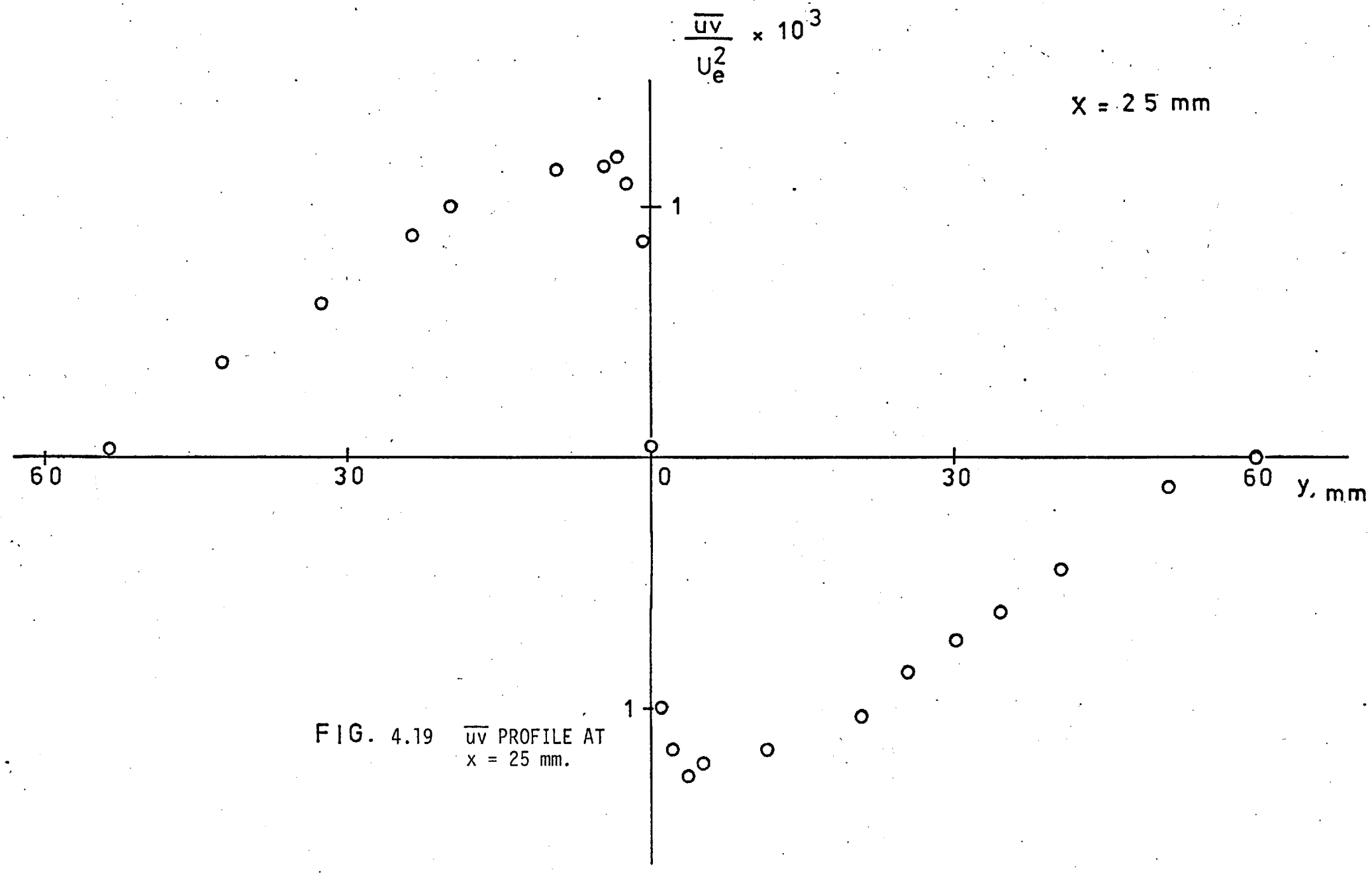

FIG. 4.19 $\overline{uv}$ PROFILE AT x = 25 mm.

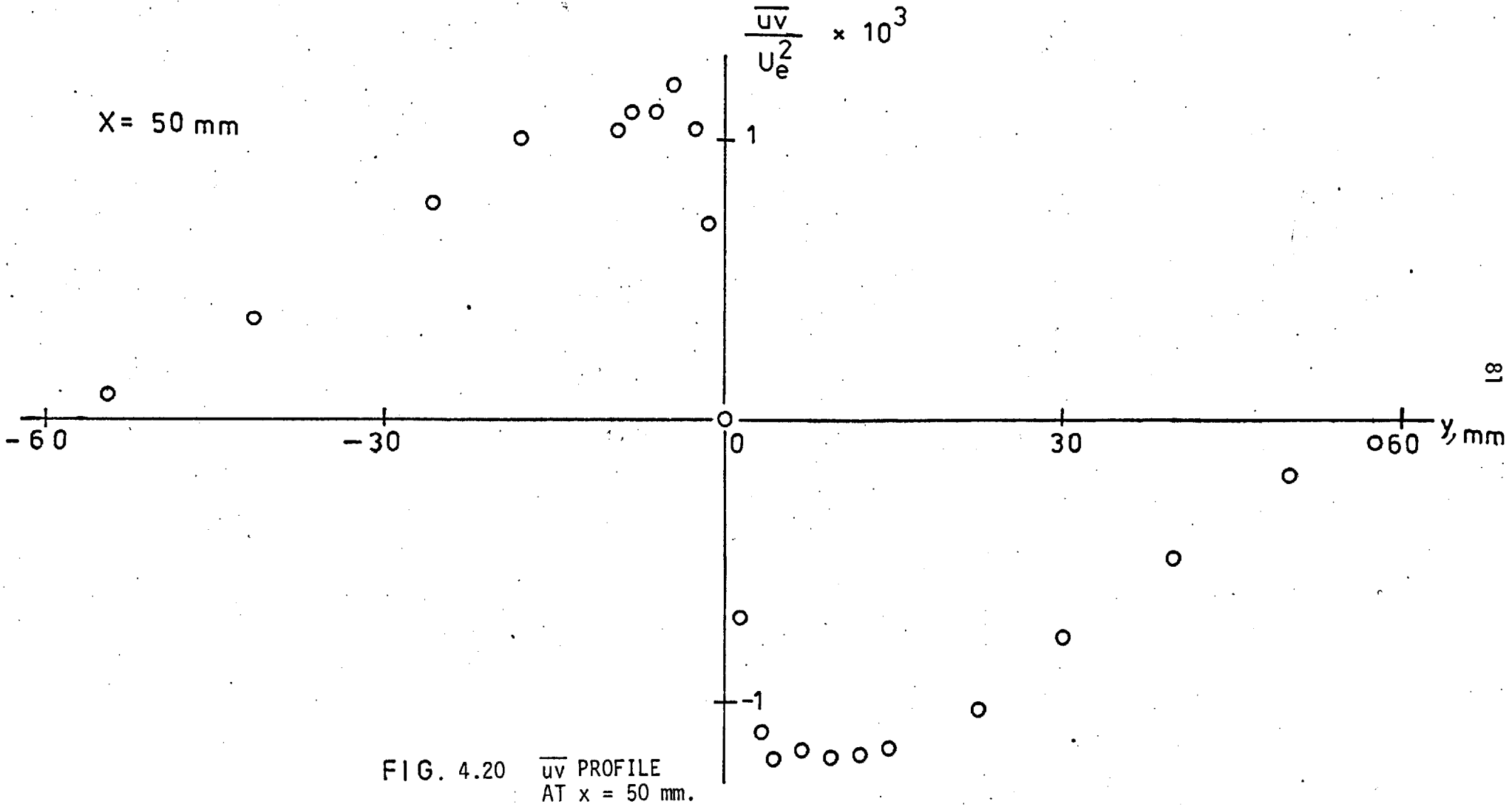

FIG. 4.20 $\overline{uv}$ PROFILE AT x = 50 mm.

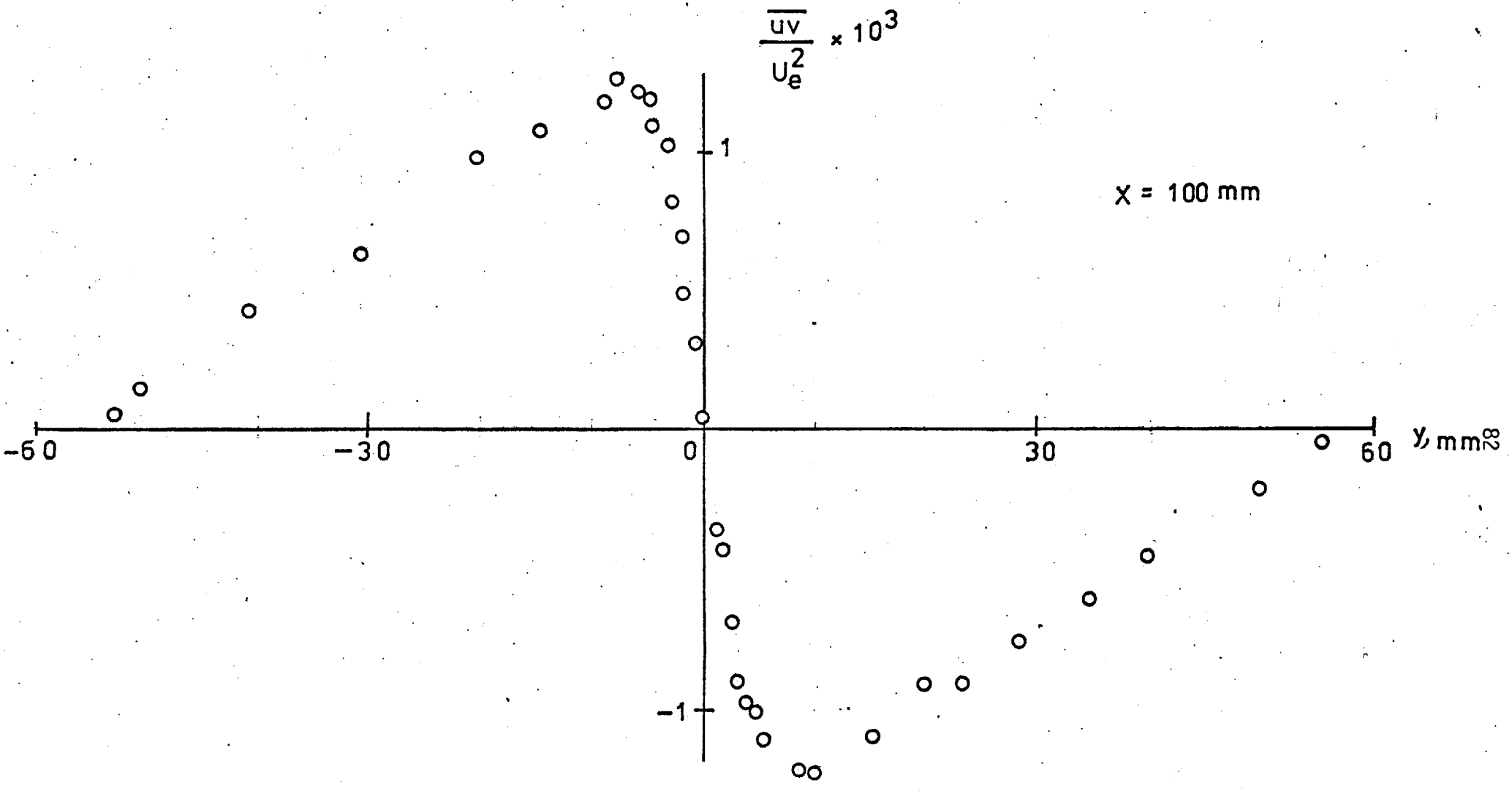

FIG. 4.21 $\overline{uv}$ PROFILE AT x = 100 mm.

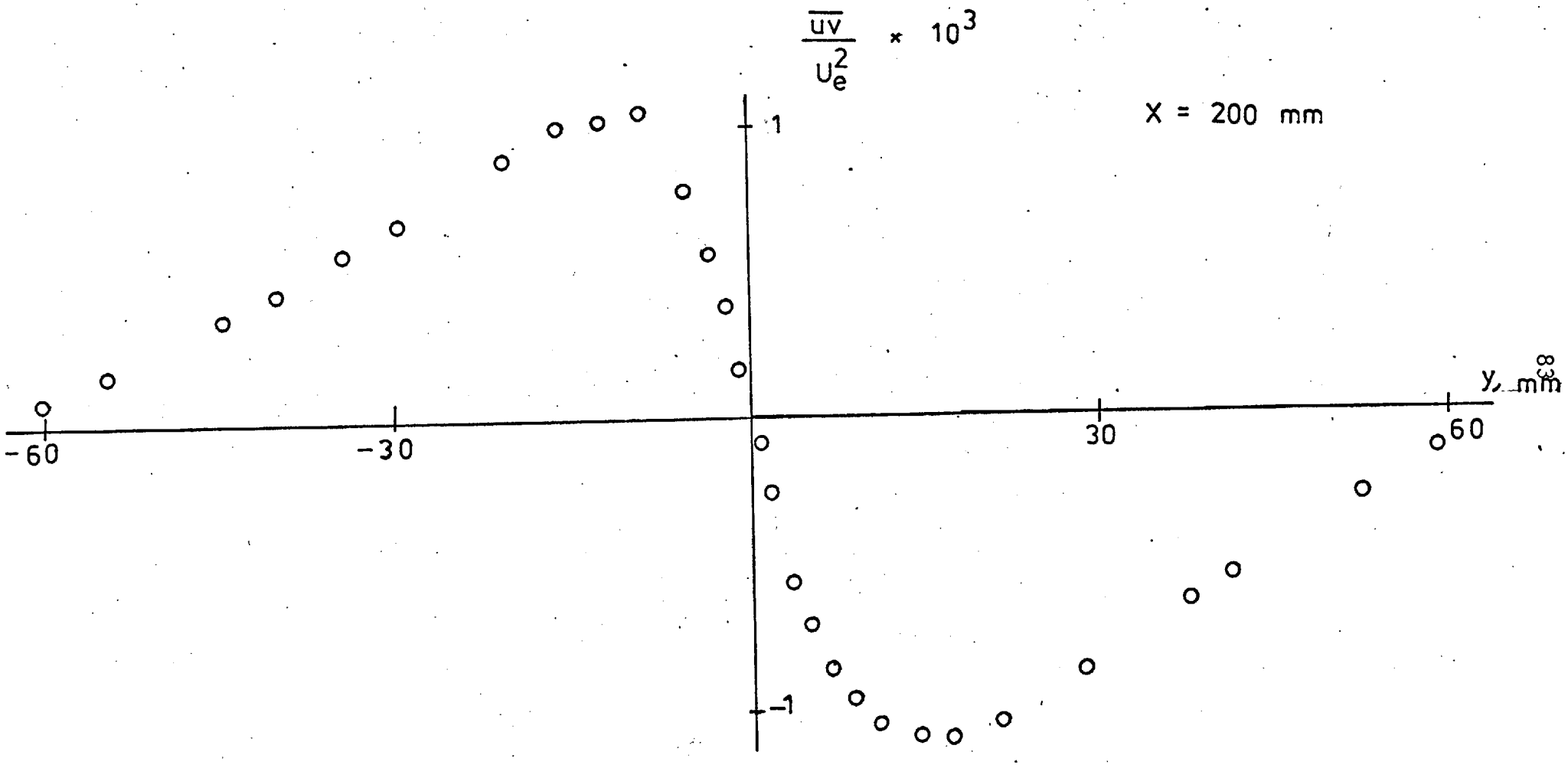

FIG. 4.22 $\overline{uv}$ PROFILE AT x = 200 mm.

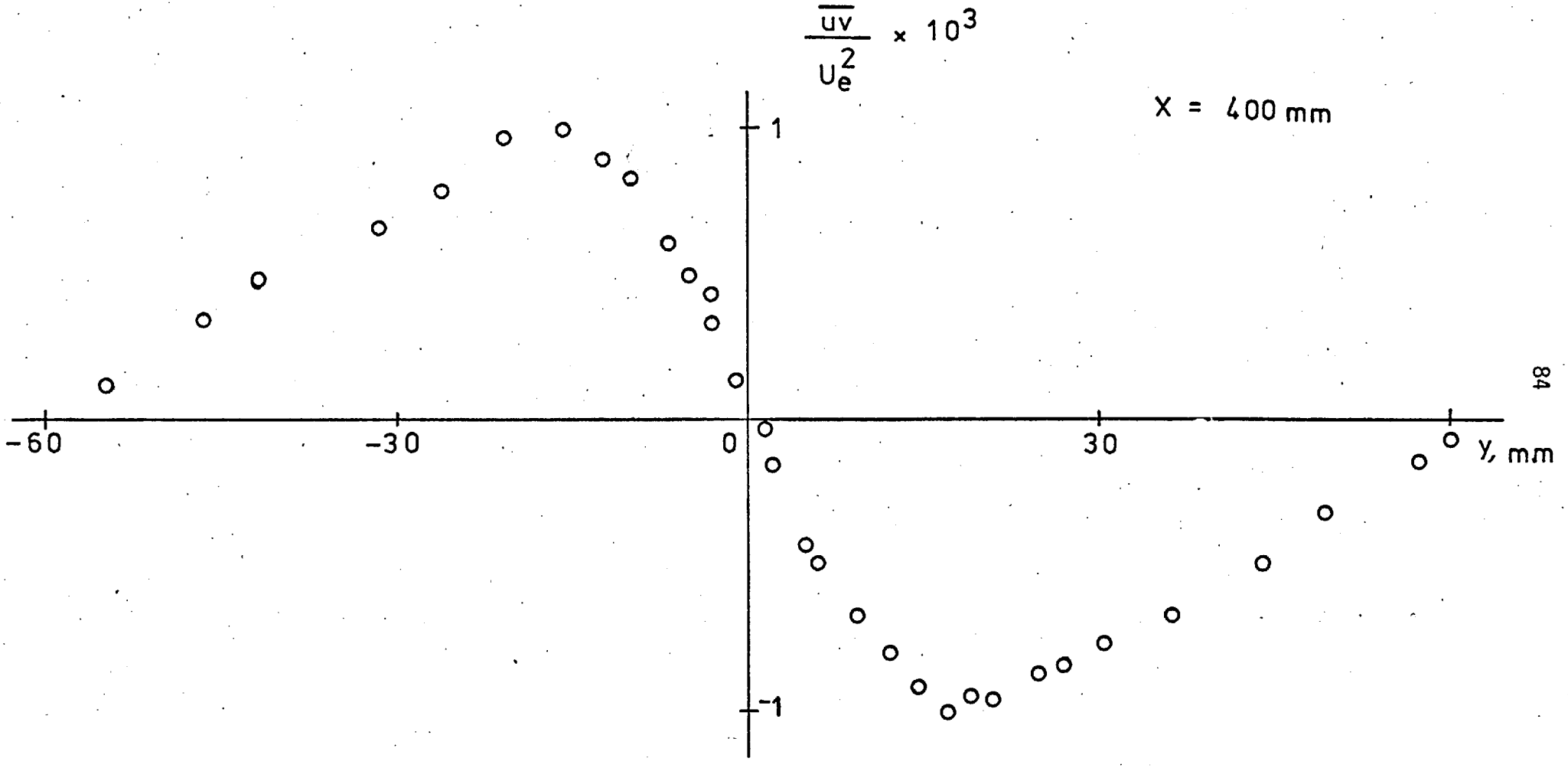

FIG. 4.23 $\overline{uv}$ PROFILE AT x = 400 mm.

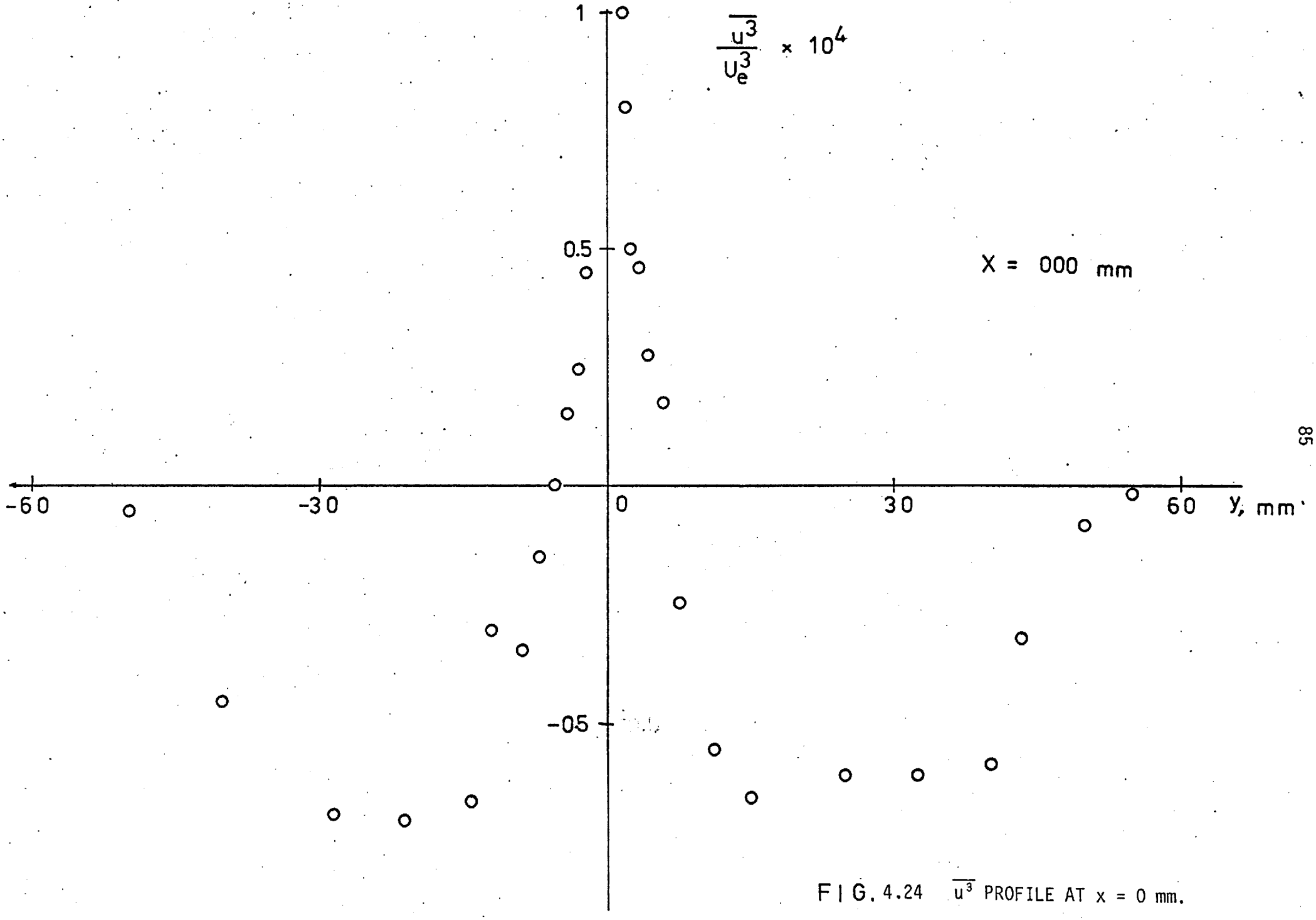

FIG. 4.24 $\overline{u^3}$ PROFILE AT x = 0 mm.

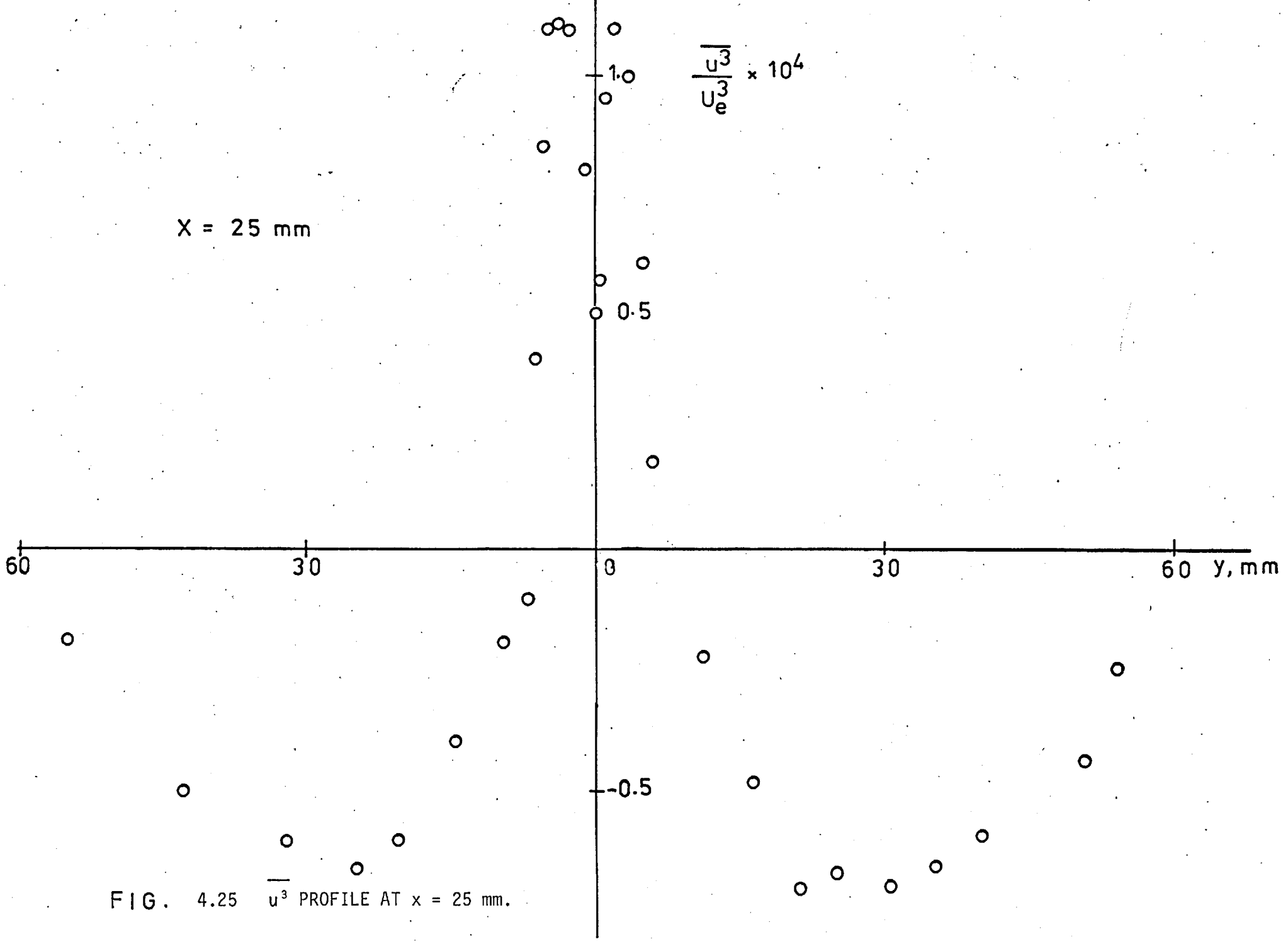

FIG. 4.25 $\overline{u^3}$ PROFILE AT x = 25 mm.

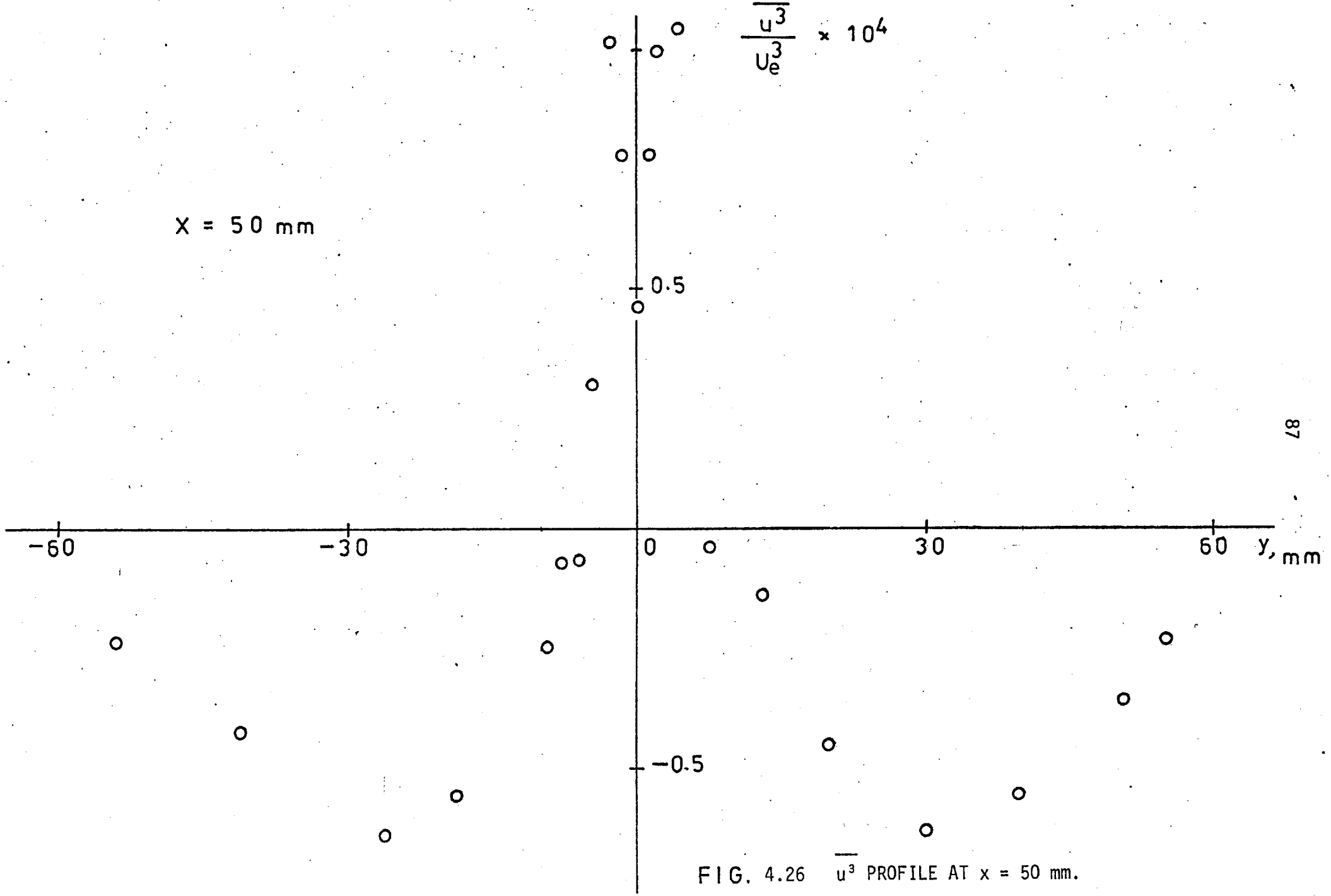

FIG. 4.26 $\overline{u^3}$ PROFILE AT x = 50 mm.

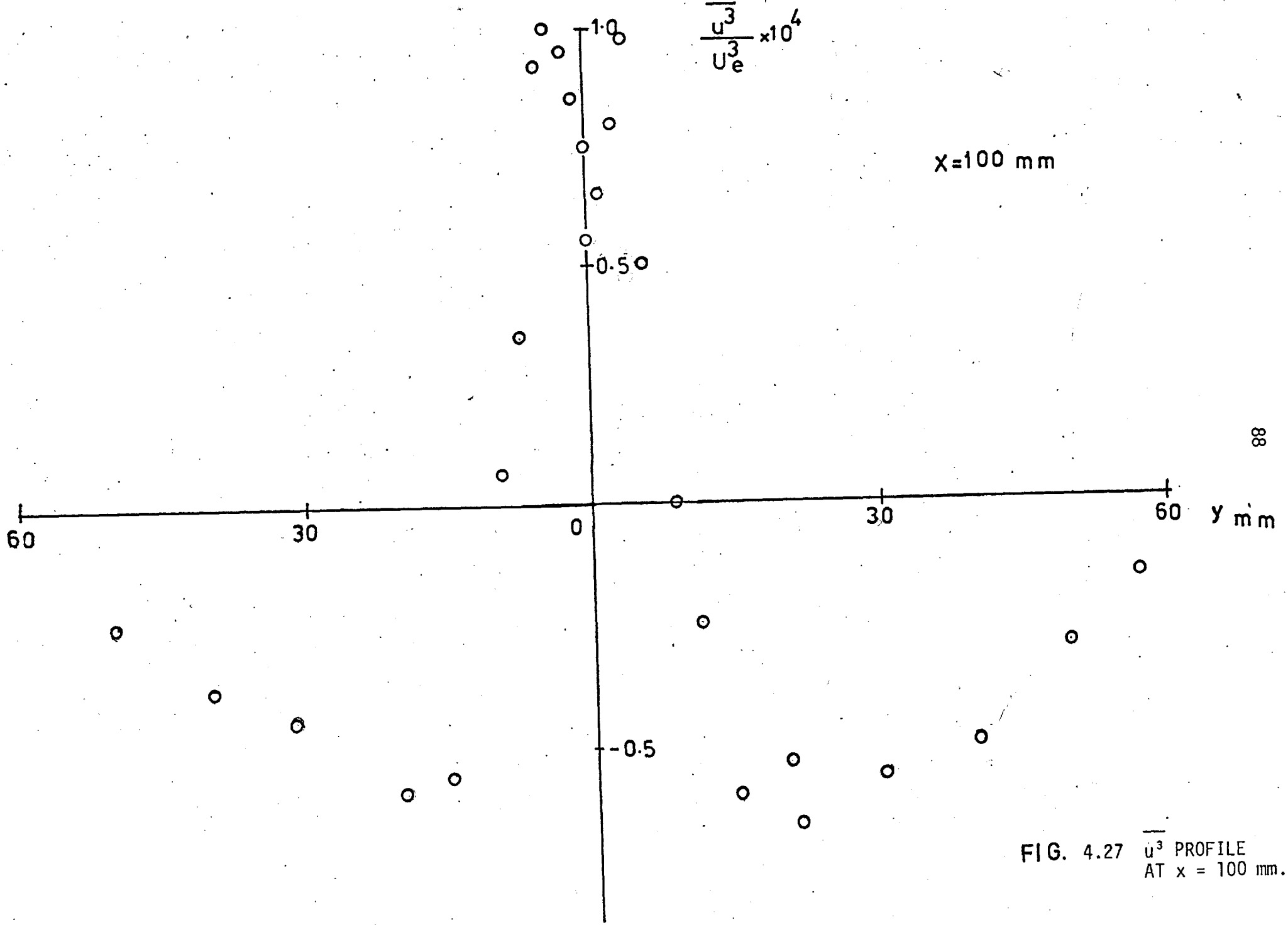

FIG. 4.27 $\overline{u^3}$ PROFILE AT x = 100 mm.

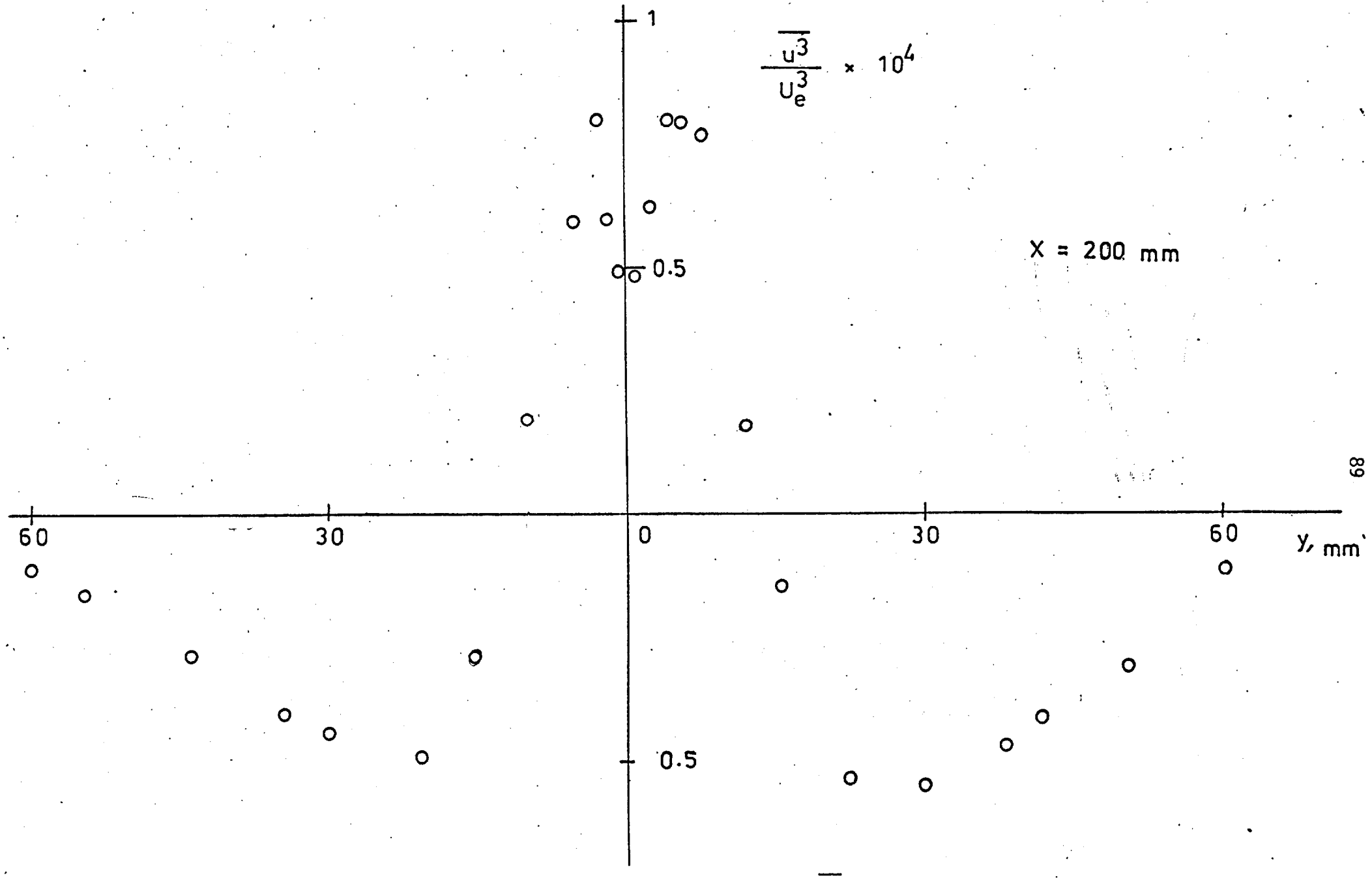

FIG. 4.28 $\overline{u^3}$ PROFILE AT x = 200 mm.

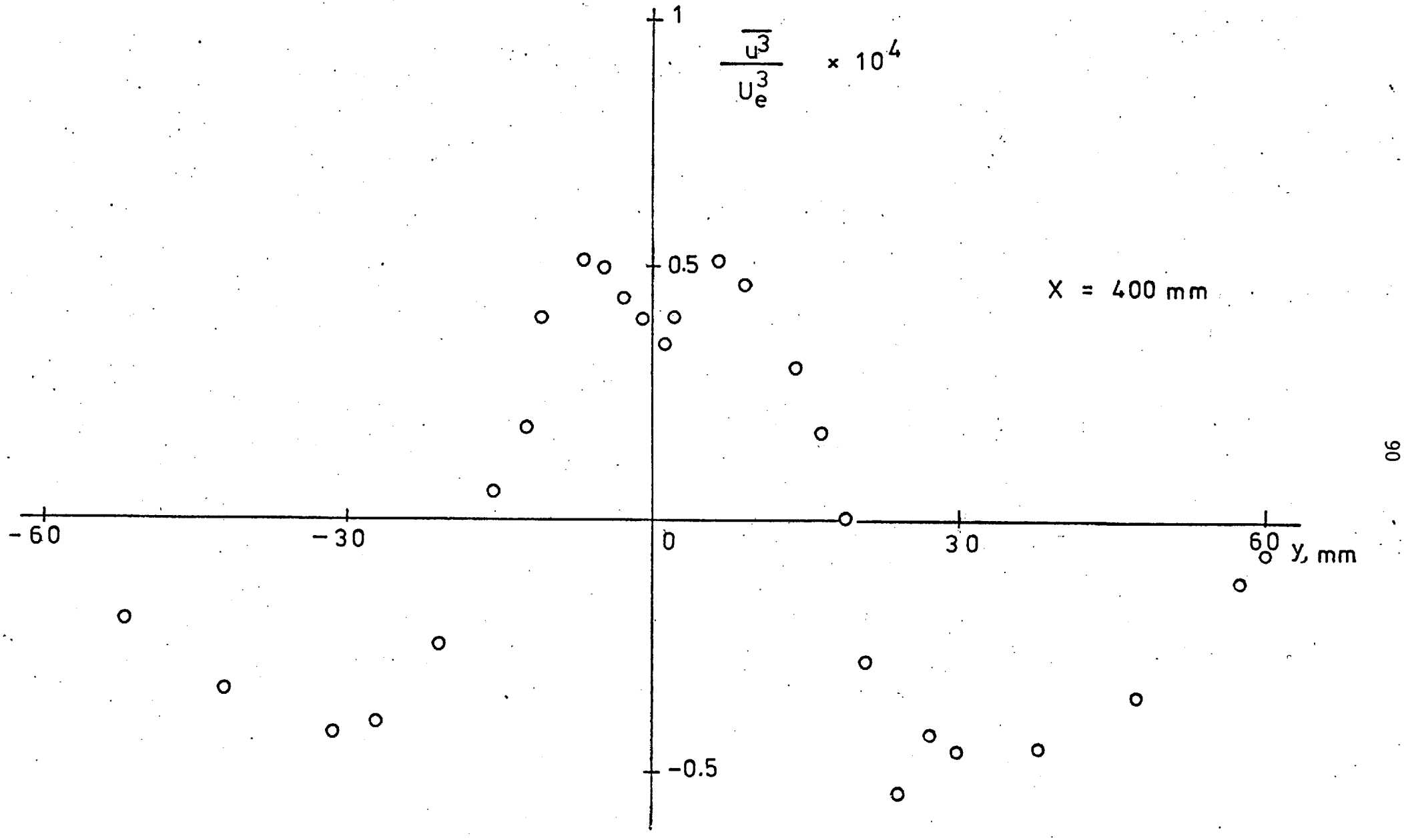

FIG. 4.29 $\overline{u^3}$ PROFILE AT x = 400 mm.

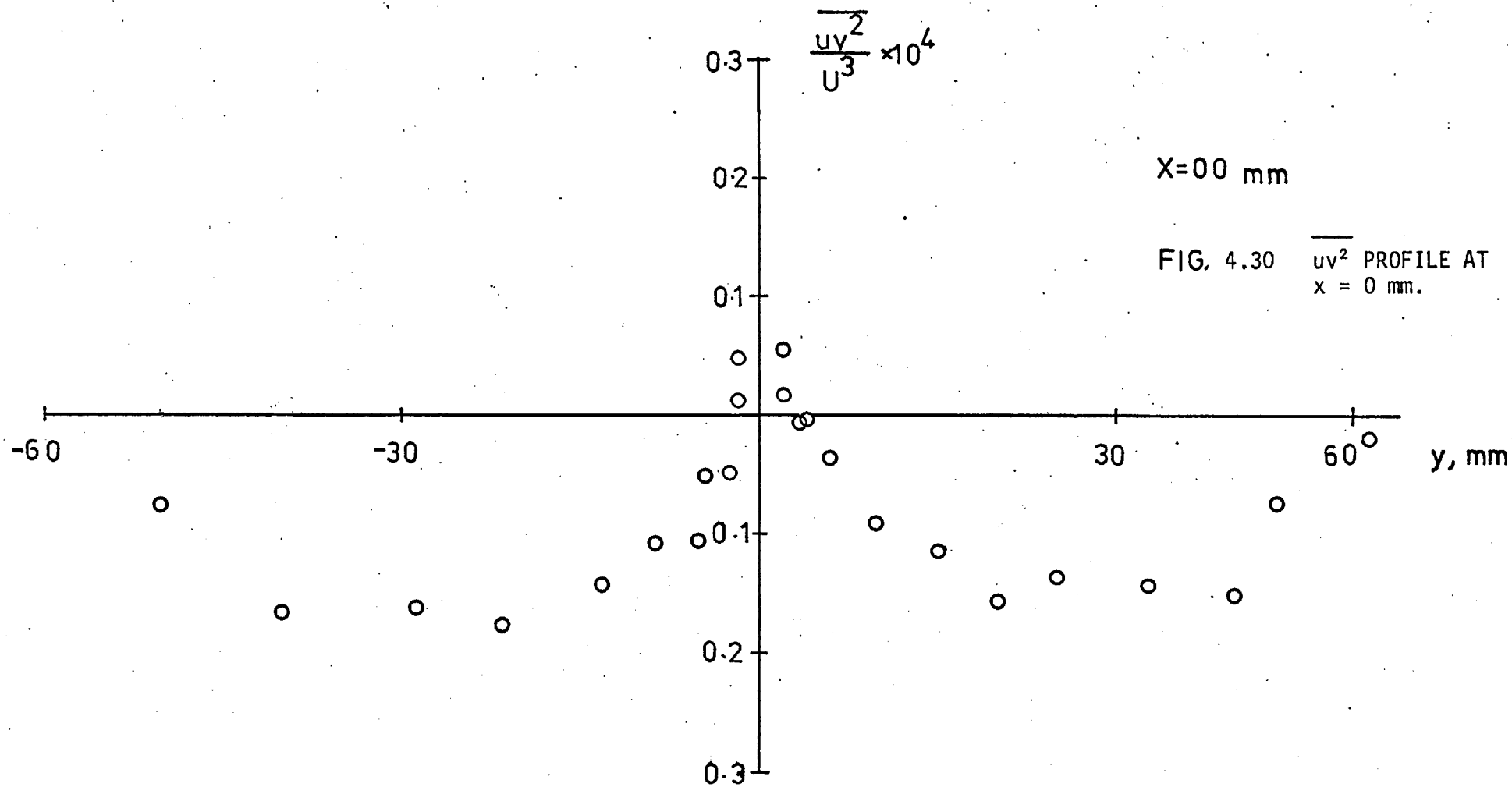

FIG. 4.30 $\overline{uv^2}$ PROFILE AT x = 0 mm.

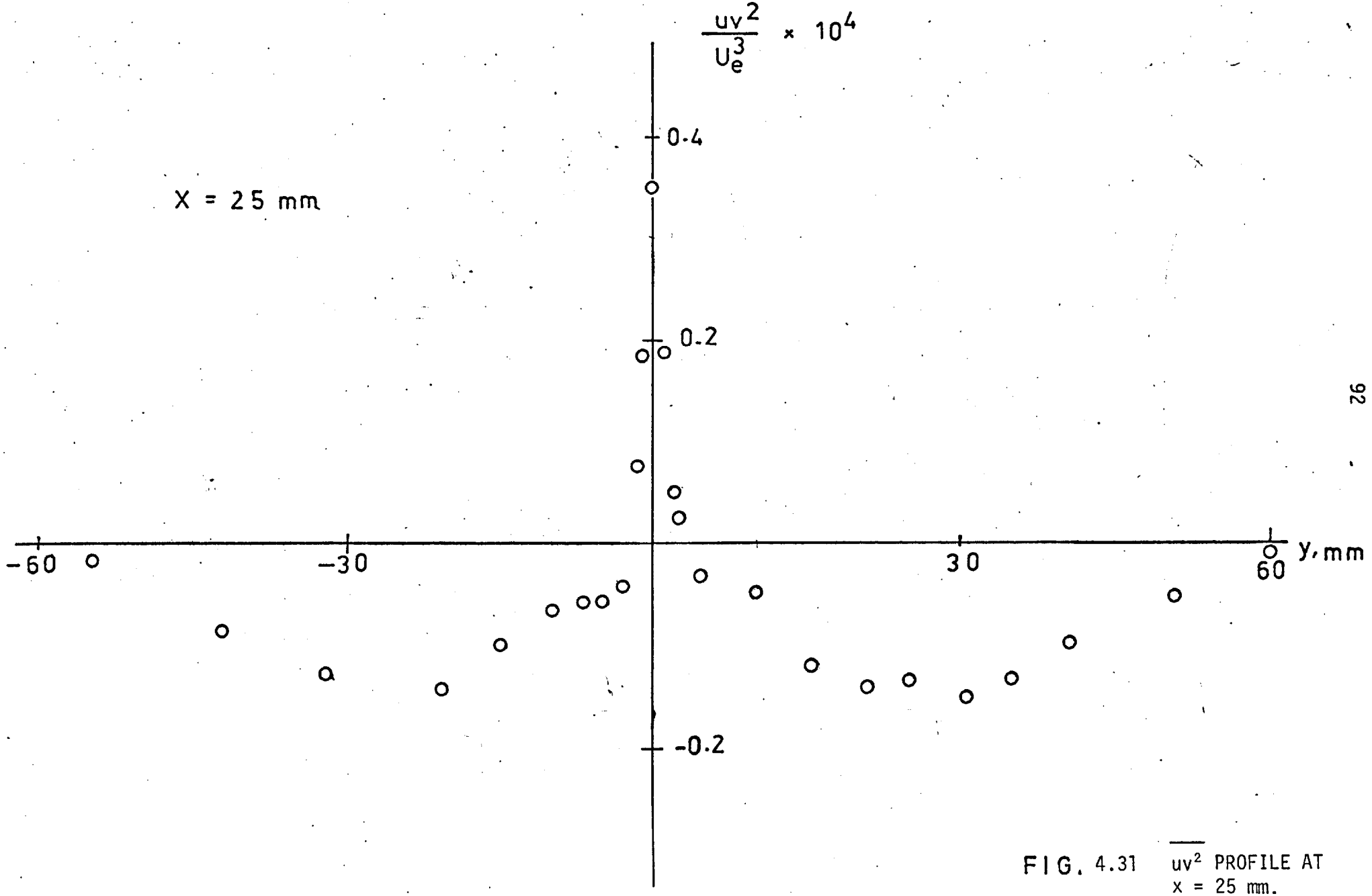

FIG. 4.31 $\overline{uv^2}$ PROFILE AT x = 25 mm.

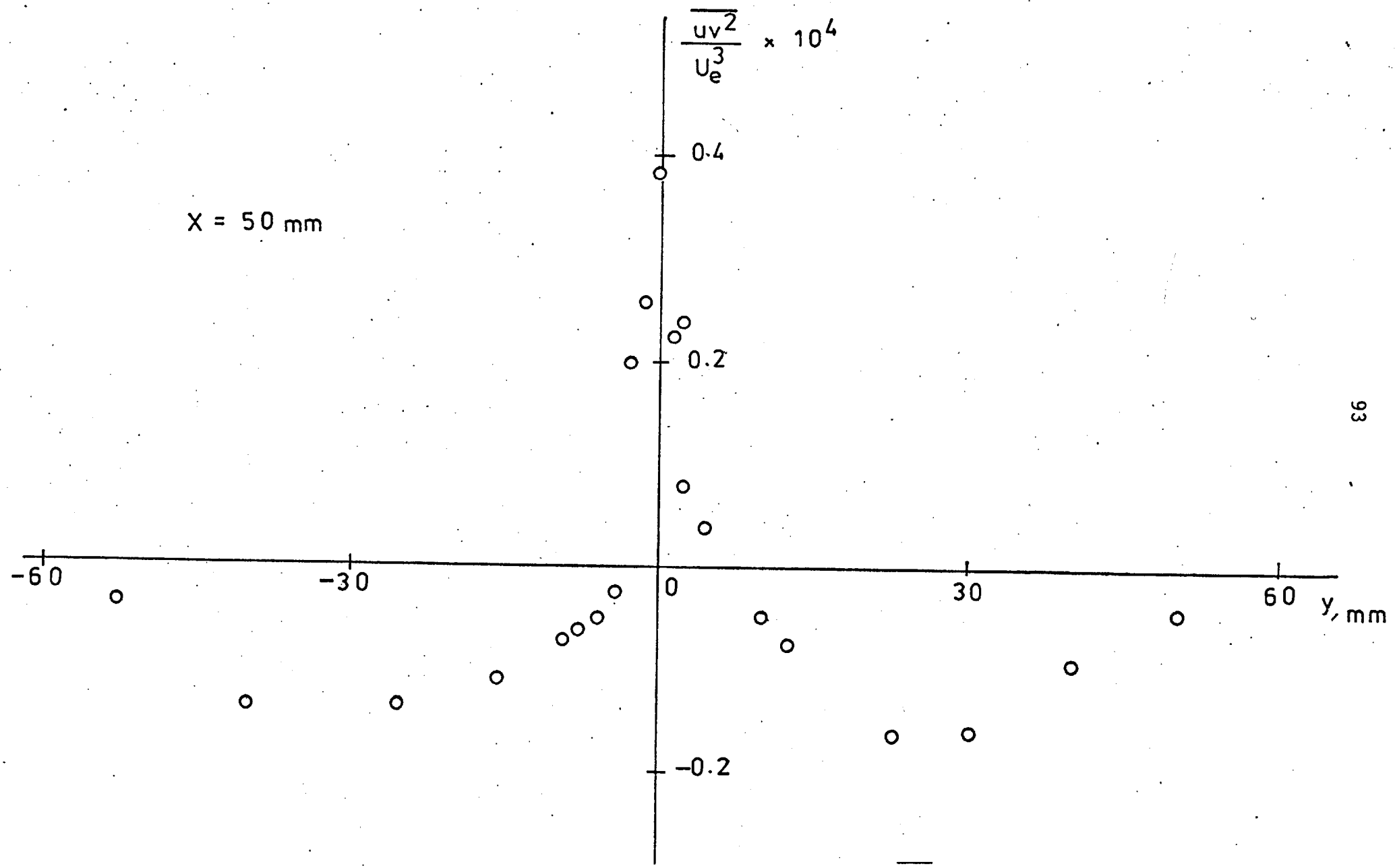

FIG. 4.32 $\overline{uv^2}$ PROFILE AT x = 50 mm.

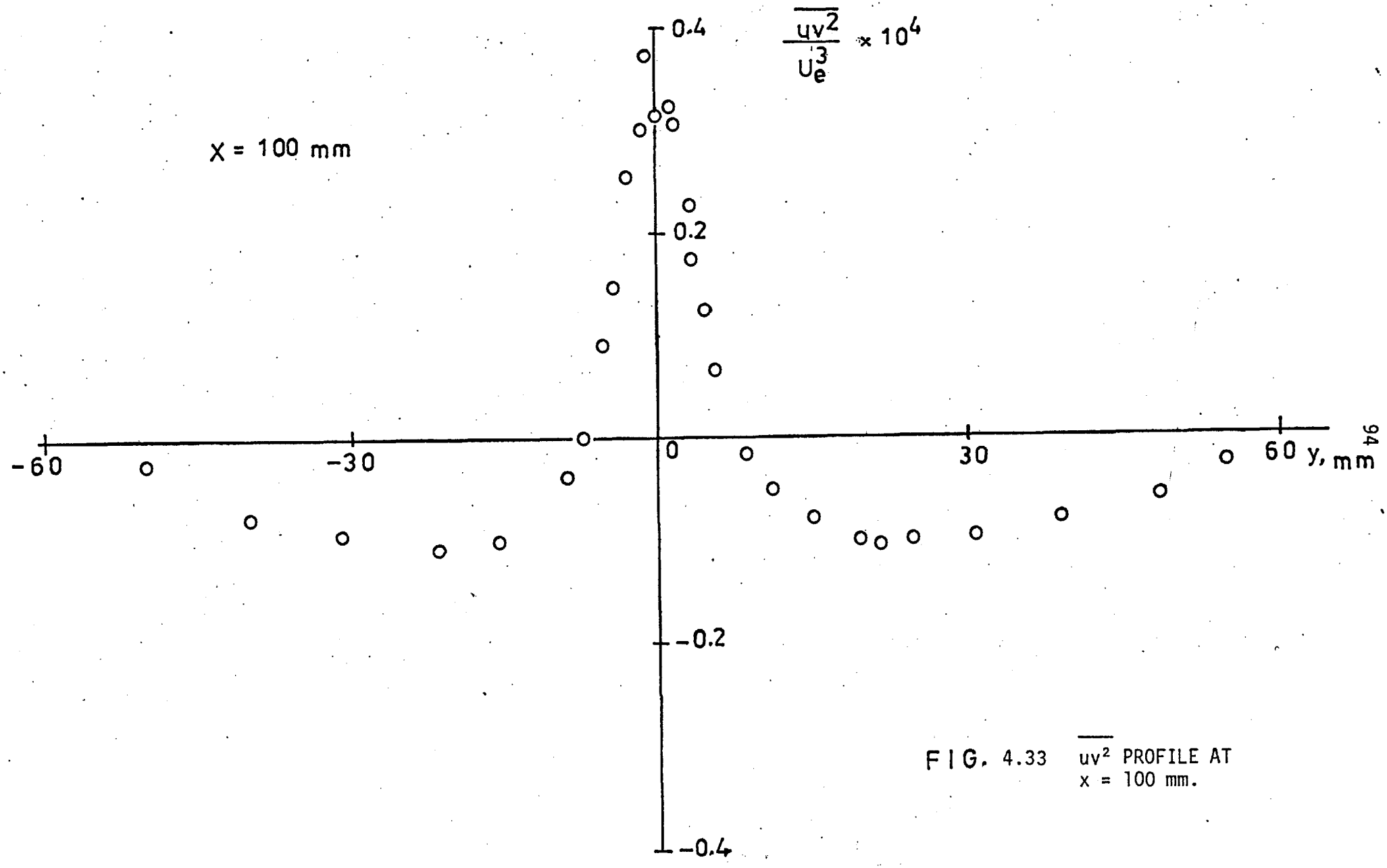

FIG. 4.33 $\overline{uv^2}$ PROFILE AT x = 100 mm.

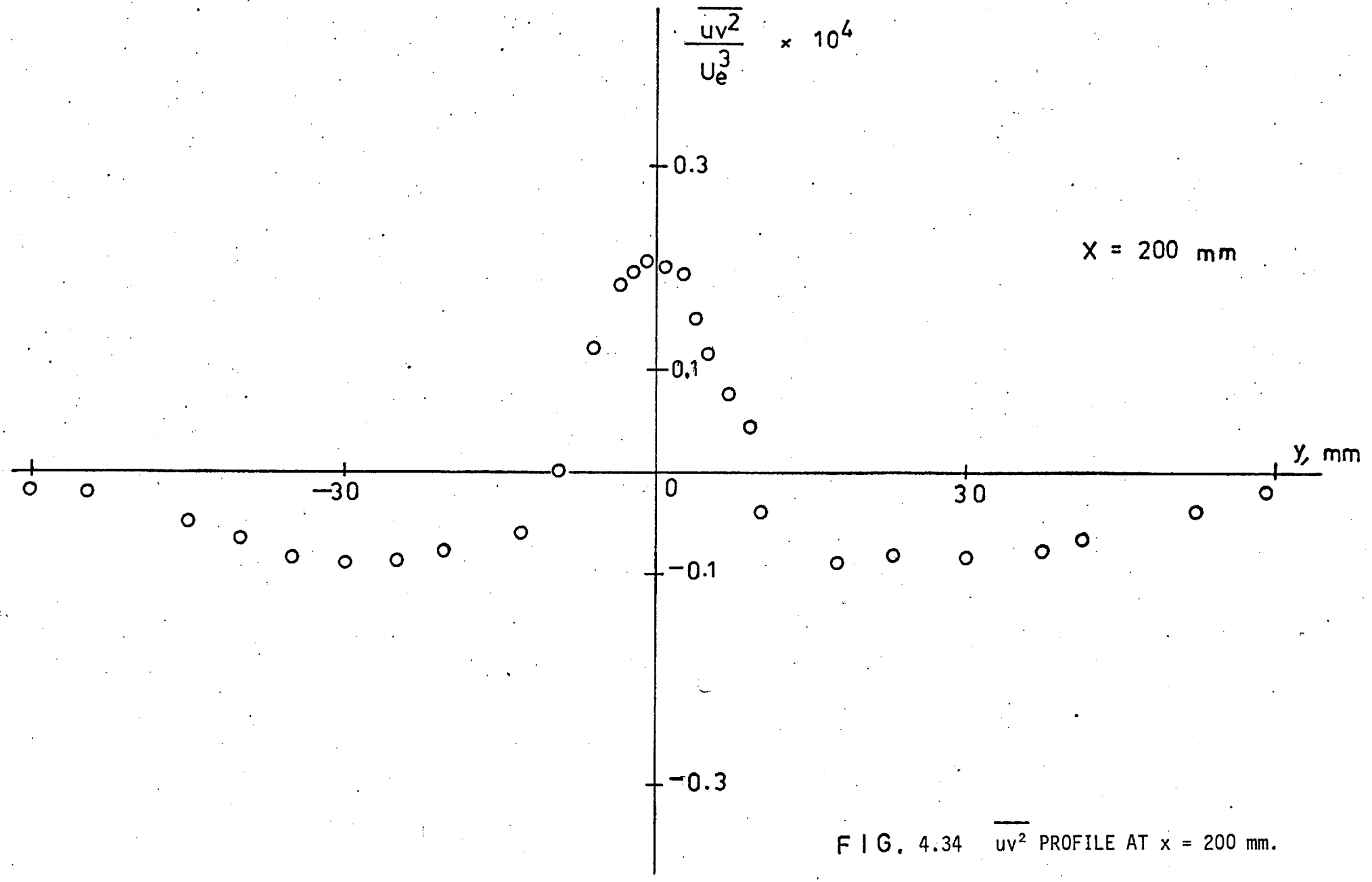

FIG. 4.34 $\overline{uv^2}$ PROFILE AT x = 200 mm.

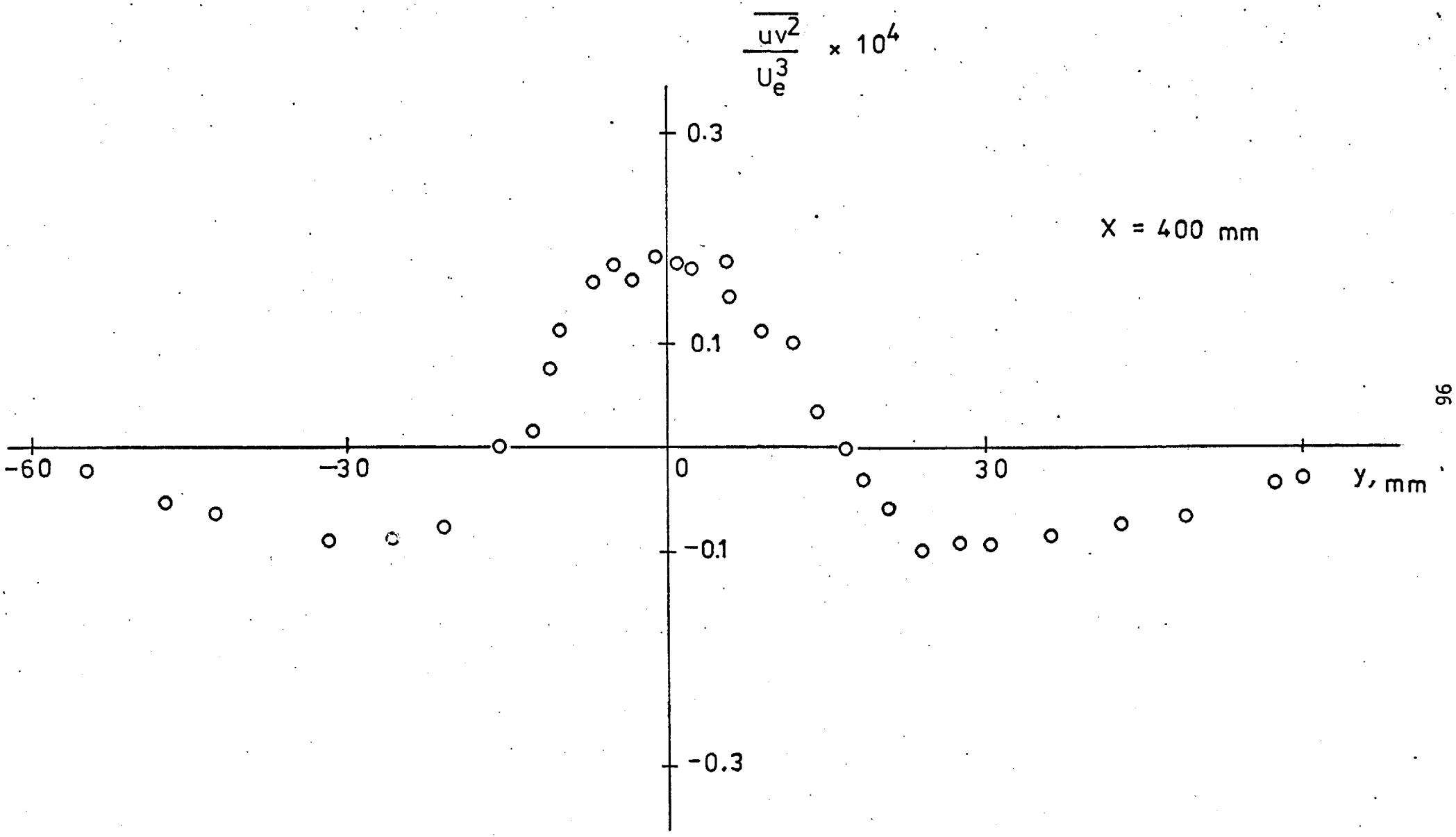

FIG. 4.35 $\overline{uv^2}$ PROFILE AT x = 400 mm.

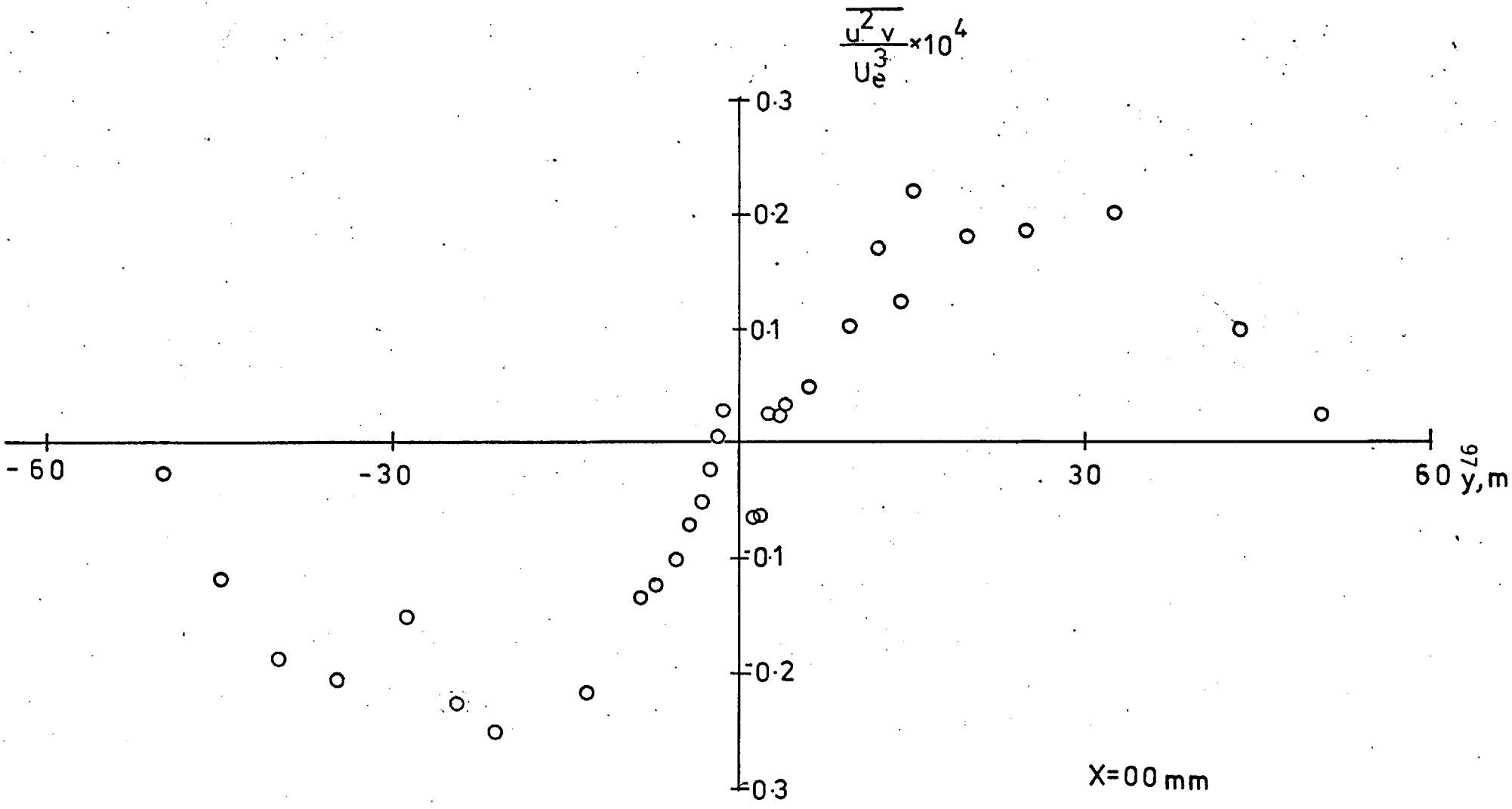

FIG. 4.36 $\overline{u^2 v}$ PROFILE AT x = 0 mm.

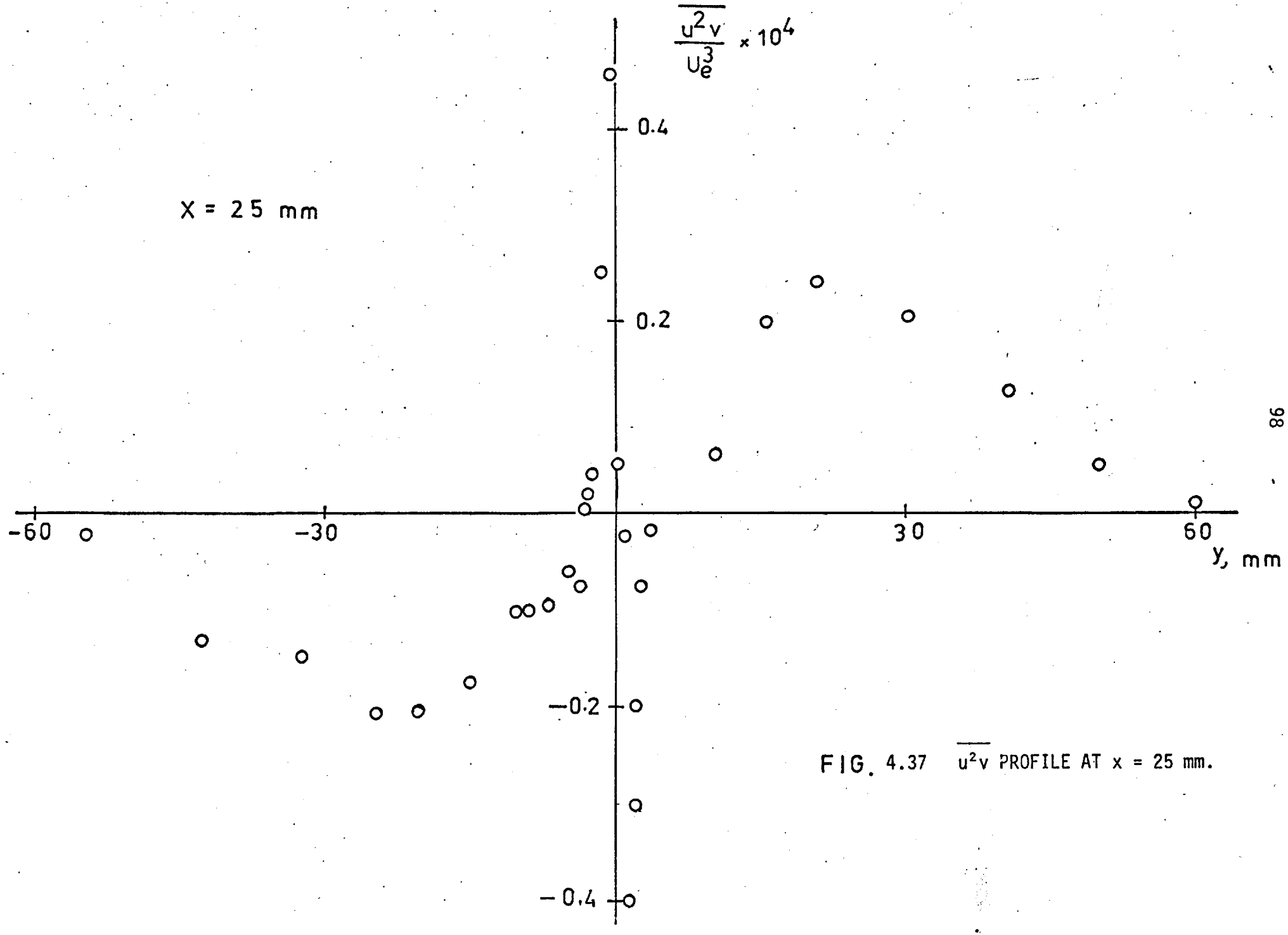

FIG. 4.37 $\overline{u^2v}$ PROFILE AT x = 25 mm.

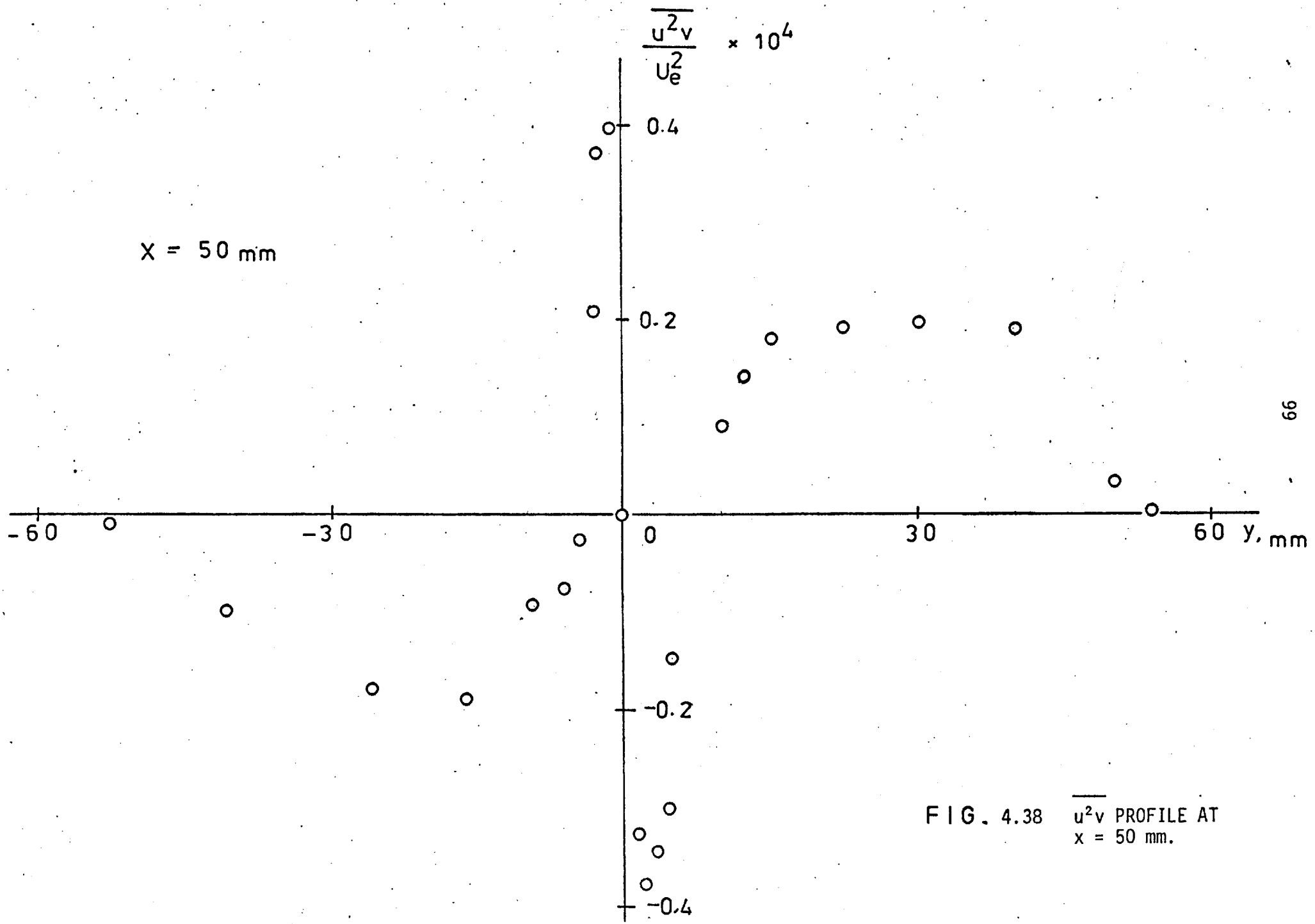

FIG. 4.38 $\overline{u^2v}$ PROFILE AT x = 50 mm.

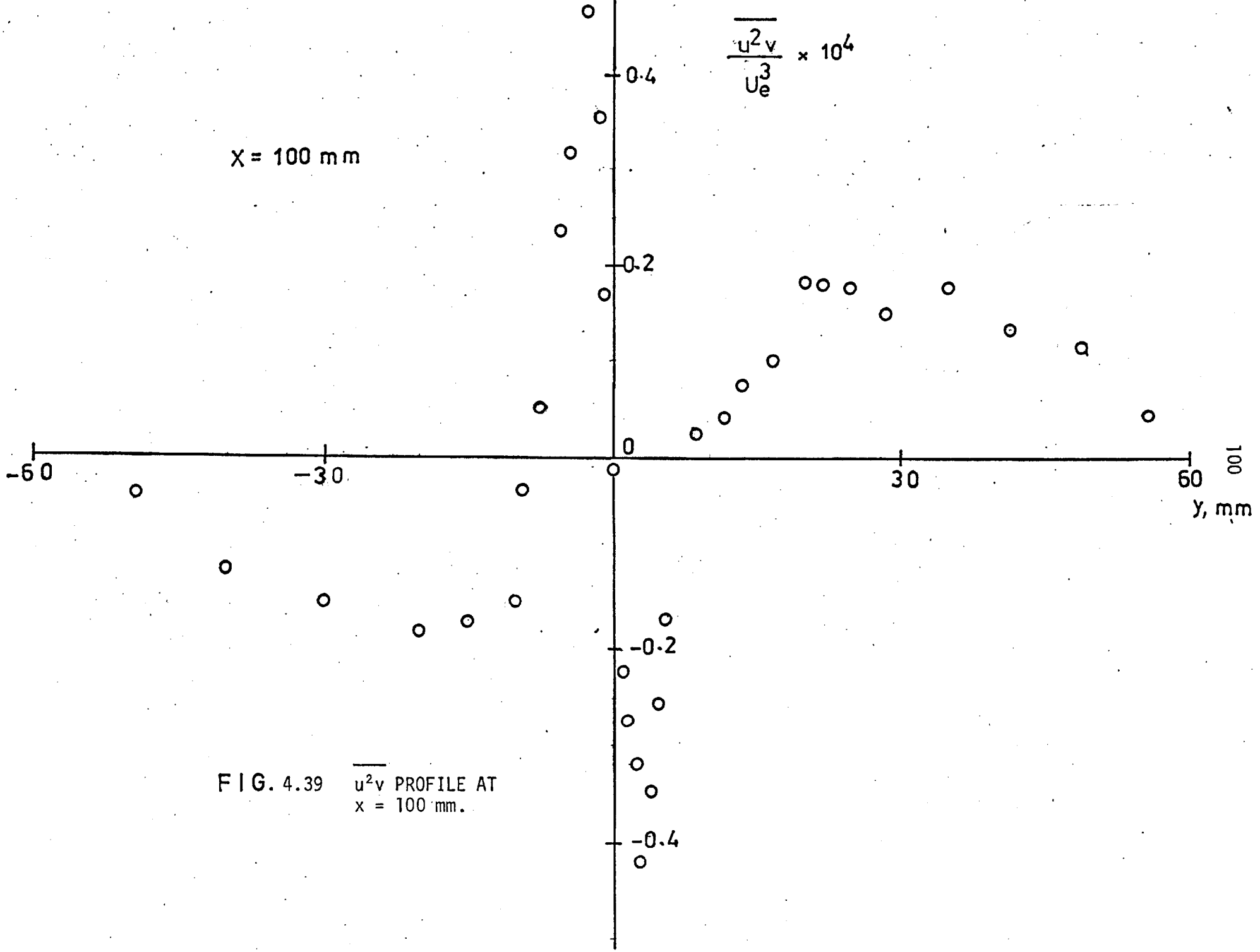

FIG. 4.39 $\overline{u^2v}$ PROFILE AT x = 100 mm.

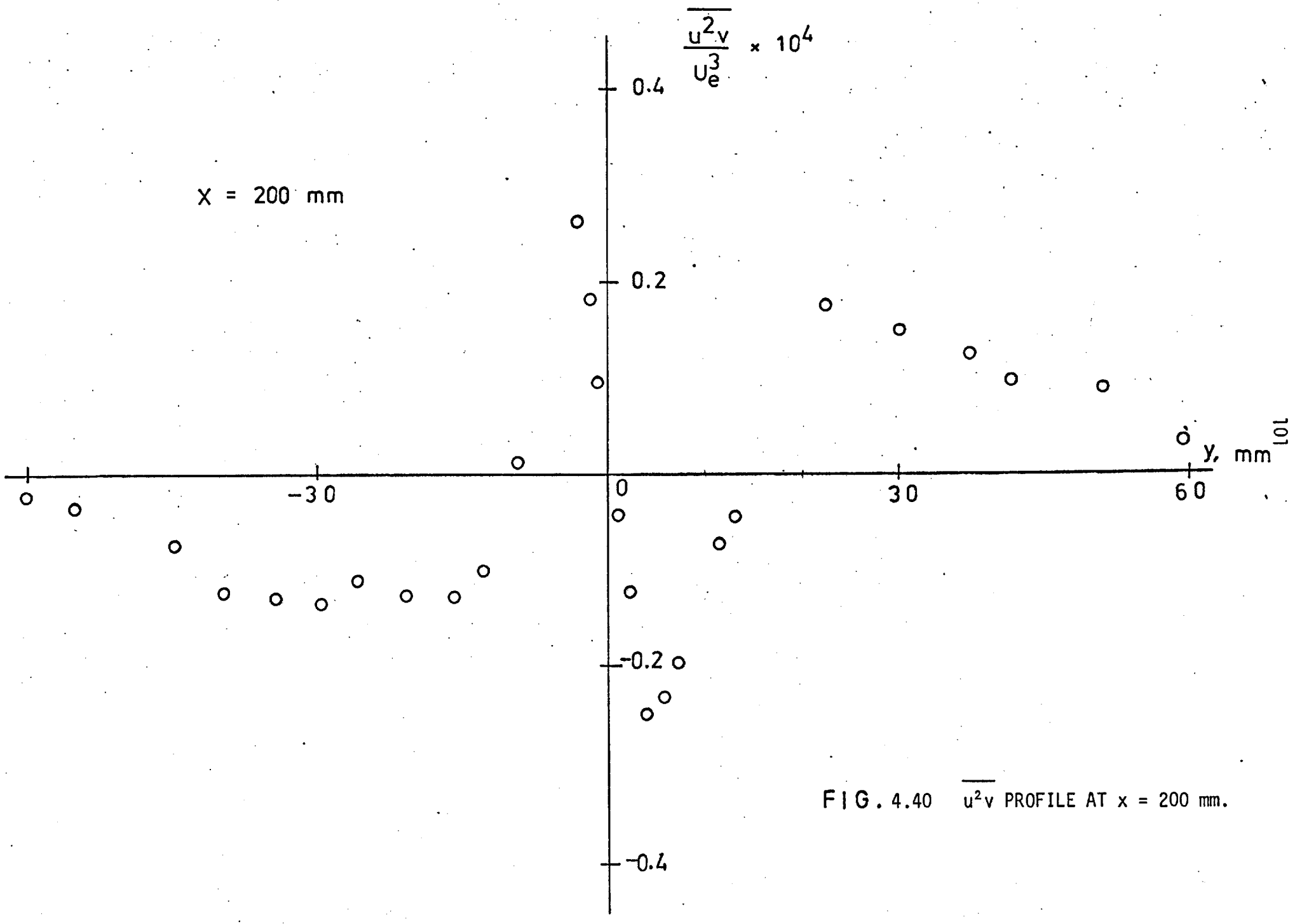

FIG. 4.40 $\overline{u^2v}$ PROFILE AT x = 200 mm.

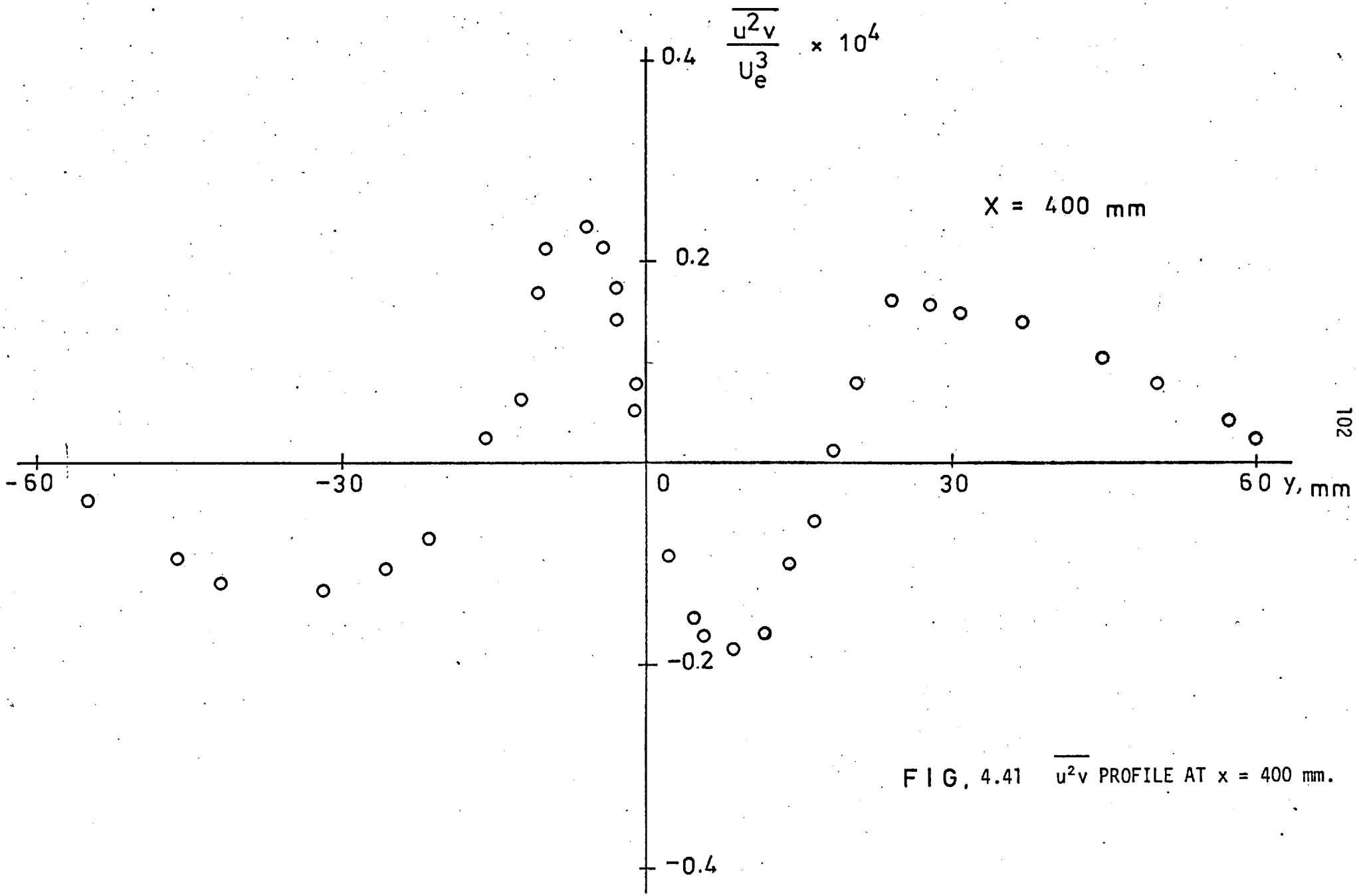

FIG. 4.41 $\overline{u^2v}$ PROFILE AT x = 400 mm.

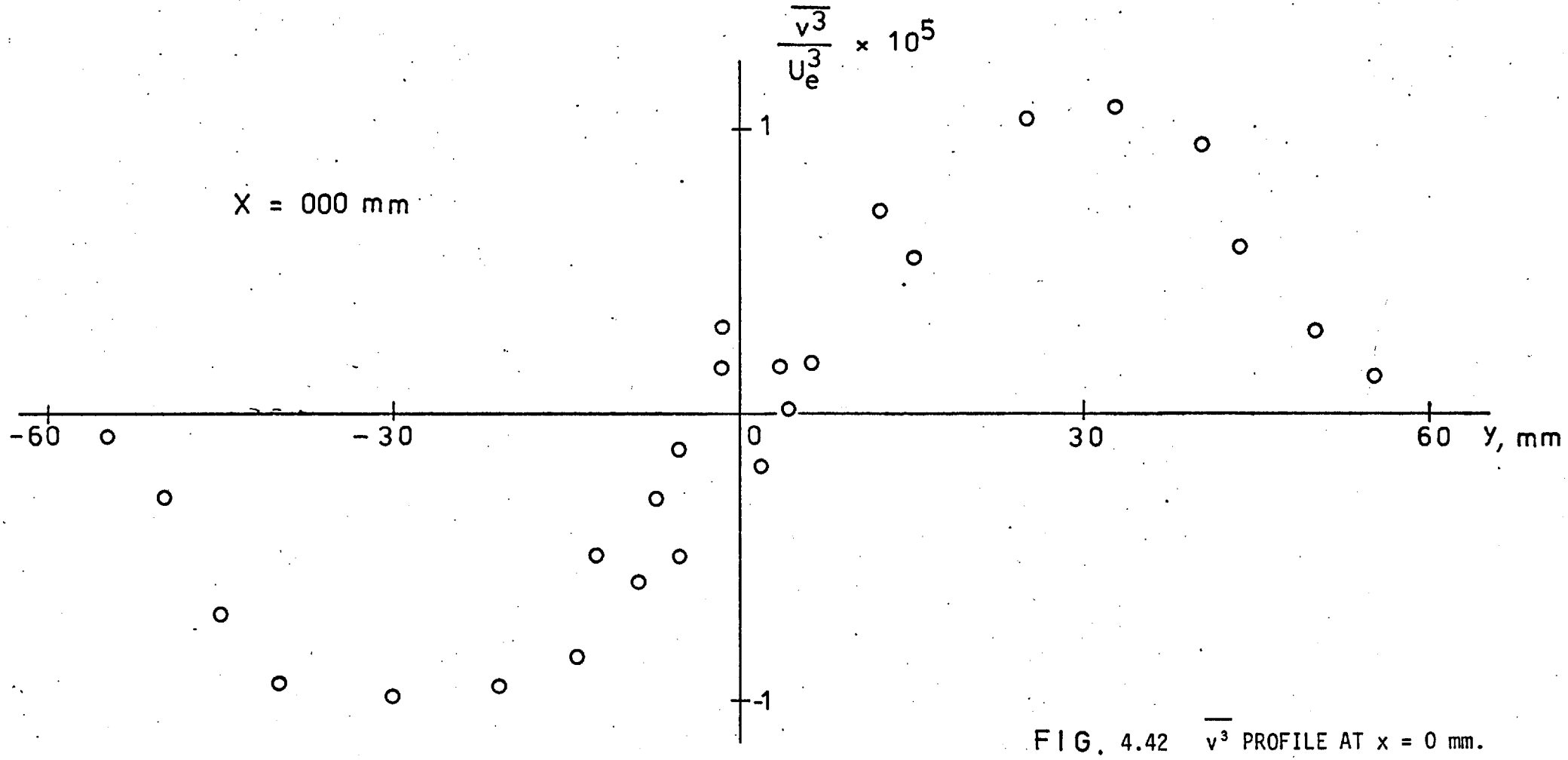

FIG. 4.42 $\overline{v^3}$ PROFILE AT x = 0 mm.

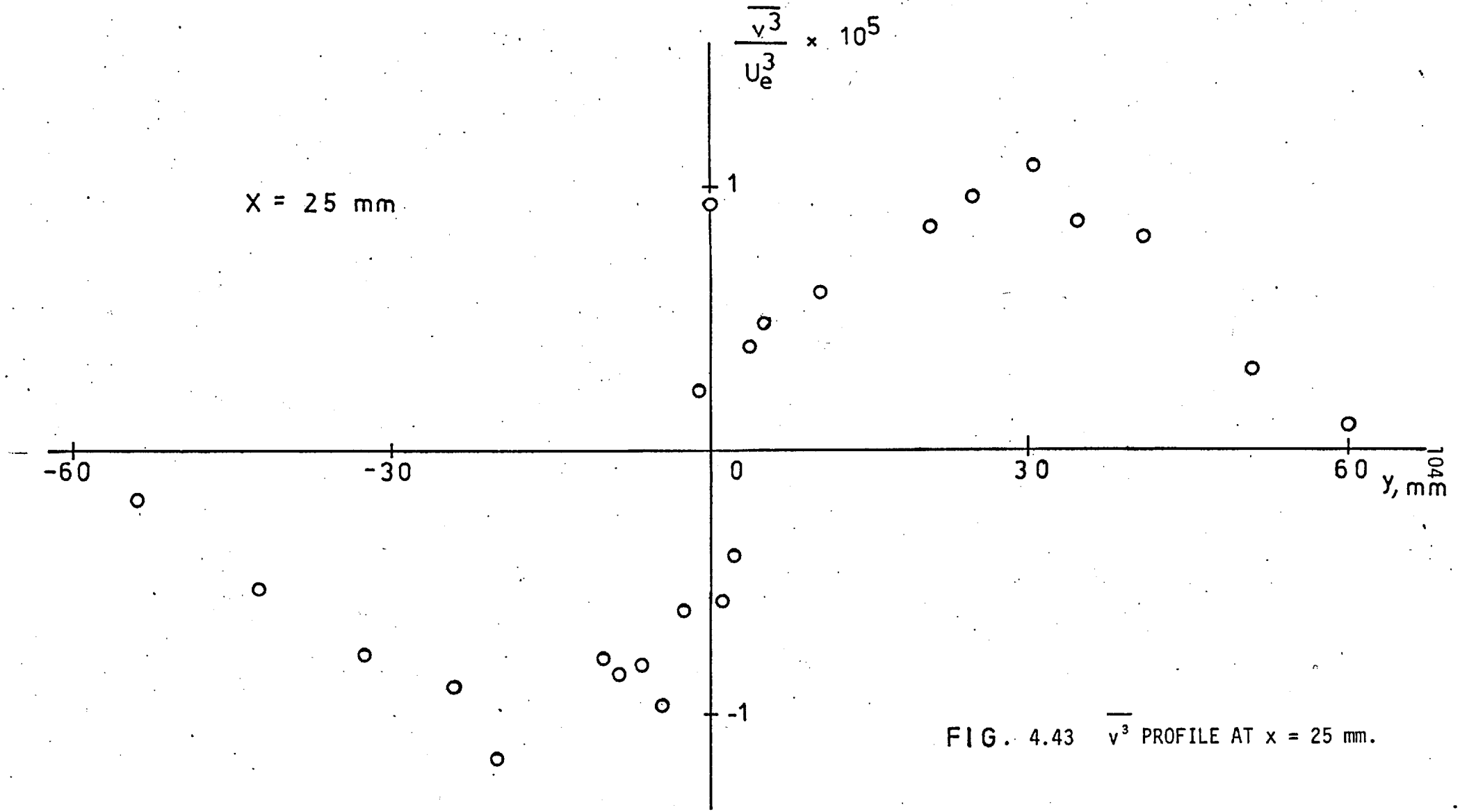

FIG. 4.43 $\overline{v^3}$ PROFILE AT x = 25 mm.

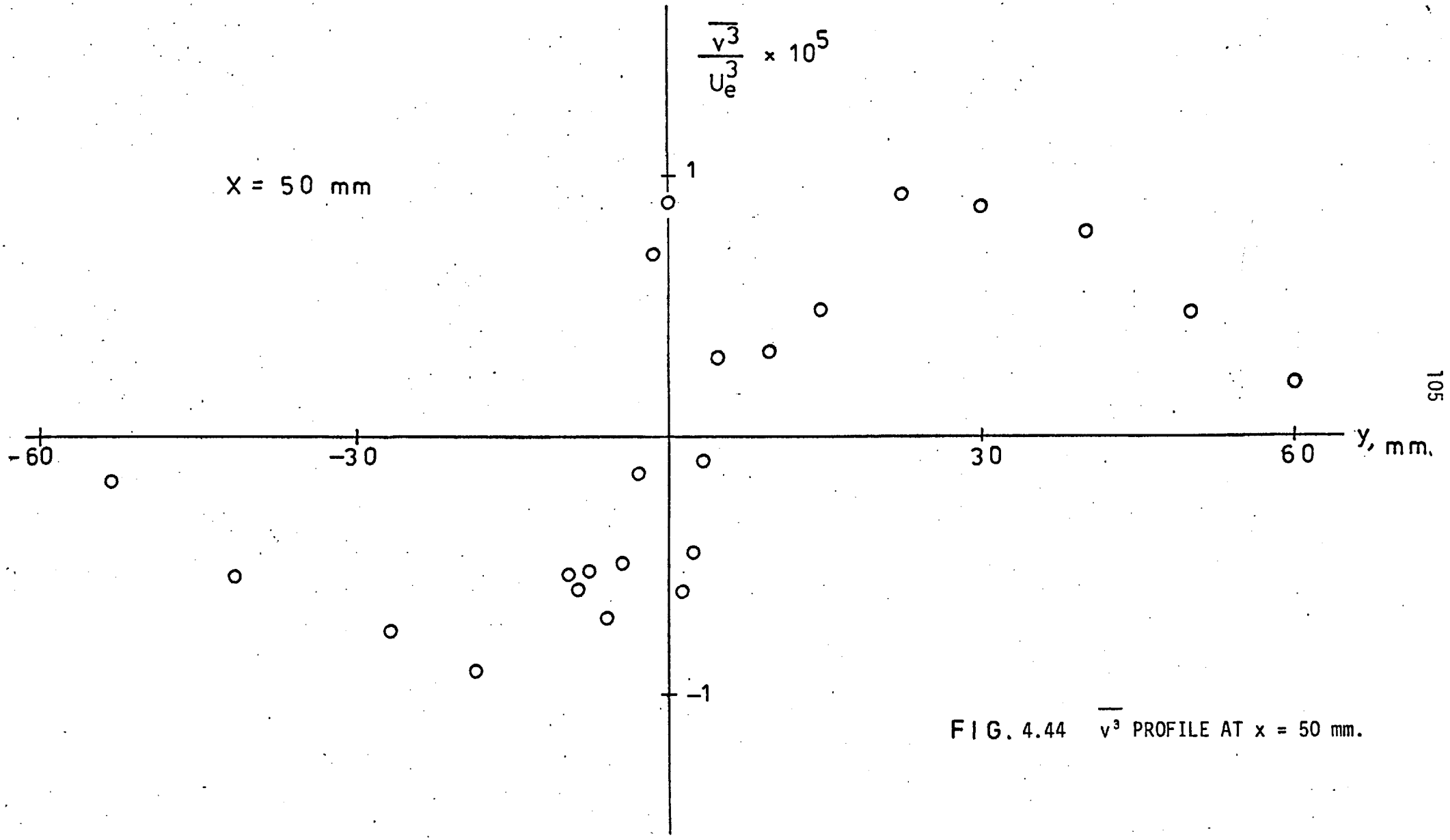

FIG. 4.44 $\overline{v^3}$ PROFILE AT x = 50 mm.

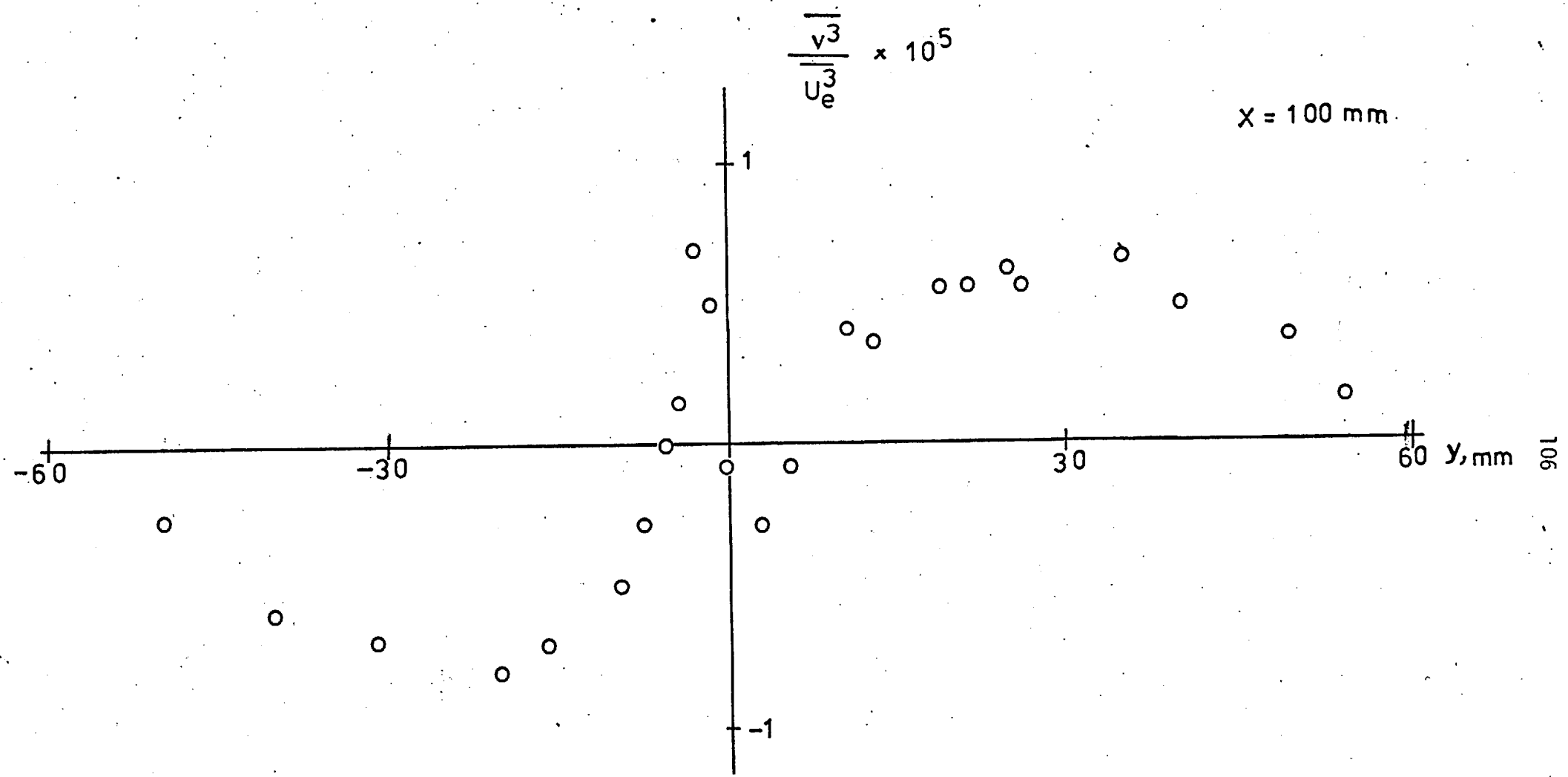

FIG. 4.45 $\overline{v^3}$ PROFILE AT x = 100 mm.

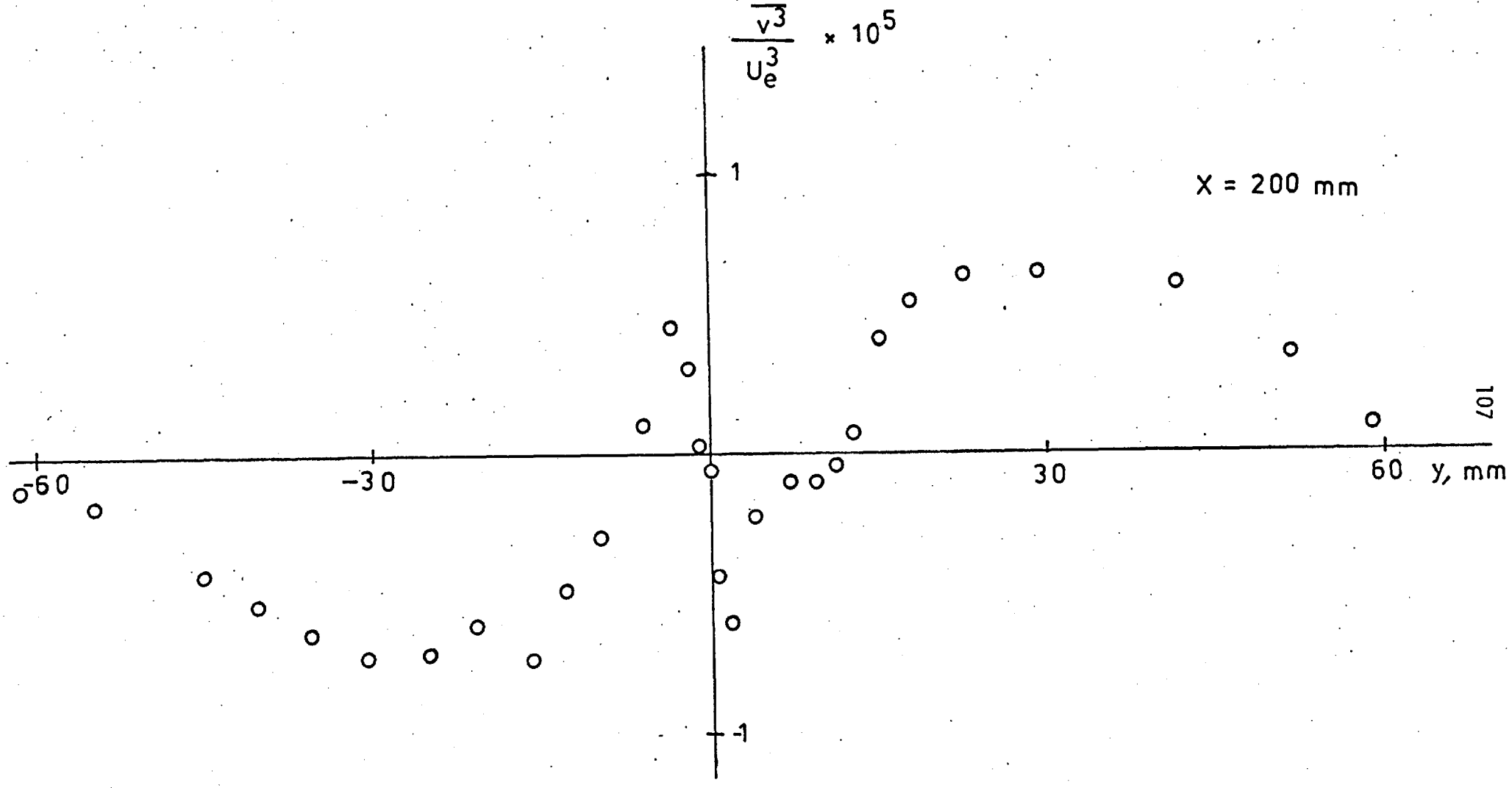

FIG. 4.46 $\overline{v^3}$ PROFILE AT x = 200 mm.

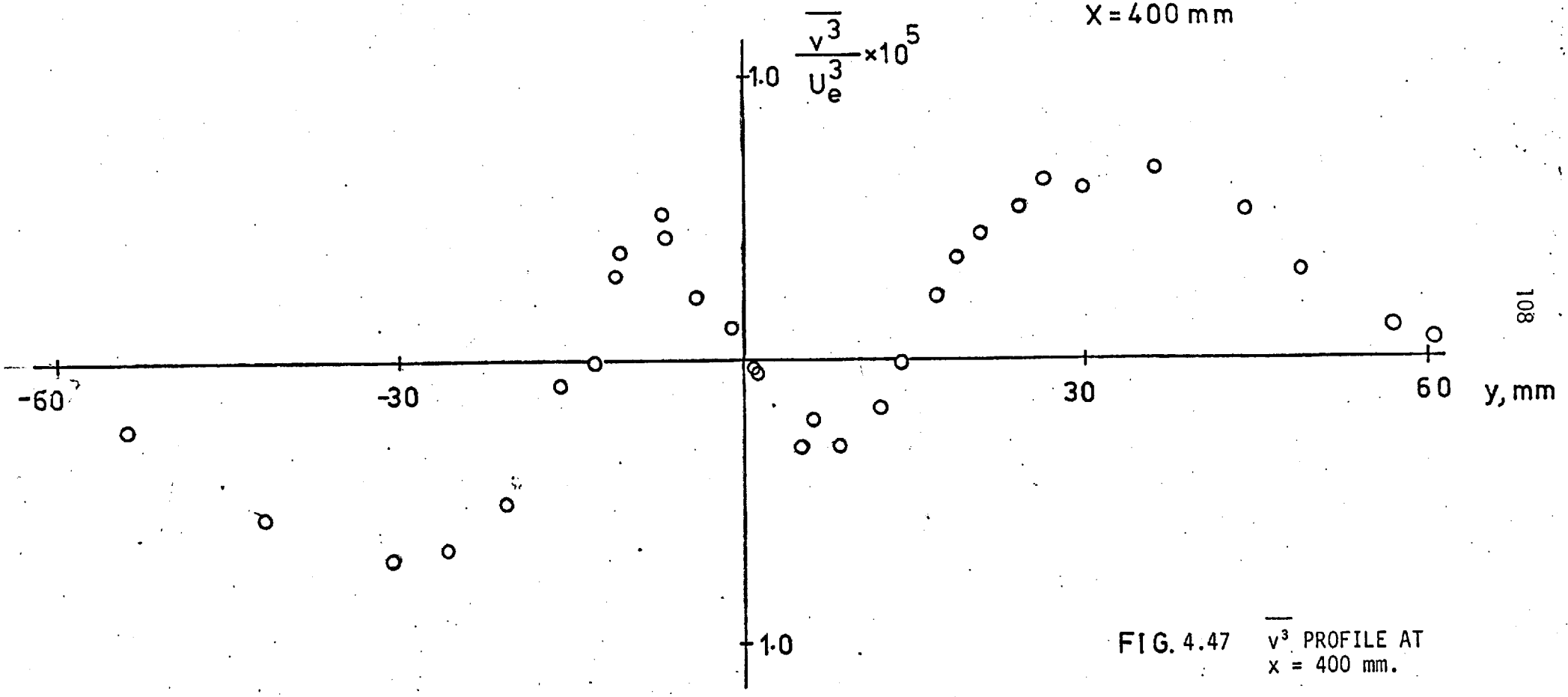

FIG. 4.47 $\overline{v^3}$ PROFILE AT x = 400 mm.

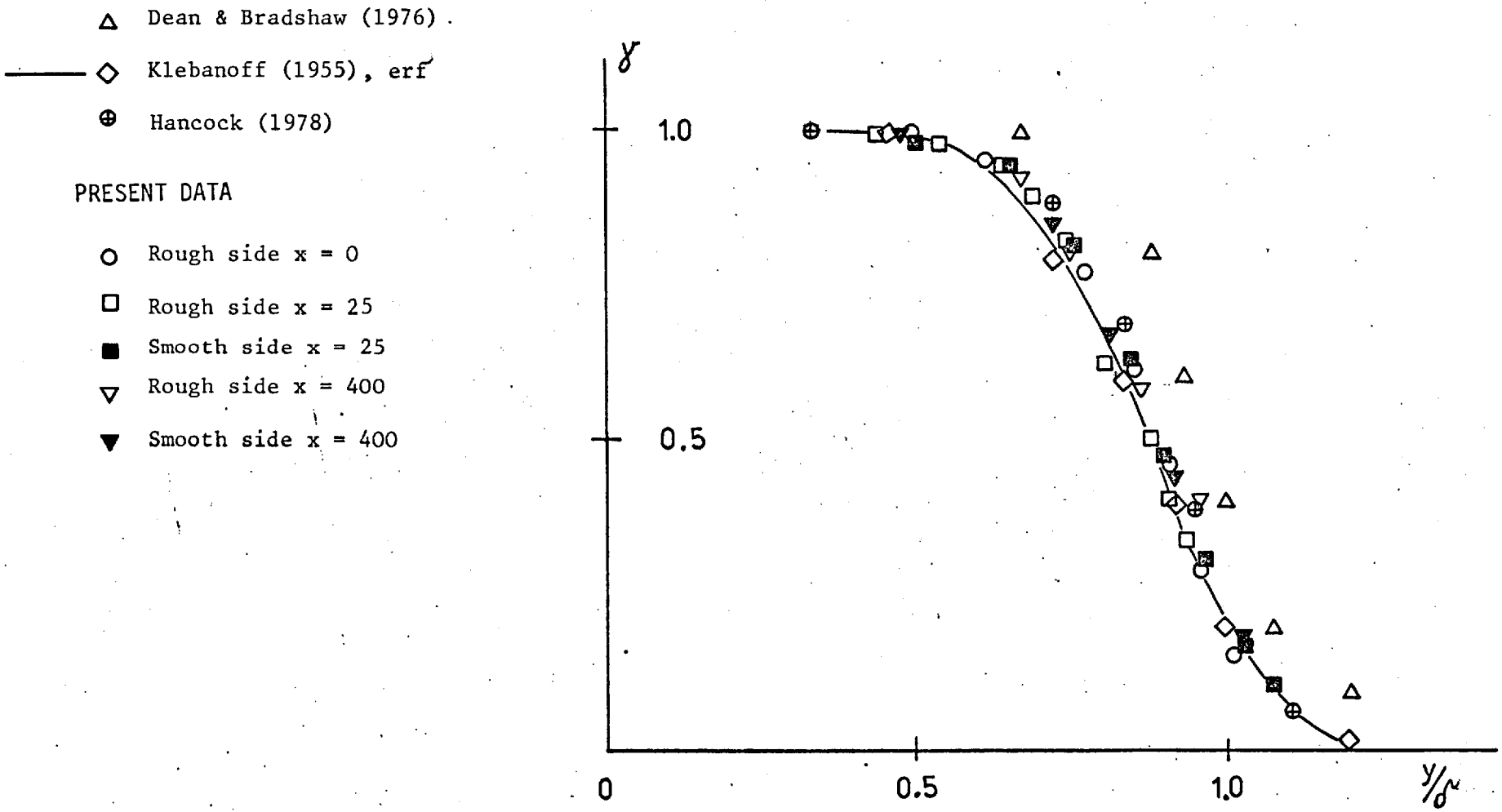

FIG. 4.48 INTERMITTENCY IN THE OUTER LAYER

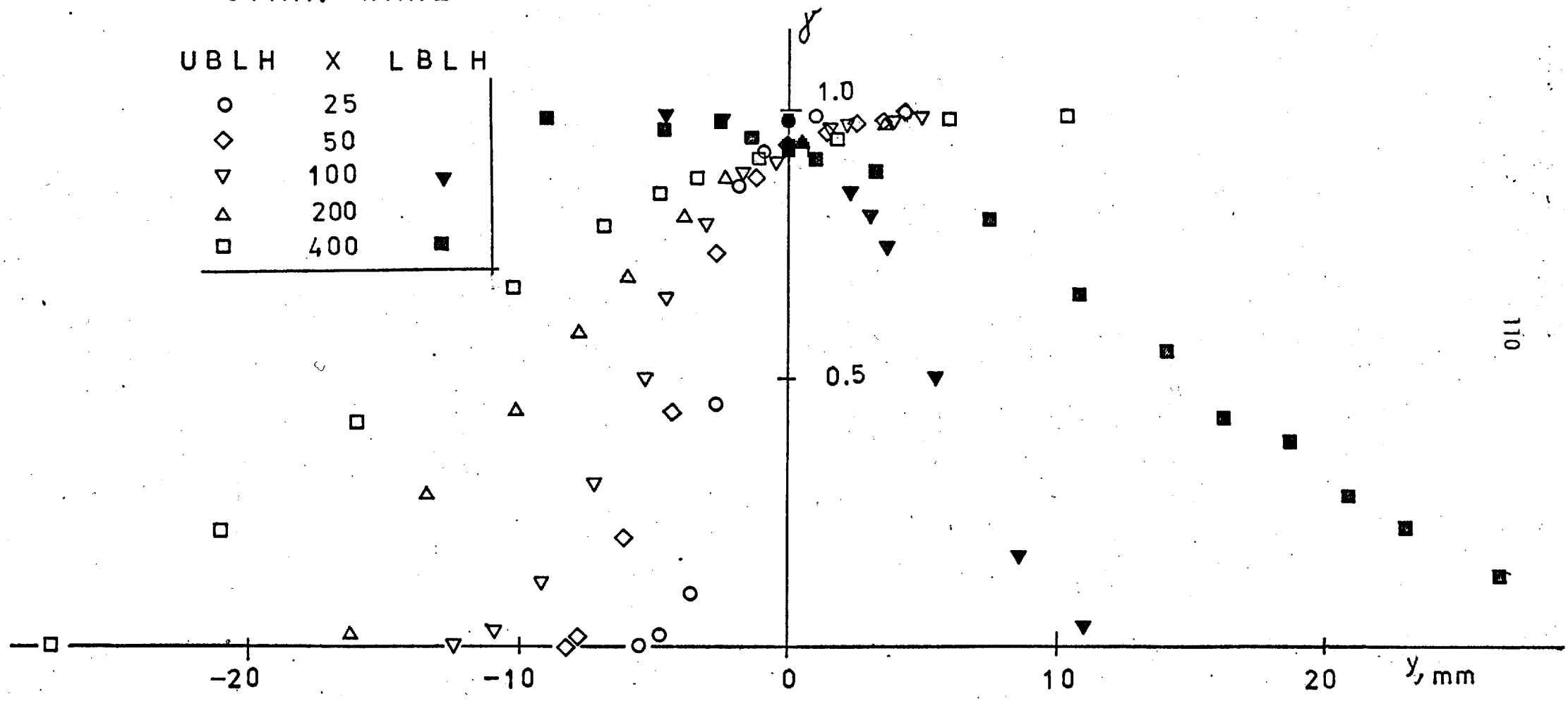

FIG. 4.49 INTERMITTENCY IN THE INNER WAKE

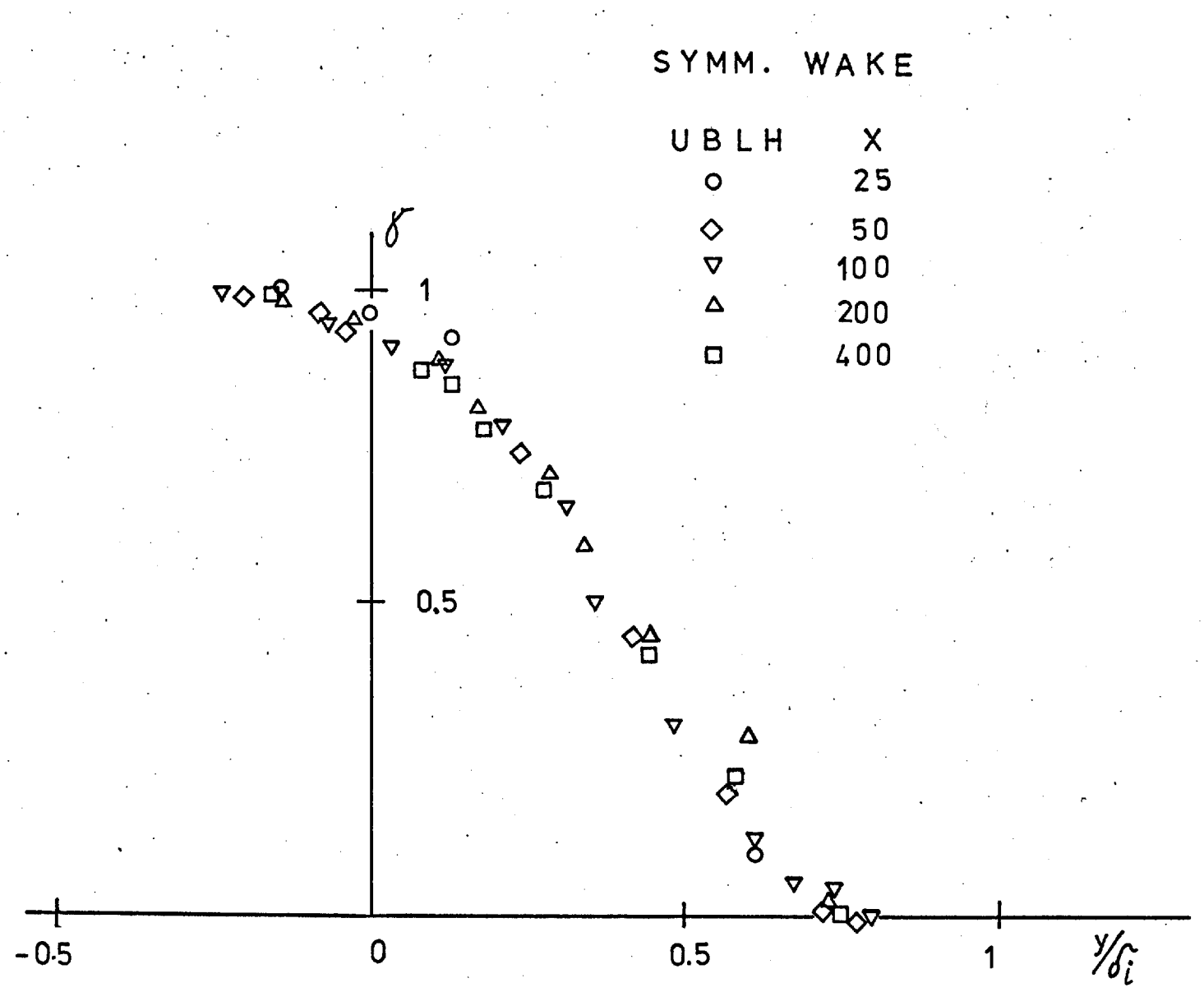

FIG. 4.50 INTERMITTENCY IN THE INNER WAKE SCALED ON INNER WAKE WIDTH

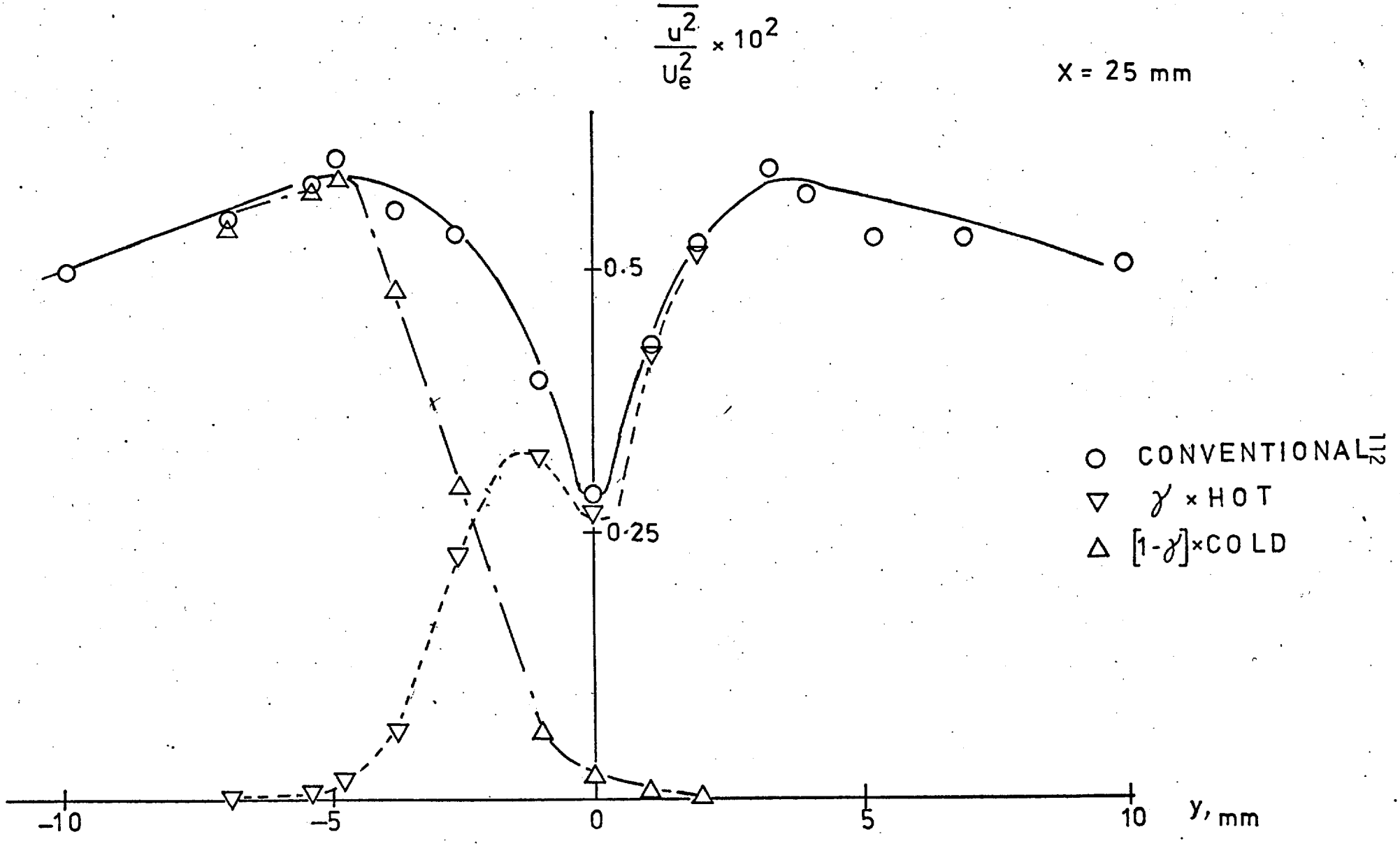

FIG. 4.51 $\overline{u^2}$ PROFILE AT x = 25 mm

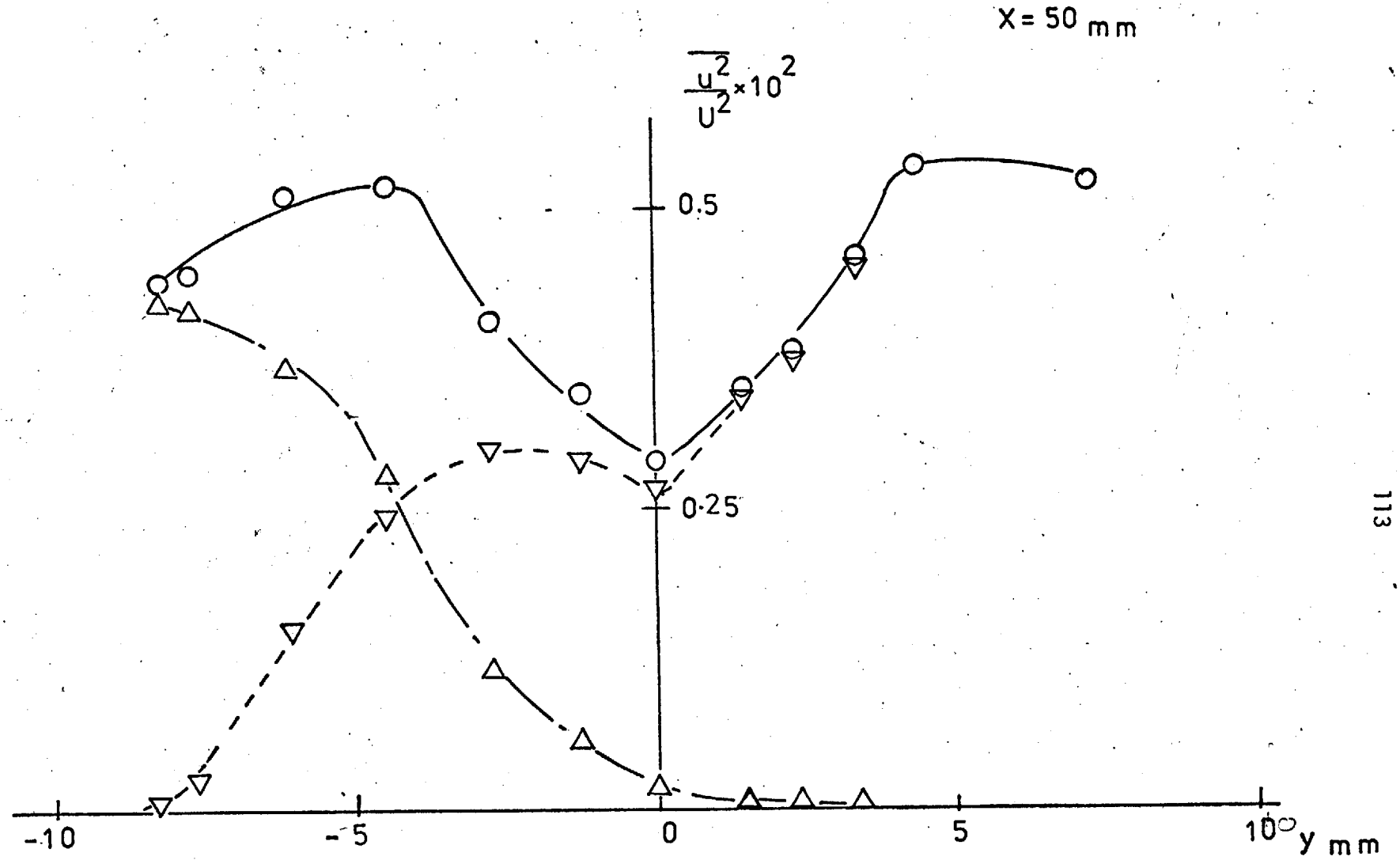

FIG. 4.52 $\overline{u^2}$ PROFILE AT x = 50 mm

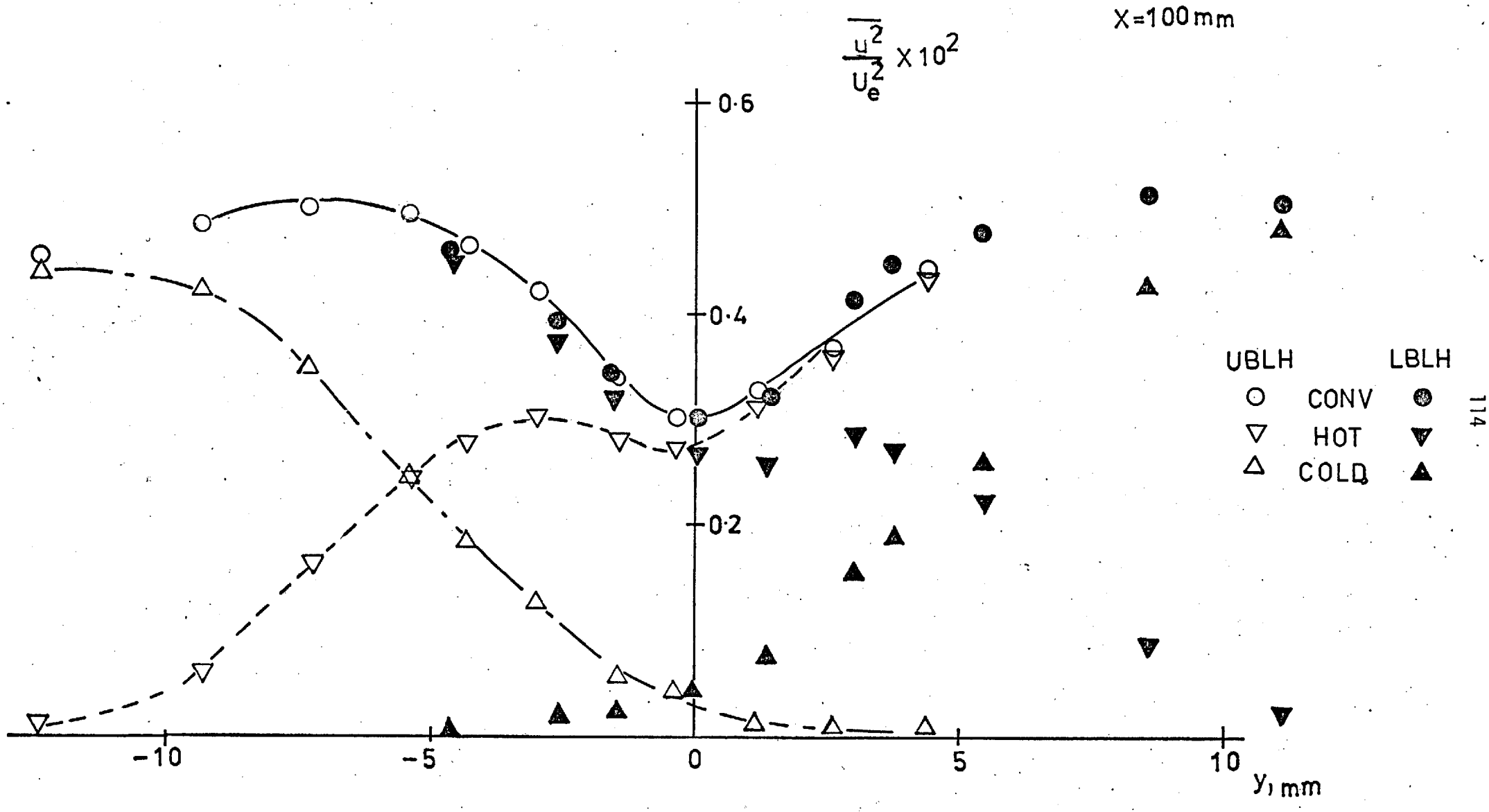

FIG. 4.53 $\overline{u^2}$ PROFILE AT x = 100 mm

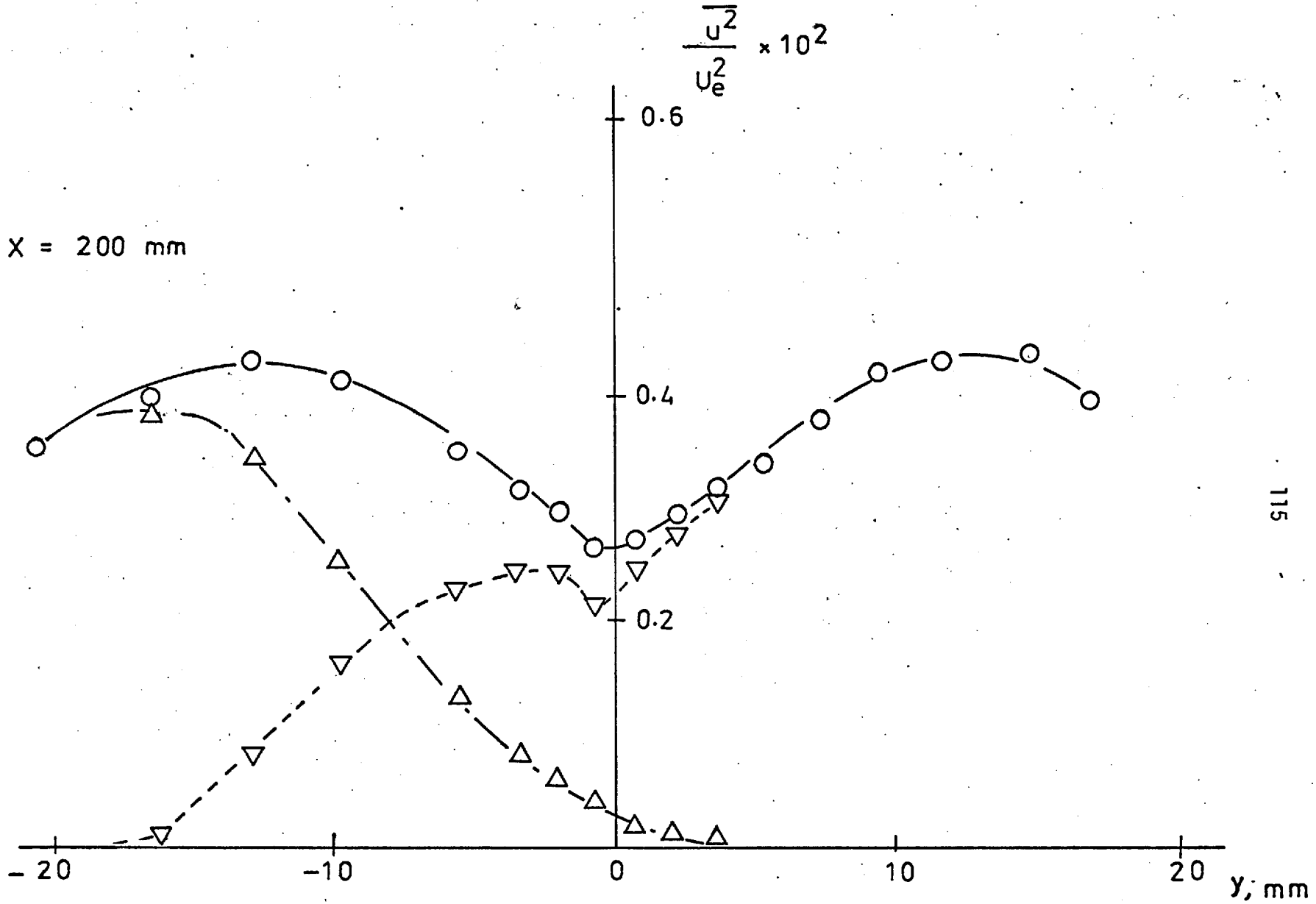

FIG. 4.54 $\overline{u^2}$ PROFILE AT x = 200 mm

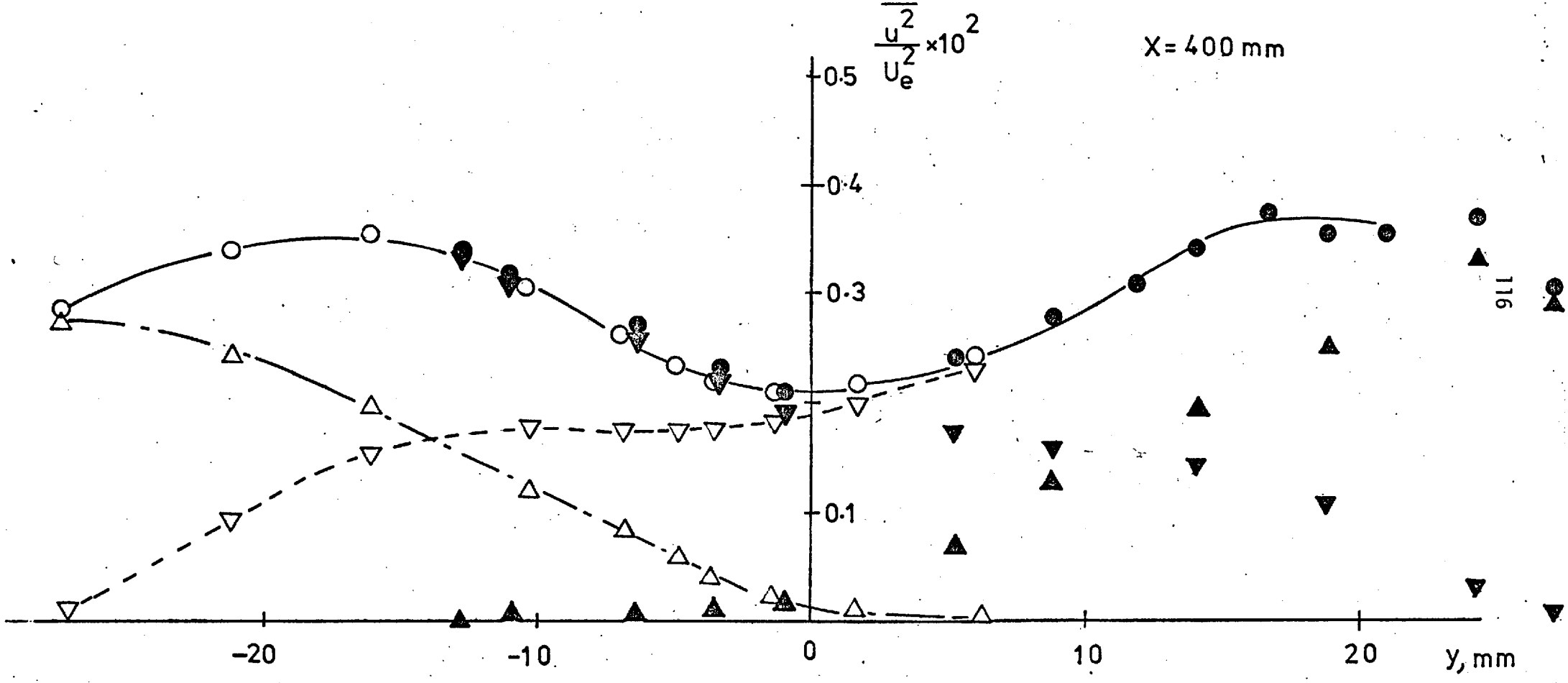

FIG. 4.55 $\overline{u^2}$ PROFILE AT x = 400 mm

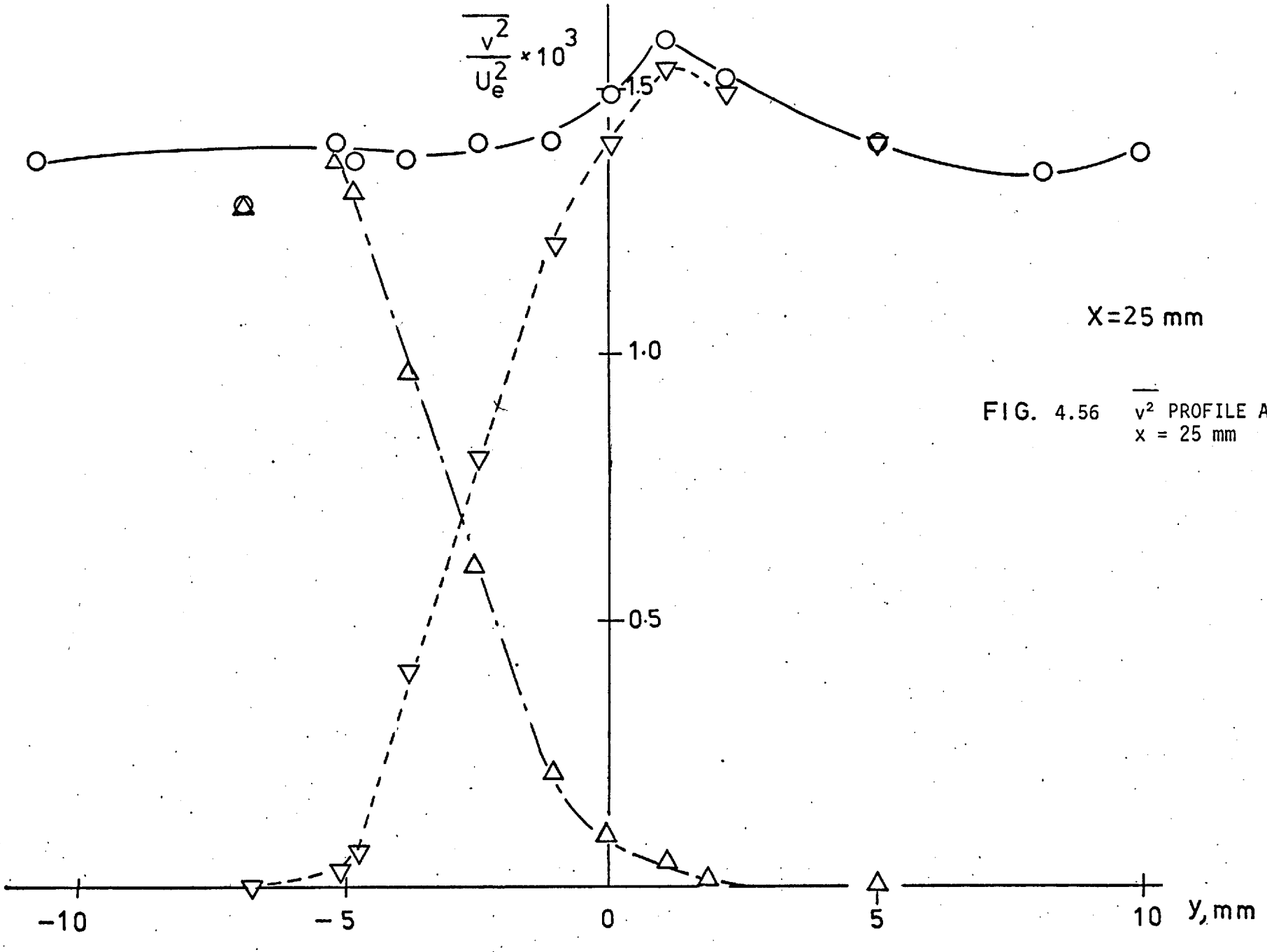

FIG. 4.56 $\overline{v^2}$ PROFILE AT x = 25 mm

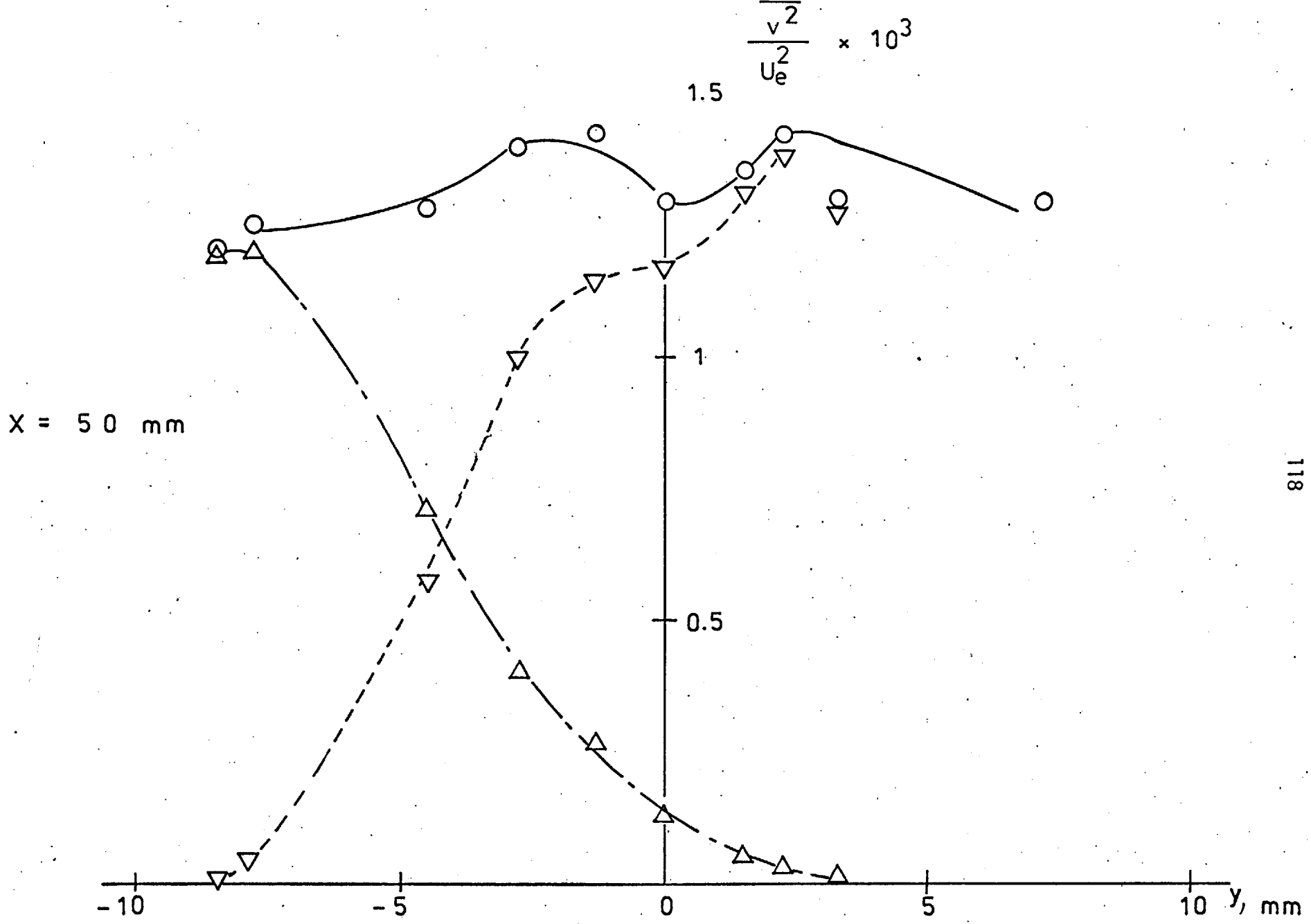

FIG. 4.57 $\overline{v^2}$ PROFILE AT x = 50 mm

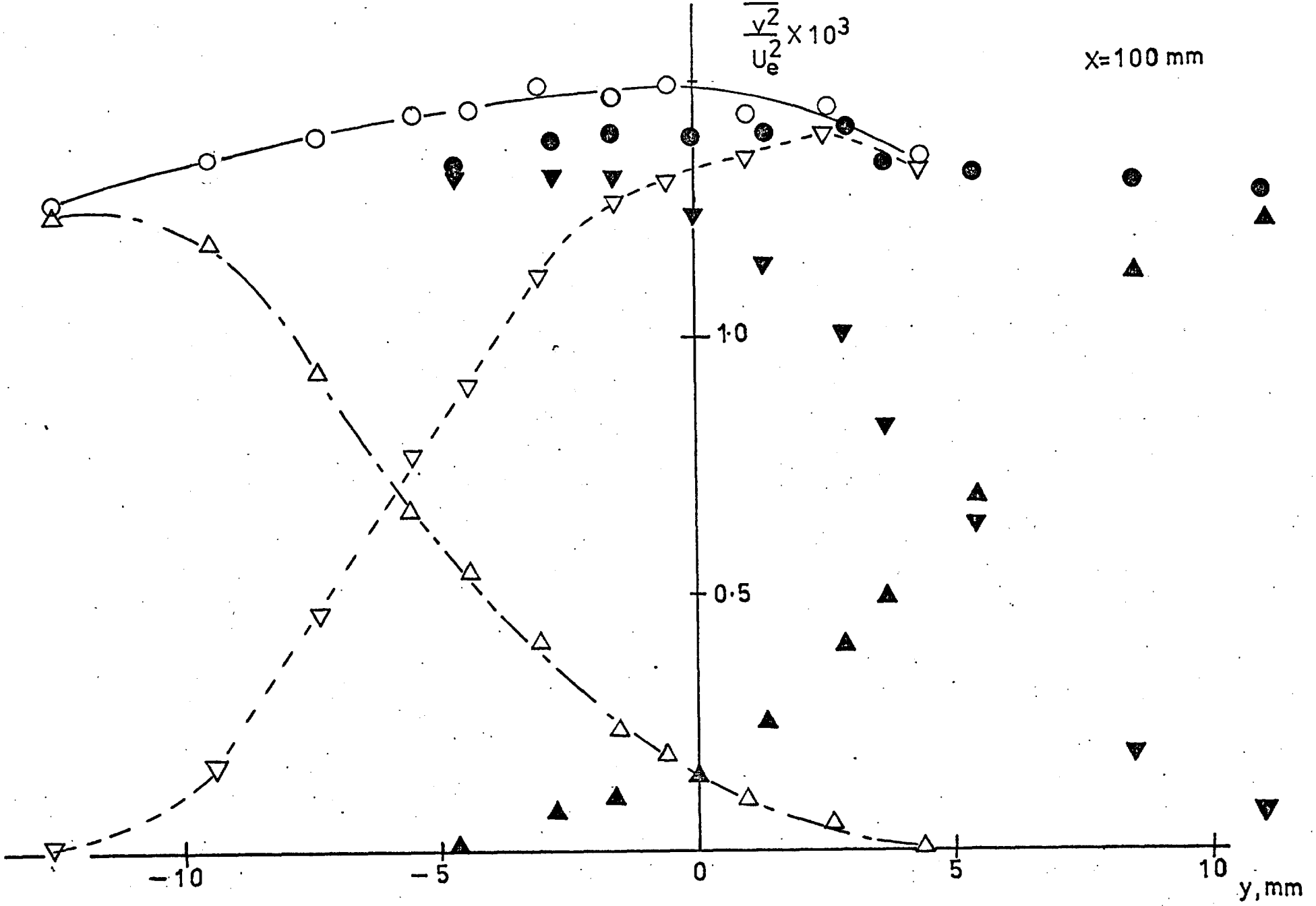

FIG. 4.58 $\overline{v^2}$ PROFILE AT x = 100 mm

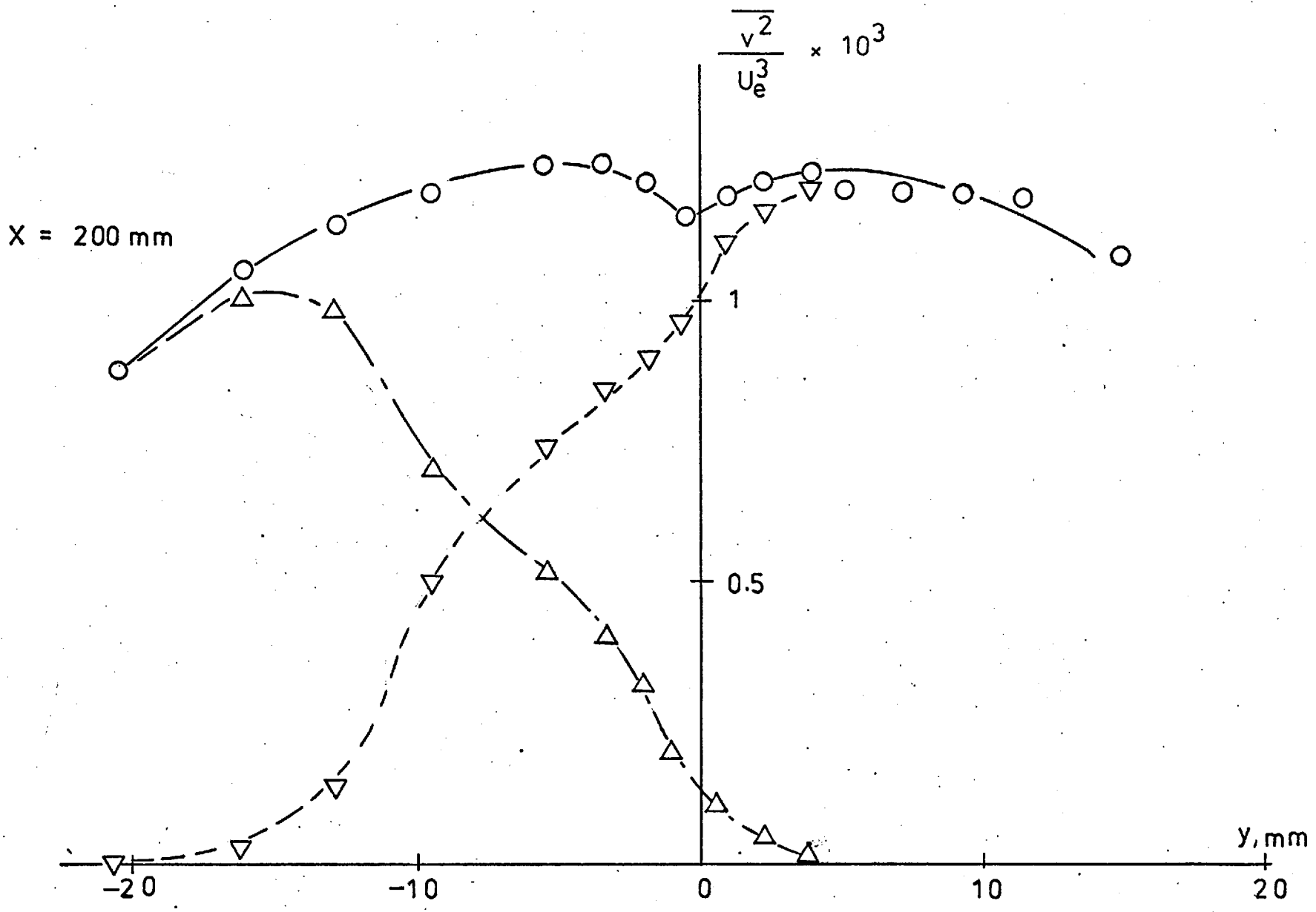

FIG. 4.59 $\overline{v^2}$ PROFILE AT x = 200 mm

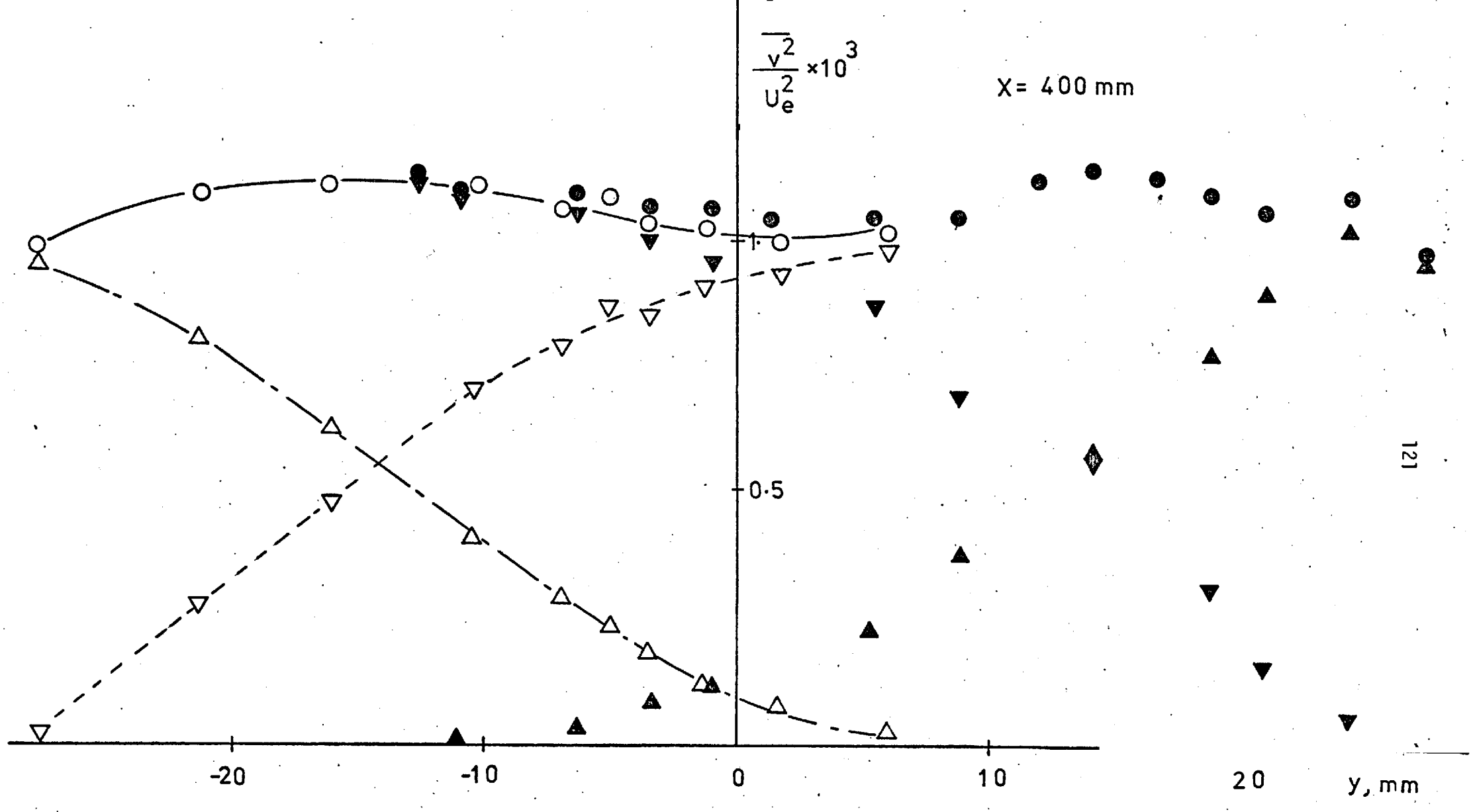

FIG. 4.60 $\overline{v^2}$ PROFILE AT x = 400 mm

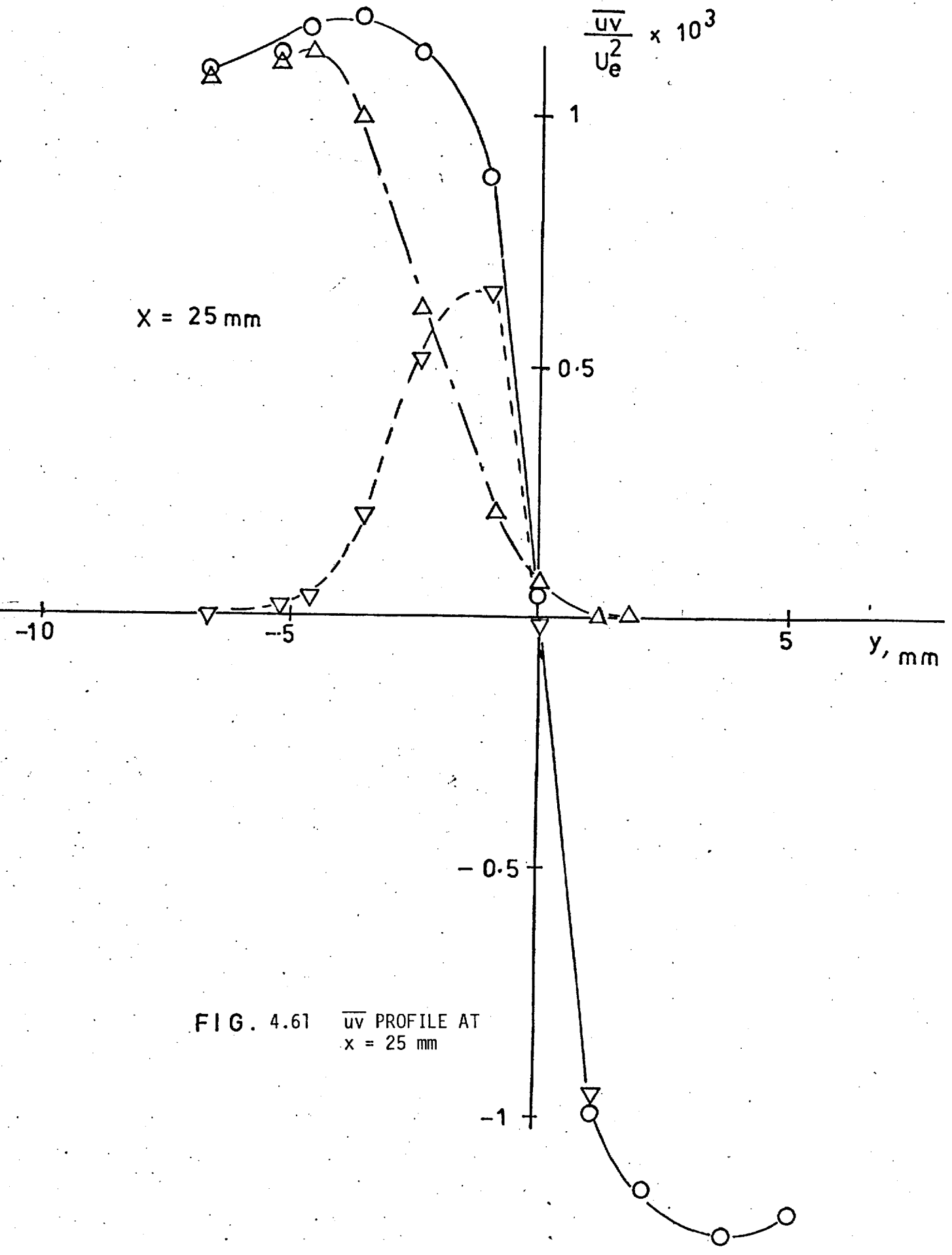

FIG. 4.61 $\overline{uv}$ PROFILE AT x = 25 mm

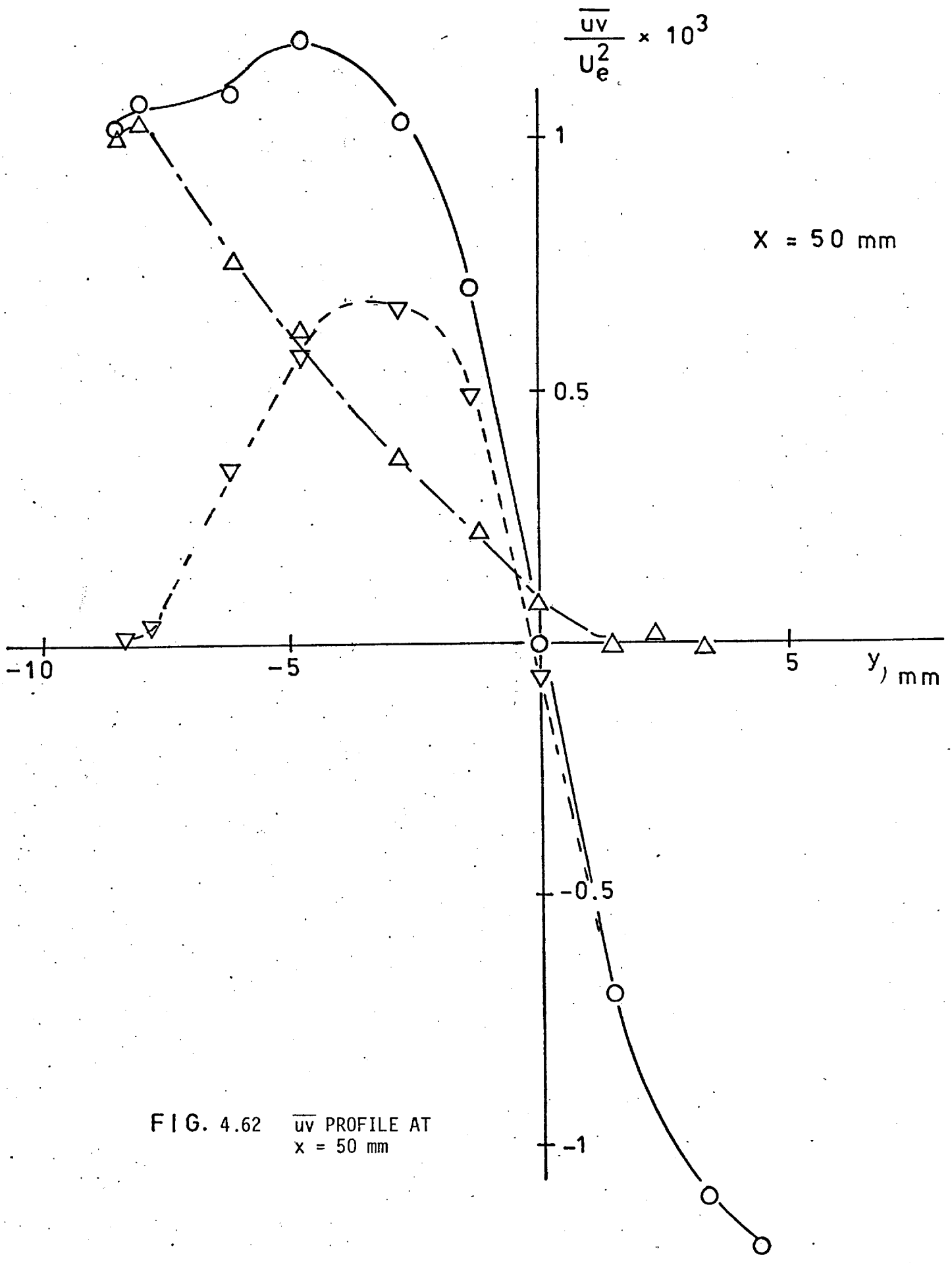

FIG. 4.62 $\overline{uv}$ PROFILE AT x = 50 mm

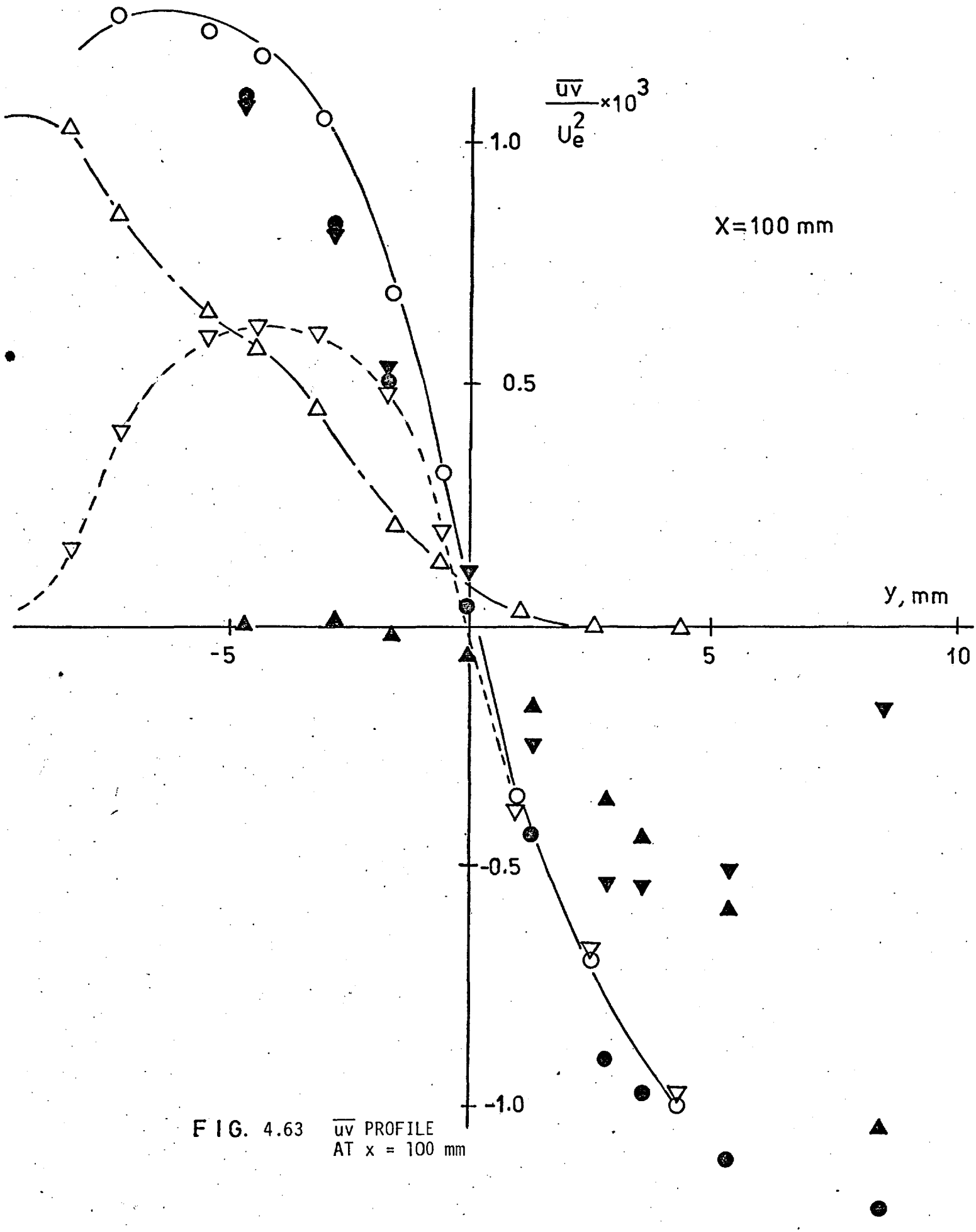

FIG. 4.63 $\overline{uv}$ PROFILE AT x = 100 mm

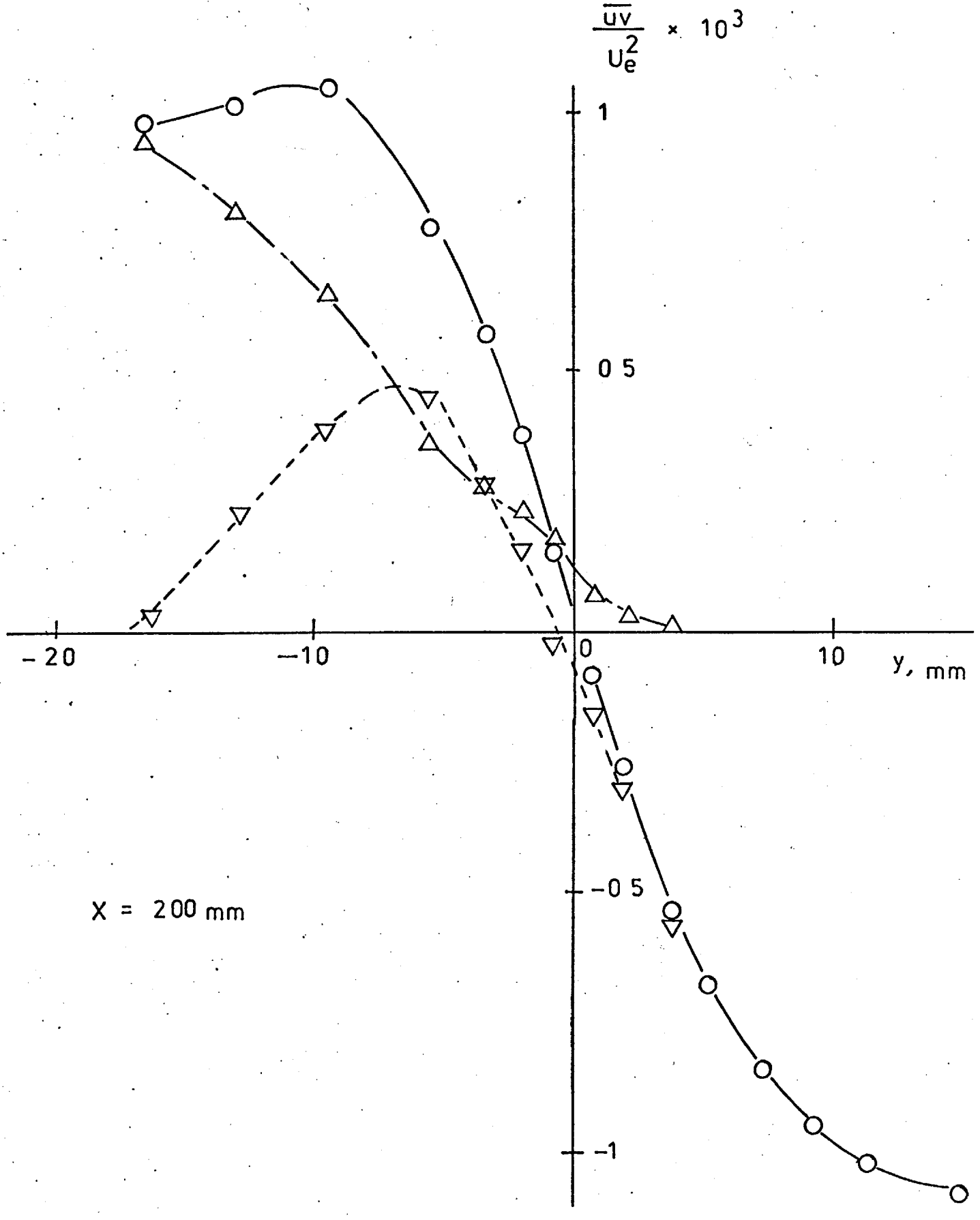

FIG. 4.64 $\overline{uv}$ PROFILE AT x = 200 mm

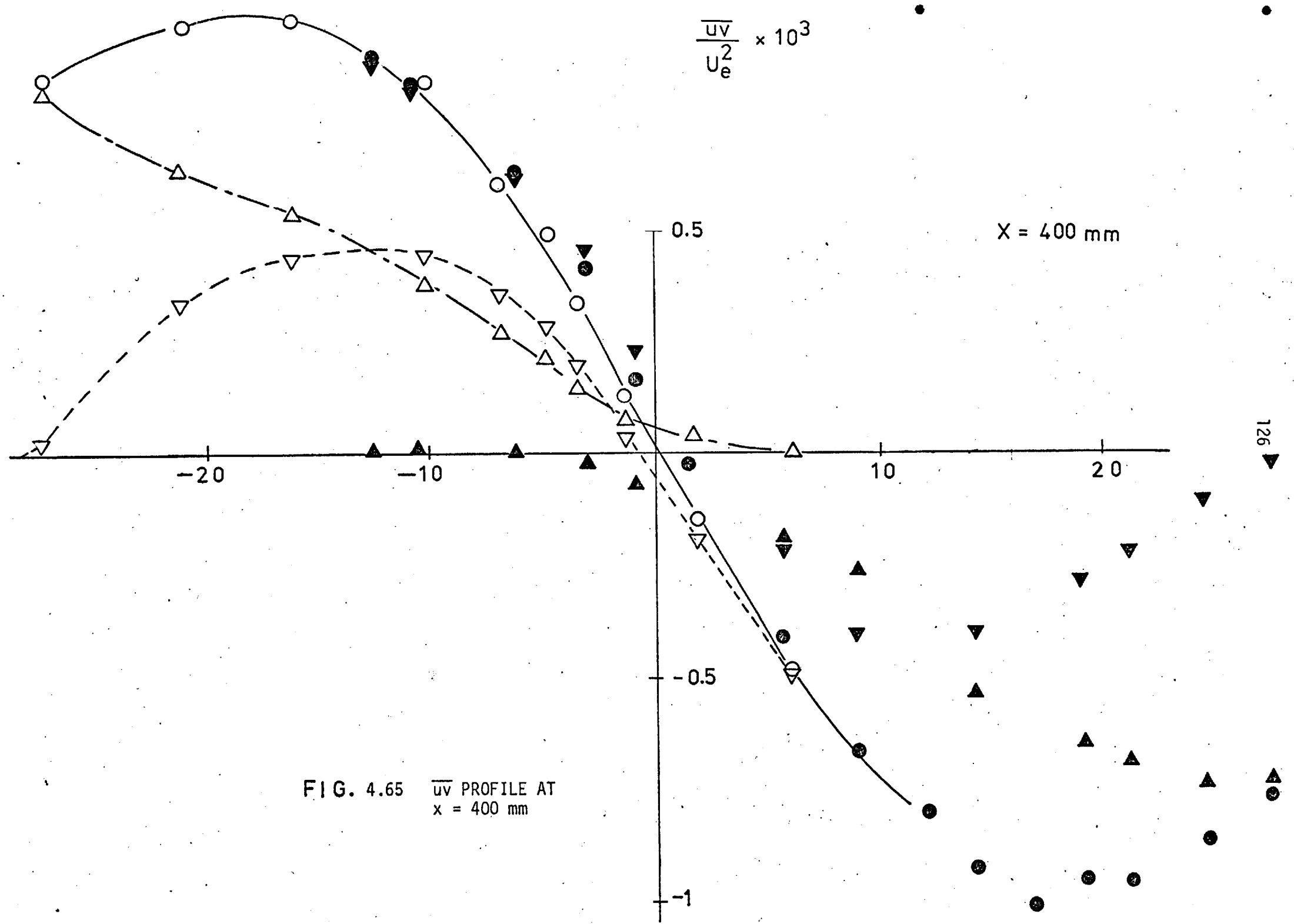

FIG. 4.65 $\overline{uv}$ PROFILE AT x = 400 mm

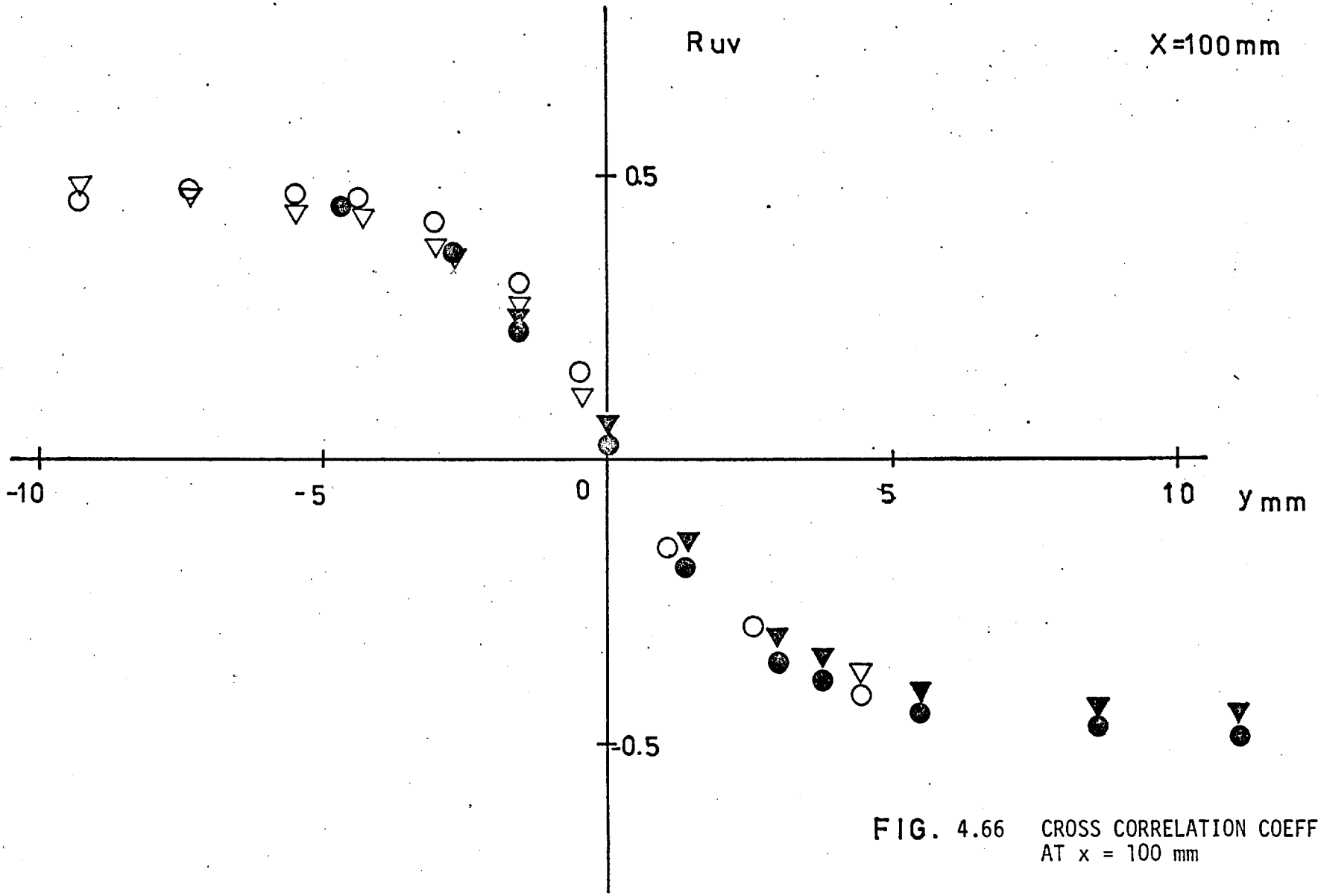

FIG. 4.66 CROSS CORRELATION COEFFICIENT
AT x = 100 mm

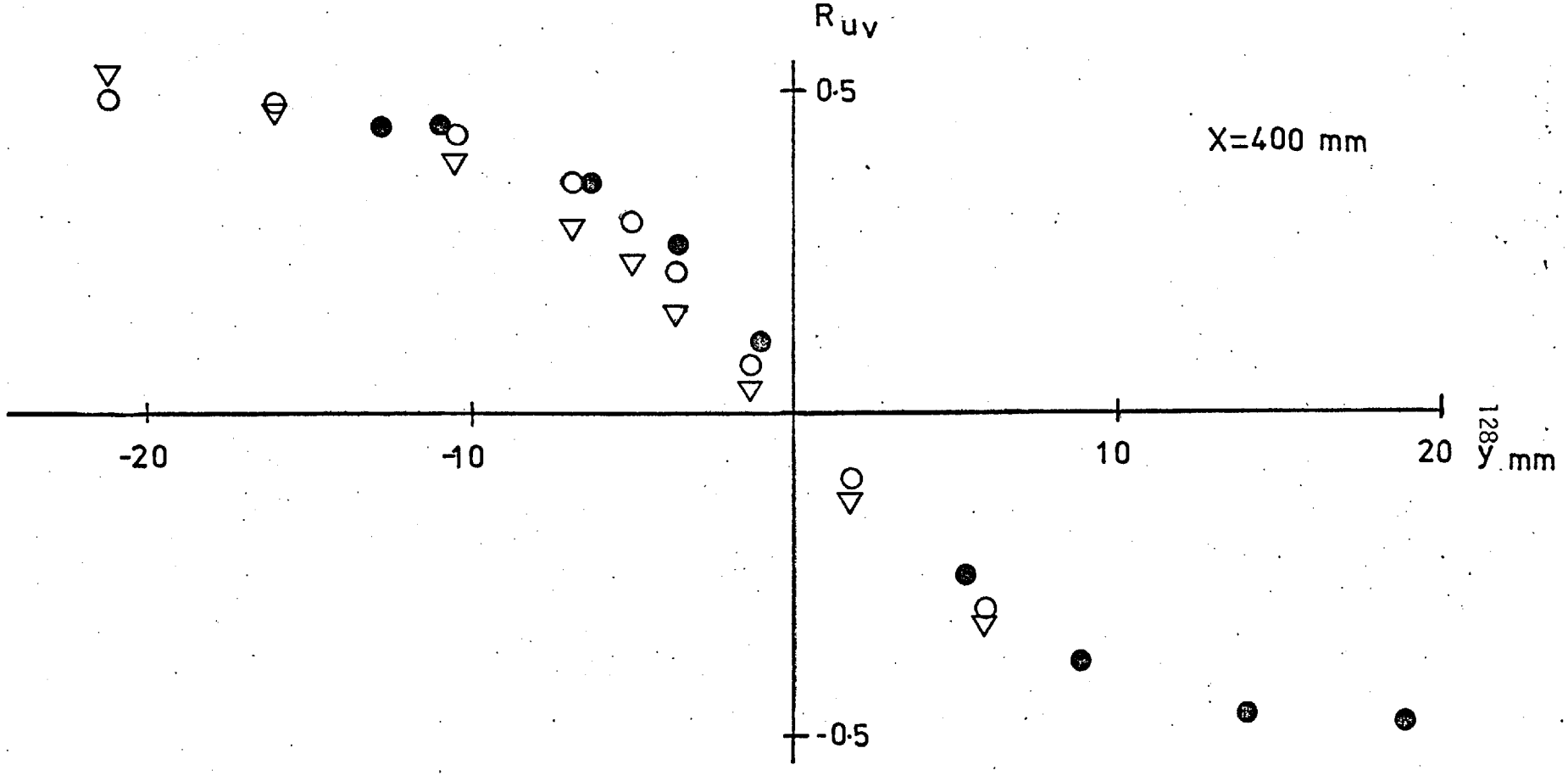

FIG. 4.67 CROSS CORRELATION COEFFICIENT AT x = 400 mm

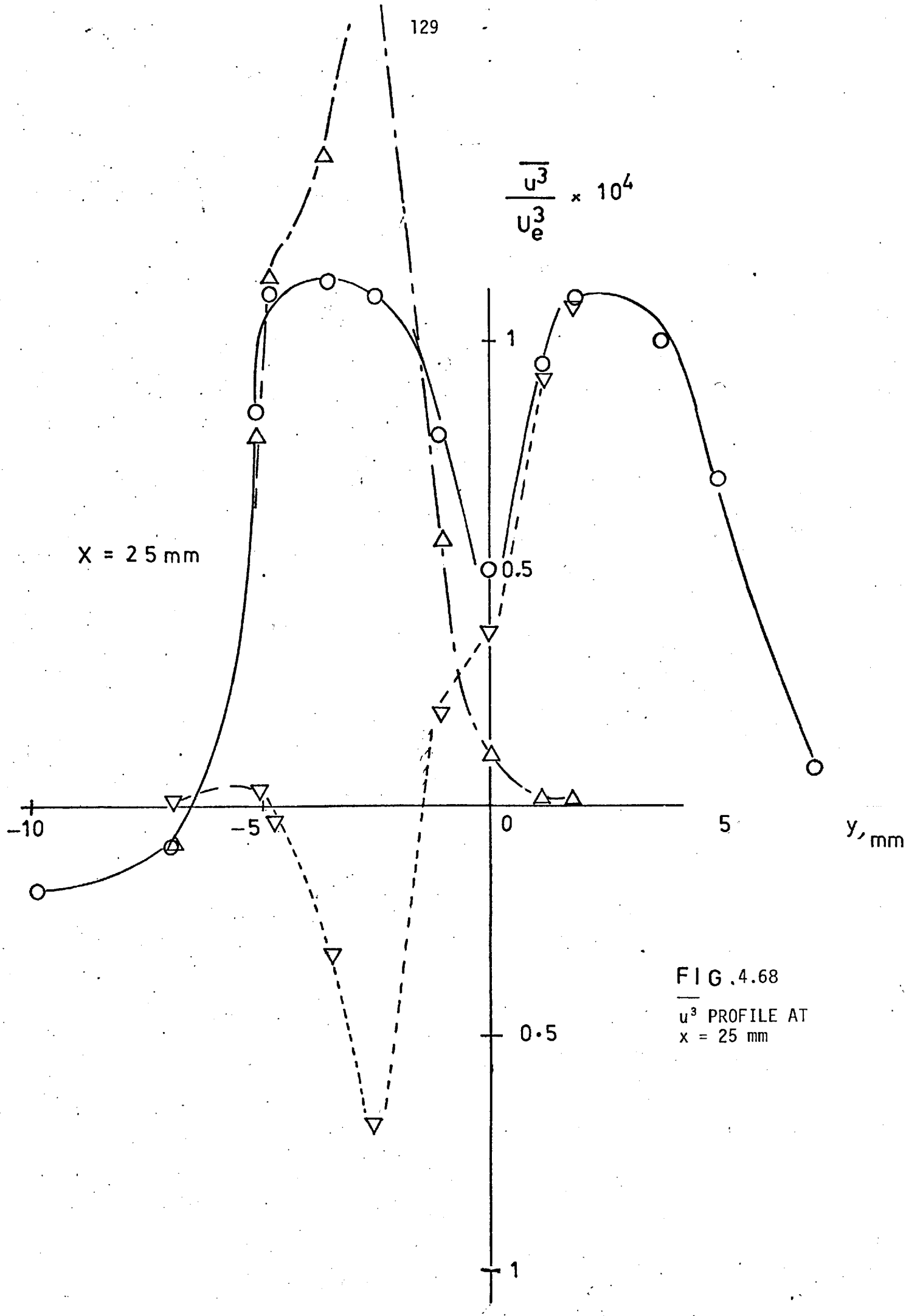

FIG.4.68

$\overline{u^3}$ PROFILE AT
x = 25 mm

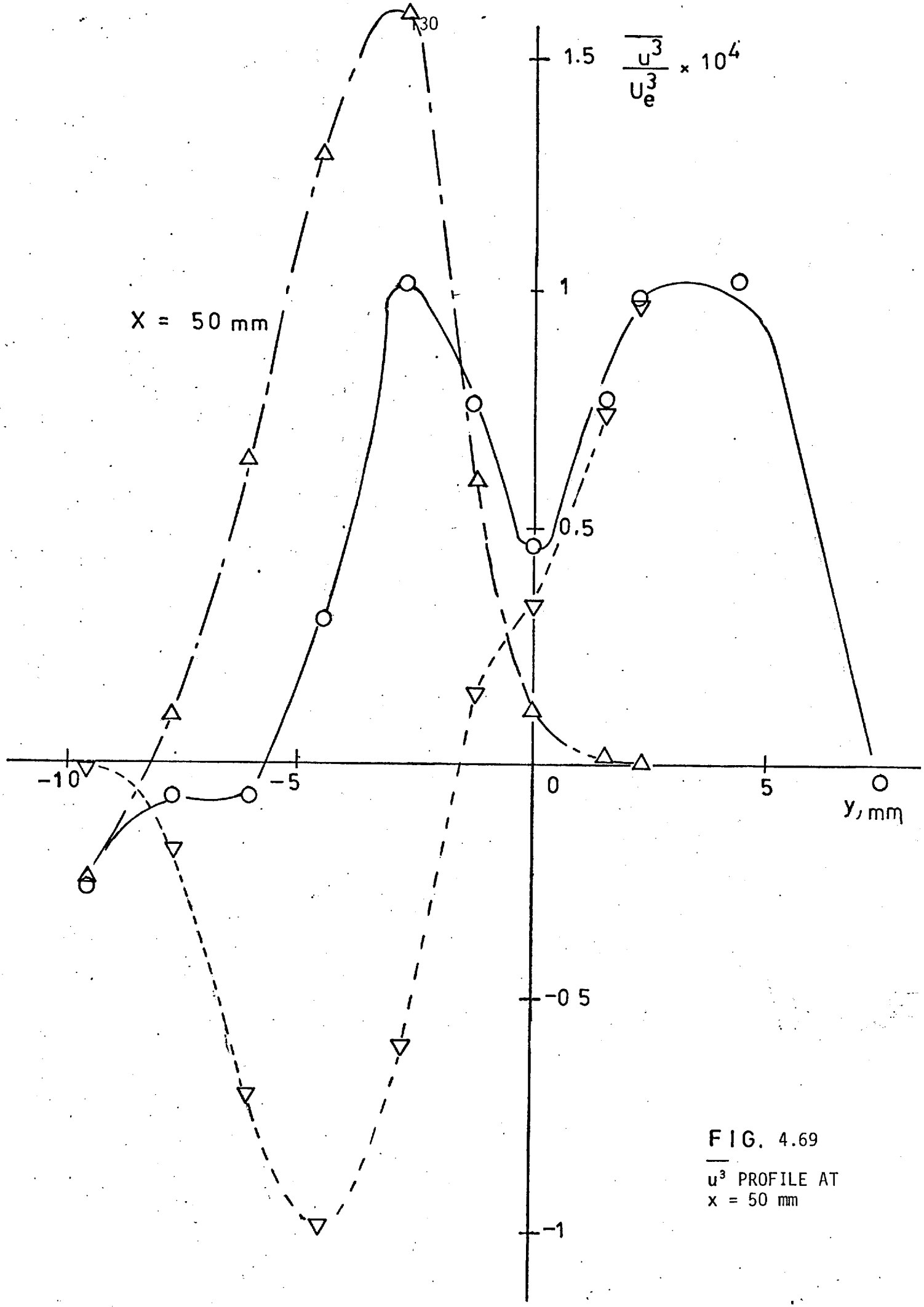

FIG. 4.69

$\overline{u^3}$ PROFILE AT x = 50 mm

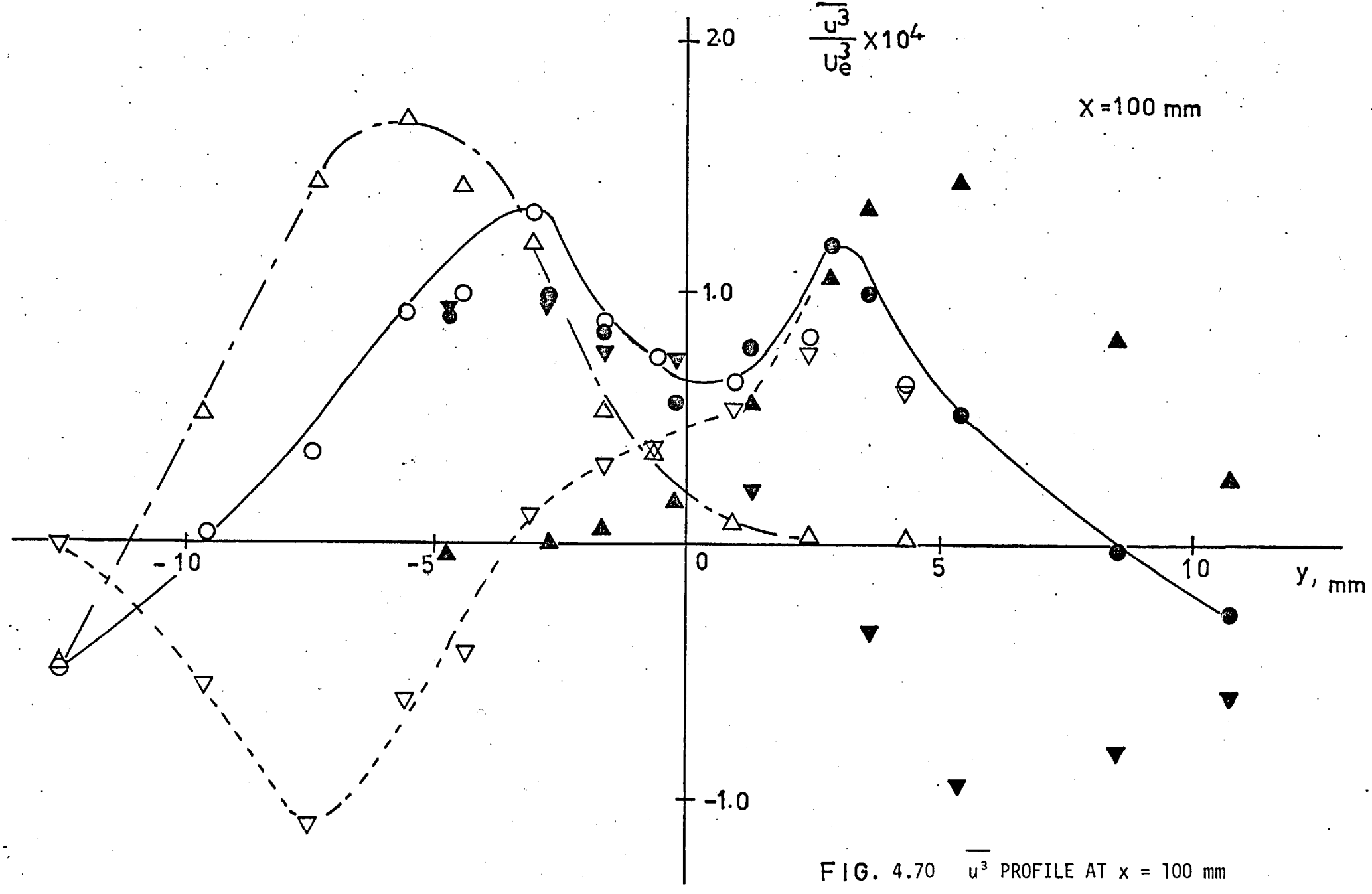

FIG. 4.70 $\overline{u^3}$ PROFILE AT x = 100 mm

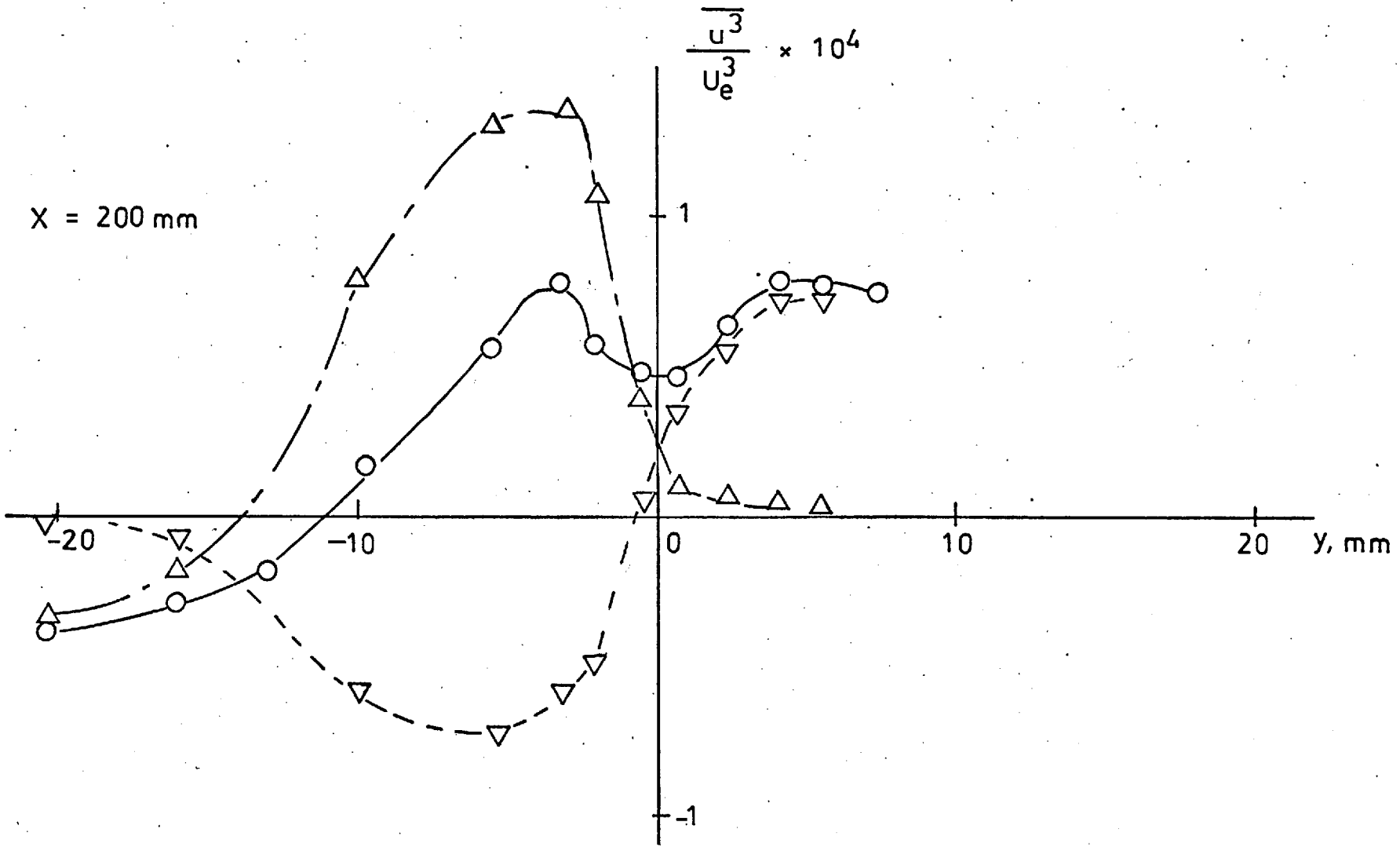

FIG. 4.71 $\overline{u^3}$ PROFILE AT x = 200 mm

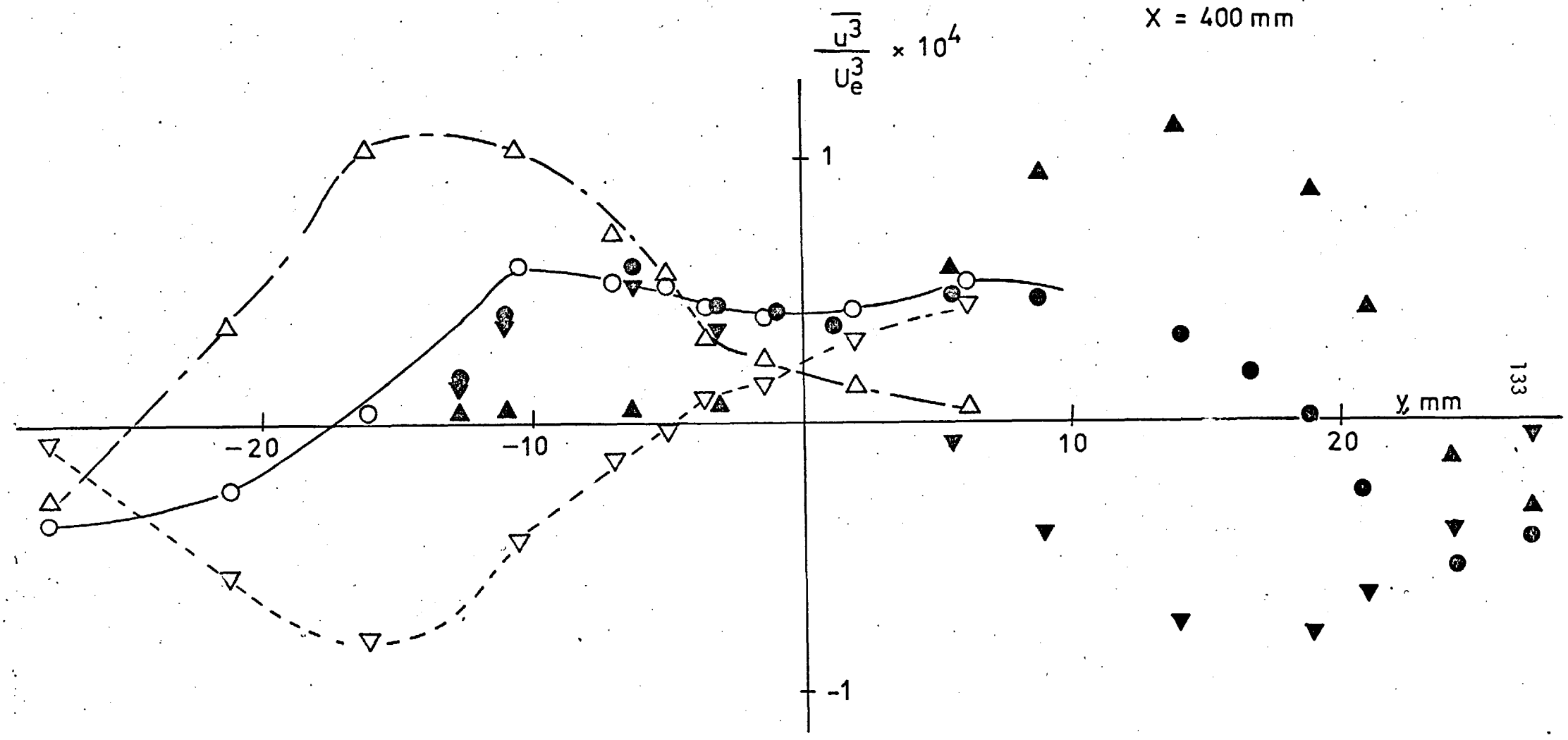

F I G. 4.72 $\overline{u^3}$ PROFILE AT x = 400 mm

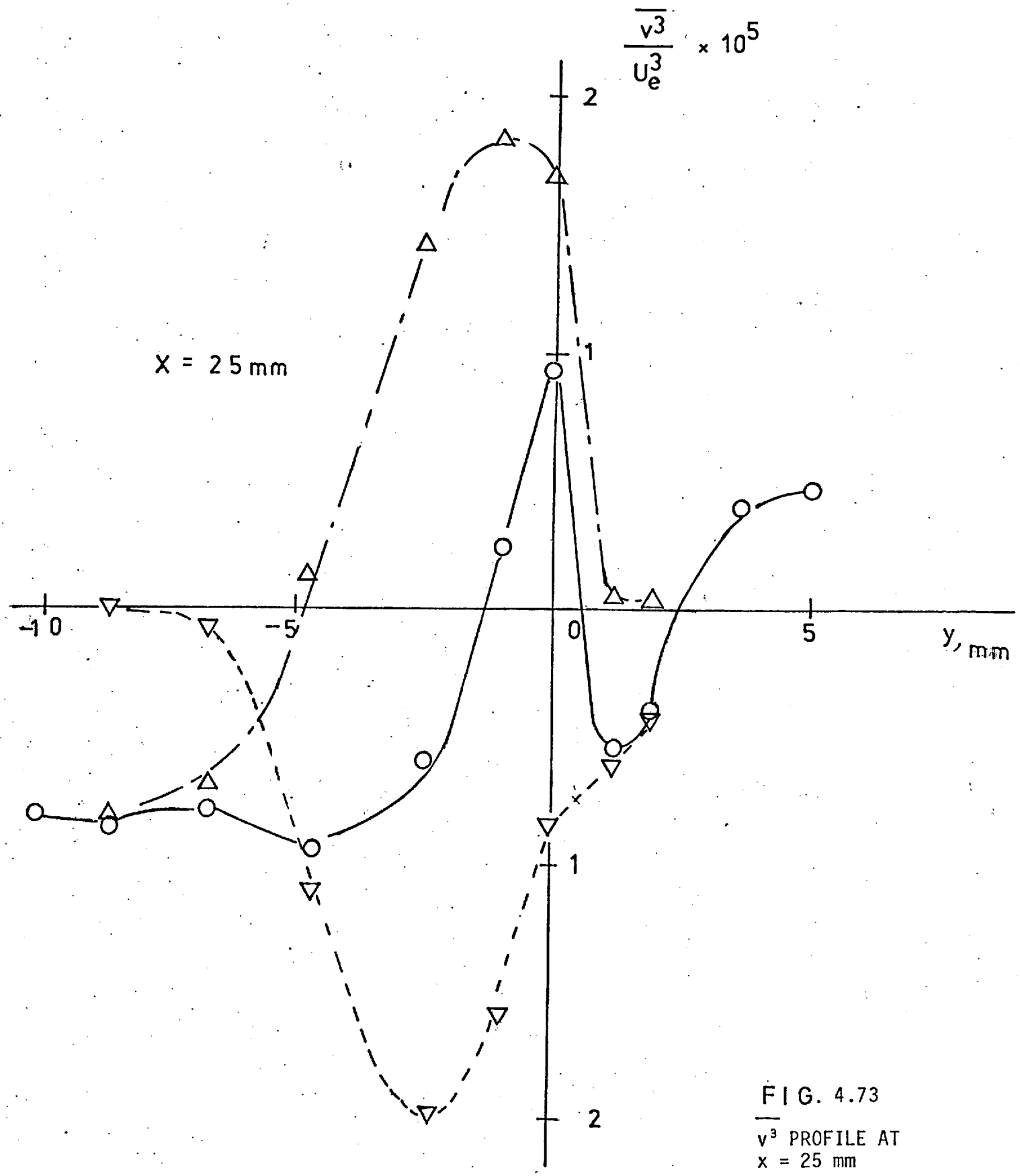

FIG. 4.73

$\overline{v^3}$ PROFILE AT
x = 25 mm

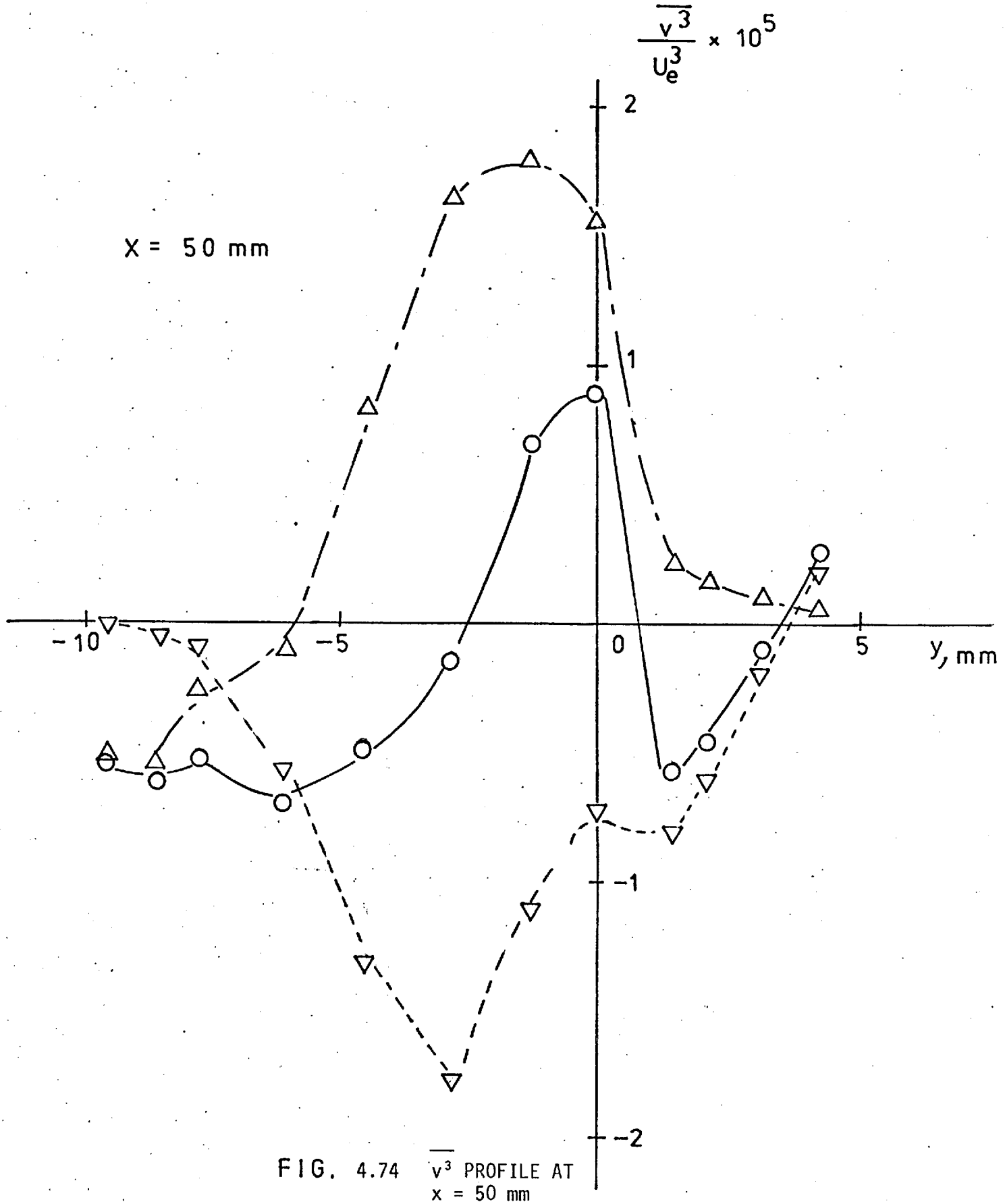

FIG. 4.74 $\overline{v^3}$ PROFILE AT x = 50 mm

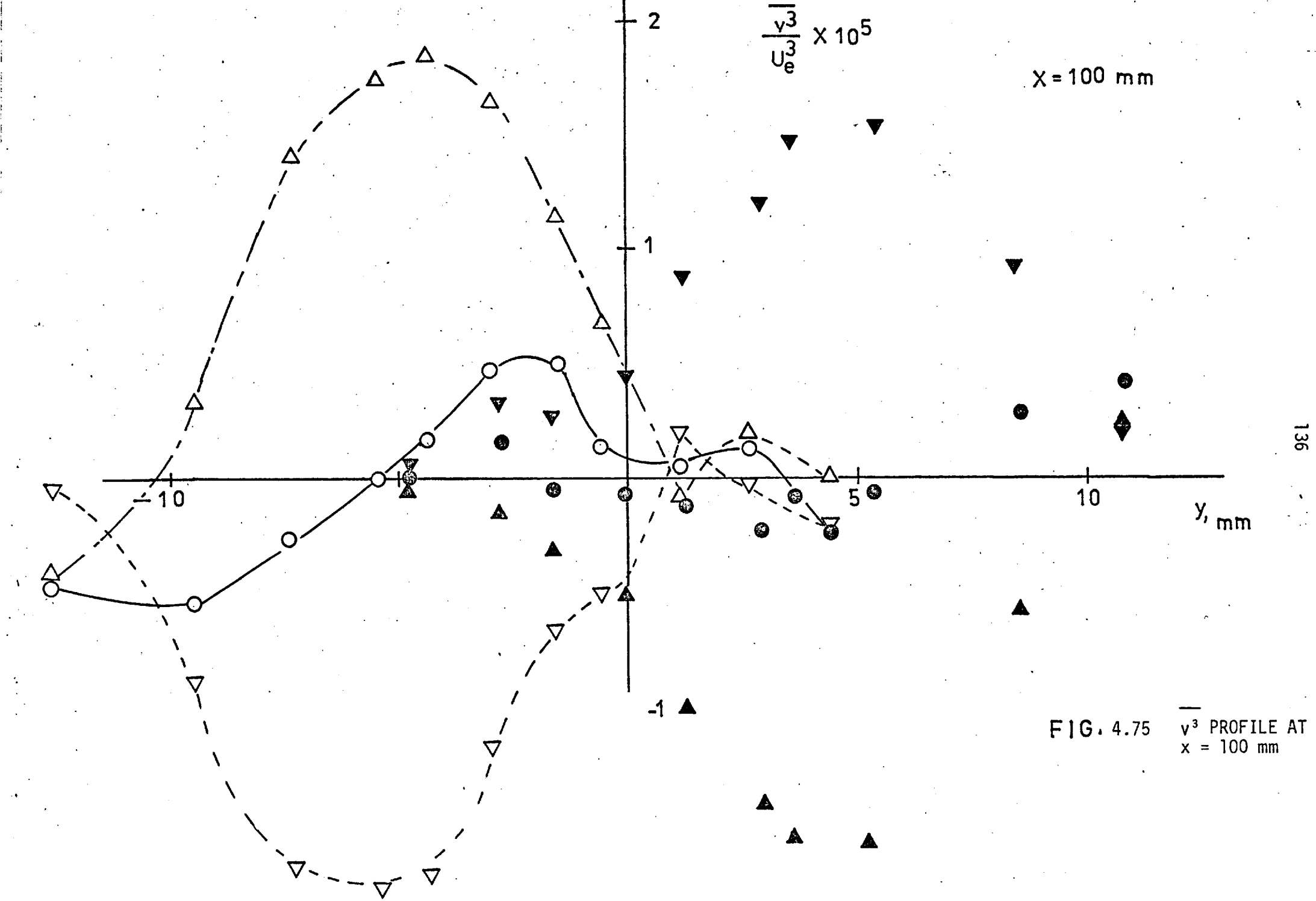

FIG. 4.75 $\overline{v^3}$ PROFILE AT x = 100 mm

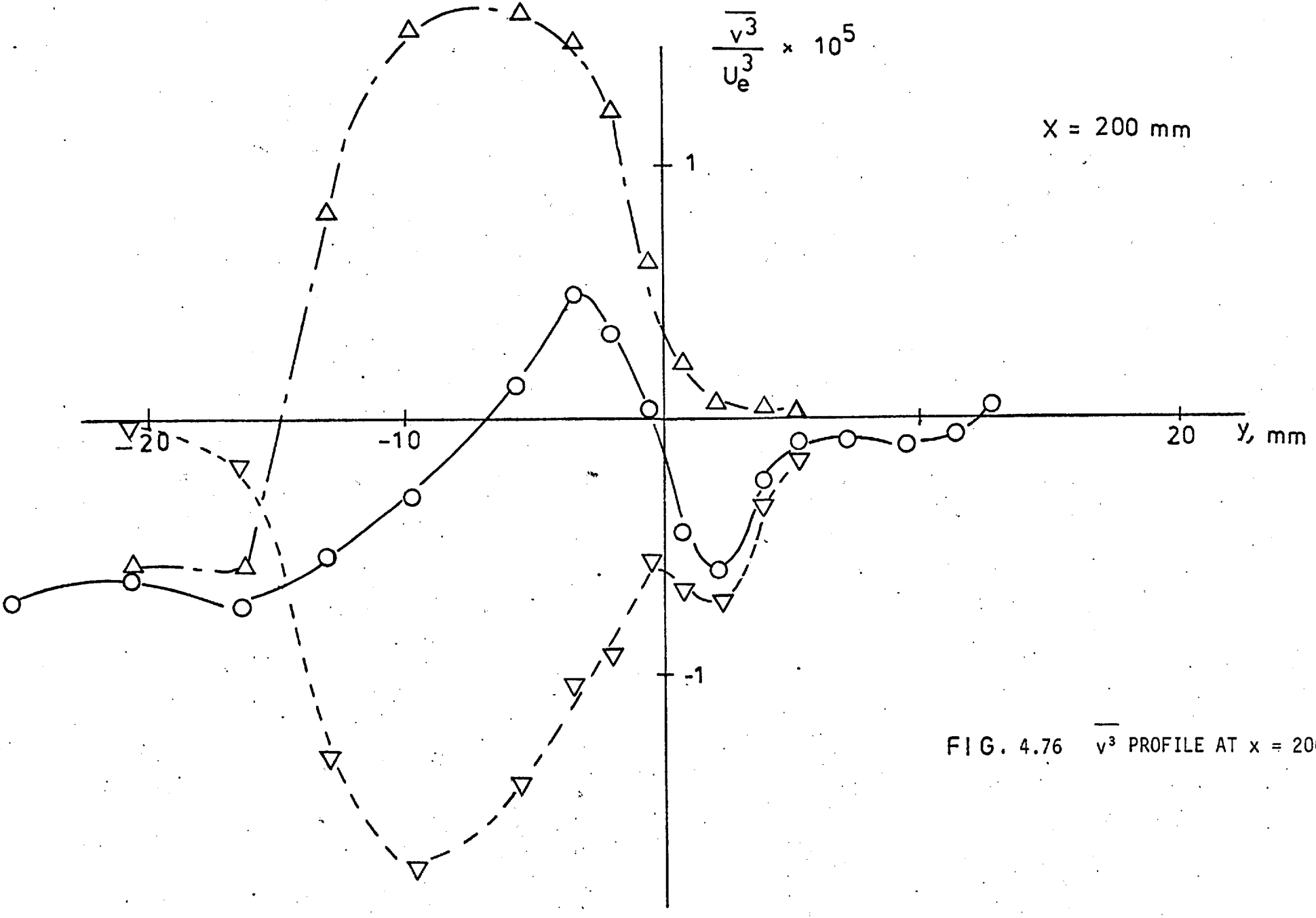

FIG. 4.76 $\overline{v^3}$ PROFILE AT x = 200 mm

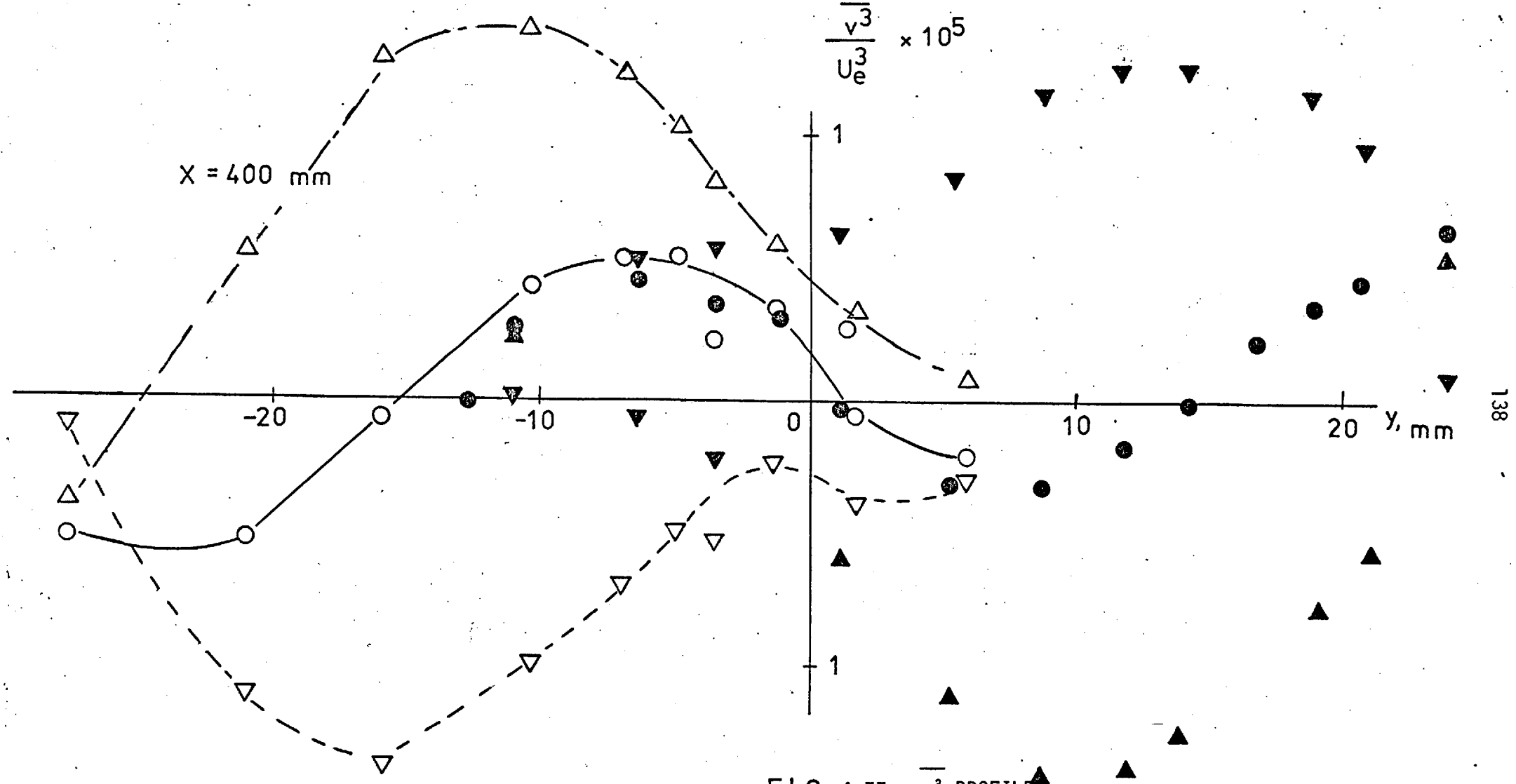

FIG. 4.77 $\overline{v^3}$ PROFILE AT x = 400 mm

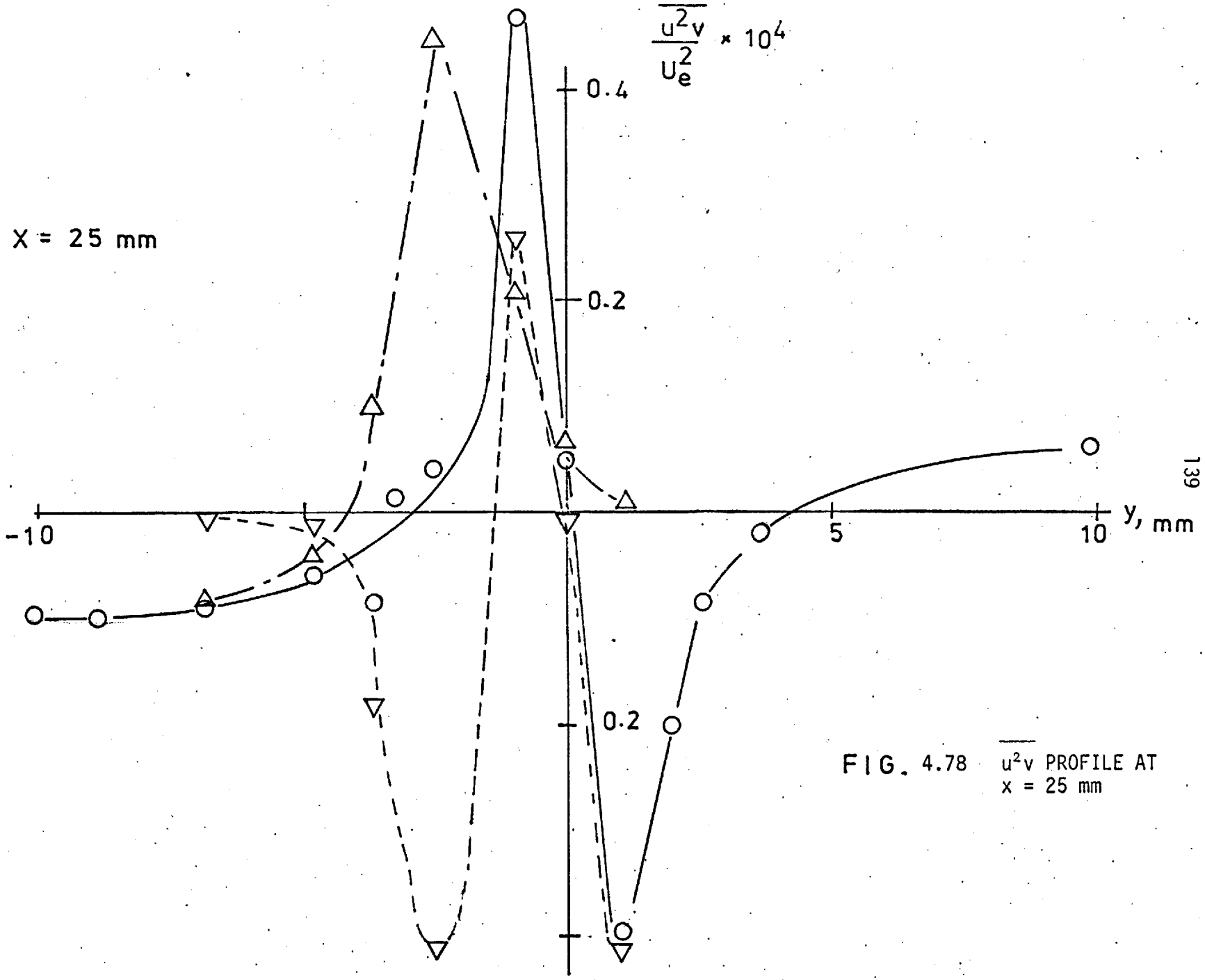

FIG. 4.78 $\overline{u^2v}$ PROFILE AT x = 25 mm

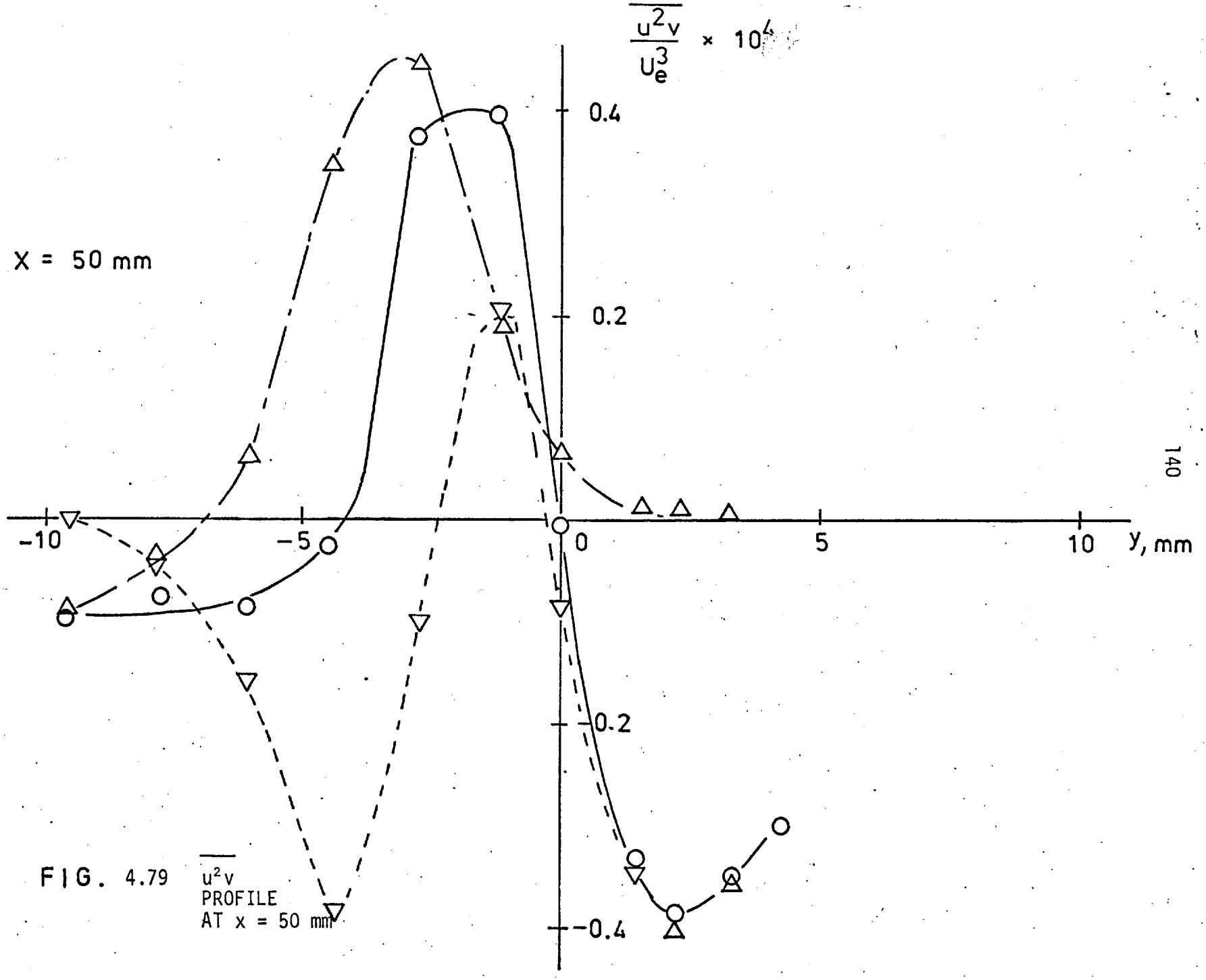

FIG. 4.79 $\overline{u^2v}$ PROFILE AT x = 50 mm

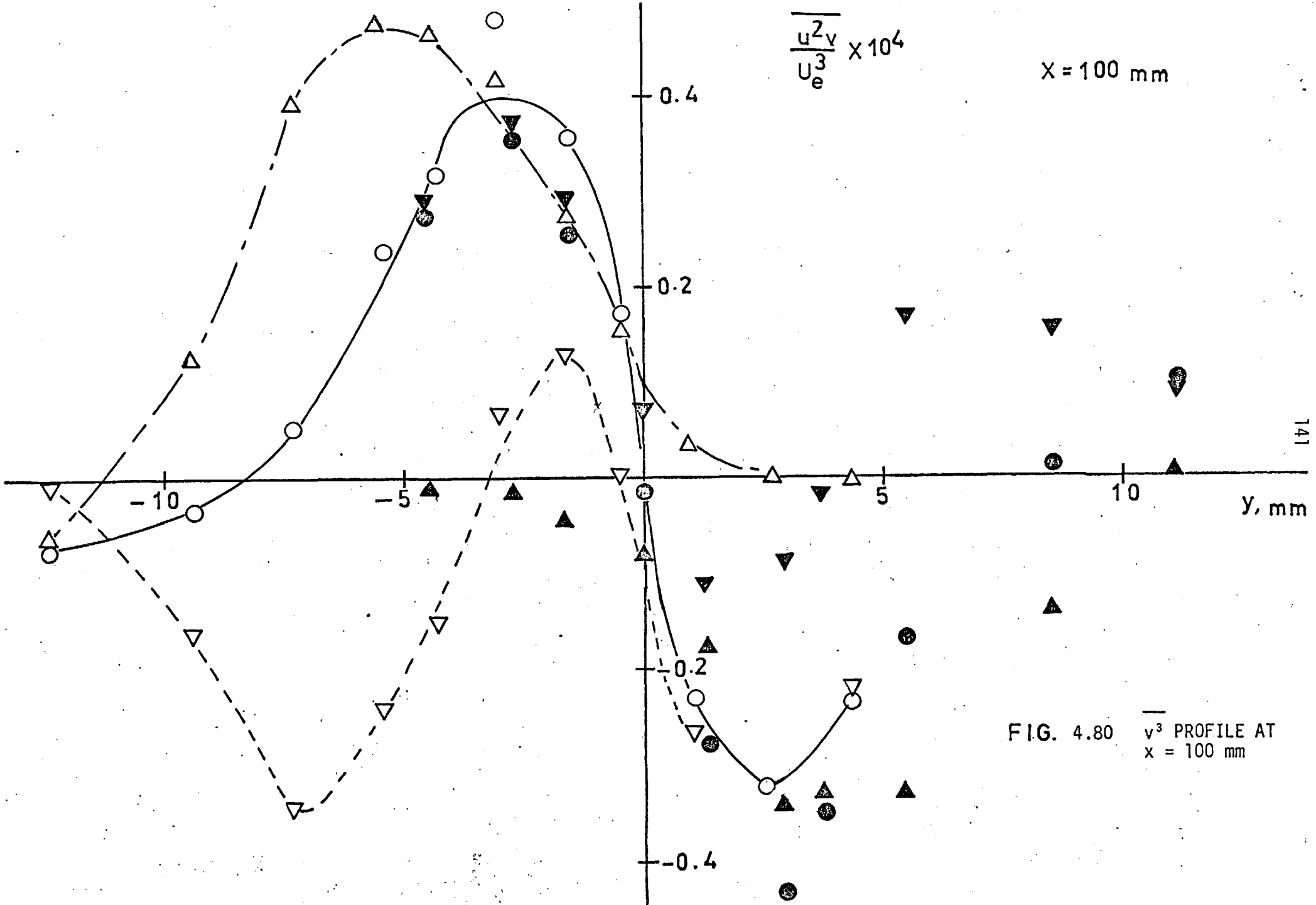

FIG. 4.80 $\overline{v^3}$ PROFILE AT x = 100 mm

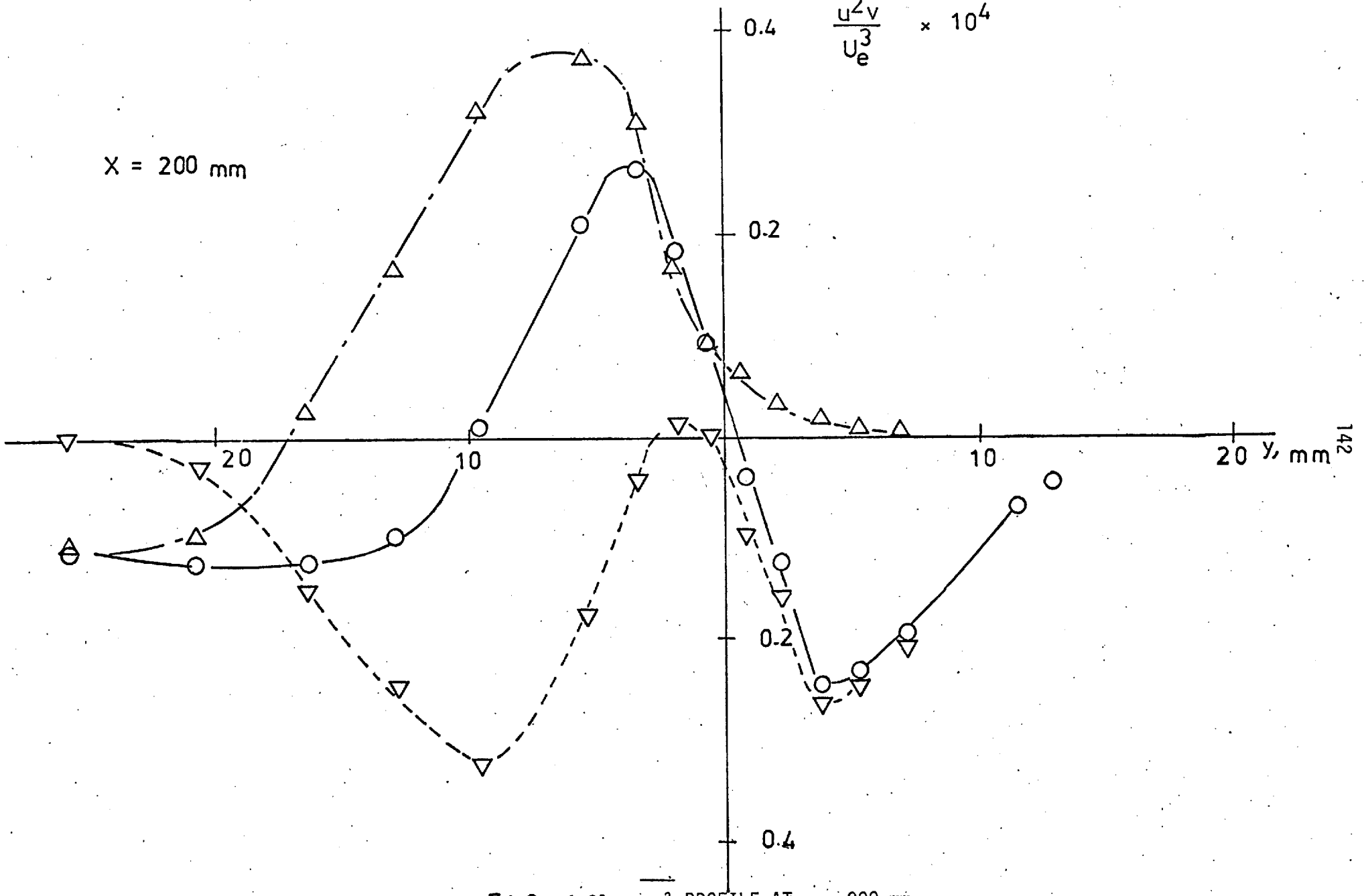

FIG. 4.81 $\overline{uv^2}$ PROFILE AT x = 200 mm

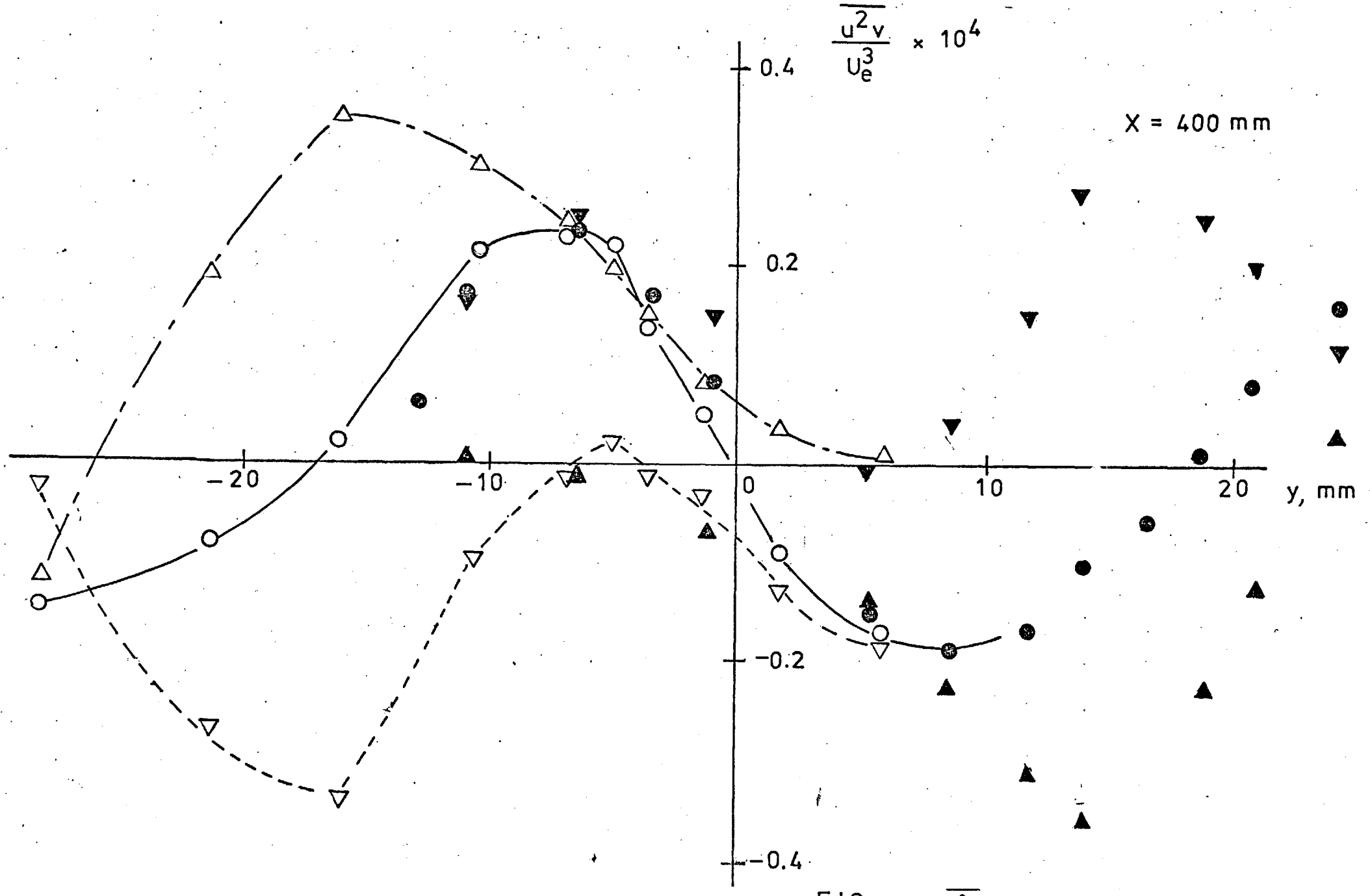

FIG. 4.82 $\overline{u^2v}$ PROFILE AT x = 400 mm

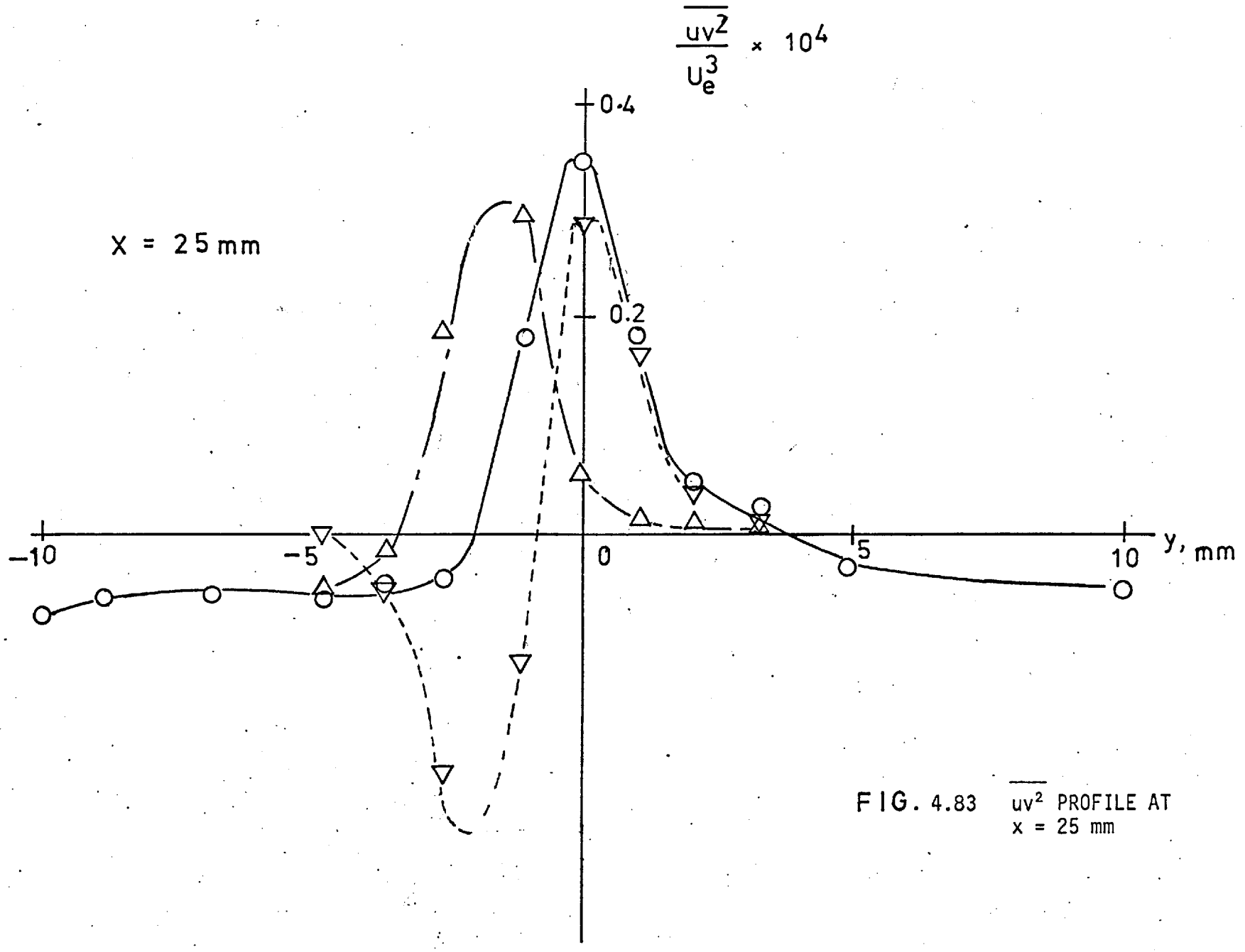

FIG. 4.83 $\overline{uv^2}$ PROFILE AT x = 25 mm

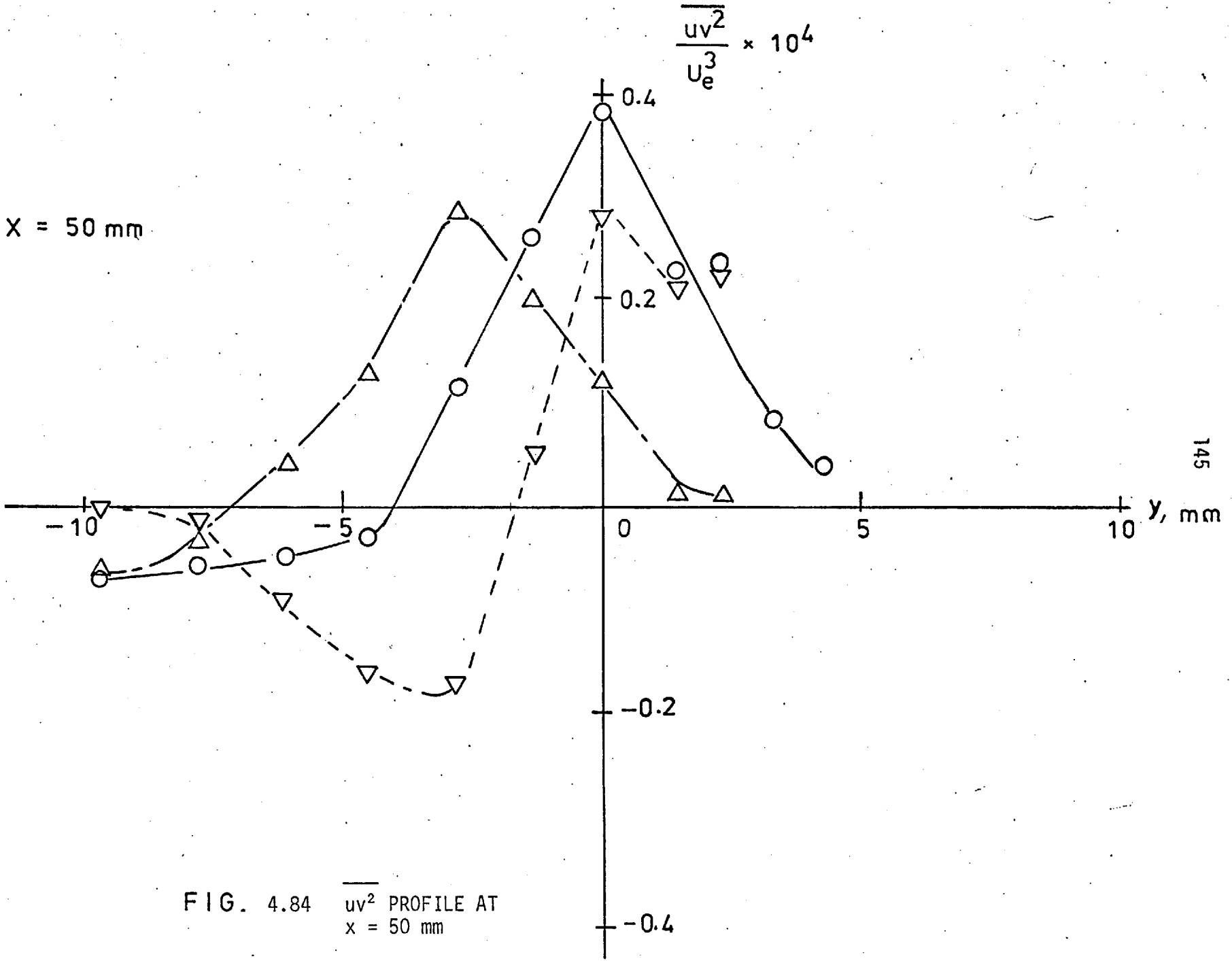

FIG. 4.84 $\overline{uv^2}$ PROFILE AT x = 50 mm

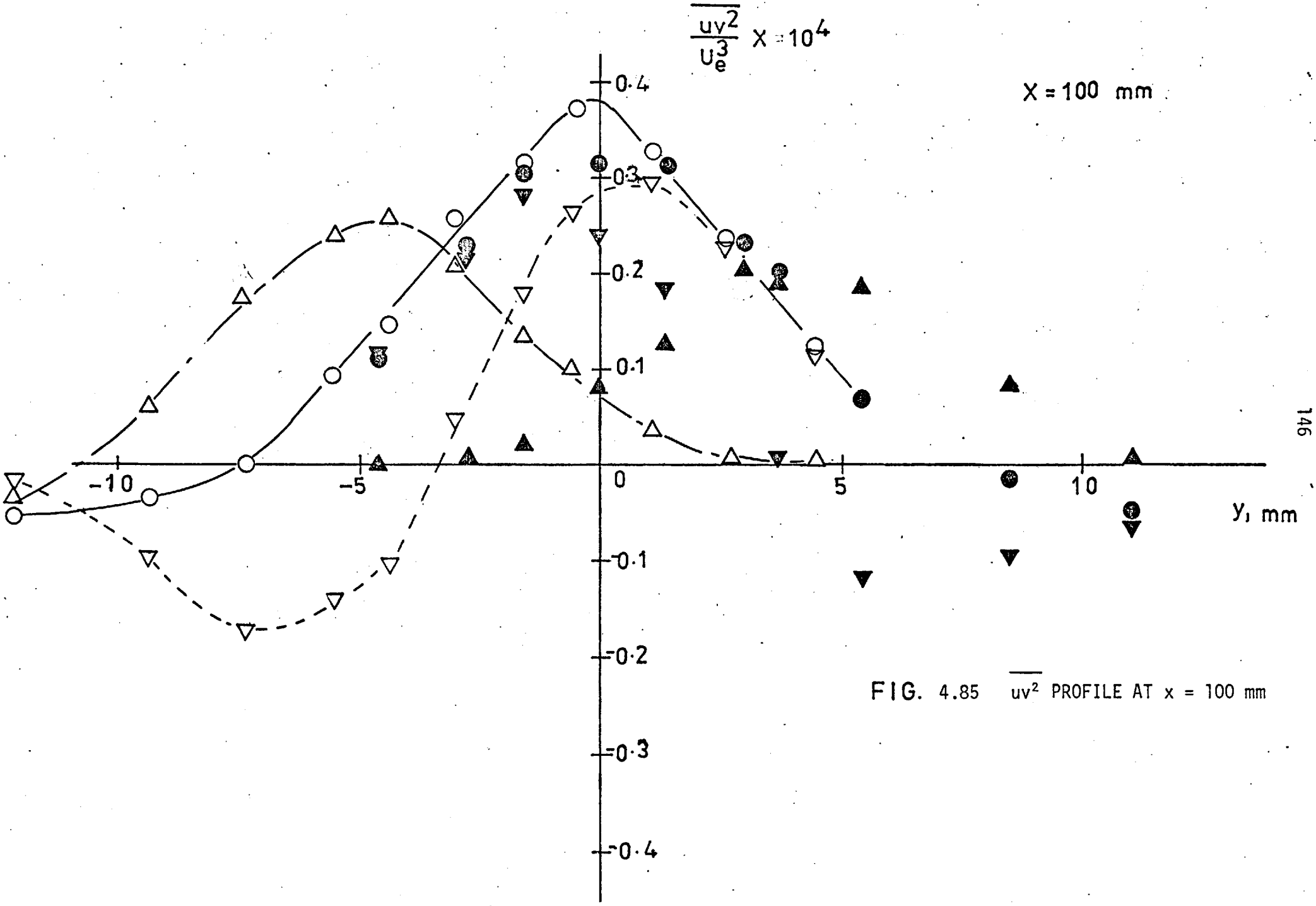

FIG. 4.85 $\overline{uv^2}$ PROFILE AT x = 100 mm

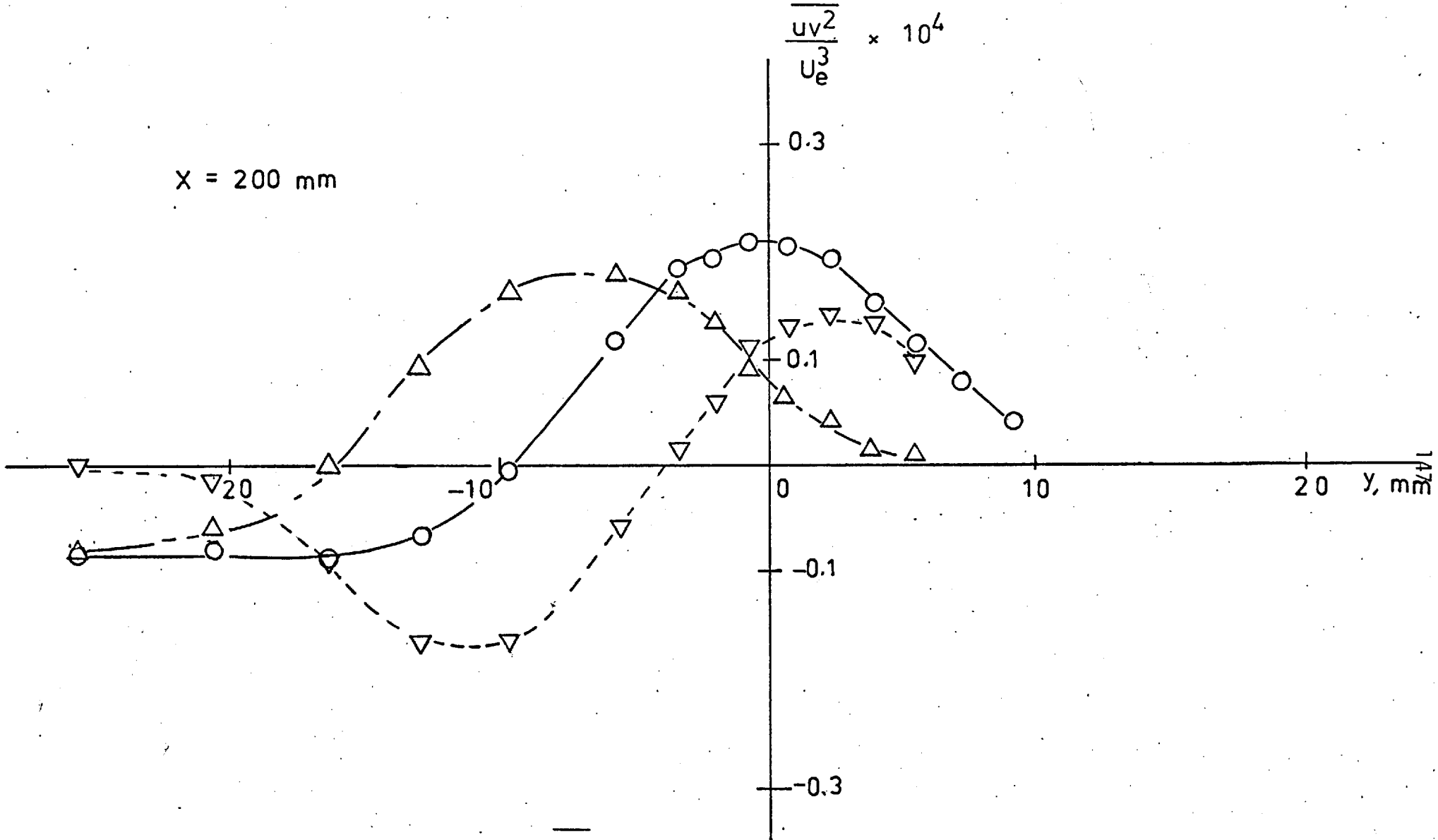

FIG. 4.86 $\overline{uv^2}$ PROFILE AT x = 200 mm

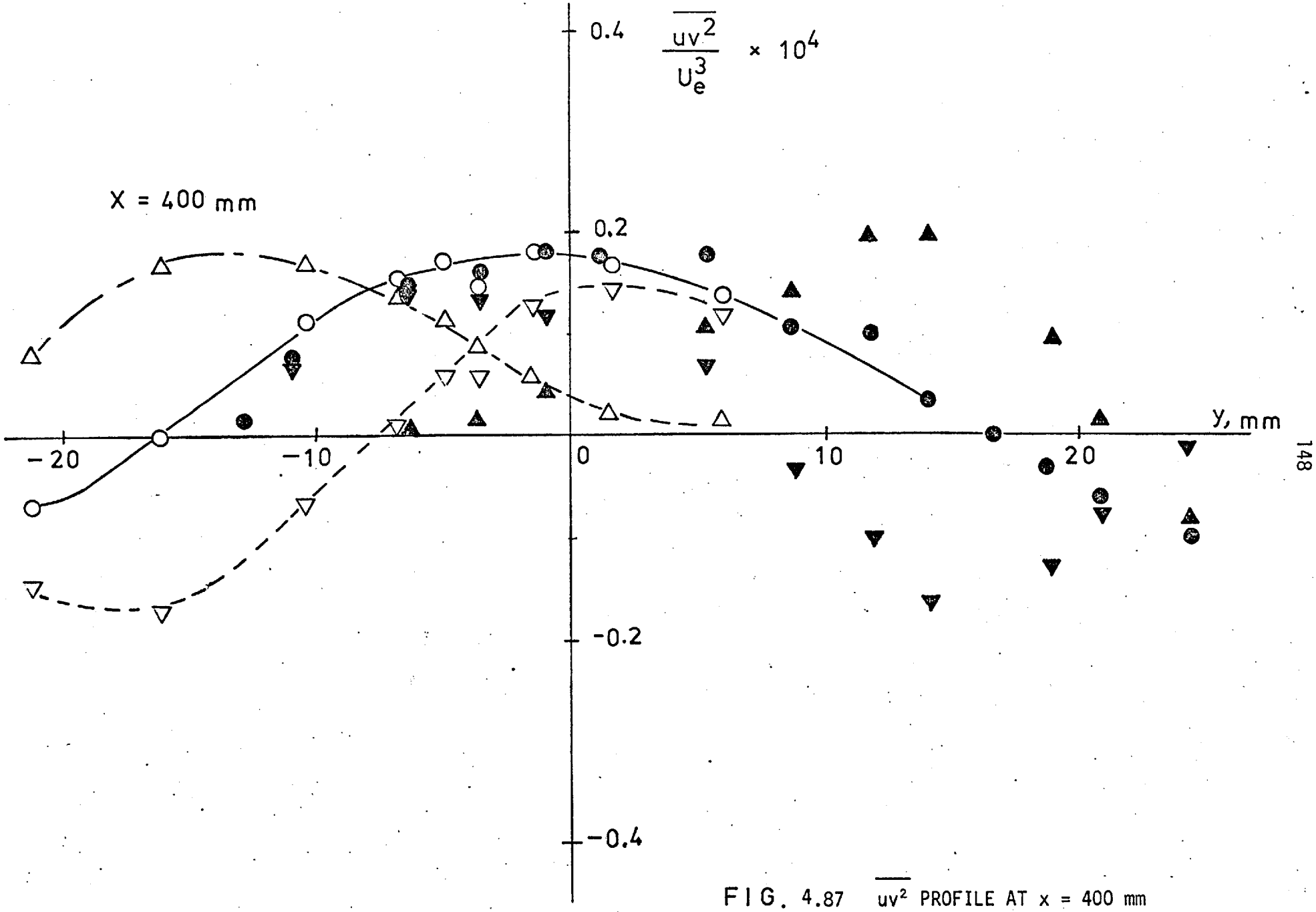

FIG. 4.87 $\overline{uv^2}$ PROFILE AT x = 400 mm

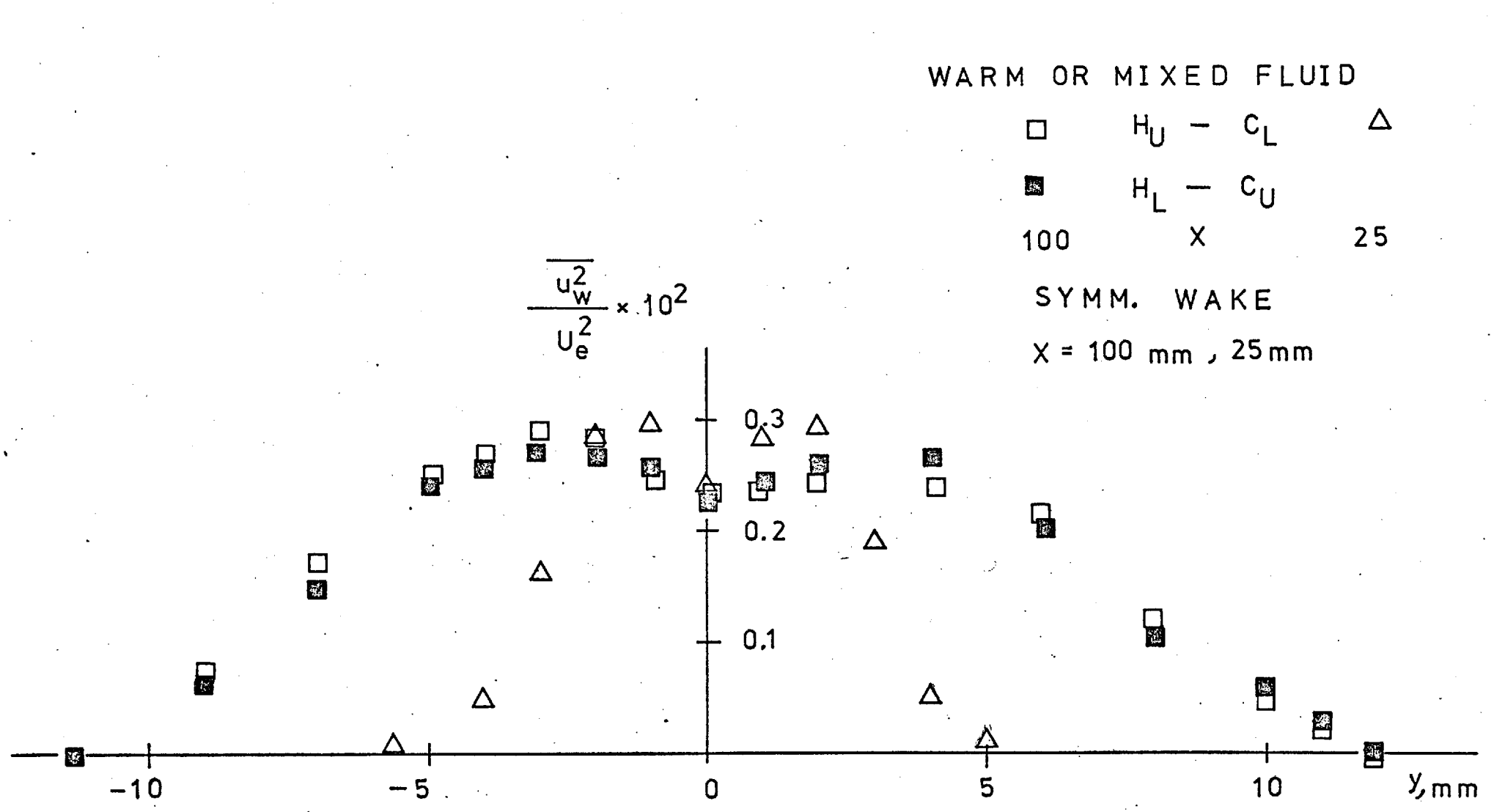

FIG. 4.88 $\overline{u_w^2}$ PROFILE

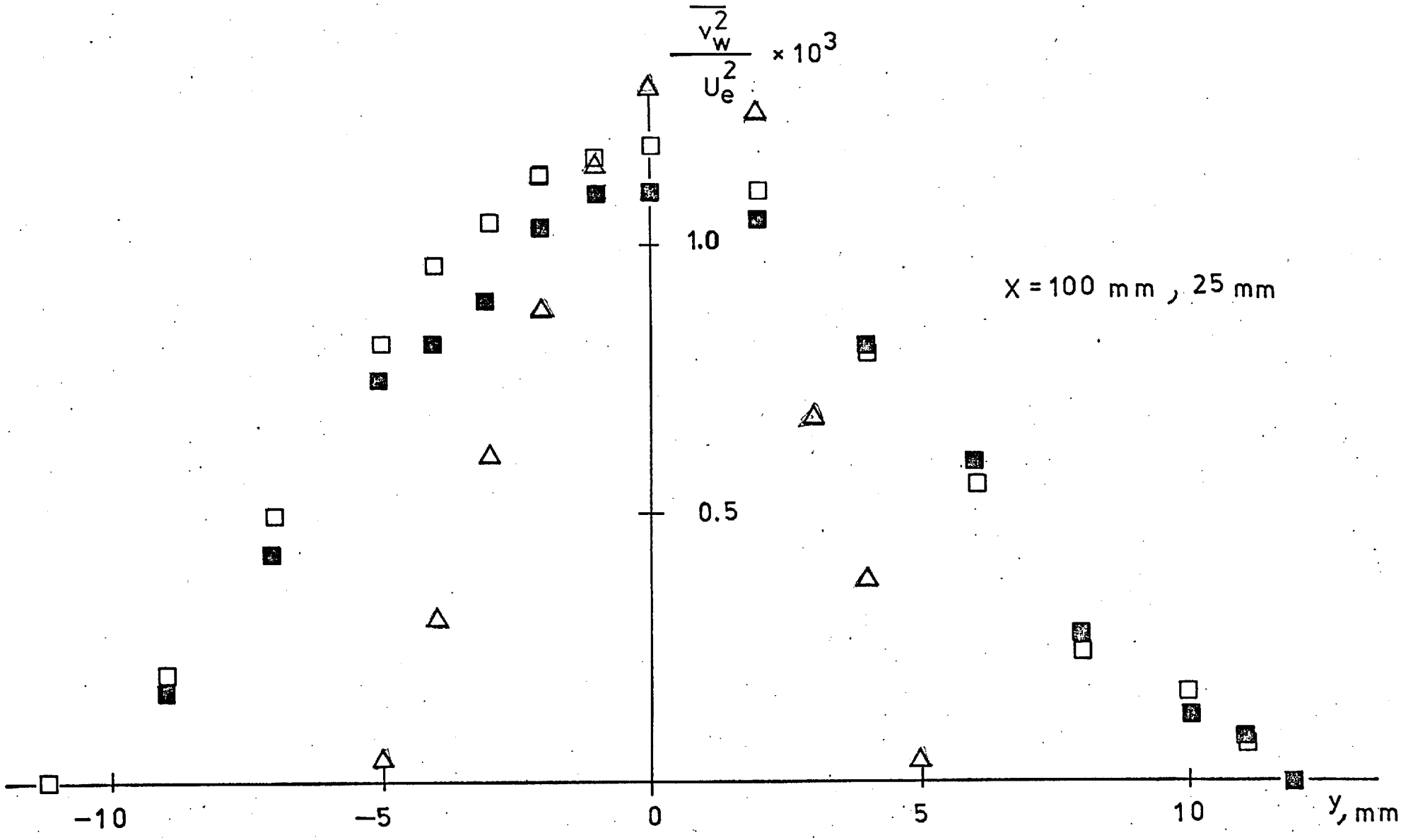

FIG. 4.89 $\overline{v_w^2}$ PROFILE

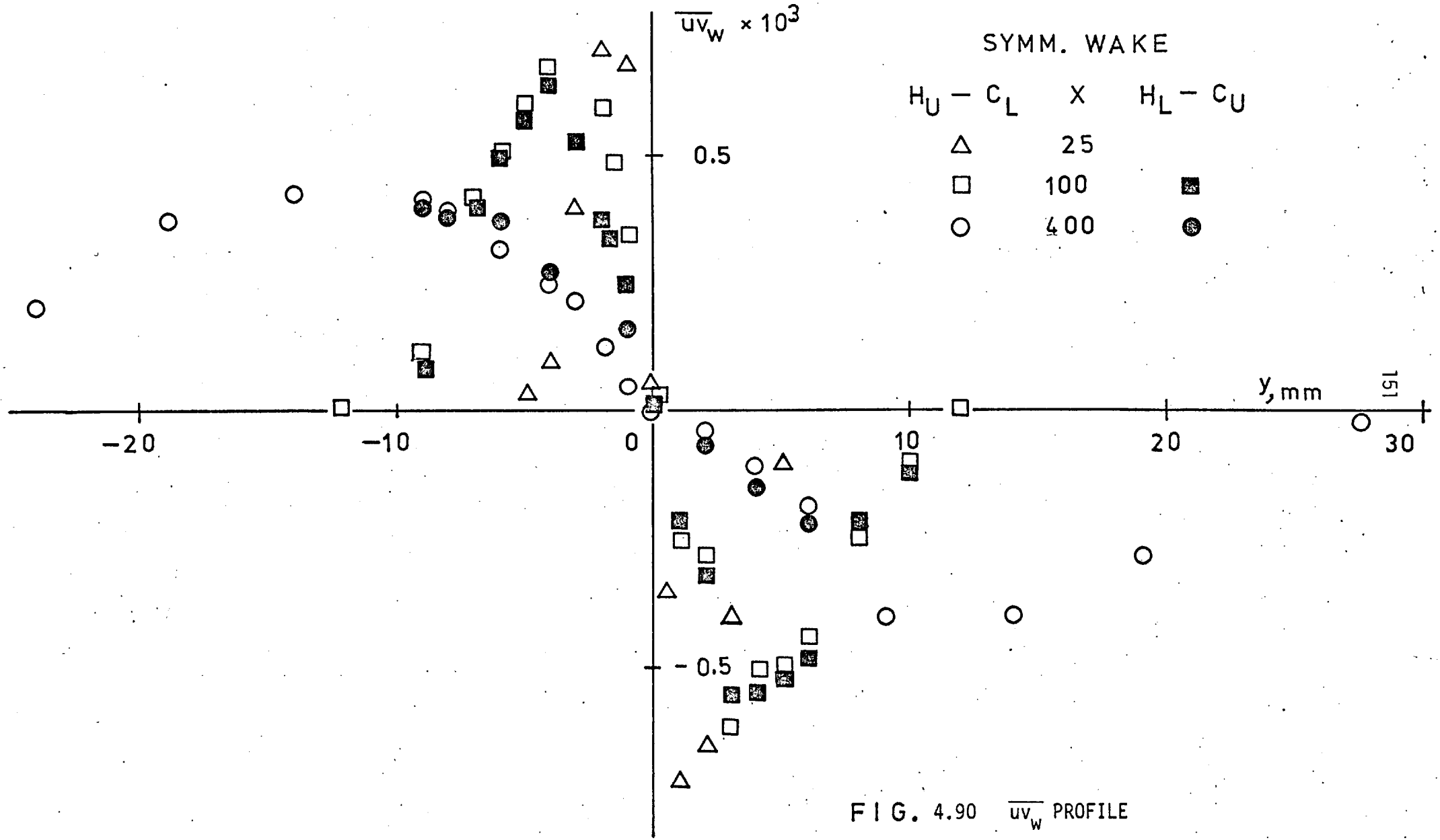

FIG. 4.90 $\overline{uv}_w$ PROFILE

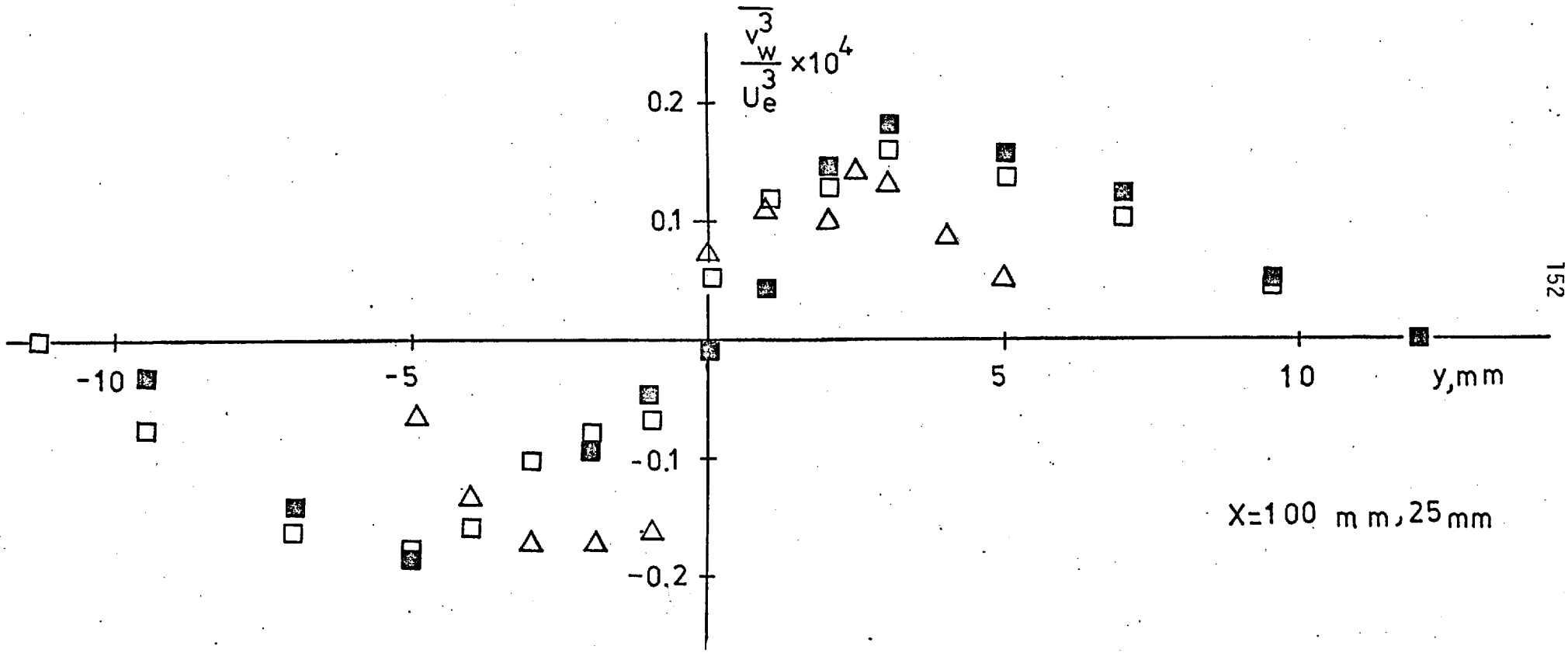

FIG. 4.91 $\overline{v_w^3}$ PROFILE

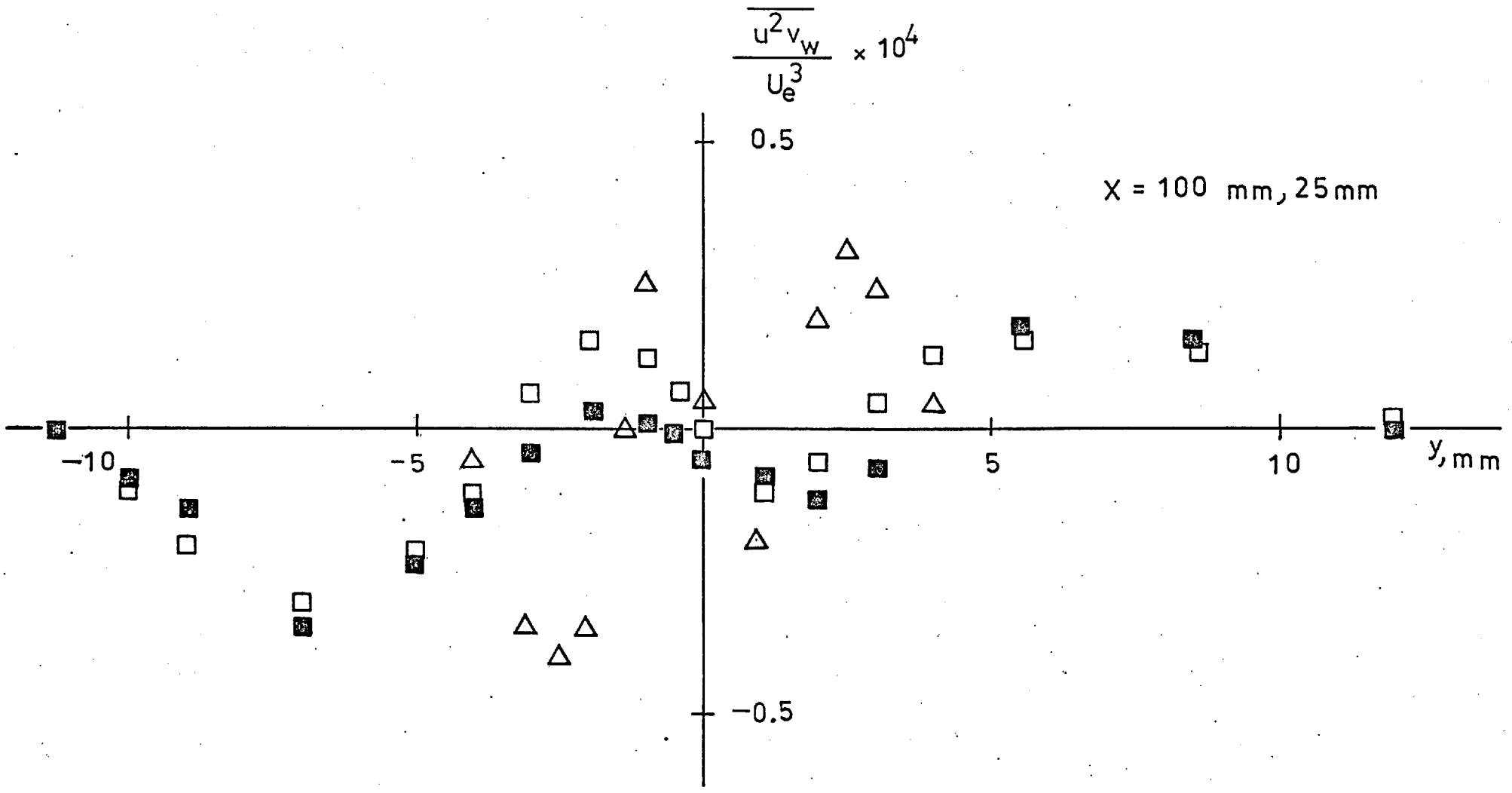

FIG. 4.92 $\overline{u^2 v_w}$ PROFILE

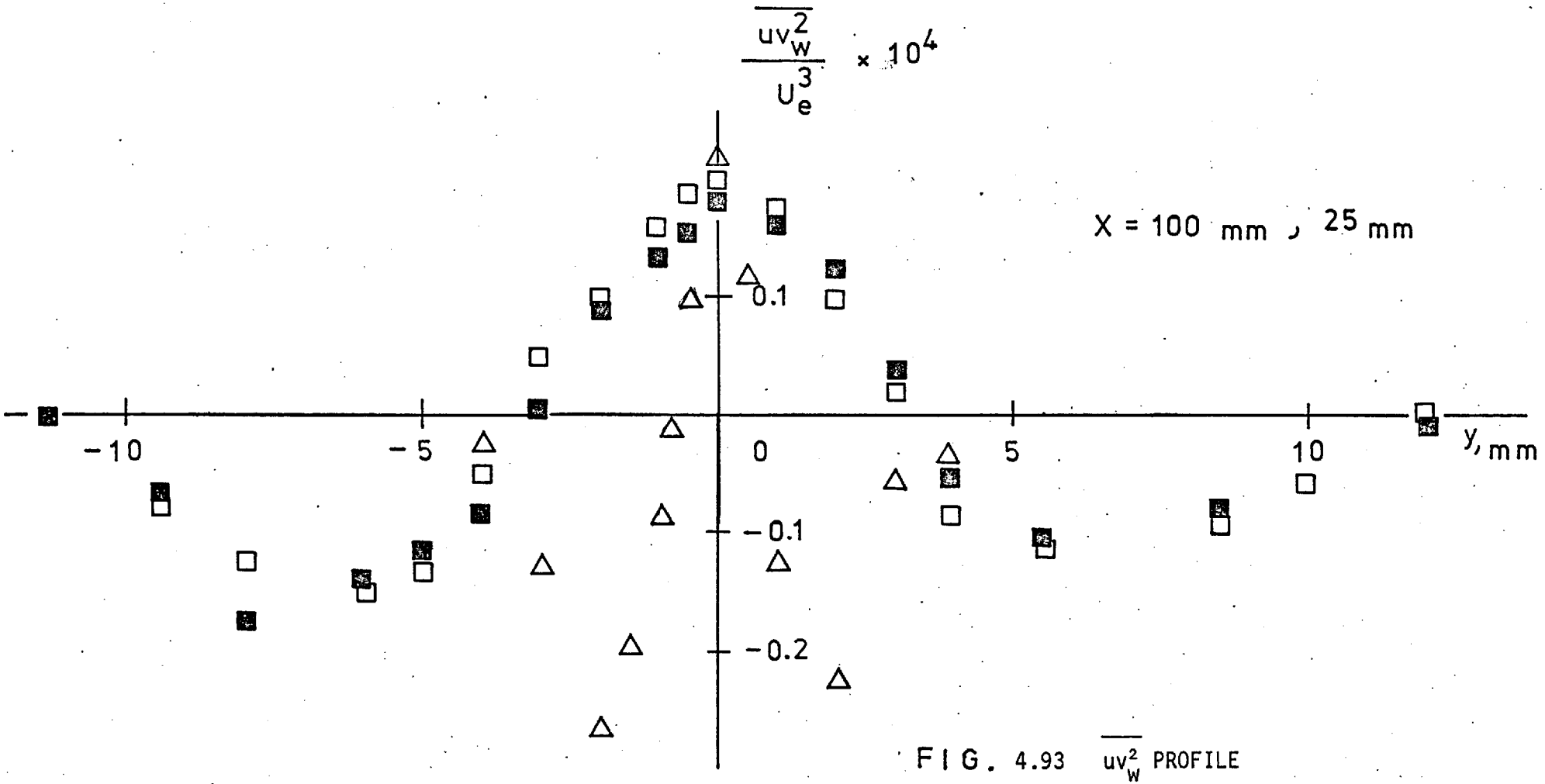

FIG. 4.93 $\overline{uv_w^2}$ PROFILE

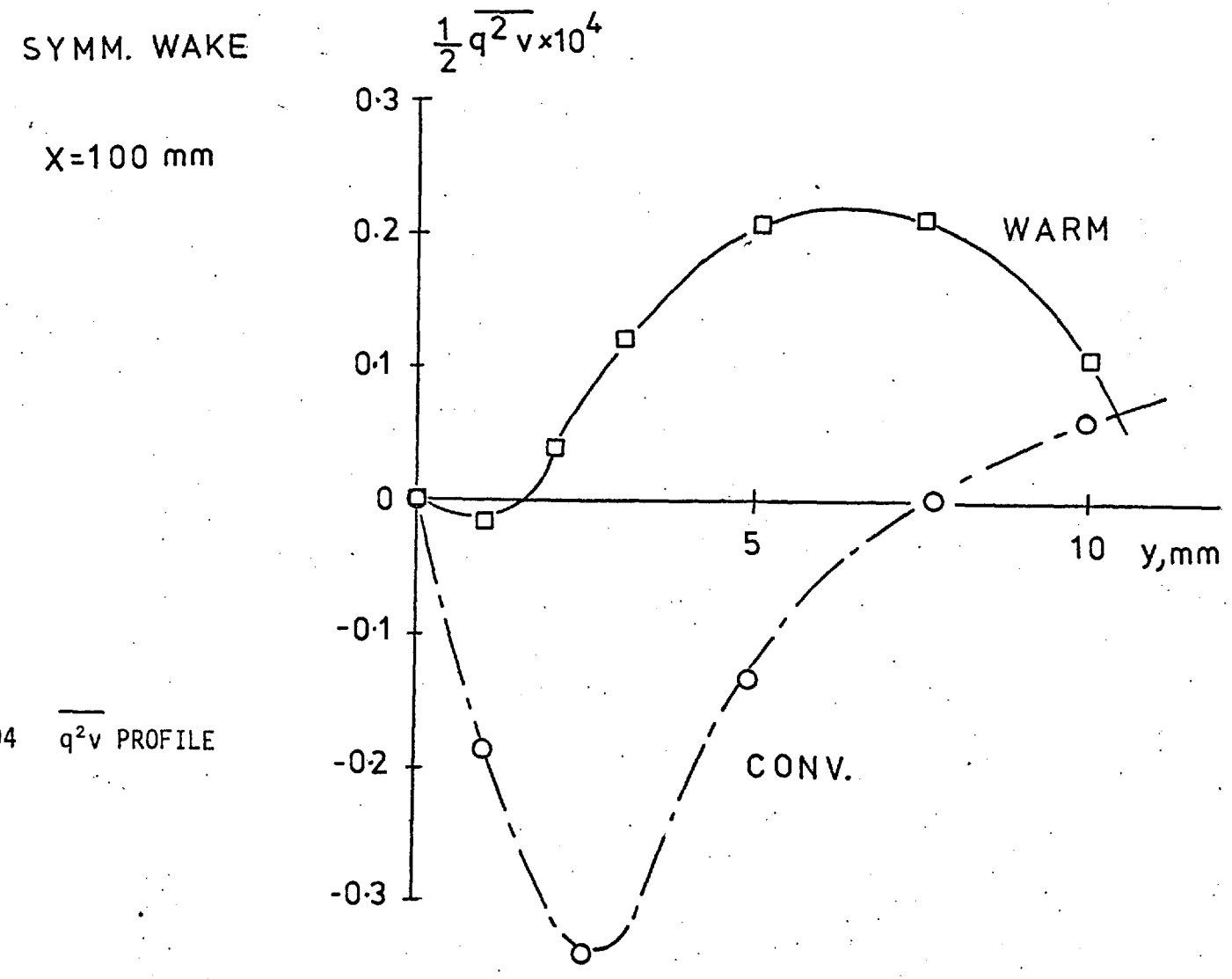

FIG. 4.94 $\overline{q^2 v}$ PROFILE

5. ASYMMETRIC WAKE RESULTS

5.1 Mean Velocities and Bulk Flow Parameters

5.1.1 General

Most of the commonly investigated interactions between adjacent turbulent flow fields have symmetry with respect to a plane or an axis. Only a few cases of flows with essential asymmetry have been examined. All the asymmetric flows have indicated some unexpected or unusual features, like the non-coincidence of the zero velocity gradient with the point of zero shear stress.

In the symmetric wake experiment, the two boundary layers which merged to form the wake had the same velocity and length scales. In the asymmetric wake, the top boundary layer develops on a rough surface and the friction velocity is much higher than in the boundary layer over a smooth surface. Therefore, an additional parameter is needed to correlate data, like the friction velocity ratio, $u_{\tau r}/u_{\tau s}$, where $u_{\tau r}$ is the friction velocity on the rough surface and $u_{\tau s}$ is the friction velocity on the smooth surface.

5.1.2 Mean Velocities

The mean velocity profiles at x = 0, 25, 50, 100, 200 and 400 mm are plotted in Figs. 5.1 to 5.6 as U/U_e versus y. It can be seen that the two dissimilar boundary layers start to interact and gradually the profile shape is reformed to a symmetric far wake but the wake at the furthest station x = 400 mm is still far from symmetric. It is also clear that the outer parts, lower and upper, do not change very much up to x = 400 as in the symmetric case. The point of minimum velocity $\partial U/\partial y = 0$ moves upwards, i.e. towards the

"rough" side, with x.

The bulk flow parameters, δ, δ^*, Θ and H are given in Table III. A comparison with values in the symmetric wake is shown in Fig. 5.7. Again, the momentum thickness does not seem to vary with x but the parameter δ^*/Θ_o retains higher values than in the symmetric case.

In Fig. 5.8, the mean V velocity is plotted, calculated from the continuity equation $\partial U/\partial x + \partial V/\partial y = 0$ for the symmetric and the asymmetric wake, as is described in Appendix H. It is clear that V is negative for $y > 0$ and positive for $y < 0$, i.e. always inwards towards the centre-line, opposing the wake growth. In the region where $\partial U/\partial x \simeq 0$, i.e. in the outer parts of the wake, V reaches an asymptotic value V_e for large positive or negative y. It is also evident that the small $\partial V/\partial x$ is negative for $y < 0$ and positive for $y > 0$ for the symmetric wake, meaning that $|V_e|$ is reduced with x. In the asymmetric wake, for small region of negative y, $\partial V/\partial x$ is positive but elsewhere is as in the symmetric case with $|V_e|$ reduced downstream.

5.1.3 Wall Shear Stress

One of the main problems in flows over rough surfaces is the determination of the wall shear stress. Perry et al (1963) suggested that the effective origin of the wall must be known before the skin friction can be determined. Antonia and Luxton (1971) proposed a method for non-equilibrium flows, (like those very near to the origin of the internal layer growing after a step change of roughness) for obtaining the effective position of the wall by trial and error, i.e. the best fit of a straight line to the log law. This method has been tried here but it was found not quite objective since there was more than one straight line fitting the log law. Therefore, the method described in Section 2.6 was adopted. In Fig. 5.9 the mean velocities

TABLE III

BULK FLOW PARAMETERS - ASYMMETRIC WAKE

x (mm)	Wake Width δ ($\delta^{LOWER}_{0.995} + \delta^{UP}_{0.995}$) (mm)	$\frac{\delta^*}{\delta}$	$\frac{\Theta}{\delta}$	$H = \frac{\delta^*}{\Theta}$
Boundary layer x =-14 mm (U)	$\delta^{UP}_{0.995} = 73.93$	0.191	0.128	1.484
Boundary layer x = 0 (L)	$\delta^{LOWER}_{0.995} = 51.53$	0.147	0.118	1.322
Boundary layer x = 0 (U)	$\delta^{UP}_{0.995} = 75.919$	0.210	0.134	1.562
25	126.0	0.175	0.118	1.475
50	126.521	0.183	0.129	1.409
100	127.52	0.172	0.125	1.378
200	127.1	0.164	0.123	1.332
400	130.0	0.147	0.115	1.281

$$\frac{\delta^*}{\delta} = \int_{-\infty}^{+\infty} \left(1 - \frac{U}{U_e}\right) dy/\delta \qquad \frac{\Theta}{\delta} = \int_{-\infty}^{\infty} \frac{U}{U_e} \left(1 - \frac{U}{U_e}\right) dy/\delta$$

(Rough) Upper Boundary Layer : $C_f = 0.0052$

(Smooth) Lower Boundary Layer : $C_f = 0.0024$

in Clauser chart co-ordinates, for the asymmetric case as well as with the symmetric, have been plotted. In addition, some cross checks have been made: the mean velocity profile at an upstream position, x =-14 mm, has been measured and by using the momentum integral equation:-

$$\frac{C_f}{2} = \frac{\tau_w}{\rho U_e^2} = \frac{d\Theta}{dx} + (2\Theta + \delta^*) \frac{1}{U_e} \frac{dU_e}{dx}$$

and taking into account the small pressure gradient which was due to the gradually reduced thickness of the flat plate at the trailing edge, an average, between the trailing edge and x = - 14 mm, C_f was found to be 0.0058 which actually is not much larger than the 0.0052 which was finally adopted. Some other tests with the use of velocity defect law $(U_e - U)/u_\tau = f(y/\delta)$ for points in the outer part of boundary layers gave a ratio of rough to smooth wall shear stress of $\sim$ 2.01 which was about 8% less than that which was found from the shear stress profiles. In Fig. 5.10 the mean velocity profile is plotted in outer layer similarity parameters.

5.1.4 The Inner Wake

Here, as in the symmetric wake case, inner layer scaling can be employed with one of the two friction velocities at the trailing edge as a velocity scale and $u_{\tau r}/u_{\tau s}$ as parameter. In Fig. 5.11, the mean velocities are presented in inner layer similarity co-ordinates with the smooth wall friction velocity $u_{\tau s}$ as velocity scale. In the same figure is the mean velocity profile for the rough boundary layer at the trailing edge plotted as $U/u_{\tau r}$ versus ln $u_{\tau r} y/\nu$. The log law:-

$$\frac{U}{u_{\tau r}} = \frac{1}{k} \ln \frac{u_{\tau r} y}{\nu} + c - \frac{\Delta U}{u_{\tau r}} \qquad (5.1)$$

for the present data seems to give:-

$$\frac{\Delta U}{u_{\tau r}} = 10.4 \qquad \text{with } k = 0.41 \text{ and } c = 5.0$$

Generally, the mean velocity profile in the inner wake region should be expressed by:-

$$\frac{U}{u_{\tau s}} = f\left[\frac{u_{\tau s} x}{\nu} \;,\; \frac{u_{\tau s} y}{\nu} \;,\; \frac{u_{\tau r}}{u_{\tau s}}\right]$$

A special case is for $y = 0$, i.e. on the centre-line, and the results from the present experiment are plotted in Fig. 5.12, together with the results from the symmetric case as in Fig. 4.5a. It seems that a good fit to the present results is:-

$$\frac{U_{\ell}}{u_{\tau s}} = A \ln \frac{u_{\tau} x}{\nu} + B' \qquad (5.2)$$

with $A \simeq 2.10$ and $B' = -1.3$ and thus after a comparison with the similar expression 4.3 of the symmetric wake, the effect of roughness just causes a shift $\Delta U_{\ell}/u_{\tau s} \simeq 2$ which is of the order of $4.8\,(u_{\tau r}/u_{\tau s} - 1)$.

Recalling again Bradshaw's argument that a small disturbance at the surface propagates outwards with an angle $\sqrt{2a_1}\; u_{\tau}/U$, assuming zero diffusion of turbulent kinetic energy and if $y = \delta_r$ is a point on the "rough" side with velocity U_i, then it follows that:-

$$\frac{d\delta_r}{dx} = \sqrt{2a_1}\,\frac{u_{\tau r}}{U_i} \tag{5.3}$$

with:-

$$\frac{U_i}{u_{\tau r}} = \frac{1}{k}\ln\frac{u_{\tau r}\,\delta_r}{\nu} + c - \frac{\Delta U}{u_{\tau r}}$$

So as in the symmetric wake:-

$$x = \frac{1}{\sqrt{2a_1}}\int_0^{\delta_r}\left(\frac{1}{k}\ln\frac{u_{\tau r}\,\delta_r'}{\nu} + c - \frac{\Delta U}{u_{\tau r}}\right)d\delta_r'$$

or:-

$$x = \frac{1}{\sqrt{2a_1}}\,\delta_r\left[\frac{1}{k}\ln\frac{u_{\tau r}\,\delta_r}{\nu} + c - \frac{\Delta U}{u_{\tau r}} - \frac{1}{k}\right]$$

and expressing this in terms of $u_{\tau s}\,\delta_r/\nu$ gives:-

$$\frac{u_{\tau s}\,x}{\nu} = \frac{u_{\tau s}\,\delta_r}{\nu}\,\frac{1}{\sqrt{2a_1}}\left[\frac{1}{k}\ln\frac{u_{\tau s}\,\delta_r}{\nu} + \frac{1}{k}\ln\frac{u_{\tau r}}{u_{\tau s}} + c - \frac{\Delta U}{u_{\tau r}}\right] \tag{5.4}$$

The expression for a point $y = \delta_s$ on the "smooth" side is similar to the symmetric wake case and it is given by equation 4.8. In Fig. 5.13 both are plotted as $\ln(u_{\tau s}\,\delta_i/\nu)$ versus $\ln(u_{\tau s}\,x/\nu)$. They are parallel. In the same graph, the experimental results of the asymmetric wake are plotted together with those of the symmetric case for comparison. Again, the edges of the inner wake $y = \delta_{Ur}$ and δ_{Us} have been taken as the last

points before the departure from the log law straight line. The edge of the "smooth" side inner wake and that of the "rough" side tend to the same asymptotic value for large x where the asymmetric wake becomes symmetric.

Bradshaw's hypothesis seems to agree quite well for the "rough" edge while for the "smooth" edge only the tendency is the same. In the same Fig., 5.13, the total inner wake width $\delta_U = \delta_{Us} + \delta_{Ur}$ is plotted as well.

5.2 Conventional Turbulent Quantities

The results to be considered here have been taken from measurements at x = 0 mm, where the two boundary layers have not yet left the solid surface, and at three downstream stations in the wake x = 25 mm, x = 100 mm and x = 400 mm. As indicated in the following graphs, the measurements have been taken with two different heating conditions for reasons explained in Section 3.2. This does not affect the conventional turbulent quantities, but the two conditions are distinguished in all the graphs as an indication of the repeatability of results. In addition, at x = 0 mm, measurements were made with the x-wire probe in its standard position and rotated 180^0 (if the mean of the two results for $\overline{uv}$ is taken, yaw calibration drift cancels out to a first approximation). This was done to ensure the greatest possible accuracy in $\overline{uv}$ on the rough wall since the determination of the rough wall shear stress was based entirely on $\overline{uv}$ measurements. All the quantities are normalized by the free stream velocity U_e. Codes UBLH and LBLH denote "upper (rough) boundary layer heated" and "lower (smooth) boundary layer heated" respectively.

In Figs. 5.14 to 5.17, the $\overline{u^2}$ intensities are plotted against y. Since the friction coefficient on the rough side is about twice that

on the smooth side and the free stream velocity U_e the same on both sides, it is expected that for x = 0 mm, all turbulent quantities on the rough side will be related to those on the smooth side by an appropriate power of $u_{\tau r}/u_{\tau s}$. The maximum values of $\overline{u^2}$, for example, on both sides have a ratio of $u^2_{\tau r}/u^2_{\tau s}$. The present measurements show a drop of $\overline{u^2}$ very close to the wall where it is possible to have wall proximity effects or wire length effects limiting measurements of scales smaller than the wire length, or separation. At stations downstream in the wake, the wall effect ceases to exist and the errors are reduced since the eddies increase in size.

In the $\overline{u^2}$ profiles, there are clearly two peaks: one on the "smooth" side and one on the "rough". The positions of both move outward from the centre-line, with x. As the two boundary layers mix, the intensity on the smooth side increases slightly while that on the rough side decreases after an initial rise. At the last station, x = 400 mm, where the inner wake has spread outside the constant stress layer, even the maximum intensity on the smooth side has started to fall and some small changes in the outer layer on the "smooth" side start to appear and cause small loss of turbulent kinetic energy by advection. Near the centre-line, the values on the "rough" side are decreasing rapidly which means that a gain by advection occurs. Generally, a normal transport of turbulent kinetic energy from the "rough" side, starting from regions near the centre-line, towards the "smooth" side should be expected up to the station where any asymmetry will have diminished. At x = 400 mm, the flow is still far from symmetric. However, some small changes in the outer layer on the smooth side have already started at x = 400 mm and perturbations have started to spread outside the inner wake on the smooth side only.

The distributions of $\overline{v^2}$ which are presented in Figs. 5.18 to

5.21 show the same trend as $\overline{u^2}$. The scatter is higher here. At x = 25 mm, the $\overline{v^2}$ has a maximum value at y = 0 while at the same point, $\overline{u^2}$ seems to have a minimum. However, since $\overline{u^2}$ is about twice the $\overline{v^2}$, the overall kinetic energy has a minimum.

In Figs. 5.22 to 5.25 are the shear stress profiles (strictly $\overline{uv}$ profiles). The values of shear stress obtained with a rotated cross-wire agree quite well with those of non-rotated wire. It was considered that the proper value of the wall shear stress was $-\overline{uv}/U_e^2 = 0.0026$. The maximum shear stress at the smooth wall is in good agreement with that obtained from the mean velocity profiles using Clauser charts. At x = 25 mm, the "rough" side retains its minimum value but the smooth side (i.e. y < 0) has almost double its boundary layer maximum value. It is obvious that some fluid from the upper side crossed the centre-line with change of sign of the shear stress. The conditionally sampled results discussed in Section 5.3 give more details. At x = 100 mm, both peaks have reduced and the shapes of distributions are deformed more. At x = 400 mm, any trace of the inner wake edge on the smooth side has disappeared.

In all stations in the wake, it is clear that the point of zero shear stress does not coincide with the point of zero velocity gradient $\partial U/\partial y$. This implies that in a small area, there is a negative eddy viscosity or an imaginary mixing length. Physically, it means that there is a negative kinetic energy production or "energy reversal" as it has been called by Palmer and Keffer (1972): this in itself is not a noteworthy phenomenon and does not imply abnormality of the turbulence; only an abnormality in the relation between turbulence and mean velocity gradient.

In Fig. 5.25a, $\overline{u^2}/u_\tau^2$, $\overline{v^2}/u_\tau^2$ and $\overline{uv}/u_\tau^2$ are plotted versus y/δ for the "smooth" and "rough" boundary layers at x = 0 mm. In the outer

part, both "smooth" and "rough" values nearly coincide. In the inner layer (i.e. $y/\delta < 0.2$), $\overline{v^2}$ and $\overline{u^2}$ on the "rough" wall are smaller than the "smooth" wall values, while the $\overline{uv}$ values are the same roughly for both.

Figs. 5.26 to 5.29 display the variation of shear correlation coefficient $\overline{uv}/\sqrt{\overline{u^2}}\sqrt{\overline{v^2}}$ across the wake. At the boundary layer, over a considerable region of the "rough" side it is constant, but generally it is less than the smooth wall. Near the rough wall, it increases because the shear stress increases faster than $\sqrt{\overline{u^2}}$ and $\sqrt{\overline{v^2}}$. At x = 25 mm on the "smooth" side and very close to the centre-line, there is a local increase of R_{uv}. As will be shown later, in this region the shear stress is transported in the y direction by turbulent diffusion faster than the kinetic energy ($V_\tau > V_q$).

In the next set of figures, the triple velocity products are presented: their physical meanings were explained in Section 4.2. The $\overline{u^3}$ distributions in Figs. 5.30 to 5.33 show, as the symmetric wake ones, a change of sign close to the wall. The short bursts are again present especially very close to the rough wall (x = 0 mm) where $\overline{u^3}$ reaches very high positive values, i.e. for y less than where the sign of $\overline{u^3}$ changes the bursts going towards the wall, while for greater y, they are going outwards. Even for the first station in the wake, x = 25 mm, the values of $\overline{u^3}$ on the "rough" side are still high, indicating that bursts persist.

At x = 100 mm, the distribution starts taking the usual wake shape as in the symmetric case. A similar behaviour is observed at x = 400 mm.

Figs. 5.34 to 5.37 show the distribution of $\overline{u^2v}$ which represents the transport of u^2 by v and contributes to the diffusion term in the kinetic energy transport equation. The change of sign near

the wall is characteristic of all the triple correlations. So again here there are two regions: the "outer" wake (or generally "outer layer") and the "inner" wake. Bearing in mind that $\overline{u^2}$ is positive everywhere across the wake, in the outer part there is a transport of $\overline{u^2}$ towards the positive direction of v (that is, outwards) while in the region near the wall or the centre-line, there is strong transport inwards. This trend is especially pronounced for the first station in the wake x = 25 mm. The inward transport from the "rough" side seems to be stronger, in absolute terms, than the inward transport from the "smooth" side. The maximum $\overline{u^2v}$ on the rough side is 1.33 $u_{\tau r}^3/u_{\tau s}^3$ times more than the maximum $\overline{u^2v}$ on the smooth side. At x = 100 mm and x = 400 mm, the inward transport is still evident but seems to become the same in amount from either side since the general trend of the flow is to become symmetric.

The $\overline{v^3}$ distributions displayed in Figs. 5.38 to 5.41 show a different behaviour. At x = 0 mm, near the rough wall, $\overline{v^3}$ seems first to increase with increasing y and then to decrease, indicating that there is first a loss by diffusion of v^2 and then a gain. There is a high scatter in the $\overline{v^3}$ measurements but a positive excursion near $y \simeq 5$ mm was found in all three runs.

The $\overline{v^3}$ at x = 25 mm shows high negative values for - 5 mm < y < 0. It is possible some eddies from the other side crossed the centre-line and changed their v velocity sign as they did with their shear stress sign as well. It is also indicated that there is transport of v^2 by v outwards near the centre-line, with the transport towards the outer part of the smooth side being stronger. This is more evident at x = 100 mm and it results in the final form of $\overline{v^3}$ at x = 400 mm. Further elucidation of the conflicting behaviour of $\overline{u^2v}$ and $\overline{v^3}$ requires consideration of conditional averages (Section 5.3).

In Figs. 5.42 to 5.45 are the distributions of $\overline{uv^2}$, which represent the transport of shear stress uv by v which appears in the diffusion term in the shear stress transport equation. In the "rough" side $\overline{uv}$ is mostly negative which means that in the "near-wall" region, i.e. the centre-line region where $\overline{uv^2}$ is high, there is transport of $\overline{uv}$ towards the centre-line.

After that point, $\overline{uv^2}$ starts to decrease while $\overline{uv}$ is increasing up to the point where $\overline{u^2v}$ becomes zero or $\overline{uv}$ becomes maximum. Between these points, there is a transport of $\overline{uv}$ going inwards but with a gain of shear stress by diffusion. Then the $\overline{uv}$ starts to decrease and $\overline{u^2v}$ becomes negative and, consequently, there is a transport outwards to the smooth side outer layer.

The same pattern seems to be repeated at all downstream stations without the somewhat eccentric changes found in $\overline{u^2v}$ and $\overline{v^3}$.

To summarize the measurements of the conventional turbulent quantities which have been presented here in turn, the asymmetric wake flow seems to behave in a slightly different way than the symmetric. There is evidence to show that there is transportation towards the centre-line of shear stress and kinetic energy but since the transportation from the rough side is stronger, the overall picture is that there is a net transport of these two quantities from the rough side towards the outer part of the other side. The conditionally sampled results will show more details of the flow.

5.3 Conditionally Sampled Results

5.3.1 "Cold" and "Hot" Fluid Averages

As in the results discussed in Chapter 4 for the symmetric wake, the conditionally sampled averages of the asymmetric wake are

presented as a contribution to the total conventional averages. Here the results of two different experiments are considered: first the case of the upper boundary layer heated (UBLH) and, secondly, the case of the lower boundary layer heated (LBLH). The best way of discussing the results is to consider the "cold" fluid averages (i.e. unmixed fluid averages) for both UBLH and LBLH, since the "hot" fluid averages include "warm" fluid averages as well, then to consider the averages derived for the "warm" (i.e. mixed) fluid; it is always UBLH "cold" = LBLH truly "hot" and LBLH "cold" = UBLH truly "hot" (see equations 3.2.4 and 3.2.11).

The measurements have been taken at three downstream stations - $x = 25$ mm, $x = 100$ mm and $x = 400$ mm, being the same data as in Section 5.2.

The intermittency factors γ_U and γ_L for the two heating cases, UBLH and LBLH respectively, are displayed in Fig. 5.46. γ_L values are higher than the γ_U ones at symmetric y, while γ_U values are considerably higher than the corresponding at the same y, symmetric wake value. Both differences may be due to the asymmetric heat transfer behaviour of the small eddies with an effect to produce more "warm" eddies in the LBLH and UBLH in the asymmetric wake case.

If an internal layer is defined from the intermittency distribution, as in the symmetric wake, its width δ_i is a good scale for γ (see Fig. 5.47). The values of δ_i are tabulated in Table IV with $y = \delta\gamma_{Ur}$ and $y = \delta\gamma_{Us}$ being the edges on the rough and smooth sides respectively and $\delta\gamma_U$ is the total width $\delta\gamma_{Ur} + \delta\gamma_{Us}$ for the case of the UBLH. $\delta\gamma_{Lr}$, $\delta\gamma_{Ls}$ and $\delta\gamma_L$ are defined similarly.

In the same table are the values of an inner wake width obtained from the perturbation of the conventional shear stress profile. It was necessary to discriminate the two edges of the inner wake since the edge on the "rough" side is not the symmetric image of the edge on

TABLE IV

INNER WAKE WIDTHS - ASYMMETRIC WAKE

I From Intermittency

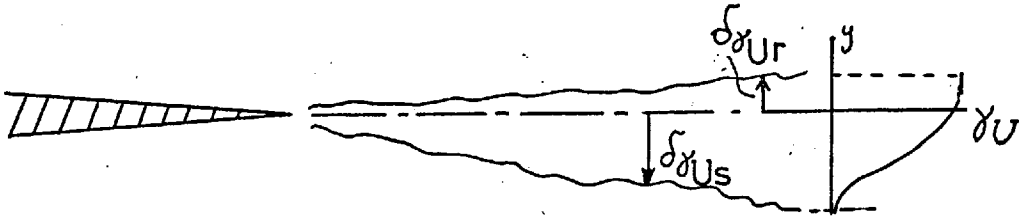

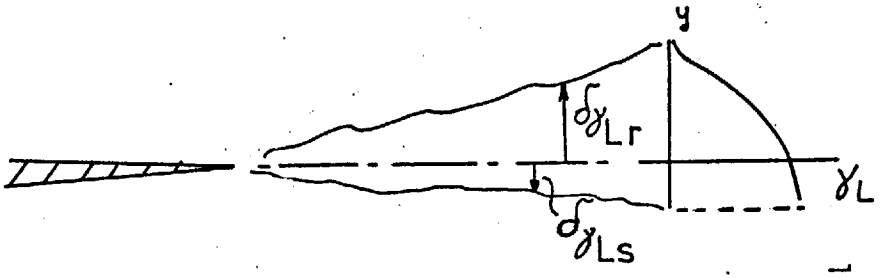

$(\delta_i =)\ \delta\gamma_U = \delta\gamma_{Ur} + \delta\gamma_{Us}$

$(\delta_i =)\ \delta\gamma_L = \delta\gamma_{Lr} + \delta\gamma_{Ls}$

δ_i	$\delta\gamma_{Ur}$ (mm)	$\delta\gamma_{Us}$ (mm)	$\delta\gamma_U$ (mm)	x (mm)	$\delta\gamma_{Lr}$ (mm)	$\delta\gamma_{Ls}$ (mm)	$\delta\gamma_L$ (mm)
	2.5	7.5	10	25	2.5	16	18
	4.0	18.0	22	100	4.0	30	34
	21.0	37.0	58	400	17.0	47	64

.... Contd.

TABLE IV (CONTD.)

II From Shear Stress

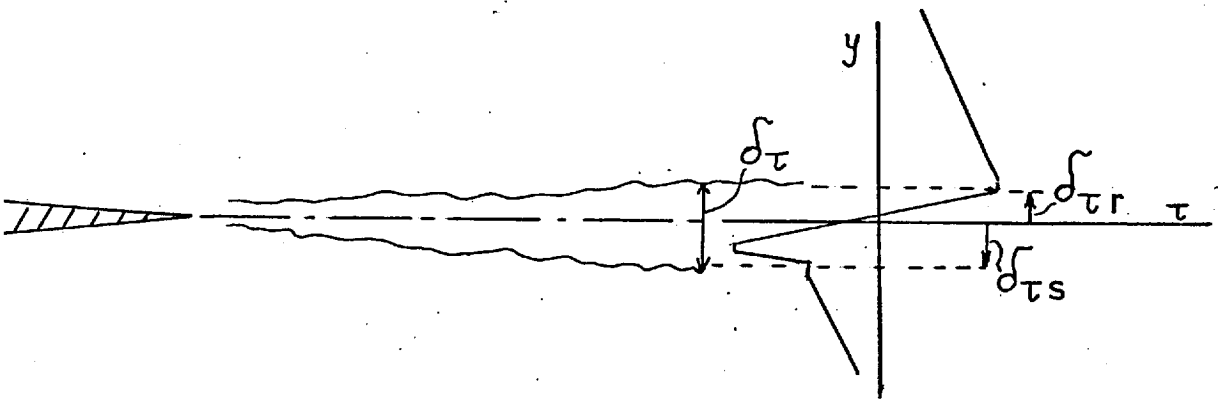

$$\delta_\tau = \delta_{\tau r} + \delta_{\tau s}$$

δ_i	$\delta_{\tau r}$ (mm)	$\delta_{\tau s}$ (mm)	δ_τ (mm)	x (mm)
	4	6	10	25
	11	14	25	100
	23	27	50	400

the "smooth" side with respect to the line y = 0. The inner wake widths defined from the intermittency and shear stress profiles are plotted in Fig. 5.13 of the earlier Section 5.1 together with those obtained from the mean velocity profiles, for direct comparison. Generally, the thermal layer (i.e. from intermittency) is wider than those of shear stress and mean velocity, as is also found at an ordinary edge, for well-known reasons. Another interesting point is that $\delta\gamma_{Ur} \simeq \delta\gamma_{Ls}$, which means that these two edges lie at symmetric positions with respect to y = 0, while the two other edges, $\delta\gamma_{Us}$ and $\delta\gamma_{Lr}$ tend to become symmetric at large x. The $\delta_{\tau r}$ seems to agree reasonably well for small x with the predictions using Bradshaw's relation, equation 5.4. The total width δ_τ (i.e. $\delta_{\tau r} + \delta_{\tau s}$) agrees quite well with the total $\delta_{\gamma U}$ (i.e. $\delta\gamma_{Ur} + \delta\gamma_{Us}$).

I UBLH Turbulent Quantities (Upper Boundary Layer Heated)

The conditional $\overline{u^2}$ intensities for the UBLH case are shown in Figs. 5.48 to 5.50. "Cold" contributions in the "hot" area, y > 0, are very small: at x = 25 mm, the intrusion of the "cold" region over the centre-line is about the same as in the symmetric wake but for x = 100 and 400 mm, it is greater. Generally, it seems that only a small amount of kinetic energy of the lower "cold" unmixed fluid is transported across the centre-line into the upper (rough wall) fluid.

The same behaviour characterizes the $\overline{v^2}$ intensities which are plotted in Figs. 5.51 to 5.53 but the intrusion of "cold" fluid into the region y > 0 carries rather more from $\overline{v^2}$ than $\overline{u^2}$.

Figs. 5.54 to 5.56 display the shear stress profiles. Again here, upper "hot" fluid changes its sign of $\overline{uv}$ inside the "hot" region y > 0 and has already started to mix with the "cold" fluid and so becoming less "hot" while the "cold" fluid which is entirely non-mixed

crosses the centre-line without any change in the shear stress sign.

It is dangerous to think of separate transport equations for "cold" and "hot" contributions to Reynolds stress because there may be a large transfer term; in particular, one should not think of $\overline{v_c^2}\,\partial U/\partial y$ as the only source term in the $\overline{uv_c}$ transport equation. However, it is noteworthy that the intrusion of "cold" fluid into a region of reversed $\partial U/\partial y$ on the "rough" side of the wake does not result in a reversal of sign of $\overline{uv_c}$ whereas in Dean and Bradshaw's duct flow, it did (see also results below for the LBLH case).

The $\overline{u^3}$ distribution in Figs. 5.57 to 5.59 shows the same behaviour as in the symmetric case which was interpreted in Section 4.3.1 as short bursts followed by long intervals of opposite-sign small u fluctuations. The bursts of "cold" fluid in the "cold" zone are going inwards towards the centre-line and they seem to increase in amplitude with x up to x = 100 mm, quite opposite to the trend in the symmetric case, and then to decrease at the same rate as in the symmetric case.

The $\overline{v^3}$ profiles are displayed in Figs. 5.60 to 5.62. The "cold" fluid in the "cold" zone again shows sweeps for $y < 0$, so kinetic energy is transferred in towards the upper fluid. The same happens to the $\overline{u^2}$ component of the kinetic energy, as is shown by the $\overline{u^2v}$ distribution in Figs. 5.63 to 5.65.

In the $\overline{uv^2}$ profiles presented in Figs. 5.66 to 5.68, the same behaviour can be observed. Shear stress from the "cold" fluid is transferred by v towards the centre-line.

II LBLH Turbulent Quantities (Lower Boundary Layer Heated)

In Figs. 5.69 to 5.71, the $\overline{u^2}$ intensities are plotted. It is obvious that "cold" (unmixed) fluid, the upper (rough wall) fluid now,

has higher turbulent kinetic energy than the lower fluid (as has been shown previously in Fig. 5.14) which seems to drop with x. The $\overline{v^2}$ intensities in Figs. 5.72 to 5.74 show the same behaviour.

The $\overline{uv}$ plots in Figs. 5.75 to 5.77 indicate something different: a non monotonic approach to zero of the "cold" fluid shear stress, inside the "hot" zone. This means that there is still "cold" fluid inside the "hot" layer, which has not been mixed up with the "hot" fluid but the latter has imposed its own sign of shear stress on it. This is quite evident in x = 25 mm and x = 400 mm, while in x = 100 mm, it is not clearly shown. Recall that the "cold" $\overline{uv}$ in the UBLH case approached zero monotonically.

In Figs. 5.78 to 5.80 are the $\overline{u^3}$ distributions. They all indicate the presence of spikes or bursts of much higher amplitude in the upper (rough wall) fluid than in the lower fluid, travelling inwards again, but their amplitude seems to drop with x quicker than that in the lower fluid (compare Figs. 5.57 - 5.59).

The $\overline{v^3}$ profiles in Figs. 5.81 to 5.83 show a similar behaviour: sweeps of "cold" fluid inside the "cold" zone y > 0.

In Figs. 5.84 to 5.86 are the $\overline{u^2v}$ distributions. They indicate an inwards transport of u^2 much more than the amount of u^2 being transported outwards, i.e. overall, the kinetic energy is transported from the "cold" zone to the "hot" or lower fluid.

"Cold" fluid shear stress is transported by v fluctuation inwards, as with the kinetic energy, as can be seen in Figs. 5.87 to 5.89 where the $\overline{uv^2}$ is displayed.

In conclusion, it can be said that both upper and lower fluid transport kinetic energy and shear stress towards the centre-line; the amounts transported being greater in the upper fluid.

5.3.2 "Warm" or Mixed Fluid Averages

In the symmetric wake, the "warm" averages were estimated by invoking the symmetry of the flow. In the asymmetric wake, for the determination of the "warm" average, it was necessary to change over the heat supply to deduce any given average. Warm = Hot_{Up} - $Cold_{Lower}$ or Warm = Hot_{Lower} - $Cold_{Up}$ (see Section 3.2).

From the results which are plotted in Figs. 5.90 to 5.97, mainly for x = 25 mm and 100 mm, it is obvious that the "warm" fluid behaves like an isolated wake, as in the symmetric case, but is generally much thicker than in the symmetric case.

The agreement of the results between the two ways of deducing the "warm" averages is quite good. Where the agreement is poor, it is mainly due to the inexact coincidence of the conventional averages, especially in the triple products.

The $\overline{u_w^2}$ peak on the rough side drops very quickly with x, more quickly than the peak in the smooth side.

The $\overline{v_w^2}$ has only one peak which drops with x. Its behaviour is similar to the symmetric v_w^2 and to $\overline{v^2}$ in an isolated wake.

The peaks in $\overline{uv_w}$ drop more or less like the peaks of $\overline{u_w^2}$.

The $\overline{v_w^3}$ behaviour is rather different from an isolated wake. The shape is the opposite of the $\overline{v^3}$ distribution of an isolated wake for 4 mm < y < 12 mm, i.e. there is an outwards transport of v_w^2 while in the conventional wake, there is an inward transport. In addition, positive $\overline{v_w^3}$ for y > 0 means that there are bursts going outwards while purely "cold" fluid indicates large ingoing sweeps. Exactly similar behaviour with the symmetric $\overline{v_w^3}$: large eddy sweeps probably propel the bursts of small eddies.

The $\overline{u^2 v_w}$ profile suggests again that generally there is a transport of kinetic energy of small eddies outwards except for a small

region near the centre-line where there is a probably small transport of kinetic energy inwards.

The $\overline{uv}_w$ is transported by v outwards near the edges of the inner wake but there is inward transport very close to the centre-line.

5.4 Conclusion to the Conditionally Sampled Results

In this chapter, the results of the conditionally sampled measurements in the asymmetric wake have been presented as "hot" (i.e. "fully hot" plus "warm"), "cold" and "warm" contributions to the total conventional averages.

The behaviour of the asymmetric wake is quite similar to that of the symmetric. The "inner" wake here is rather thicker and generally the changes are stronger. The large eddies from either side transport kinetic energy and shear stress towards the centre-line while the small eddies near the centre-line seem to do the opposite. Large eddy sweeps in the upper and lower fluid push up and down the bursts of "warm" fluid (necessarily composed of small eddies) in the thin mixed region.

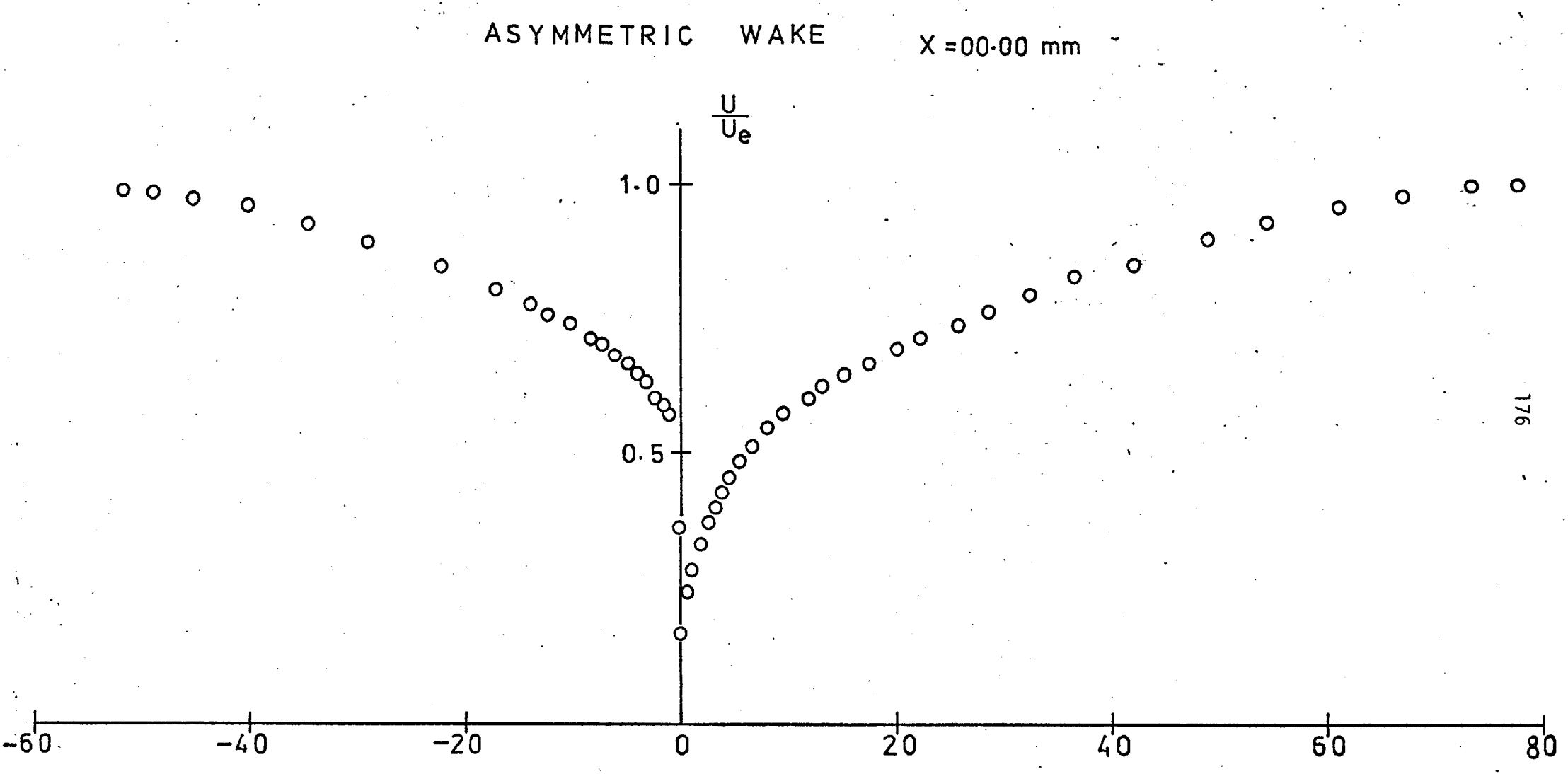

FIG. 5.1 MEAN VELOCITY PROFILE AT x = 0

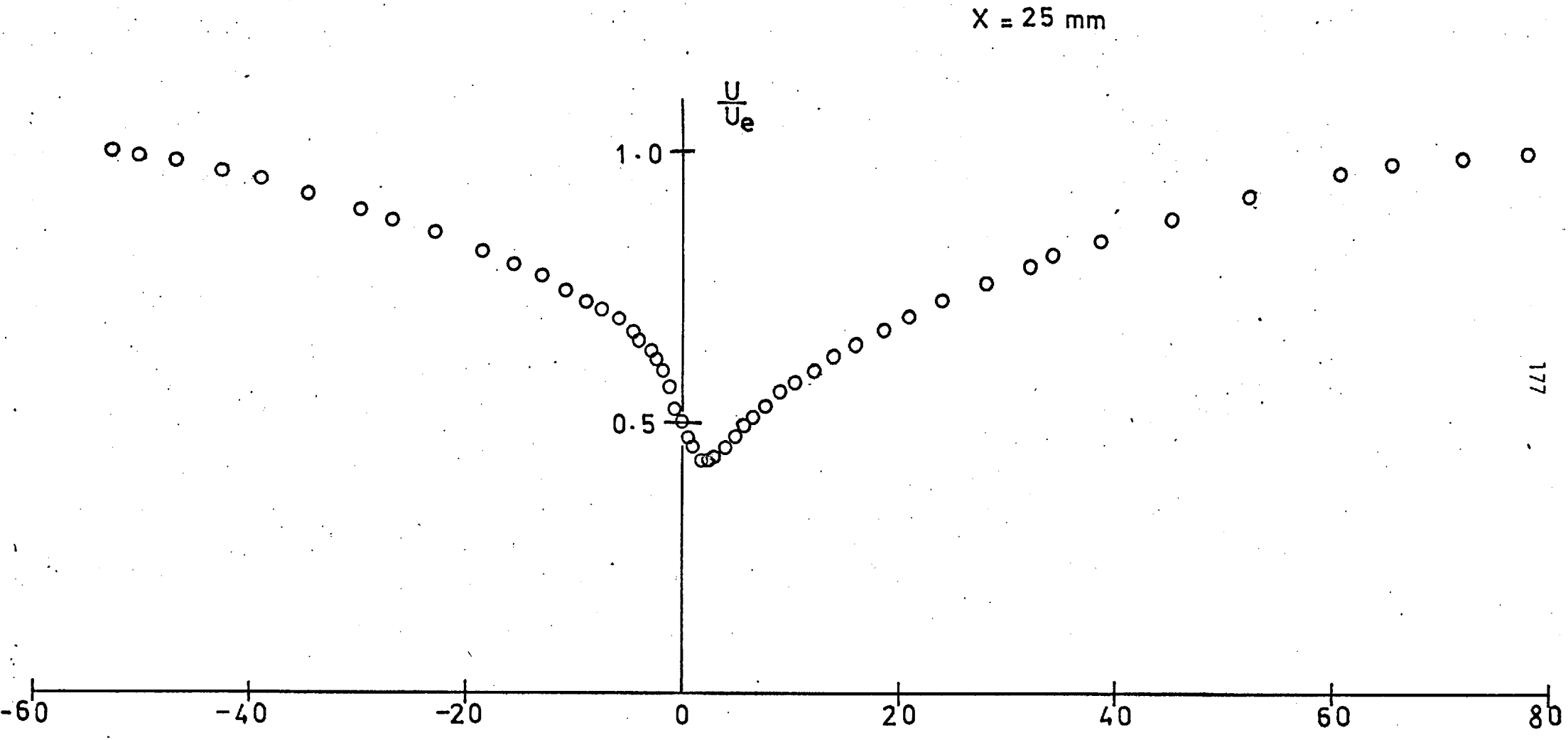

FIG. 5.2 MEAN VELOCITY PROFILE AT x = 25 mm.

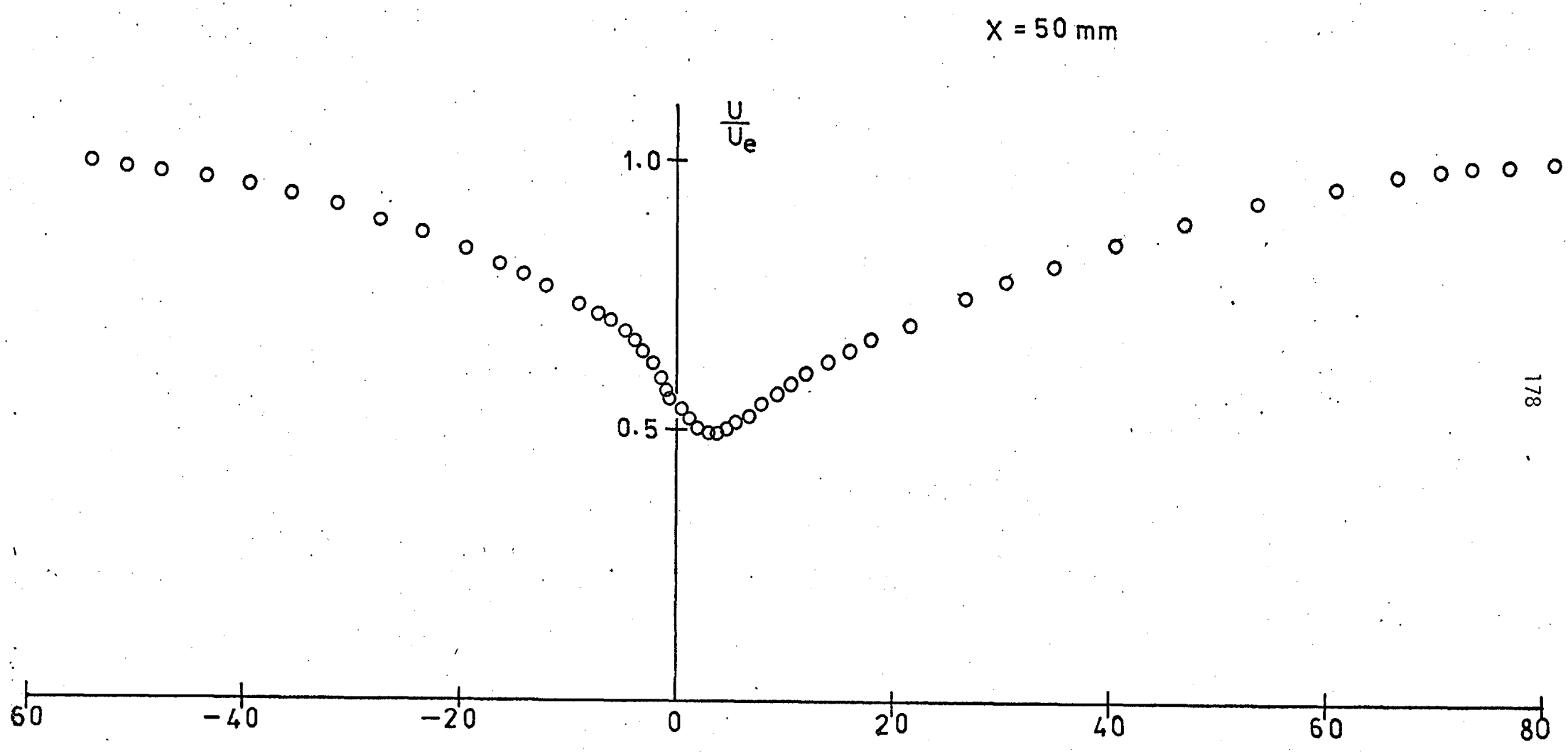

FIG. 5.3 MEAN VELOCITY PROFILE AT x = 50 mm.

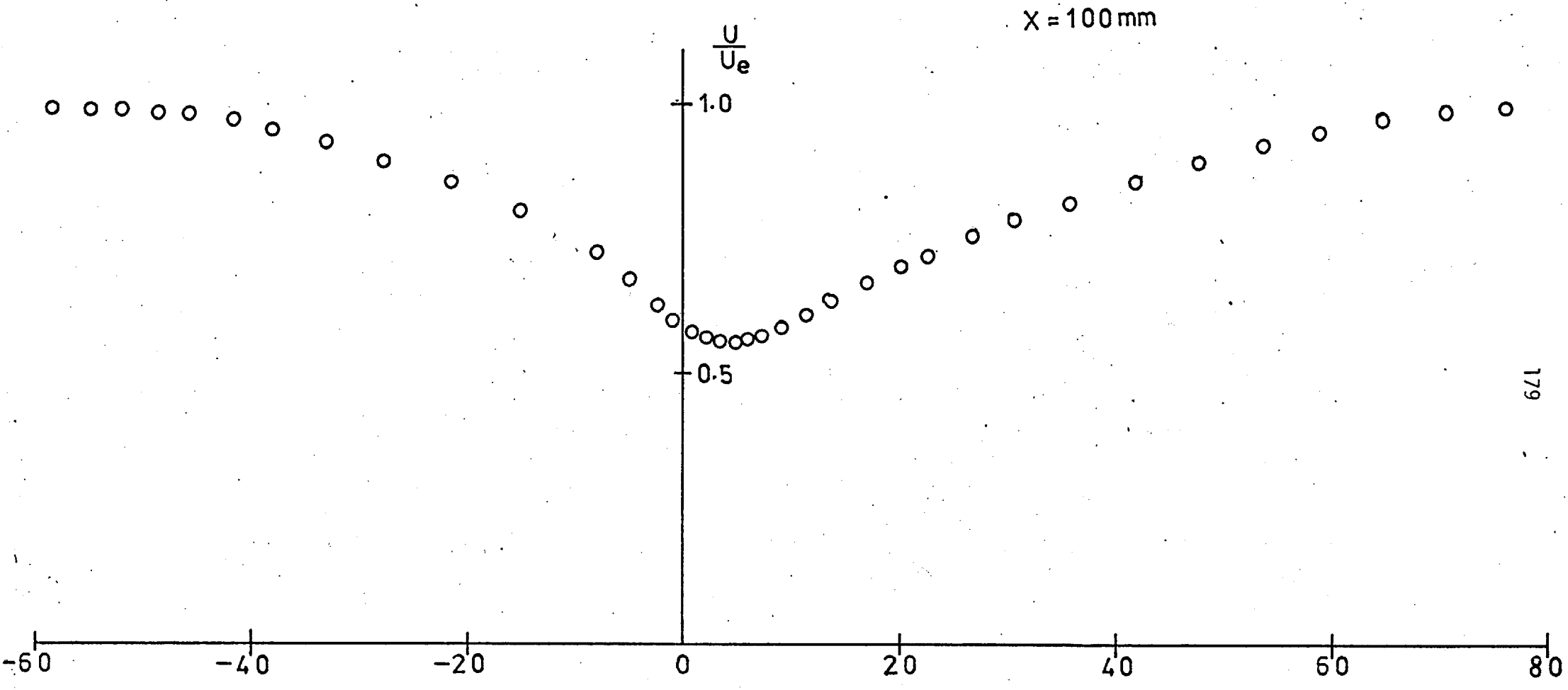

FIG. 5.4 MEAN VELOCITY PROFILE AT x = 100 mm.

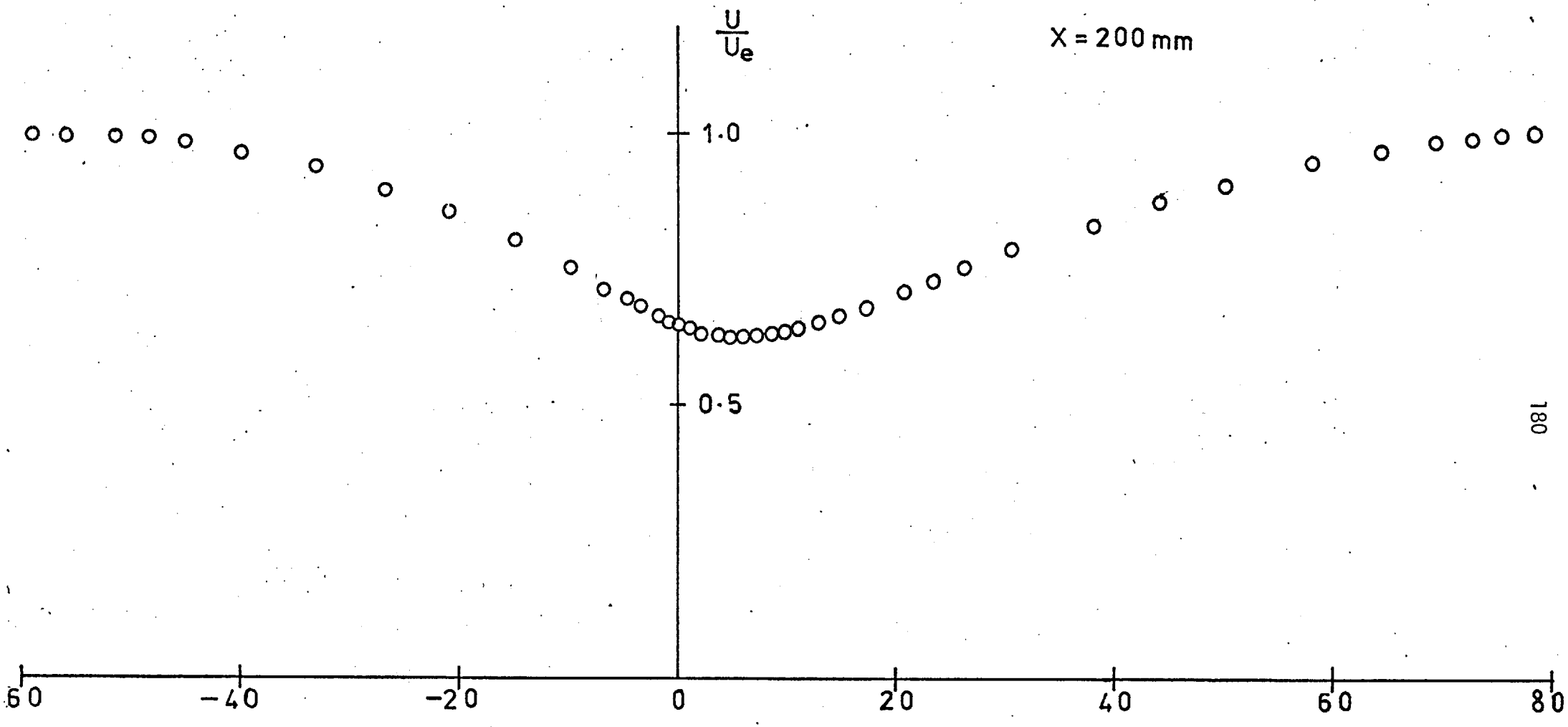

FIG. 5.5 MEAN VELOCITY PROFILE AT x = 200 mm.

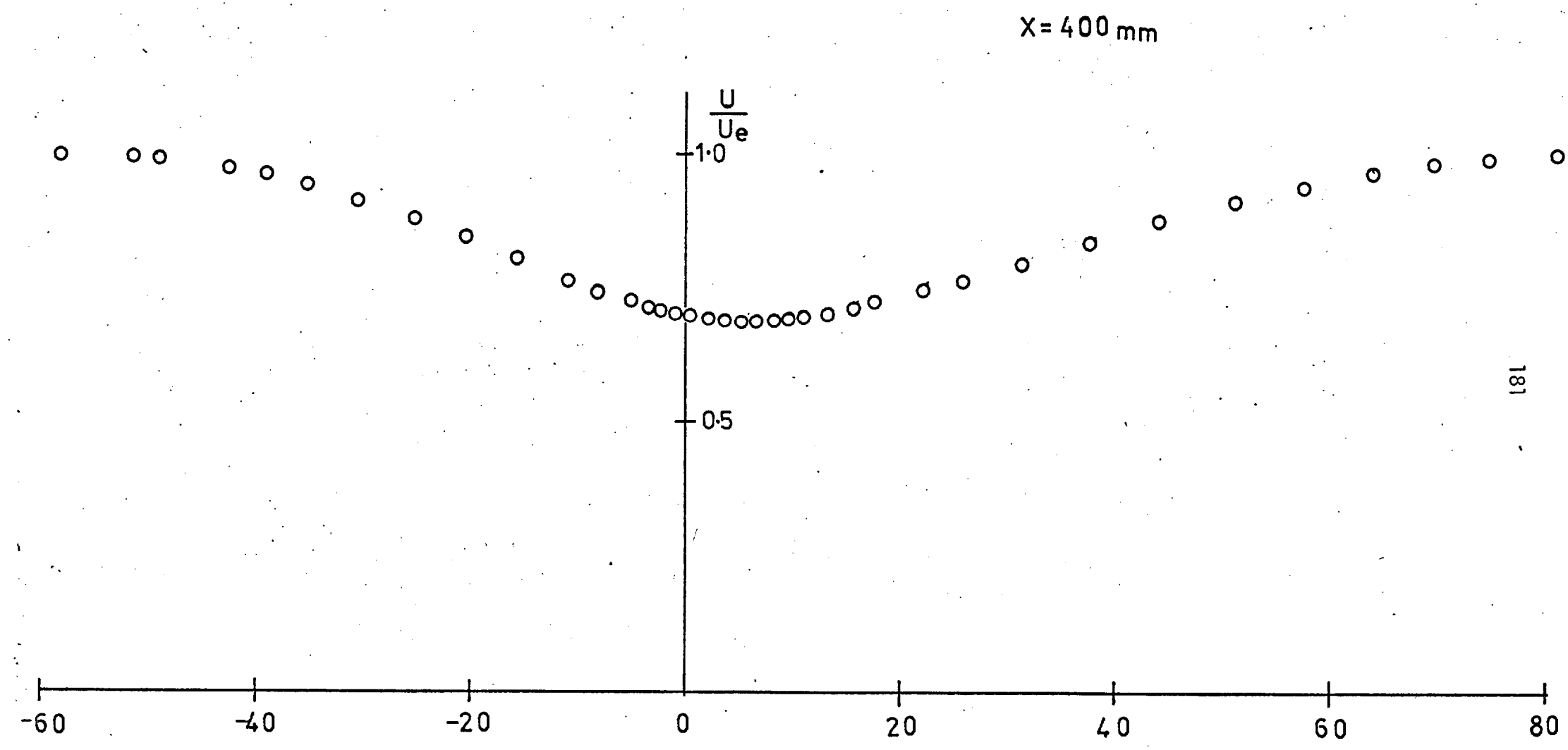

FIG. 5.6 MEAN VELOCITY PROFILE AT x = 400 mm.

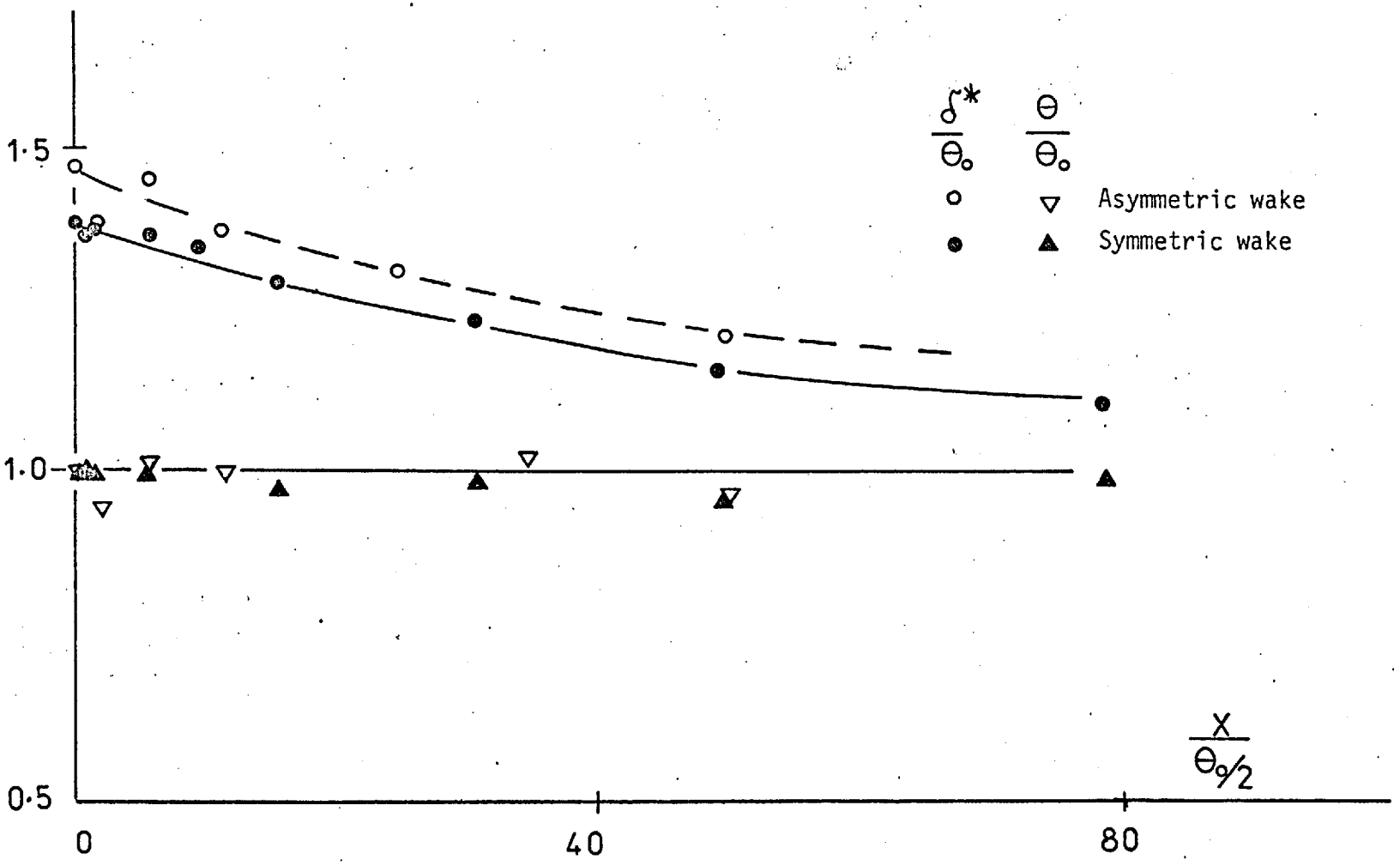

FIG. 5.7 STREAMWISE VARIATION OF δ* and θ

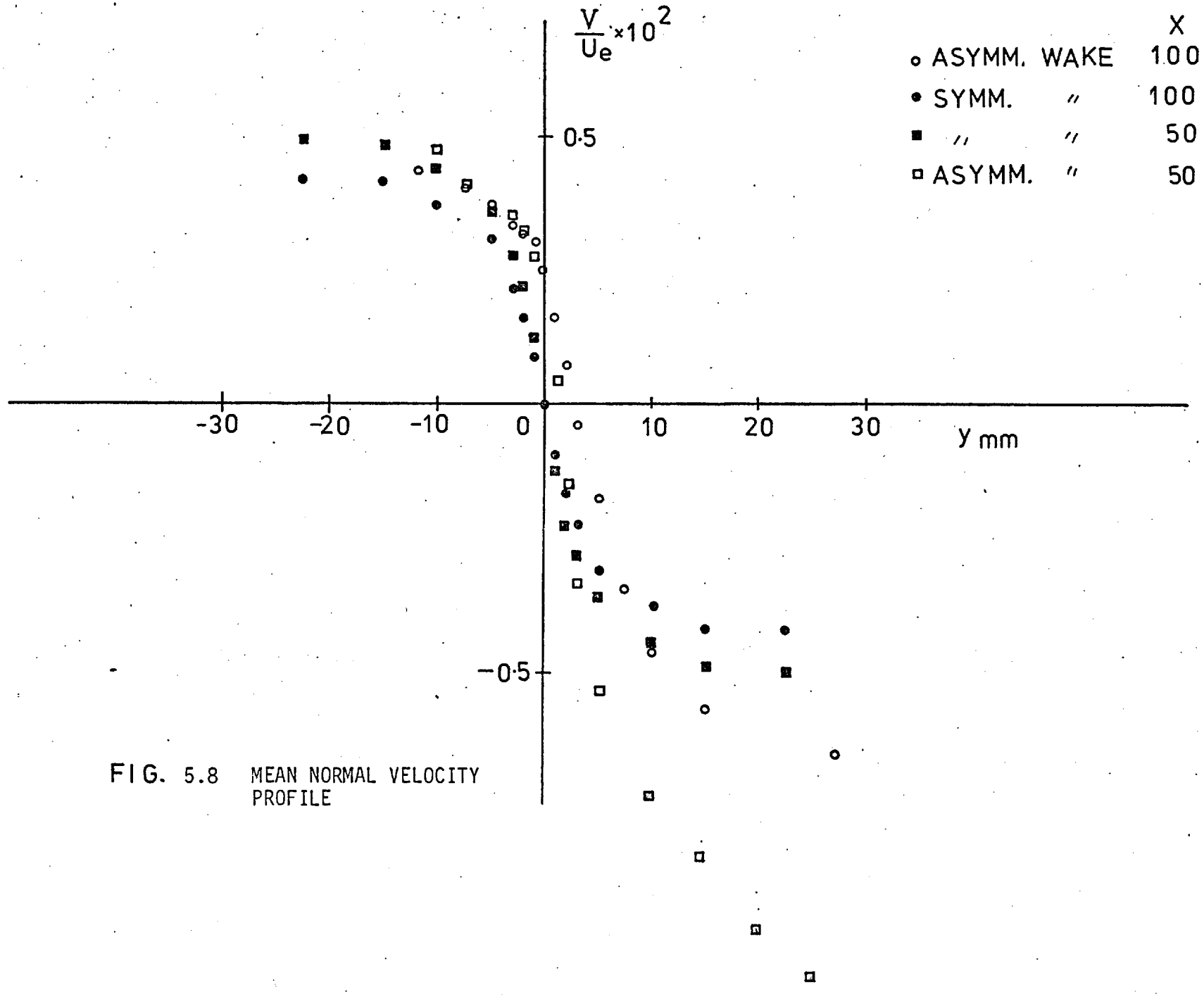

FIG. 5.8 MEAN NORMAL VELOCITY PROFILE

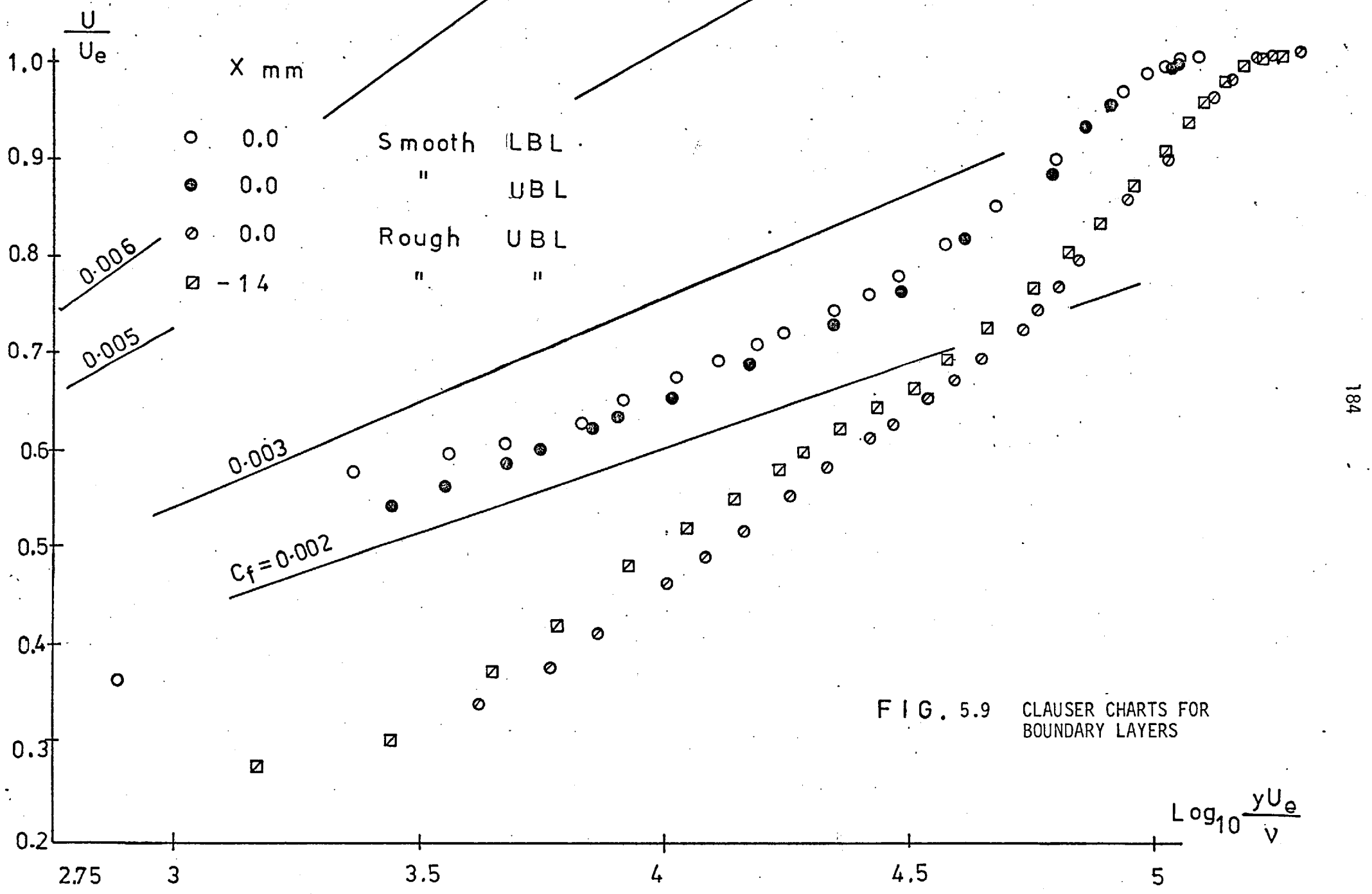

FIG. 5.9 CLAUSER CHARTS FOR BOUNDARY LAYERS

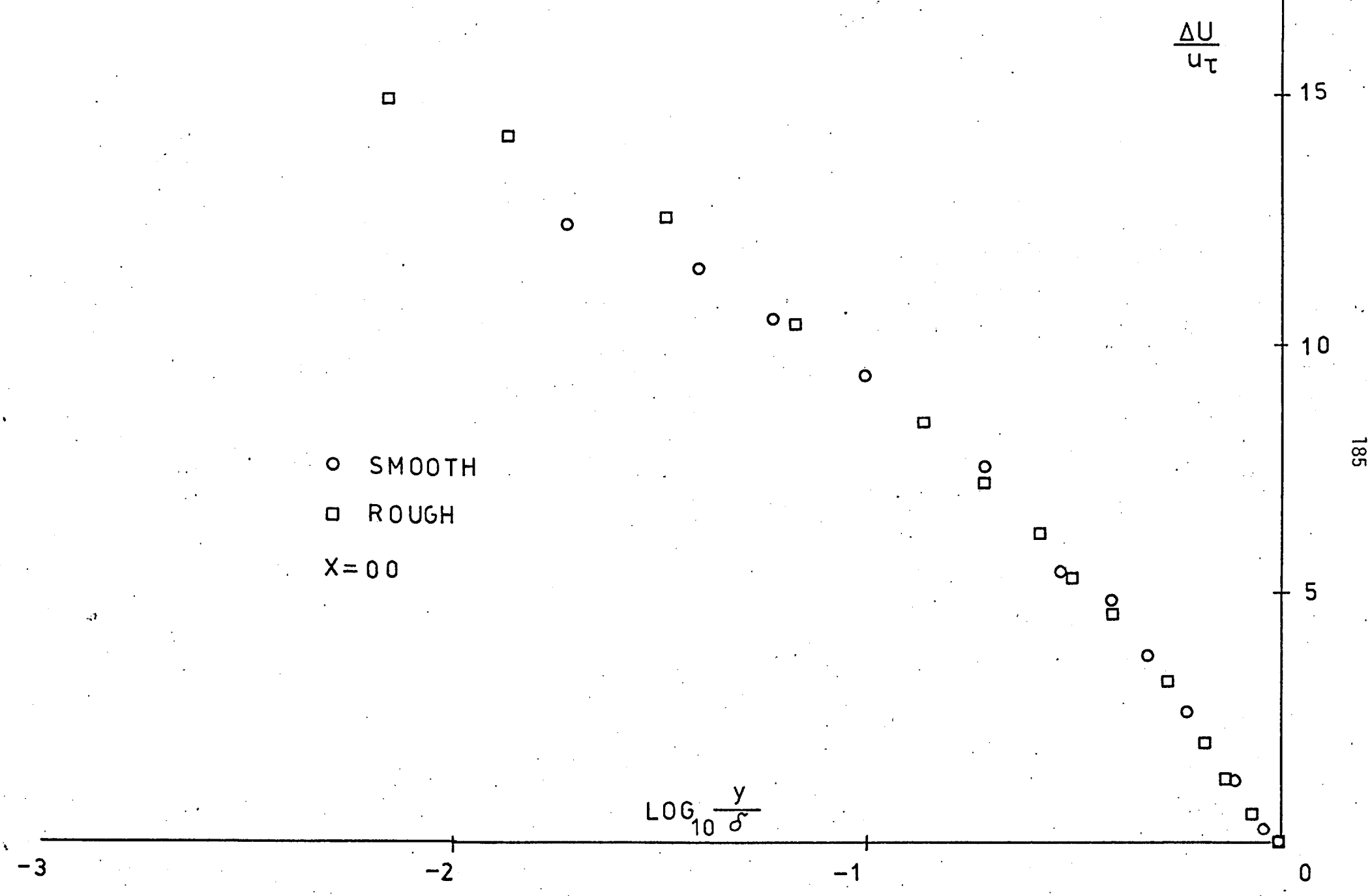

FIG. 5.10 SEMI-LOG VELOCITY PROFILES. OUTER LAYER SCALING

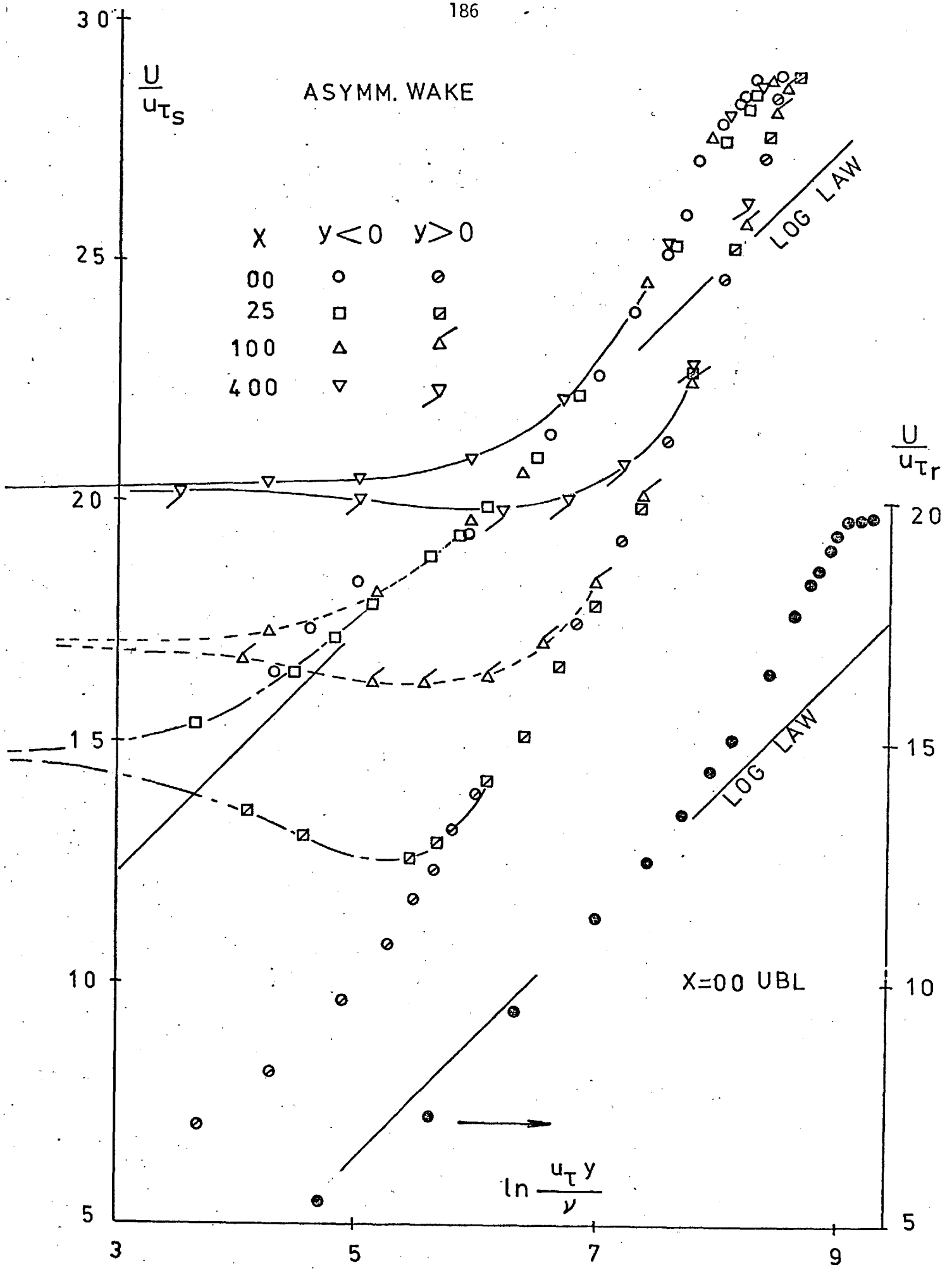

FIG. 5.11 MEAN VELOCITY PROFILE
INNER LAYER SCALING

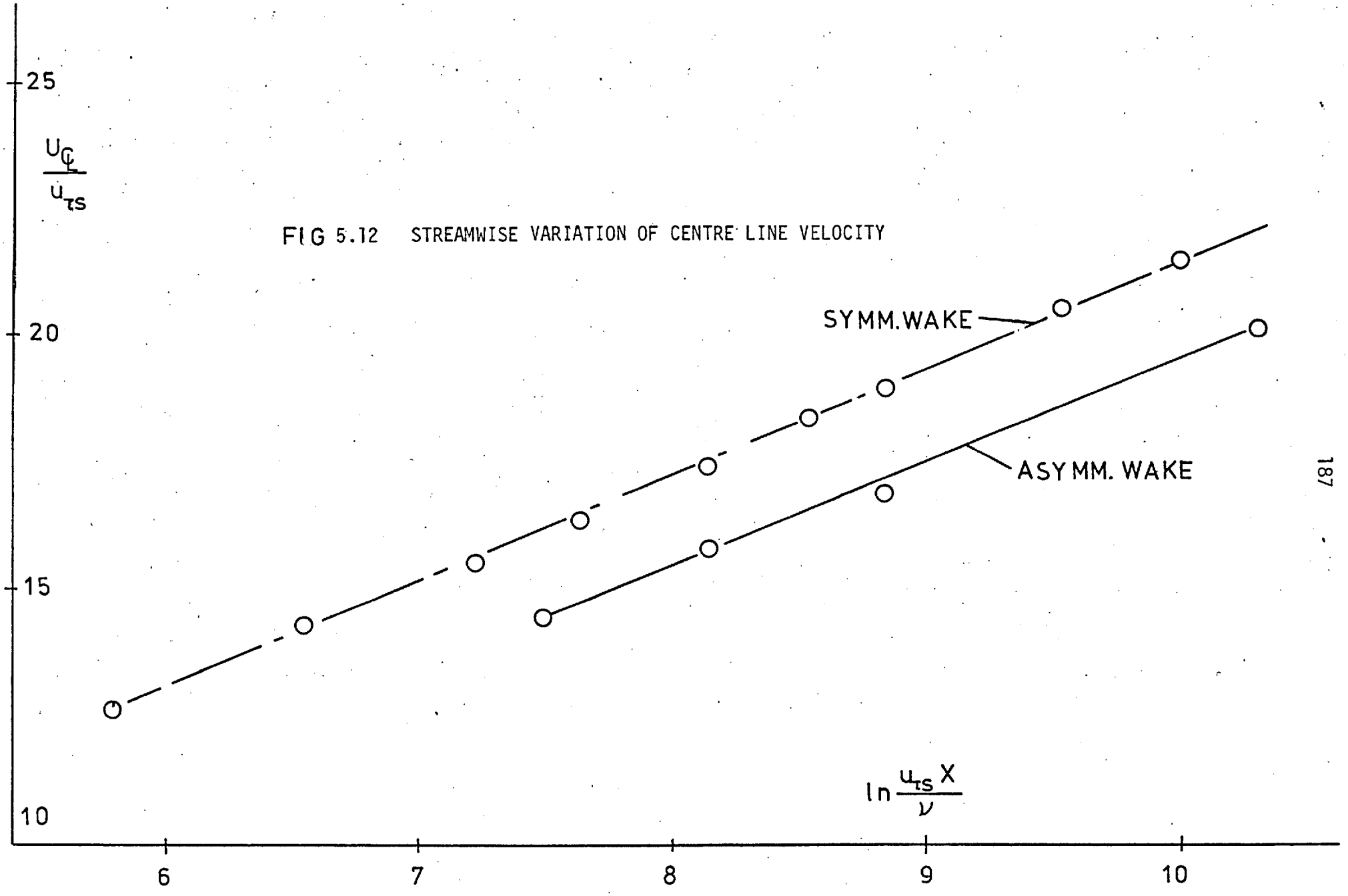

FIG 5.12 STREAMWISE VARIATION OF CENTRE LINE VELOCITY

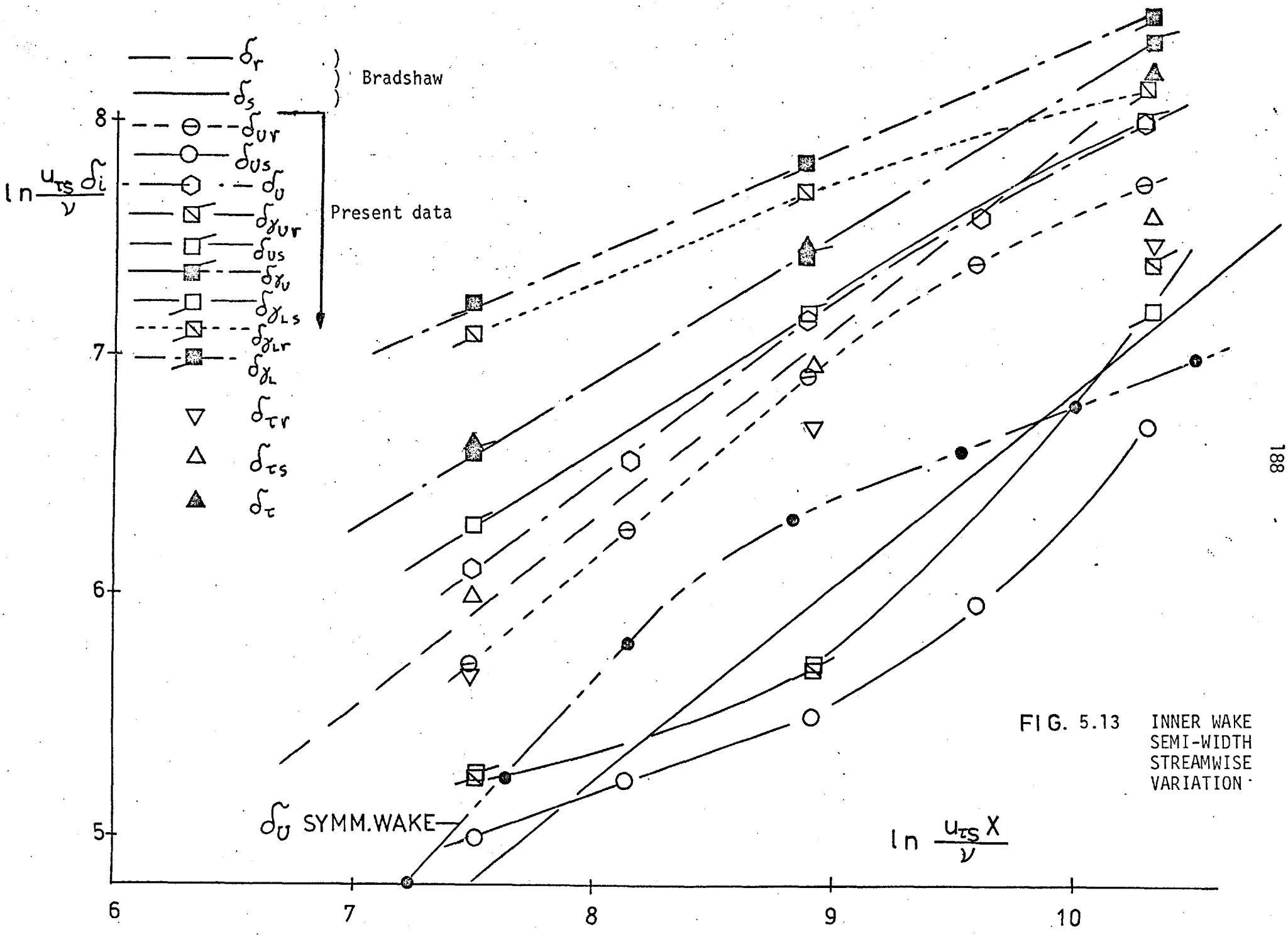

FIG. 5.13 INNER WAKE SEMI-WIDTH STREAMWISE VARIATION

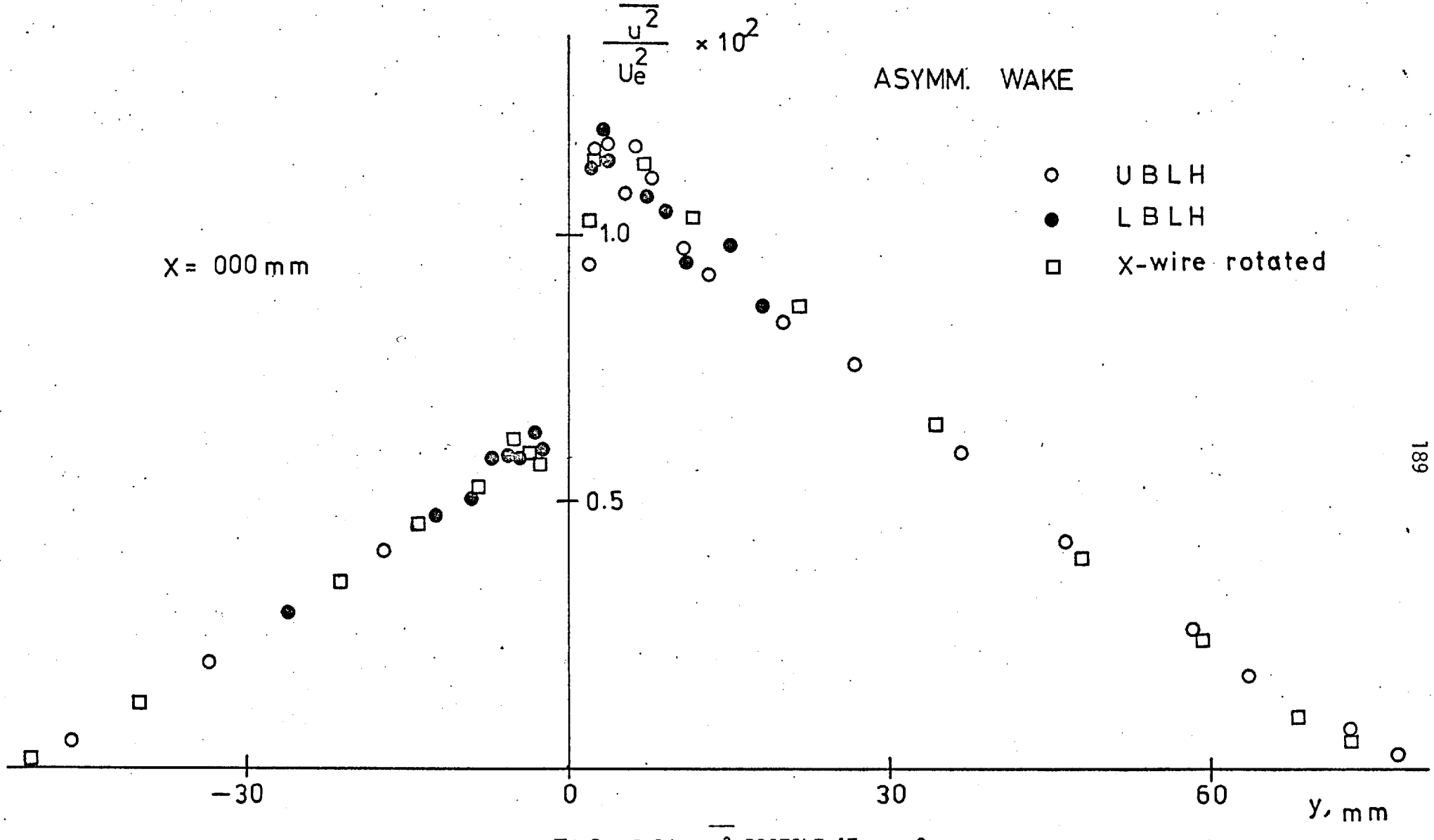

FIG. 5.14 $\overline{u^2}$ PROFILE AT x = 0 mm.

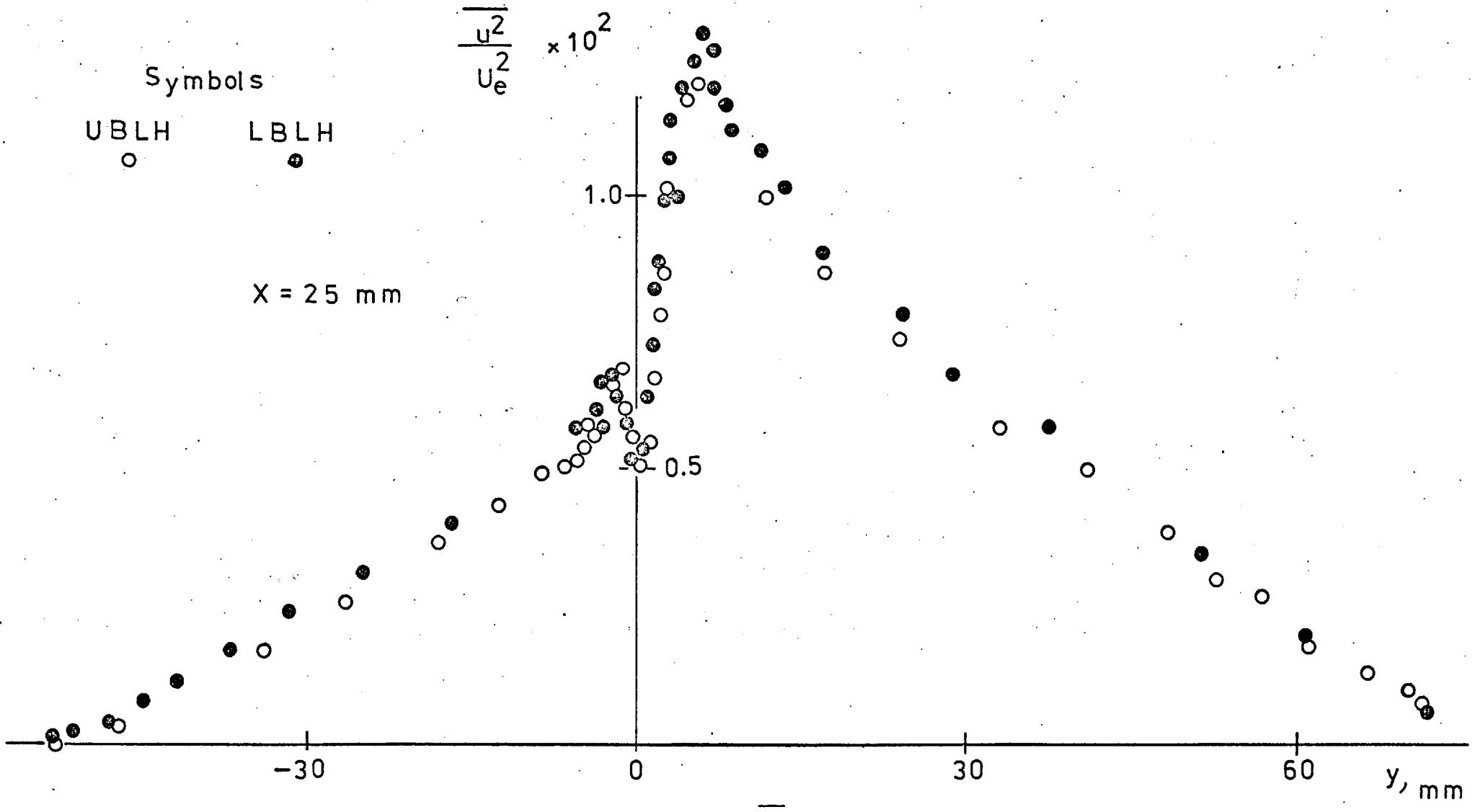

FIG. 5.15 $\overline{u^2}$ PROFILE AT x = 25 mm.

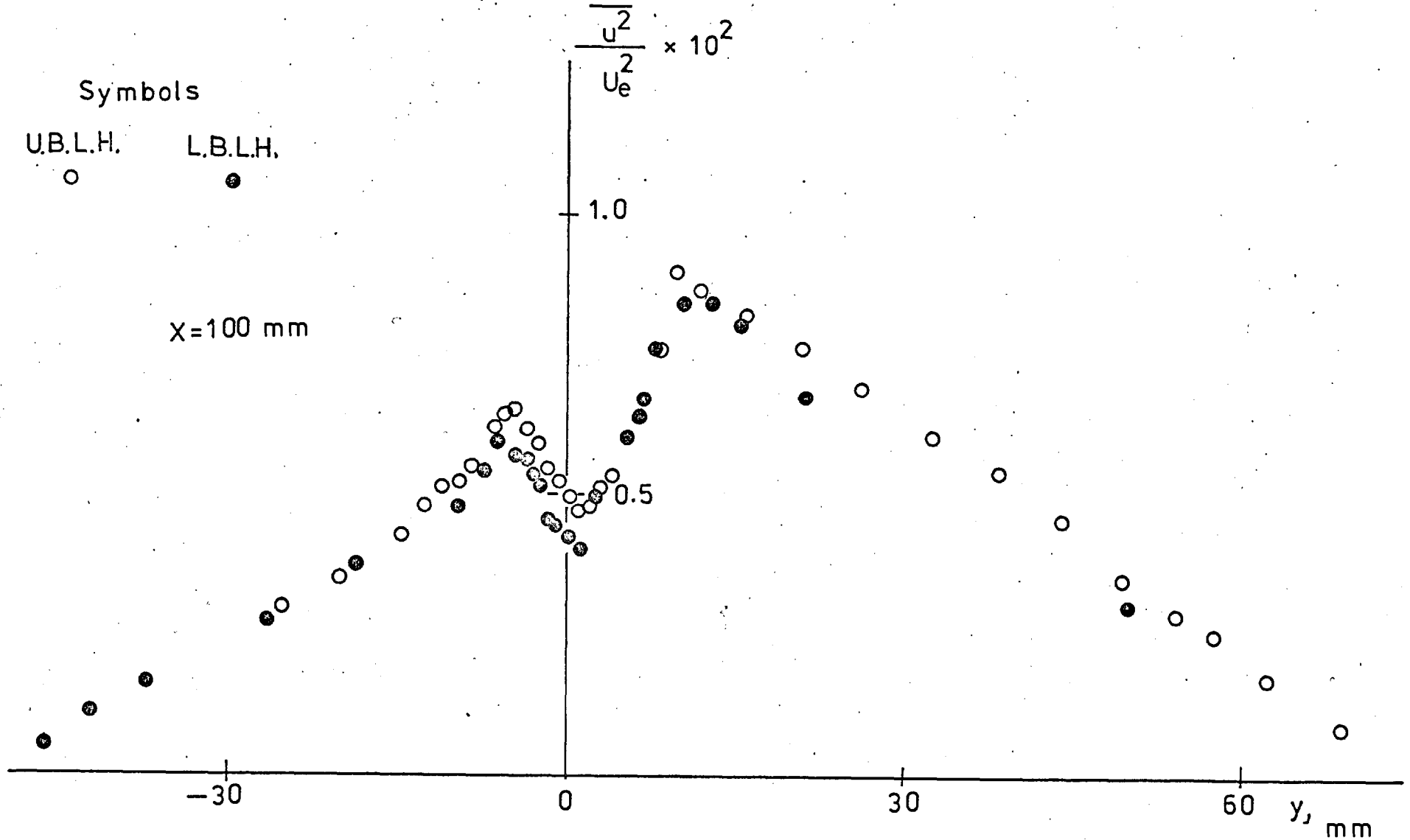

FIG. 5.16 $\overline{u^2}$ PROFILE AT x = 100 mm.

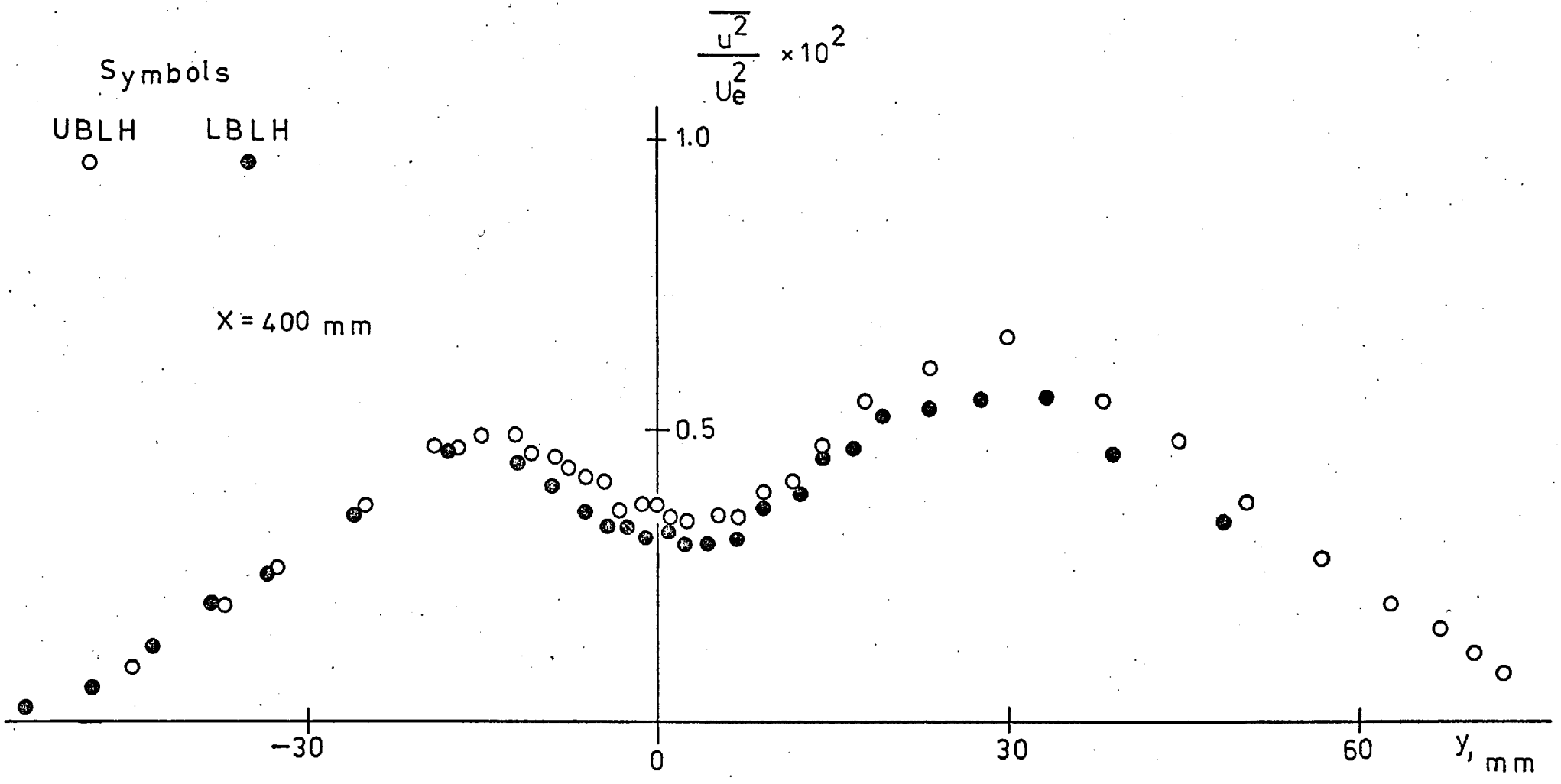

FIG. 5.17 $\overline{u^2}$ PROFILE AT x = 400 mm.

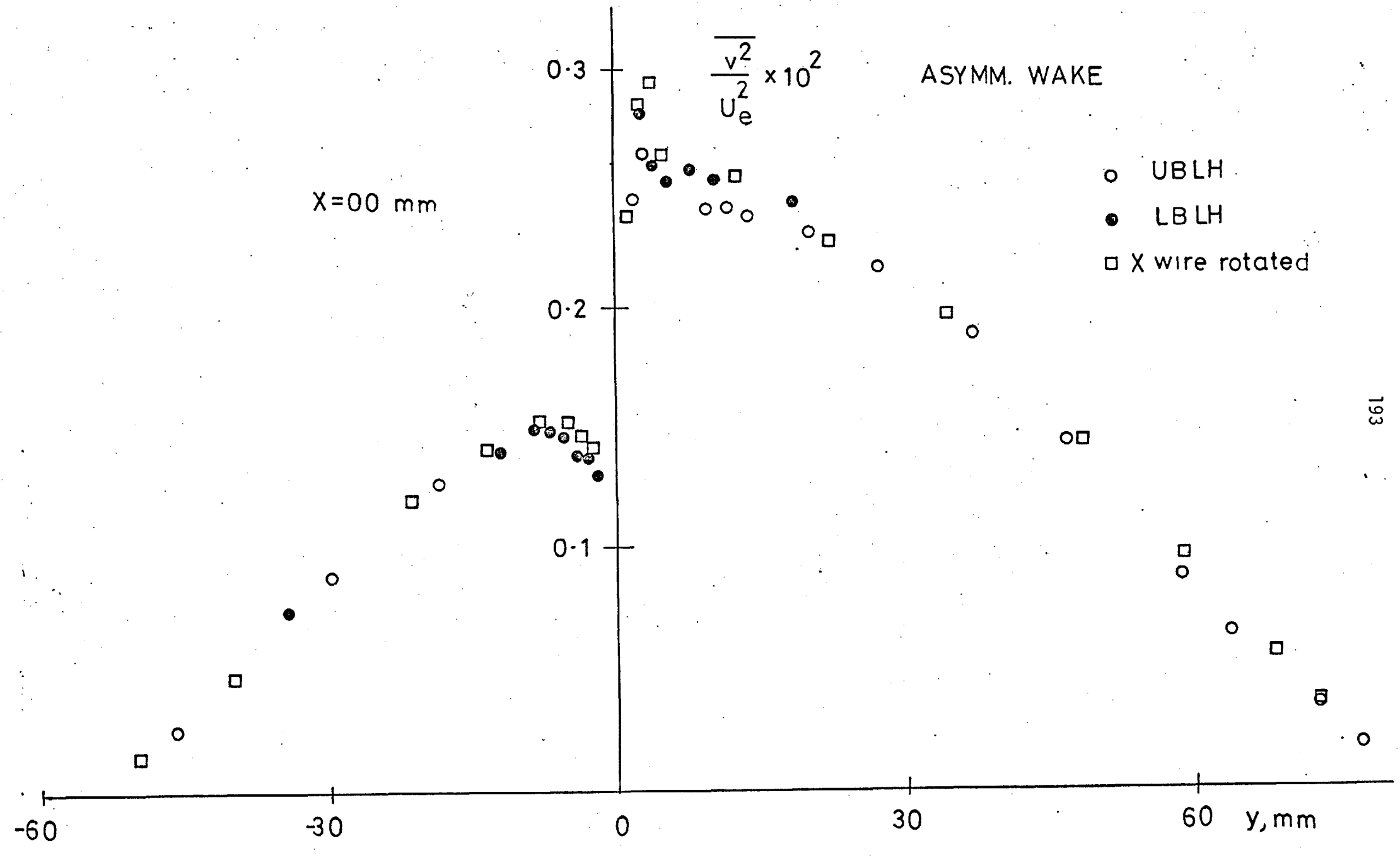

FIG 5.18 $\overline{v^2}$ PROFILE AT x = 0 mm.

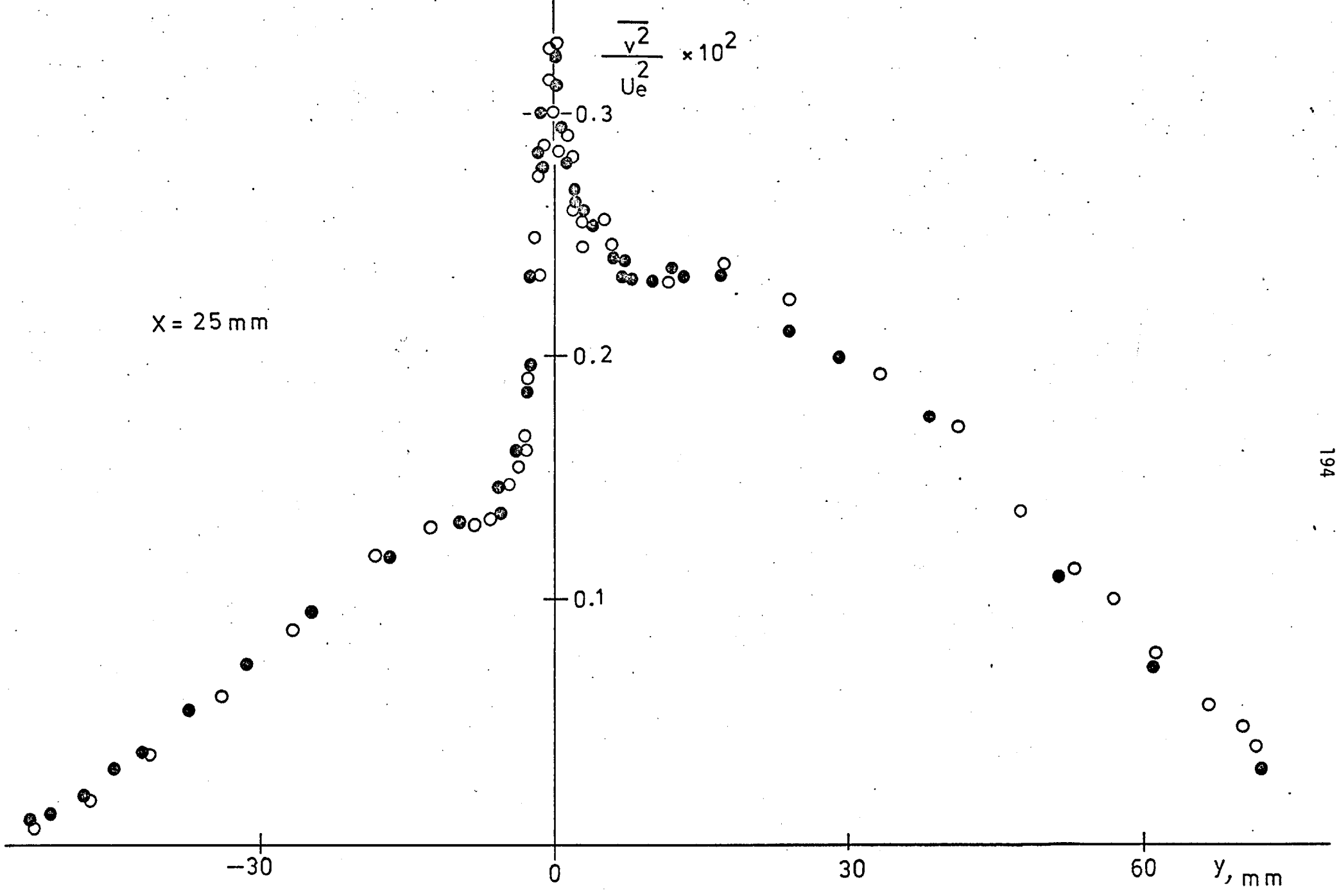

FIG. 5.19 $\overline{v^2}$ PROFILE AT x = 25 mm.

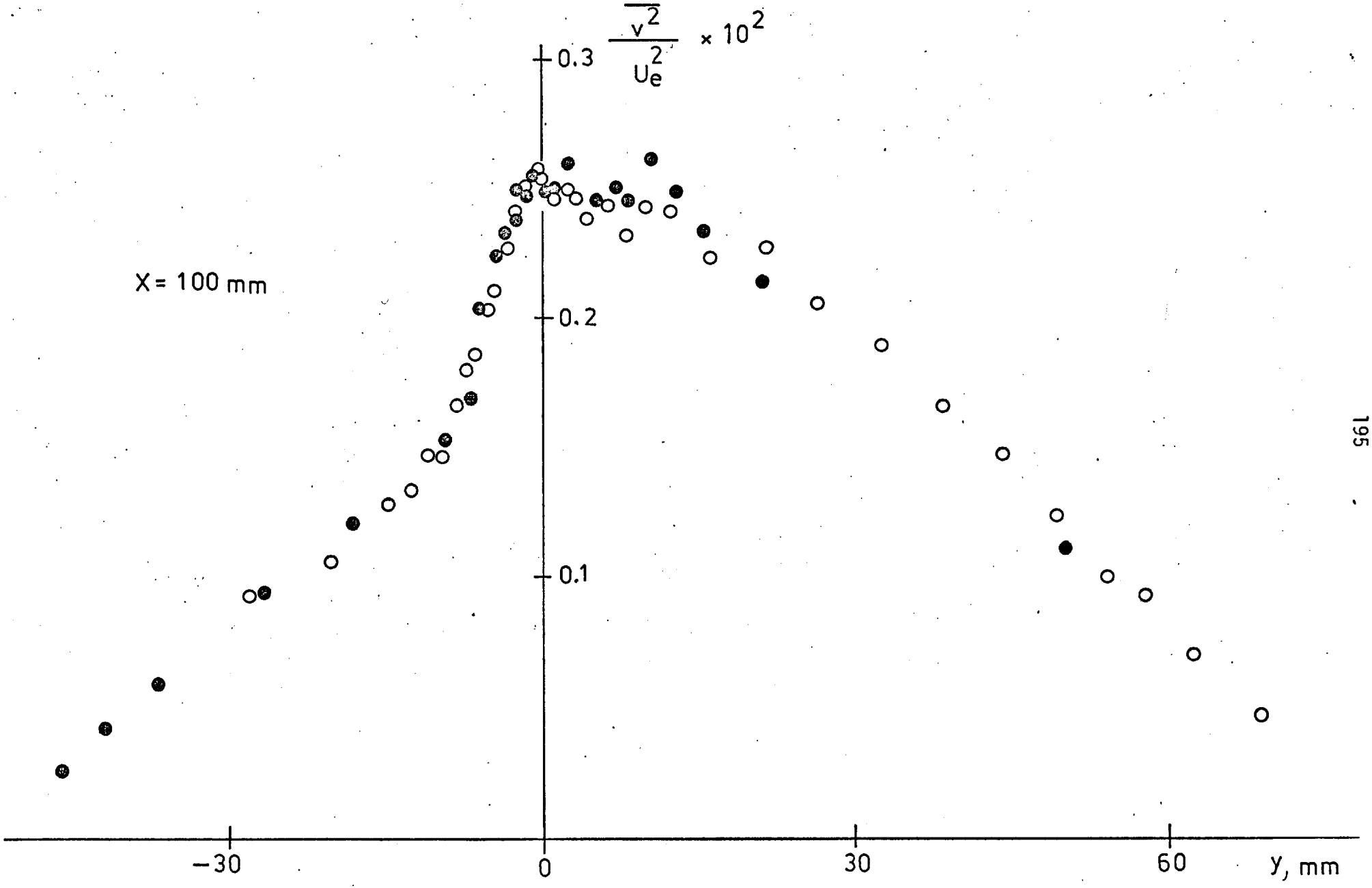

FIG. 5.20 $\overline{v^2}$ PROFILES AT x = 100 mm.

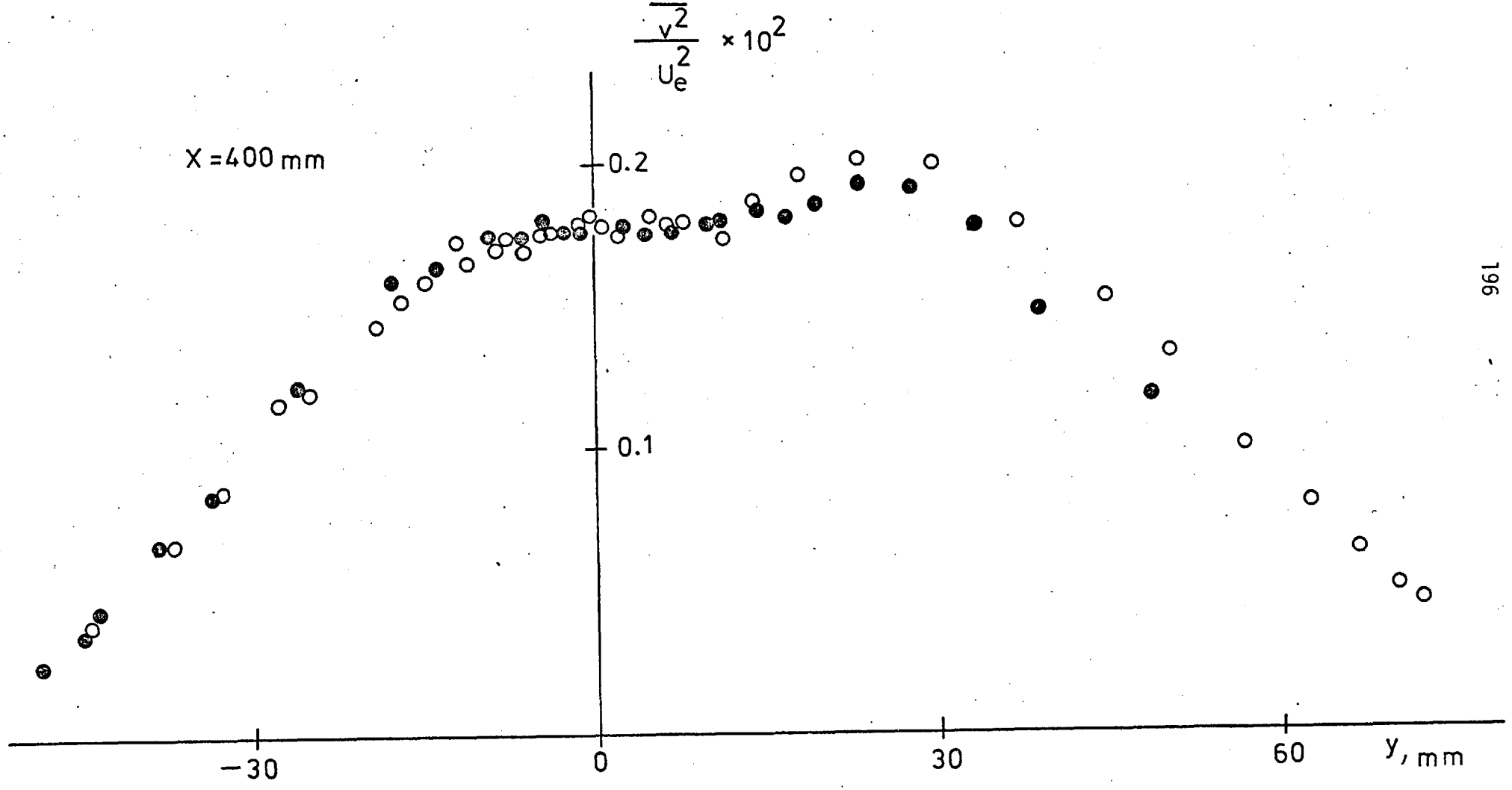

FIG. 5.21 $\overline{v^2}$ PROFILE AT x = 400 mm.

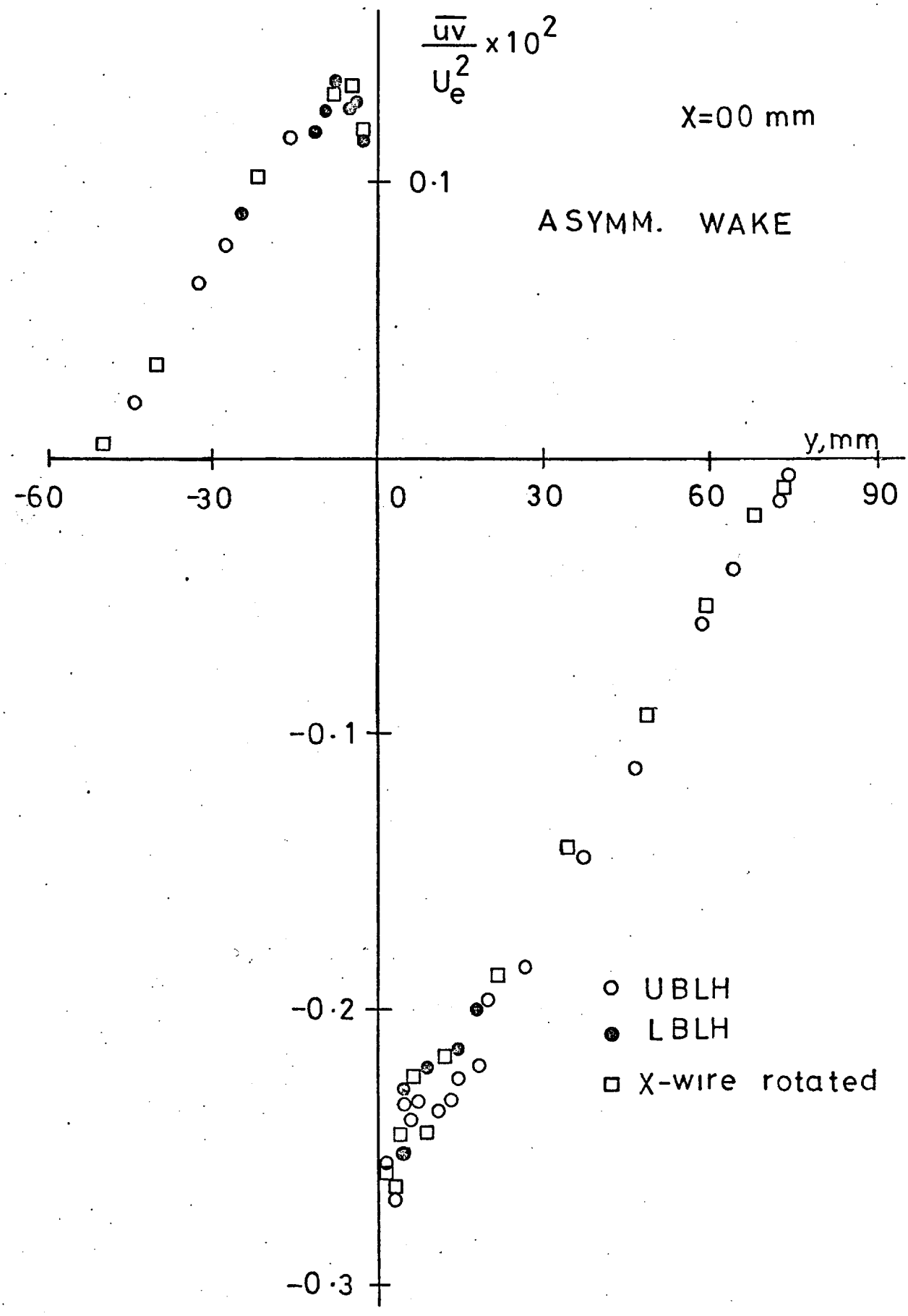

FIG. 5.22 SHEAR STRESS PROFILE AT x = 0 mm.

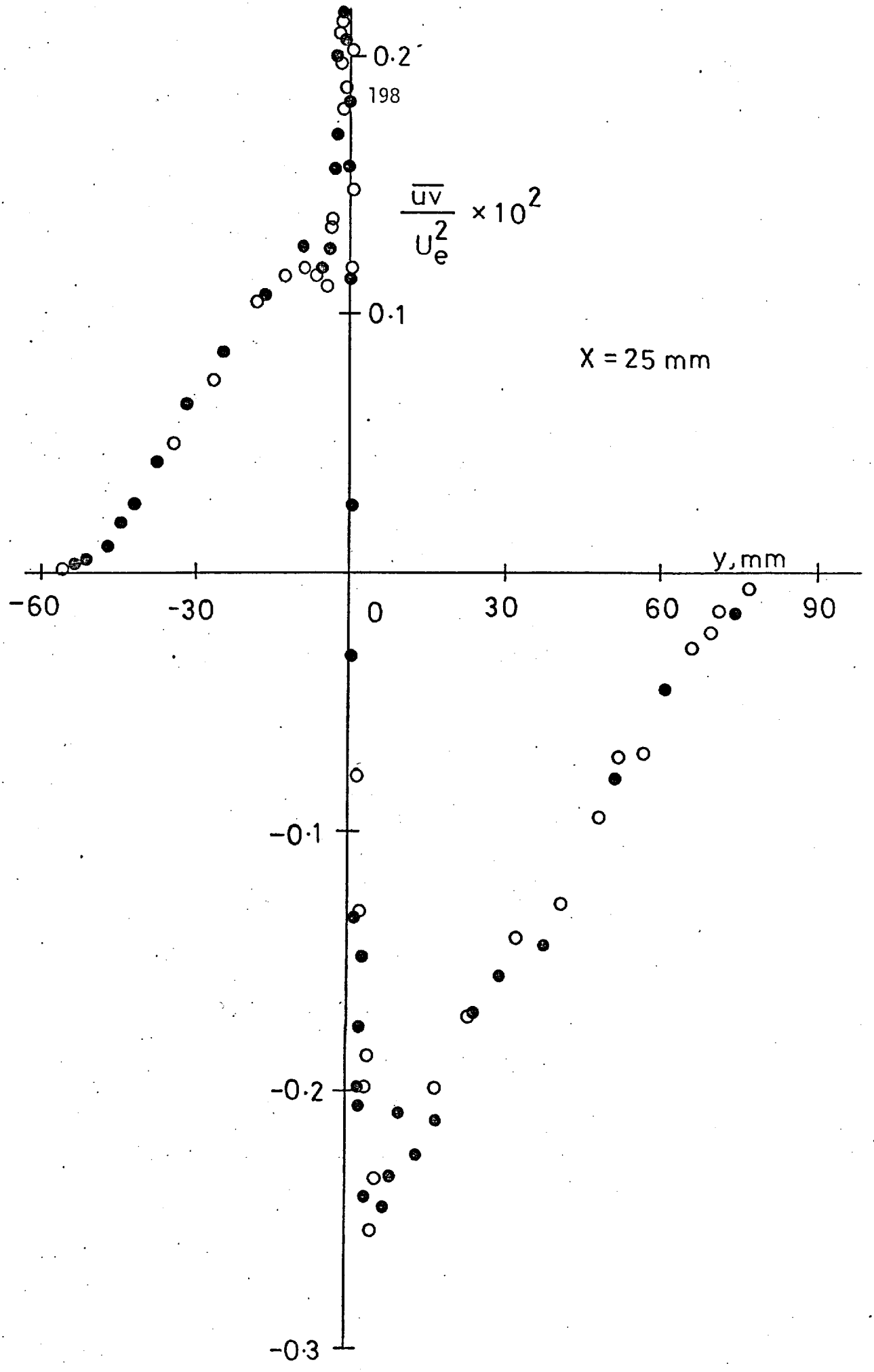

FIG. 5.23 SHEAR STRESS PROFILE AT x = 25 mm.

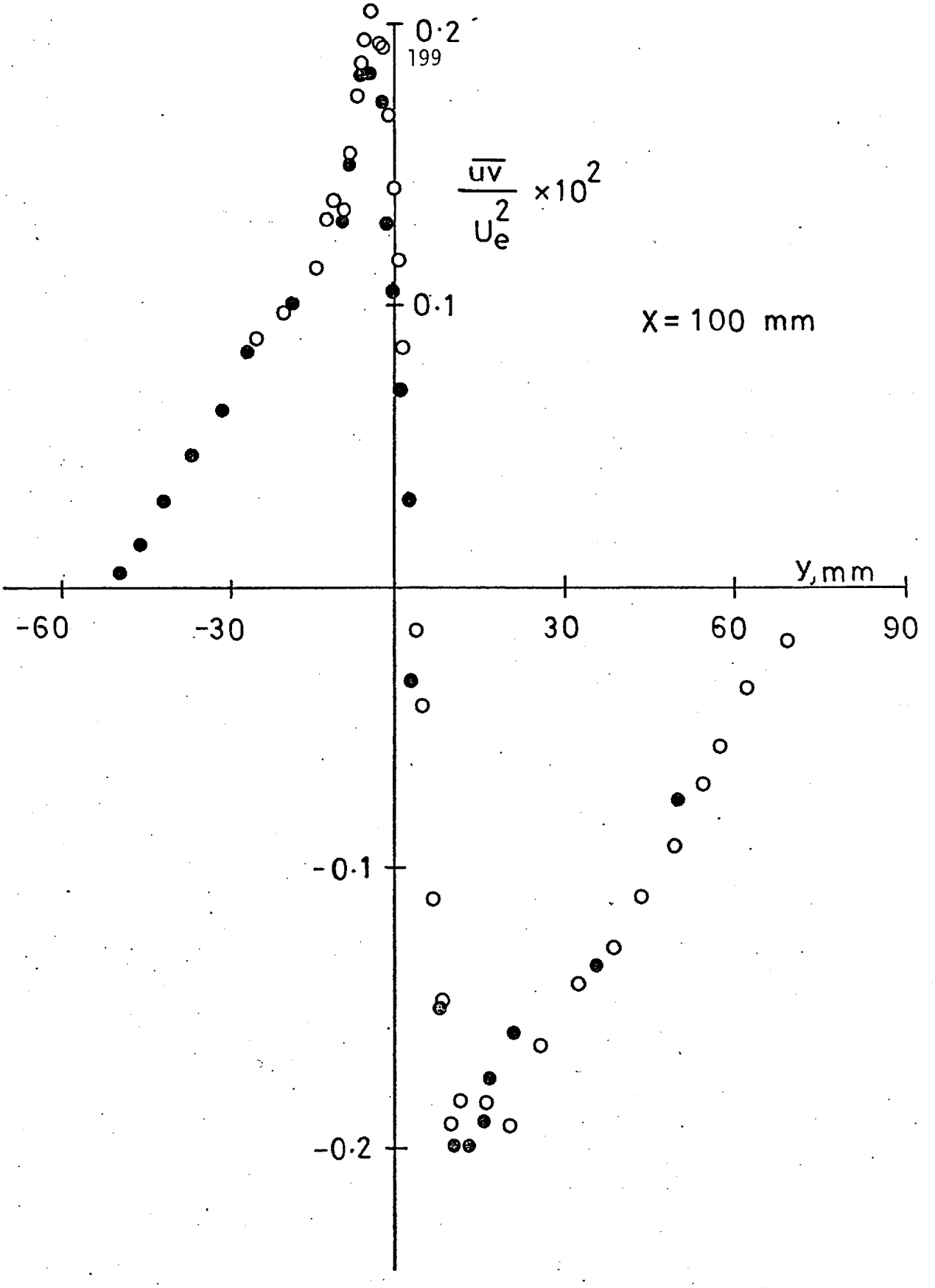

FIG. 5.24 SHEAR STRESS PROFILE AT x = 100 mm.

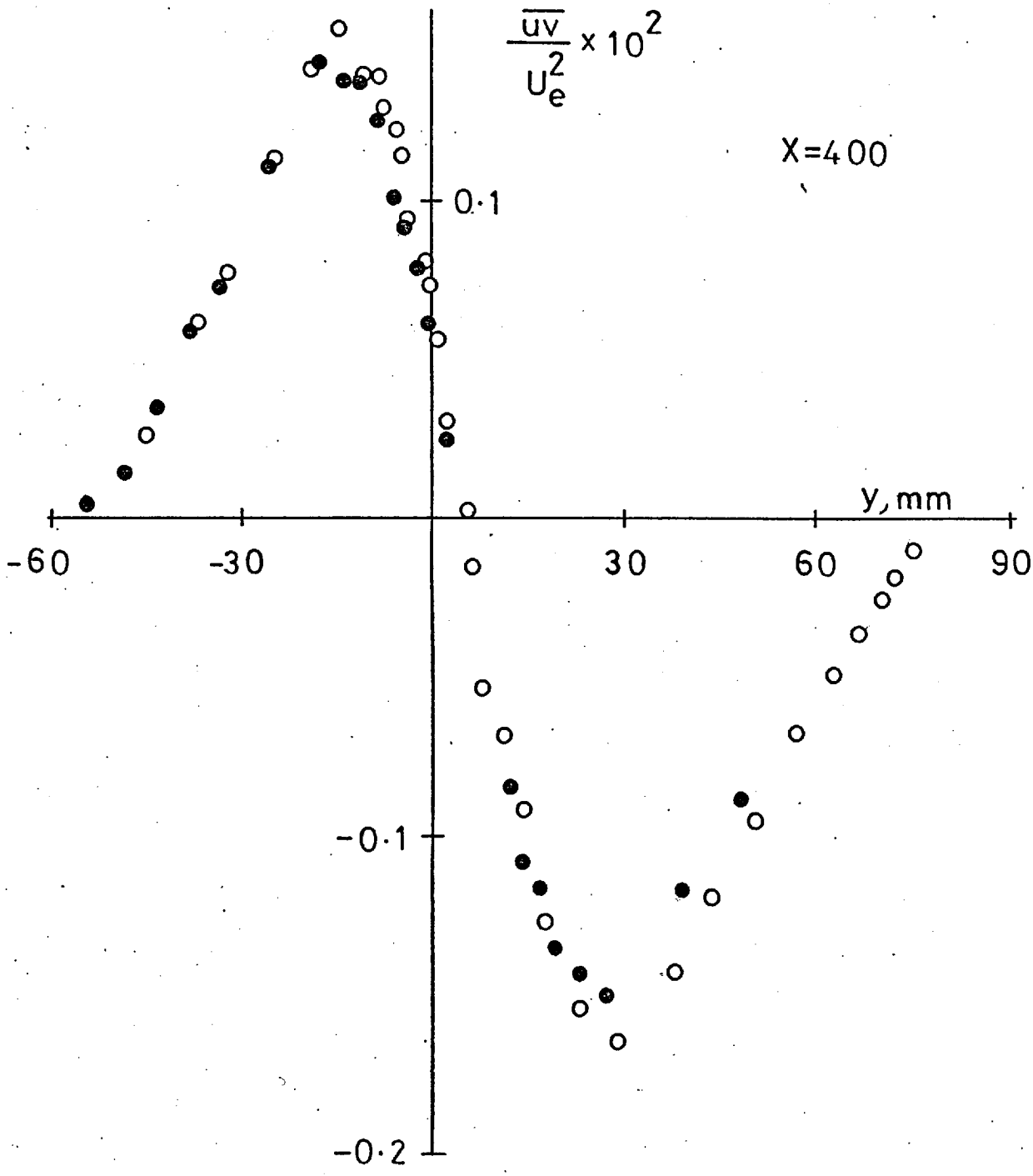

FIG. 5.25 SHEAR STRESS PROFILE AT x = 400 mm.

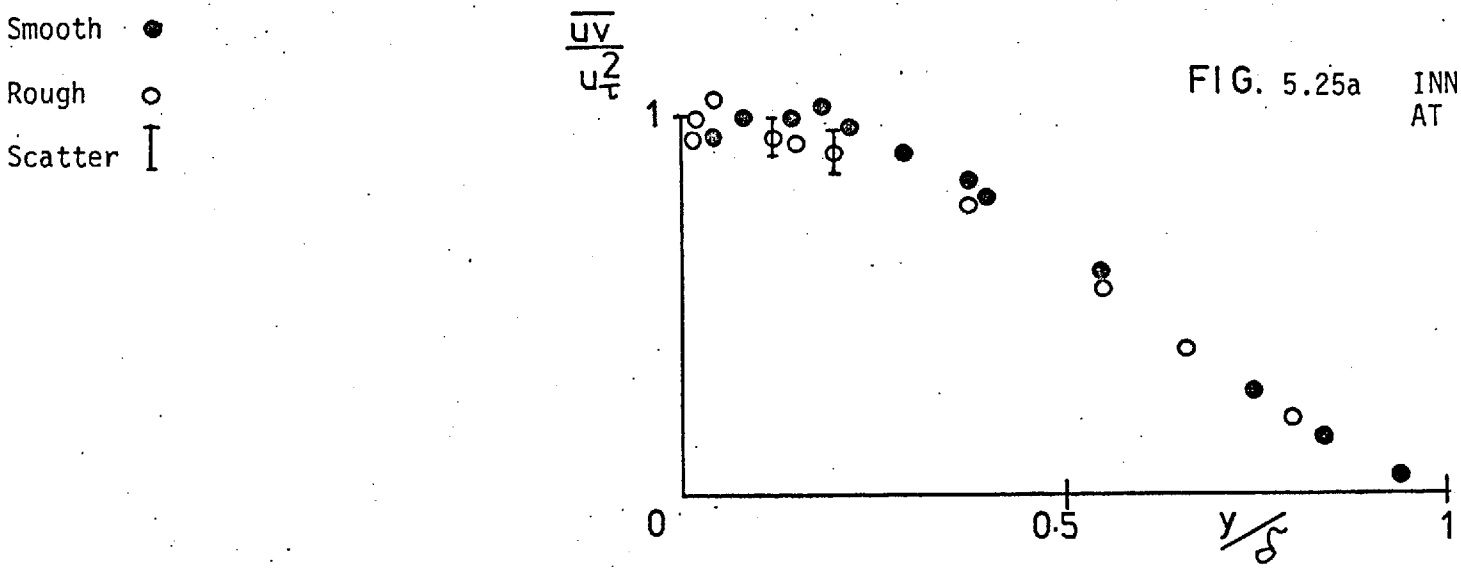

FIG. 5.25a INNER LAYER SCALING FOR $\overline{u^2}$, $\overline{v^2}$, $\overline{uv}$ AT x = 0 mm

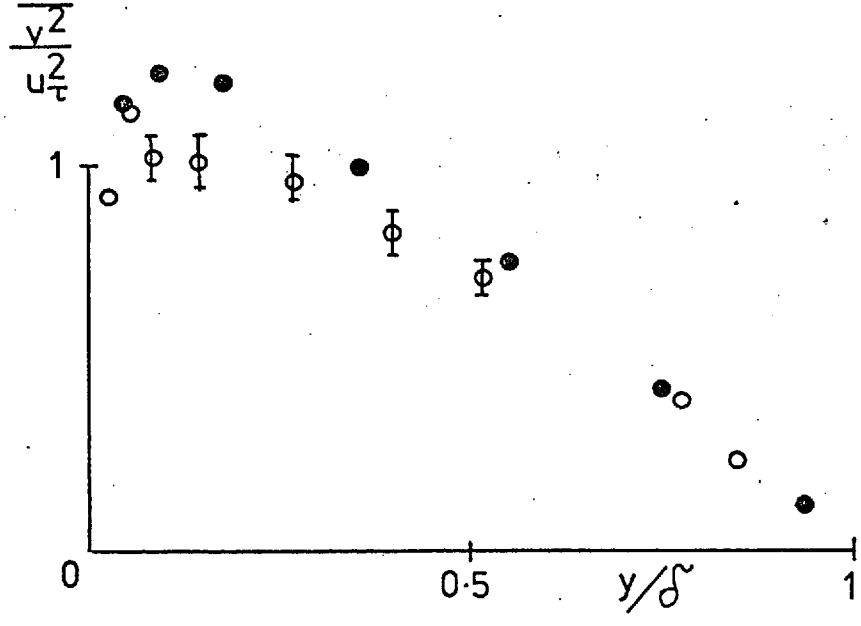

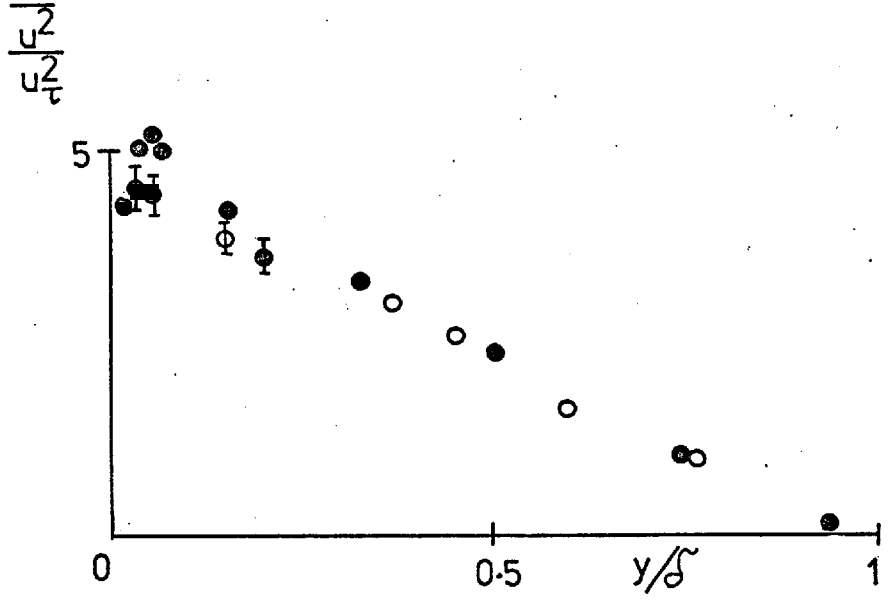

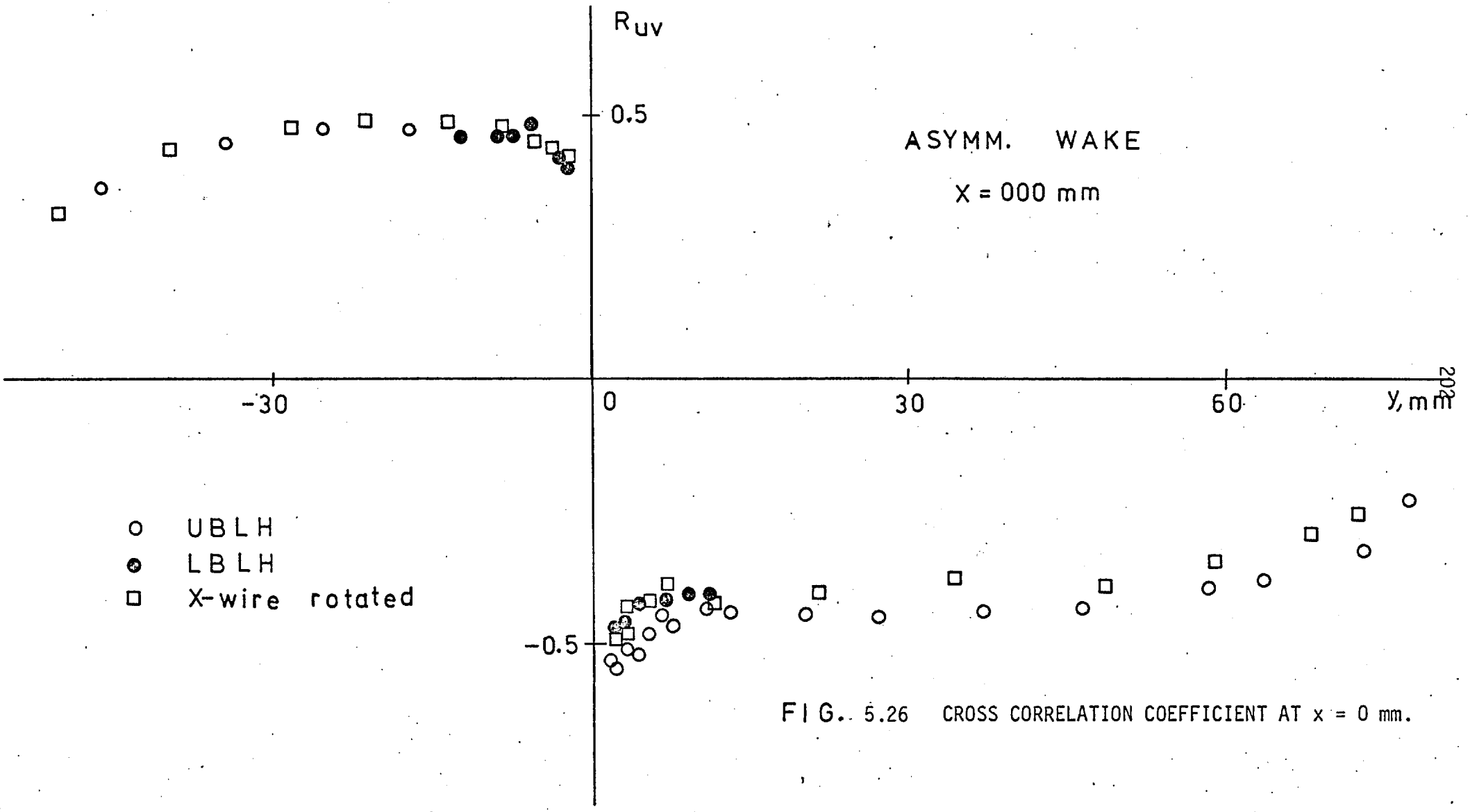

FIG. 5.26 CROSS CORRELATION COEFFICIENT AT x = 0 mm.

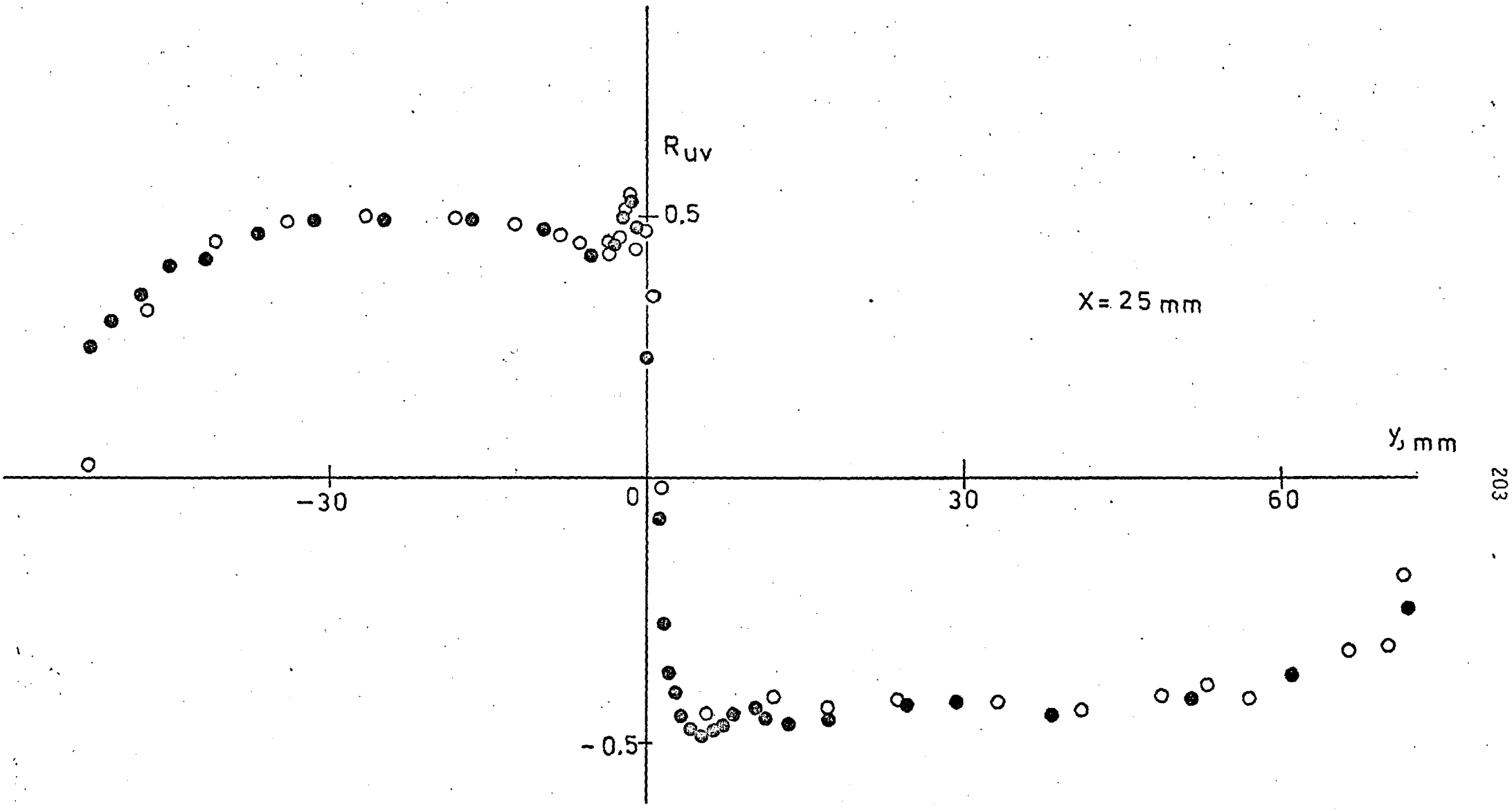

FIG. 5.27 CROSS CORRELATION COEFFICIENT AT x = 25 mm.

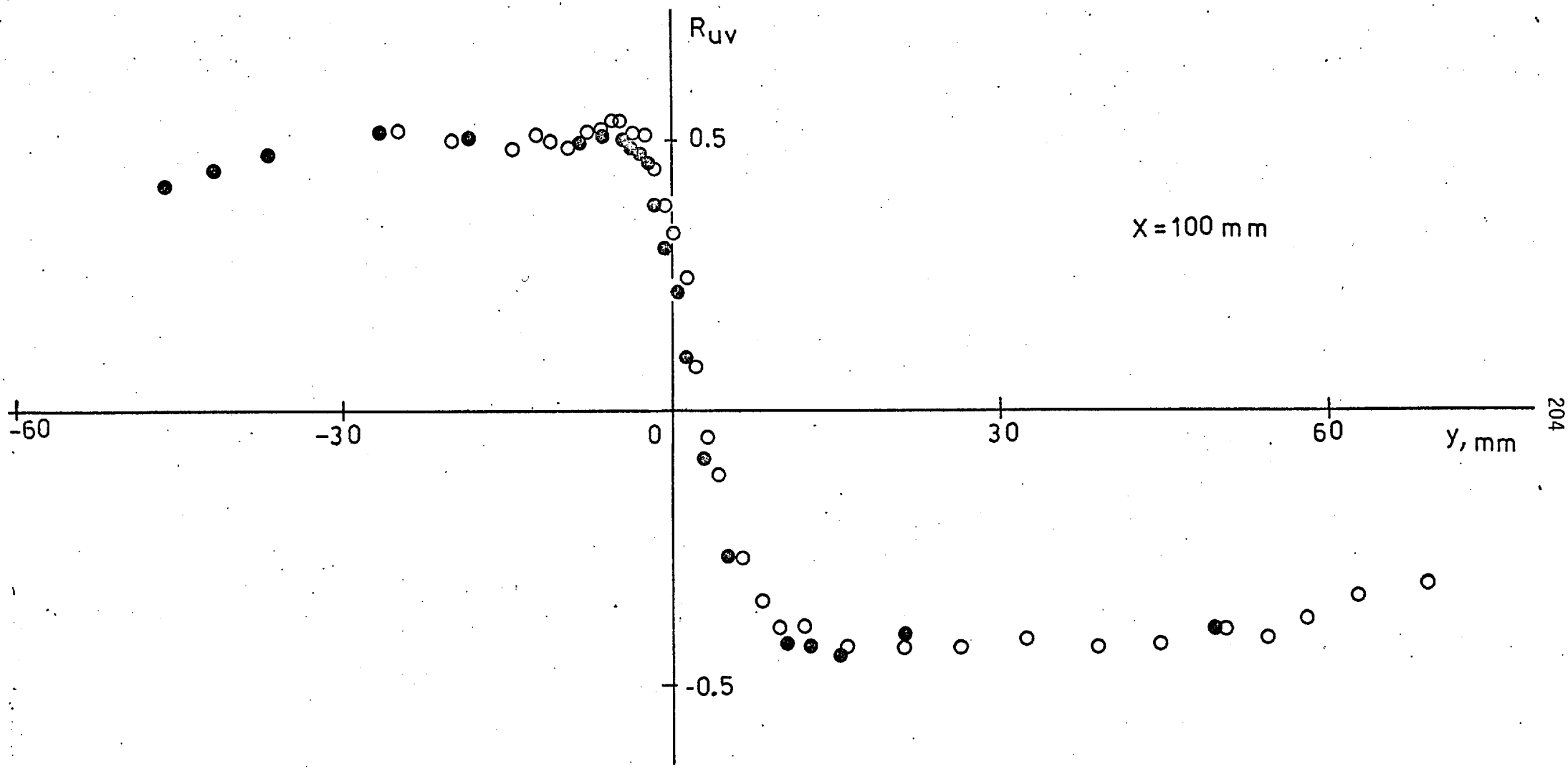

FIG. 5.28 CROSS CORRELATION COEFFICIENT AT x = 100 mm.

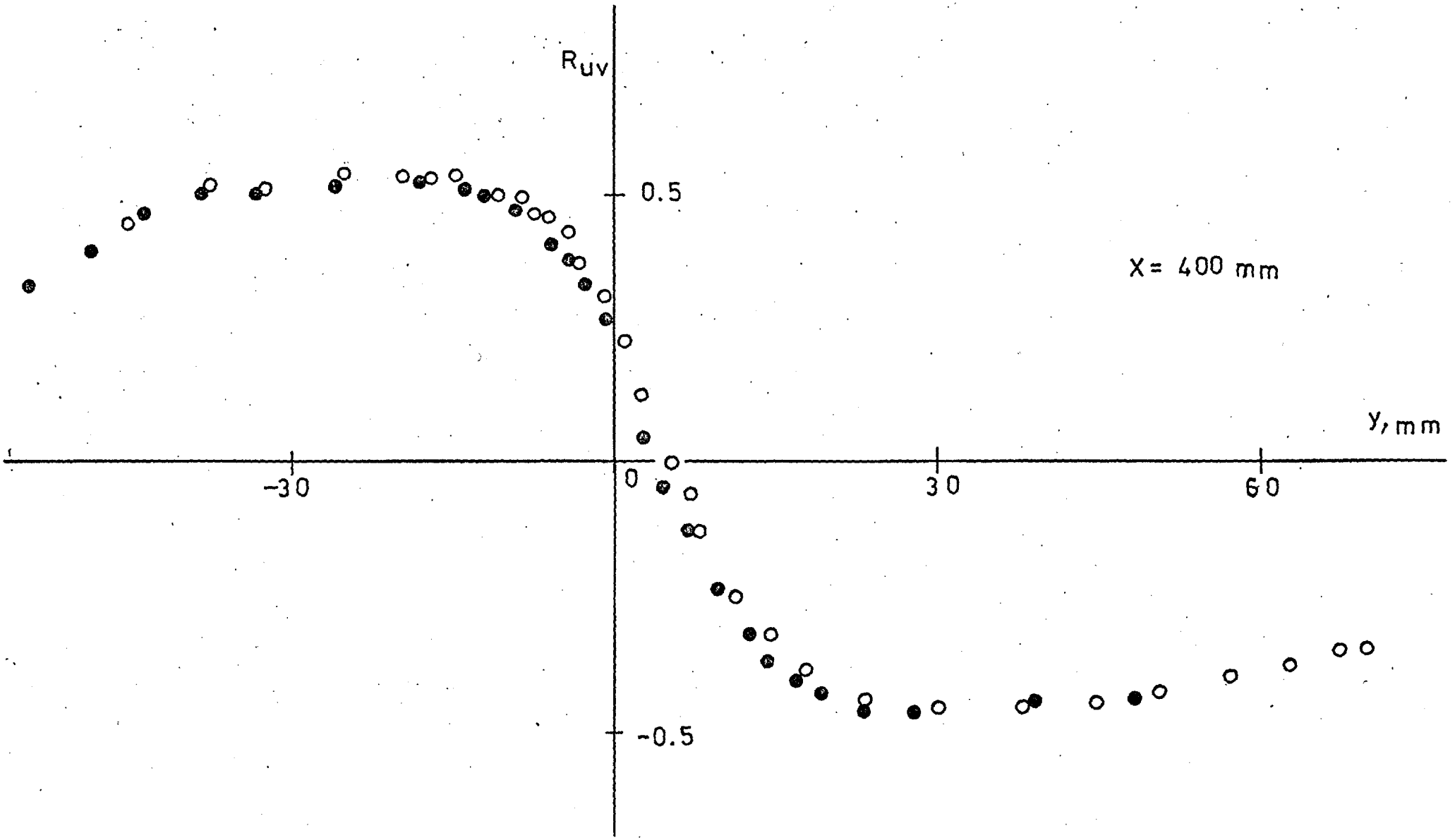

FIG. 5.29 CROSS CORRELATION COEFFICIENT AT x = 400 mm.

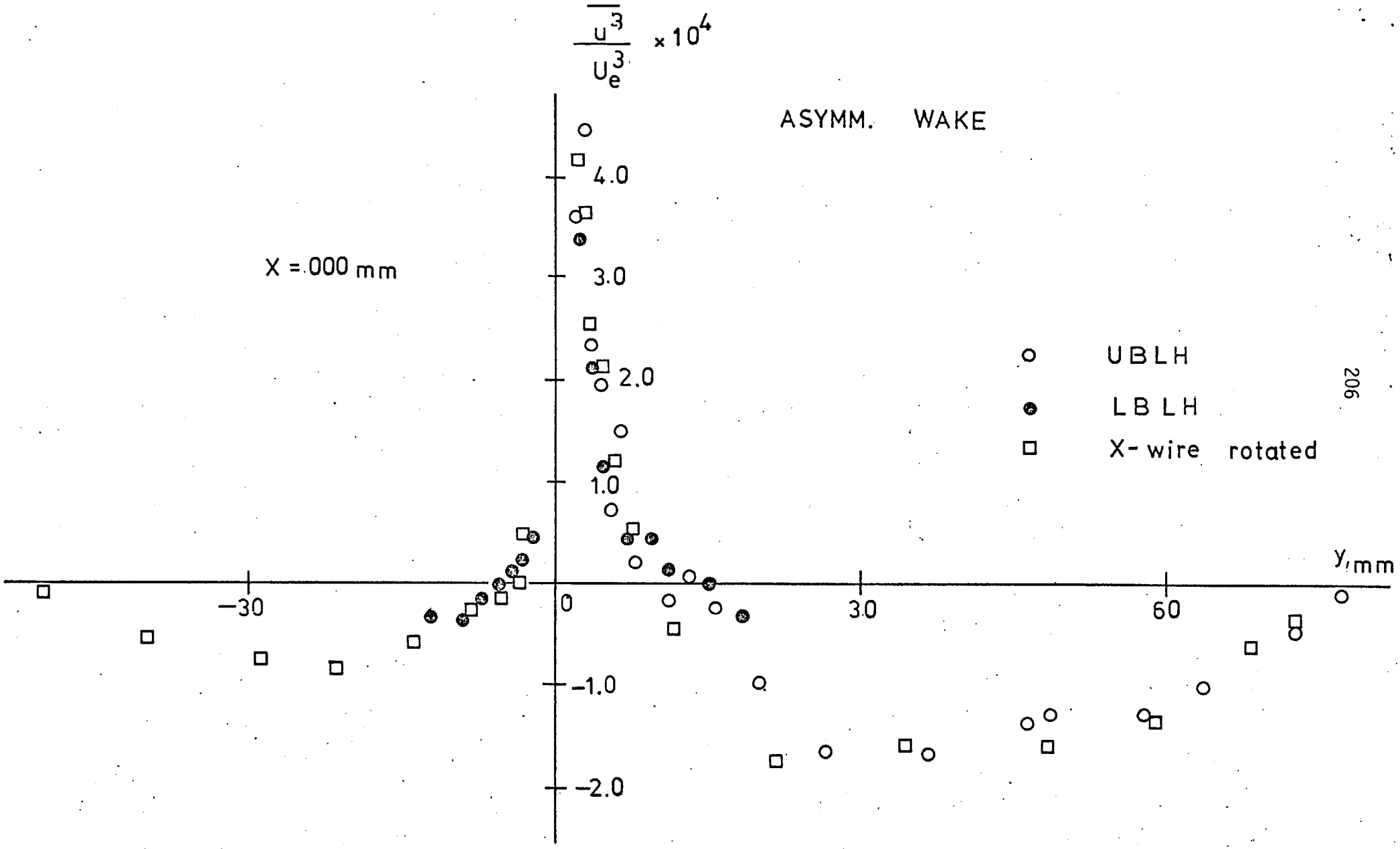

FIG. 5.30 $\overline{u^3}$ PROFILE AT x = 0 mm.

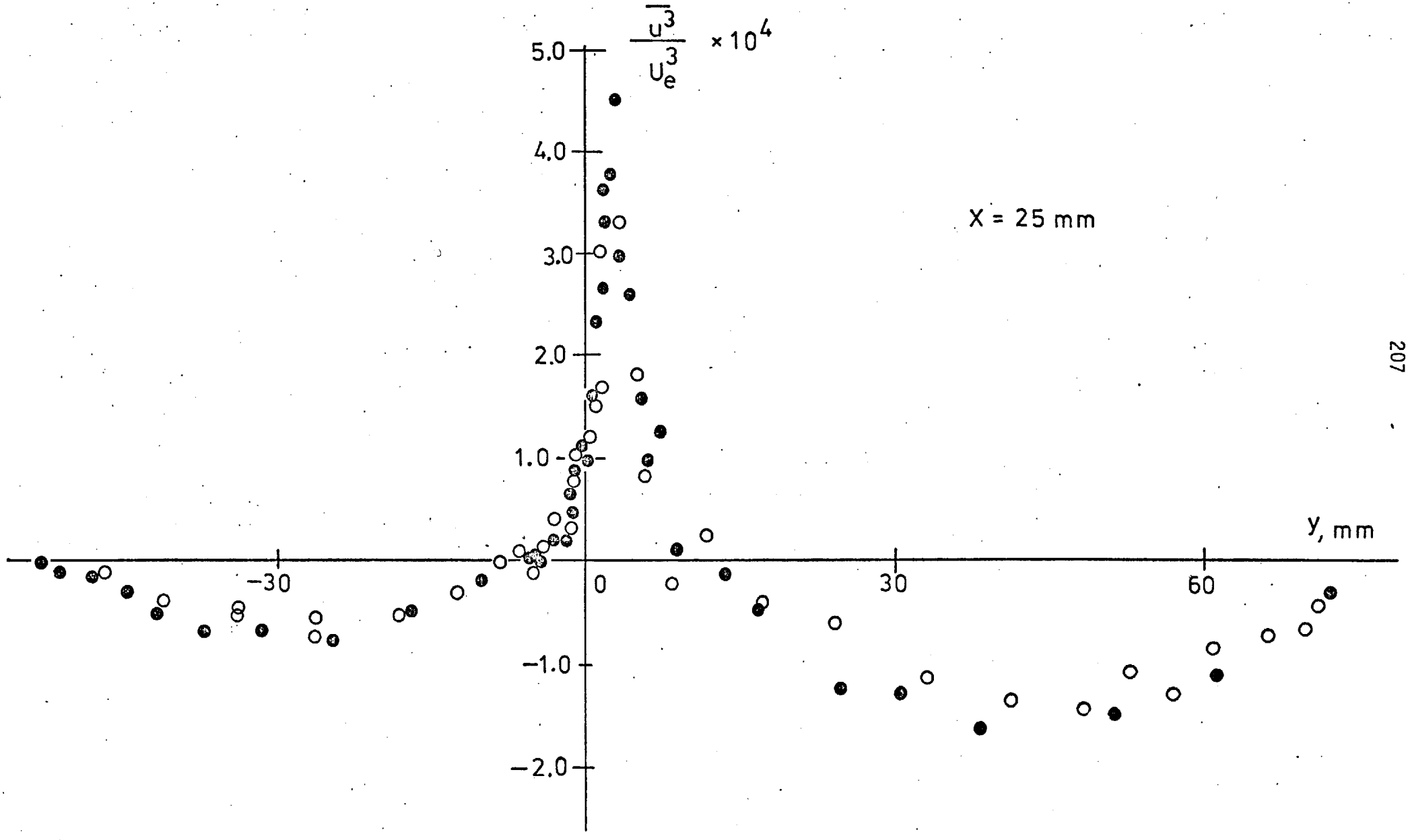

FIG. 5.31 $\overline{u^3}$ PROFILE AT x = 25 mm.

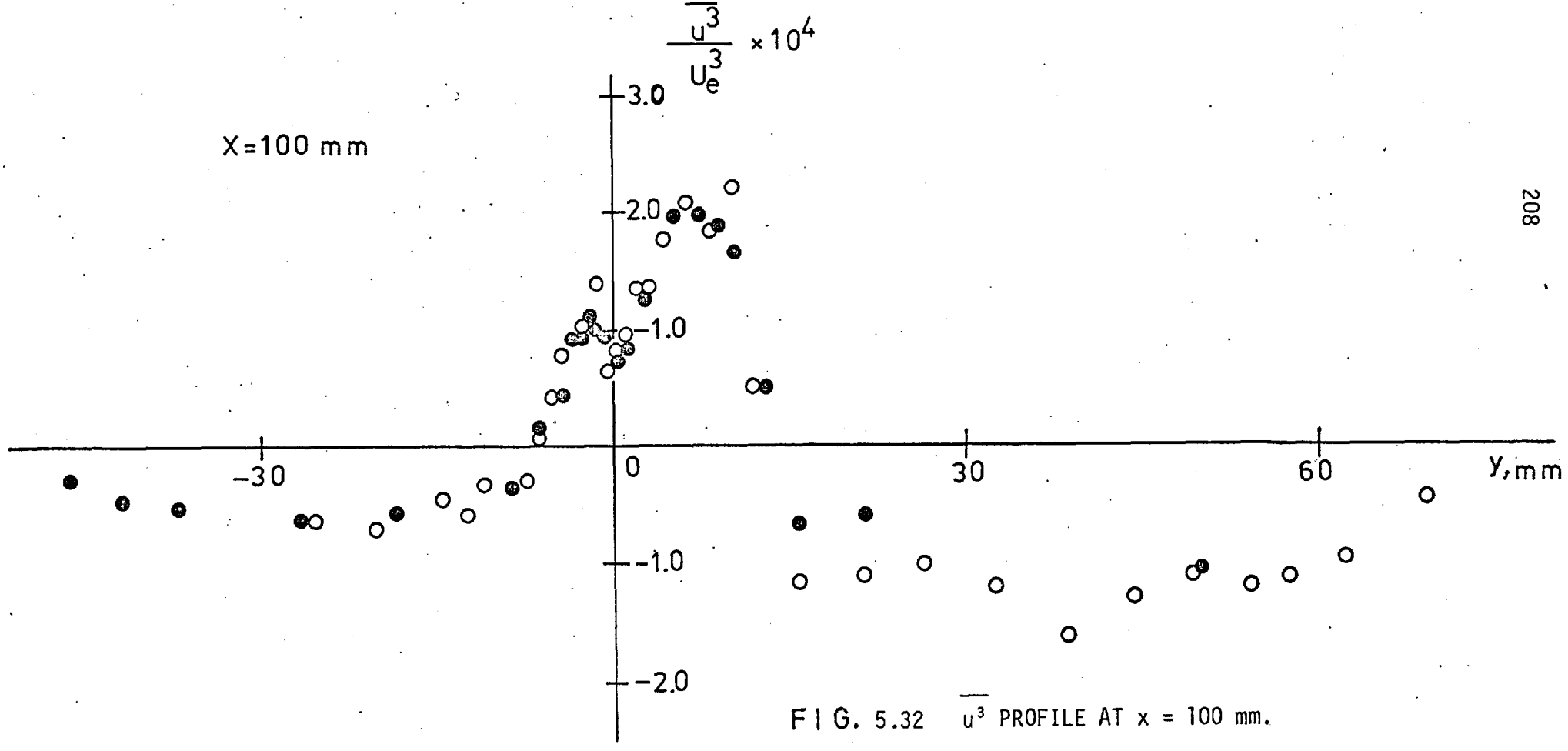

FIG. 5.32 $\overline{u^3}$ PROFILE AT x = 100 mm.

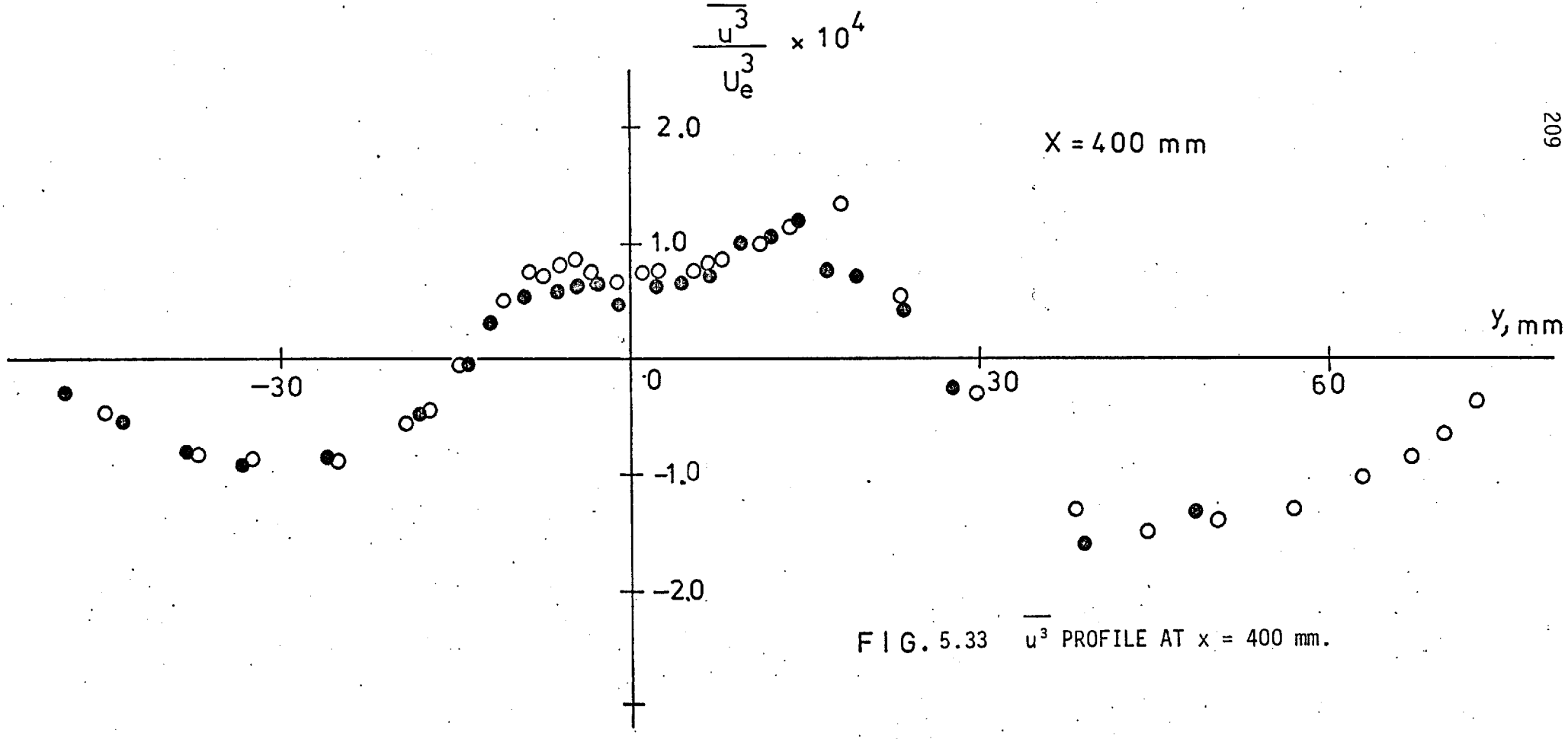

FIG. 5.33 $\overline{u^3}$ PROFILE AT x = 400 mm.

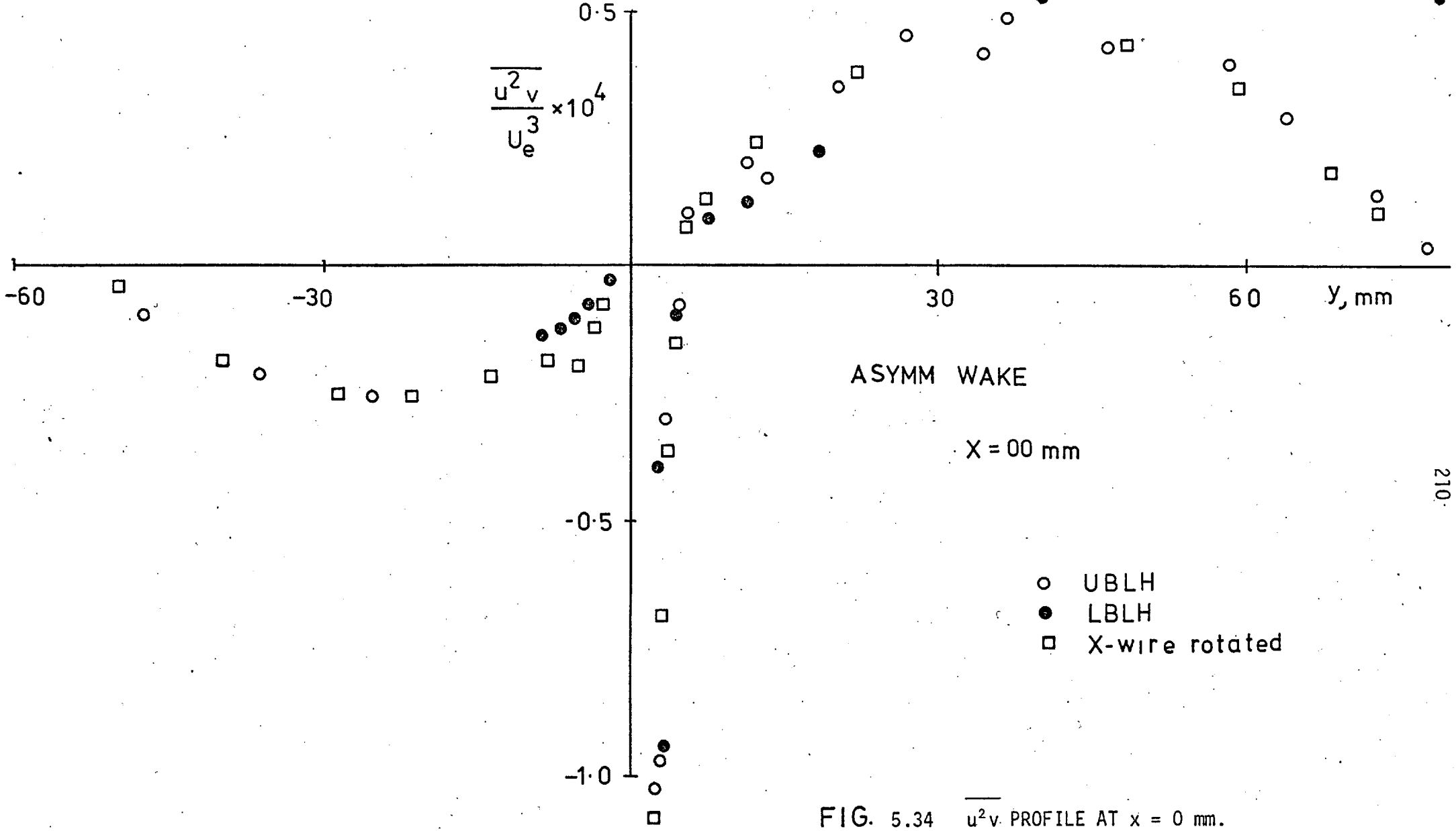

FIG. 5.34 $\overline{u^2v}$ PROFILE AT x = 0 mm.

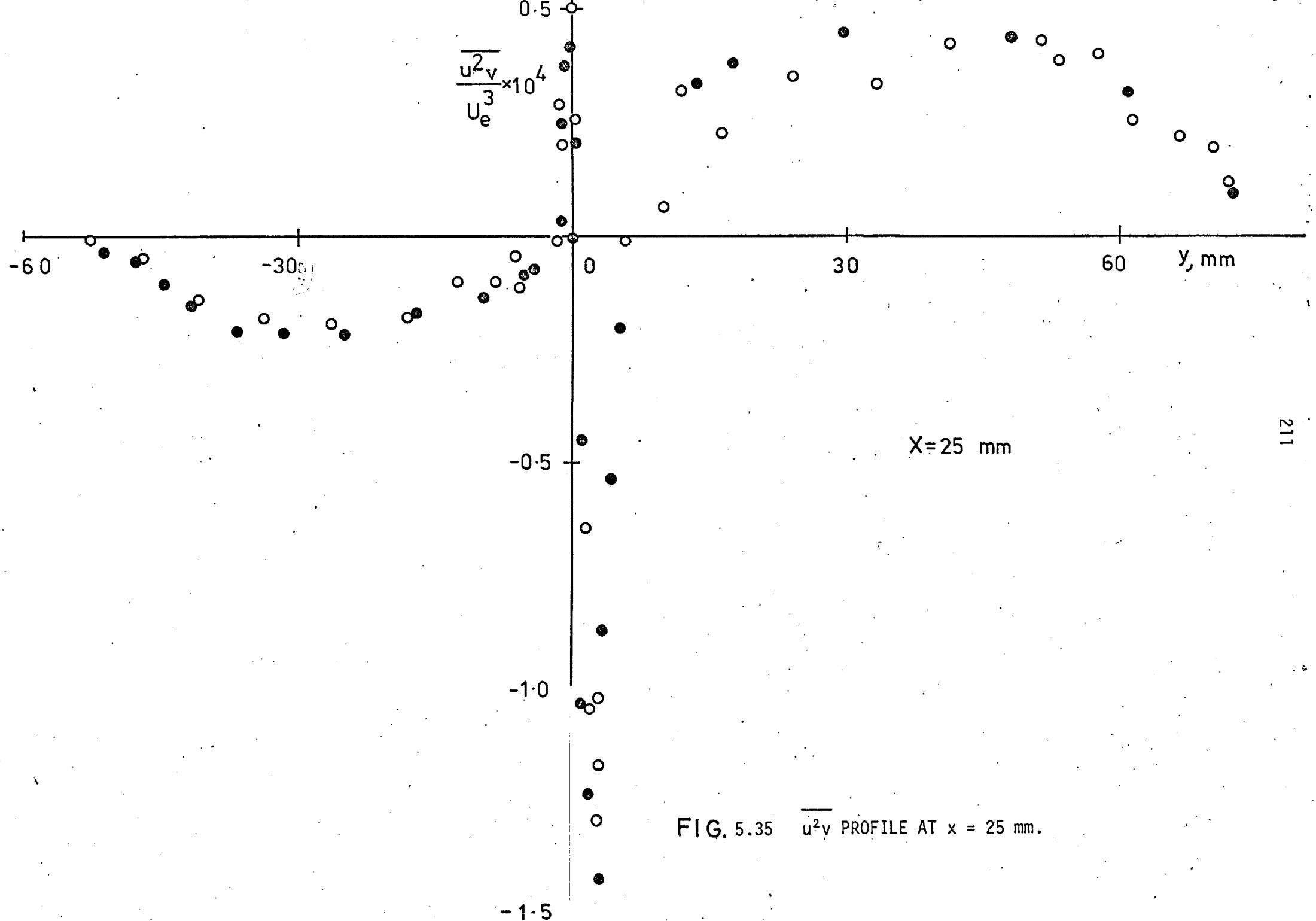

FIG. 5.35 $\overline{u^2v}$ PROFILE AT x = 25 mm.

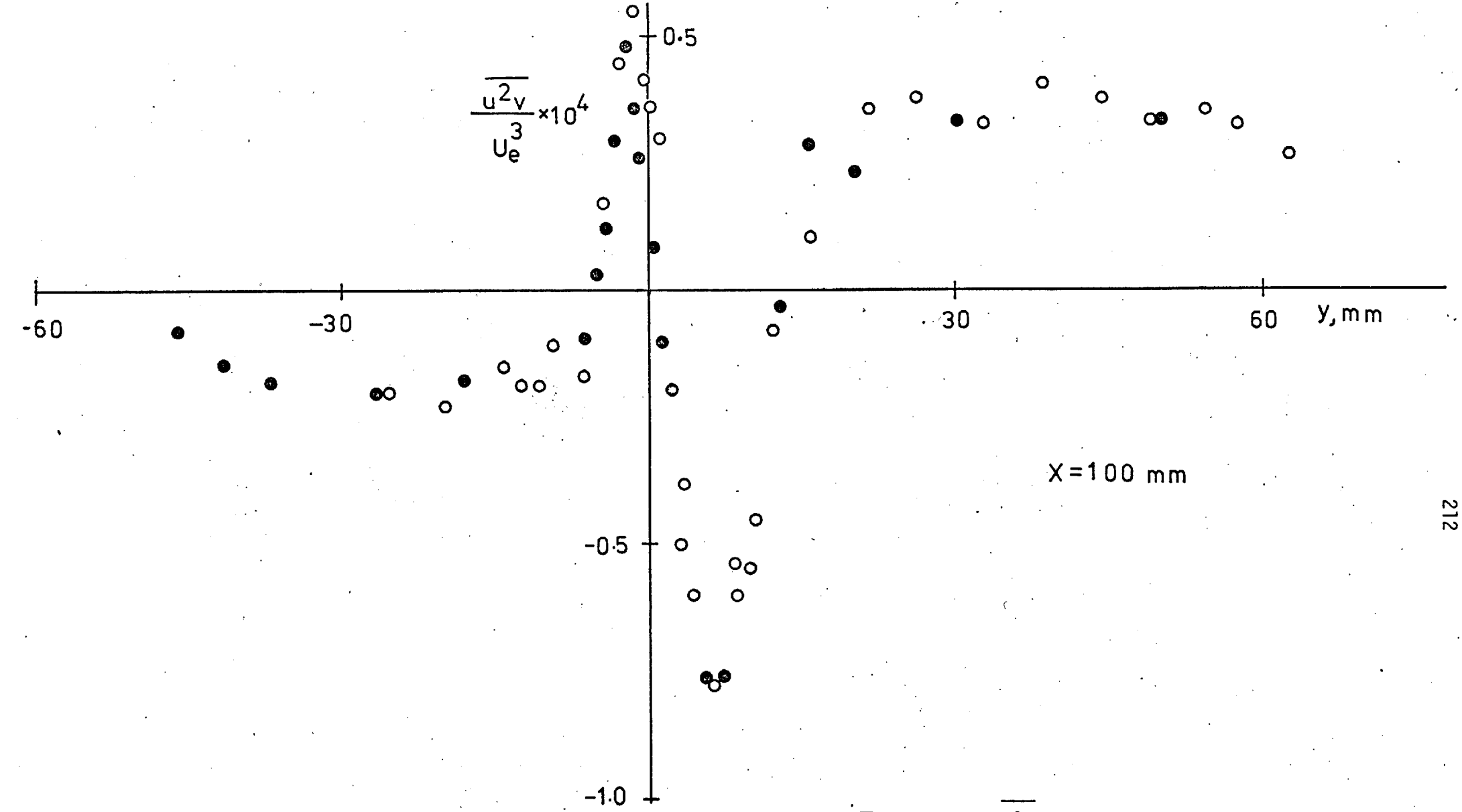

FIG. 5.36 $\overline{u^2v}$ PROFILE AT x = 100 mm.

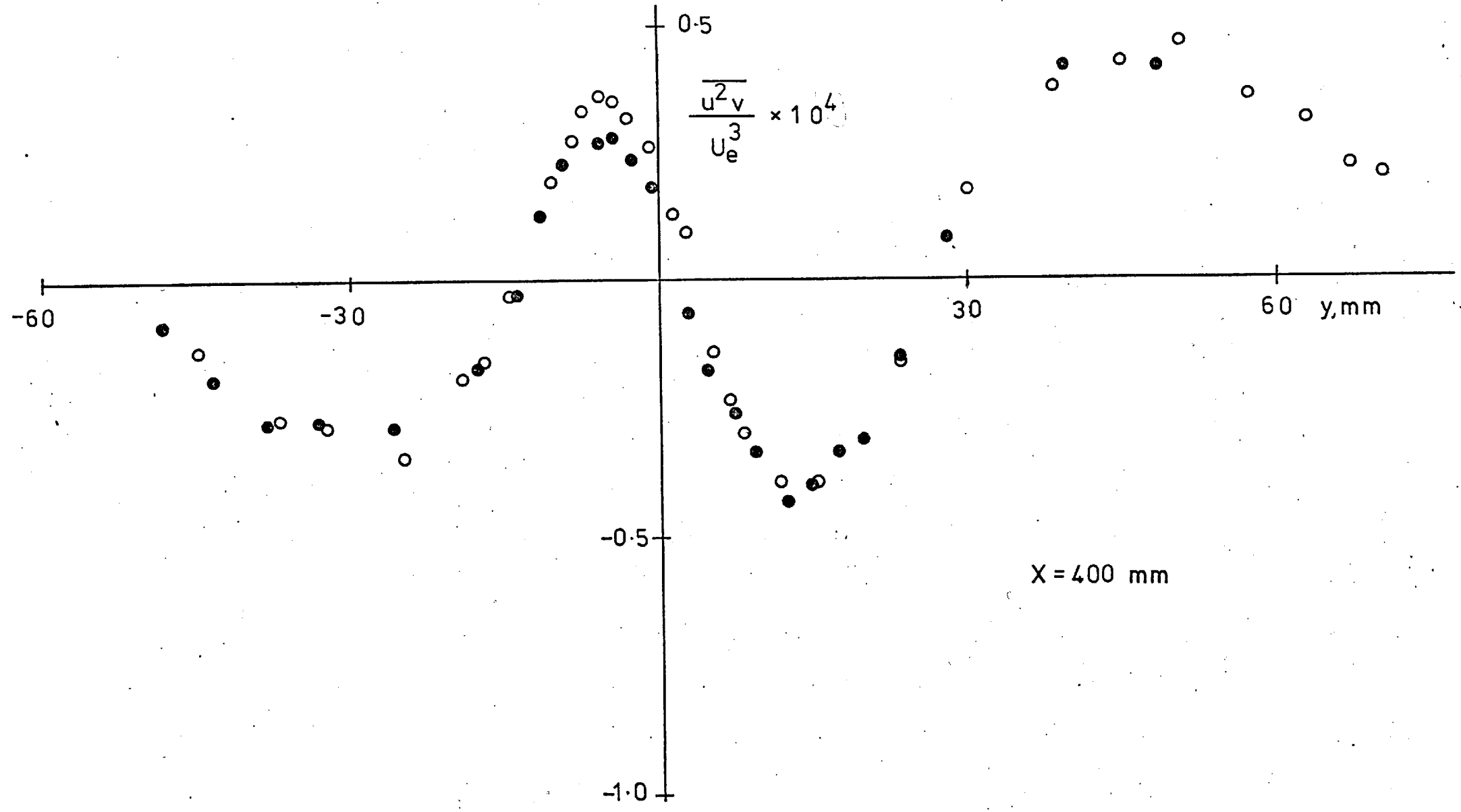

FIG. 5.37 $\overline{u^2v}$ PROFILE AT x = 400 mm.

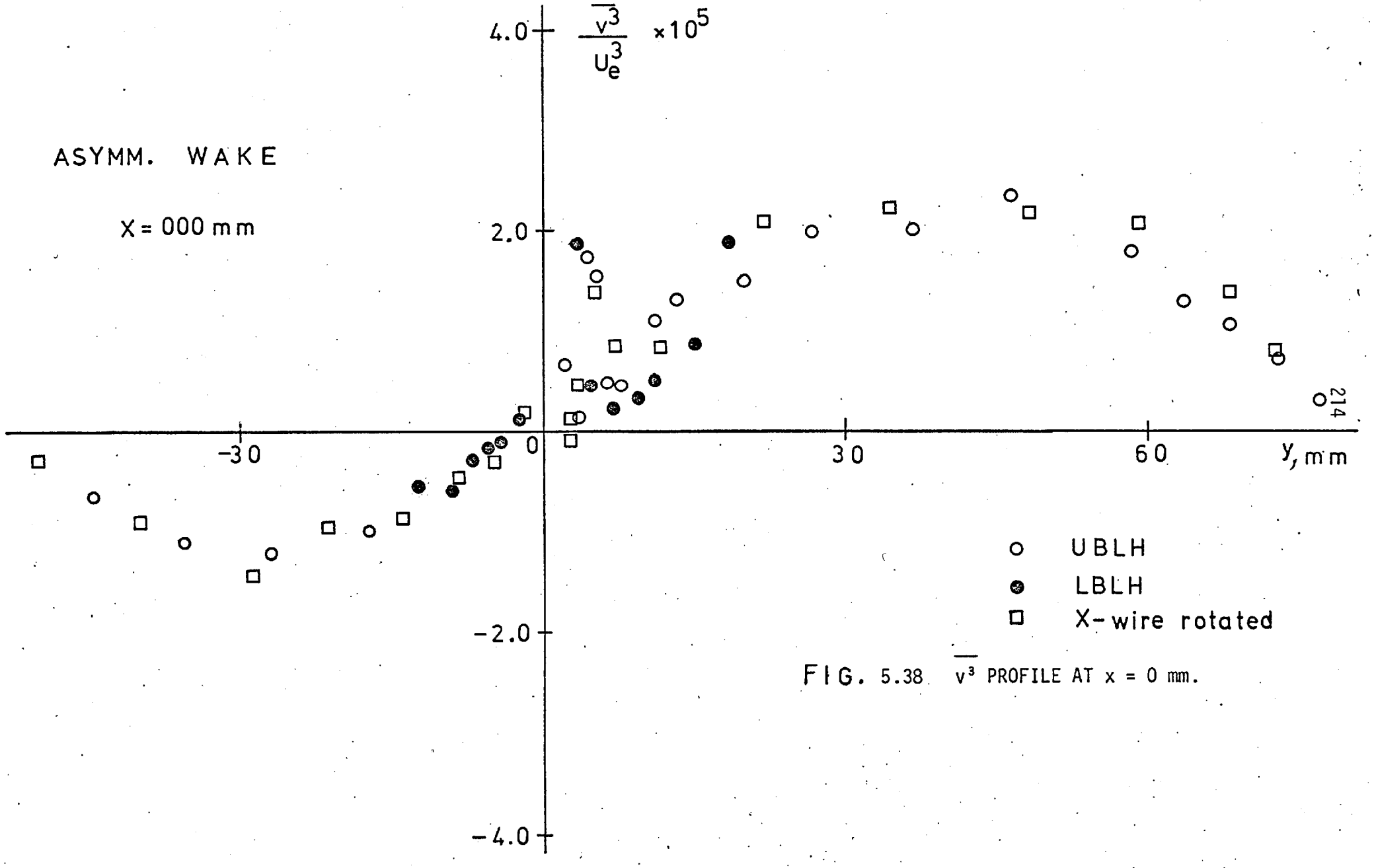

FIG. 5.38 $\overline{v^3}$ PROFILE AT x = 0 mm.

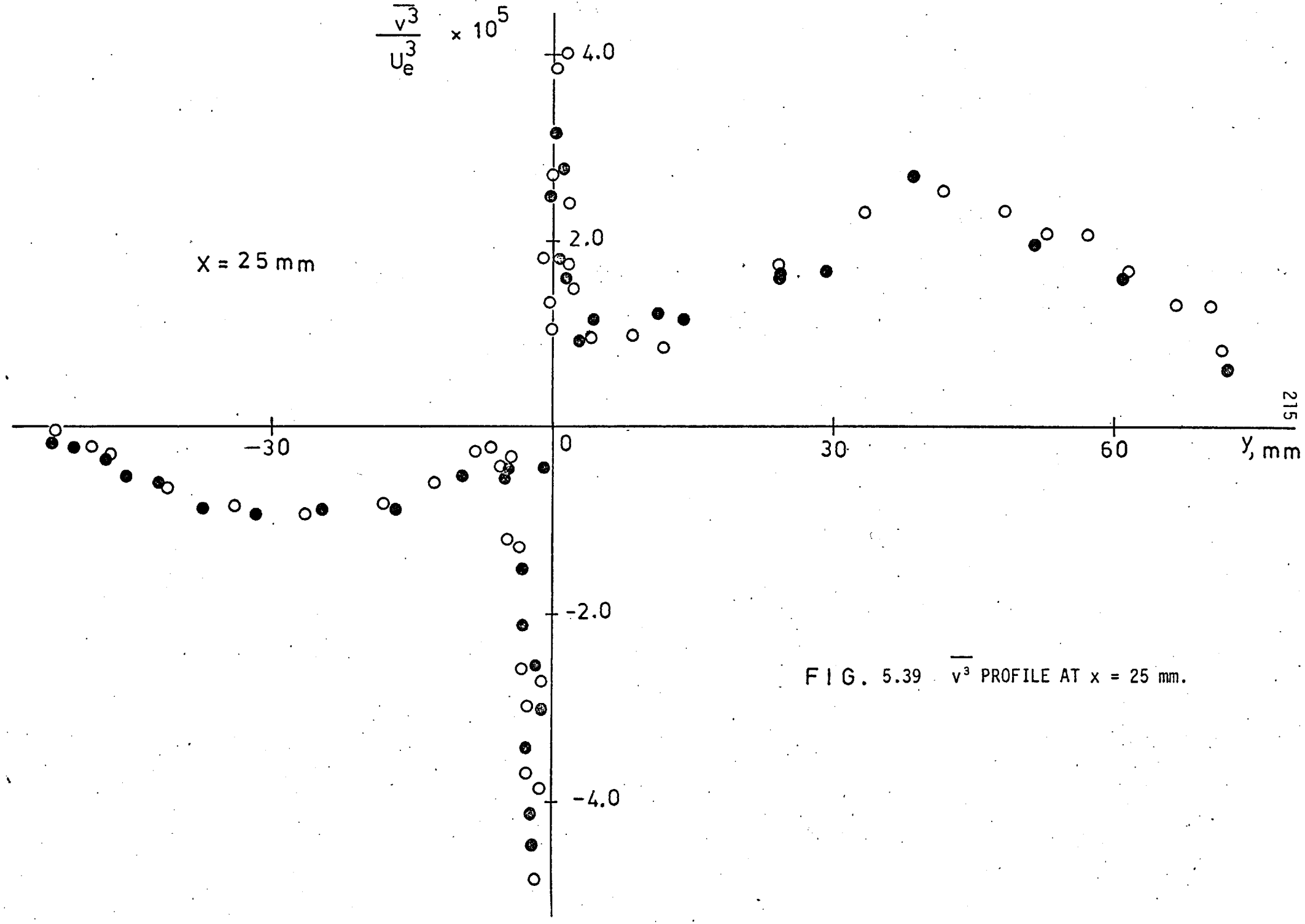

FIG. 5.39 $\overline{v^3}$ PROFILE AT x = 25 mm.

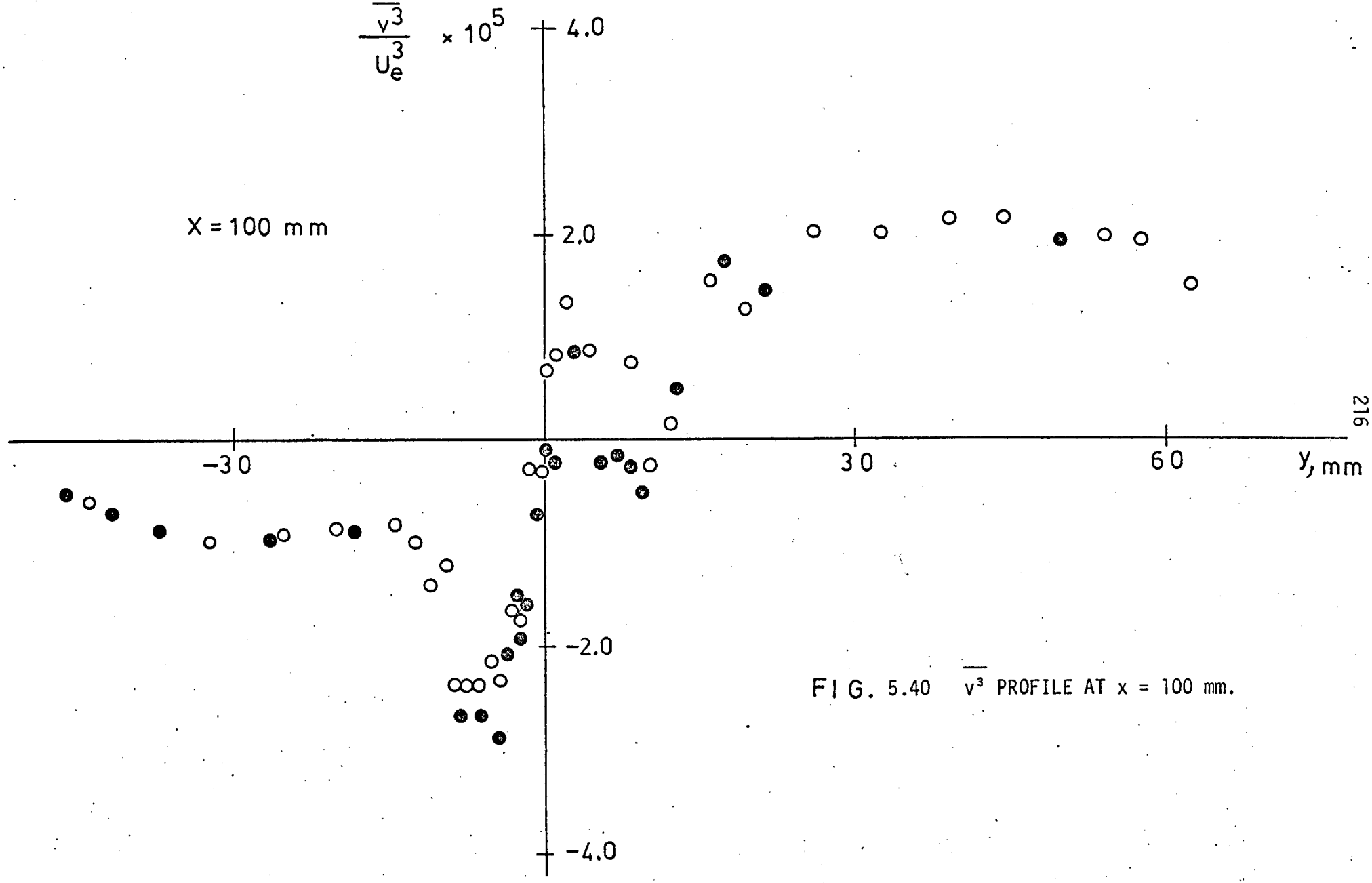

FIG. 5.40 $\overline{v^3}$ PROFILE AT x = 100 mm.

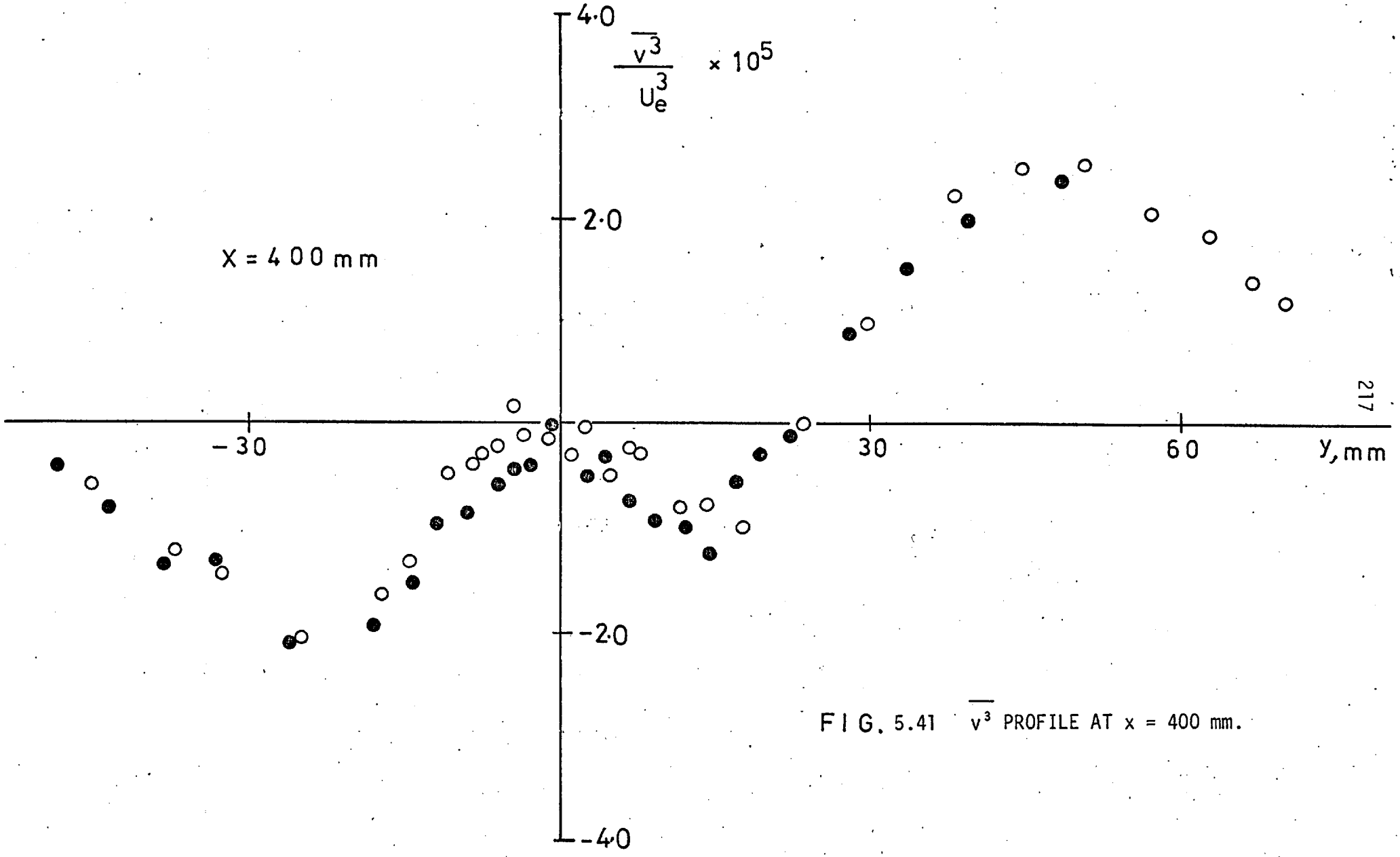

FIG. 5.41 $\overline{v^3}$ PROFILE AT x = 400 mm.

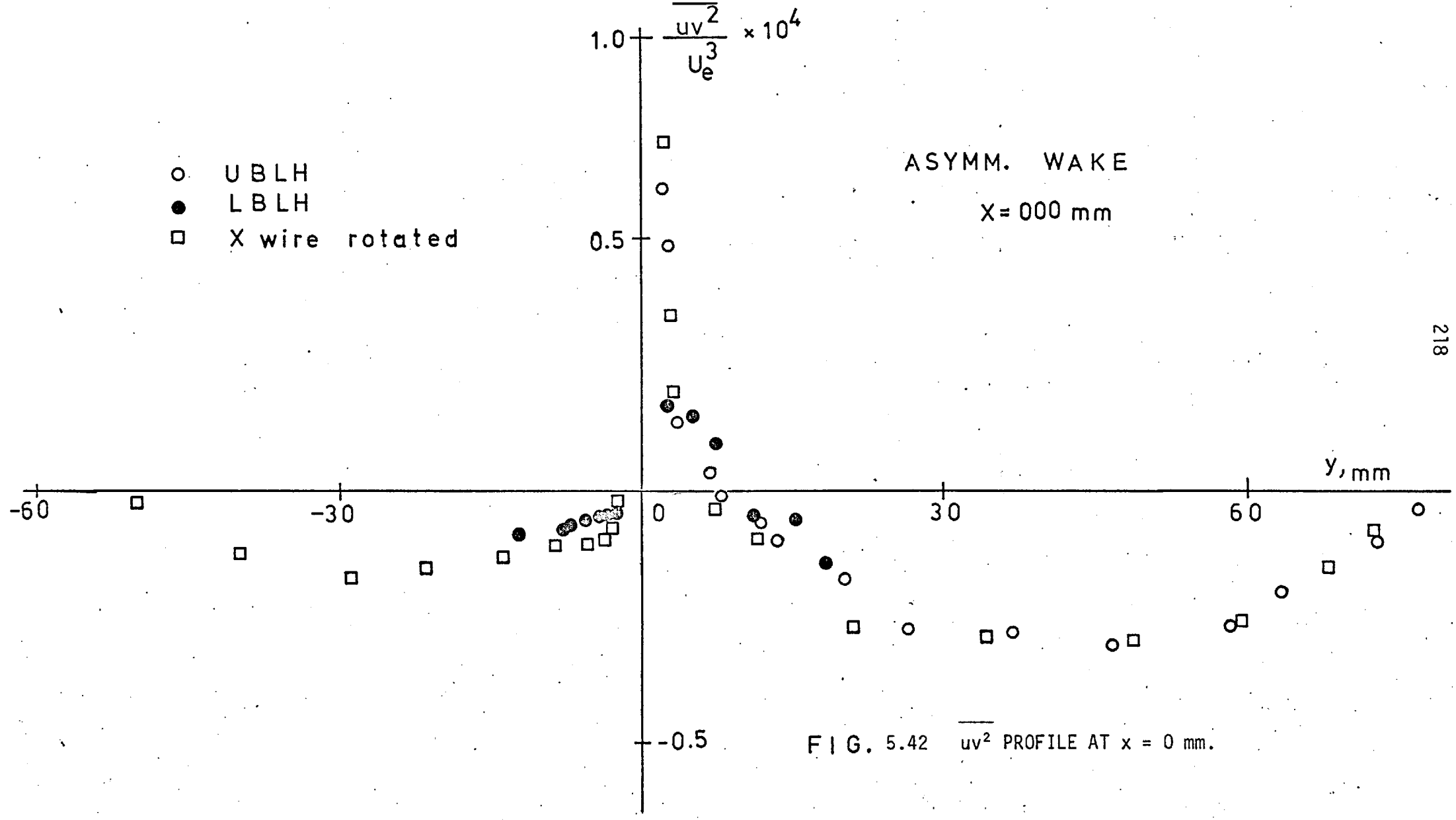

FIG. 5.42 $\overline{uv^2}$ PROFILE AT x = 0 mm.

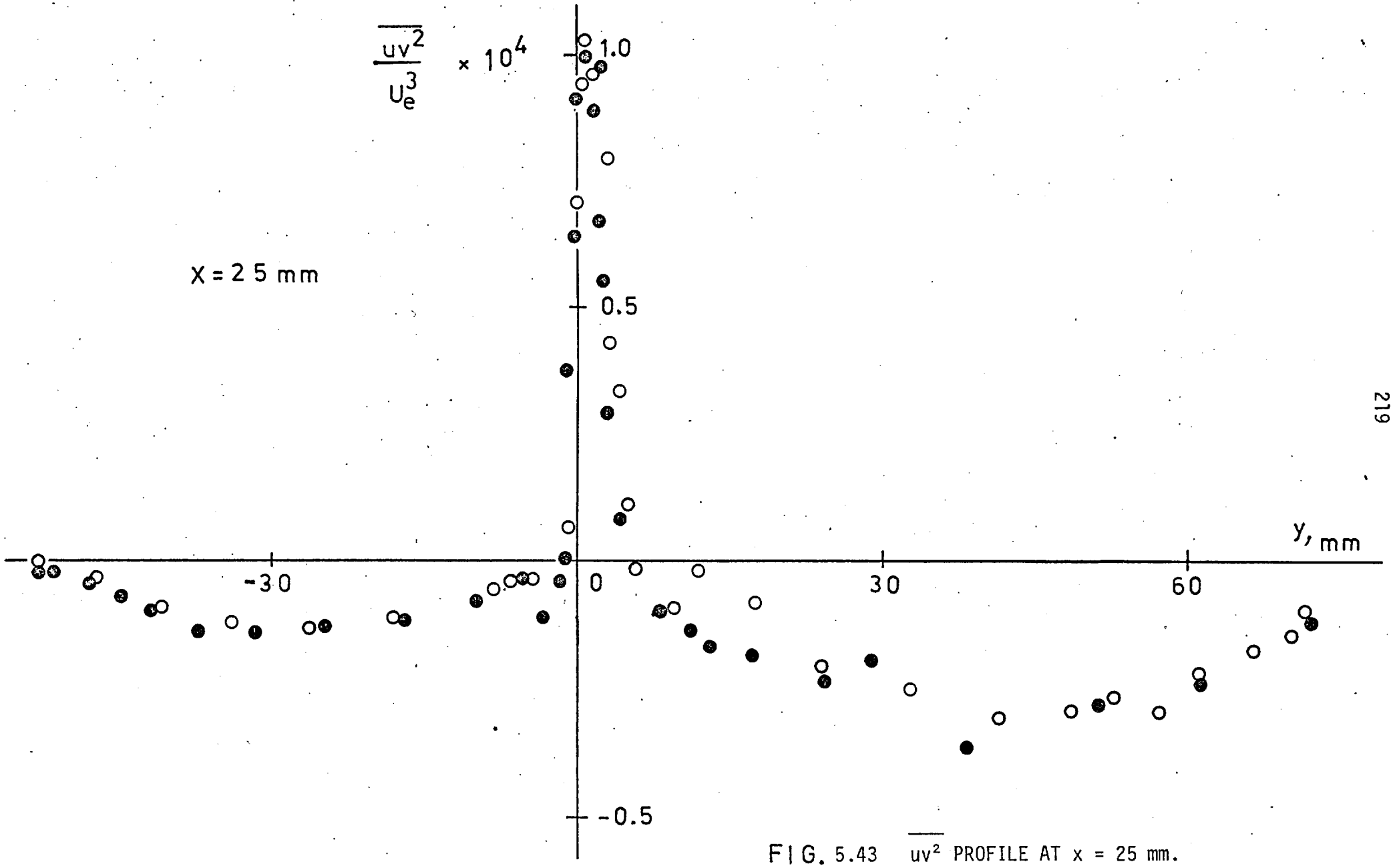

FIG. 5.43 $\overline{uv^2}$ PROFILE AT x = 25 mm.

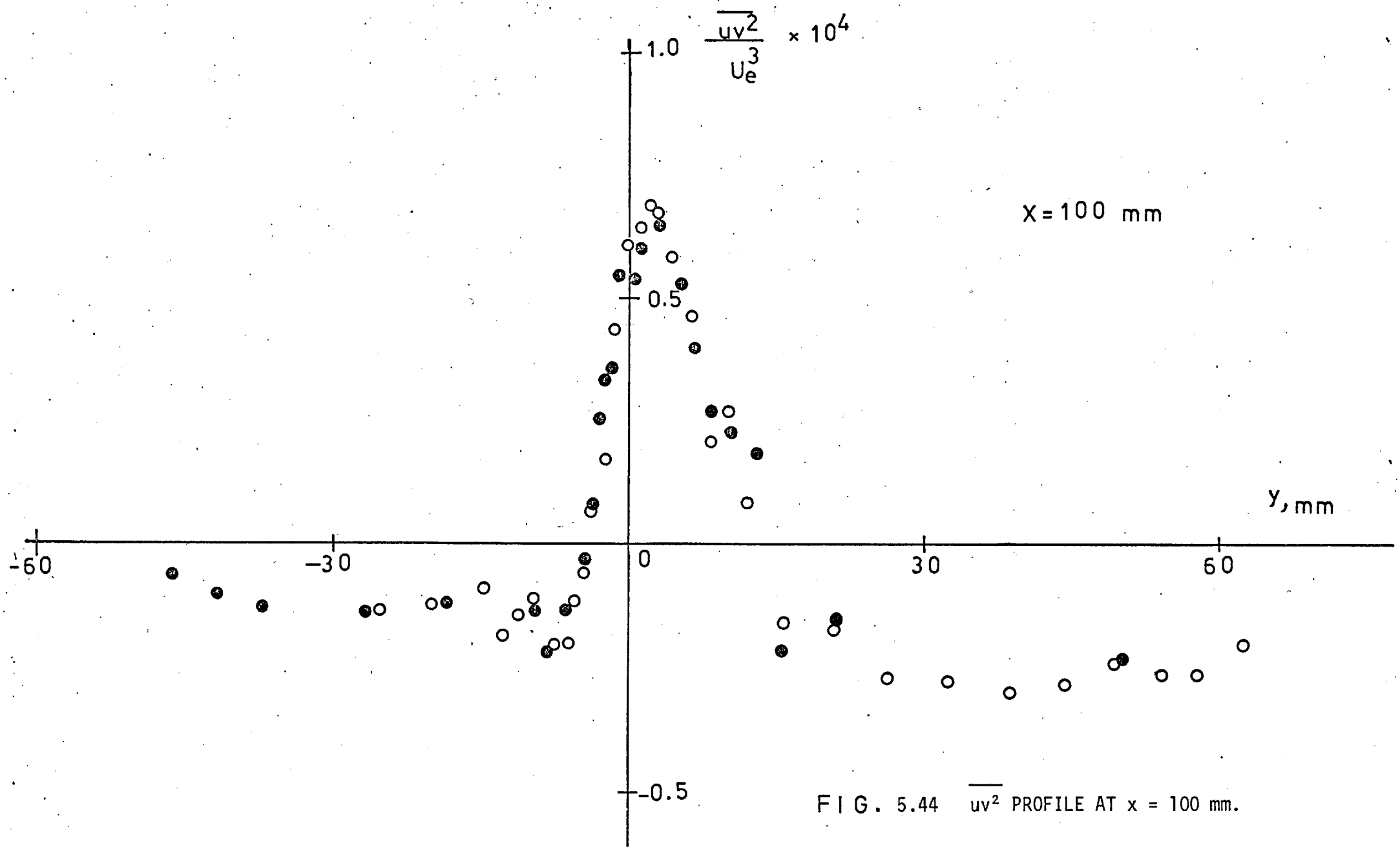

FIG. 5.44 $\overline{uv^2}$ PROFILE AT x = 100 mm.

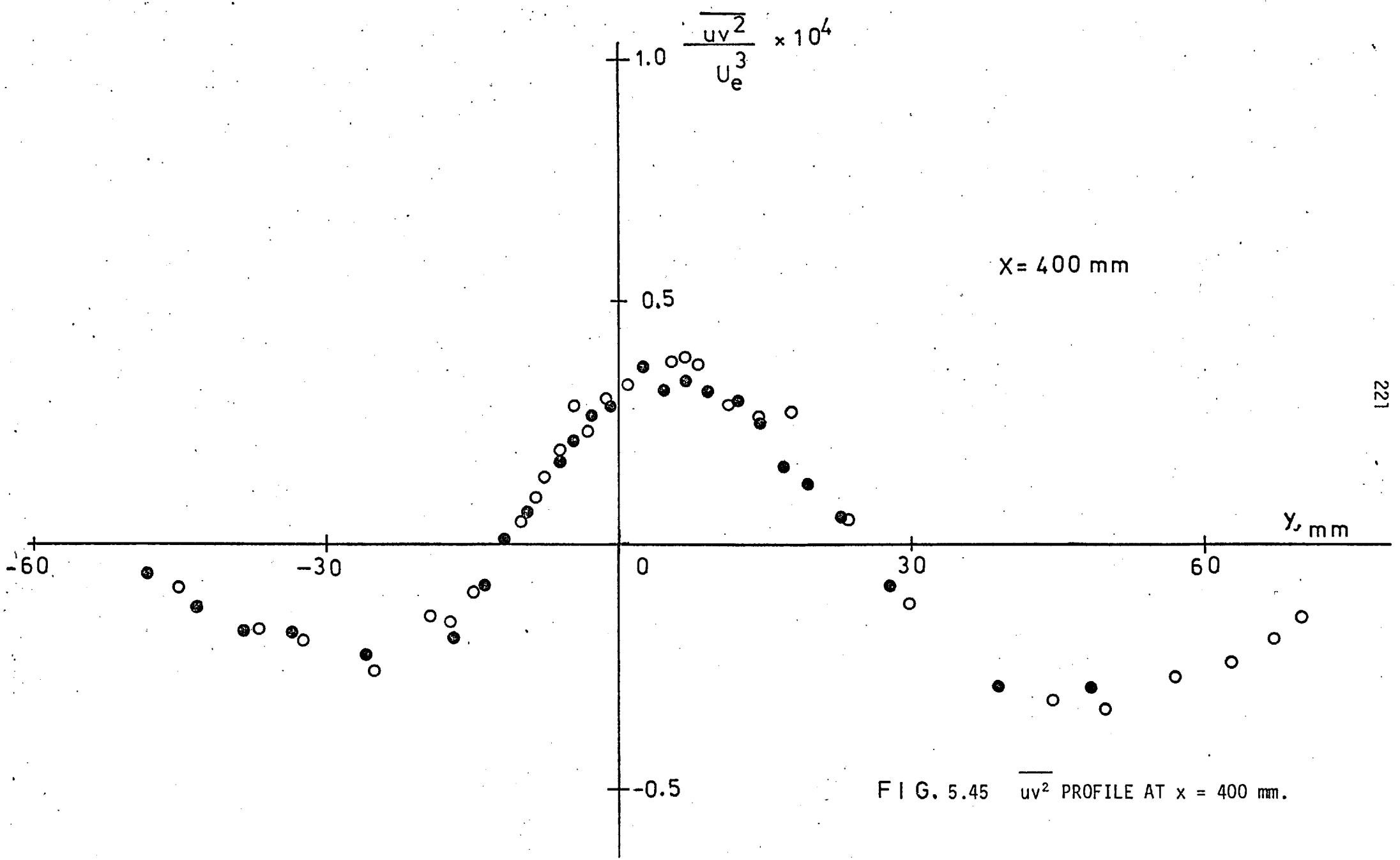

FIG. 5.45 $\overline{uv^2}$ PROFILE AT x = 400 mm.

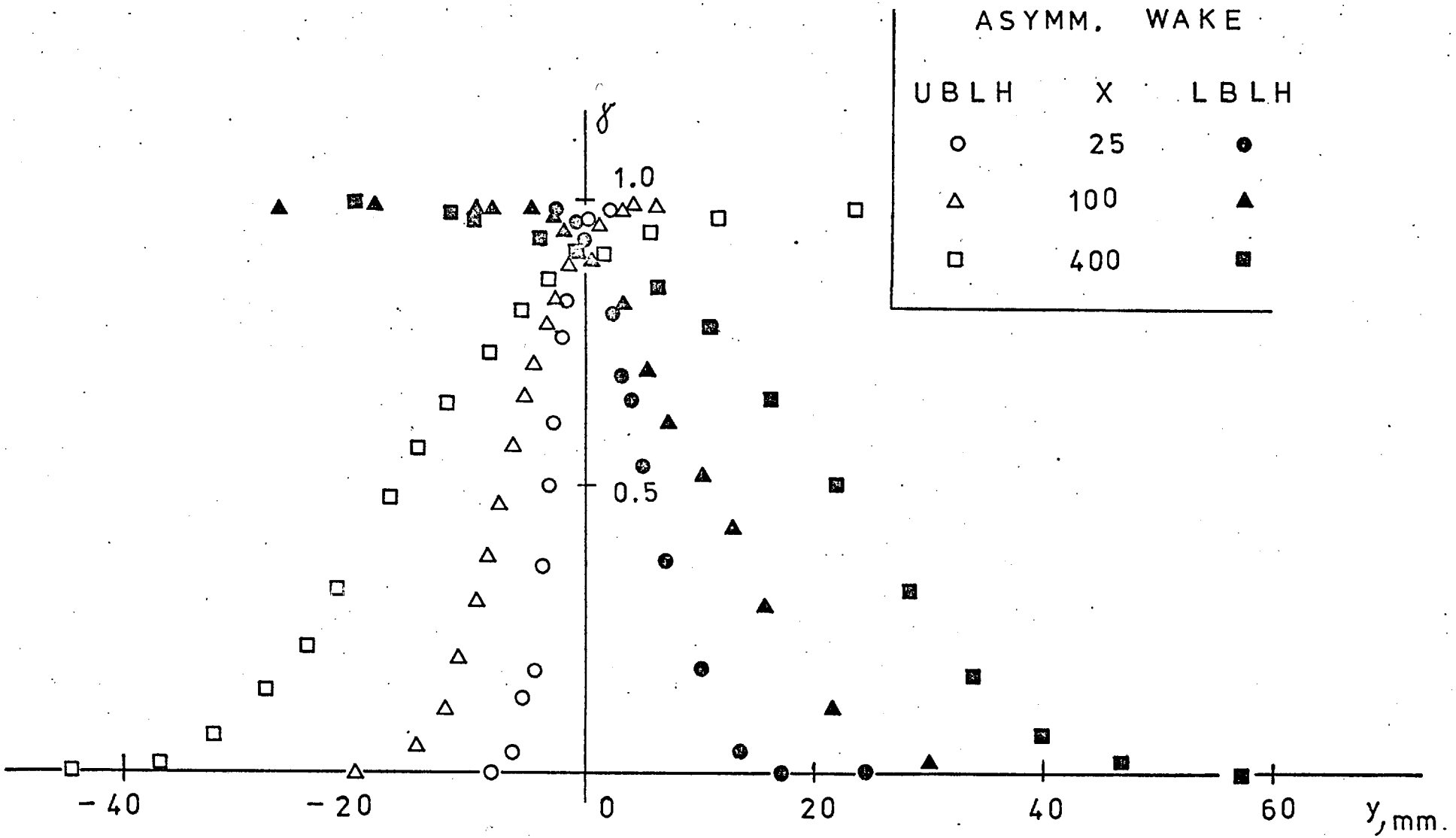

FIG. 5.46 INTERMITTENCY IN THE INNER WAKE

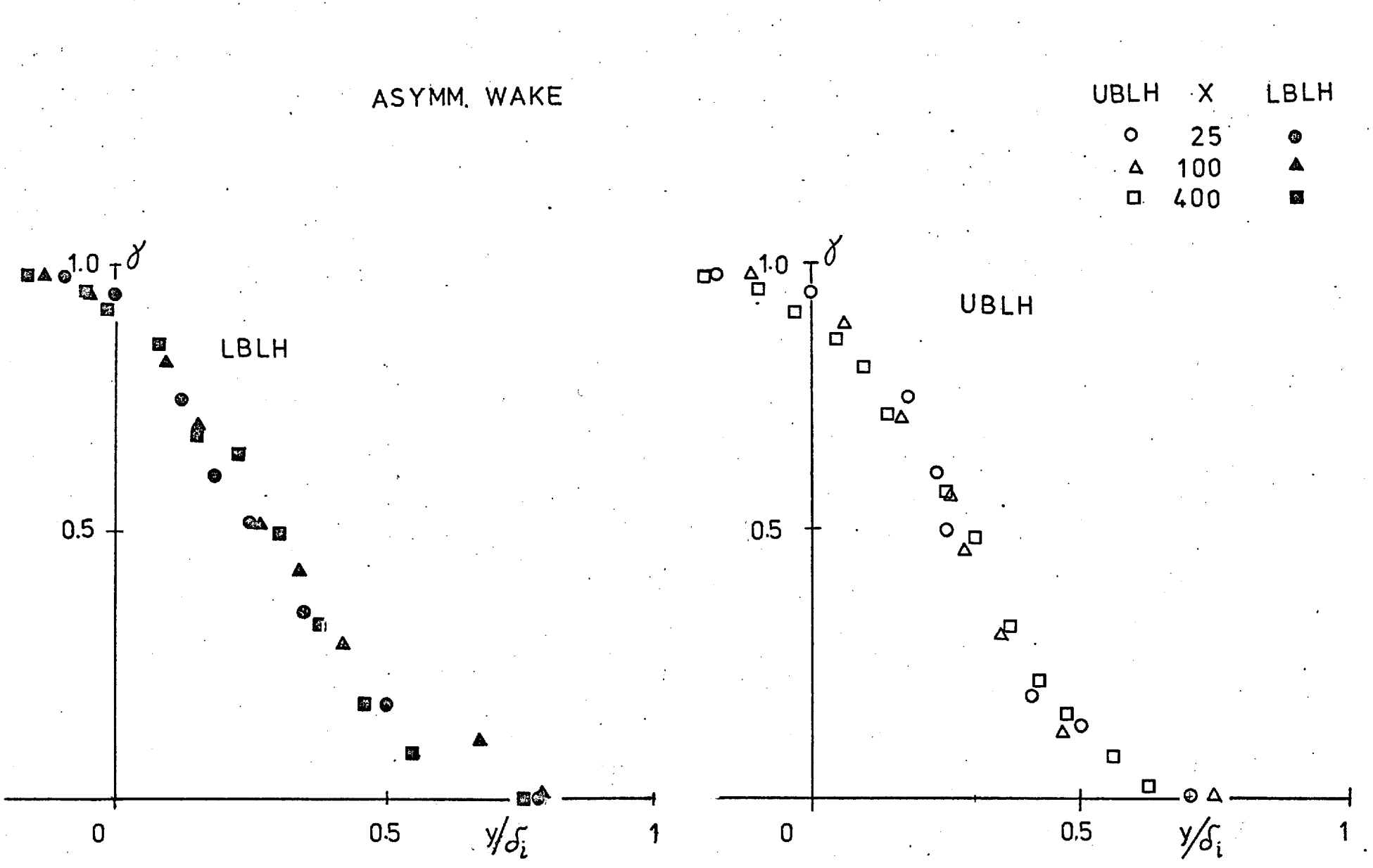

FIG. 5.47 INTERMITTENCY IN THE INNER WAKE NON-DIMENSIONALIZED BY INNER WAKE WIDTH

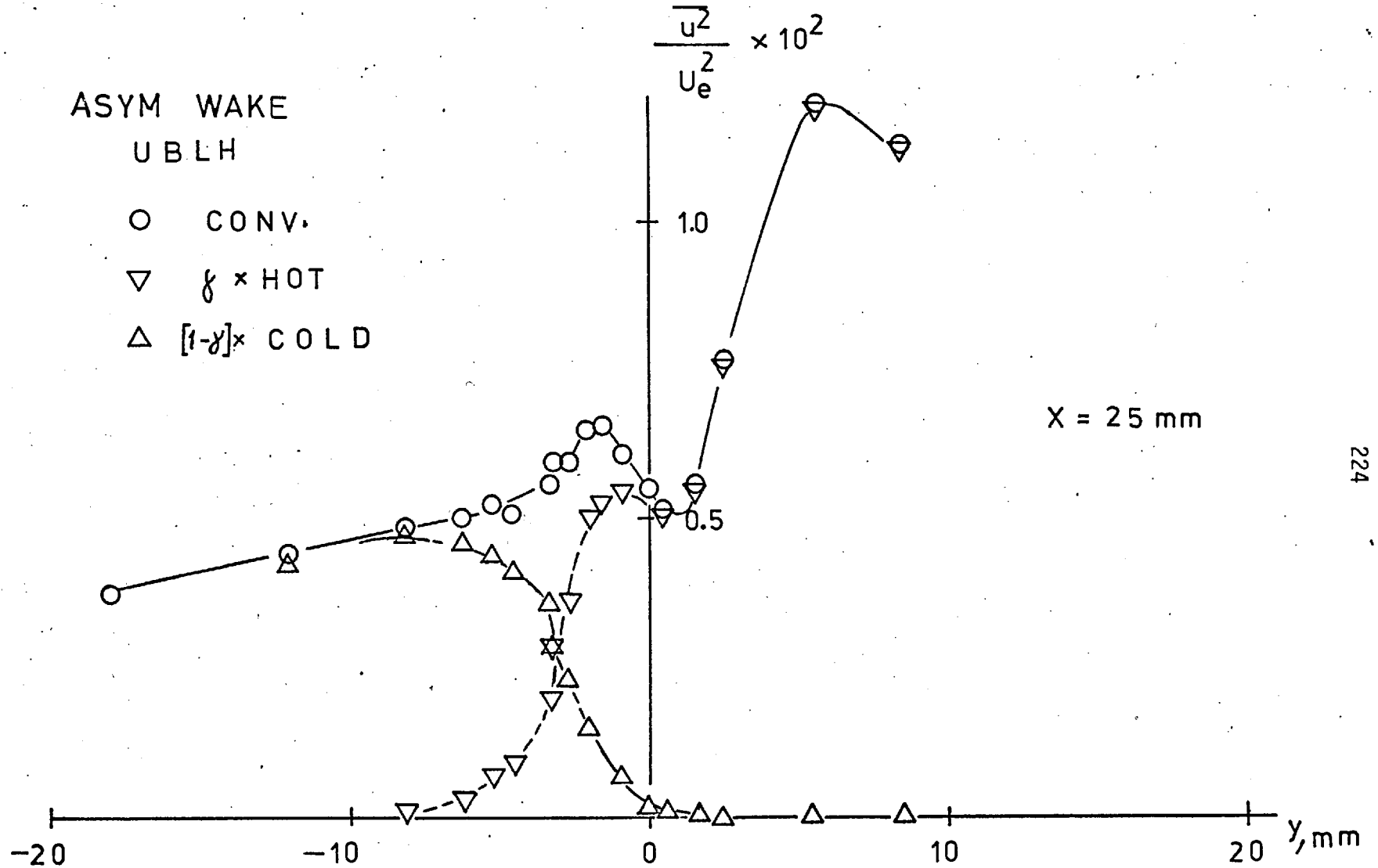

FIG. 5.48 $\overline{u^2}$ PROFILE AT x = 25 mm

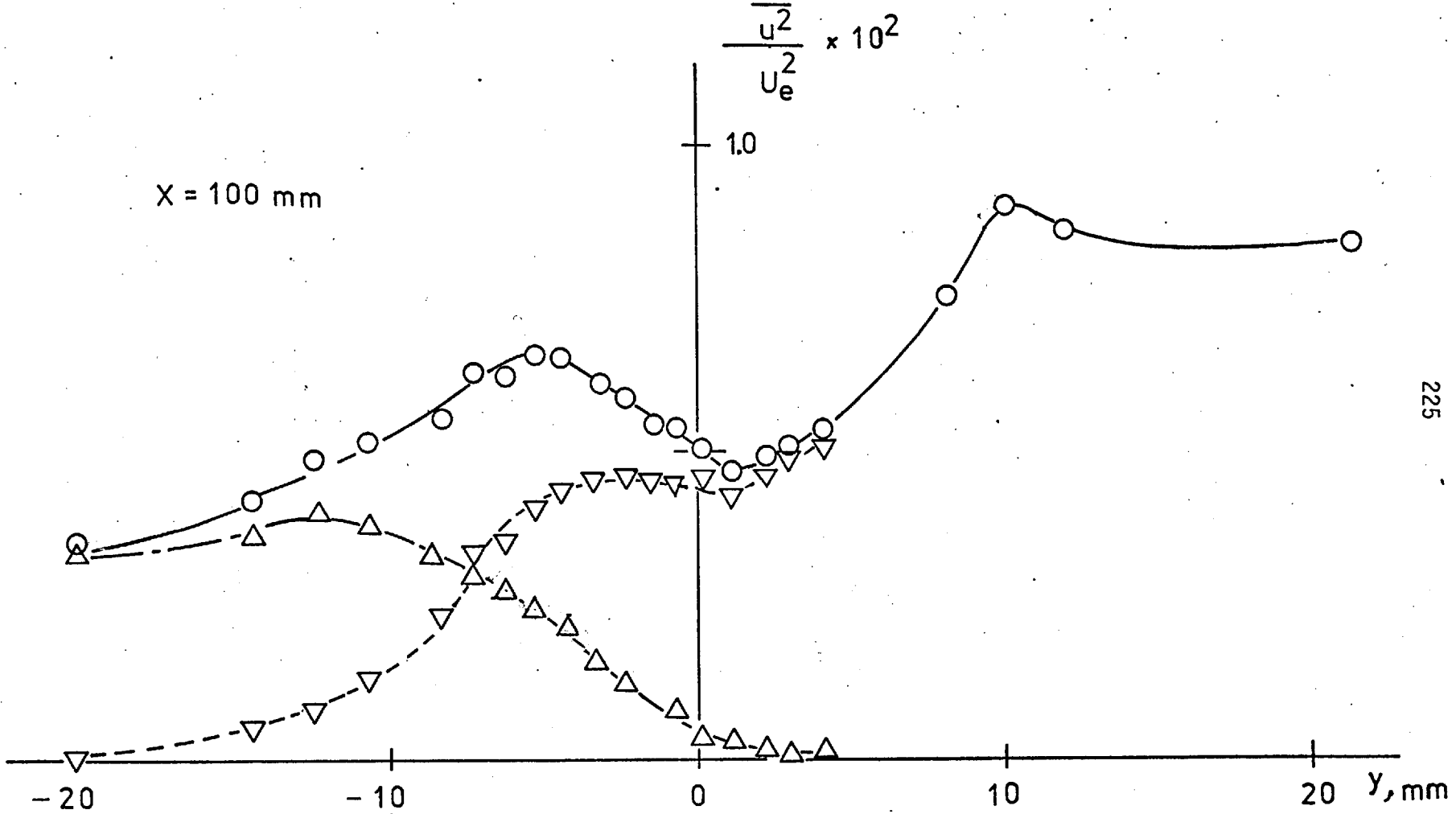

FIG. 5.49 $\overline{u^2}$ PROFILE AT x = 100 mm

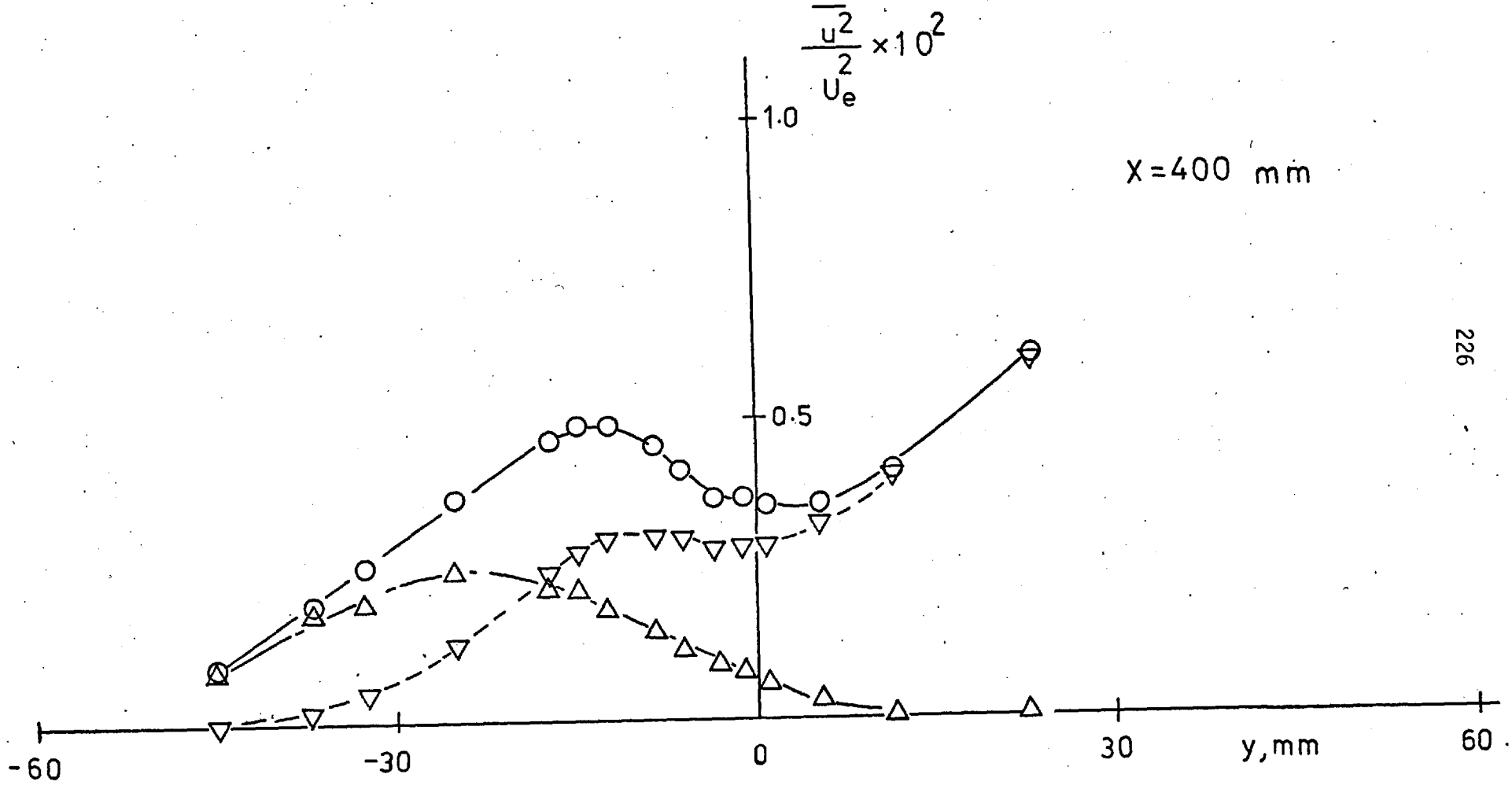

FIG. 5.50 $\overline{u^2}$ PROFILE AT x = 400 mm

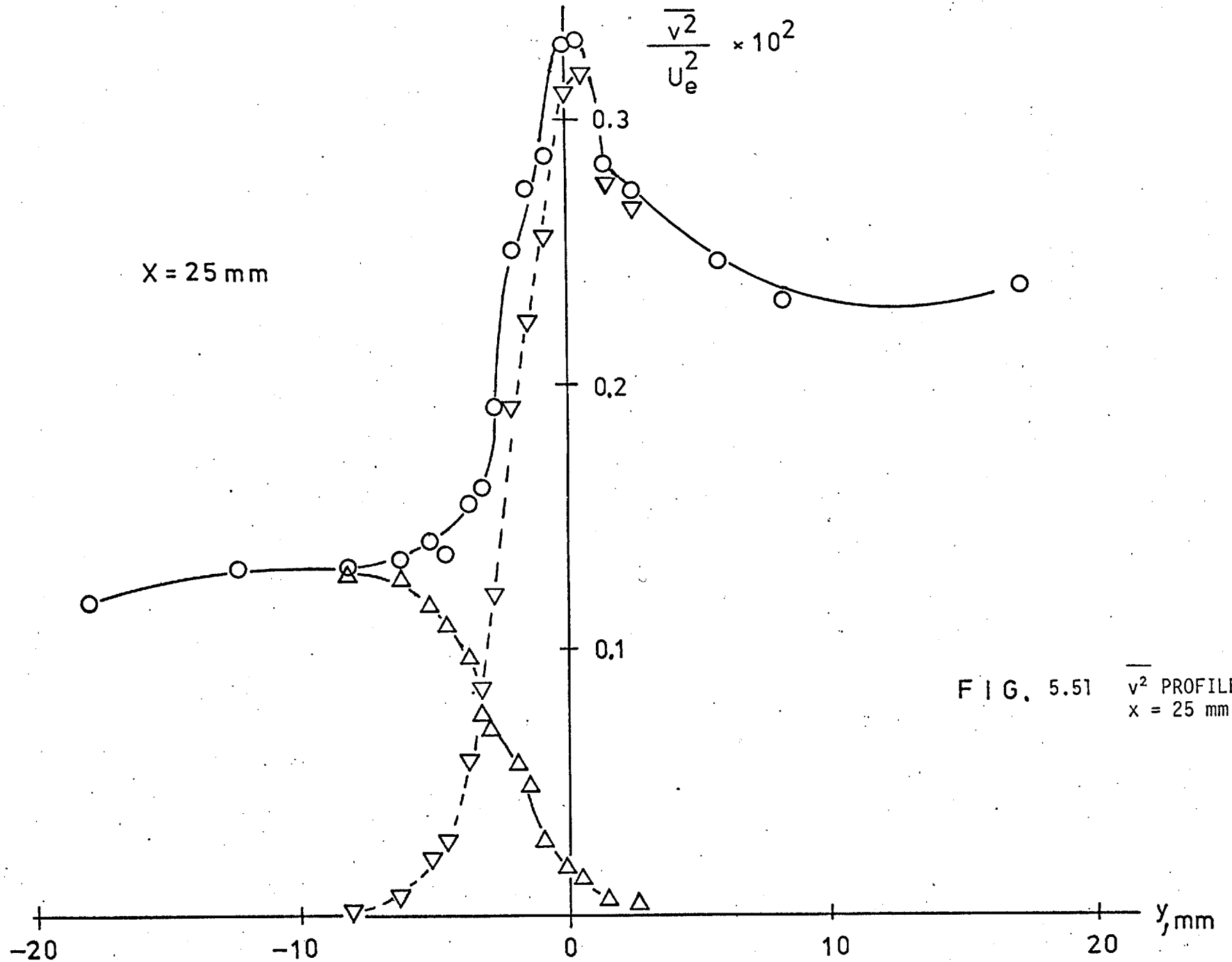

FIG. 5.51 $\overline{v^2}$ PROFILE AT x = 25 mm

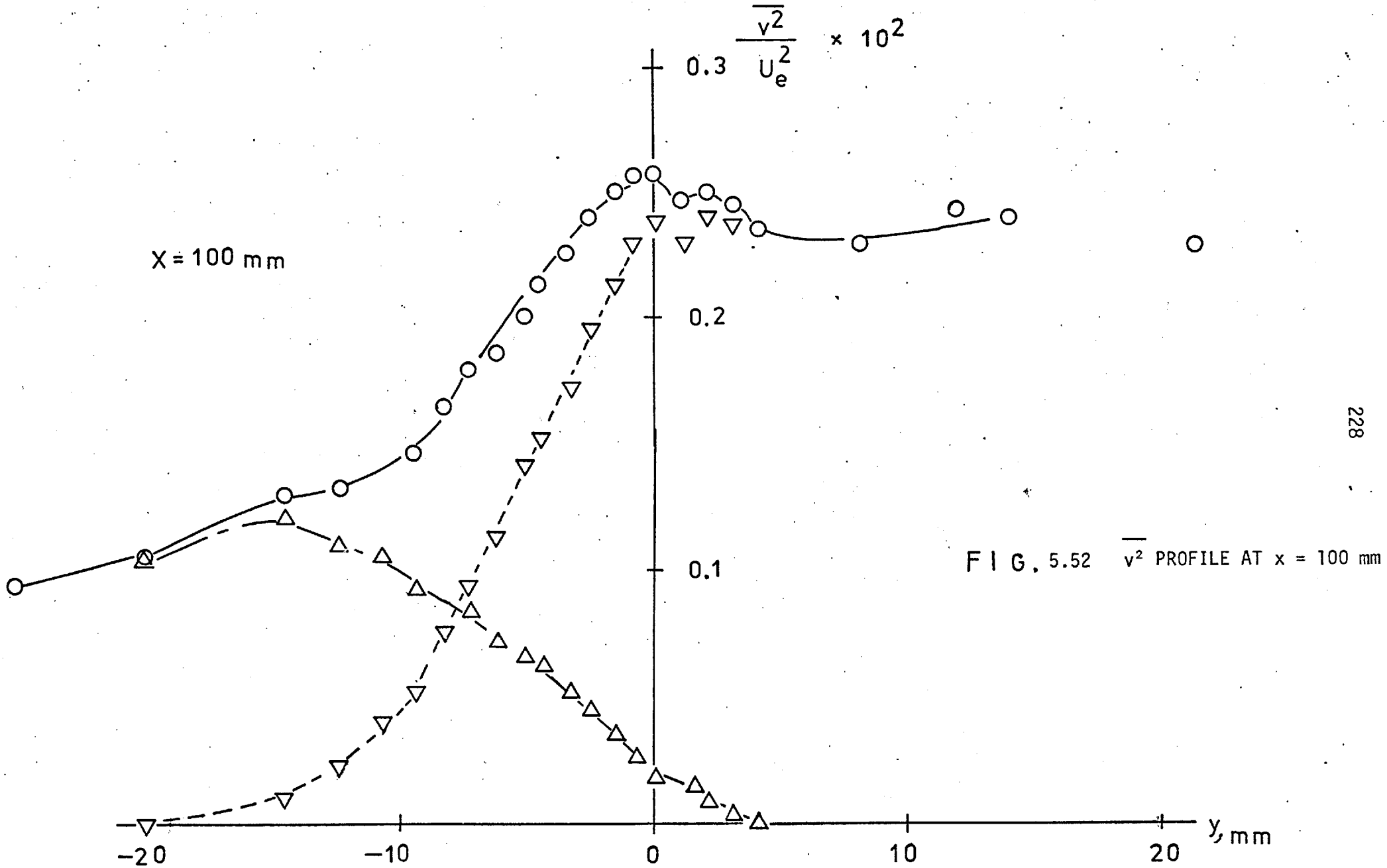

FIG. 5.52 $\overline{v^2}$ PROFILE AT x = 100 mm

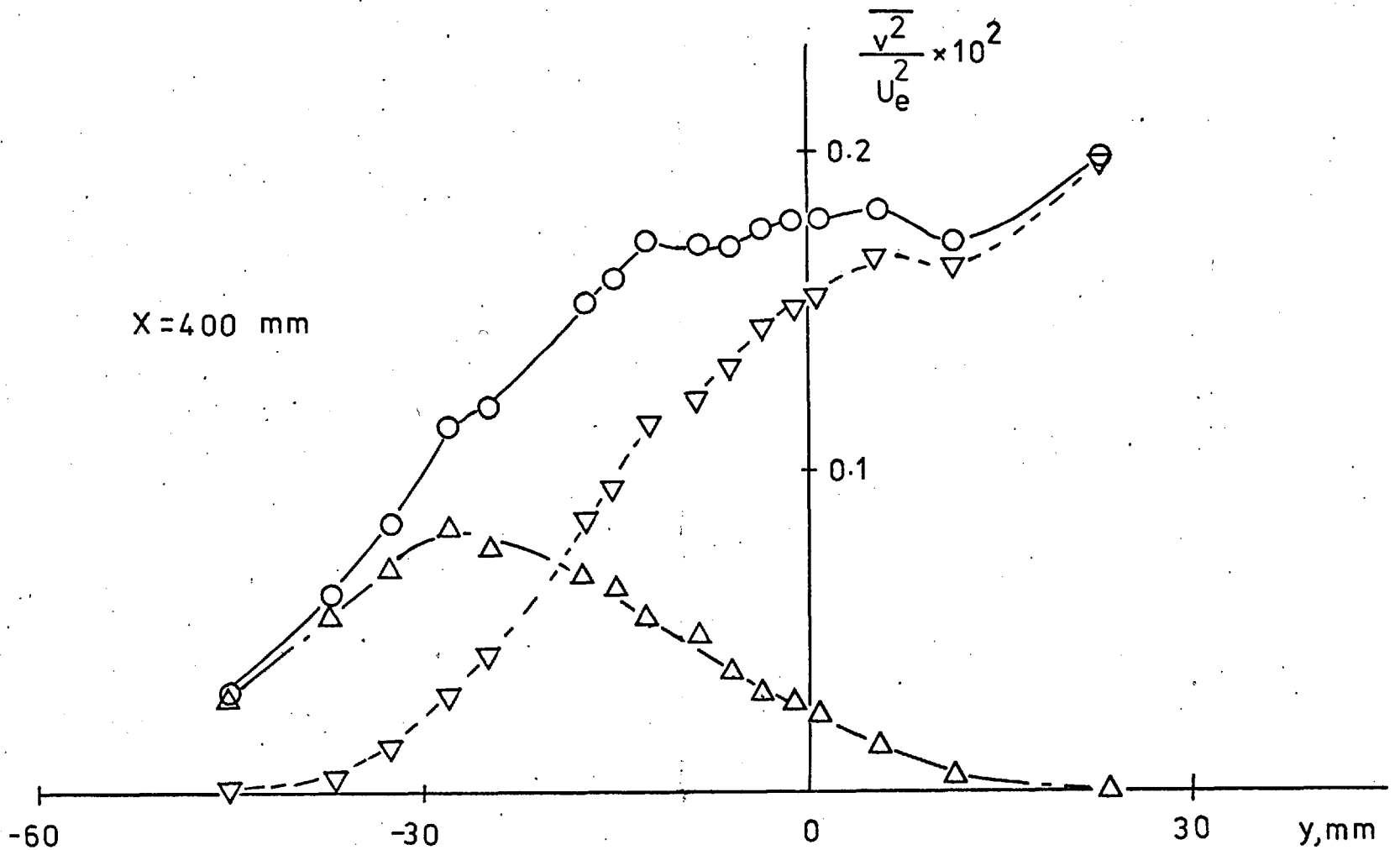

FIG. 5.53 $\overline{v^2}$ PROFILE AT x = 400 mm

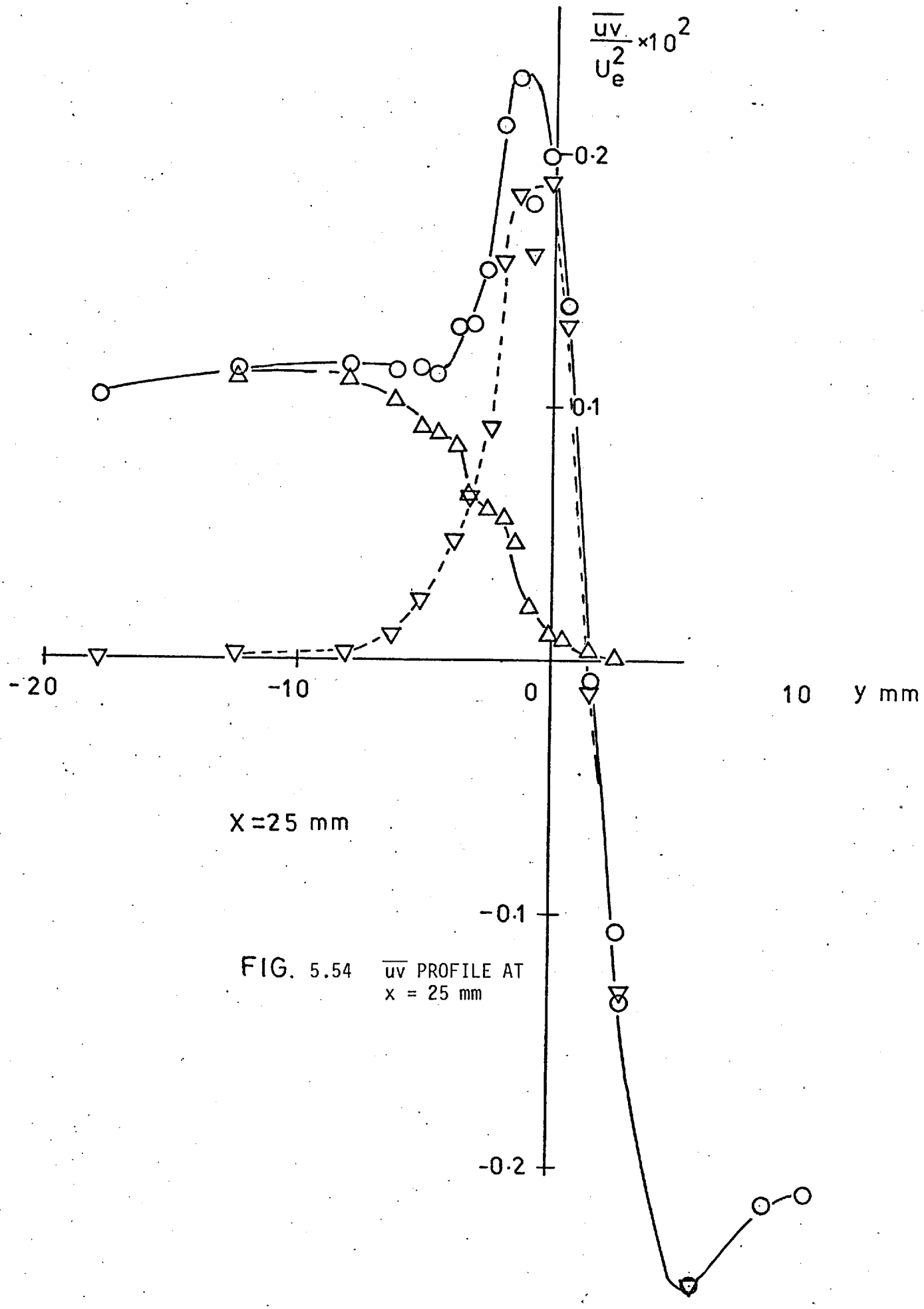

FIG. 5.54 $\overline{uv}$ PROFILE AT x = 25 mm

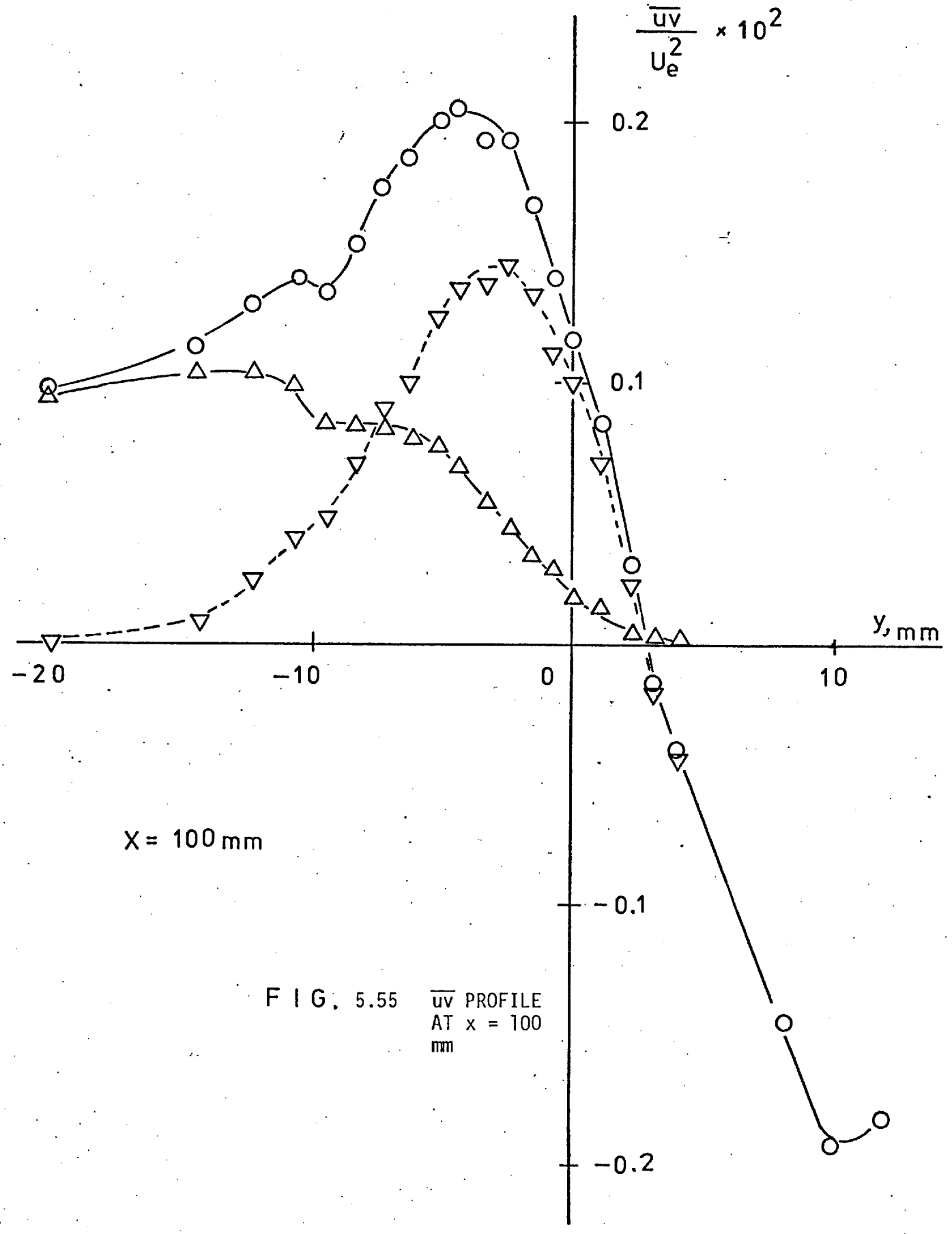

FIG. 5.55 $\overline{uv}$ PROFILE AT x = 100 mm

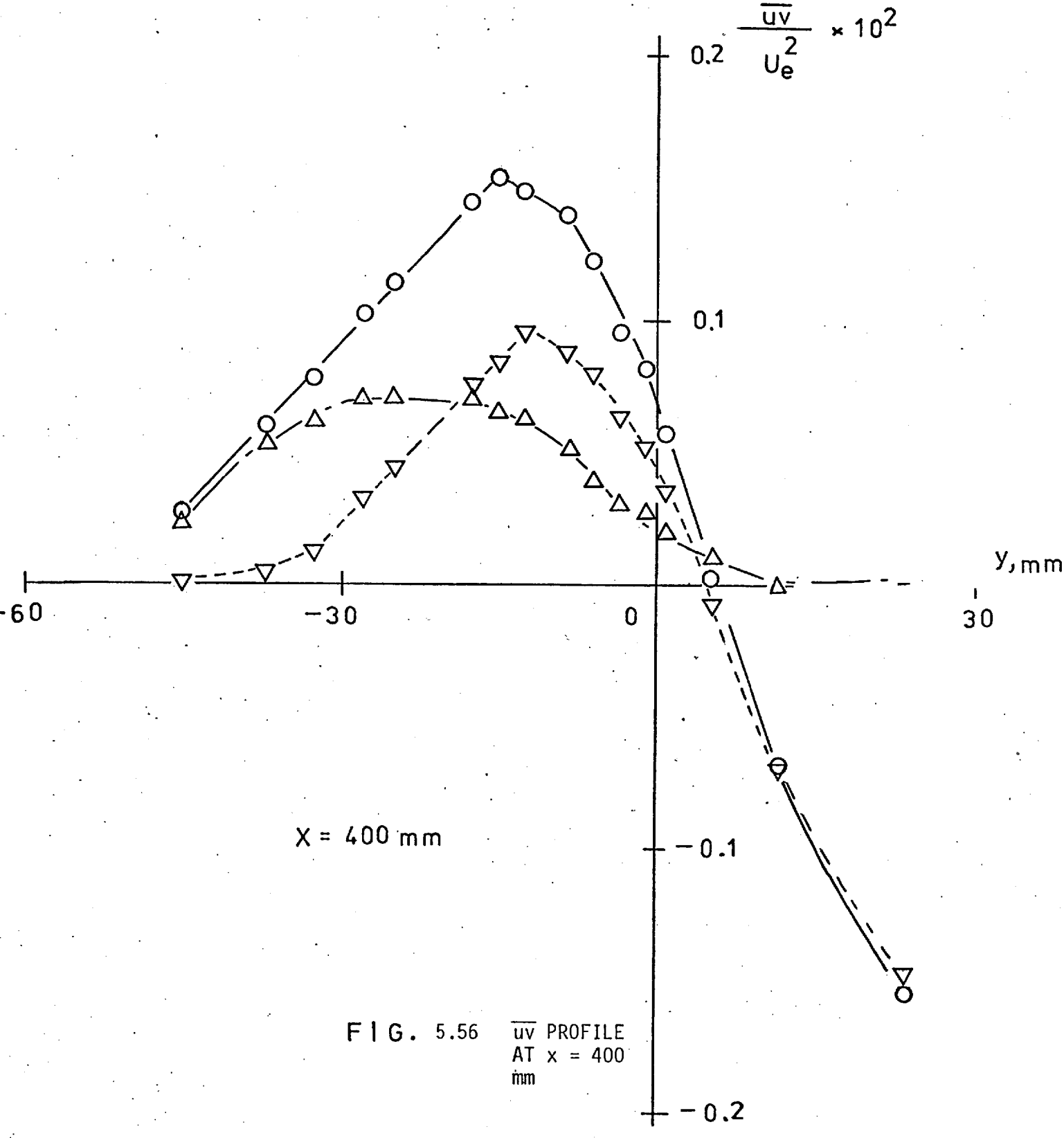

FIG. 5.56 $\overline{uv}$ PROFILE AT x = 400 mm

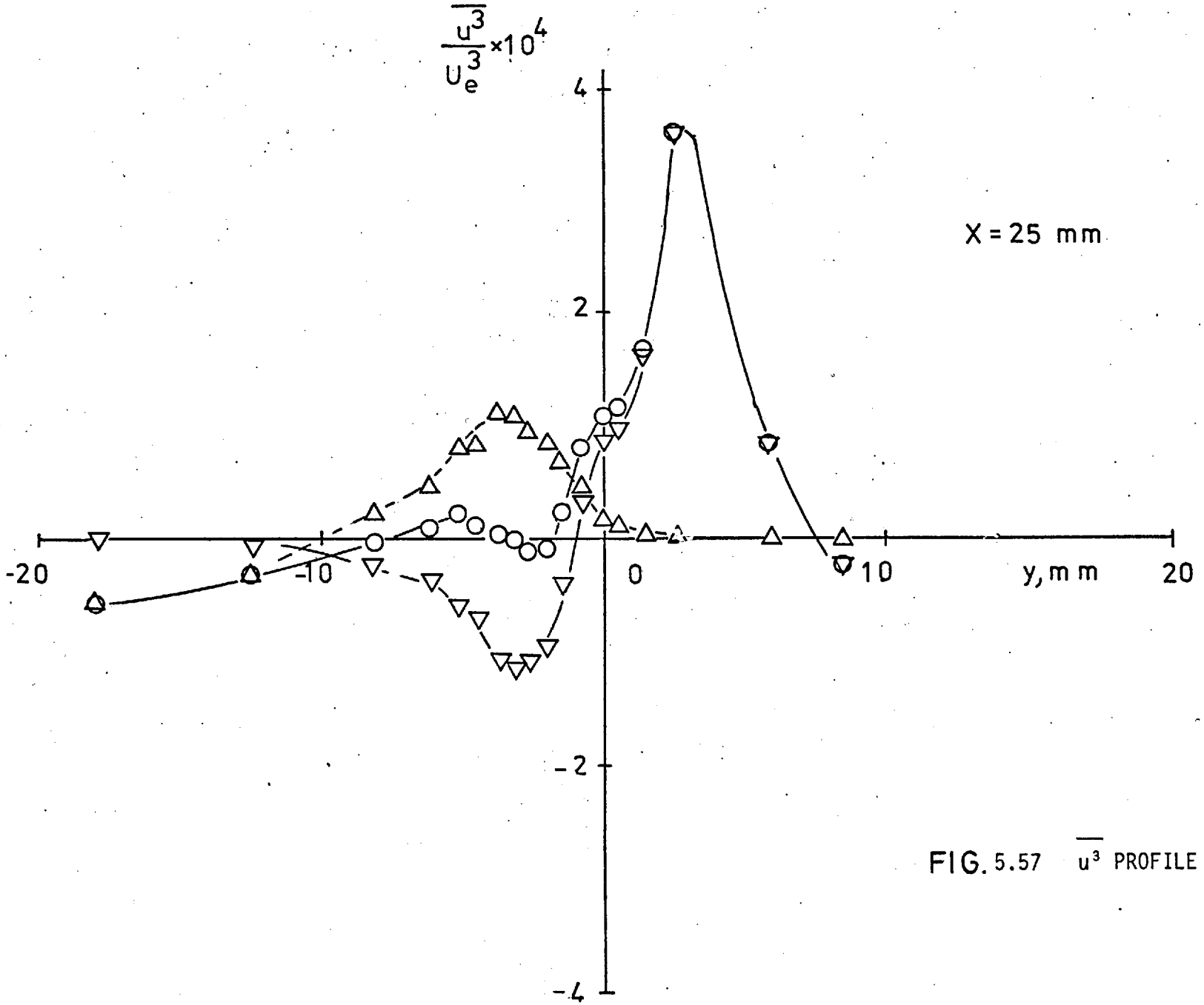

FIG. 5.57 $\overline{u^3}$ PROFILE AT x = 25 mm

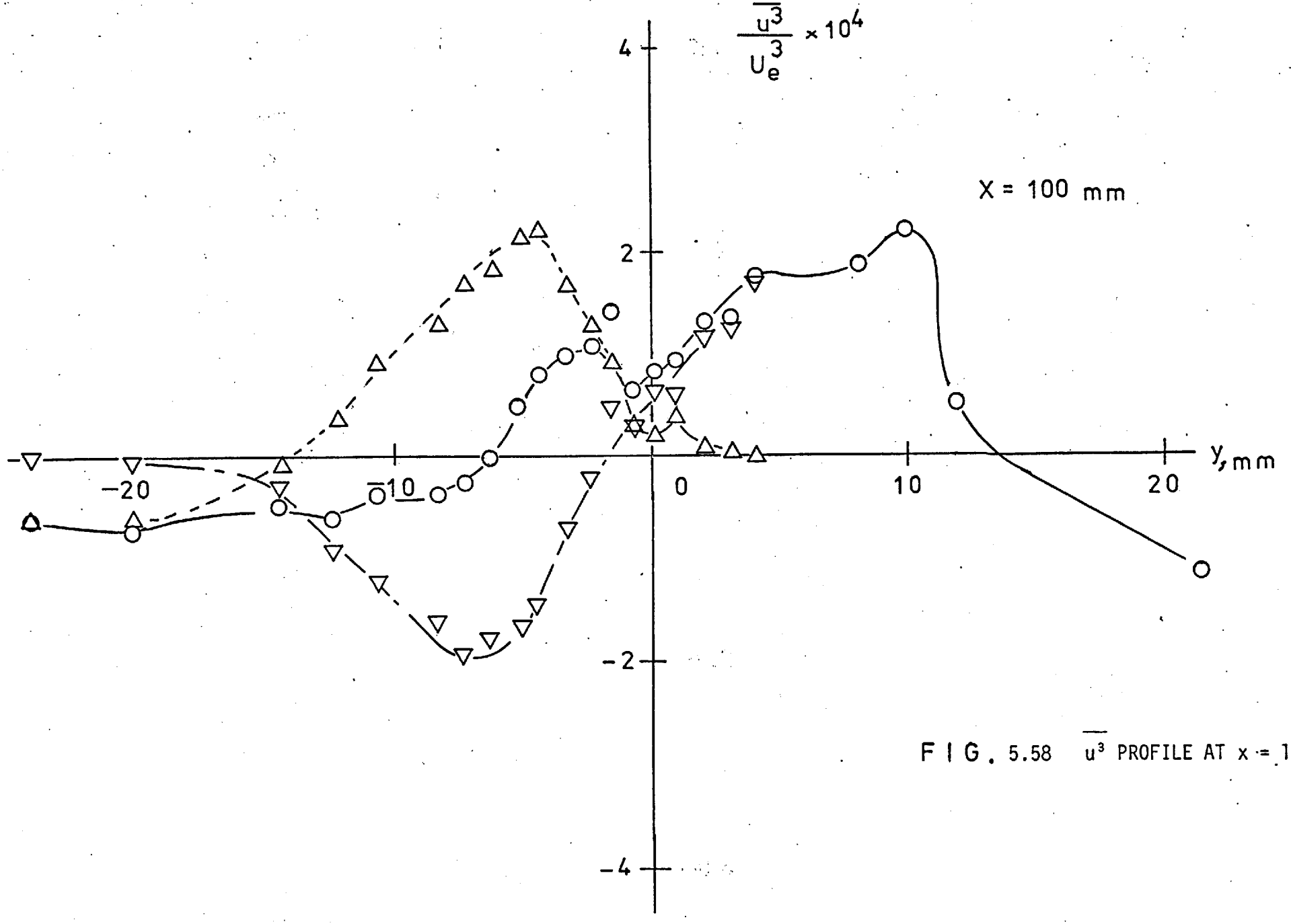

FIG. 5.58 $\overline{u^3}$ PROFILE AT x = 100 mm

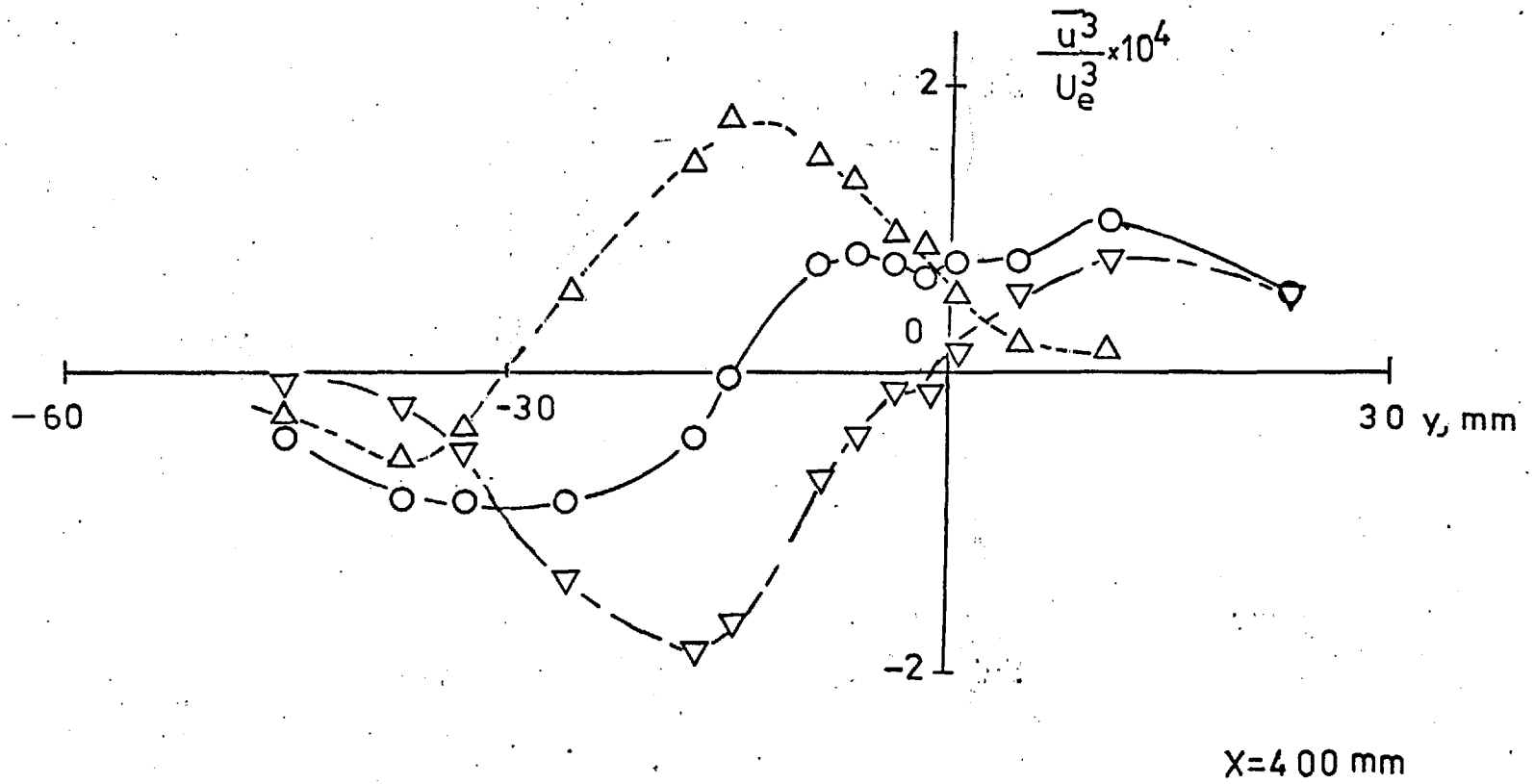

FIG. 5.59 $\overline{u^3}$ PROFILE AT x = 400 mm

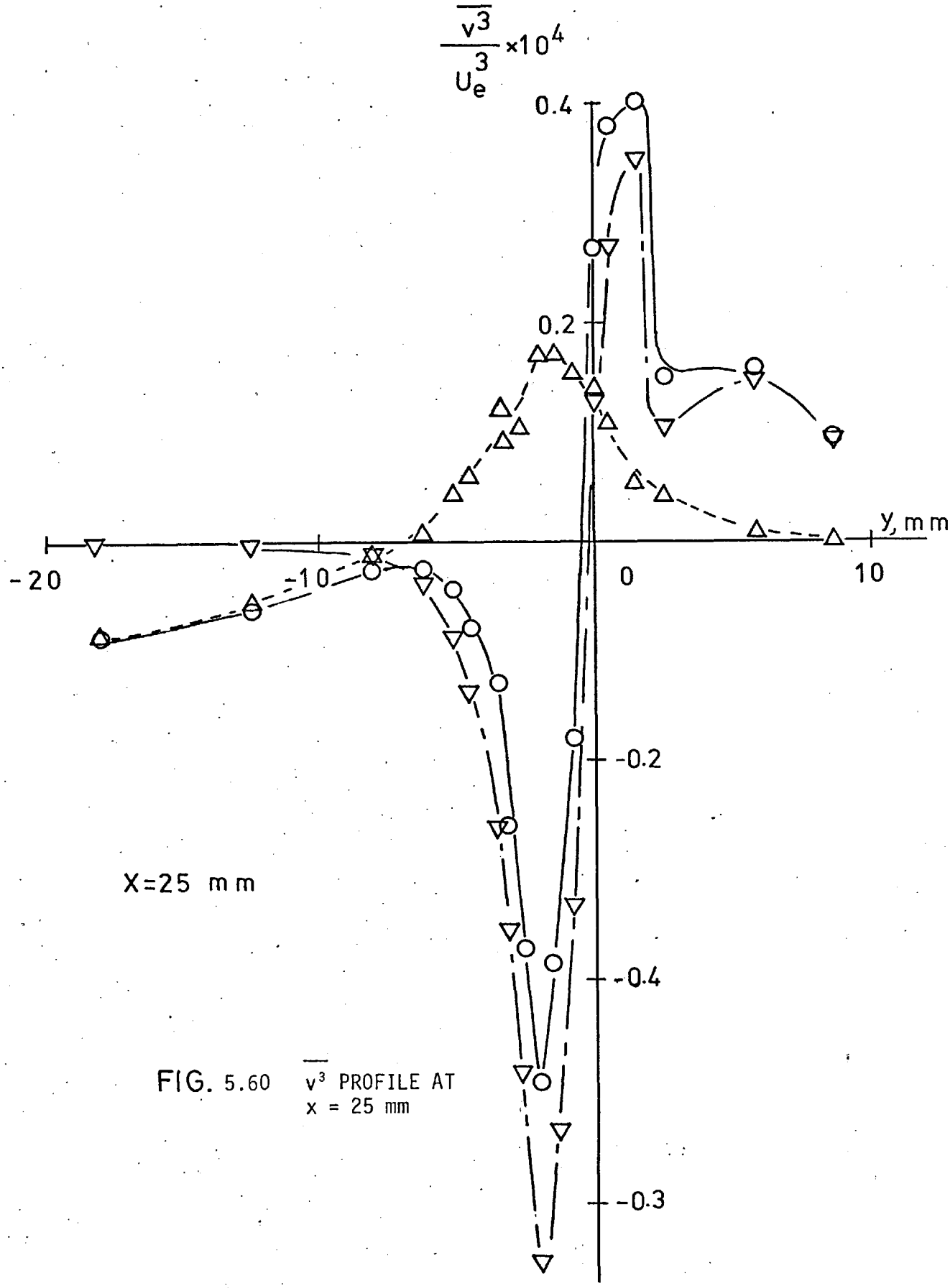

FIG. 5.60 $\overline{v^3}$ PROFILE AT x = 25 mm

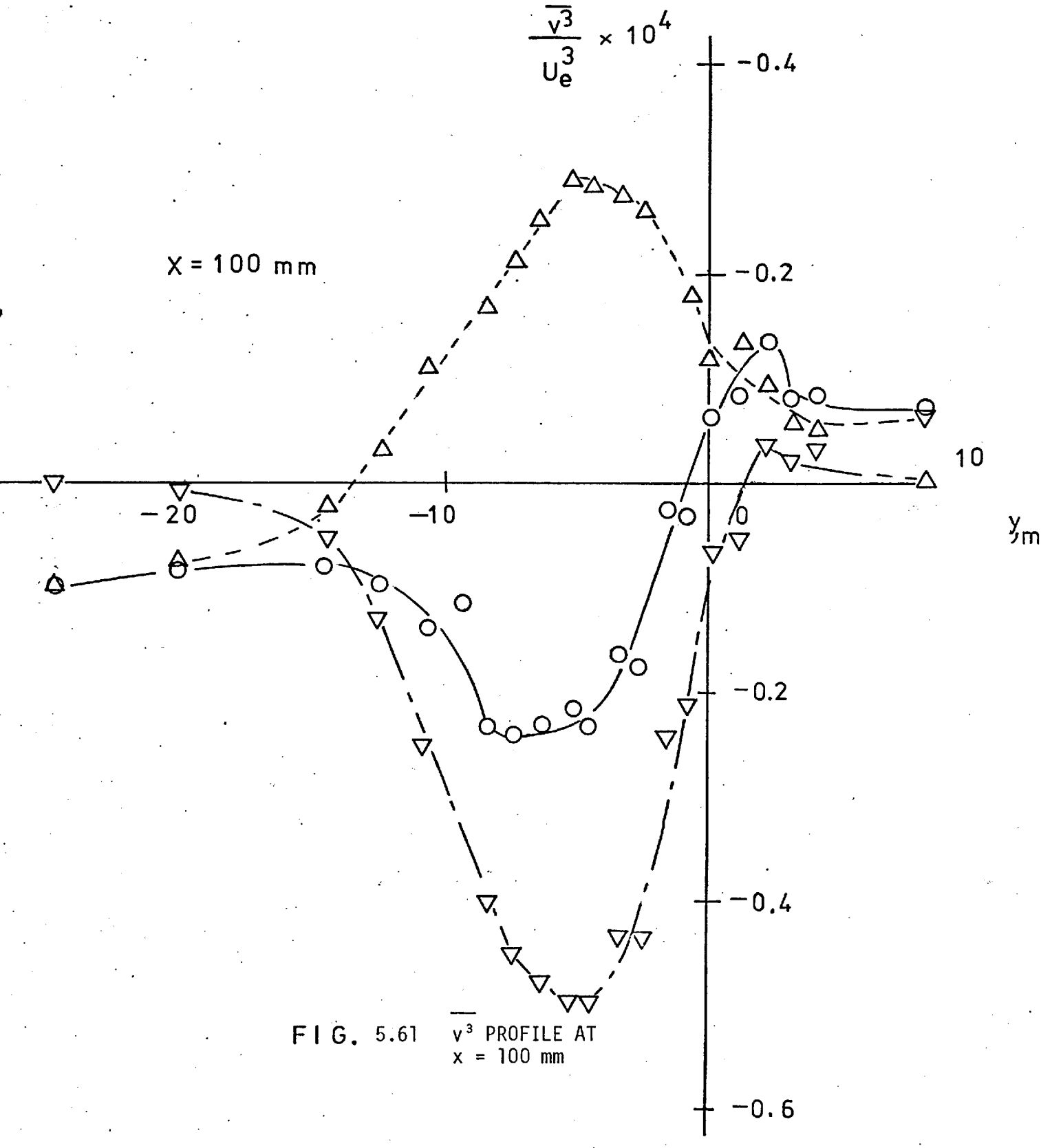

FIG. 5.61 $\overline{v^3}$ PROFILE AT x = 100 mm

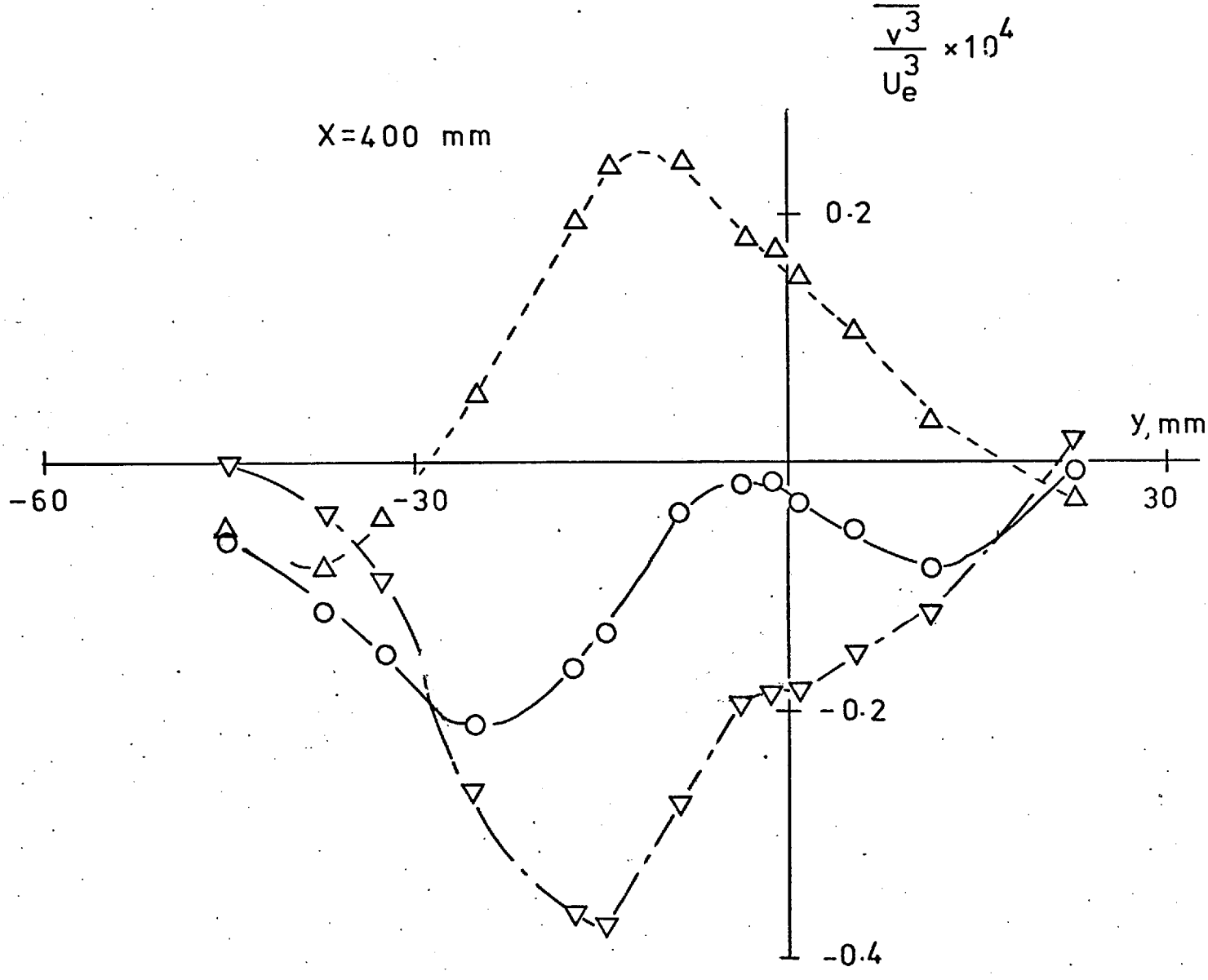

FIG. 5.62 $\overline{v^3}$ PROFILE AT x = 400 mm

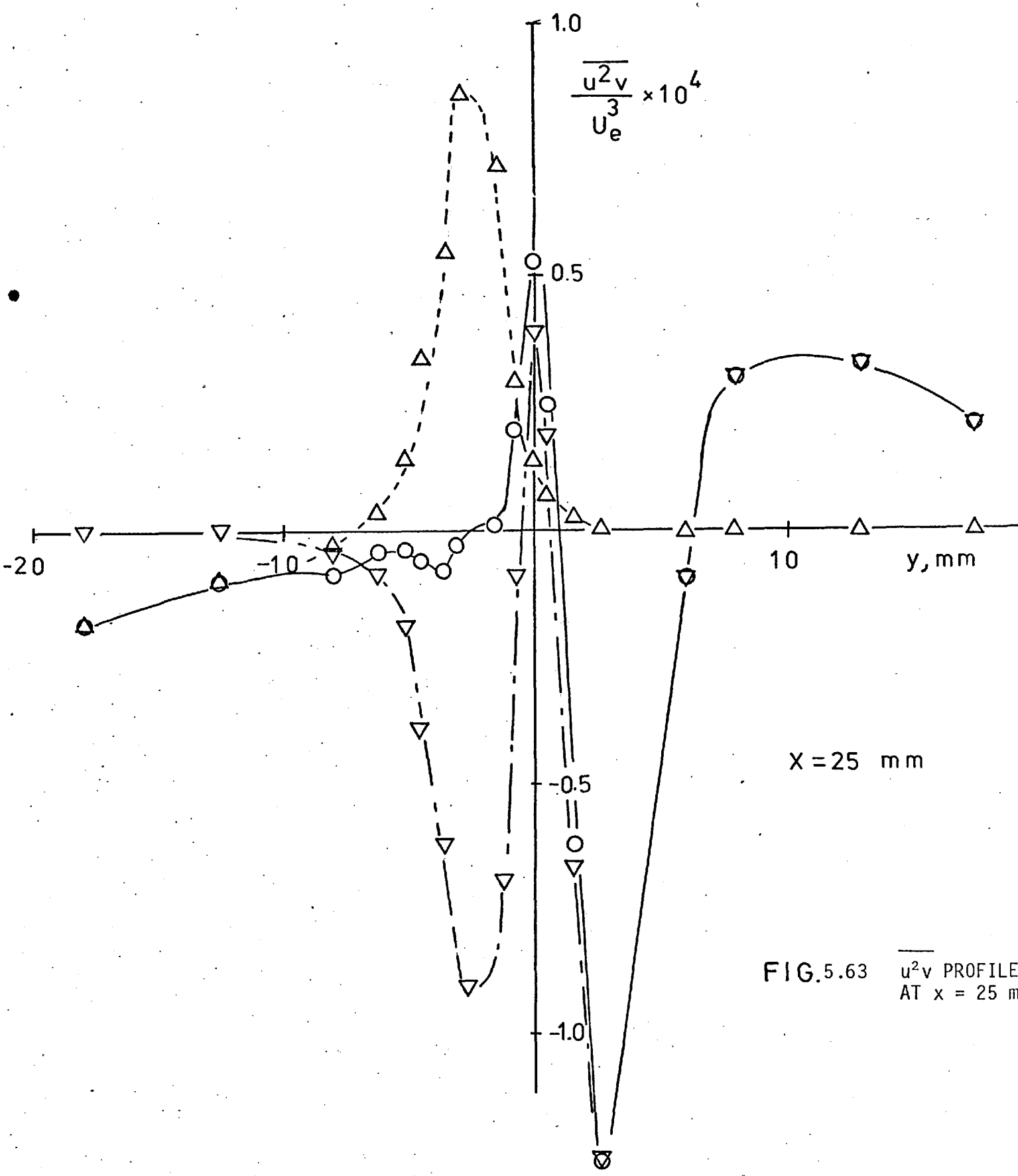

FIG. 5.63 $\overline{u^2v}$ PROFILE AT x = 25 mm

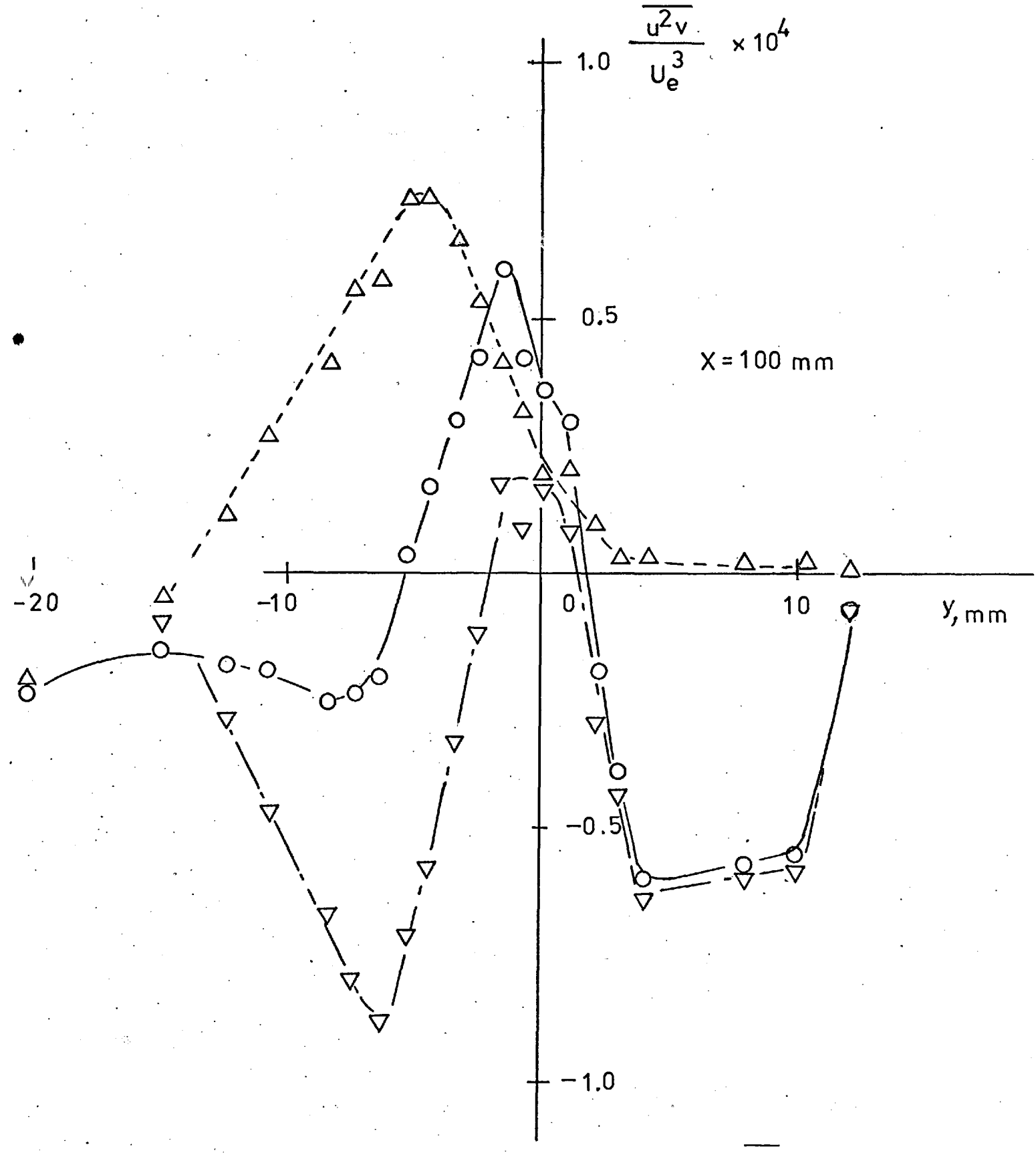

FIG. 5.64 $\overline{u^2v}$ PROFILE AT x = 100 mm

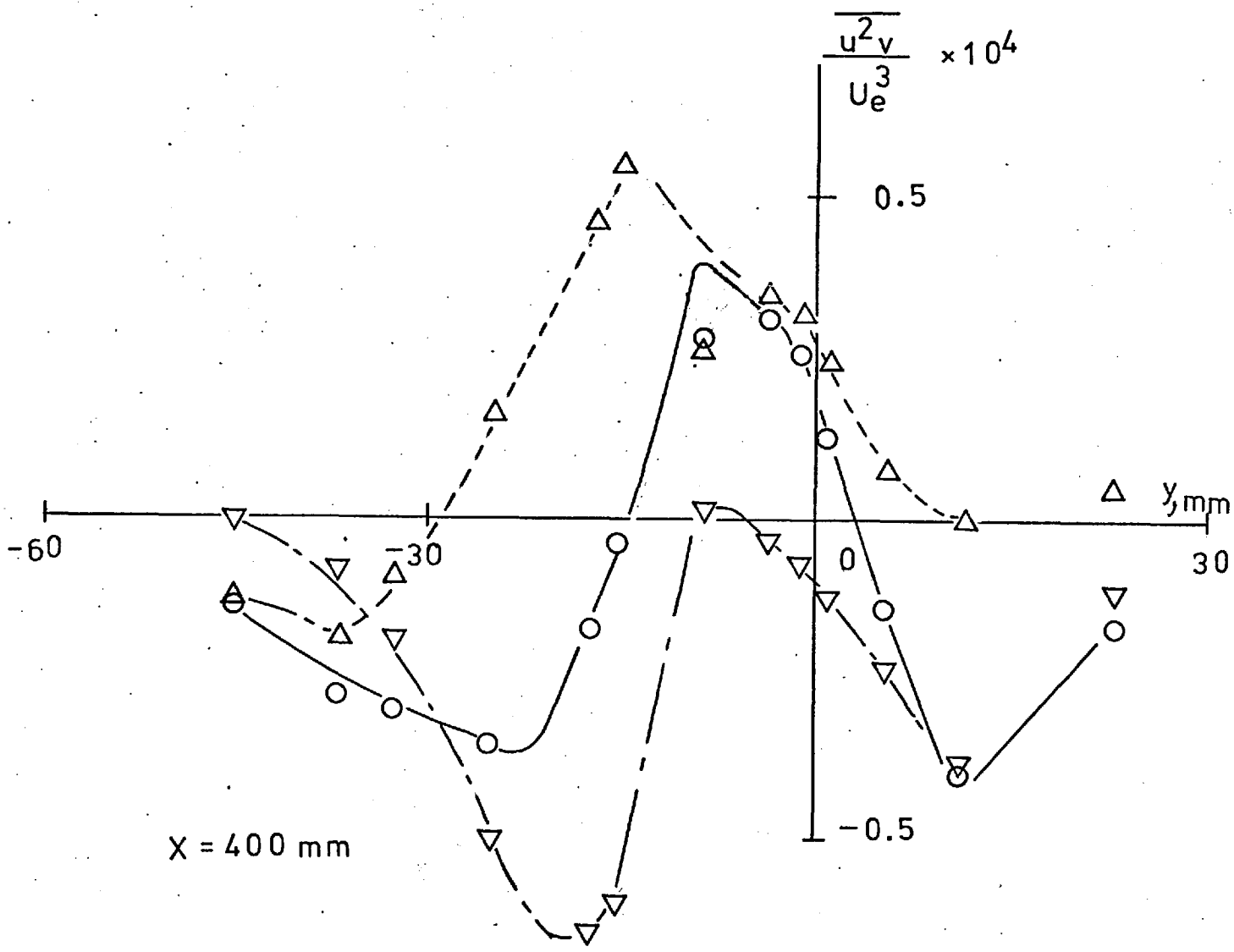

FIG. 5.65 $\overline{u^2v}$ PROFILE AT x = 400 mm

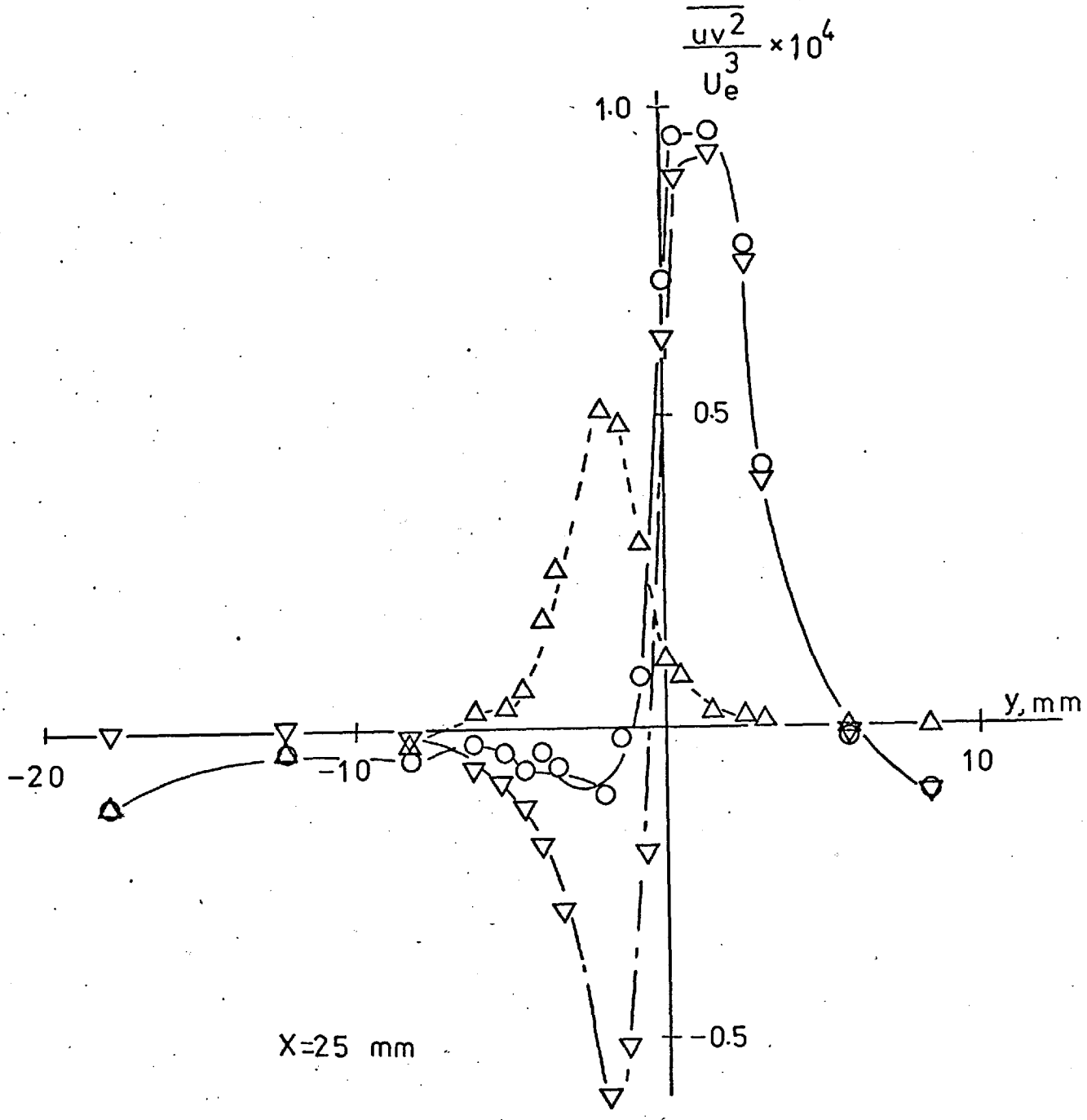

FIG. 5.66 $\overline{uv^2}$ PROFILE AT x = 25 mm

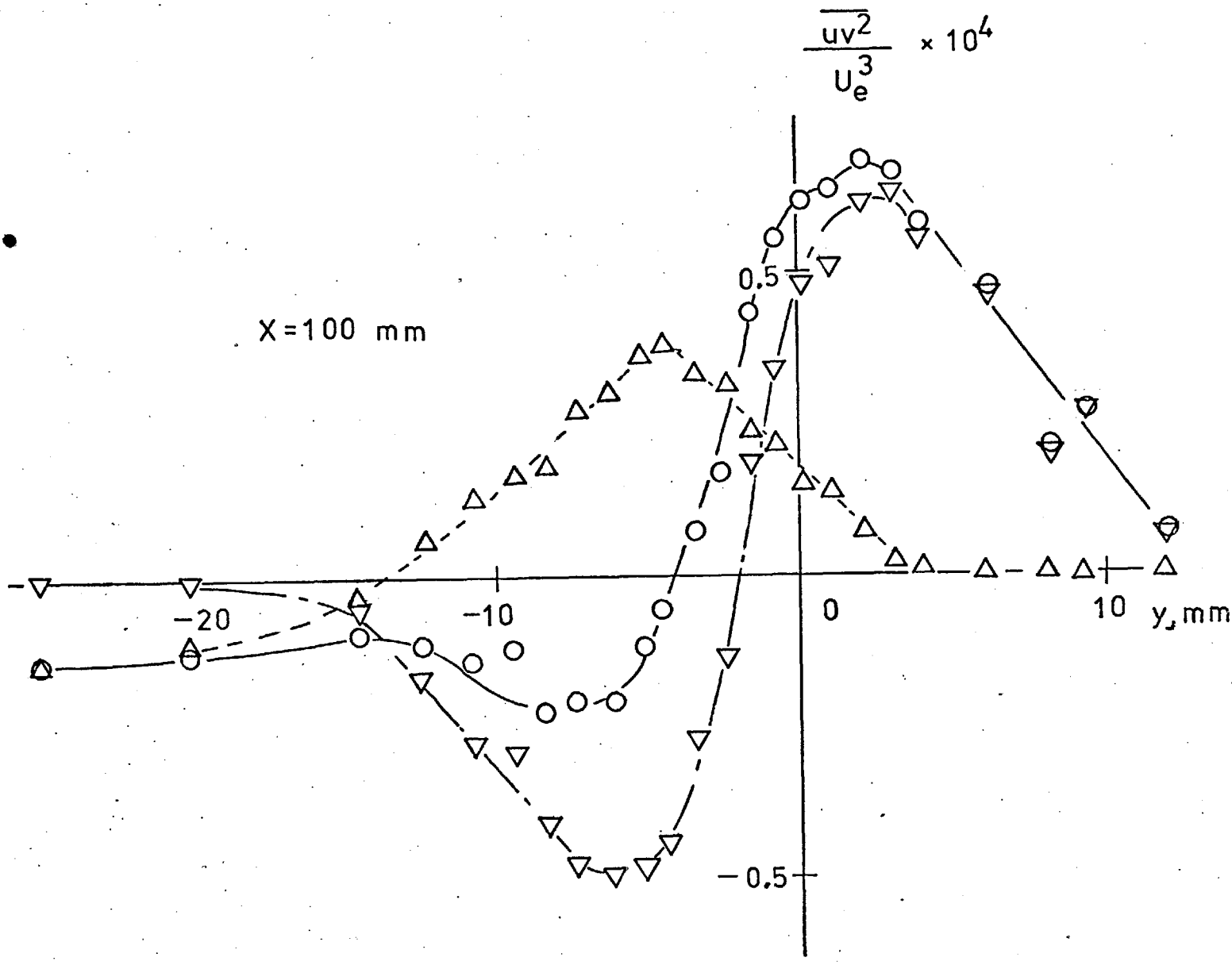

FIG. 5.67 $\overline{uv^2}$ PROFILE AT x = 100 mm

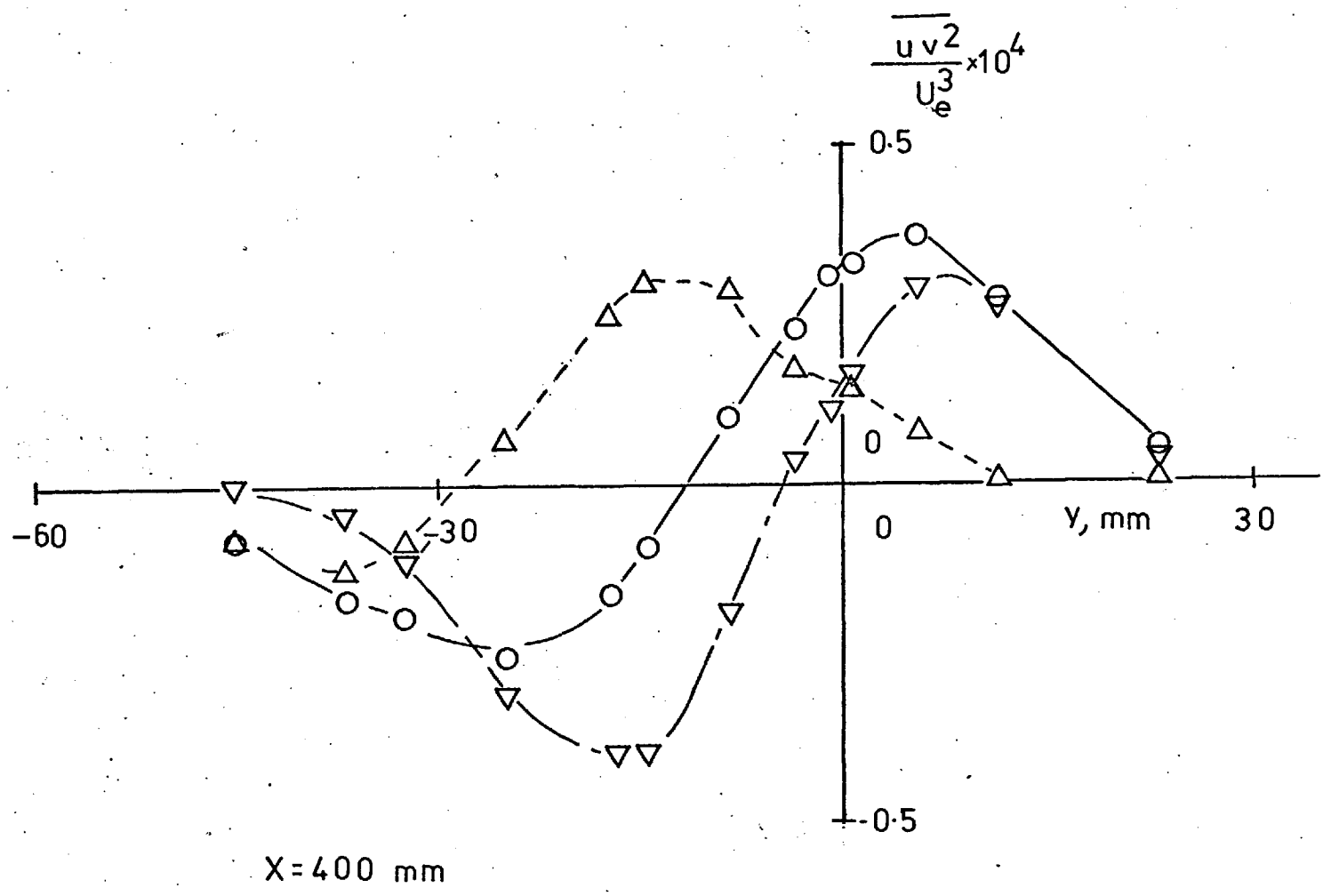

FIG. 5.68 $\overline{uv^2}$ PROFILE AT x = 400 mm

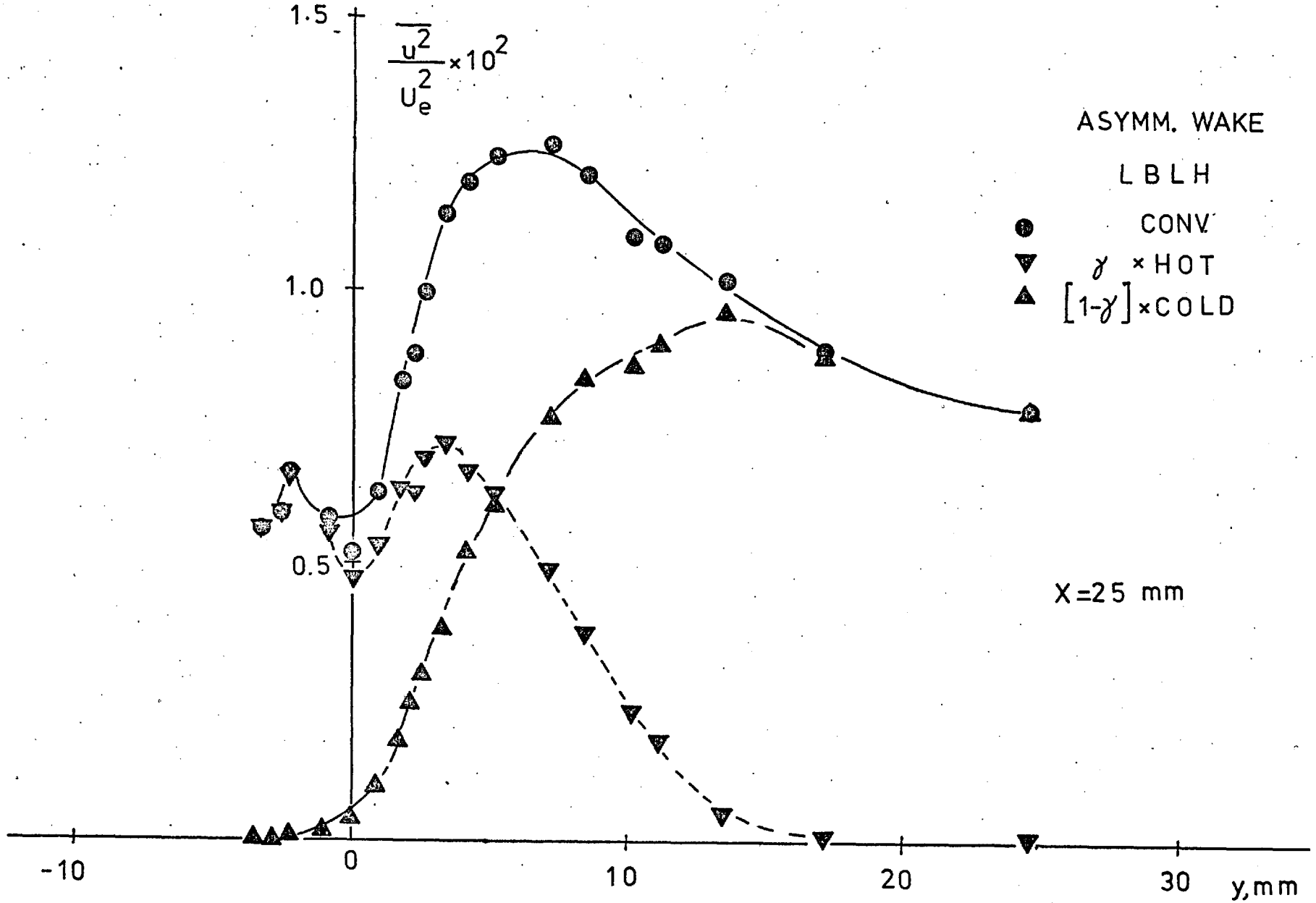

FIG. 5.69 $\overline{u^2}$ PROFILE AT x = 25 mm

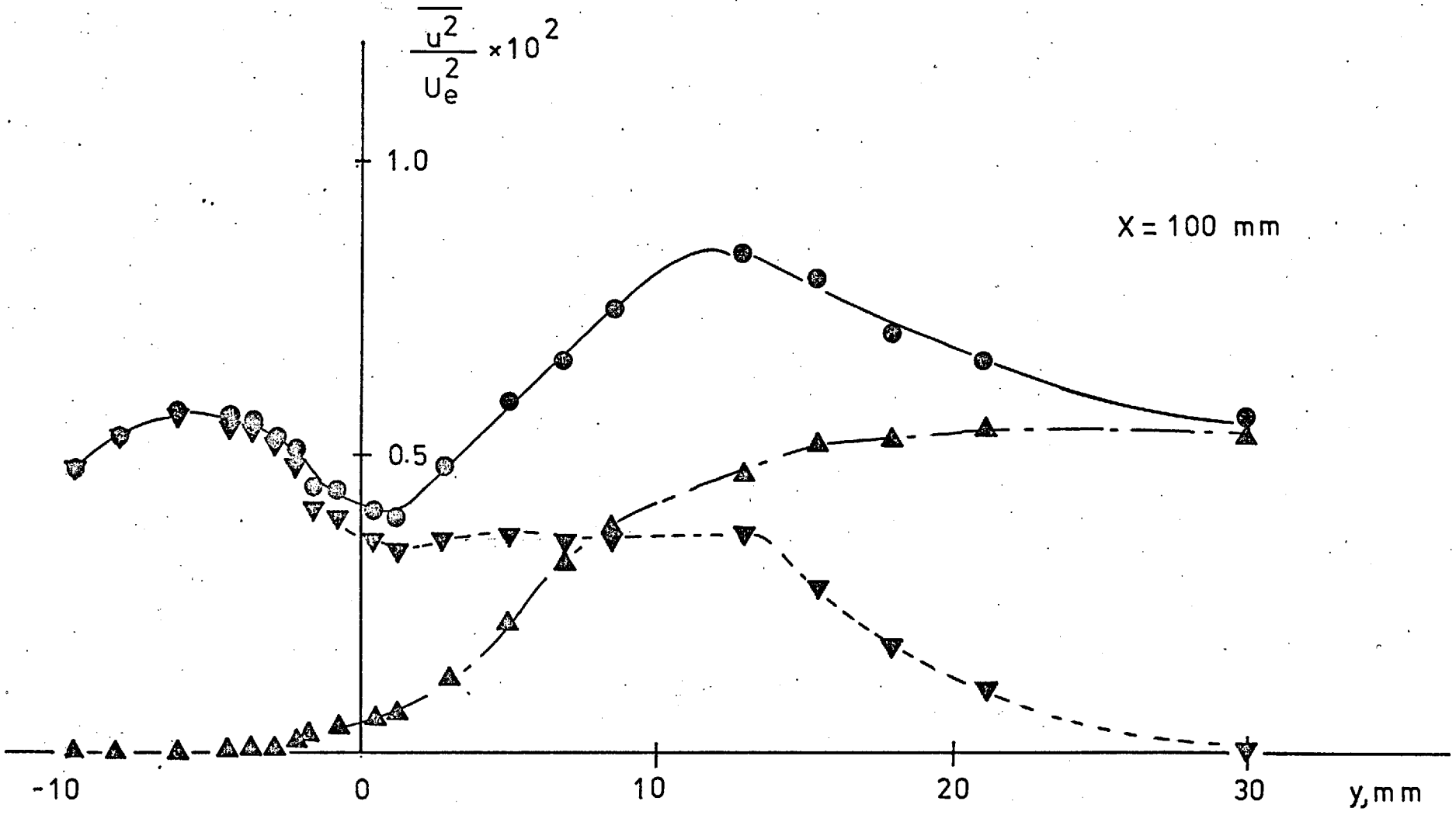

FIG. 5.70 $\overline{u^2}$ PROFILE AT x = 100 mm

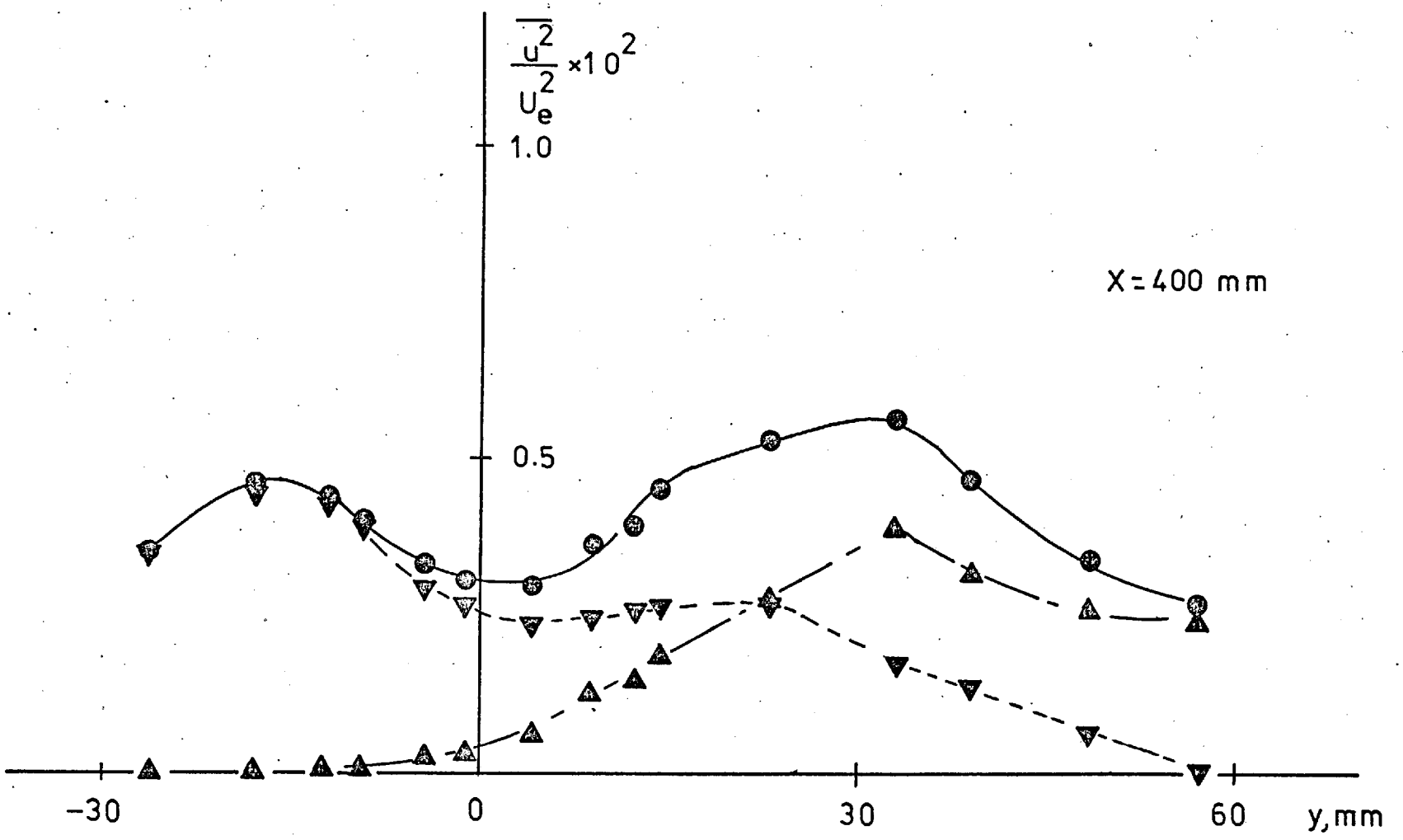

FIG. 5.71 $\overline{u^2}$ PROFILE AT x = 400 mm

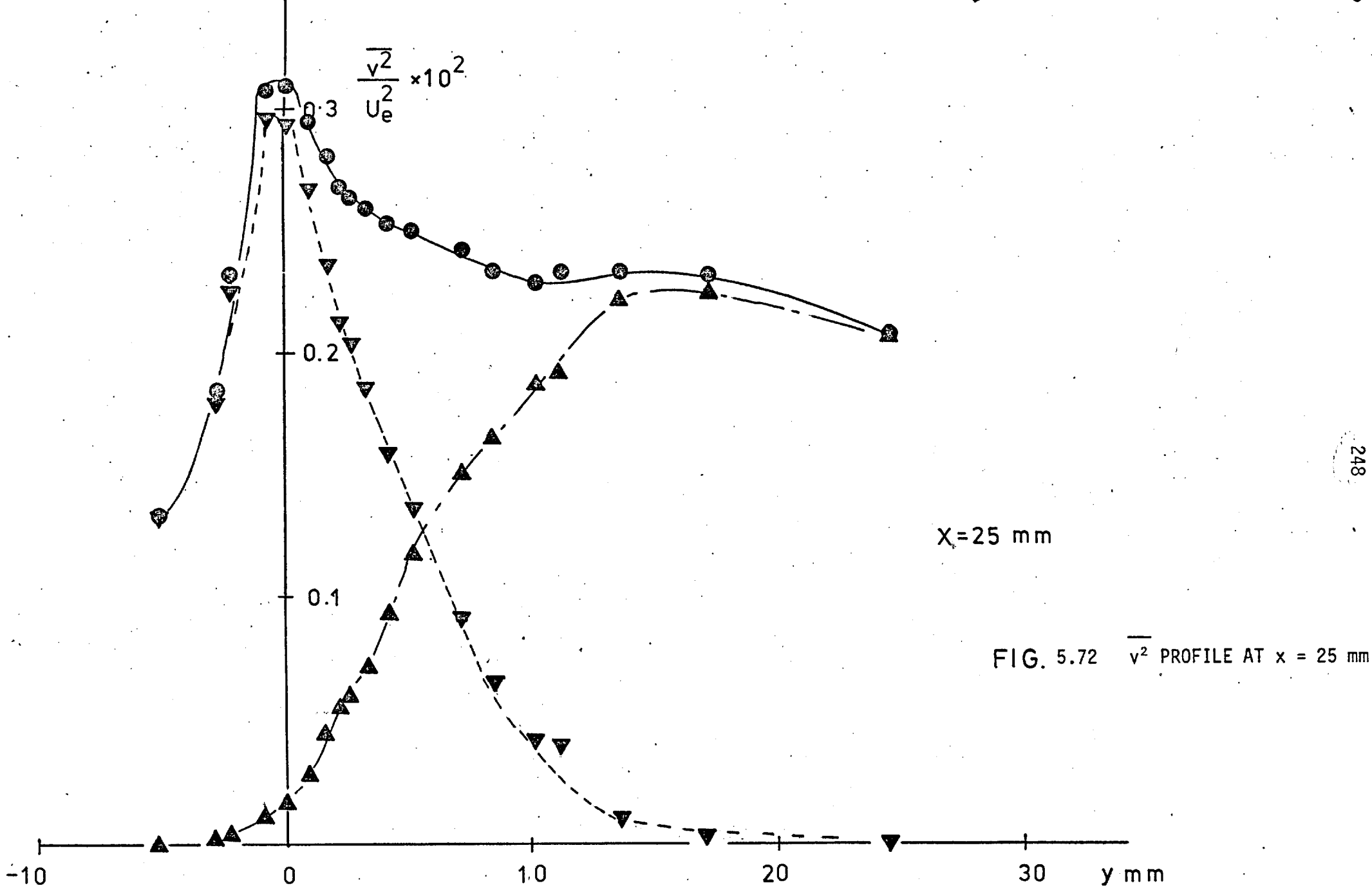

FIG. 5.72 $\overline{v^2}$ PROFILE AT x = 25 mm

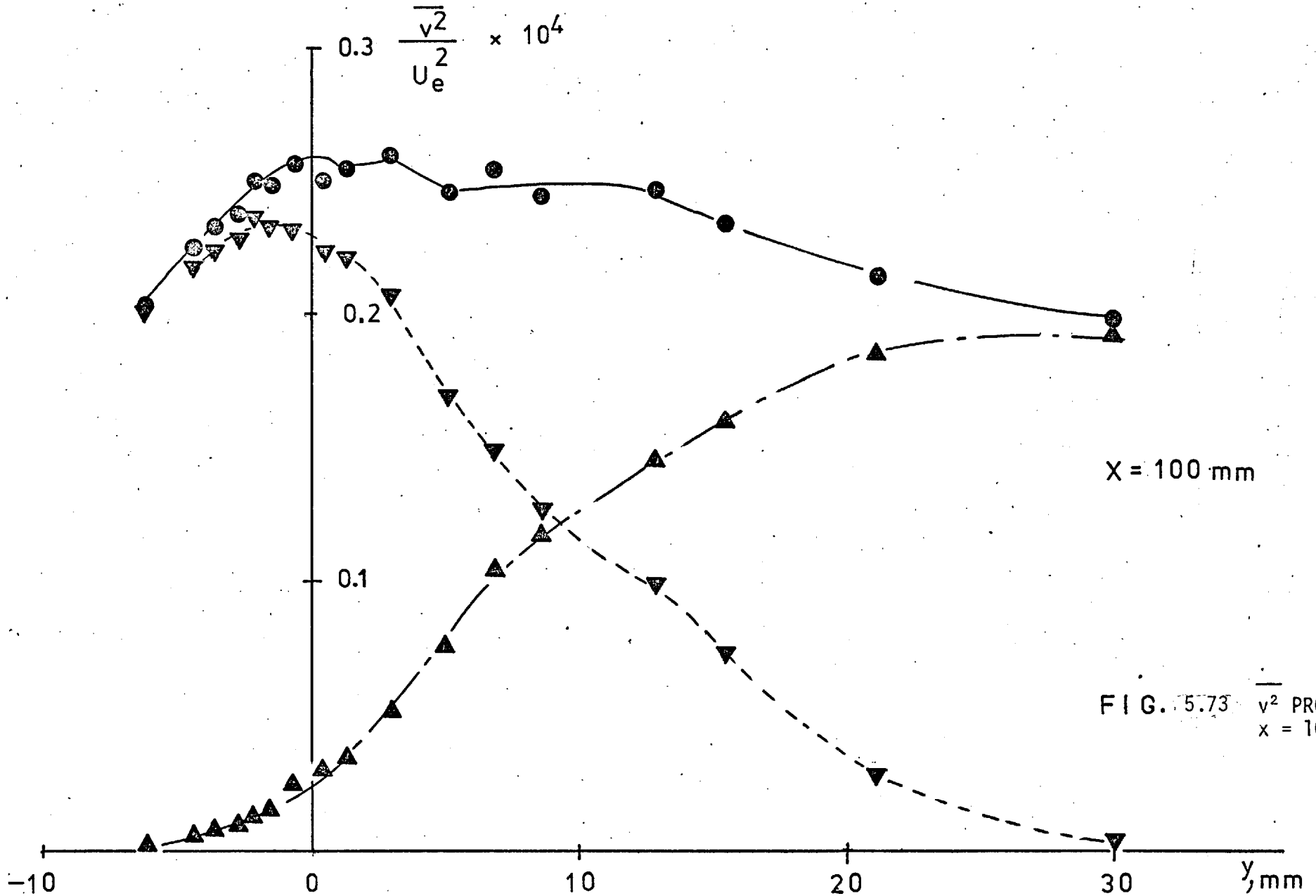

FIG. 5.73 $\overline{v^2}$ PROFILE AT x = 100 mm

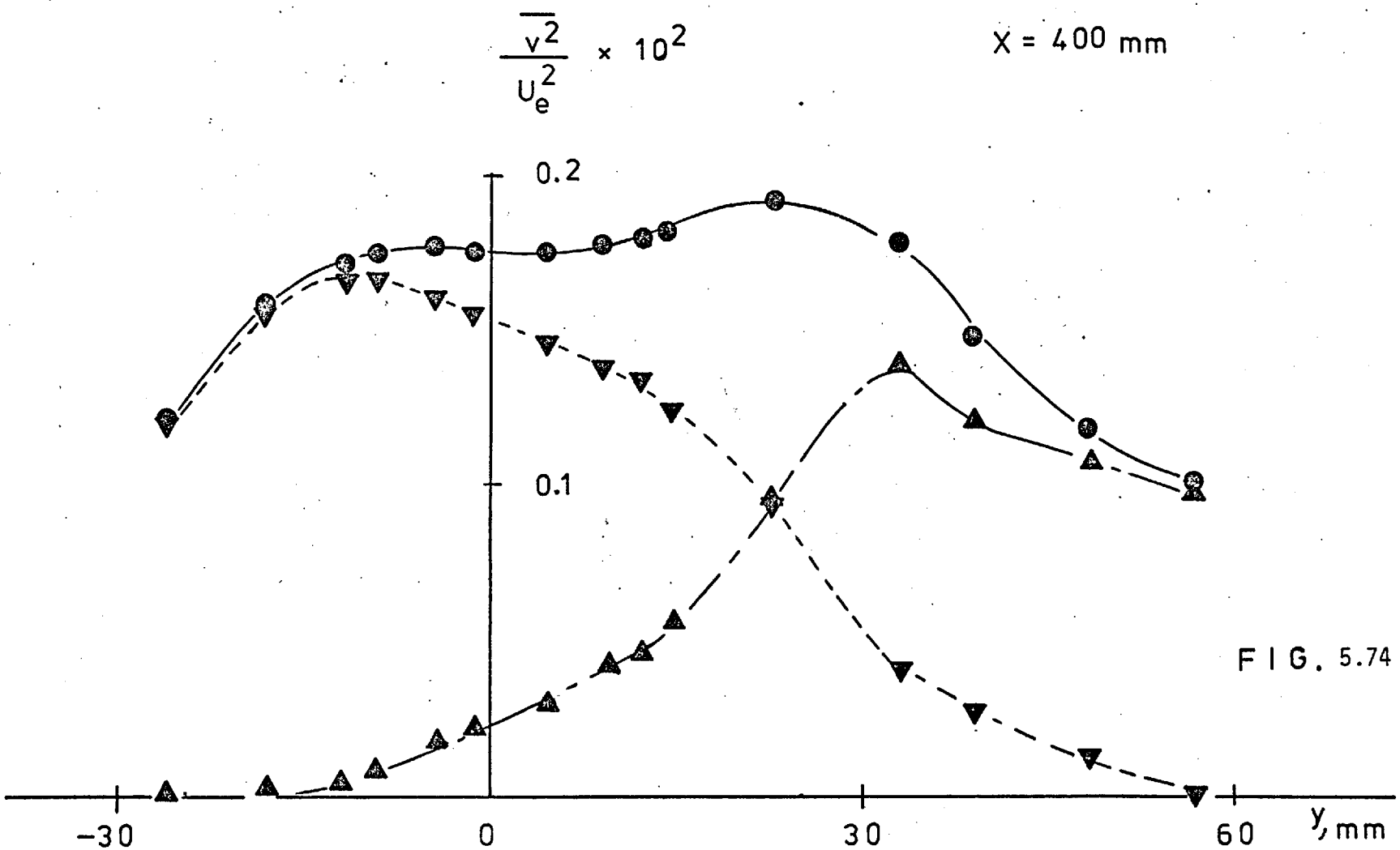

FIG. 5.74 $\overline{v^2}$ PROFILE AT x = 400 mm

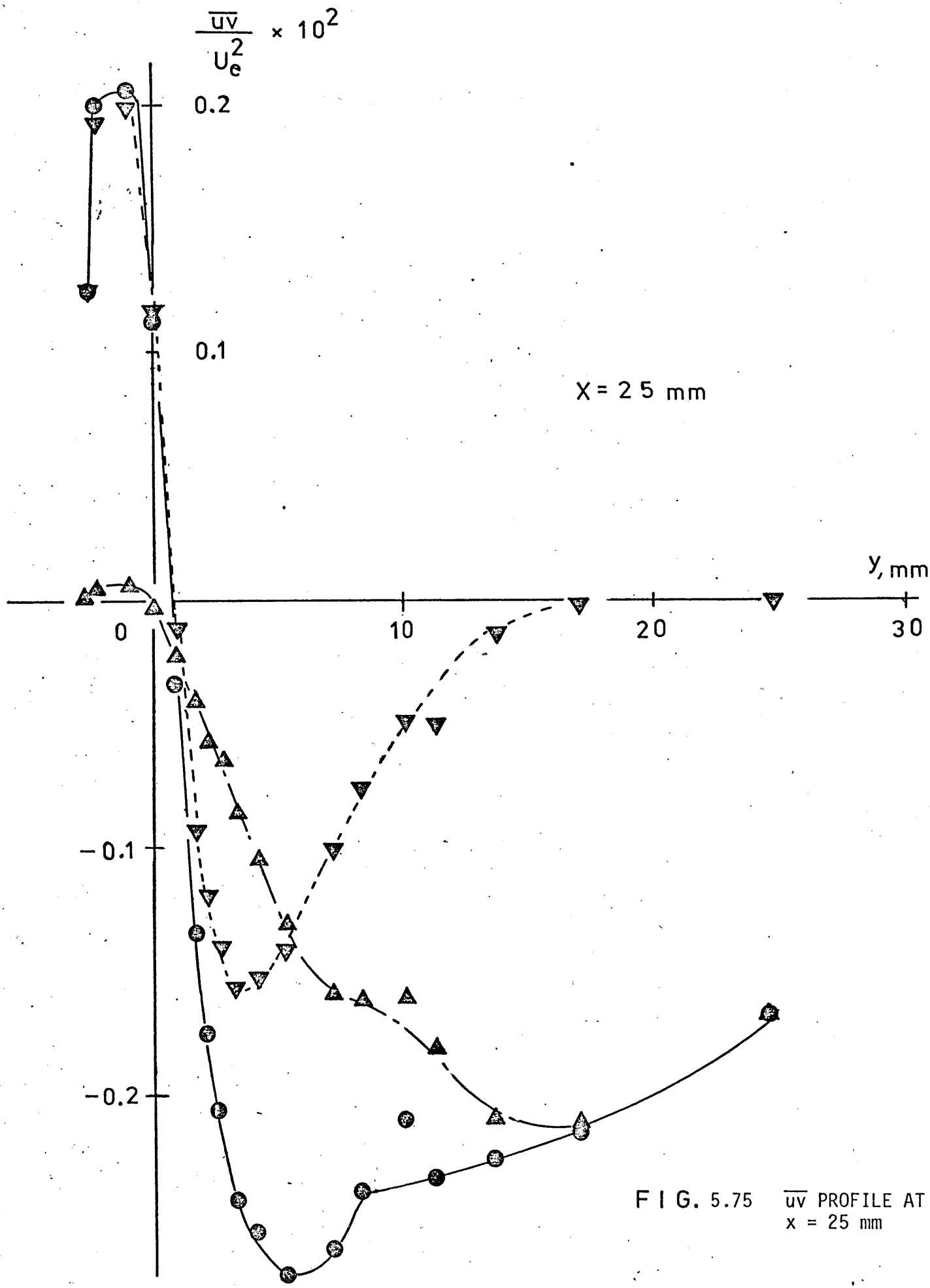

FIG. 5.75 $\overline{uv}$ PROFILE AT x = 25 mm

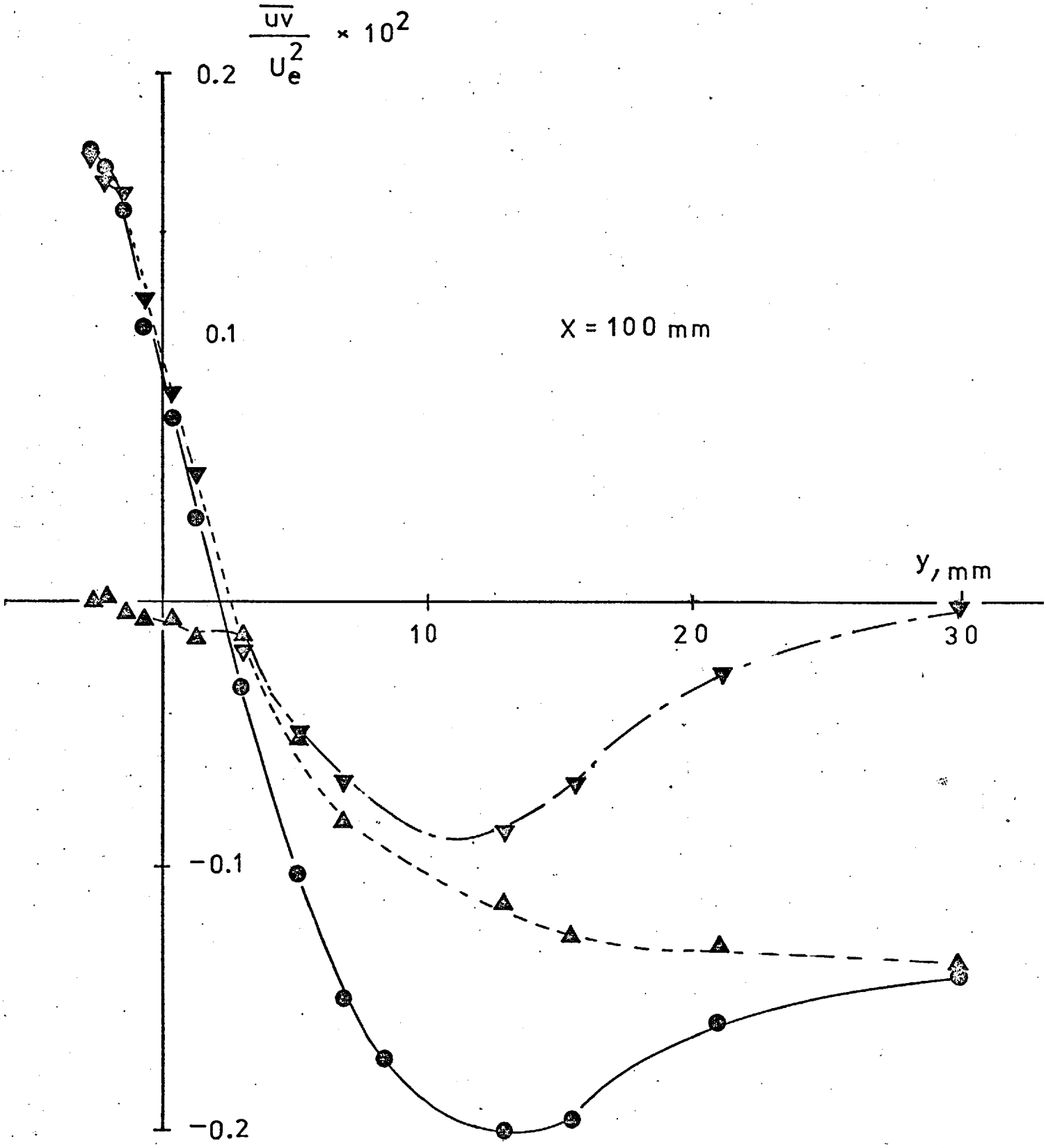

FIG. 5.76 $\overline{uv}$ PROFILE AT x = 100 mm

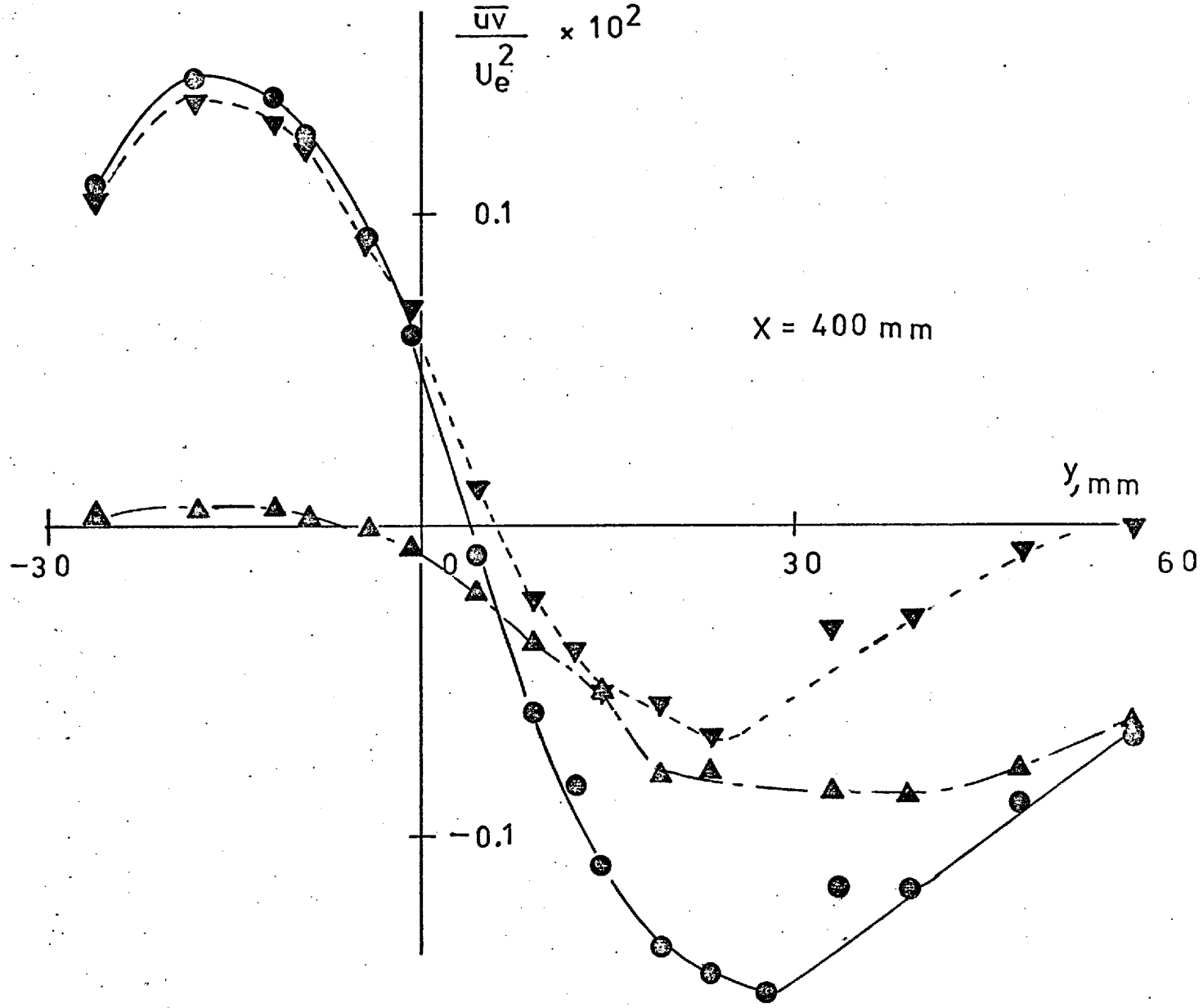

FIG. 5.77 $\overline{uv}$ PROFILE AT x = 400 mm

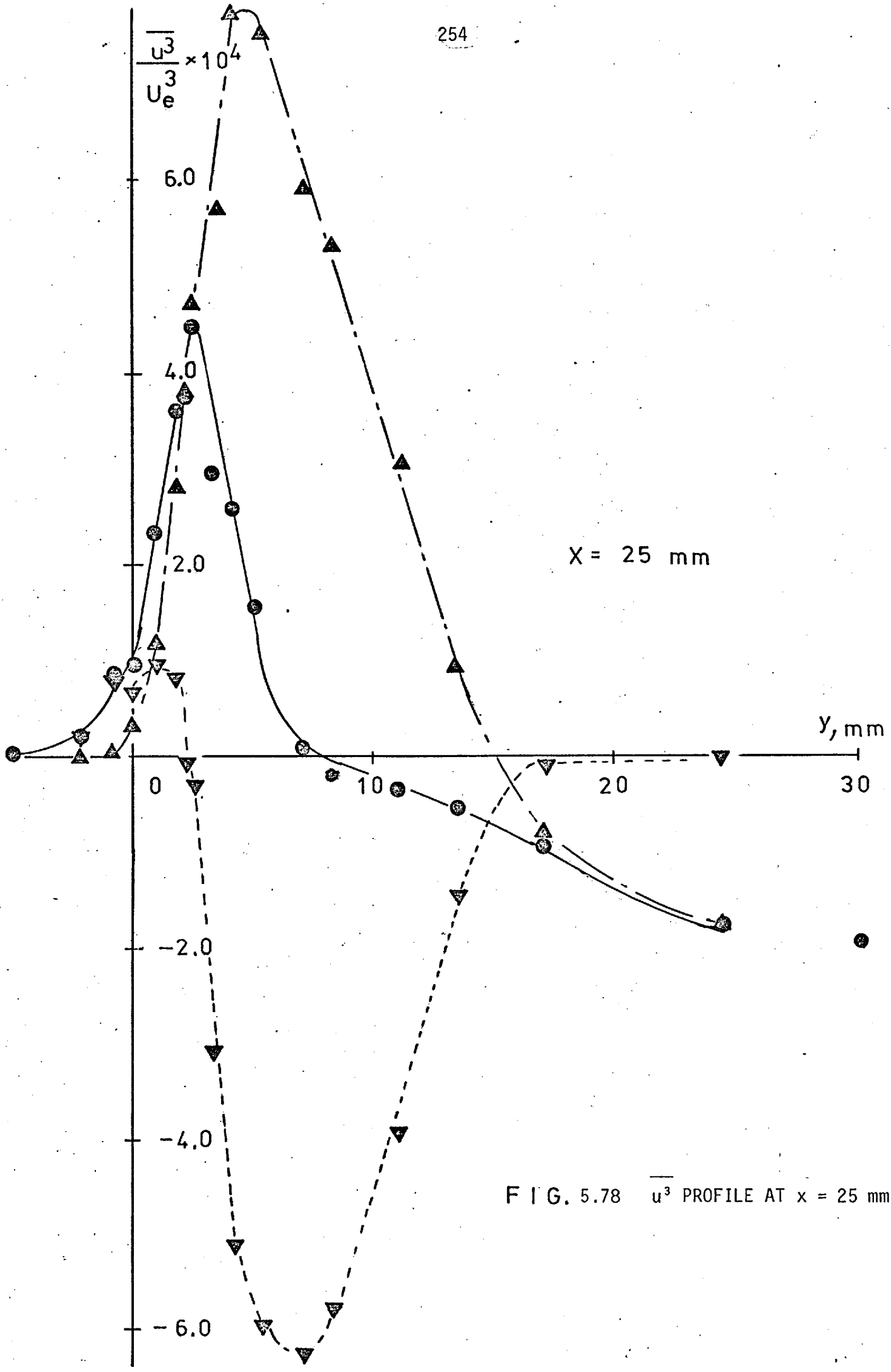

FIG. 5.78 $\overline{u^3}$ PROFILE AT x = 25 mm

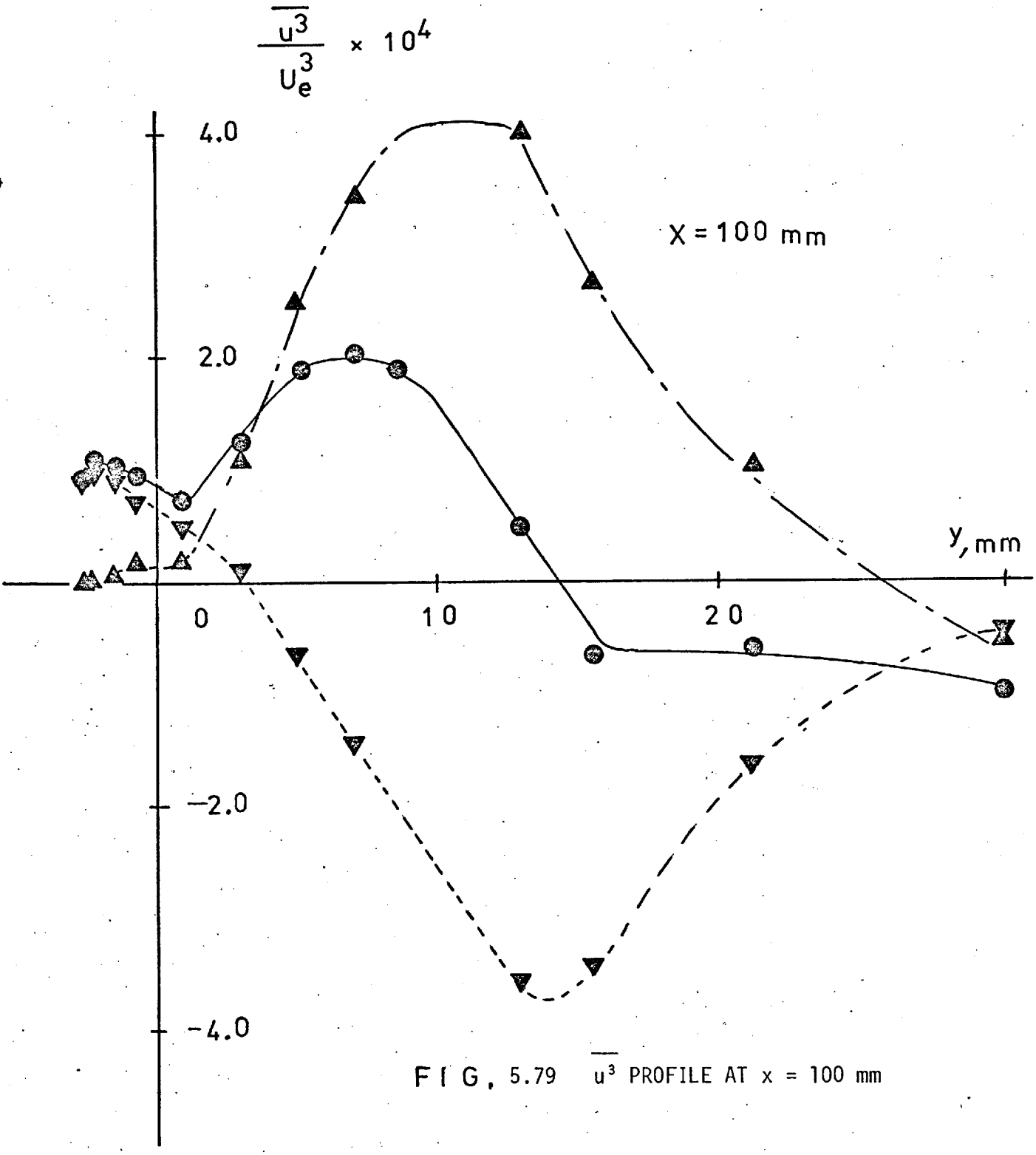

FIG. 5.79 $\overline{u^3}$ PROFILE AT x = 100 mm

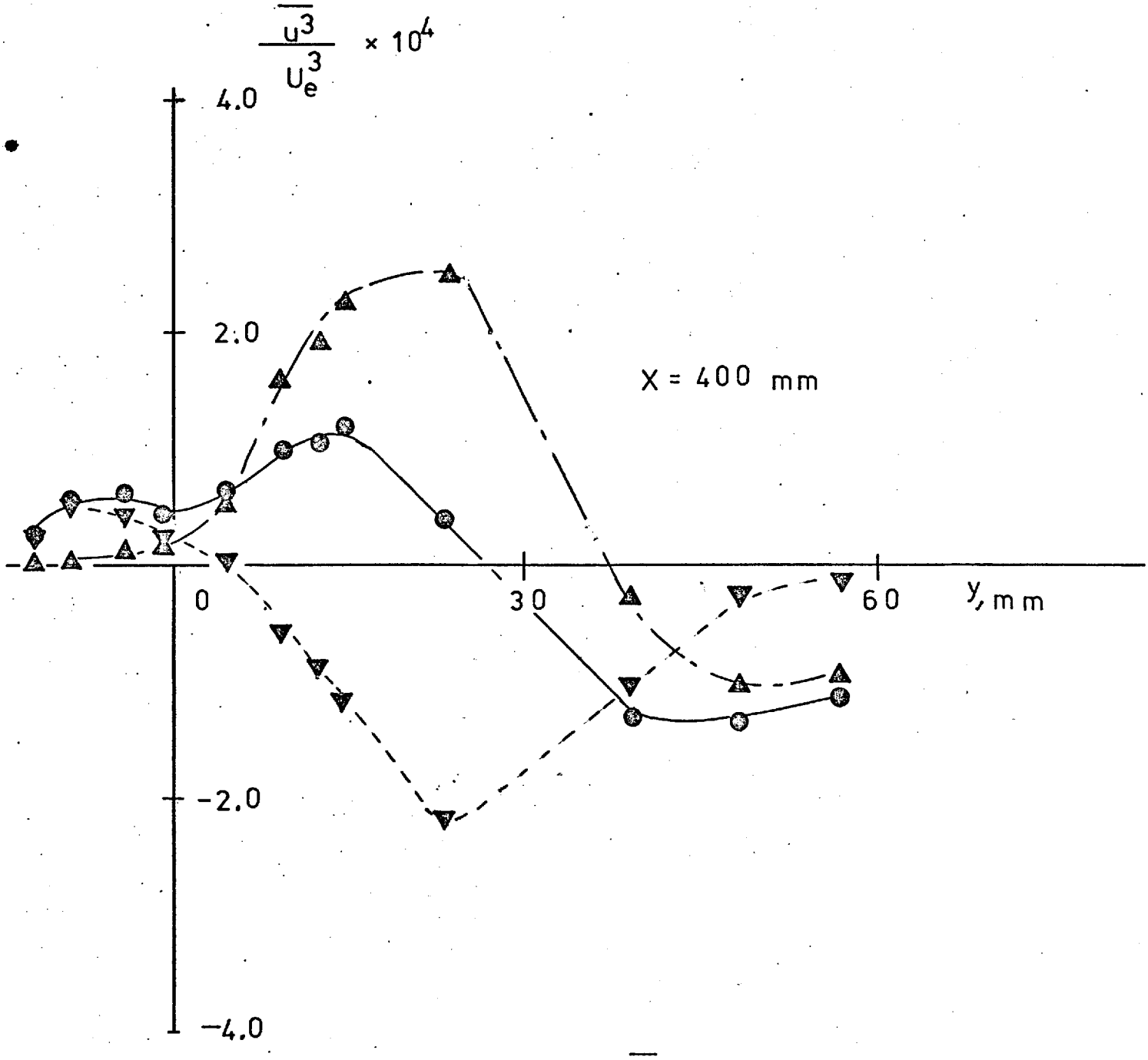

FIG. 5.80 $\overline{u^3}$ PROFILE AT x = 400 mm

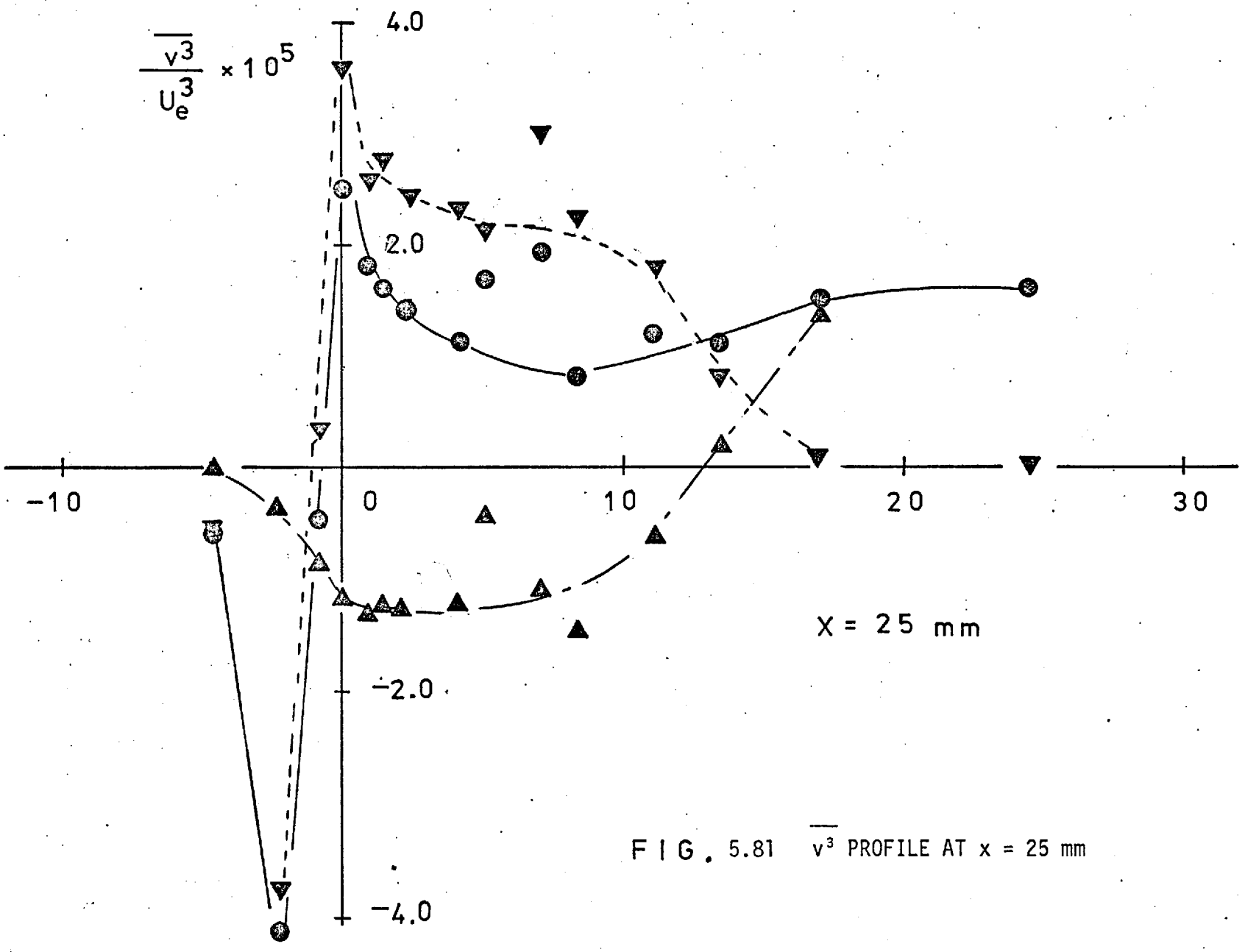

FIG. 5.81 $\overline{v^3}$ PROFILE AT x = 25 mm

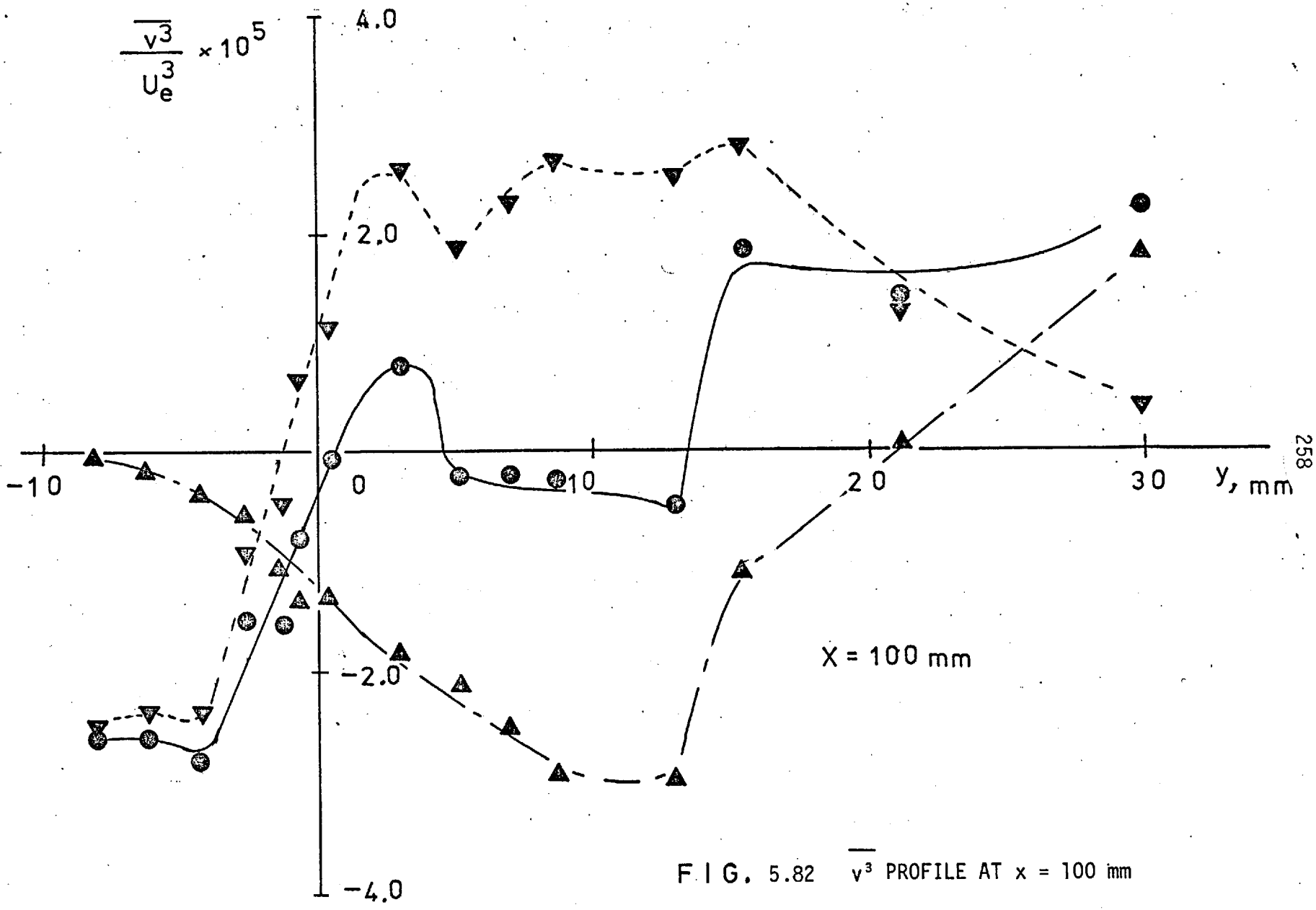

FIG. 5.82 $\overline{v^3}$ PROFILE AT x = 100 mm

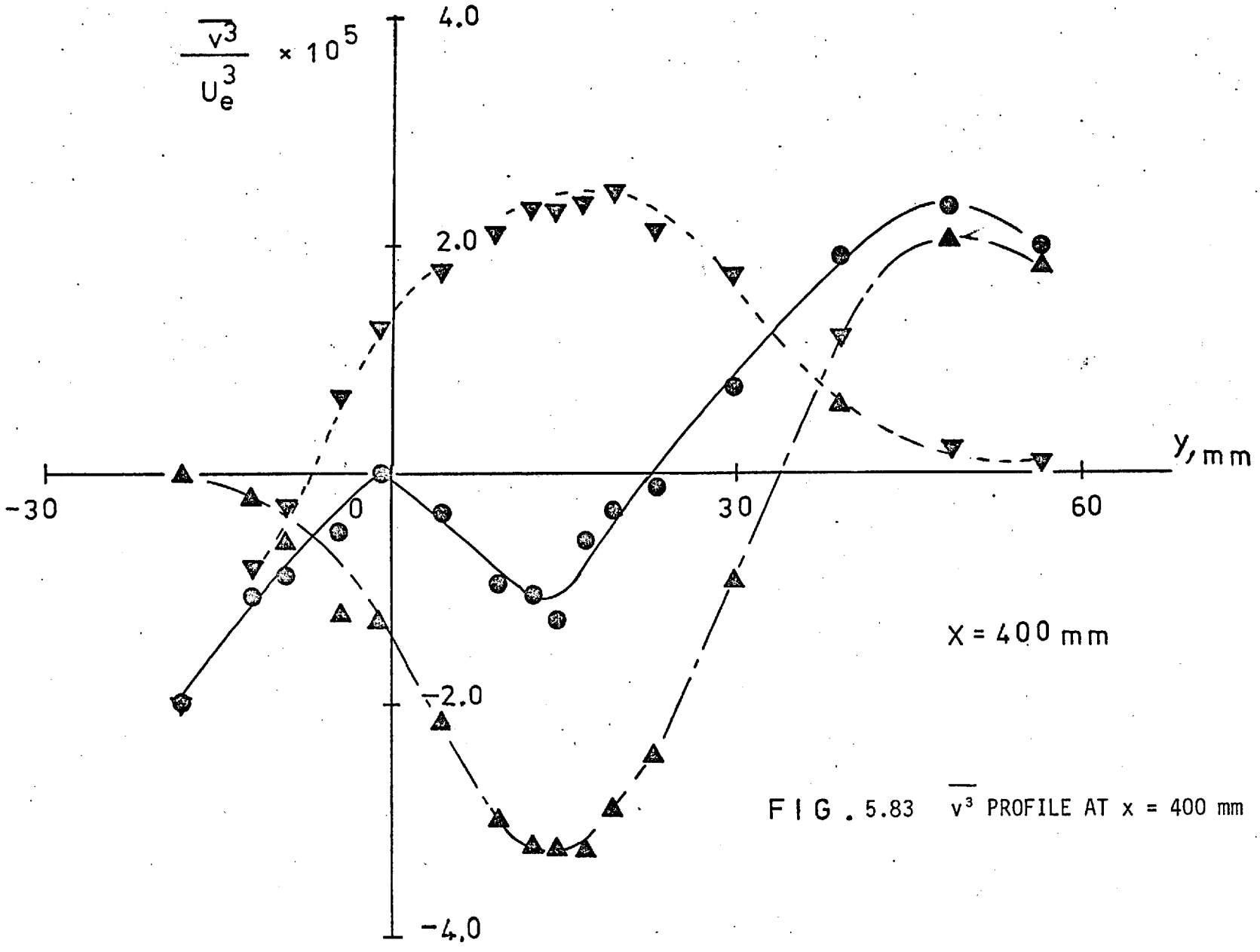

FIG. 5.83 $\overline{v^3}$ PROFILE AT x = 400 mm

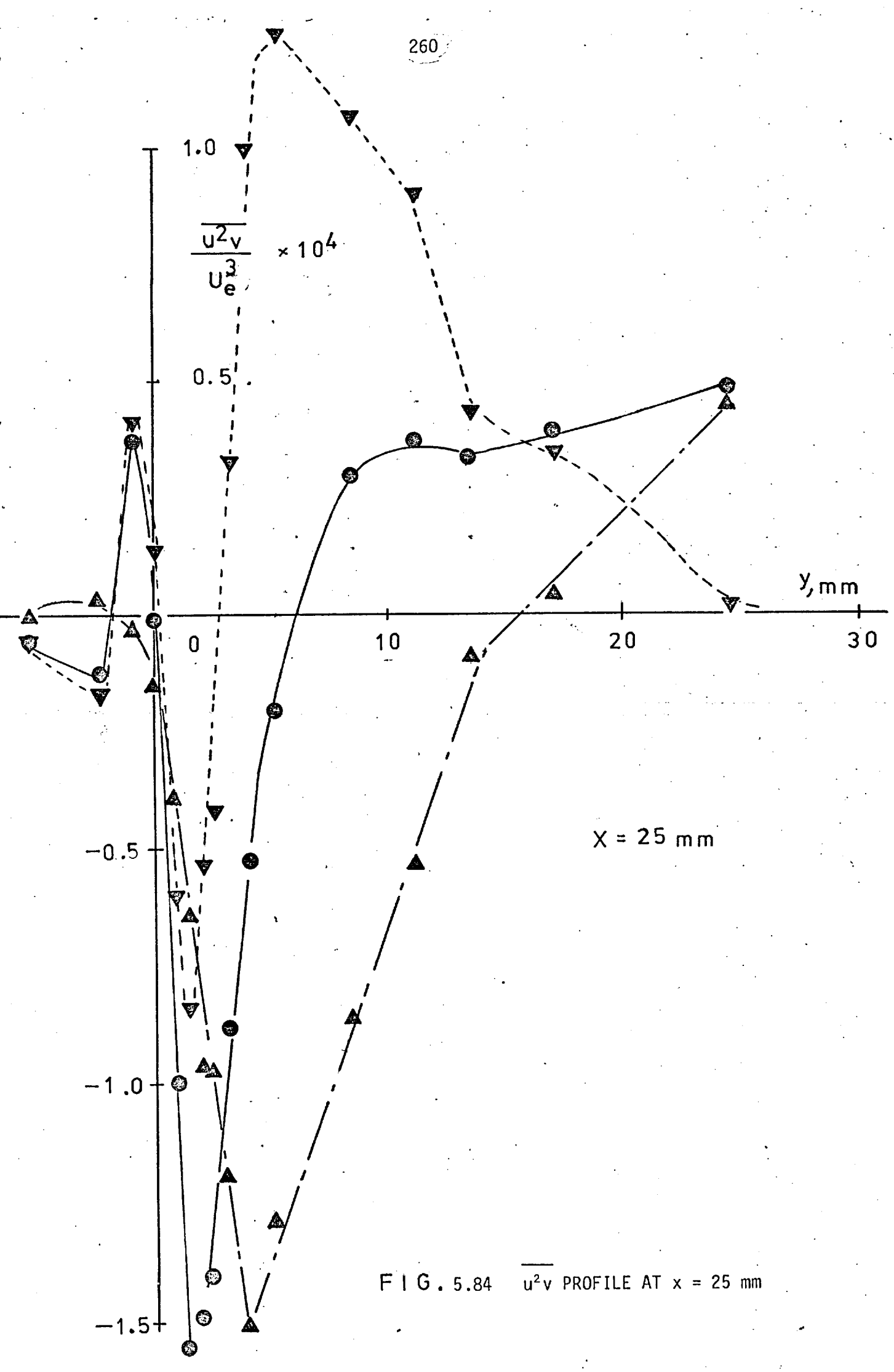

FIG. 5.84 $\overline{u^2v}$ PROFILE AT x = 25 mm

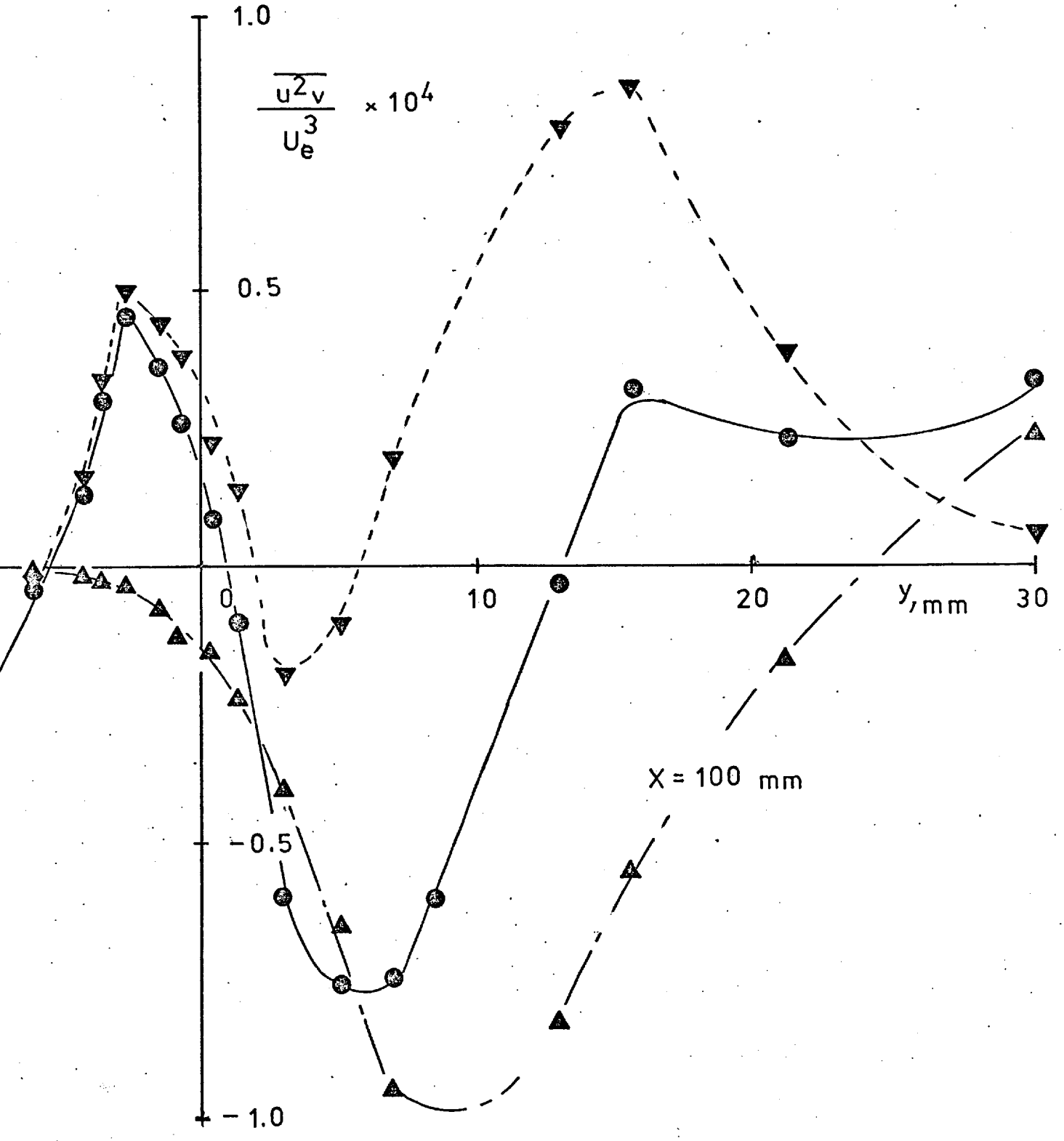

FIG. 5.85 $\overline{u^2v}$ PROFILE AT x = 100 mm

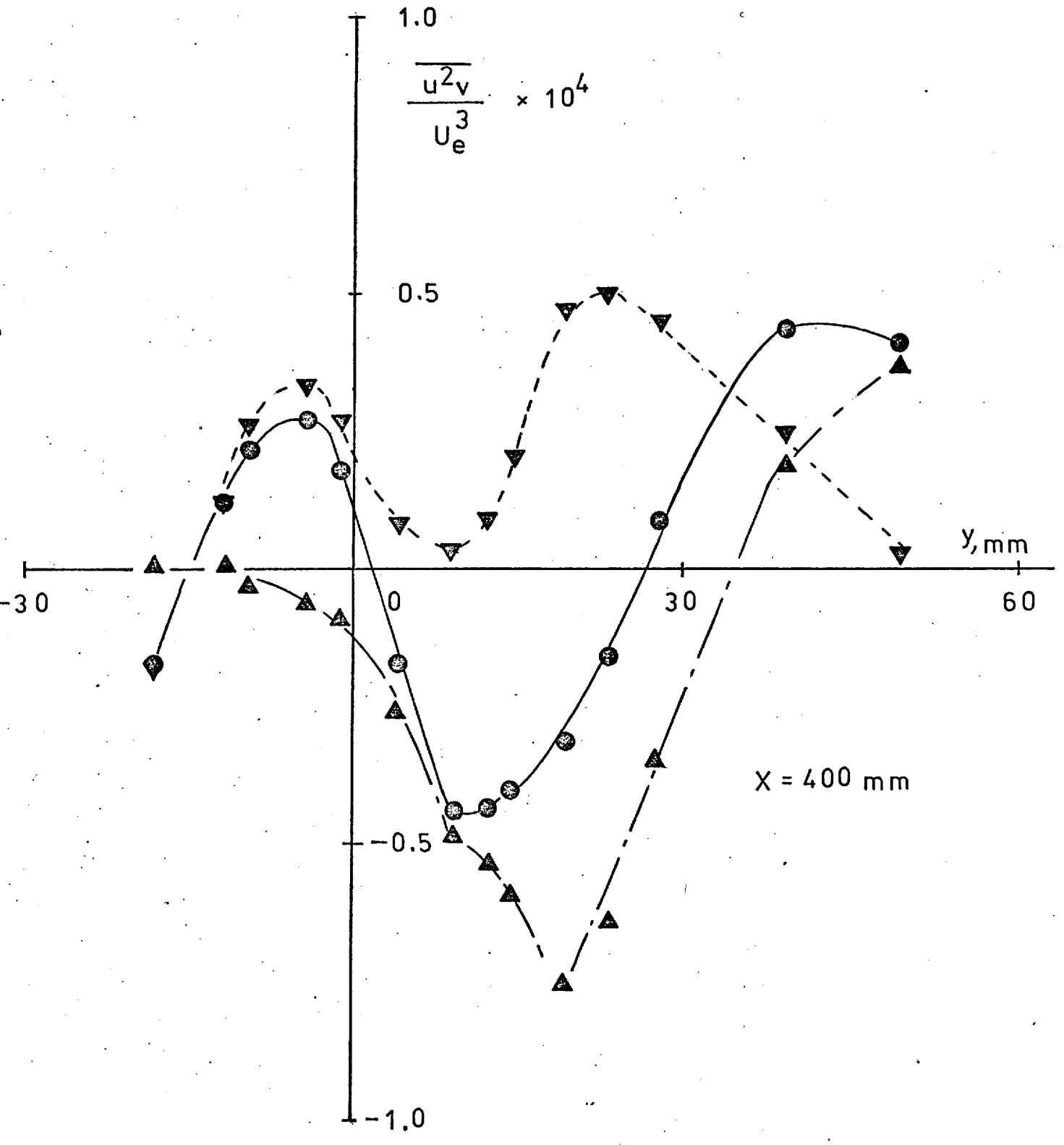

FIG. 5.86 $\overline{u^2v}$ PROFILE AT x = 400 mm

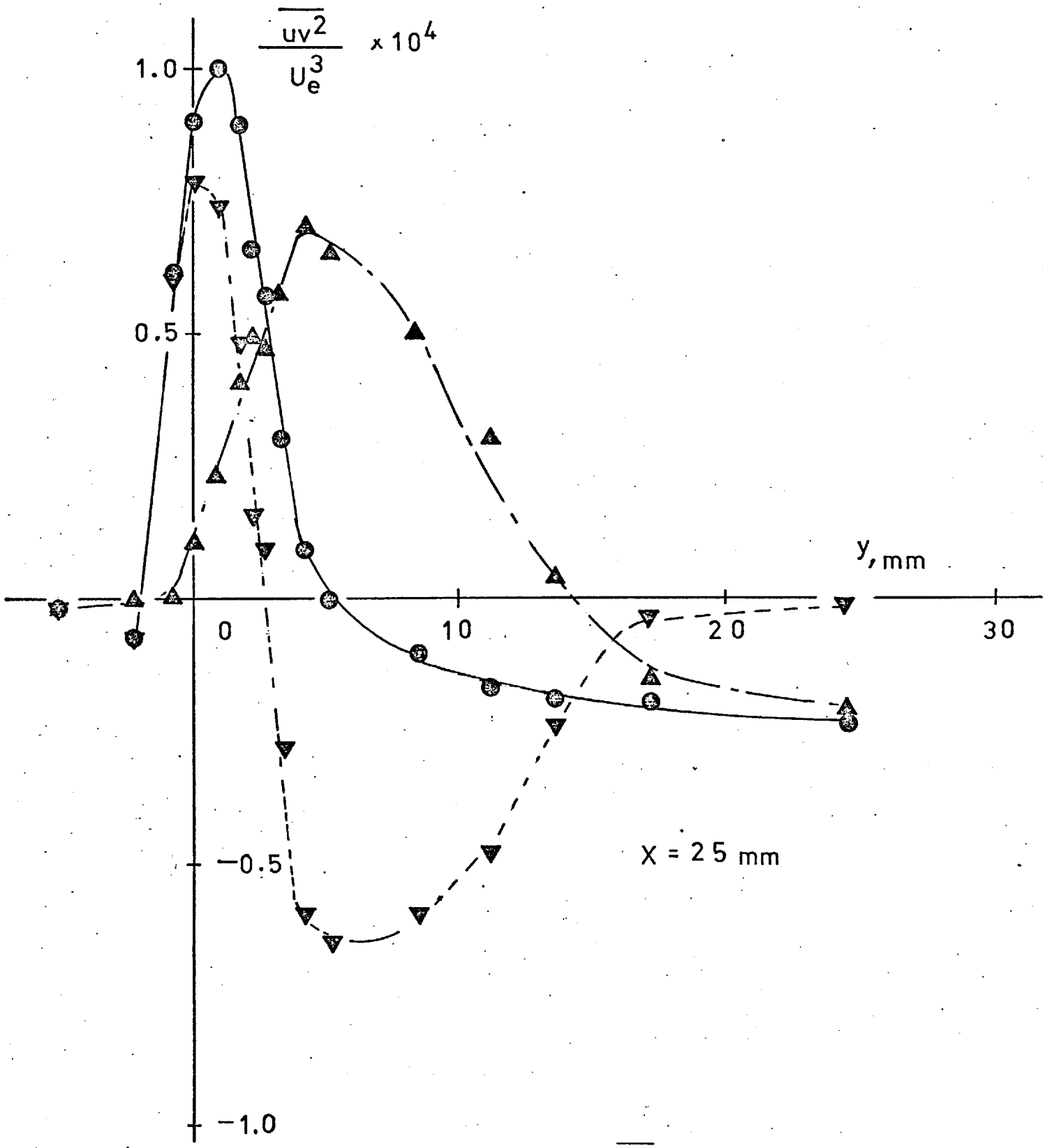

FIG. 5.87 $\overline{uv^2}$ PROFILE AT x = 25 mm

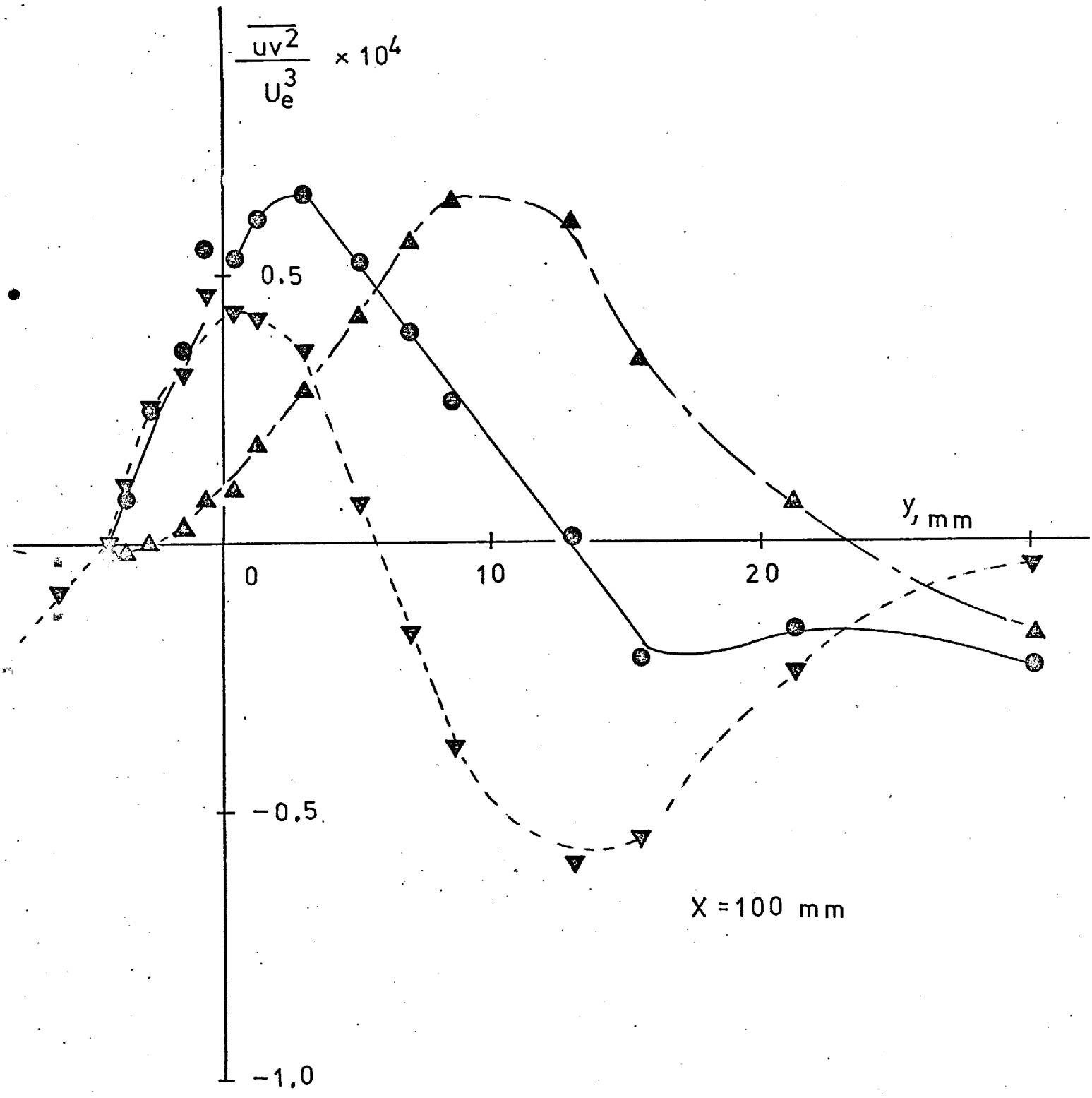

FIG. 5.88 $\overline{uv^2}$ PROFILE AT x = 100 mm

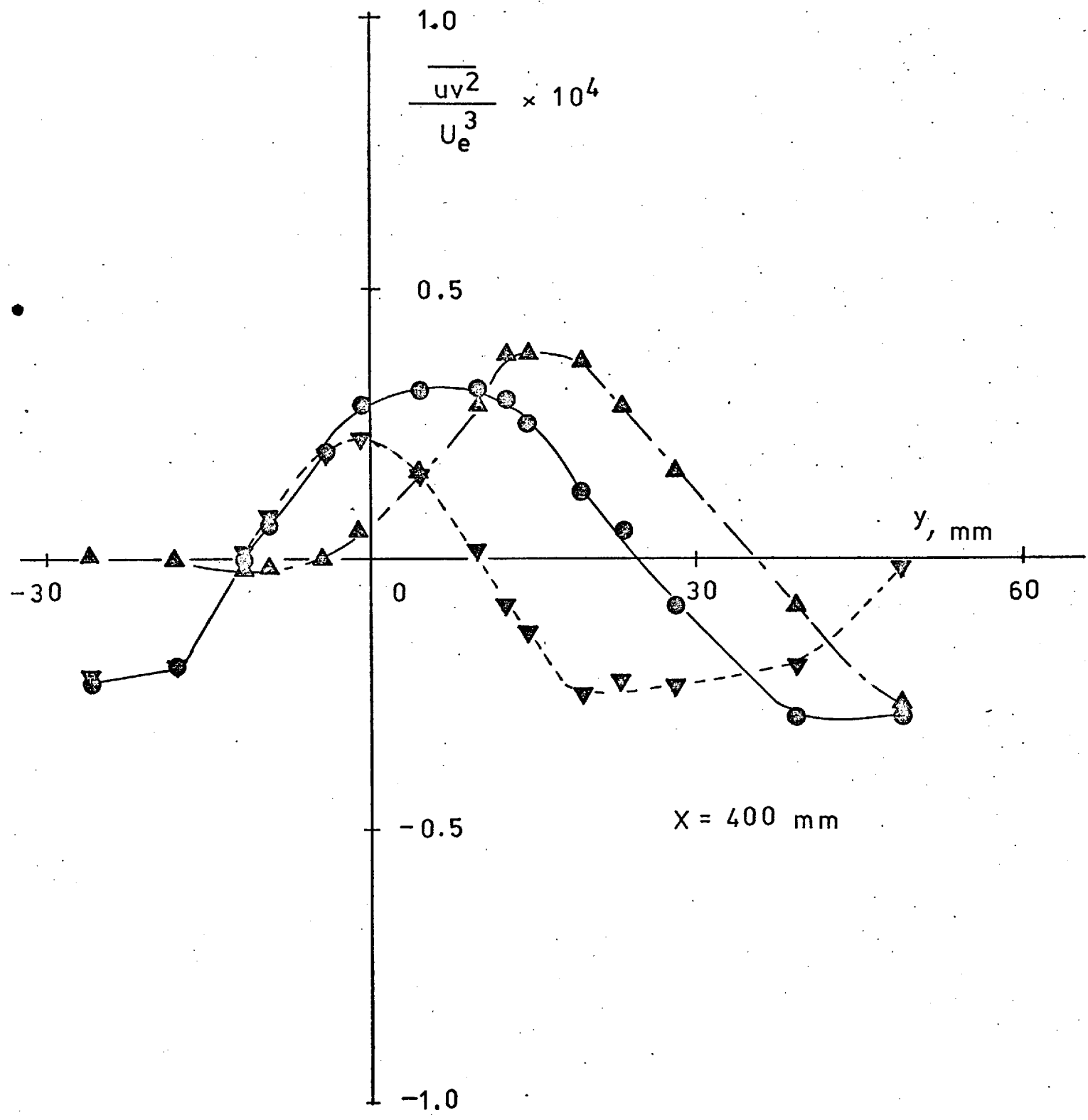

FIG. 5.89 $\overline{uv^2}$ PROFILE AT x = 400 mm

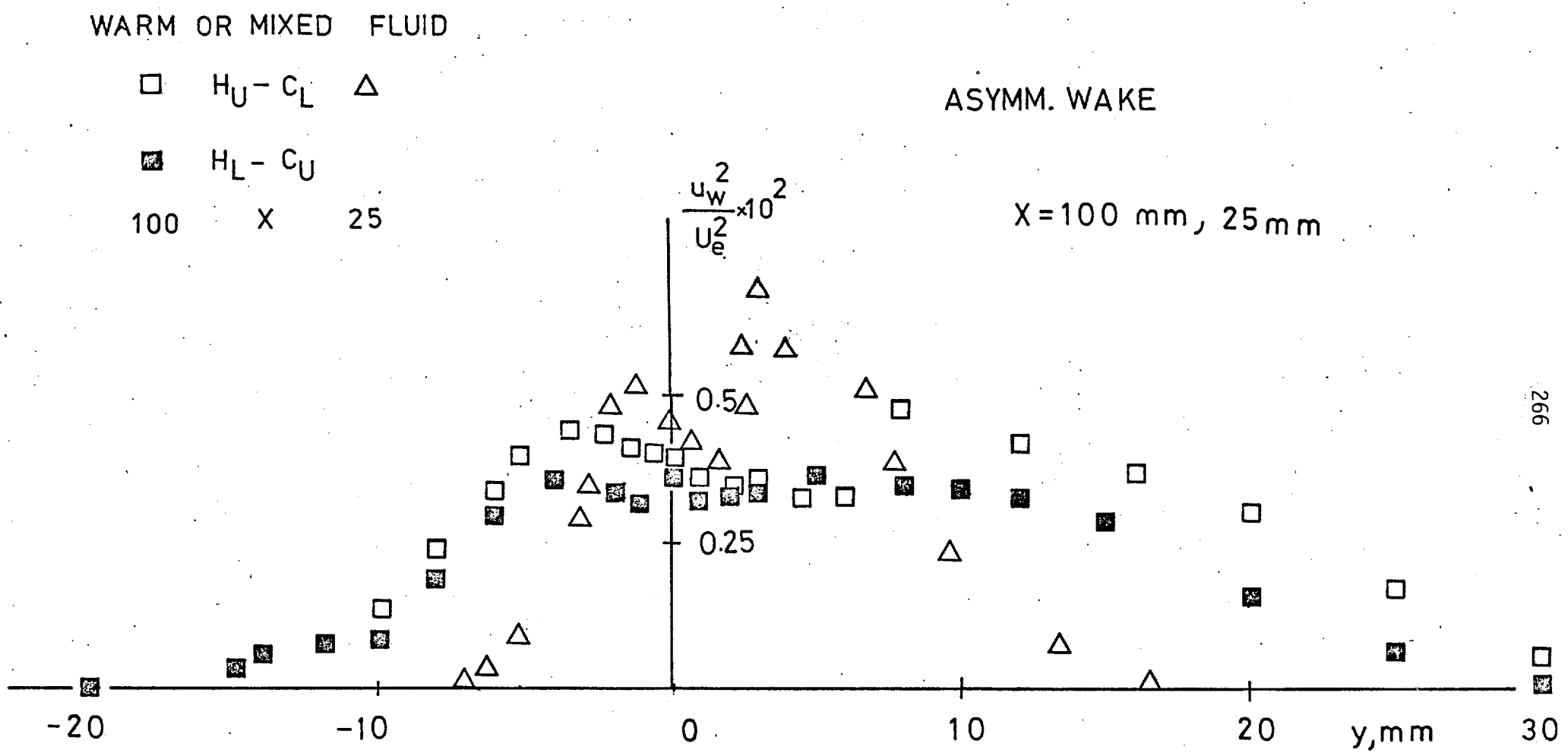

FIG. 5.90 $\overline{u_w^2}$ PROFILE

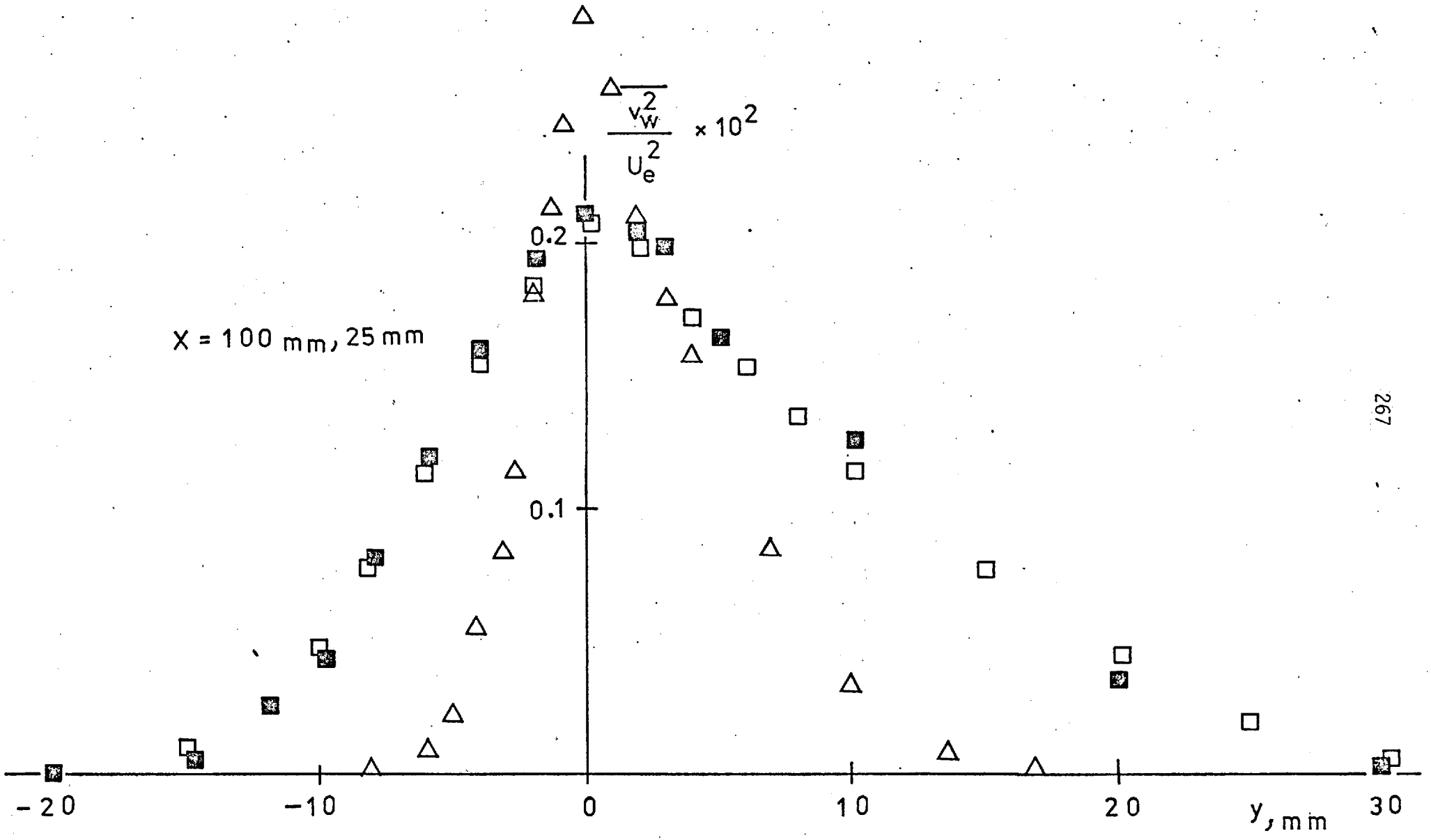

FIG. 5.91 $\overline{v_w^2}$ PROFILE

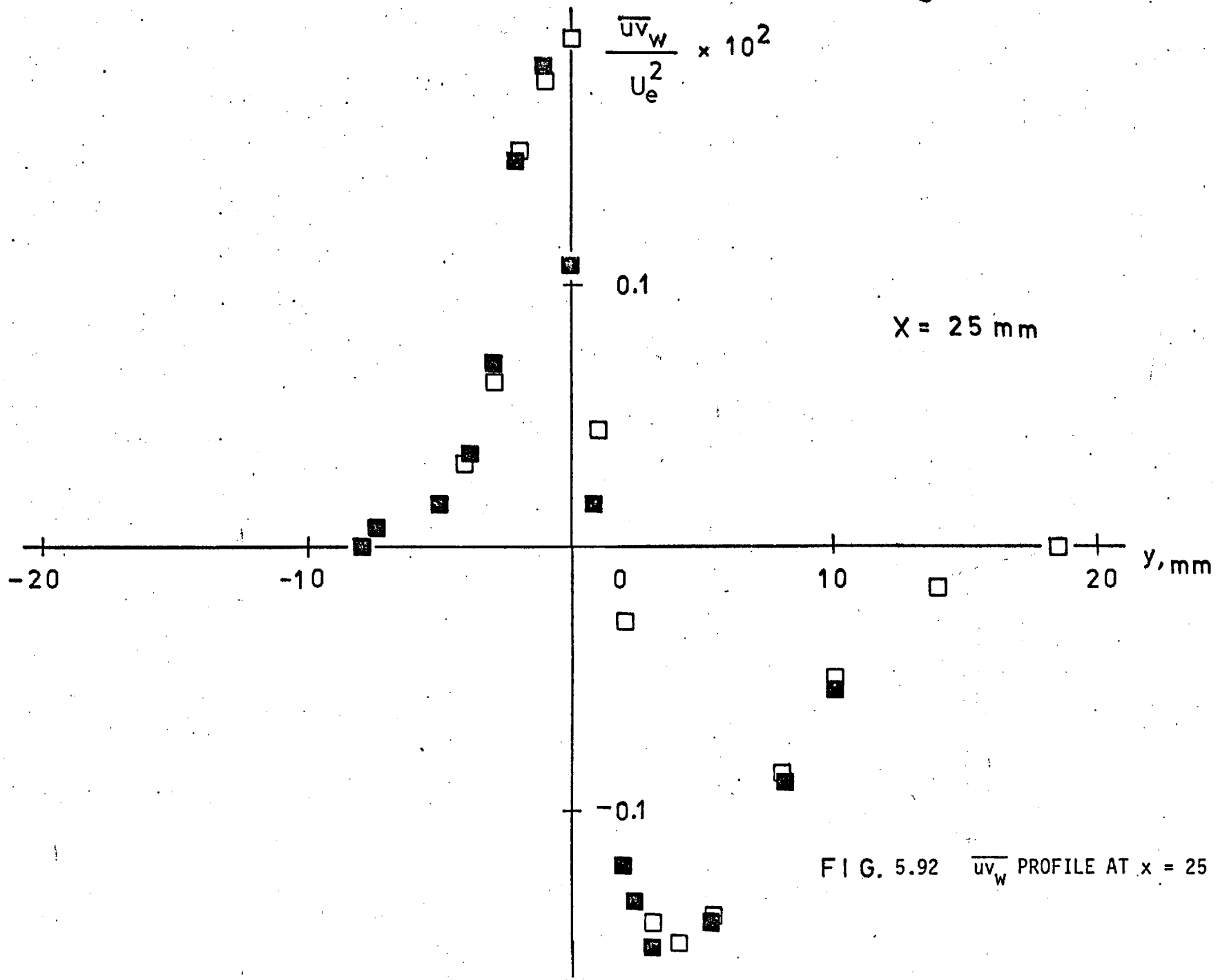

FIG. 5.92 $\overline{uv}_w$ PROFILE AT x = 25 mm

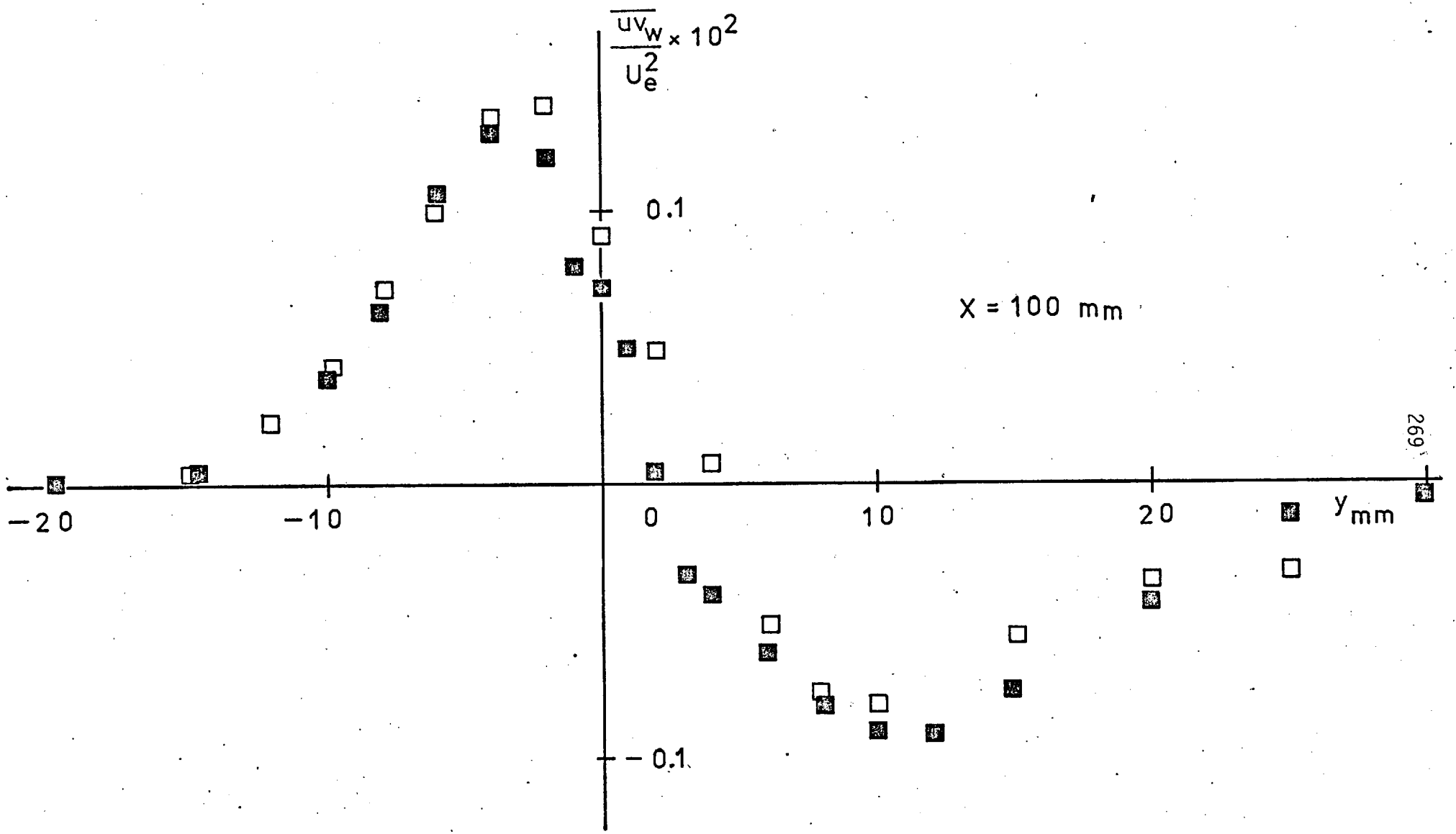

FIG. 5.93 $\overline{uv_w}$ PROFILE AT x = 100 mm

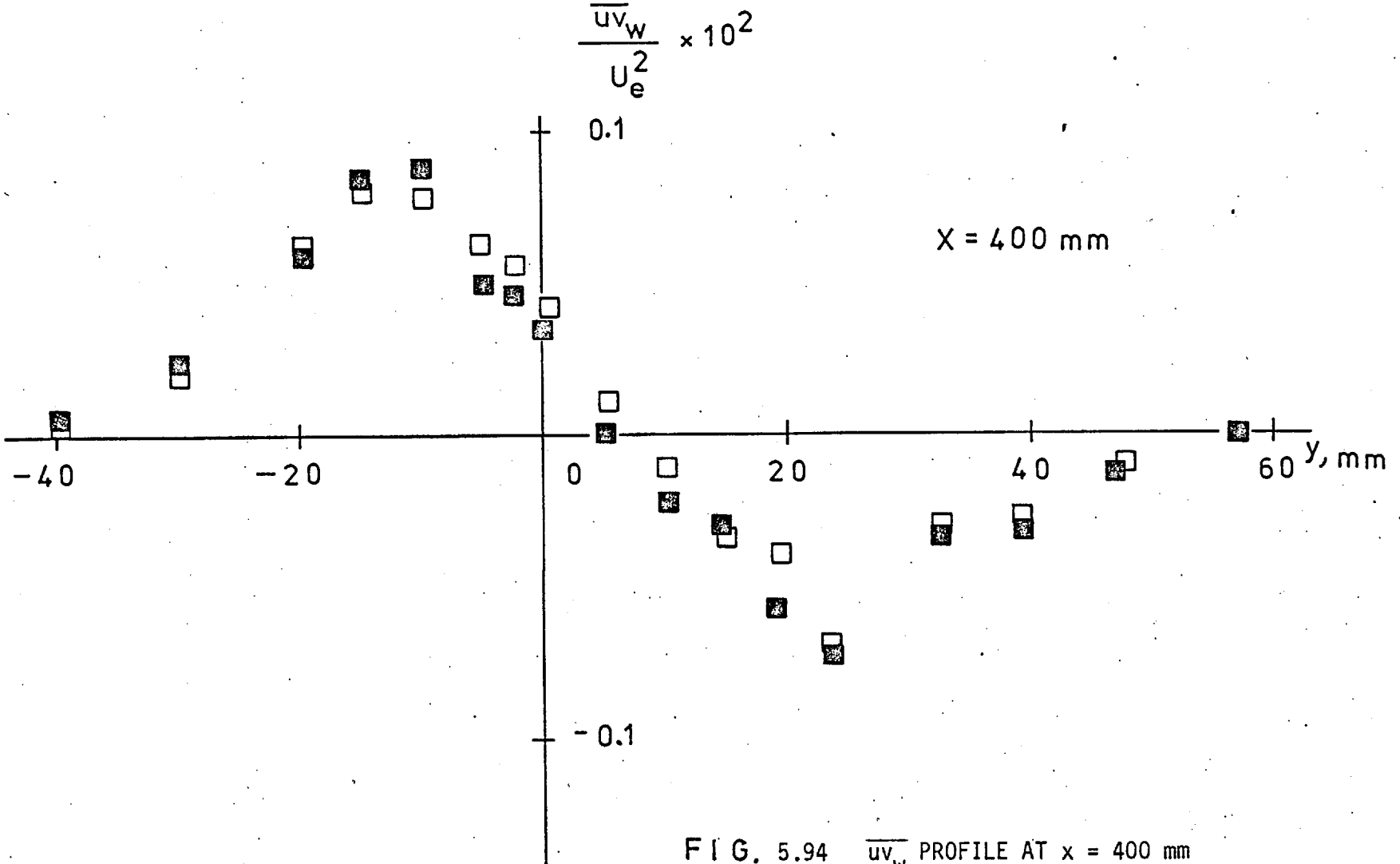

FIG. 5.94 $\overline{uv_w}$ PROFILE AT x = 400 mm

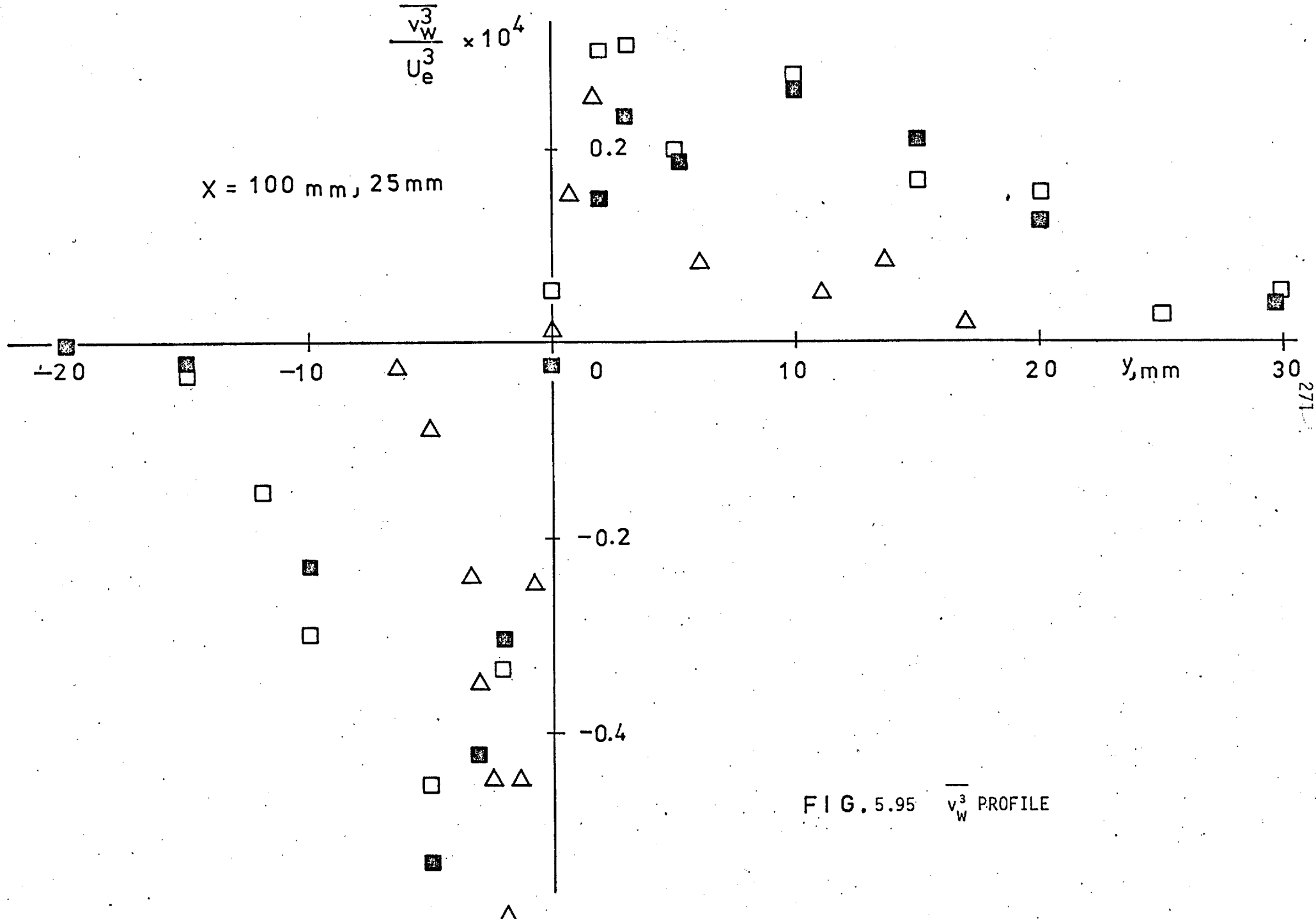

FIG. 5.95 $\overline{v_w^3}$ PROFILE

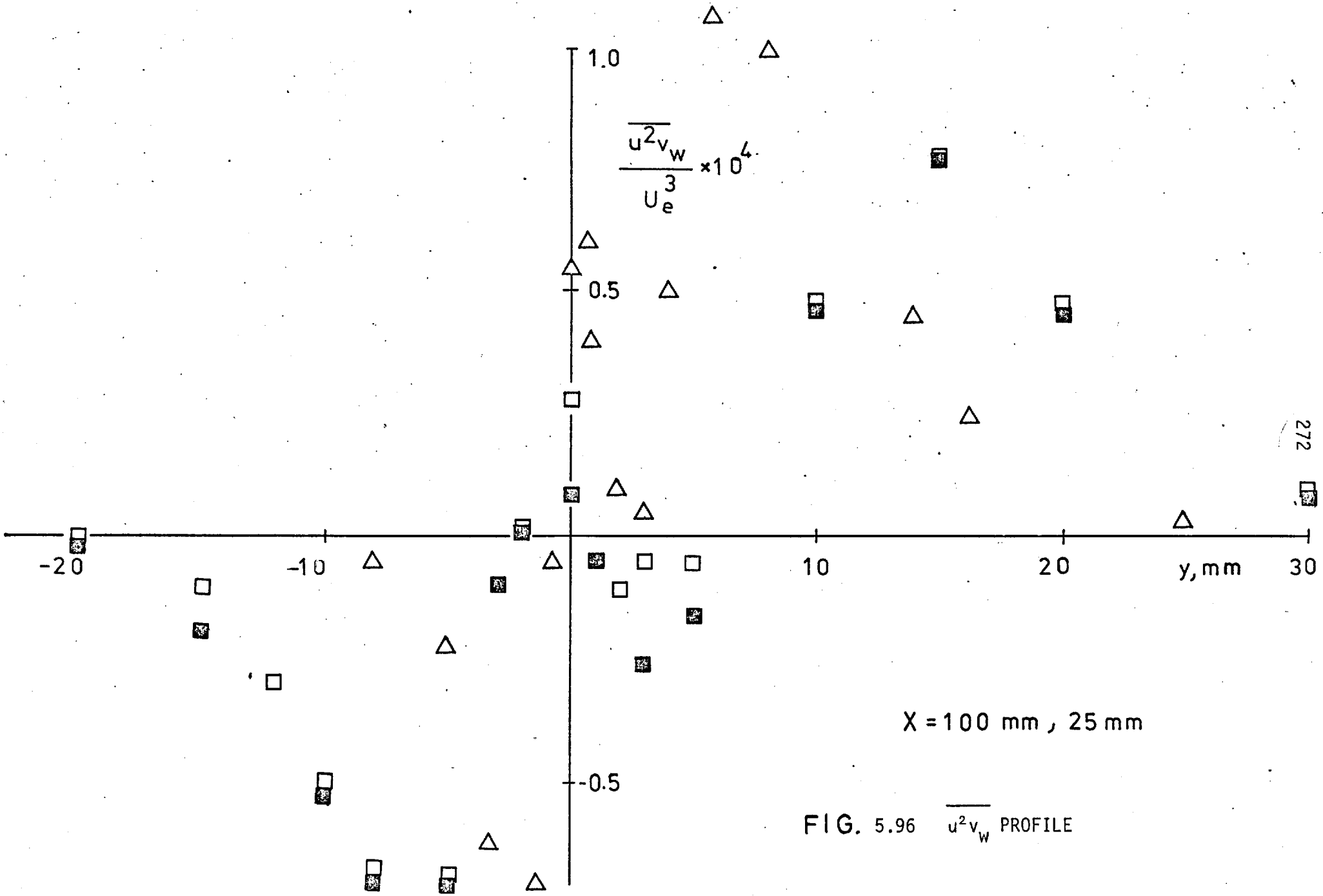

FIG. 5.96 $\overline{u^2 v_w}$ PROFILE

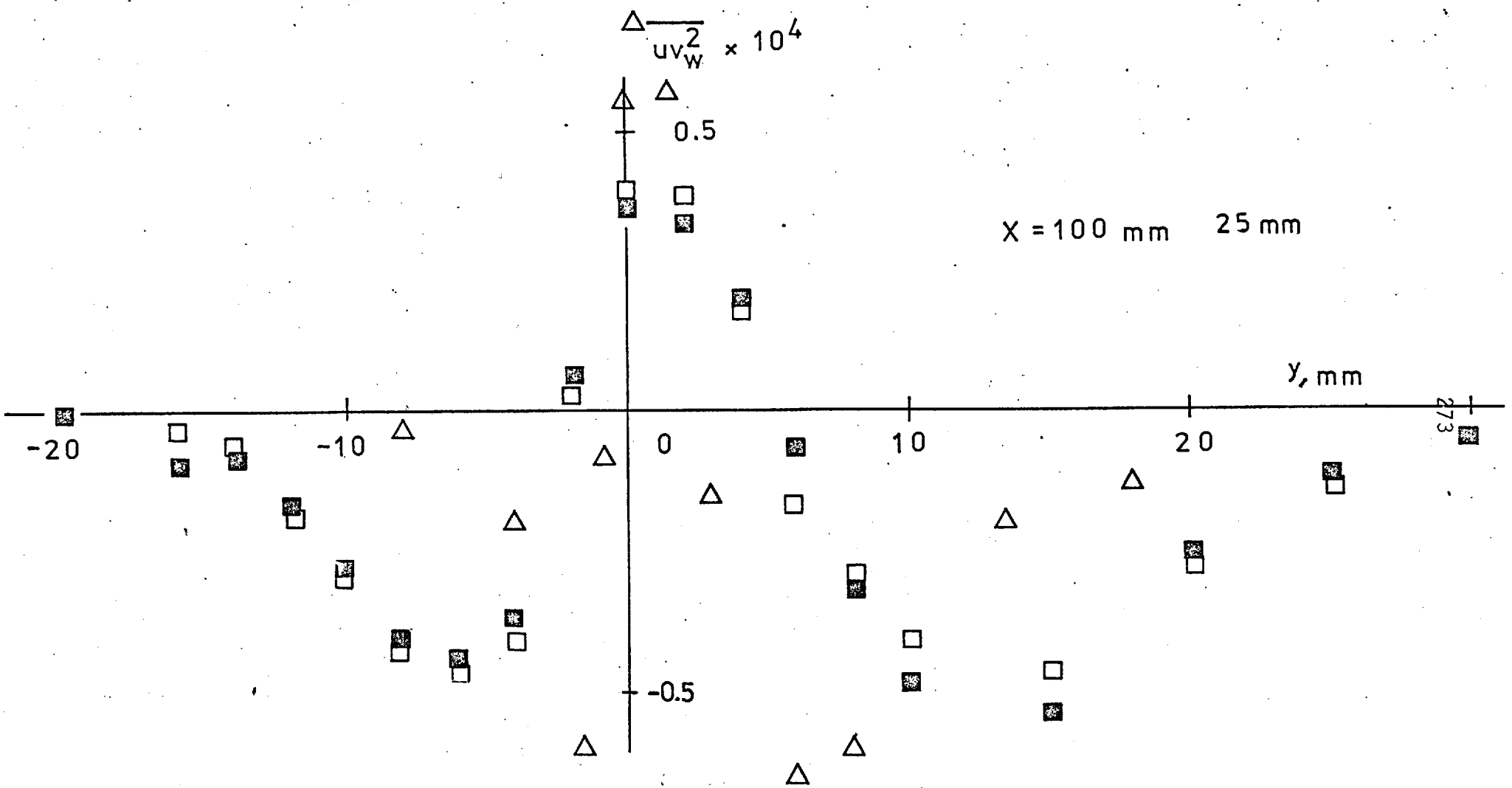

FIG. 5.97 $\overline{uv_w^2}$ PROFILE

6. THERMAL FIELD RESULTS

6.1 General

In the present experiment, heat was used as a tracer to tag the fluid and heat transfer investigation was not one of the objectives. However, during the progress of the investigation, it was felt that more information about the thermal field would be useful. In this chapter, the heat transfer results will be presented.

In the present experimental research, it is expected that the fluid motion is not affected by the temperature field, i.e. absence of buoyancy forces or compressibility effects.

An obvious characteristic feature of the thermal field is its asymmetry even in the symmetric flow case and, consequently, it is expected again that the point of zero mean temperature gradient ($\partial T/\partial y$) does not coincide with the point where $\overline{v\theta}$ is zero, thus leading to a negative thermal diffusivity, exactly as in any asymmetric flow field. This situation has been observed by Beguier et al (1975) and Beguier et al (1976). Fulachier et al (1977) investigated the flow field of a slightly heated jet and showed that the large eddies were responsible for the "negative" production of the temperature fluctuations. This argument is mainly based on the concept of a "double" structure of the flow where the high frequency components are related to the small eddies which are in equilibrium with the local mean gradient and low frequency components to the large eddies.

All the present results relate to a constant heat input which has been introduced at the leading edge. Thus, the "hot" boundary layer fluid entrained "cold" free stream fluid. The symmetric wake results, for the case of the upper boundary layer heated mainly, are presented firstly and the asymmetric ones secondly for the two ways of

heating (upper or lower boundary layer heated).

6.2 Symmetric Wake

In Fig. 6.1, the mean temperature profiles for various downstream stations are plotted as $\Delta T = T - T_e$ against y. For x = 0, $\partial T/\partial y$ at $y \simeq 0$ is quite big indicating that the flat plate behaves more or less as a heat insulator between the upper (heated) and the lower (unheated) flow, although there is an inevitable heat loss by conduction through the plate as seen by the tail in ΔT for $y < 0$, i.e. the lower stream. But it is quite unlikely that this small $\partial T/\partial y$ will produce any considerable temperature fluctuation or even interfere with the discrimination technique of "hot" and "cold" eddies. The max ΔT drops with x since a normal transport and diffusion to the unheated layer is expected. The $\partial T/\partial y$ drops as well with x indicating that the production of temperature fluctuations decreases. In the outer part of the wake, the profiles remain roughly constant with x as in the case of the U profiles. In Fig. 6.2, the $\overline{\theta^2}$ profiles are displayed. There are clearly two peaks of high temperature fluctuations, one in the outer part corresponding to the turbulent/non-turbulent or heated/unheated fluid interface, and another in the inner wake around the centre-line corresponding to that heated non-heated interface. Both maxima drop with x and tend to move outwards to the colder regions.

In Figs. 6.3 to 6.13, the second and third order temperature velocity correlations are presented for both ways of heating. They are all terms in the $\overline{\theta^2}$, $\overline{u\theta}$ or $\overline{v\theta}$ transport equations which are given in Appendix G. The terms $\overline{u\theta}$ and $\overline{v\theta}$ respectively are the longitudinal and lateral turbulent heat fluxes and are presented in Figs. 6.3 and 6.4.

Generally $\overline{u\theta}$ is higher than $\overline{v\theta}$ (by about twice) and both exhibit the same trend. Their correlation coefficients $\overline{u\theta}/\sqrt{\overline{u^2}}\sqrt{\overline{\theta^2}}$ and

$\overline{v\theta}/\sqrt{\overline{v^2}}\sqrt{\overline{\theta^2}}$ are plotted in Figs. 6.5 to 6.8 for x = 100 and x = 400.

The $\overline{v\theta^2}$ correlation represents the normal transport by v fluctuations of θ^2 appearing in the diffusion term $\partial\overline{v\theta^2}/\partial y$. The $\overline{u\theta^2}$ is the longitudinal transport by u of θ^2 and it appears in the longitudinal diffusion term $\partial\overline{u\theta^2}/\partial x$ in the θ^2 transport equation. In the present case or anywhere where the thin shear layer approximation is valid $\partial\overline{u\theta^2}/\partial x << \partial\overline{v\theta^2}/\partial y$. Both $\overline{v\theta^2}$ and $\overline{u\theta^2}$ are plotted in Figs. 6.9 and 6.10.

The next three figures, Figs. 6.11, 6.12 and 6.13, show the variation of $\overline{u^2\theta}$, $\overline{v^2\theta}$ and $\overline{uv\theta}$. The first is the transport of $u\theta$ by u and appears in the diffusion term of the $\overline{u\theta}$ transport equation. The second, $\overline{v^2\theta}$, is the transport of $v\theta$ by v and occurs in the diffusion term of the $\overline{v\theta}$ transport equation. Finally, $\overline{uv\theta}$ is the transport of $v\theta$ by u or $u\theta$ by v and appears in both transport equations.

From all the above considerations of the behaviour of the thermal field in the symmetric wake flow, it is obvious that there are essential differences between temperature and momentum or kinetic energy transport. For example, near the central line, $\overline{v\theta^2}$ is positive meaning that temperature fluctuations are transported towards positive v, i.e. upwards, while kinetic energy and shear stress are transported inwards towards the centre-line from both directions. But this difference is mainly the result of another basic difference, in the boundary conditions; Reynolds' analogy applies only if the velocity and temperature boundary conditions are equivalent.

6.3 Asymmetric Wake

In the first two figures, Fig. 6.14 and 6.15, the mean temperatures with respect to the free stream value are plotted for the heating conditions: UBLH and LBLH. The max value is higher in the case of LBLH since the boundary layer is thinner and the heat input is

the same in both situations. They both exhibit the same trend as in the symmetric case, except that the $\partial T/\partial y$ in the latter case is rather higher than in the asymmetric UBLH and LBLH cases.

Also similar to the symmetric case is the behaviour of $\overline{\theta^2}$, see Figs. 6.16 to 6.18, across the wake for x = 25, 100 and 400 mm.

It is useful to check any effects of buoyancy in the present experimental investigation. From Figs. 6.19 to 6.22, where the $\overline{v\theta}$ distribution is presented, we see that $\overline{v\theta}/_{max}/U_e = 0.35 \times 10^{-2}\ ^oC$, at x = 100. The flux Richardson number, which characterises the ratio of buoyant production to the stress production of turbulent kinetic energy, is:-

$$R_f \equiv \frac{g}{\Delta\theta} \frac{\overline{v\theta}}{\overline{uv}\,\frac{\partial U}{\partial y}} = \frac{g}{\Delta\theta} \frac{\delta}{U_e^{\,2}} \frac{\overline{v\theta}}{U_e \frac{\overline{uv}}{U_e^{\,2}} \frac{1}{U_e} \frac{\partial U}{\partial y}\,\delta}$$

and gives a value of 1.30×10^{-3} for the asymmetric case. Of the same order of magnitude is the R_f in the symmetric case: thus buoyant production is negligible.

In Figs. 6.23 to 6.26, the $\overline{u\theta}$ profiles are presented. At x = 0 , close to the wall there is sudden decrease of $\overline{u\theta}$, quite similar to that observed in the $\overline{uv}$ distribution: this could be the effect of roughness. It is still evident at x = 25. The rest of the profiles all have similar trends.

The next figures, Figs. 6.22 to 6.34, display the correlation coefficients, $R_{u\theta}$ and $R_{v\theta}$. Generally, the correlation between u and θ is higher than between v and θ.

Finally in Figs. 6.35 to 6.49, the quantities $\overline{v\theta^2}$, $\overline{u\theta^2}$, $\overline{u^2\theta}$, $\overline{v^2\theta}$ and $\overline{uv\theta}$ appear, with the meaning described in the previous section, i.e. all are terms of the diffusion in the various transport equations.

Their trends are similar to those in the symmetric case.

6.4 Further Results and Discussion

From the results previously considered, it is obvious that the velocity and thermal field do not indicate strong similarities between them because there is a difference in the mean flow normal gradients $\partial U/\partial y$ and $\partial T/\partial y$. The $\partial T/\partial y$ is shown in Figs. 6.50 and 6.51 for the symmetric and asymmetric wake. In the same figures, the thermal eddy diffusivity, $\nu_\theta = -\overline{v\theta}/(\partial T/\partial y)$, is plotted. This demonstrates simply that when $\partial T/\partial y$ is tending to zero, ν_θ tends to infinity because $\overline{v\theta}$ does not tend to zero at the same point. Generally, any attempt to connect locally the $\overline{v\theta}$ with the mean temperature gradient will fail in restricted regions of flows exhibiting asymmetric boundary conditions exactly as happens when one attempts to relate the shear stress to the local mean velocity gradient.

The structural parameter V_θ defined as the lateral transport velocity of $v\theta$, i.e. $V_{\theta v} = \overline{v^2\theta}/\overline{v\theta}$, and plotted in Fig. 6.52, indicates a higher transport velocity, $V_{v\theta}$, for the asymmetric wake and always positive around the centre-line, i.e. towards the higher temperature.

The transport velocity of θ^2, $V_\theta = \overline{v\theta^2}/\overline{\theta^2}$, (Fig. 6.53), indicates the same trend with $V_{v\theta}$ for the region near the centre-line where the asymmetric reaches a value twice that of symmetric value. But for high negative y it is negative, i.e. θ^2 is transport towards the "cold" zone with roughly the same values for symmetric and asymmetric. The $\overline{\theta^2}$ balance of the various terms involved in the $\overline{\theta^2}$ transport equations are plotted in Figs. 6.54 and 6.55. The transport equation of $\overline{\theta^2}$ is the equation (G.10) of Appendix G. The production term consists of $-\overline{\theta u}\,(\partial T/\partial x)$ and $-\overline{\theta v}\,(\partial T/\partial y)$, i.e. $\overline{\theta^2}$ is produced by the interaction of the heat flux terms $\overline{\theta u}$ and $\overline{\theta v}$ and the mean temperature

gradients, $\partial T/\partial x$ and $\partial T/\partial y$, respectively. However, in the present case, the longitudinal variation of T is very weak compared with the normal one and, consequently, $-\overline{\theta v}\ (\partial T/\partial y)$ is the term dominating the production. Similar argument can be applied to the diffusion terms: $\overline{\partial u\theta^2/\partial x} << \overline{\partial v\theta^2/\partial y}$.

The molecular dissipation or diffusion is also completely neglected since it is two orders of magnitude less than the other terms. In the graphs, all terms have been non-dimensionalised by $\delta/U_e\ (\Delta T^2_{max})$ at $x = 0$. The thermal dissipation or destruction ε_θ is obtained by difference. The production near the edges of the internal thermal layer is very small but it increases towards the centre-line where it reaches its maximum value. There, the diffusion is negligible and the advection is rather small and thus the equilibrium hypothesis can be held with small error, smaller than anywhere else. The advection is always a loss near the edges of the layer being quite large near the lower edge. There is a small gain by advection near the centre-line. The diffusion near the edges behaves like an isolated shear layer, i.e. exhibits a small gain. For $y > 0$, this gain is increased with decreasing y but at $y = 0$, a loss by diffusion starts to be important.

Very similar behaviour characterises the asymmetric wake $\overline{\theta^2}$ balance.

The turbulent Prandtl number, Pr_t, defined as the ratio $\overline{uv}\ \partial T/\partial y/\overline{v\theta}\ \partial U/\partial y$ of momentum diffusivity to thermal diffusivity, has been evaluated for the outer part of the wake only where it has a value of approximately 0.8. Any attempt to evaluate it in the inner wake is fruitless since the quantities involved are zero at different points and, thus, Pr_t jumps from zero to infinity a few times, and in between the uncertainty is unavoidably large.

SYMM. WAKE

FIG. 6.1

MEAN TEMPERATURE PROFILES

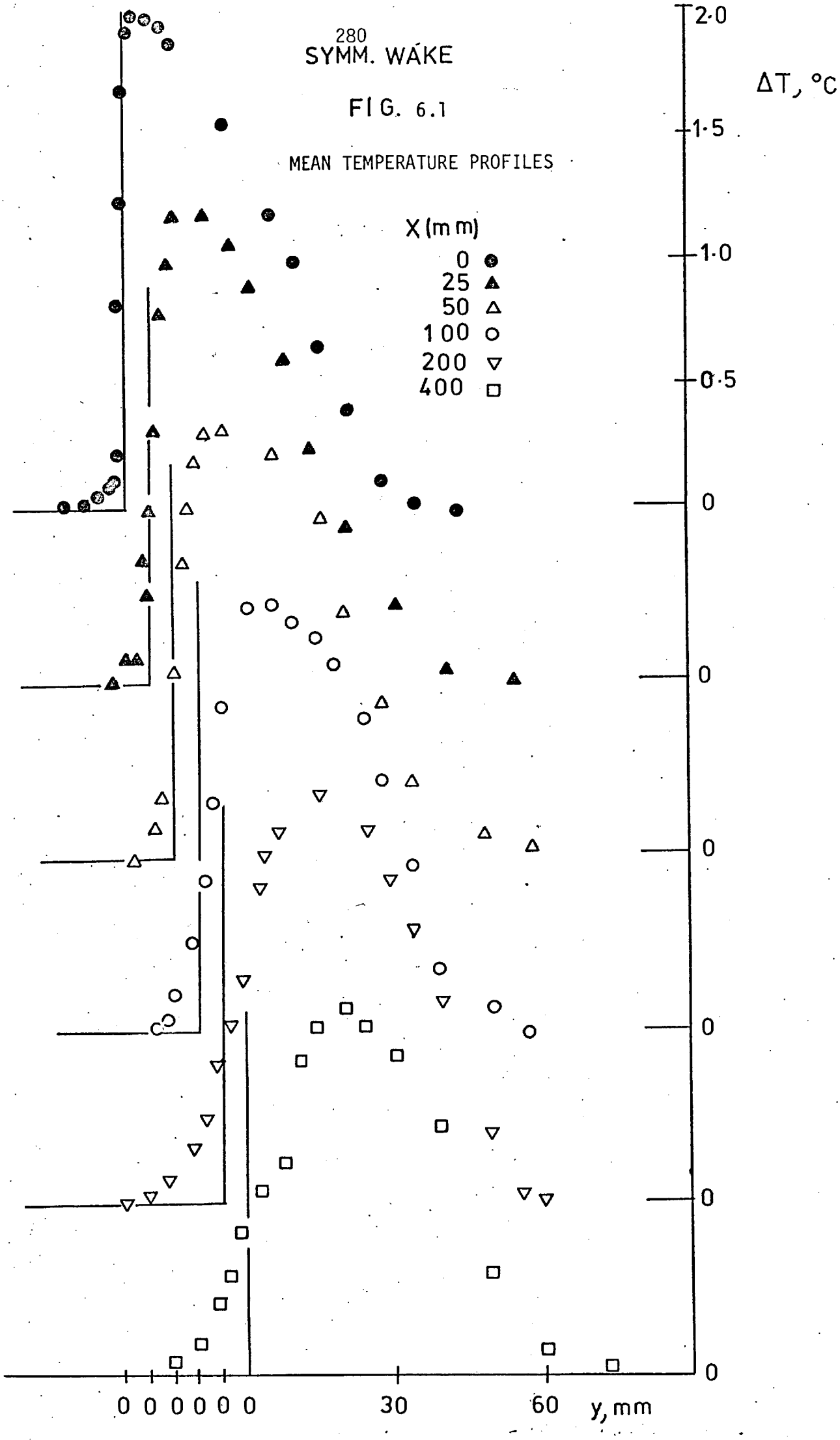

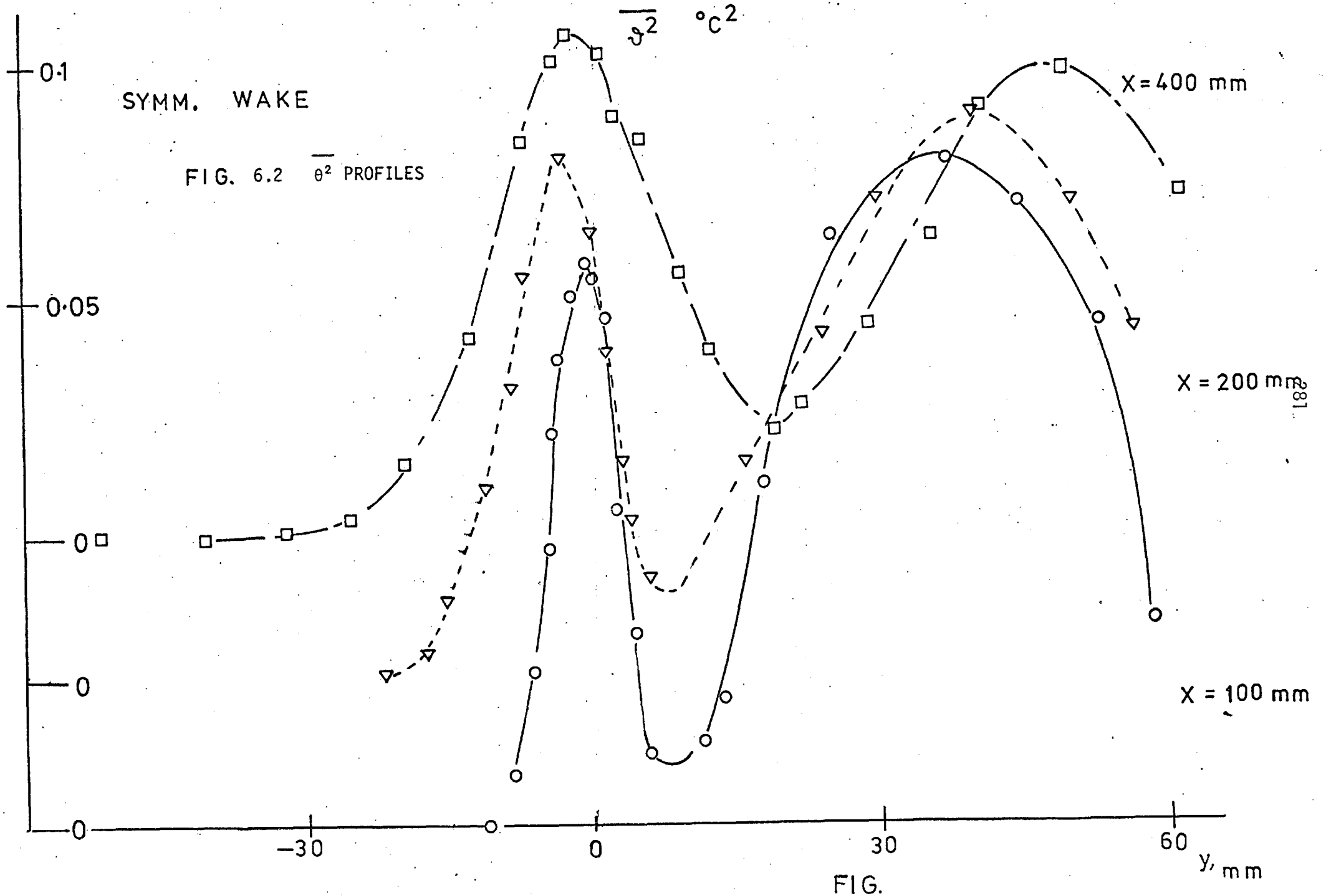

FIG. 6.2 $\overline{\theta^2}$ PROFILES

FIG.

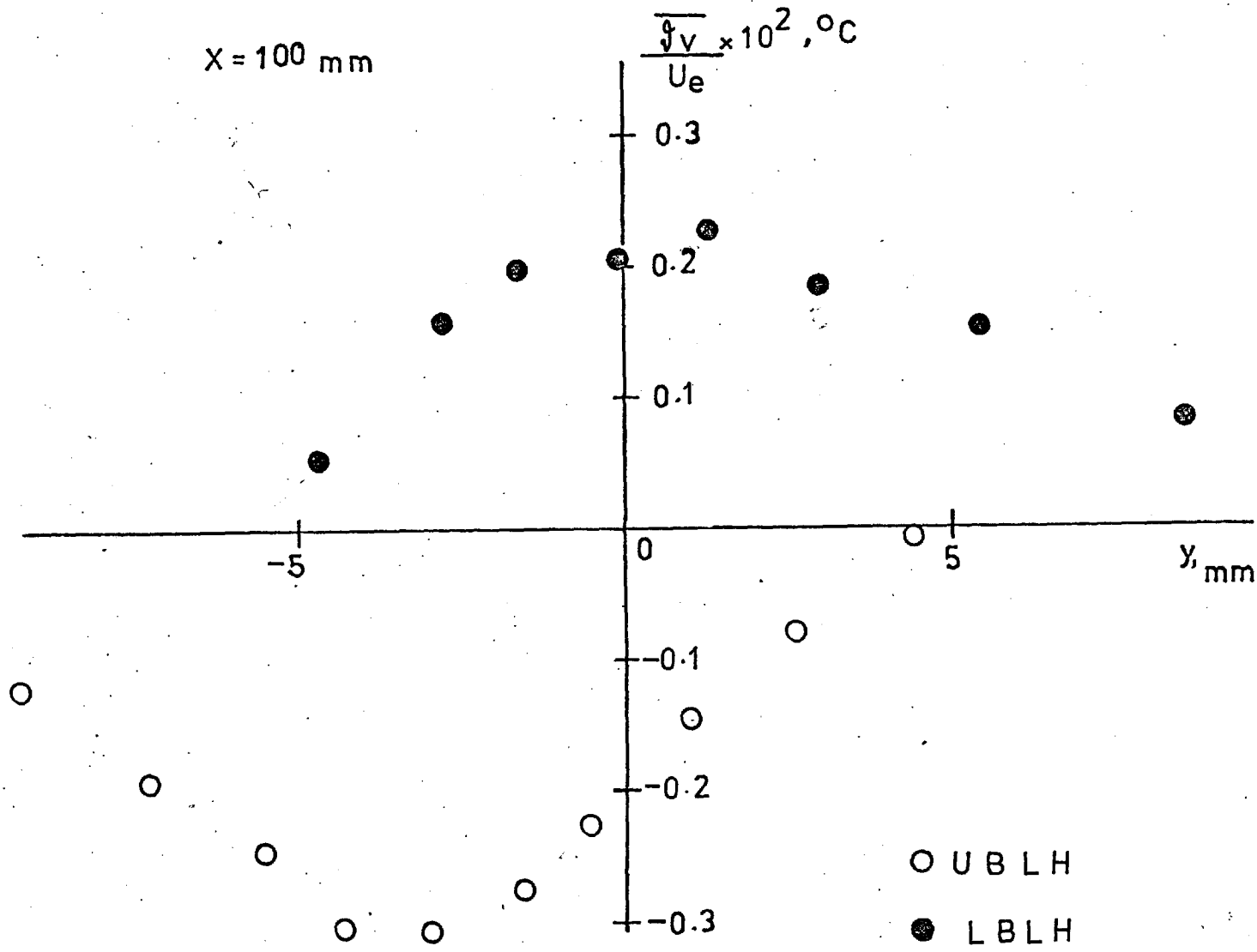

FIG. 6.3 NORMAL TURBULENT HEAT FLUX

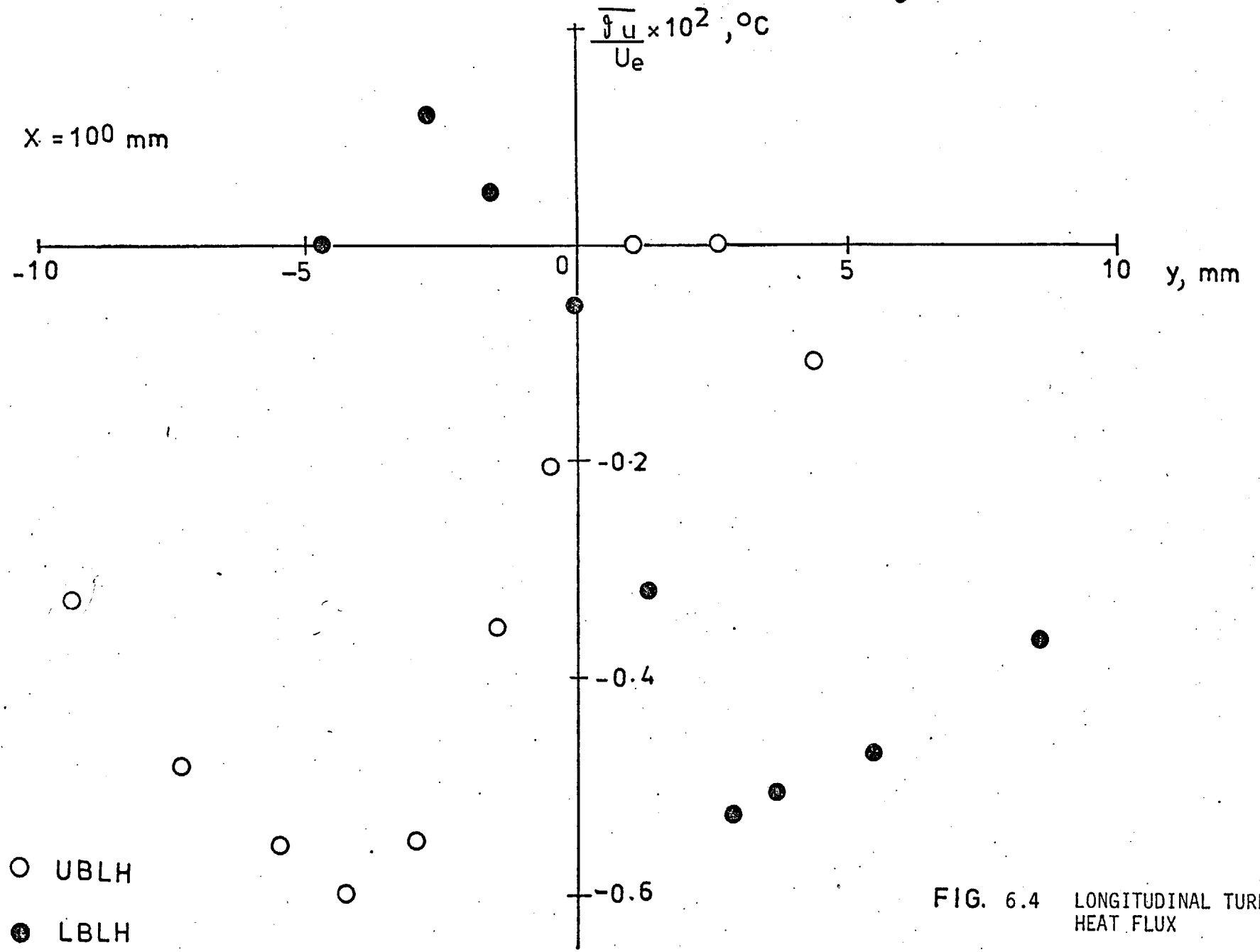

FIG. 6.4 LONGITUDINAL TURBULENT HEAT FLUX

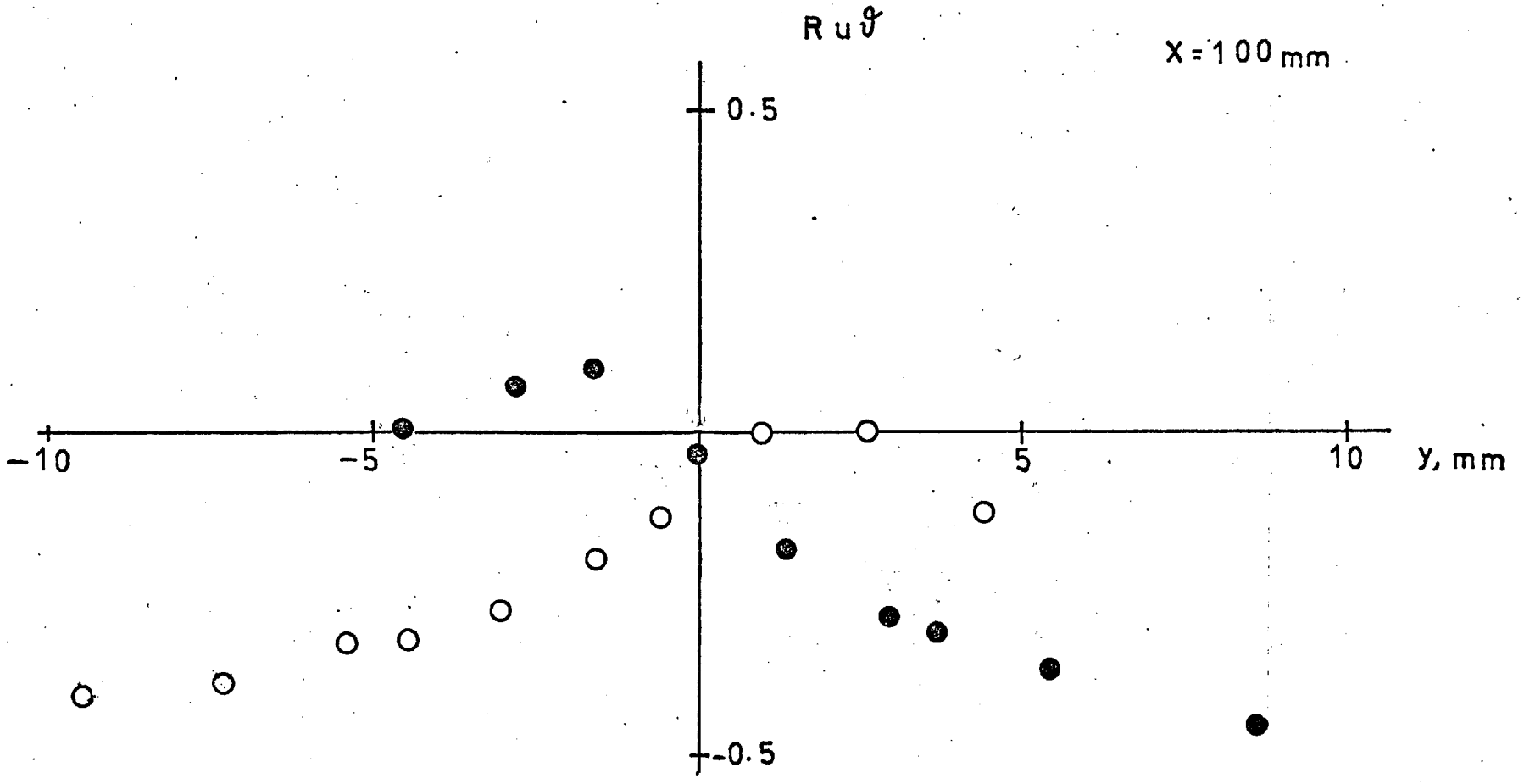

FIG. 6.5 u, θ CORRELATION COEFFICIENT AT x = 100 mm

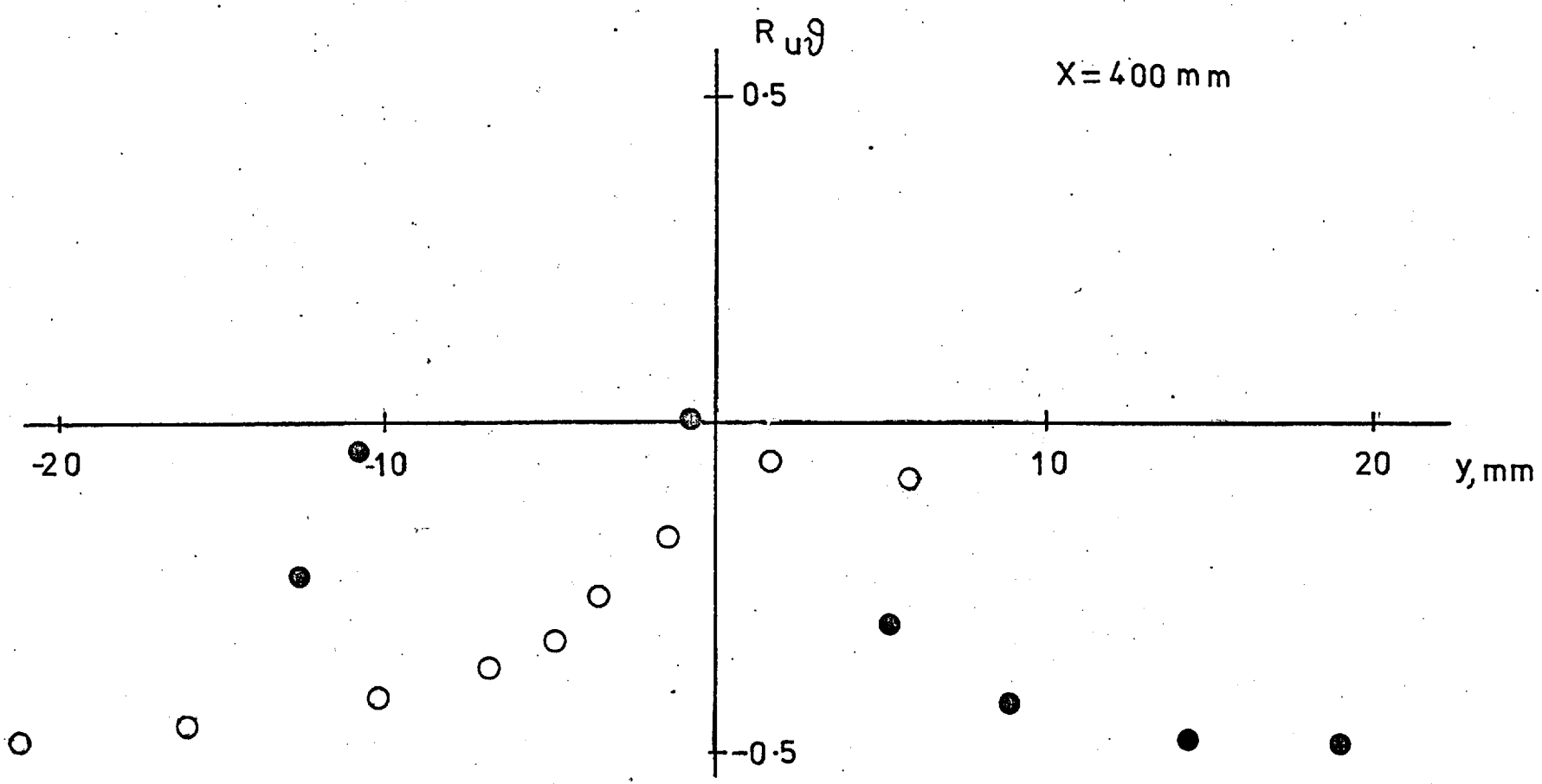

FIG. 6.6 u, θ CORRELATION COEFFICIENT AT x = 400 mm

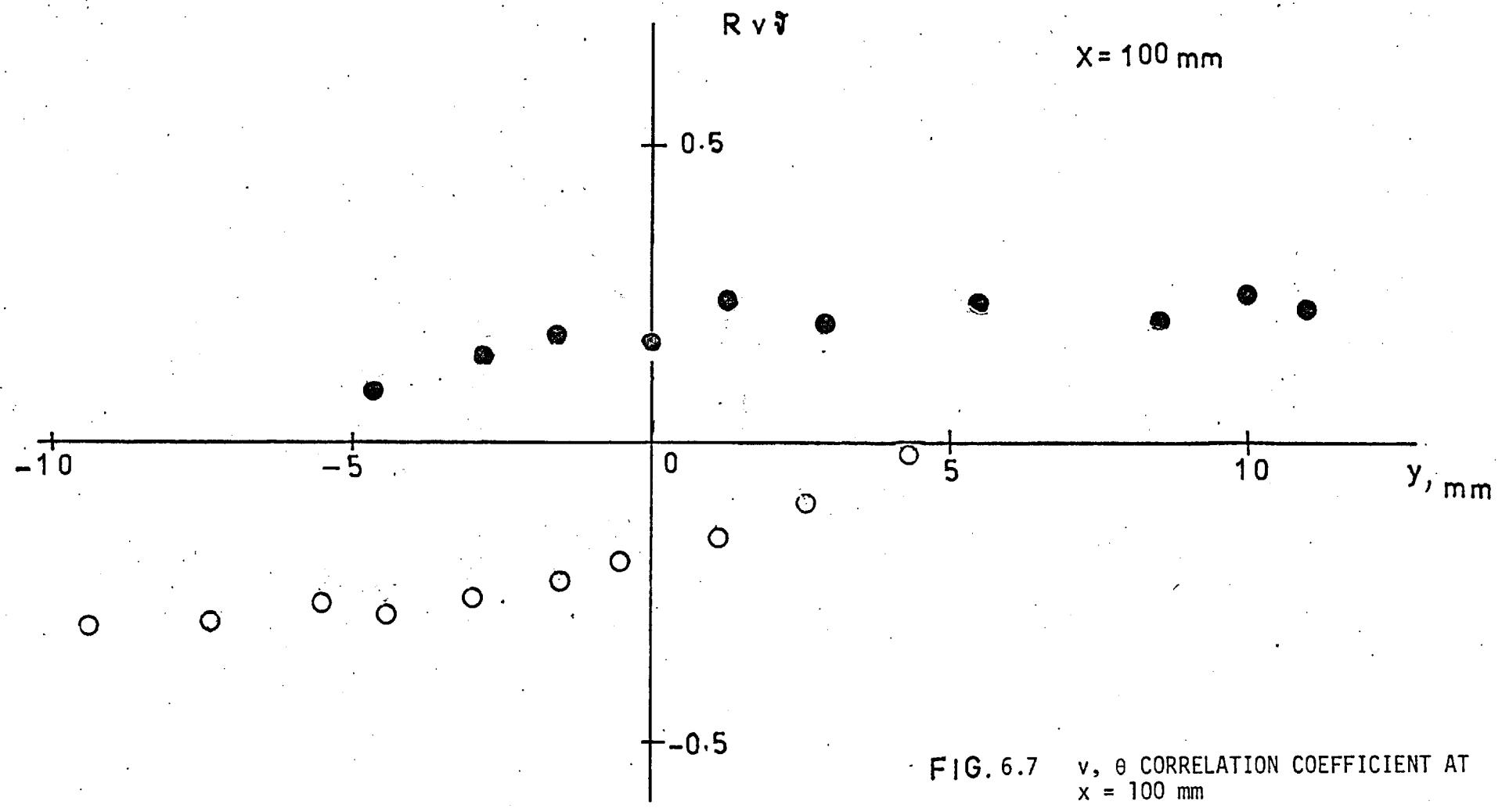

FIG. 6.7 v, θ CORRELATION COEFFICIENT AT x = 100 mm

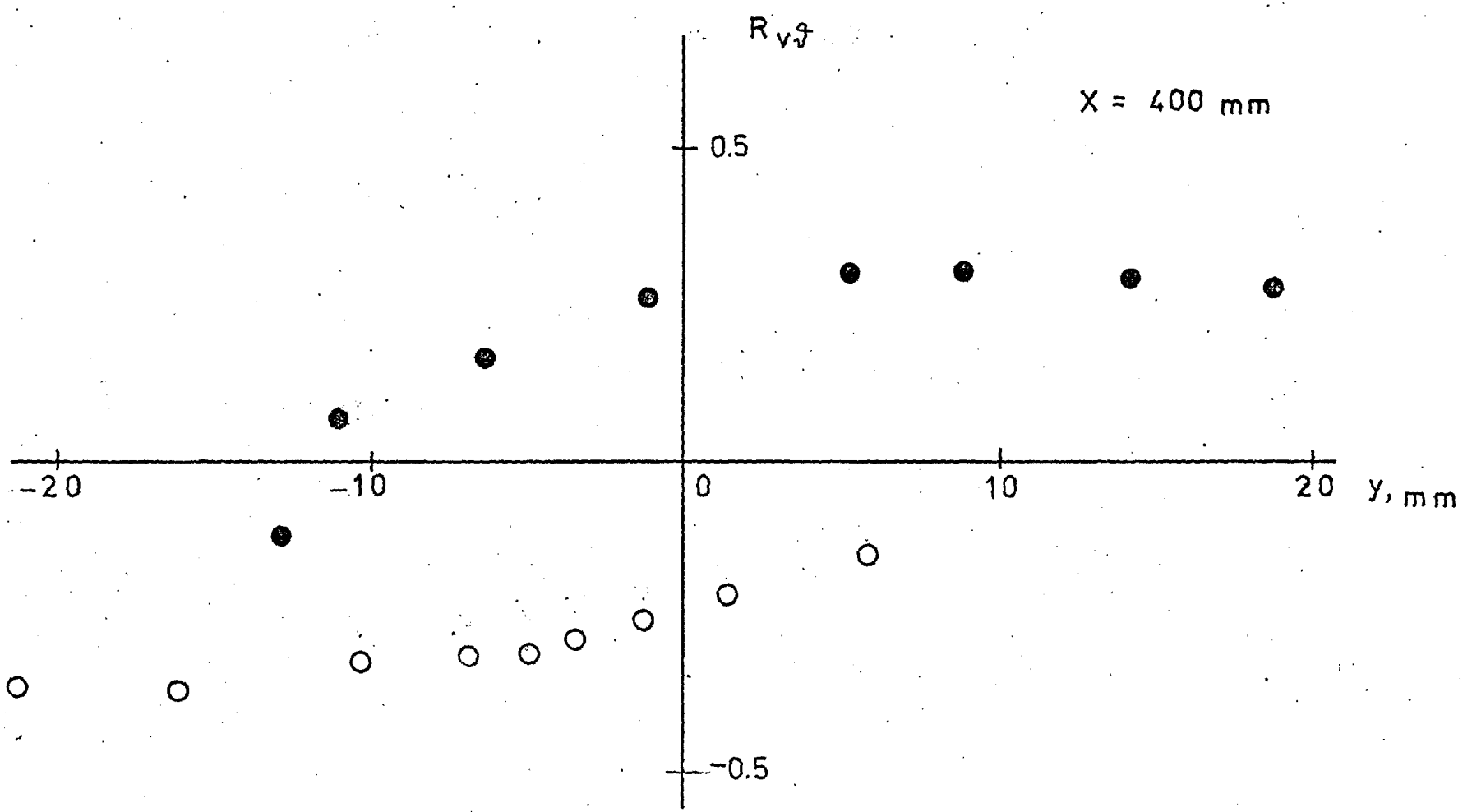

FIG. 6.8 v, θ CORRELATION COEFFICIENT AT x = 400 mm

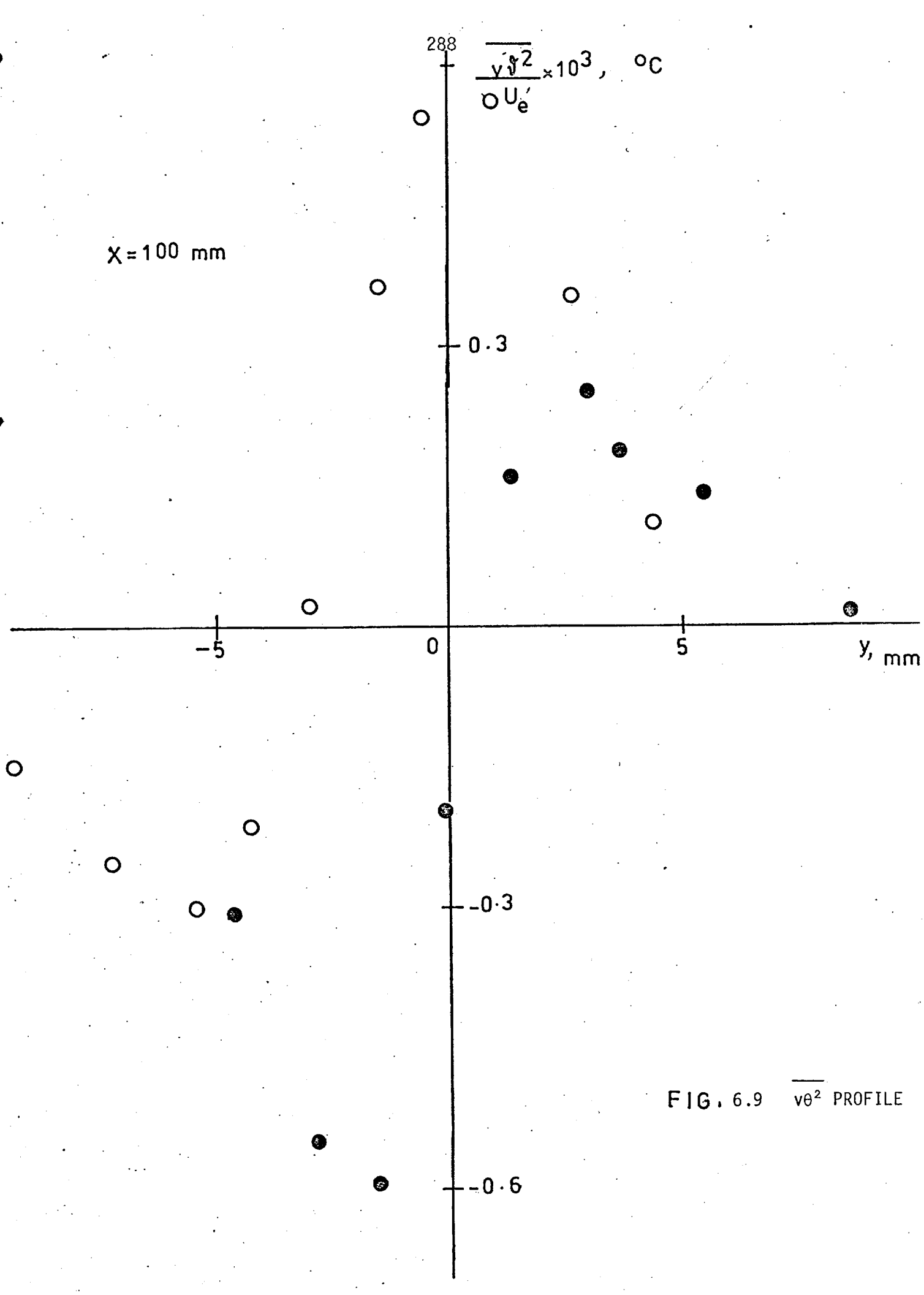

FIG. 6.9 $\overline{v\theta^2}$ PROFILE

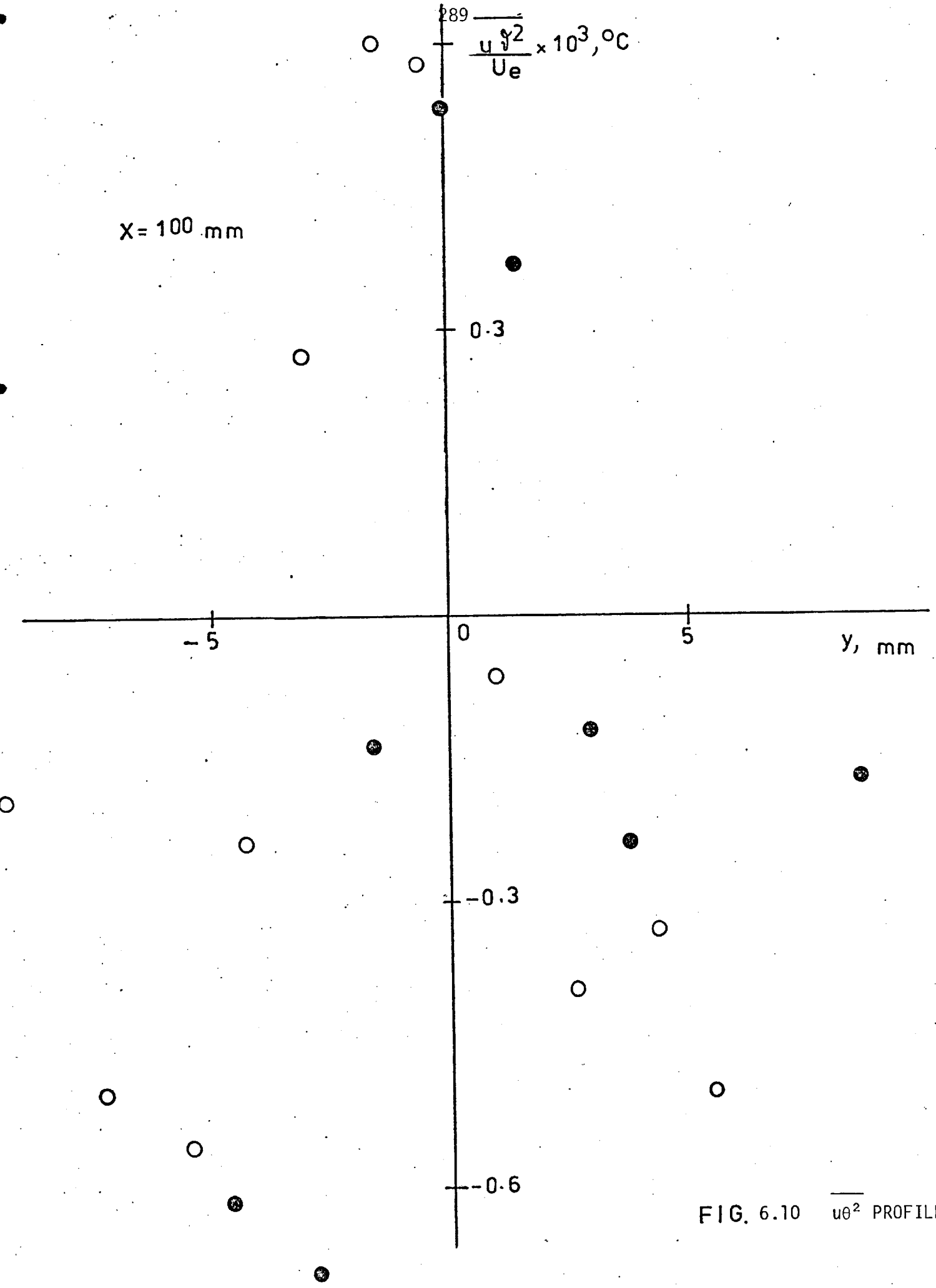

FIG. 6.10 $\overline{u\theta^2}$ PROFILE

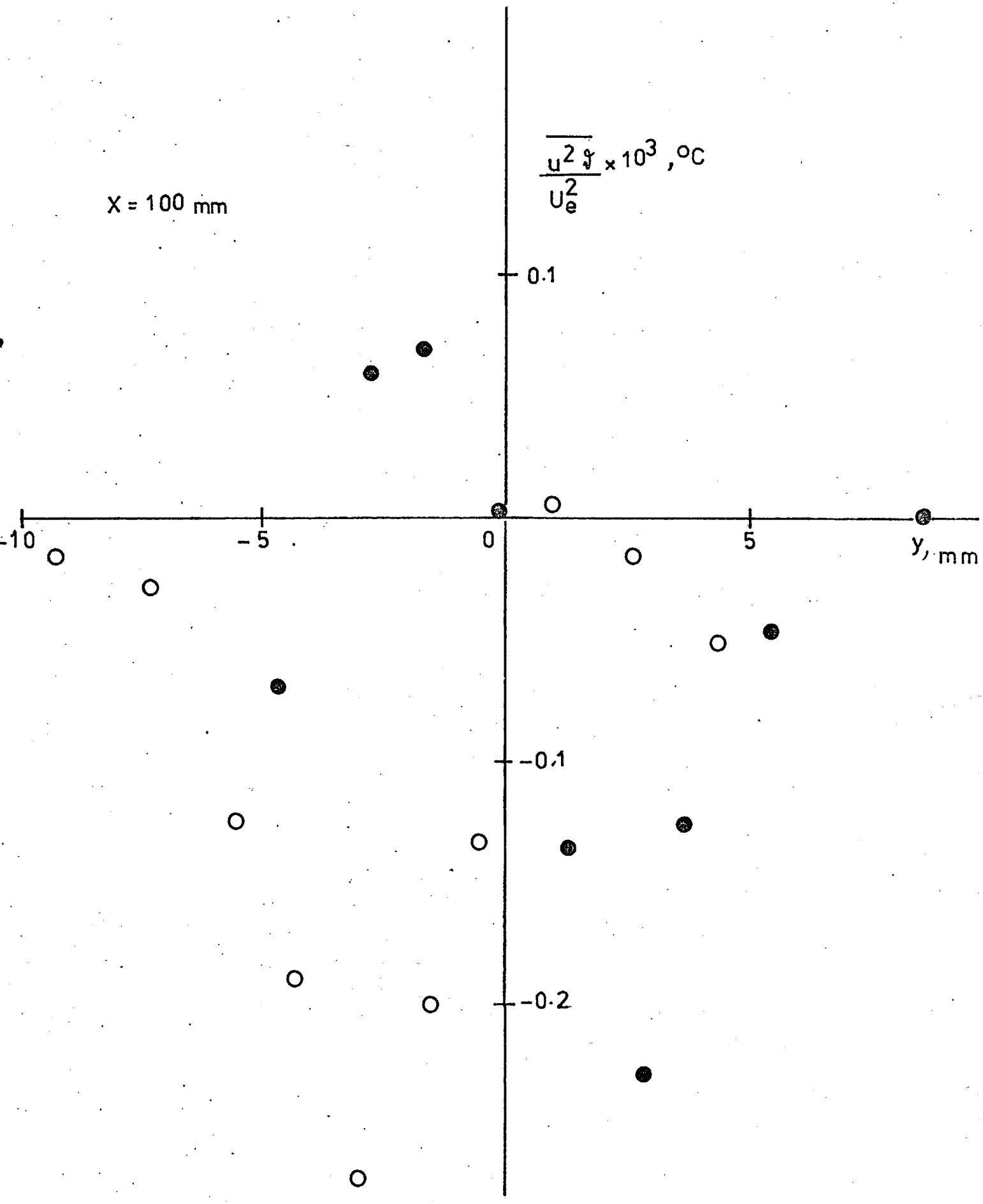

FIG. 6.11 $\overline{u^2\theta}$ PROFILE

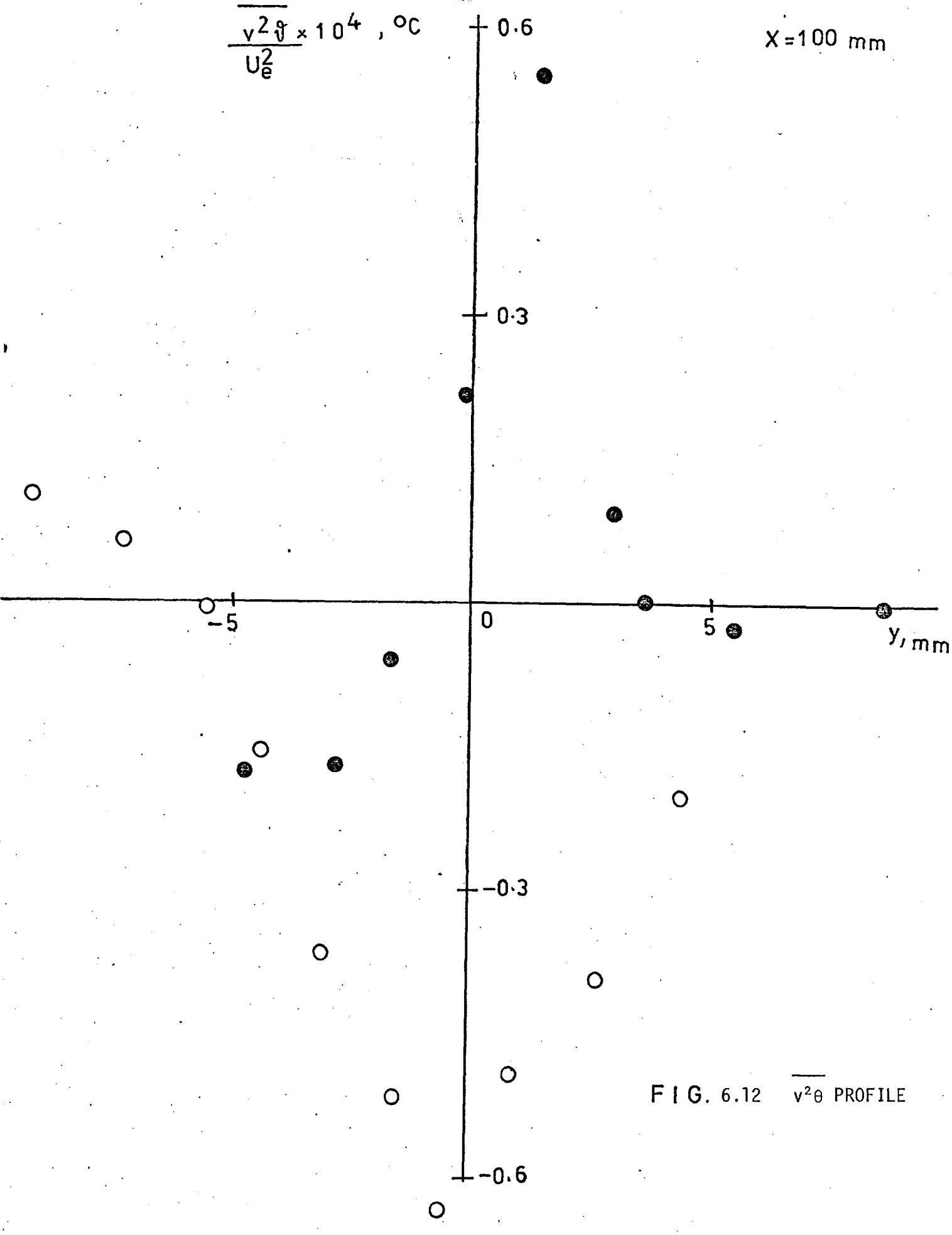

FIG. 6.12 $\overline{v^2\theta}$ PROFILE

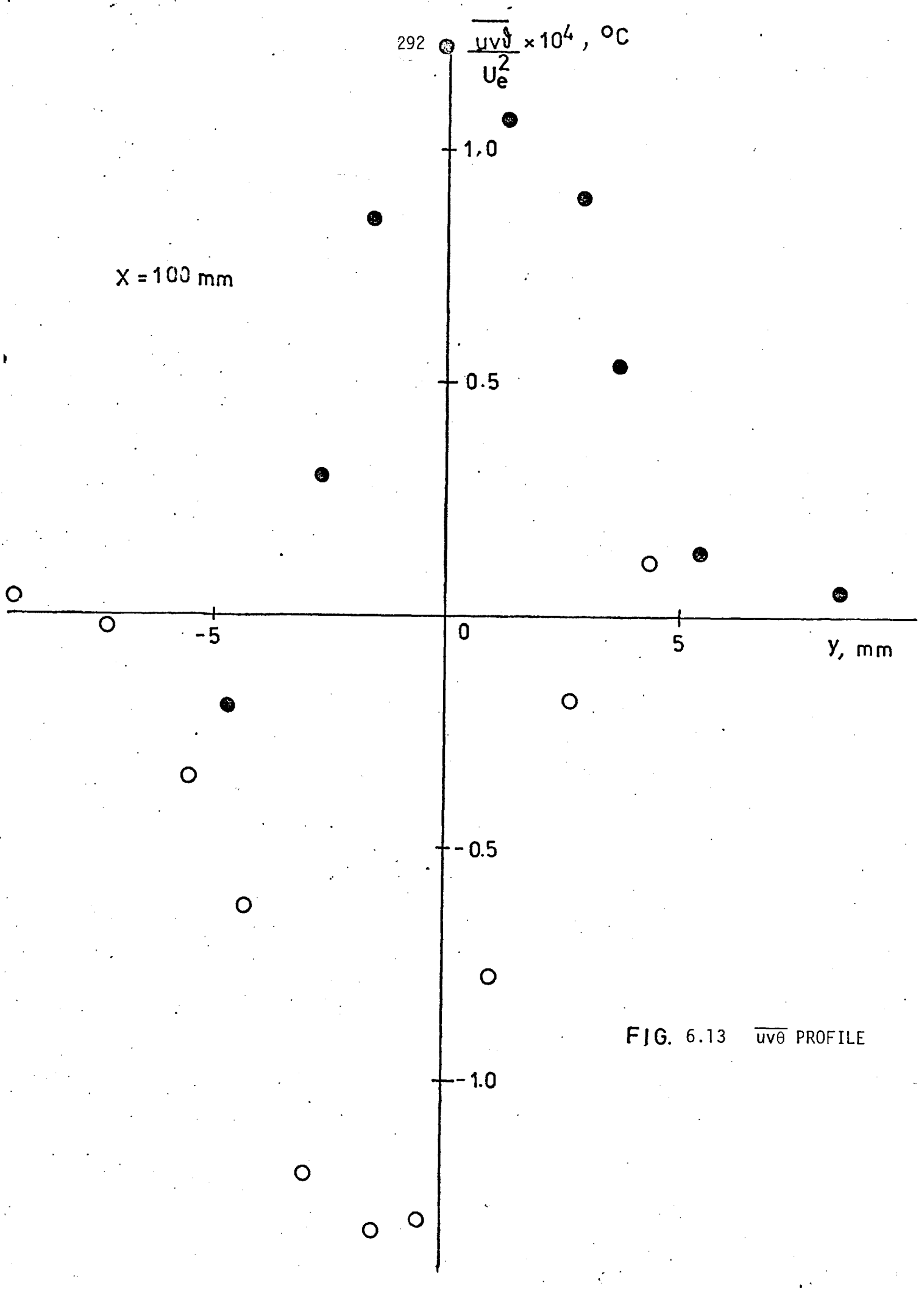

FIG. 6.13 $\overline{uv\theta}$ PROFILE

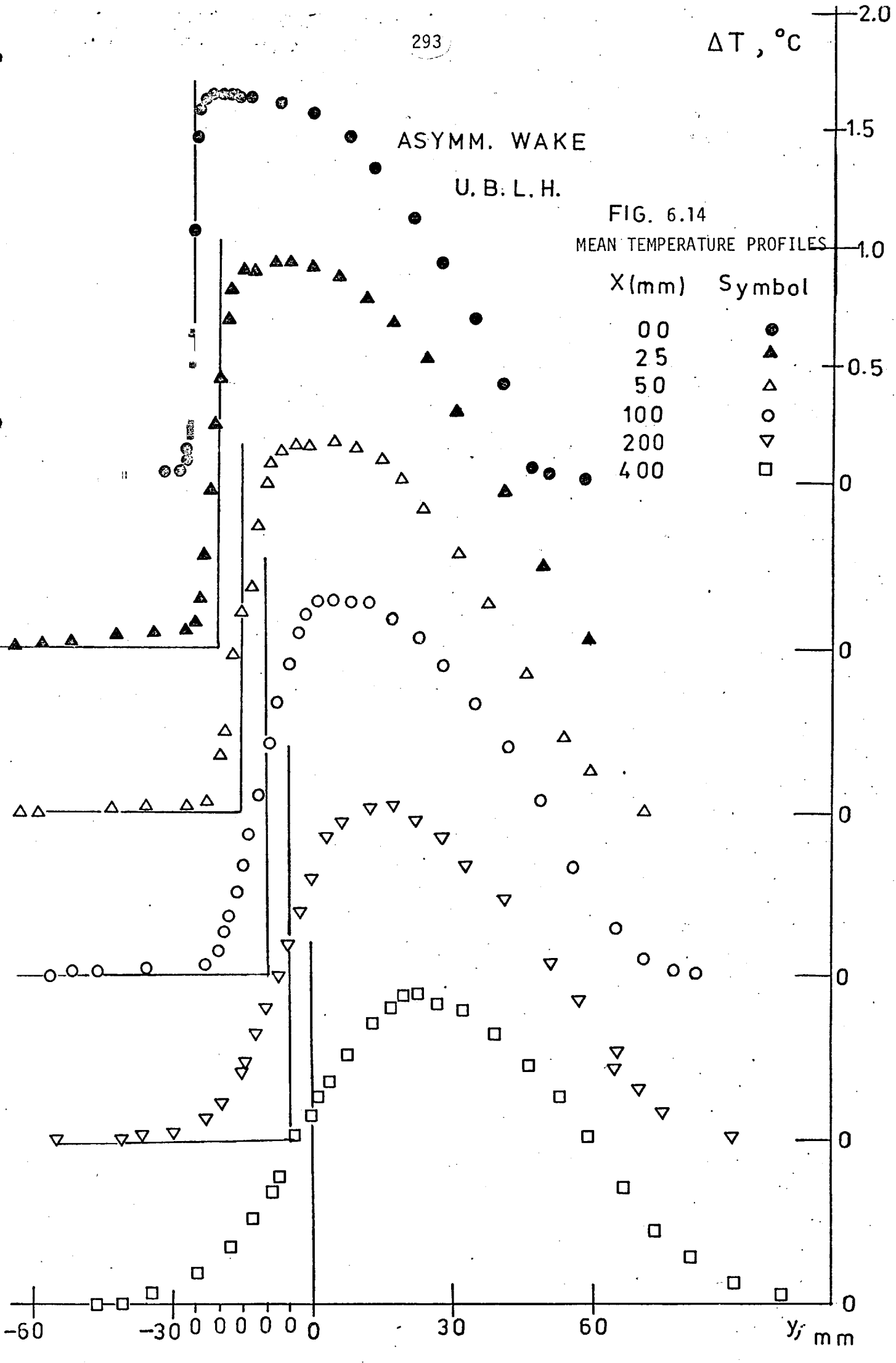
ΔT, °C
2.0
1.5
1.0
0.5
0
0
0
0
0
0
ASYMM. WAKE
U.B.L.H.
FIG. 6.14
MEAN TEMPERATURE PROFILES
X(mm) Symbol
00
25
50
100
200
400
-60
-30
30
60
y, mm

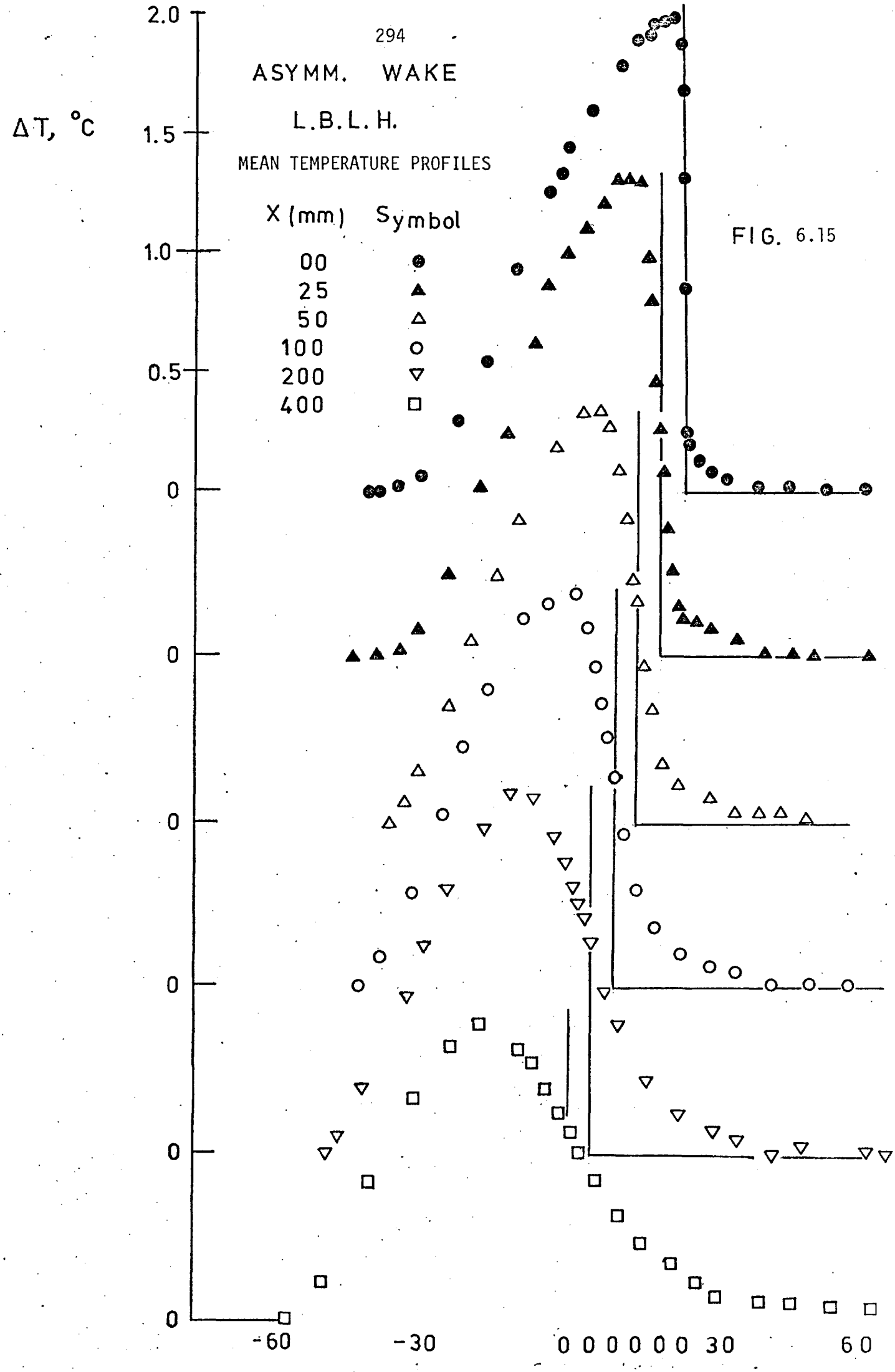
ASYMM. WAKE
L.B.L.H.
MEAN TEMPERATURE PROFILES
X (mm) Symbol
00
25
50
100
200
400
ΔT, °C
2.0
1.5
1.0
0.5
0
0
0
0
0
-60
-30
0 0 0 0 0 0 30
60

FIG. 6.15

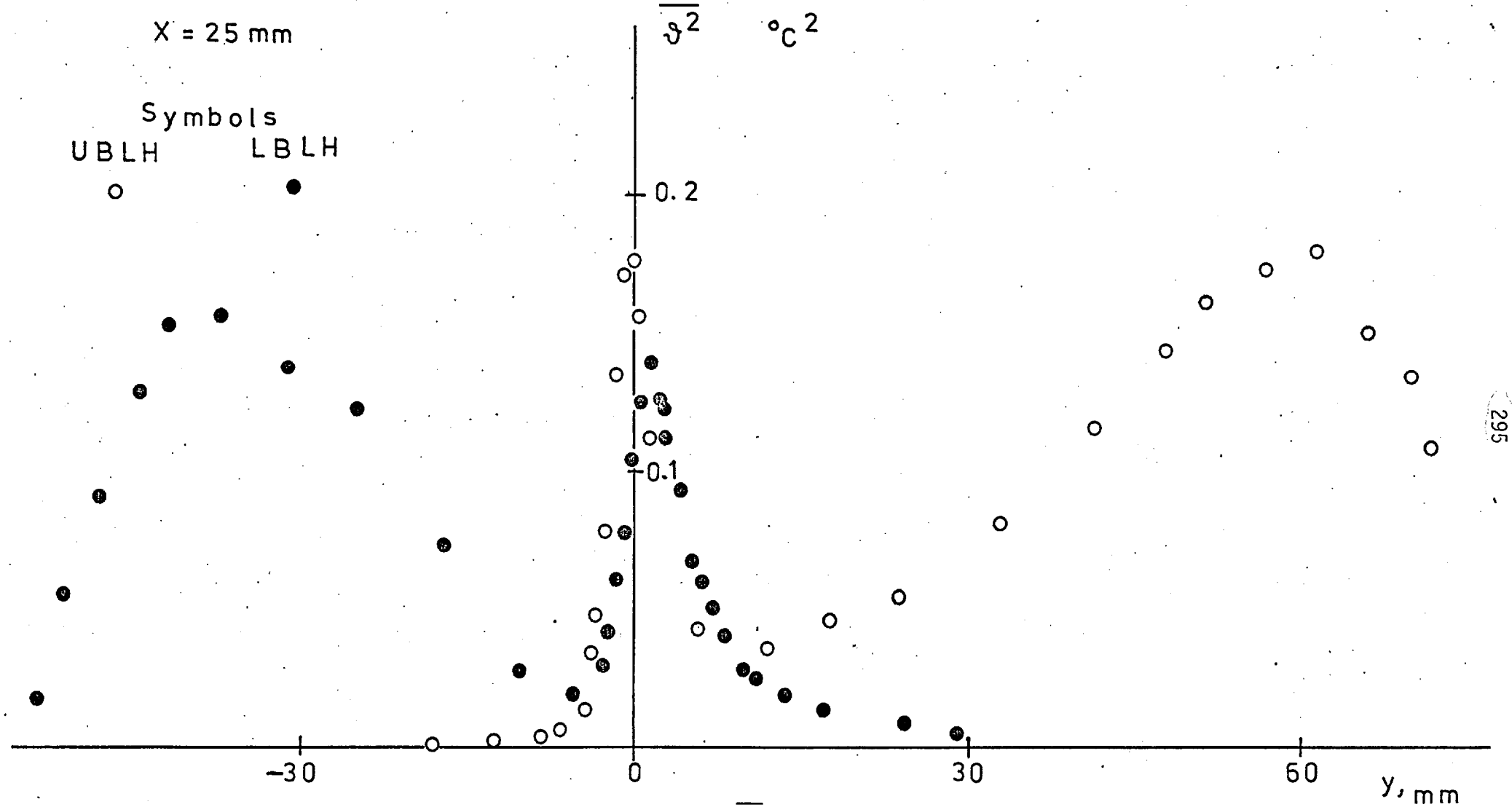

FIG. 6.16 $\overline{\theta^2}$ PROFILE

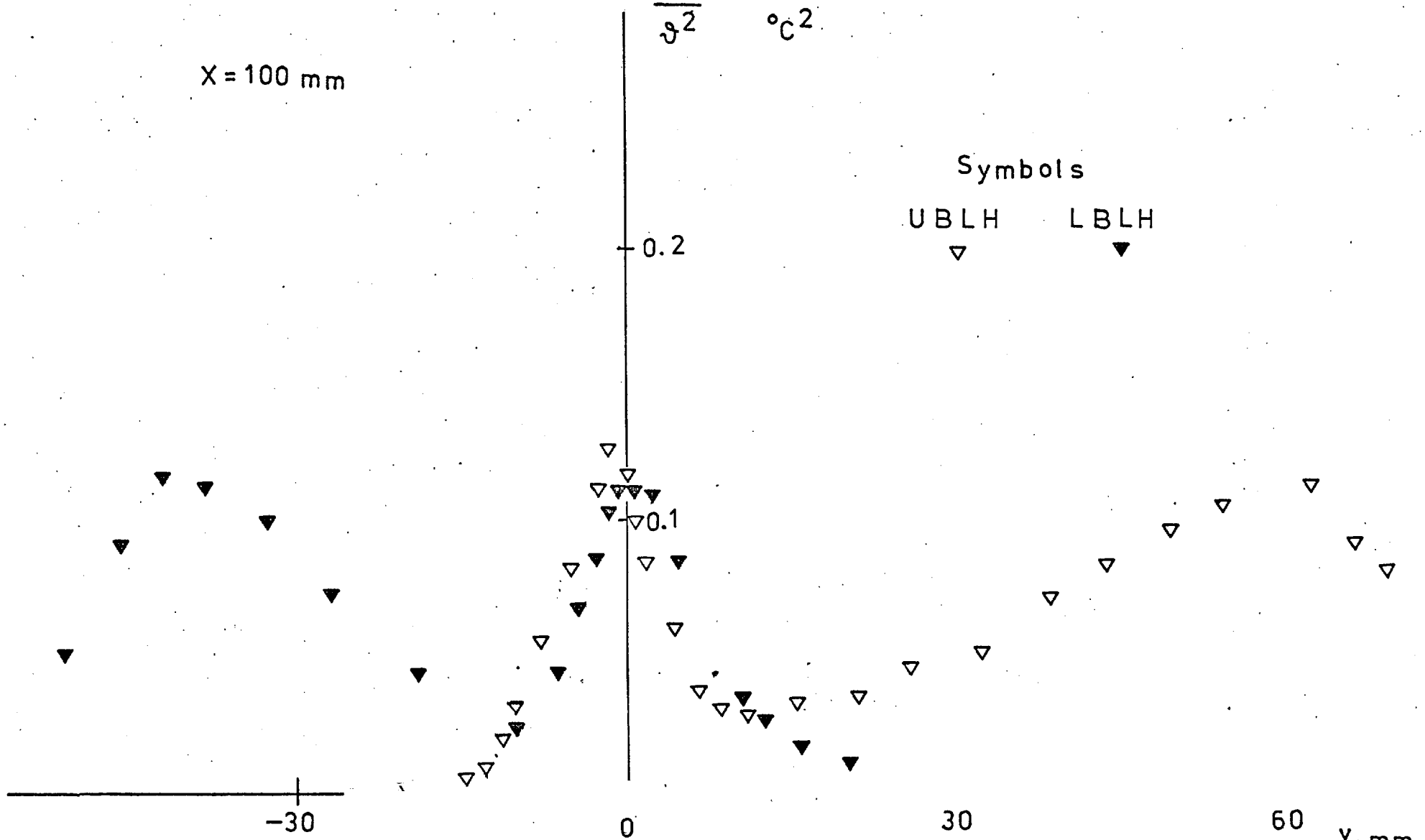

FIG. 6.17 $\overline{\theta^2}$ PROFILE

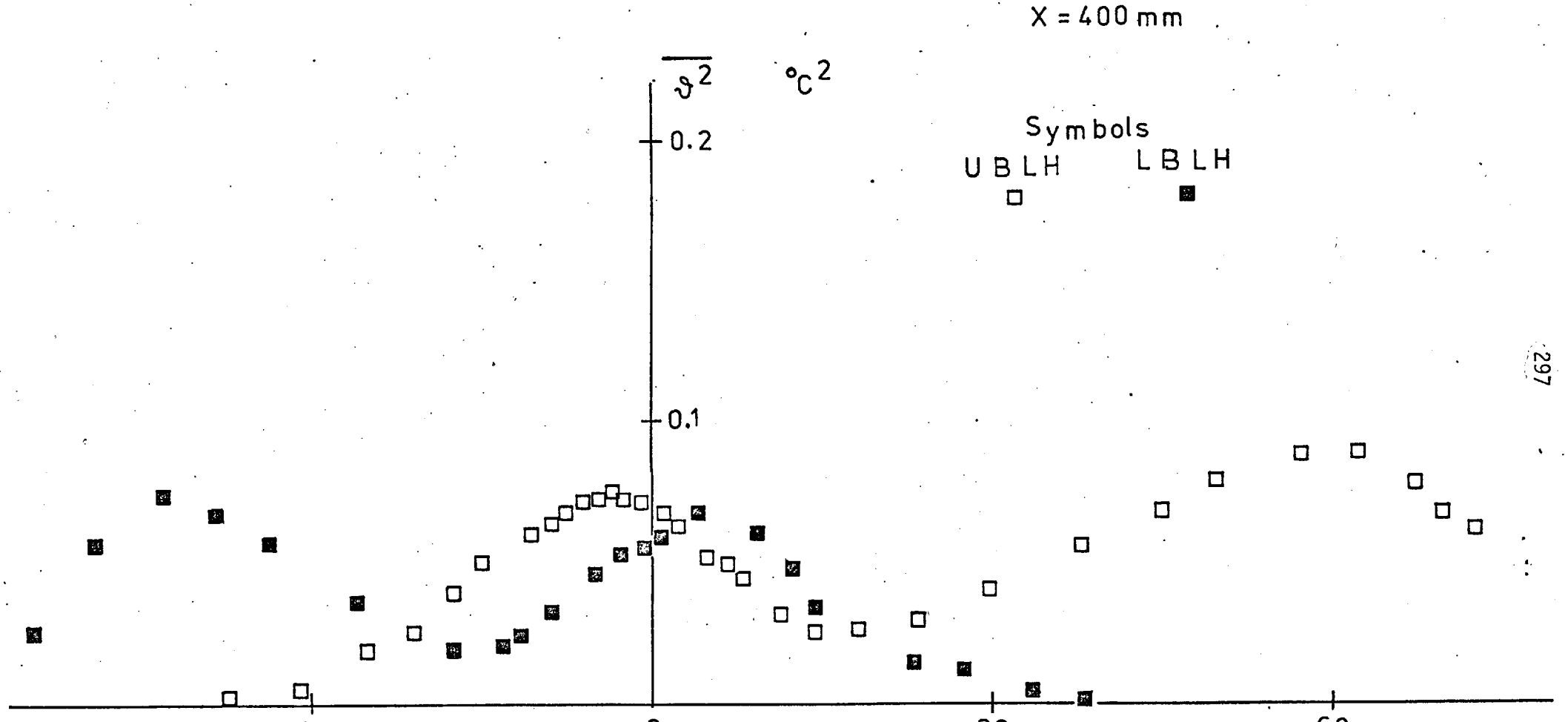

FIG. 6.18 $\overline{\theta^2}$ PROFILE

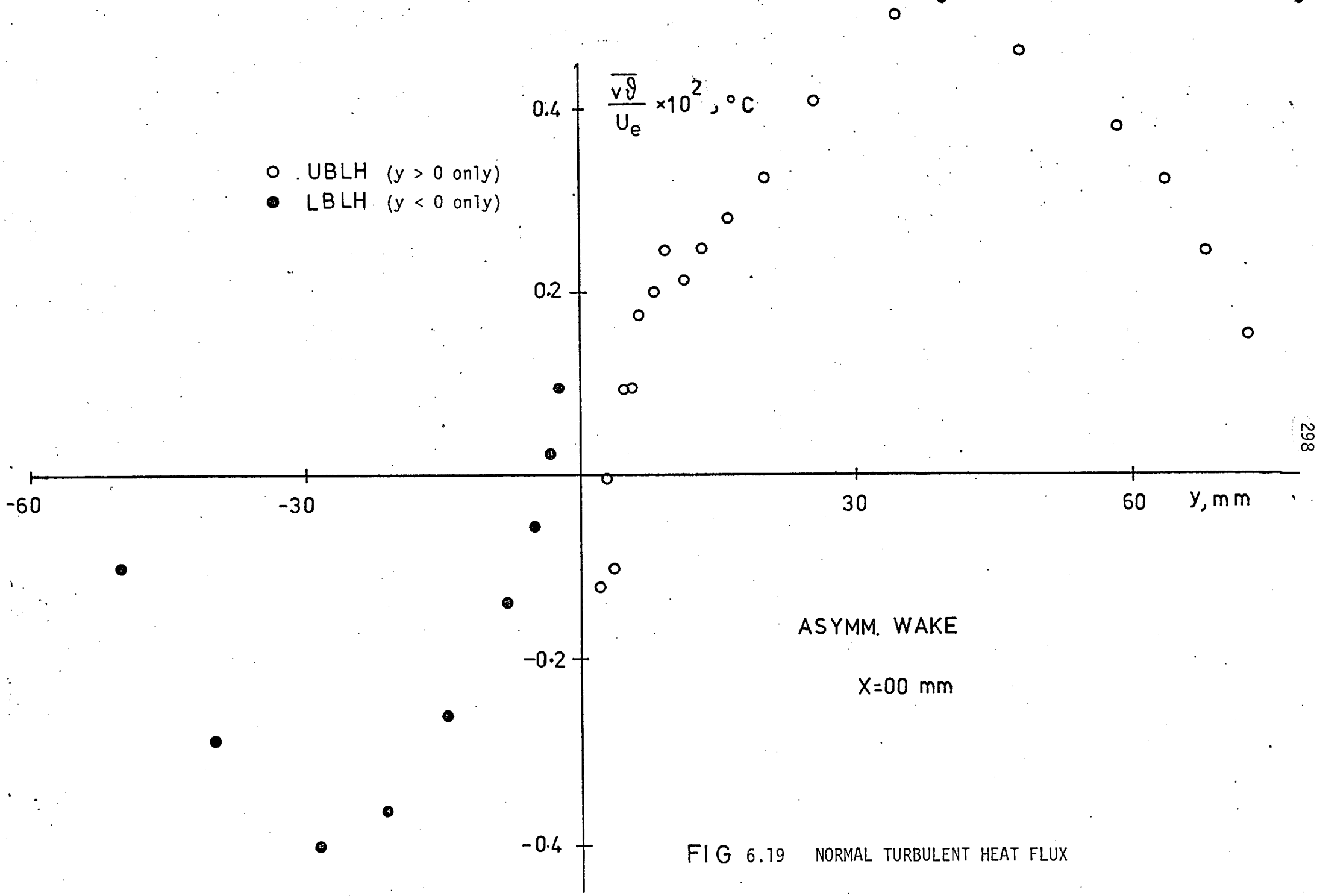

FIG 6.19 NORMAL TURBULENT HEAT FLUX

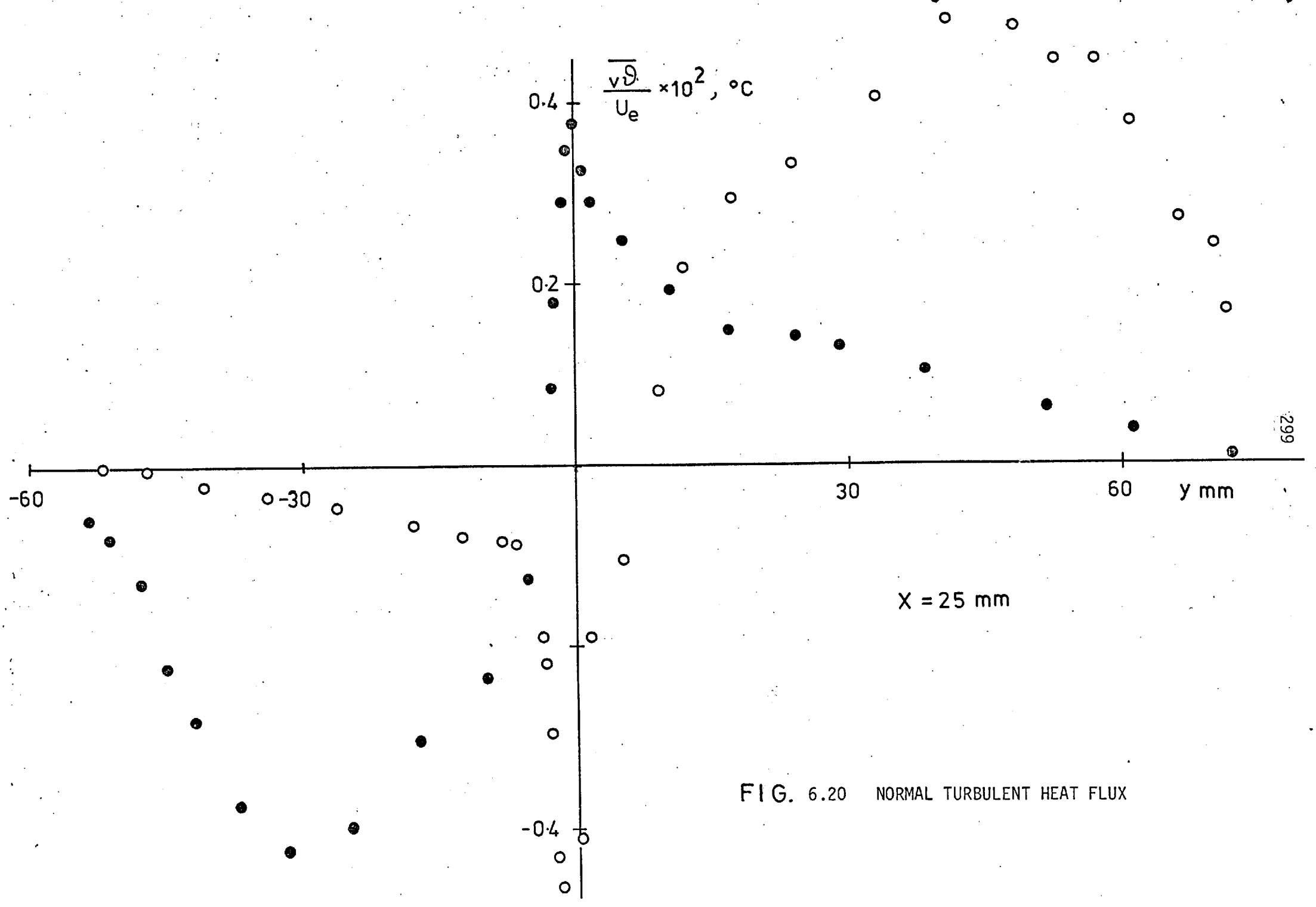

FIG. 6.20 NORMAL TURBULENT HEAT FLUX

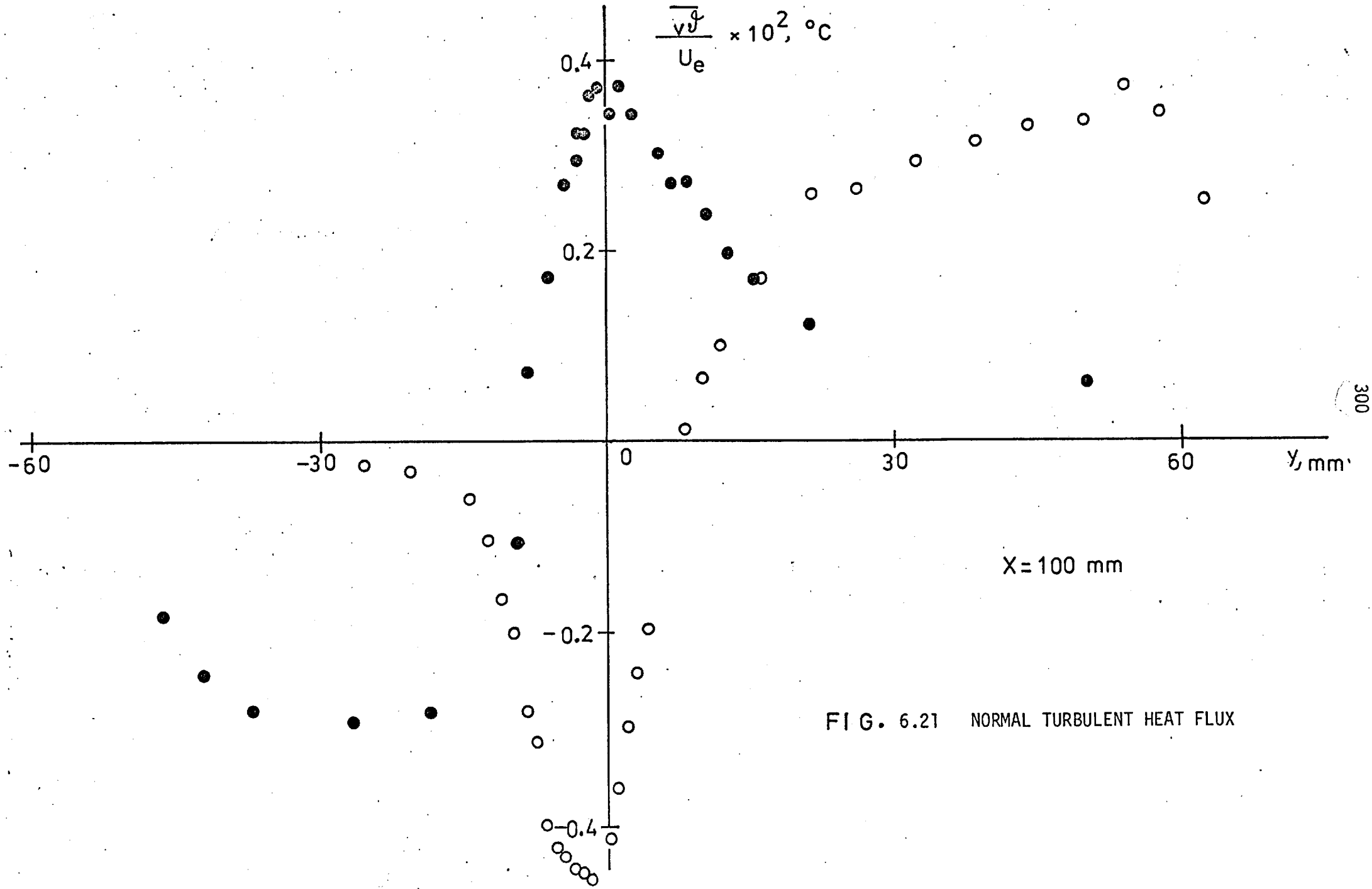

FIG. 6.21 NORMAL TURBULENT HEAT FLUX

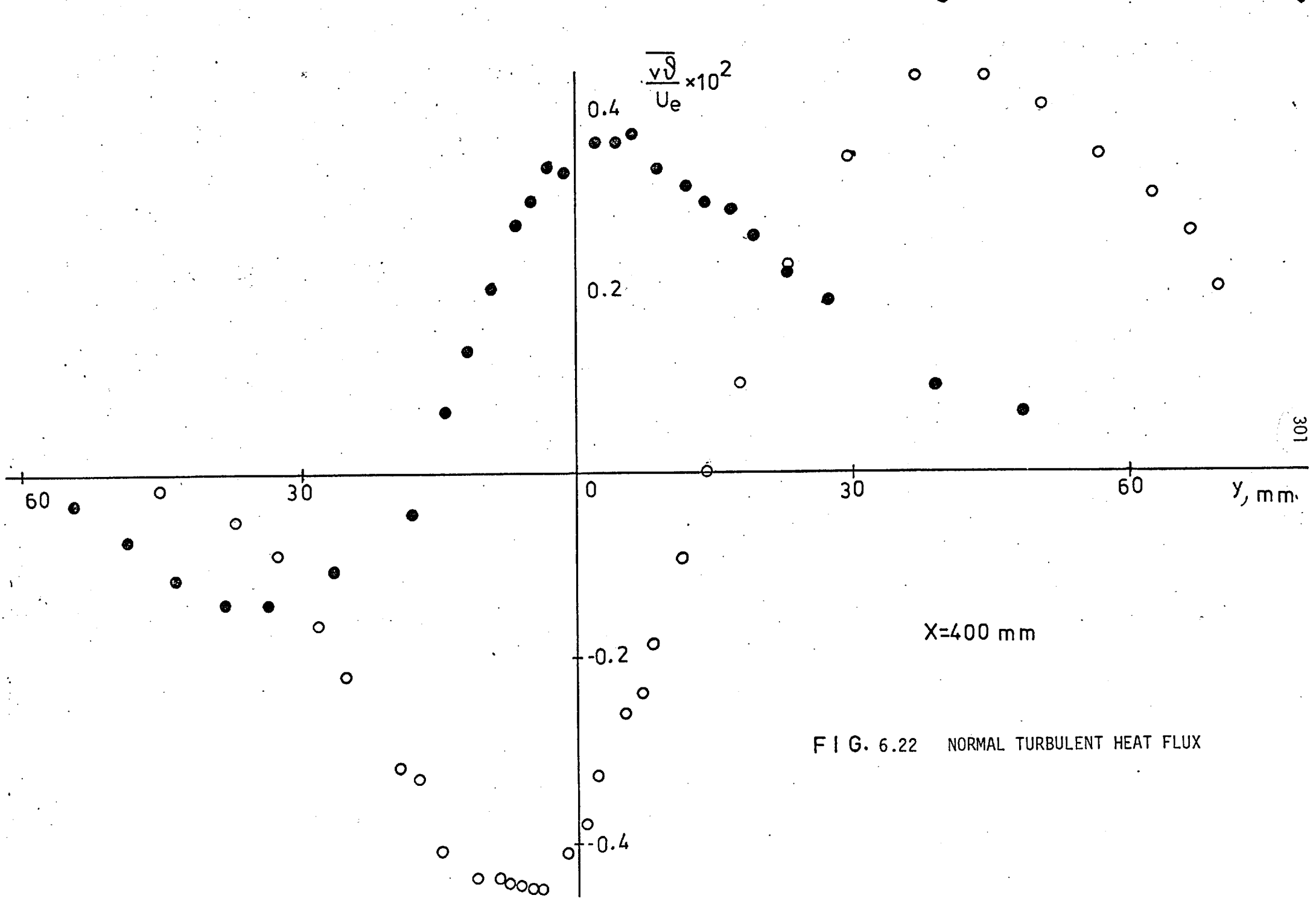

FIG. 6.22 NORMAL TURBULENT HEAT FLUX

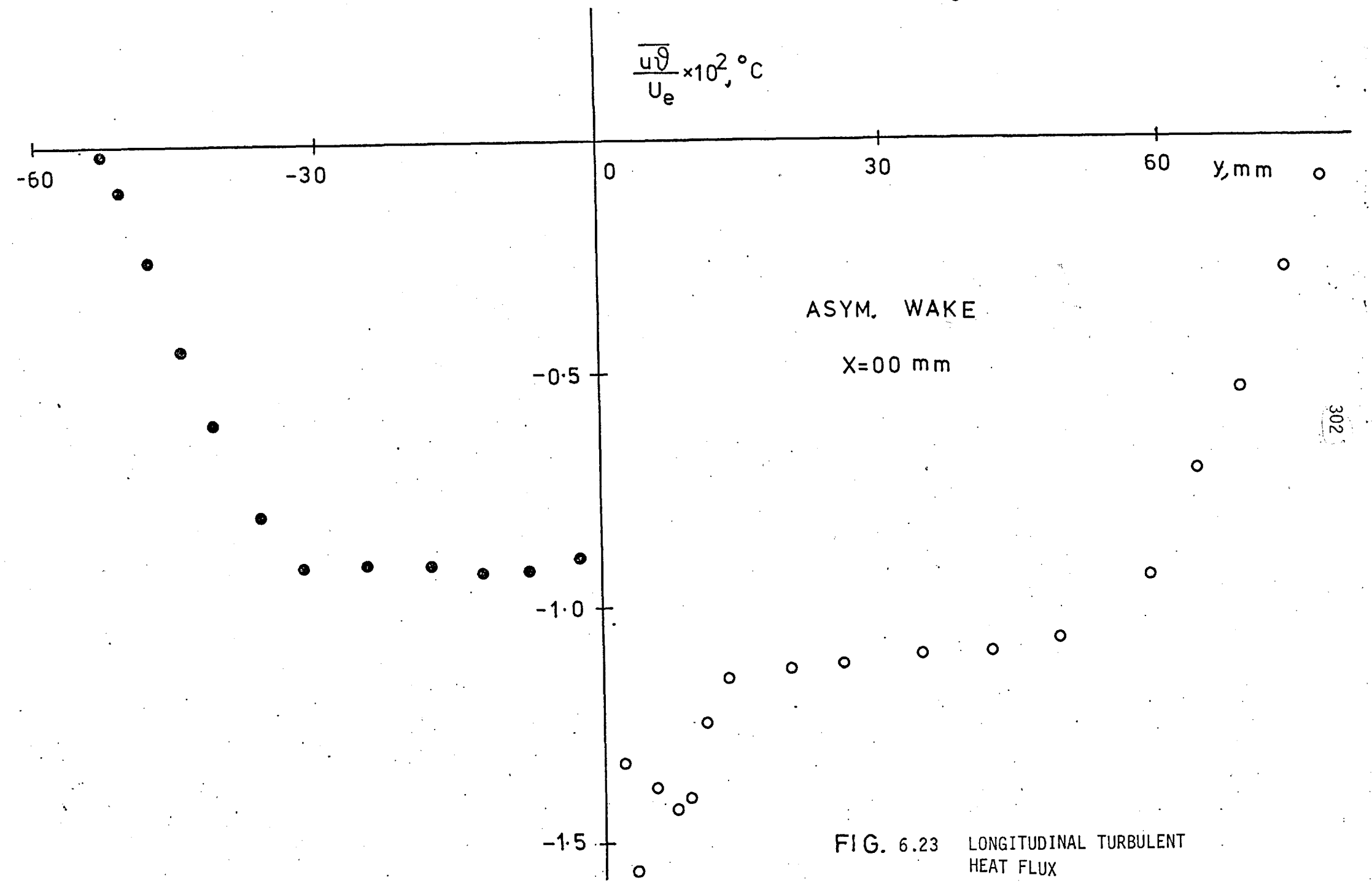

FIG. 6.23 LONGITUDINAL TURBULENT HEAT FLUX

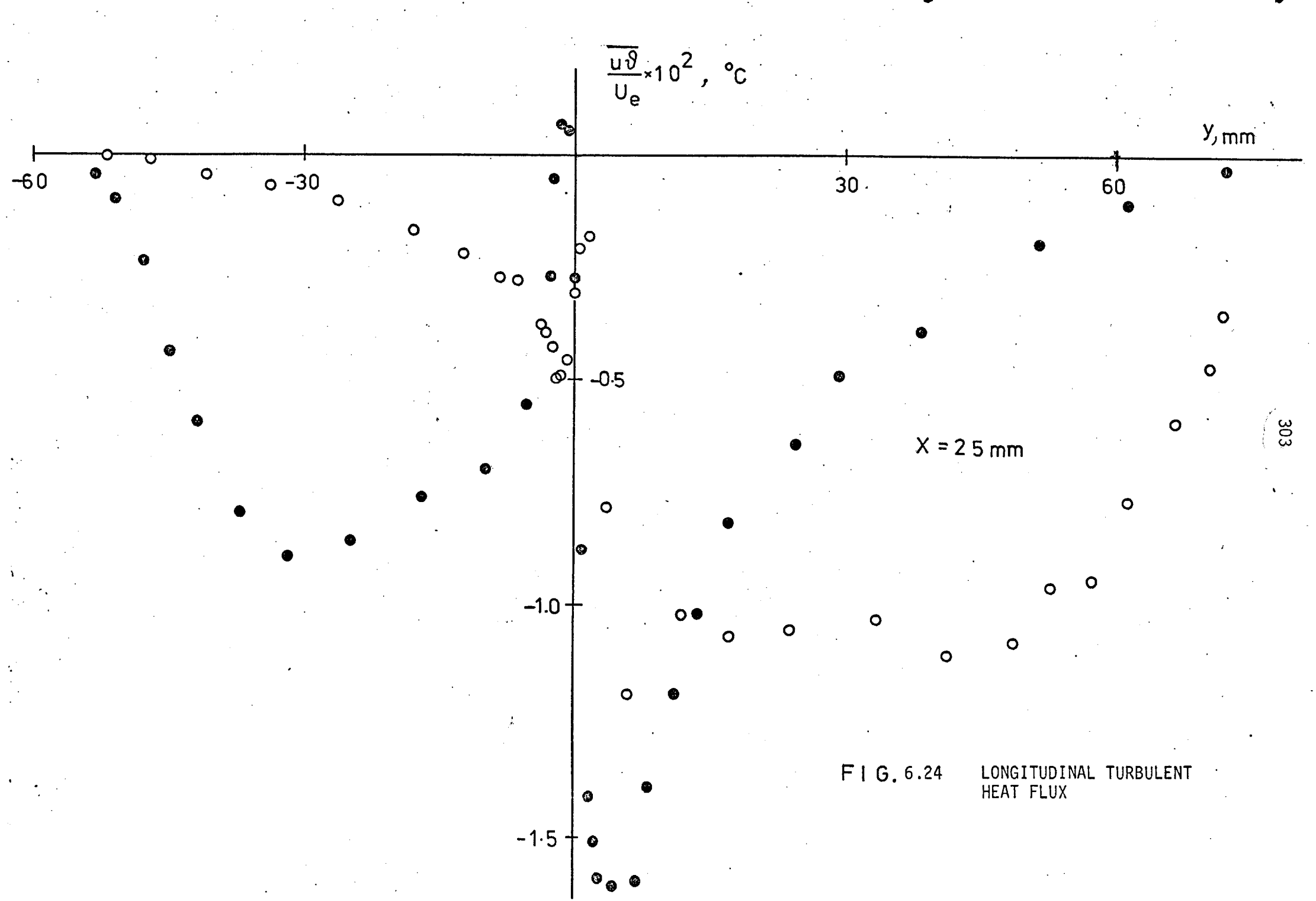

FIG. 6.24 LONGITUDINAL TURBULENT HEAT FLUX

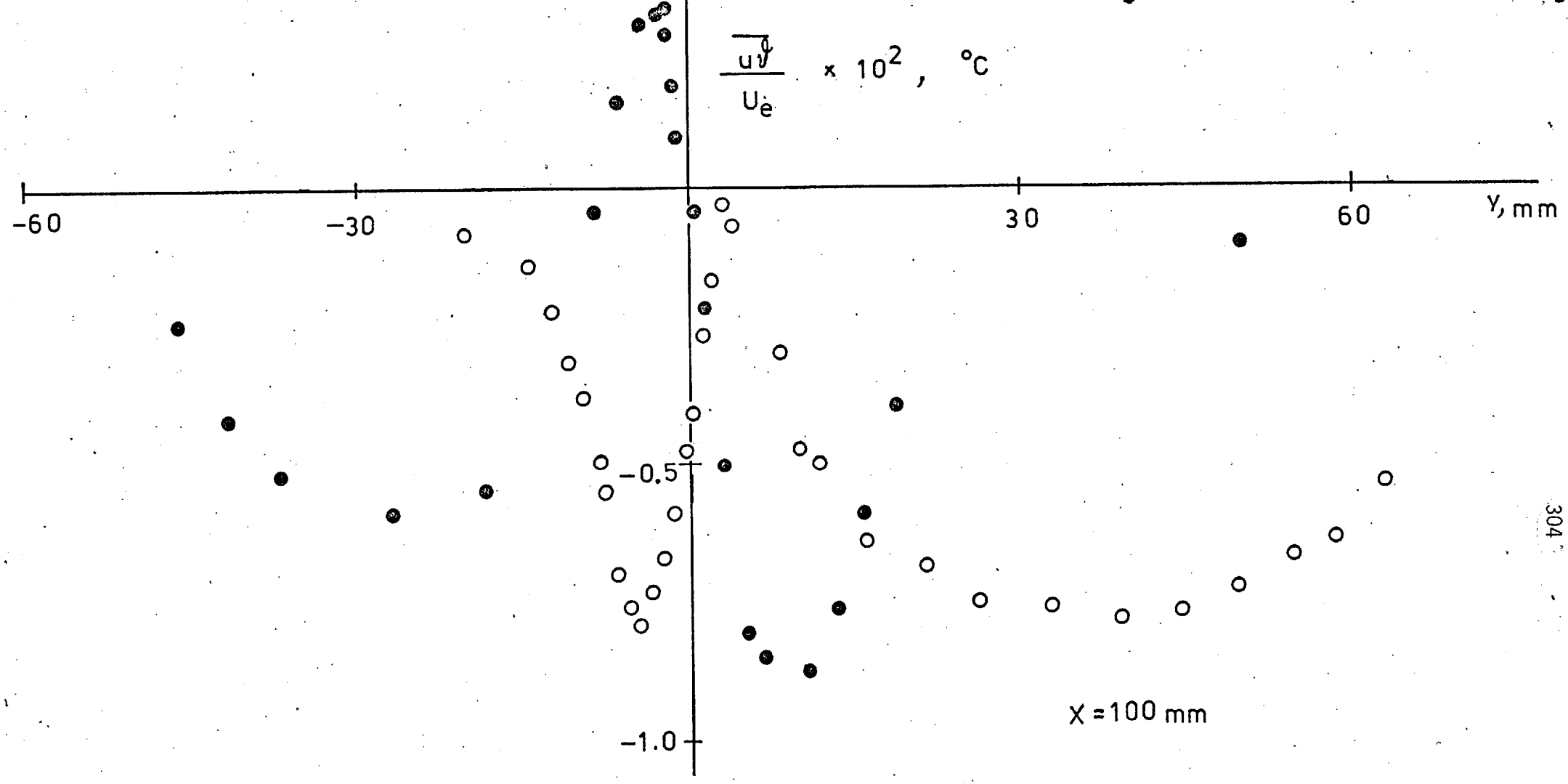

FIG. 6.25 LONGITUDINAL TURBULENT HEAT FLUX

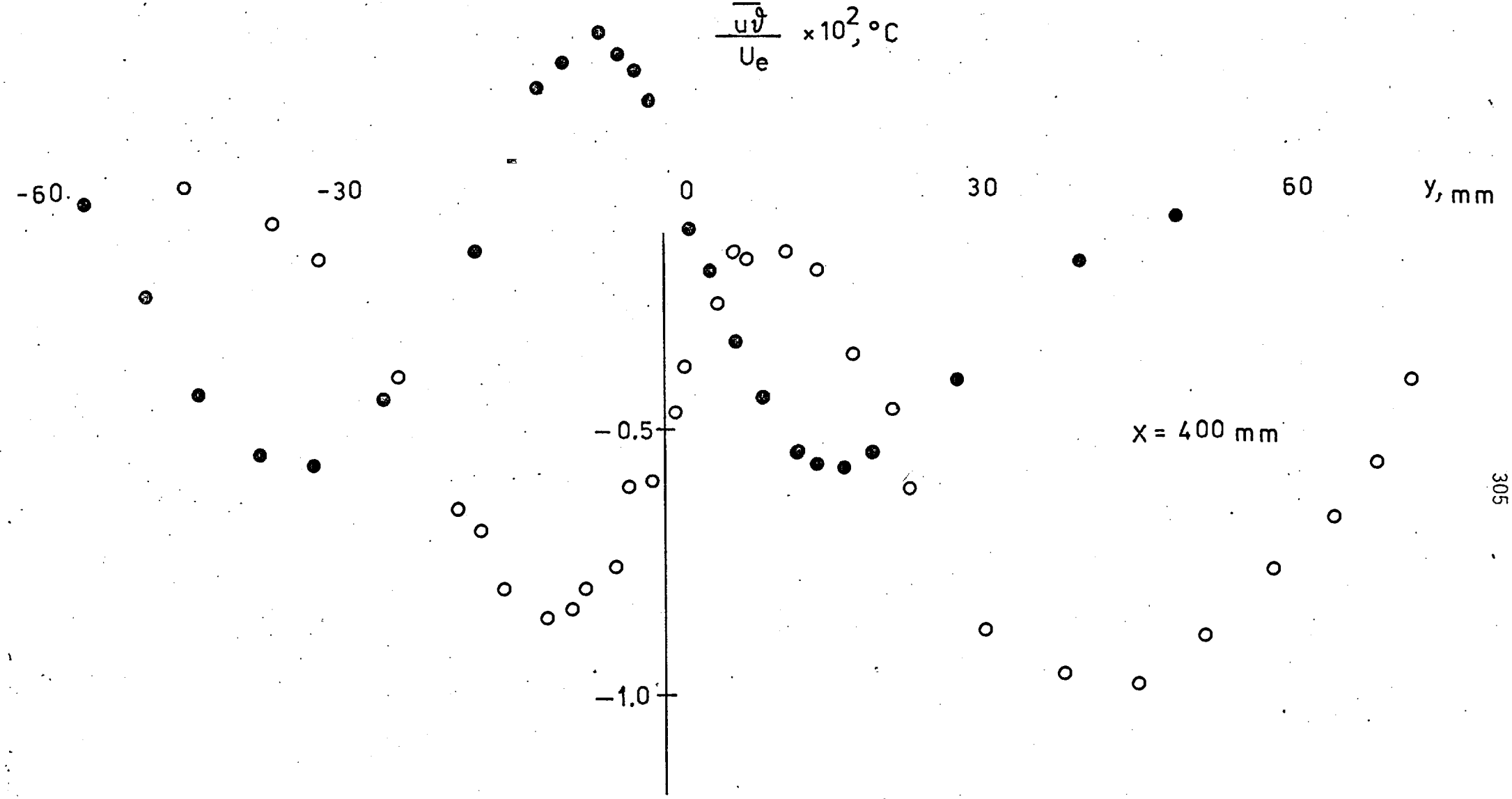

FIG. 6.26 LONGITUDINAL TURBULENT HEAT FLUX

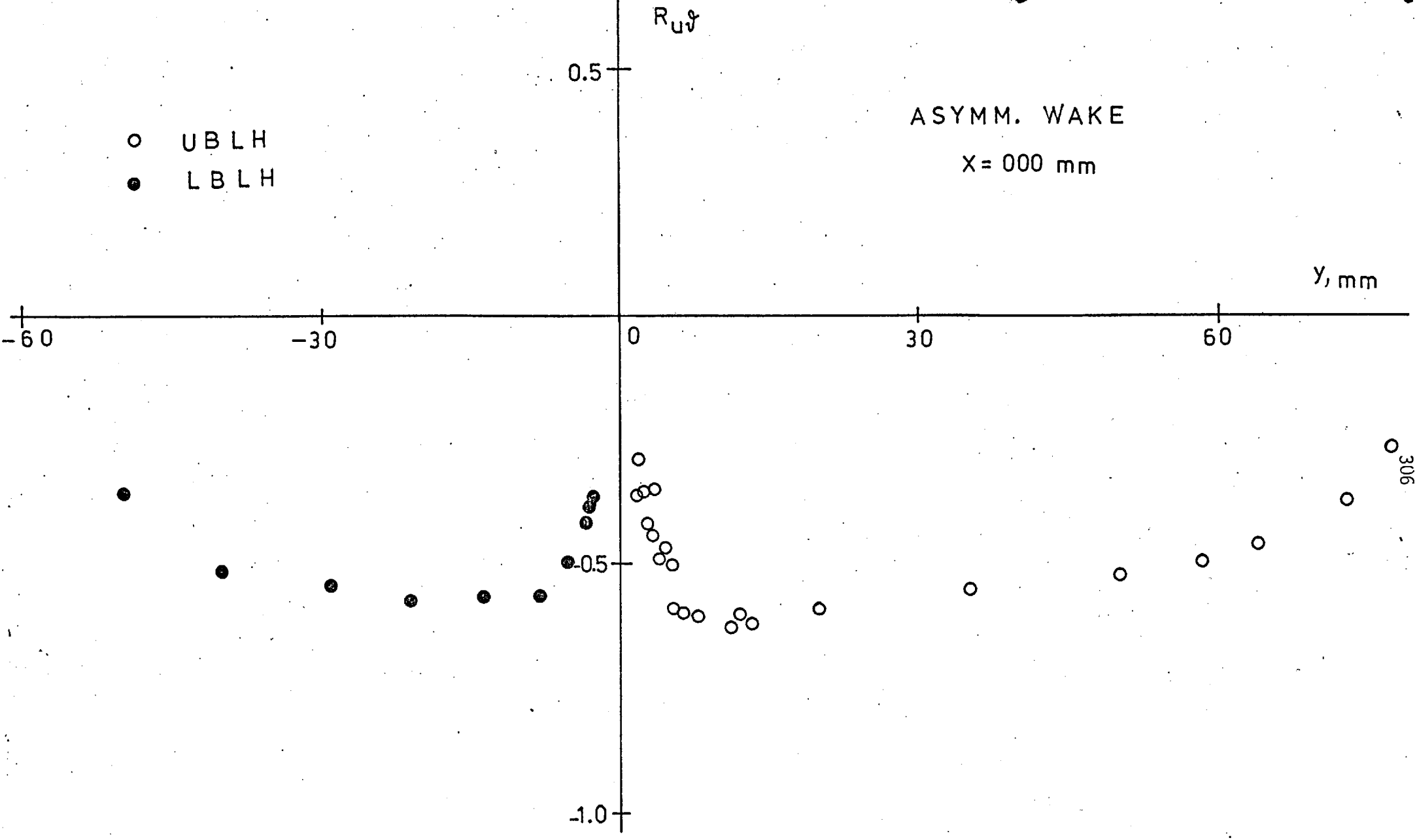

FIG. 6.27 u, θ CORRELATION COEFFICIENT

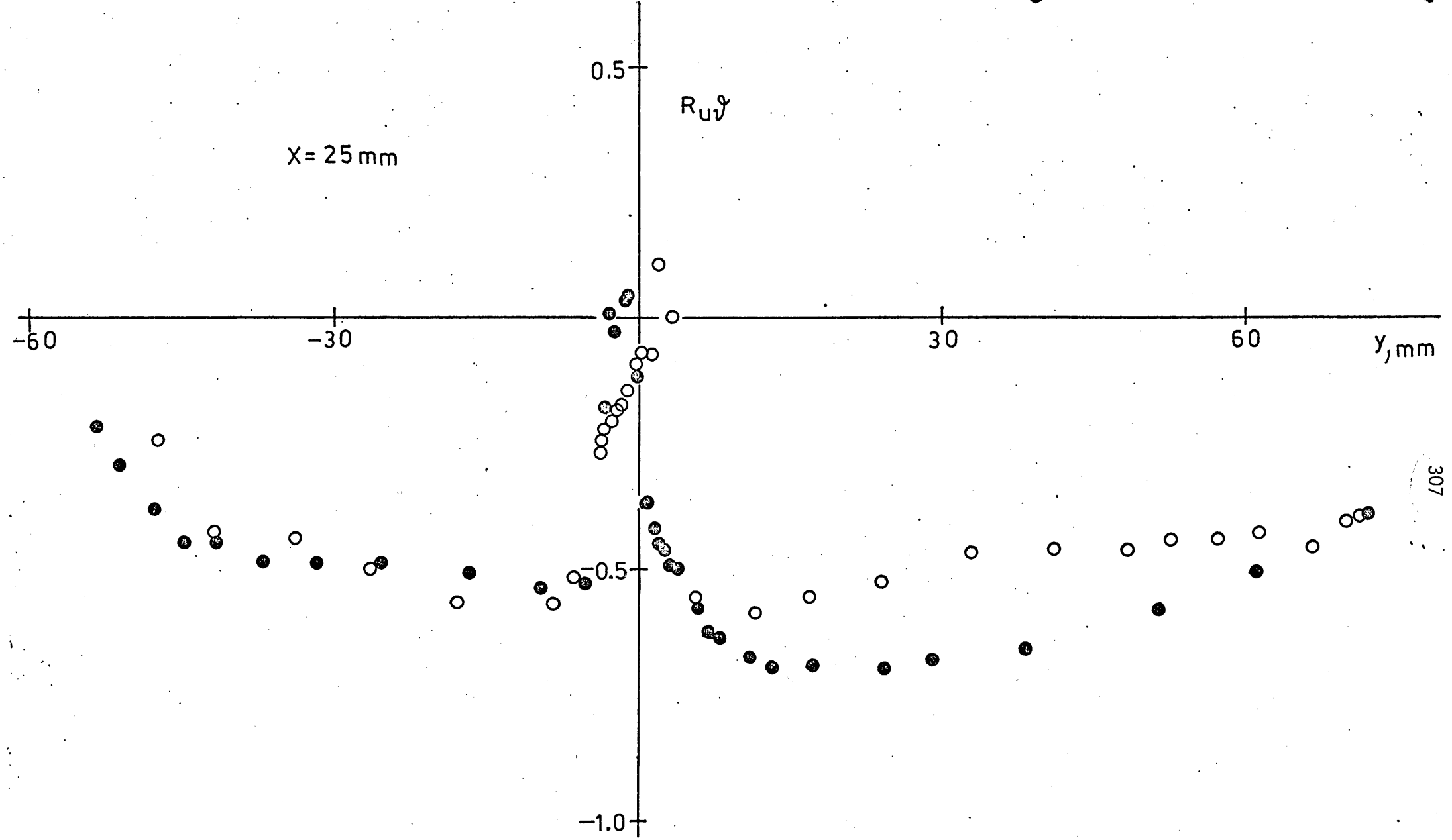

FIG. 6.28 u, θ CORRELATION COEFFICIENT

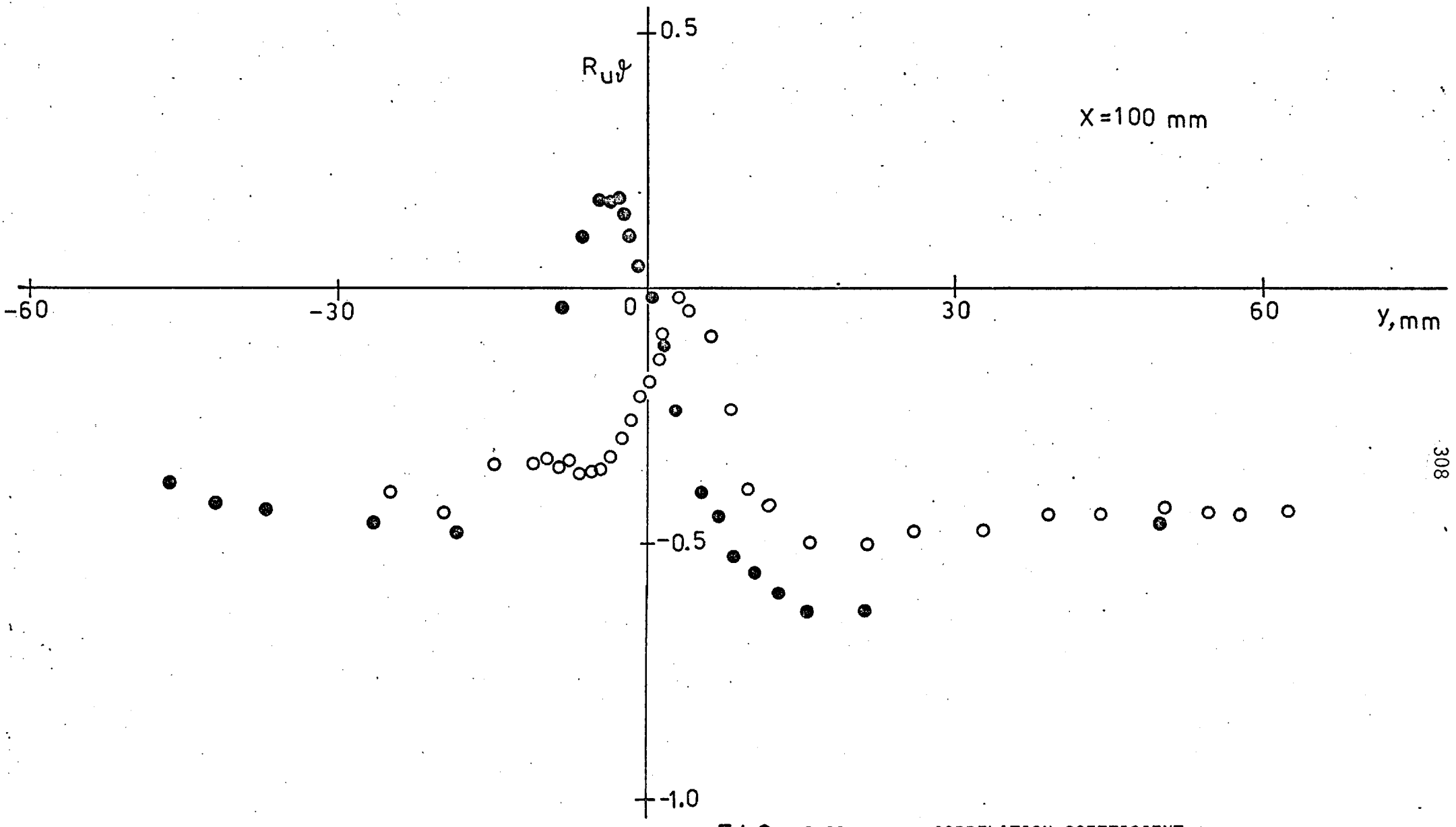

FIG. 6.29 u, θ CORRELATION COEFFICIENT

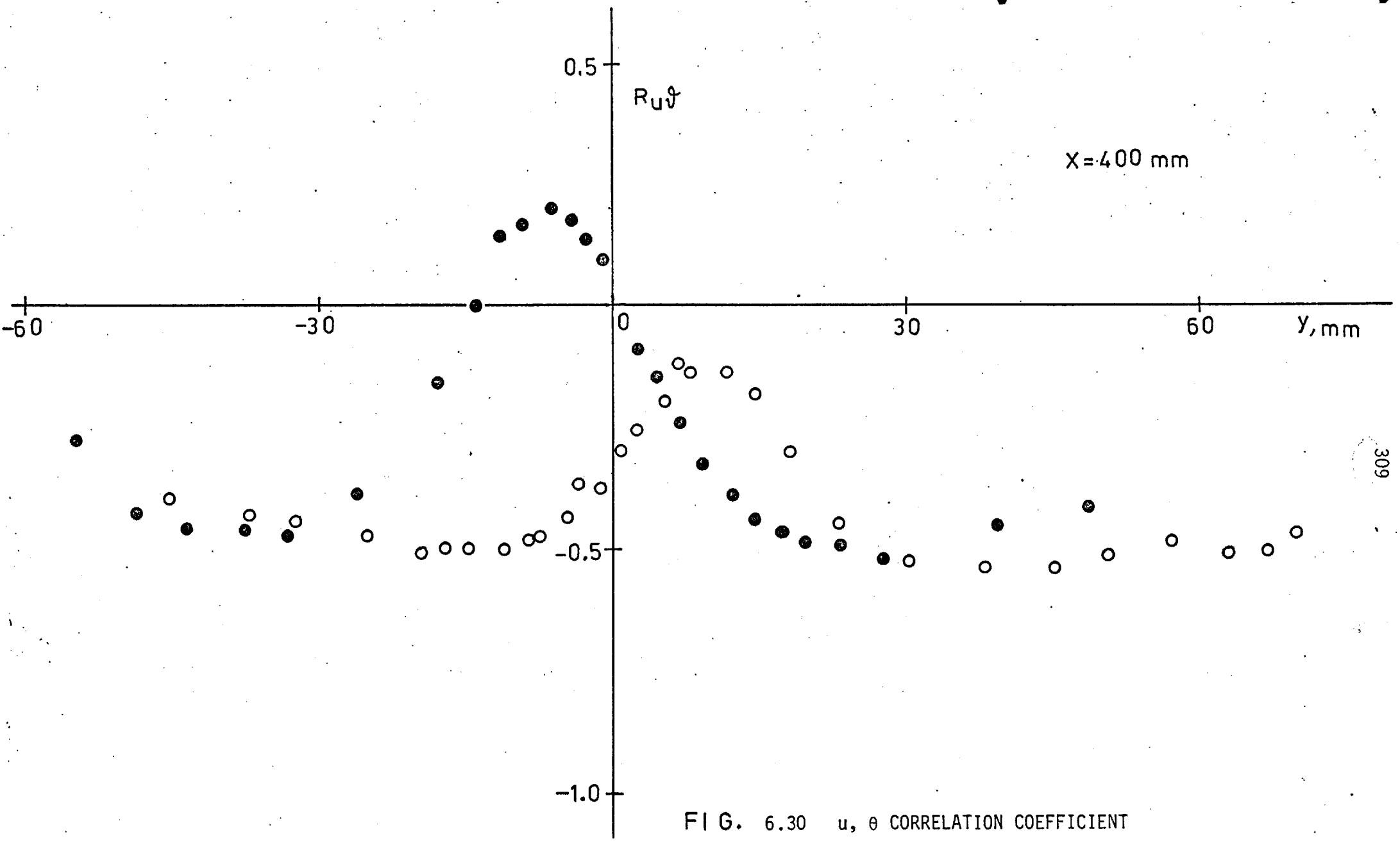

FIG. 6.30 u, θ CORRELATION COEFFICIENT

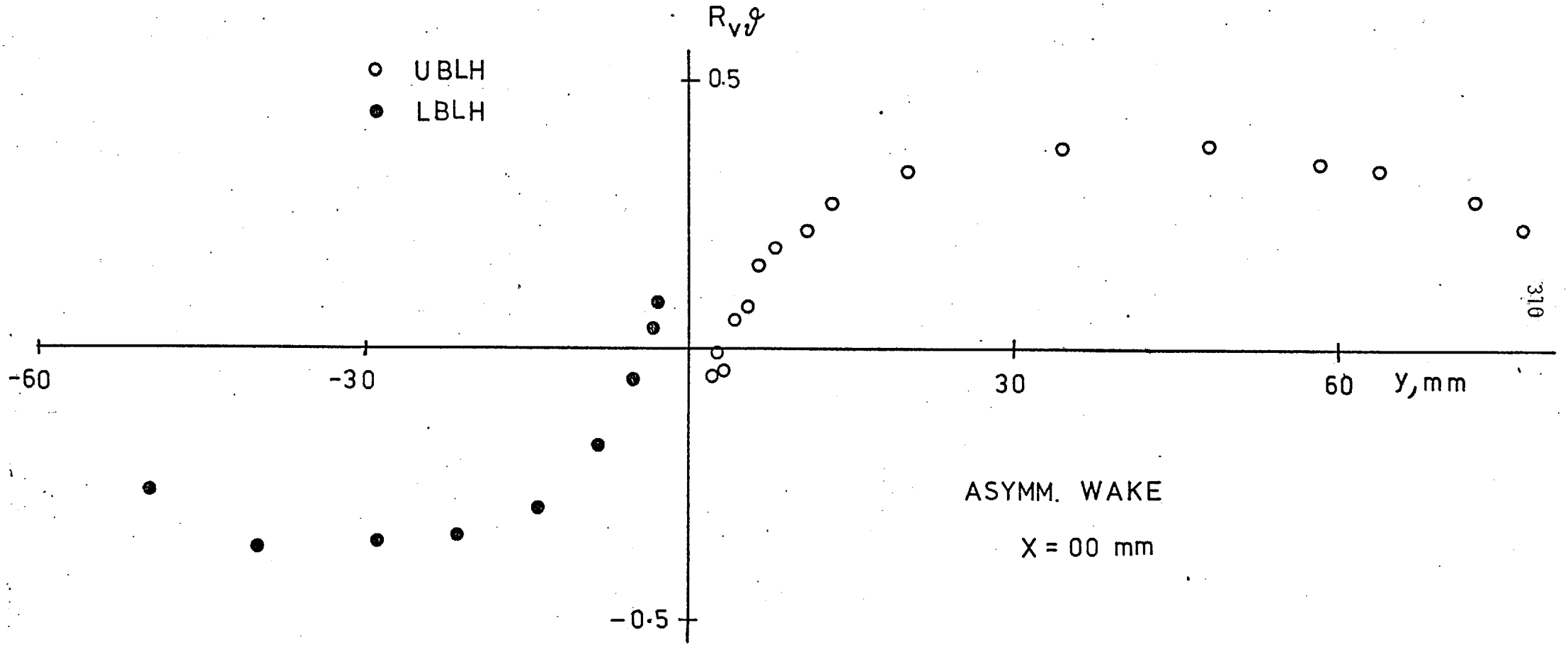

FIG. 6.31 v, θ CORRELATION COEFFICIENT

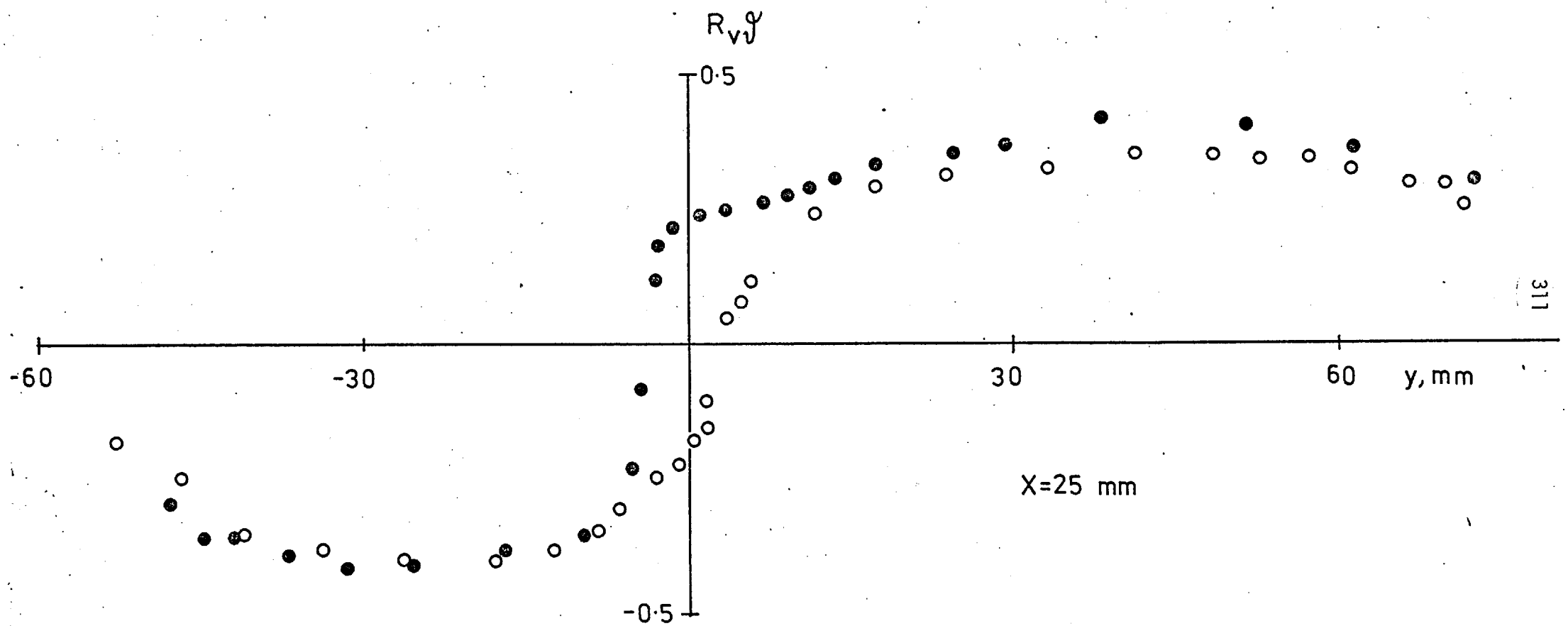

FIG. 6.32 v, θ CORRELATION COEFFICIENT

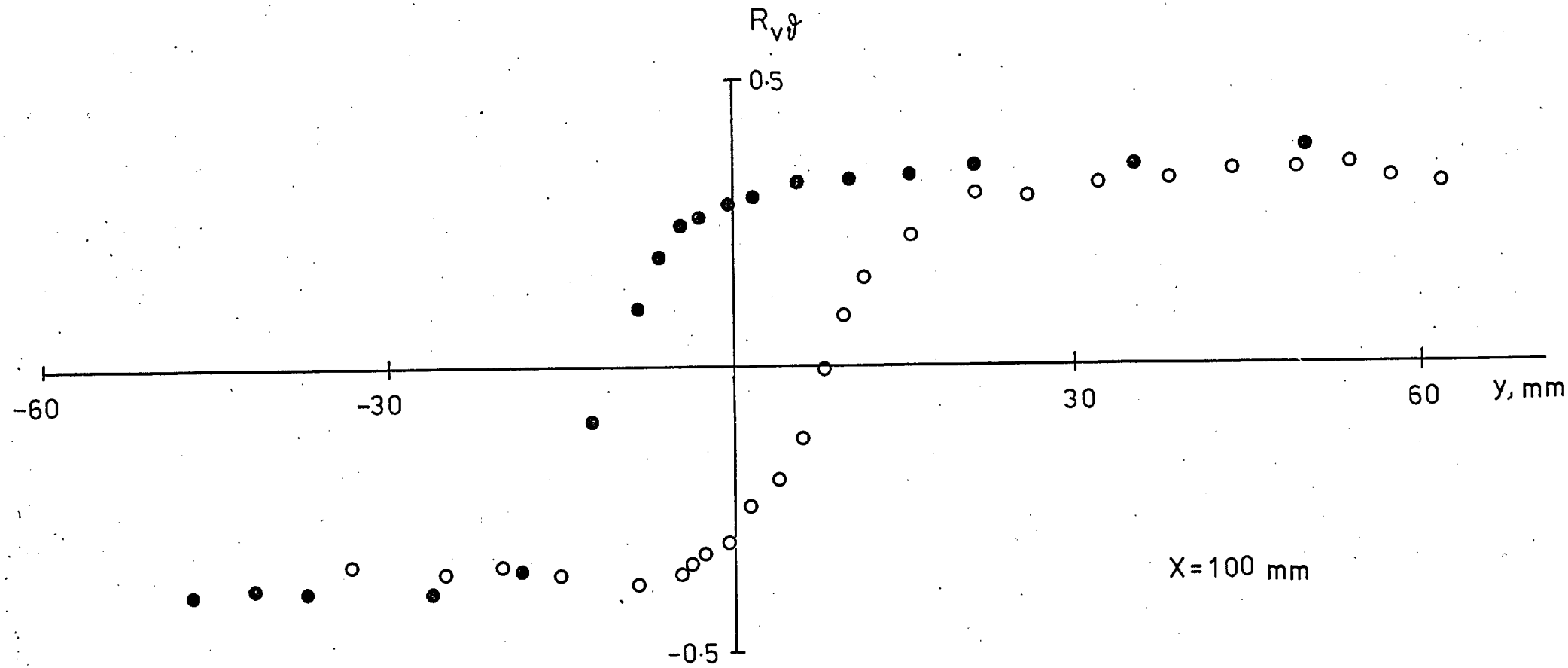

FIG. 6.33 v, θ CORRELATION COEFFICIENT

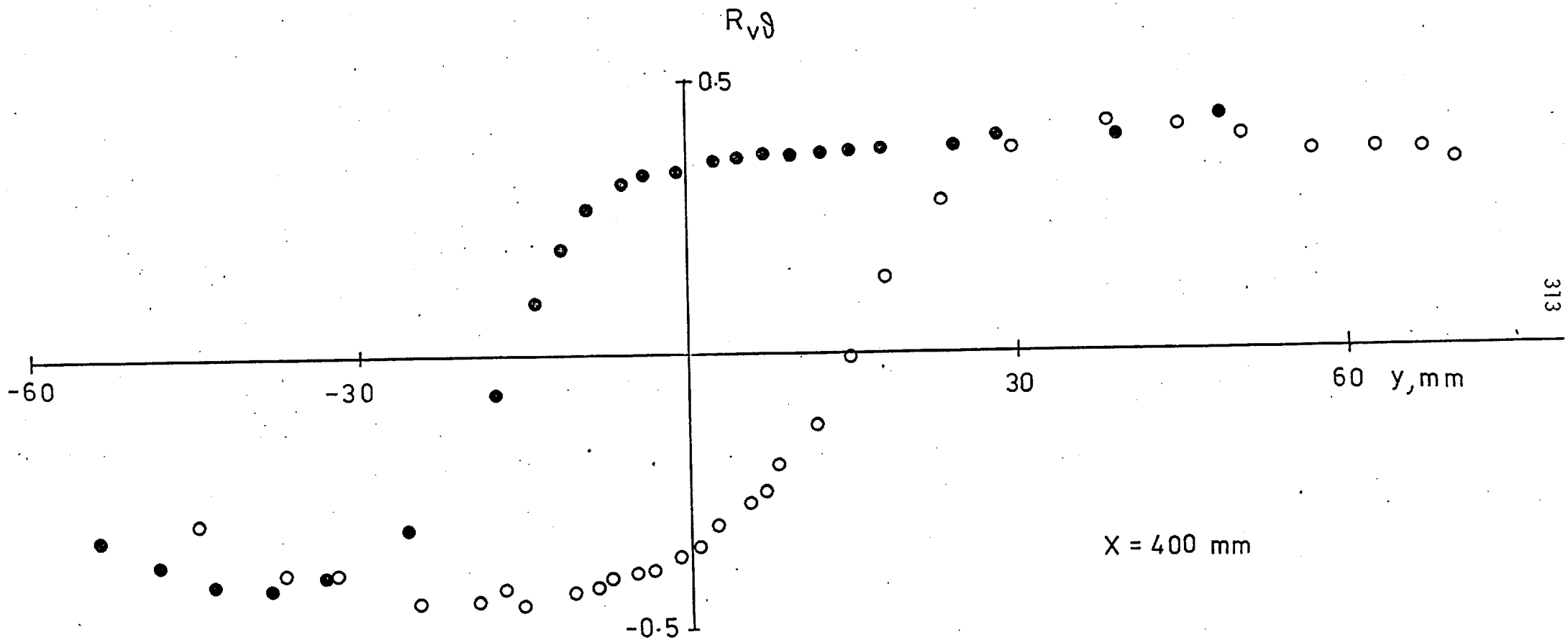

FIG. 6.34 v, θ CORRELATION COEFFICIENT

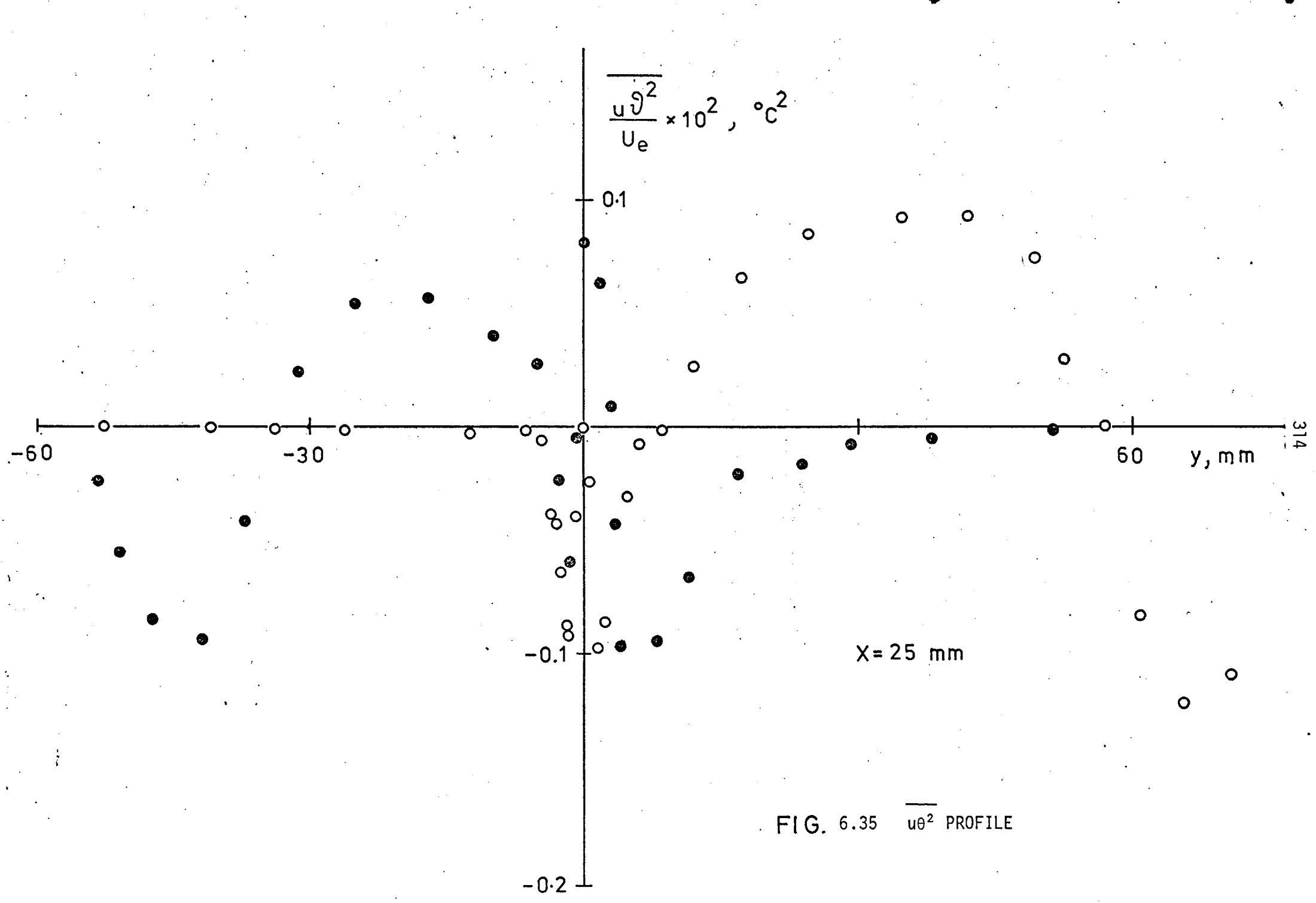

FIG. 6.35 $\overline{u\theta^2}$ PROFILE

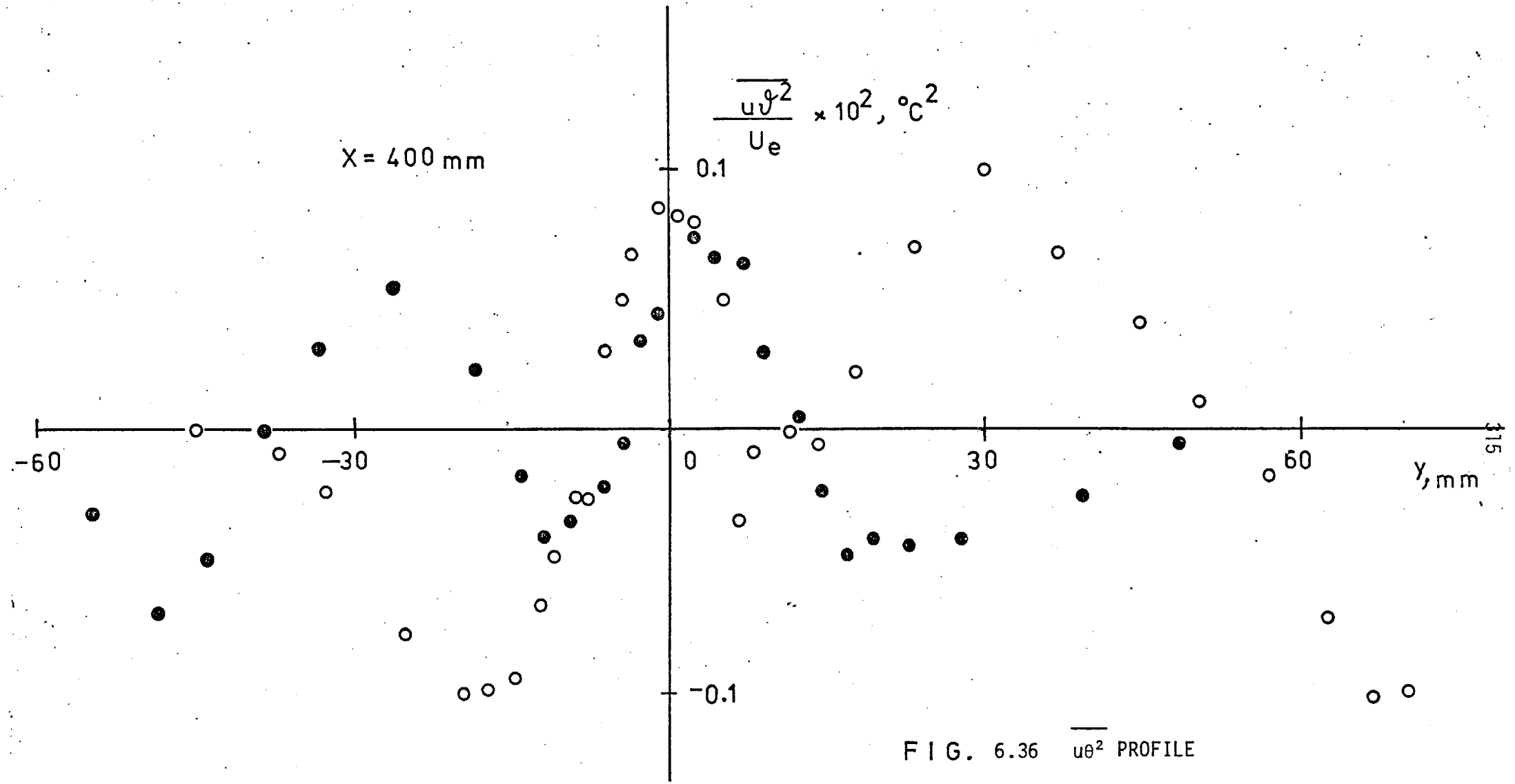

FIG. 6.36 $\overline{u\theta^2}$ PROFILE

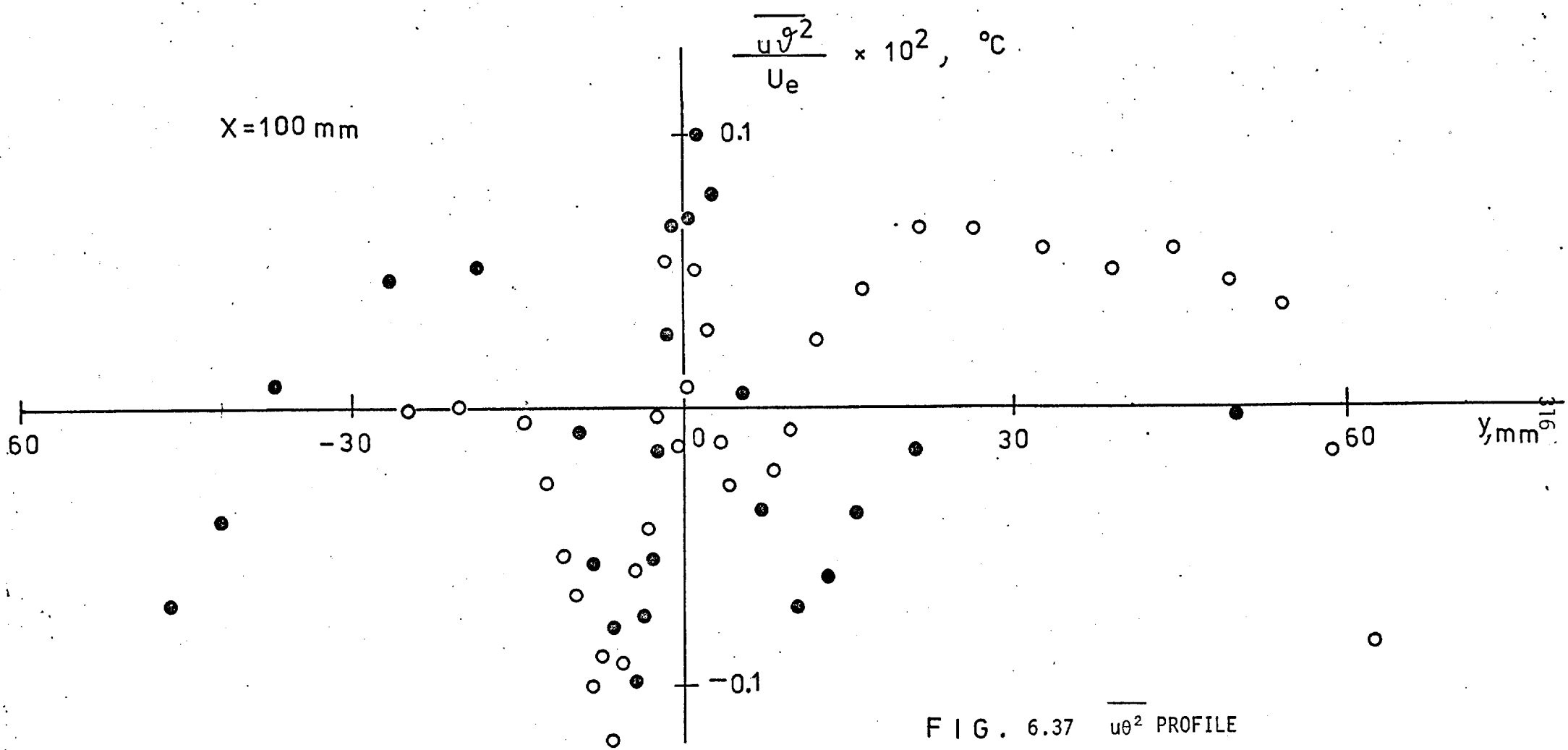

FIG. 6.37 $\overline{u\theta^2}$ PROFILE

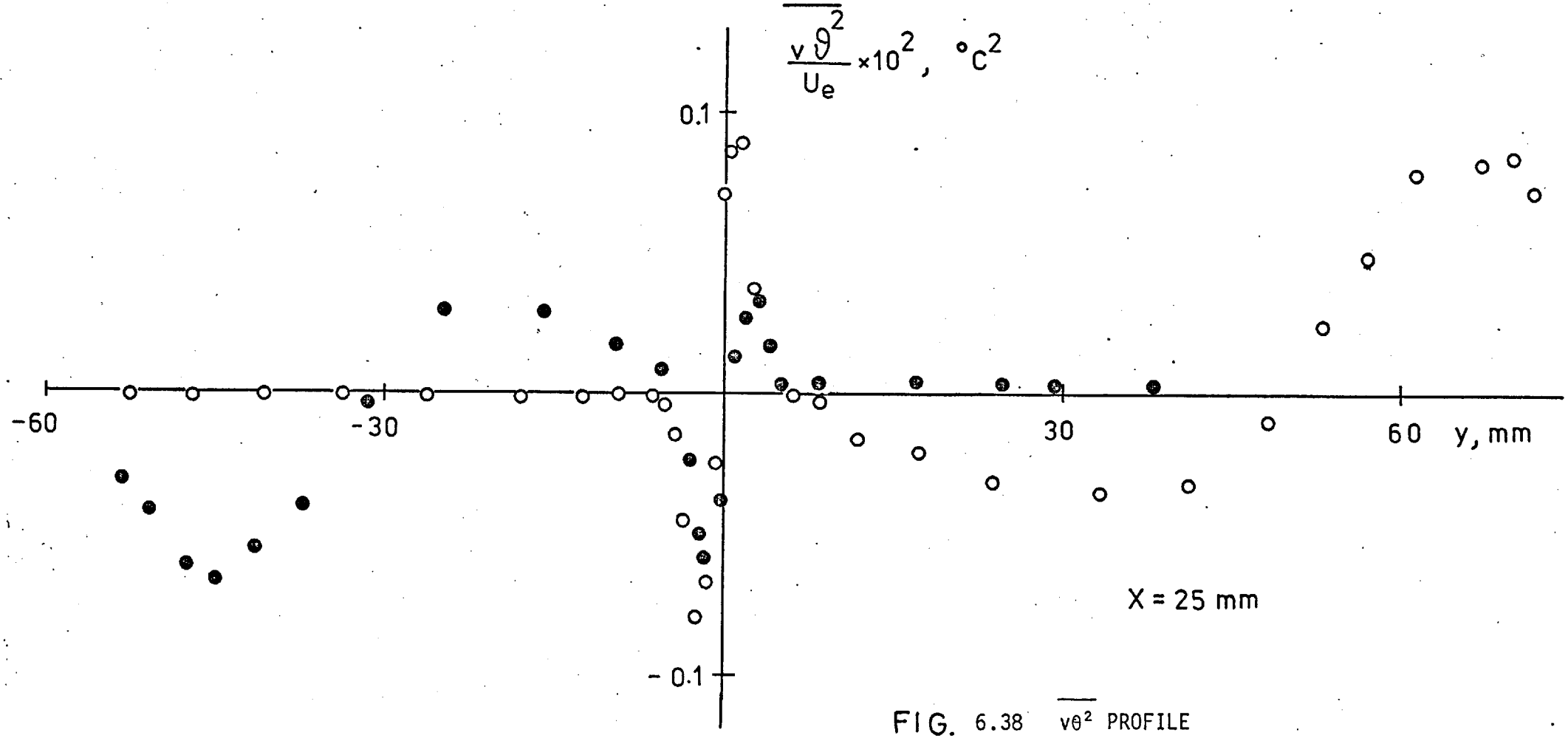

FIG. 6.38 $\overline{v\theta^2}$ PROFILE

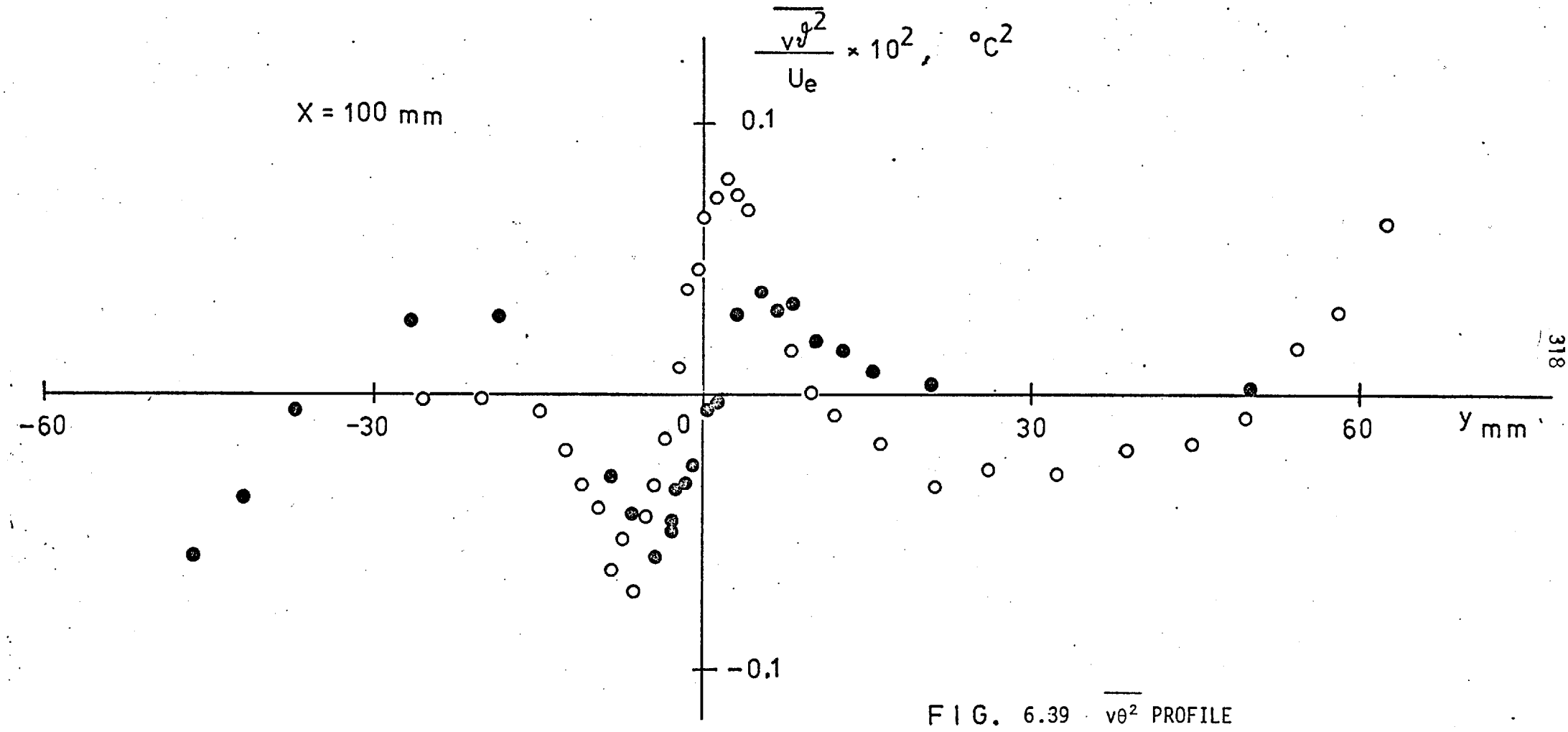

FIG. 6.39 $\overline{v\theta^2}$ PROFILE

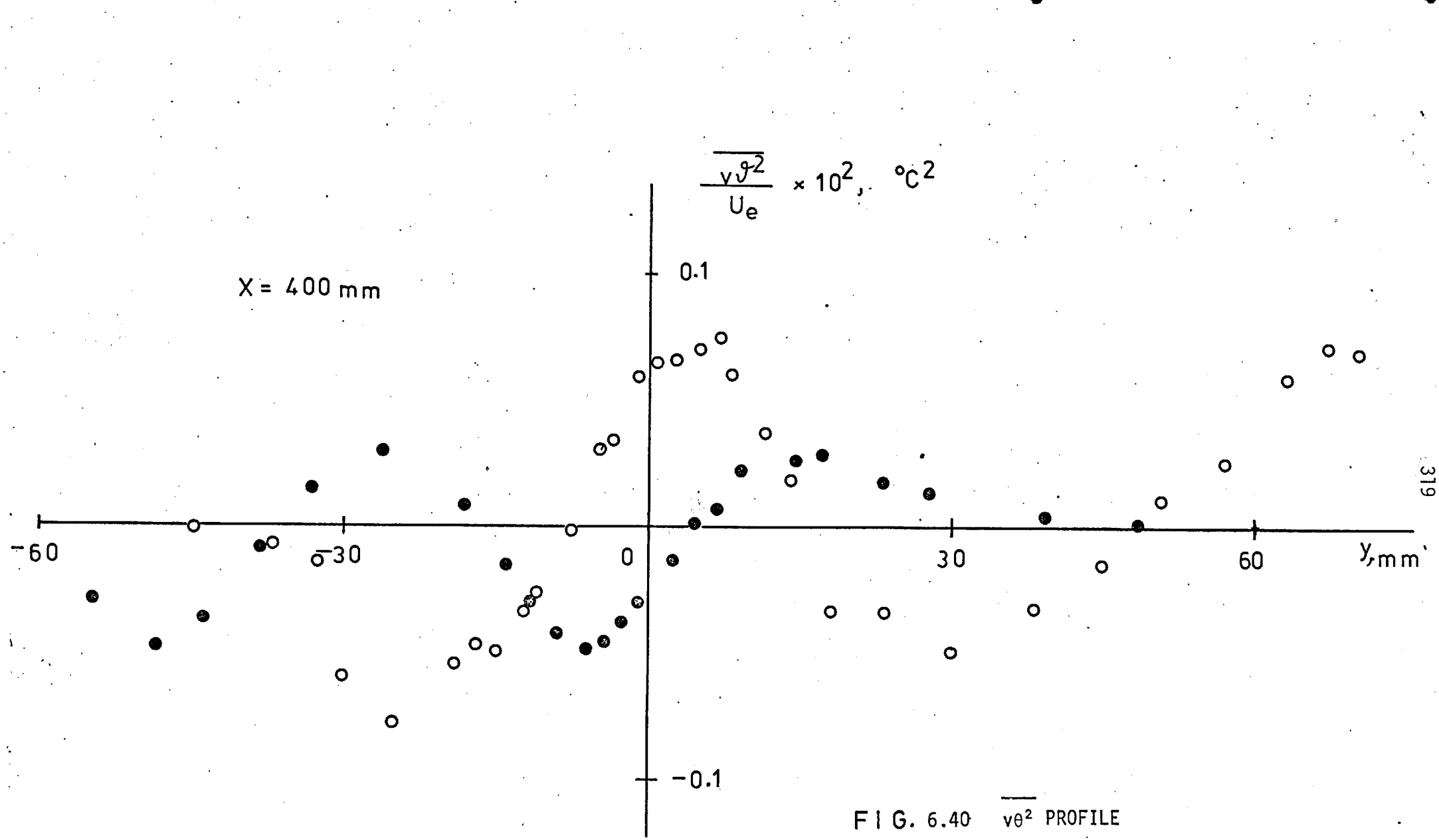

FIG. 6.40 $\overline{v\theta^2}$ PROFILE

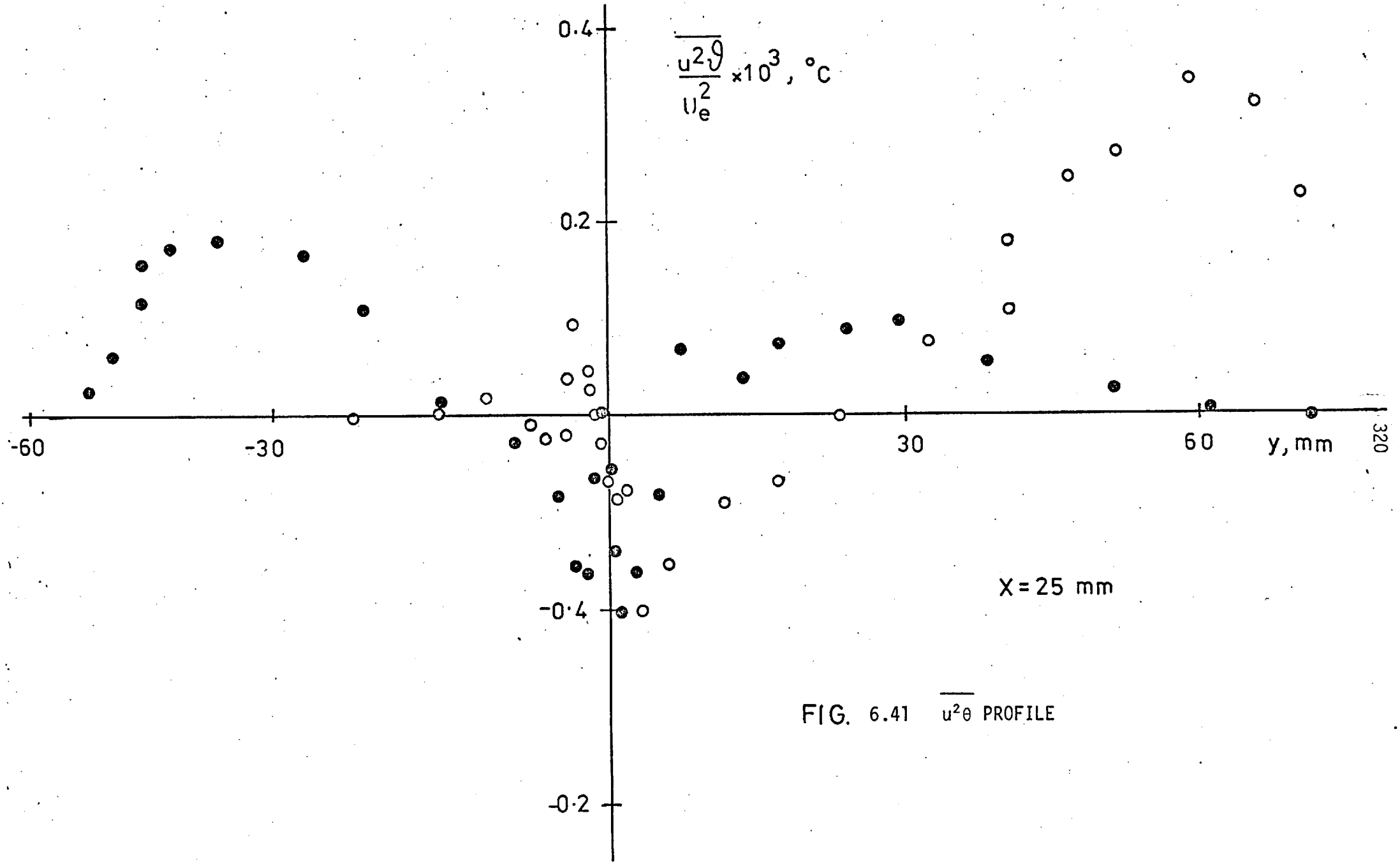

FIG. 6.41 $\overline{u^2\theta}$ PROFILE

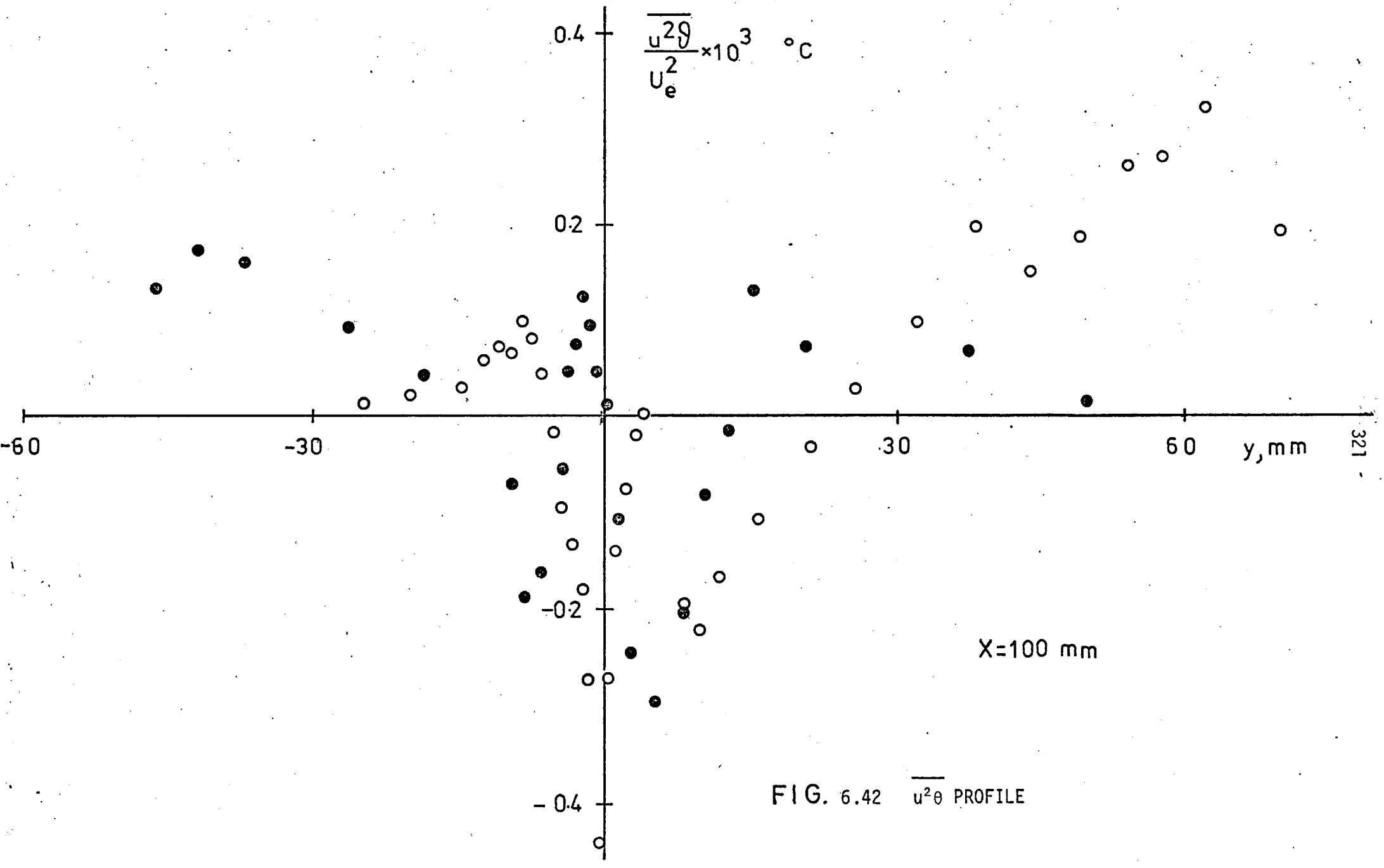

FIG. 6.42 $\overline{u^2\theta}$ PROFILE

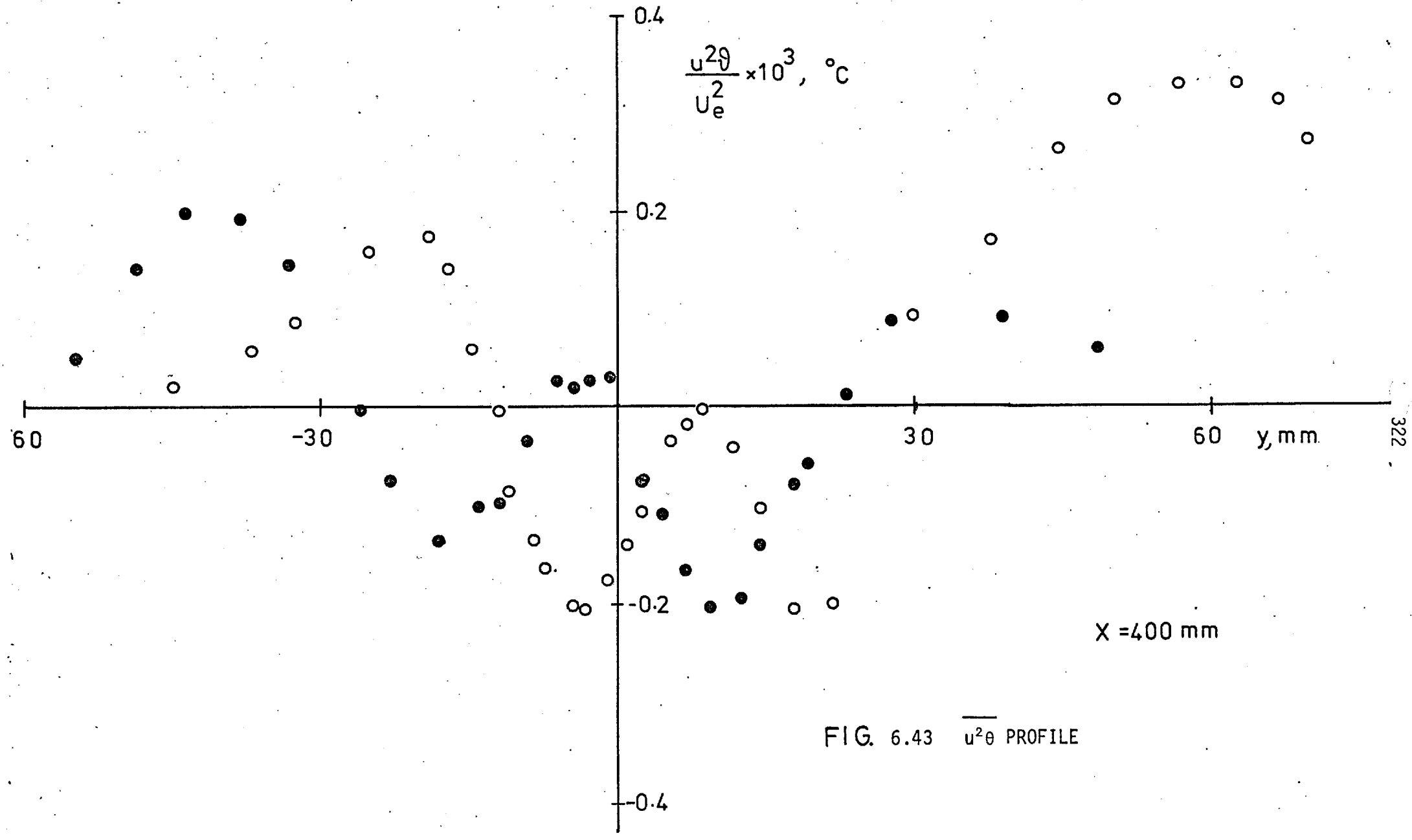

FIG. 6.43 $\overline{u^2\theta}$ PROFILE

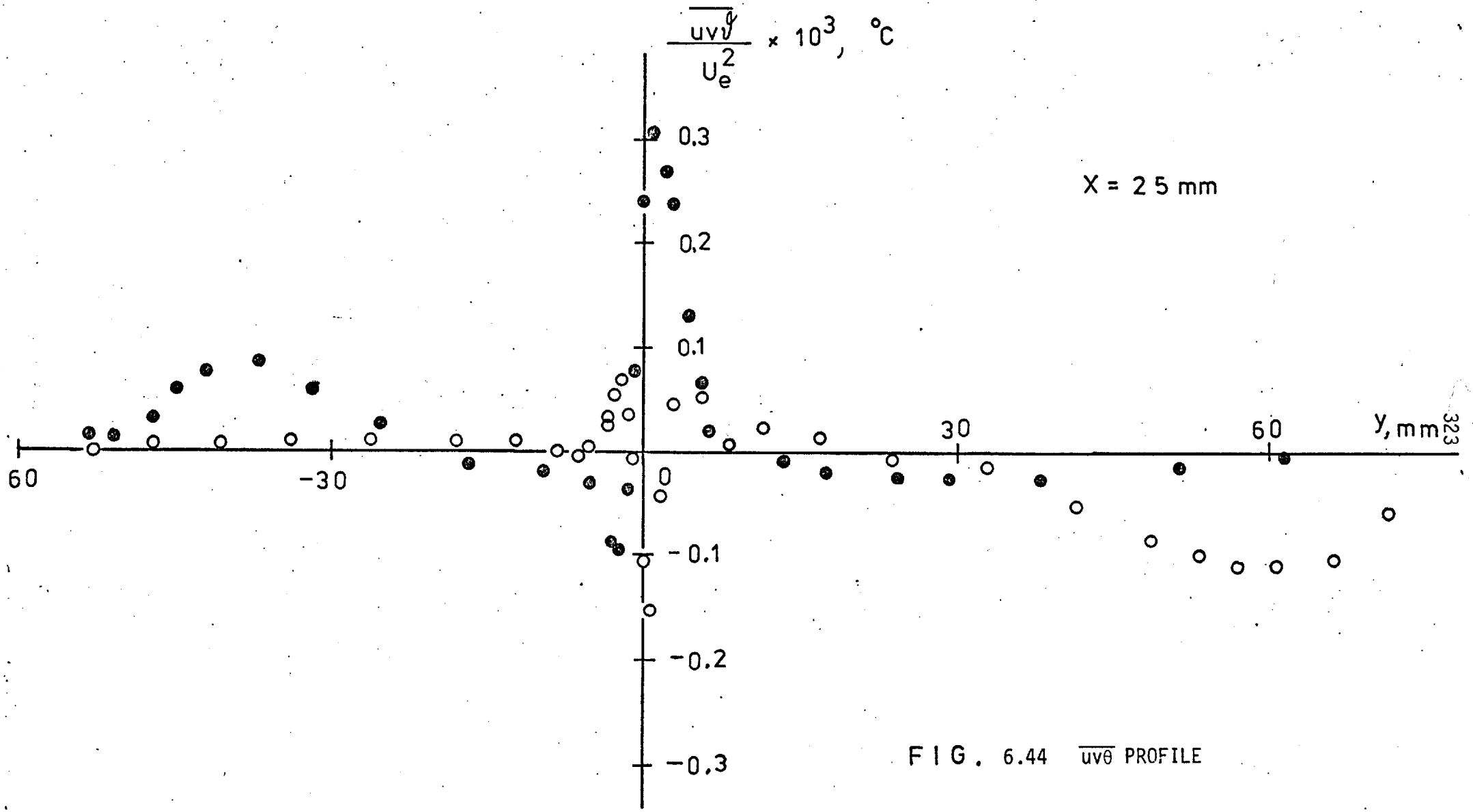

FIG. 6.44 $\overline{uv\theta}$ PROFILE

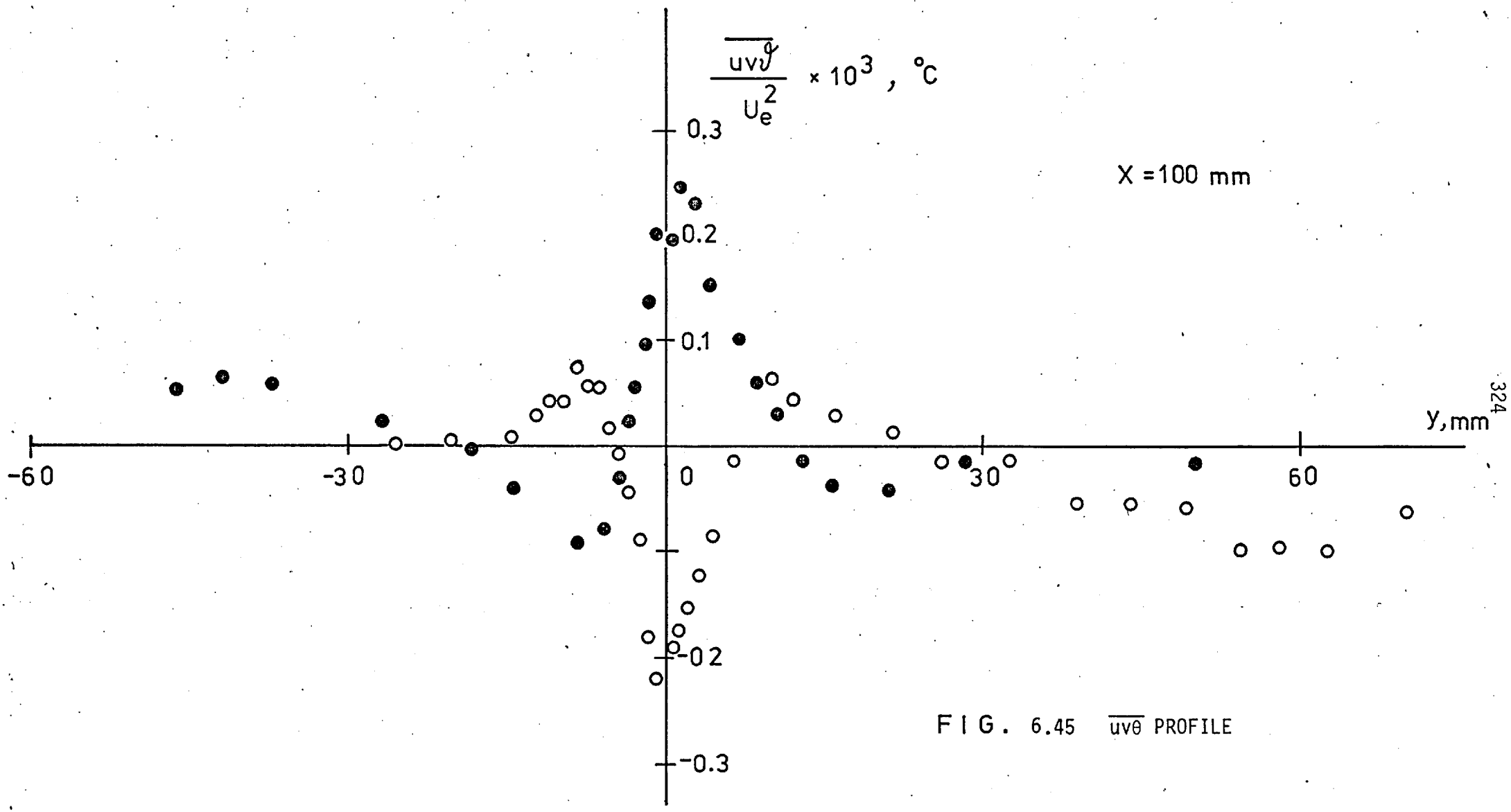

FIG. 6.45 $\overline{uv\theta}$ PROFILE

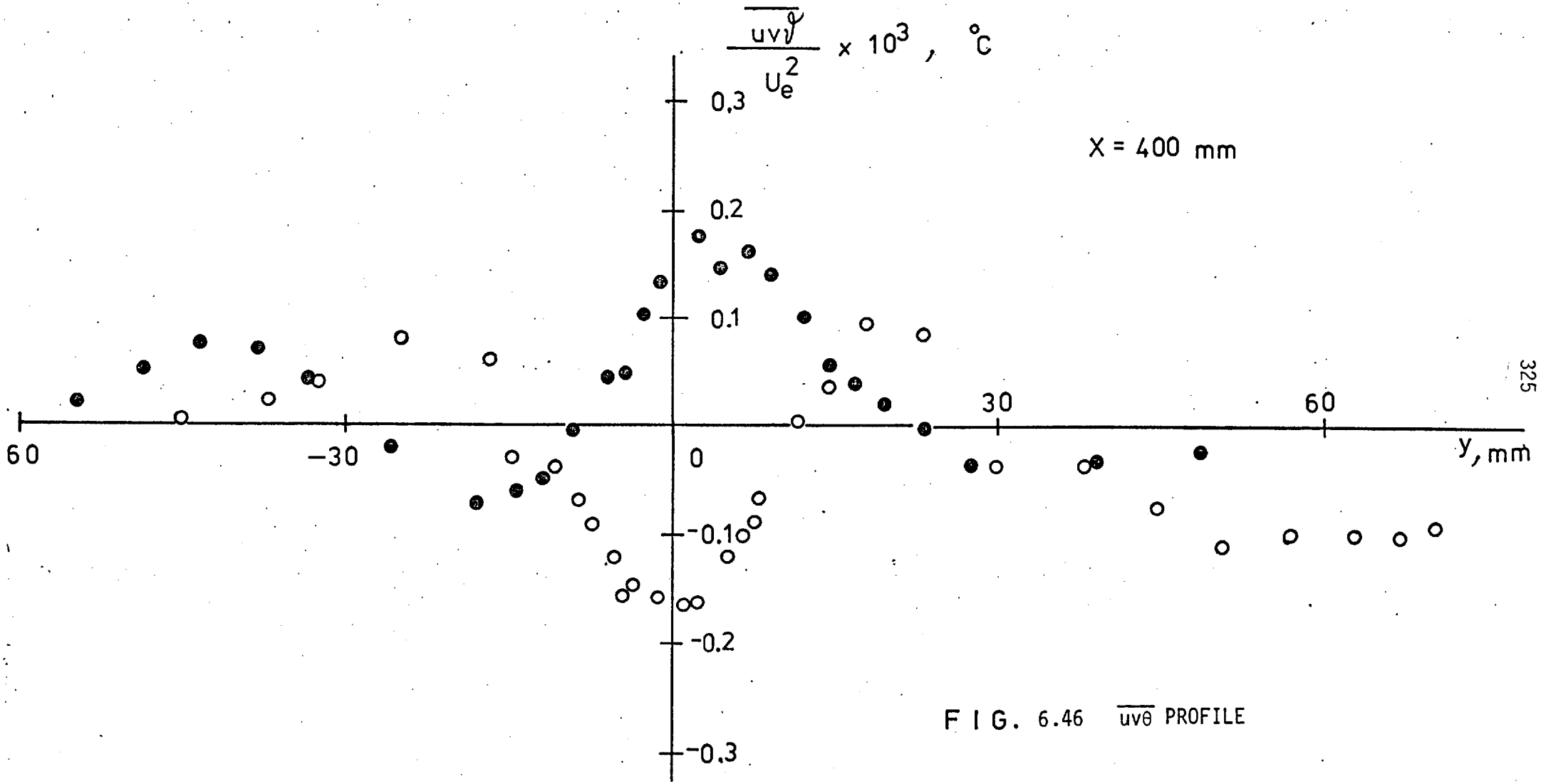

FIG. 6.46 $\overline{uv\theta}$ PROFILE

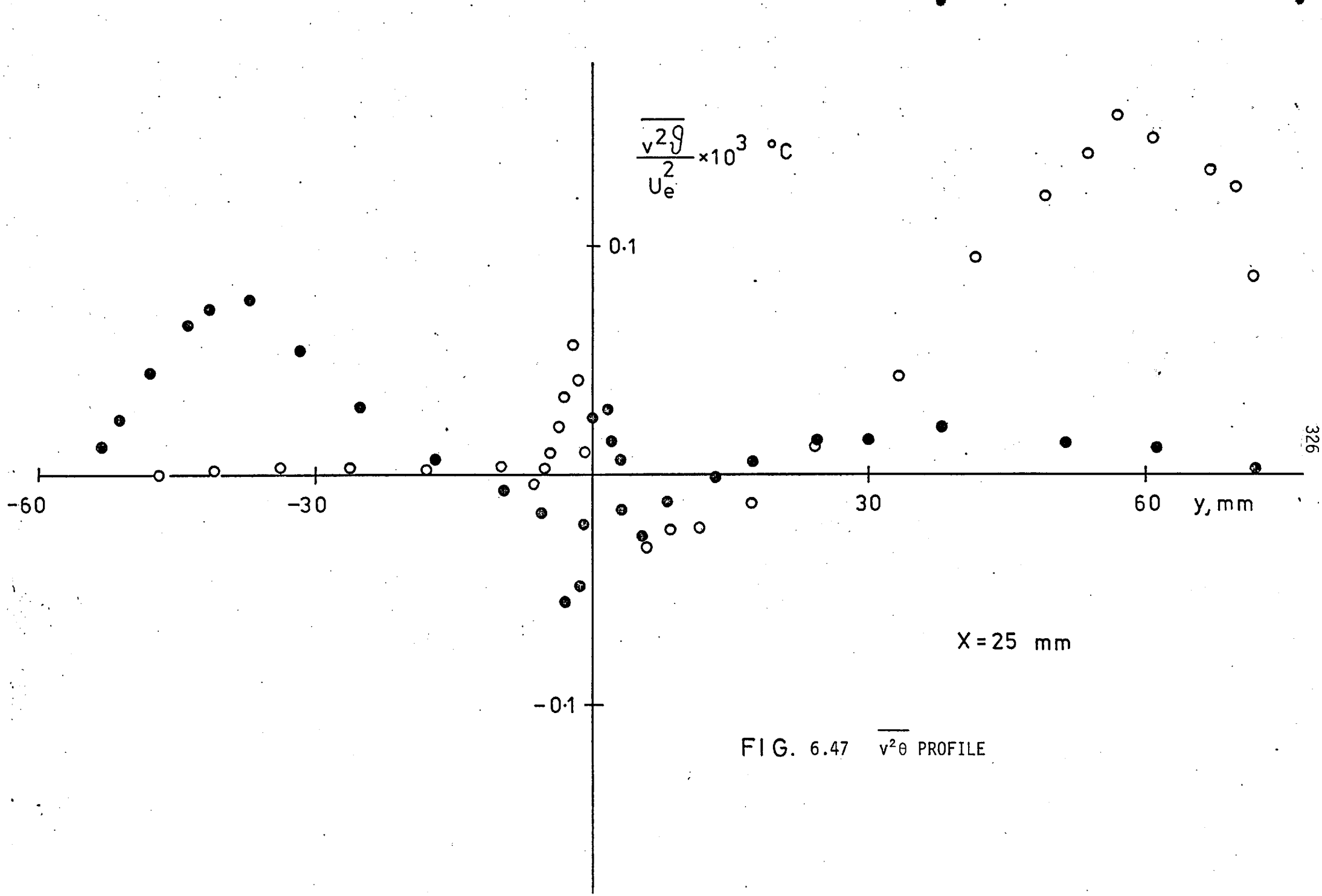

FIG. 6.47 $\overline{v^2\theta}$ PROFILE

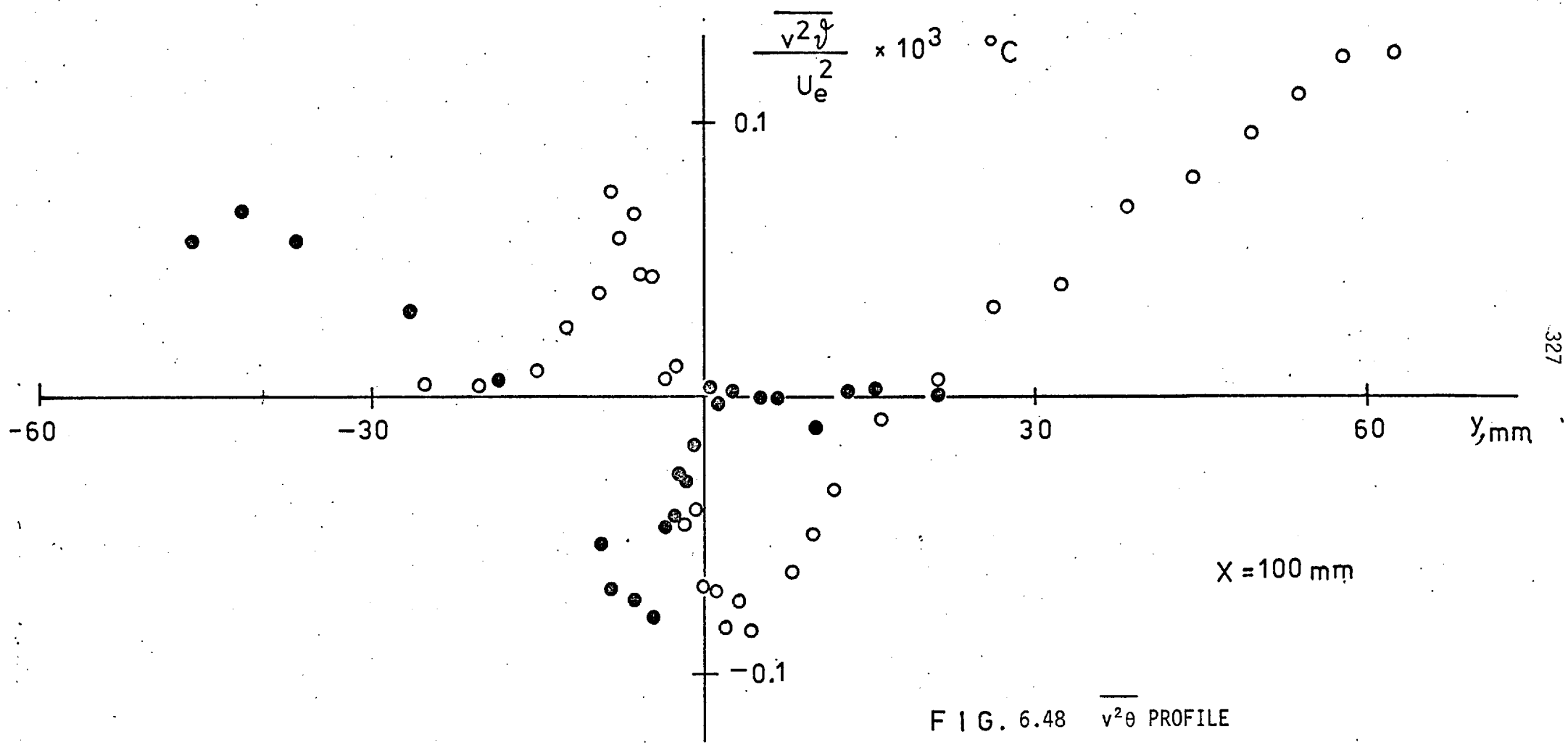

FIG. 6.48 $\overline{v^2\theta}$ PROFILE

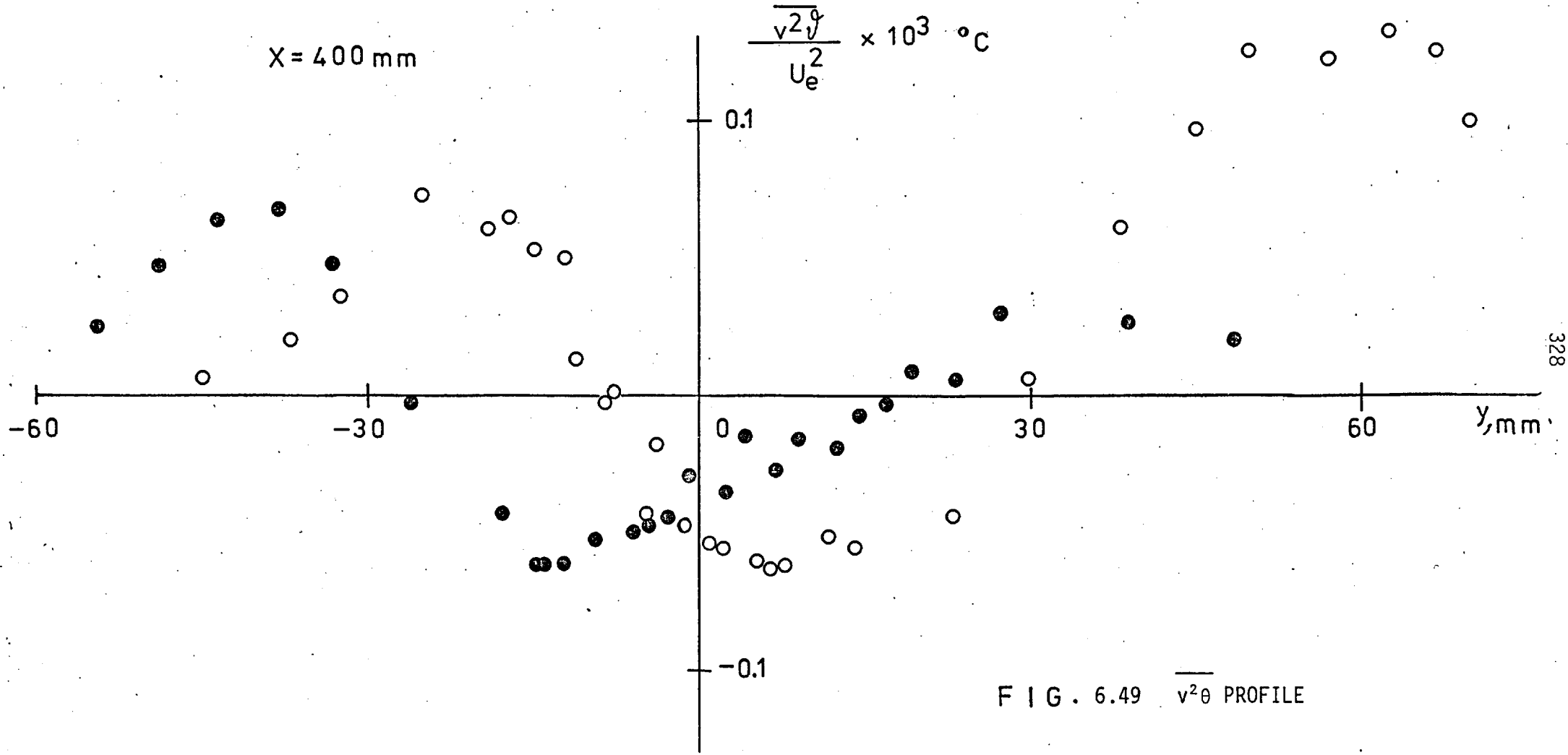

FIG. 6.49 $\overline{v^2\theta}$ PROFILE

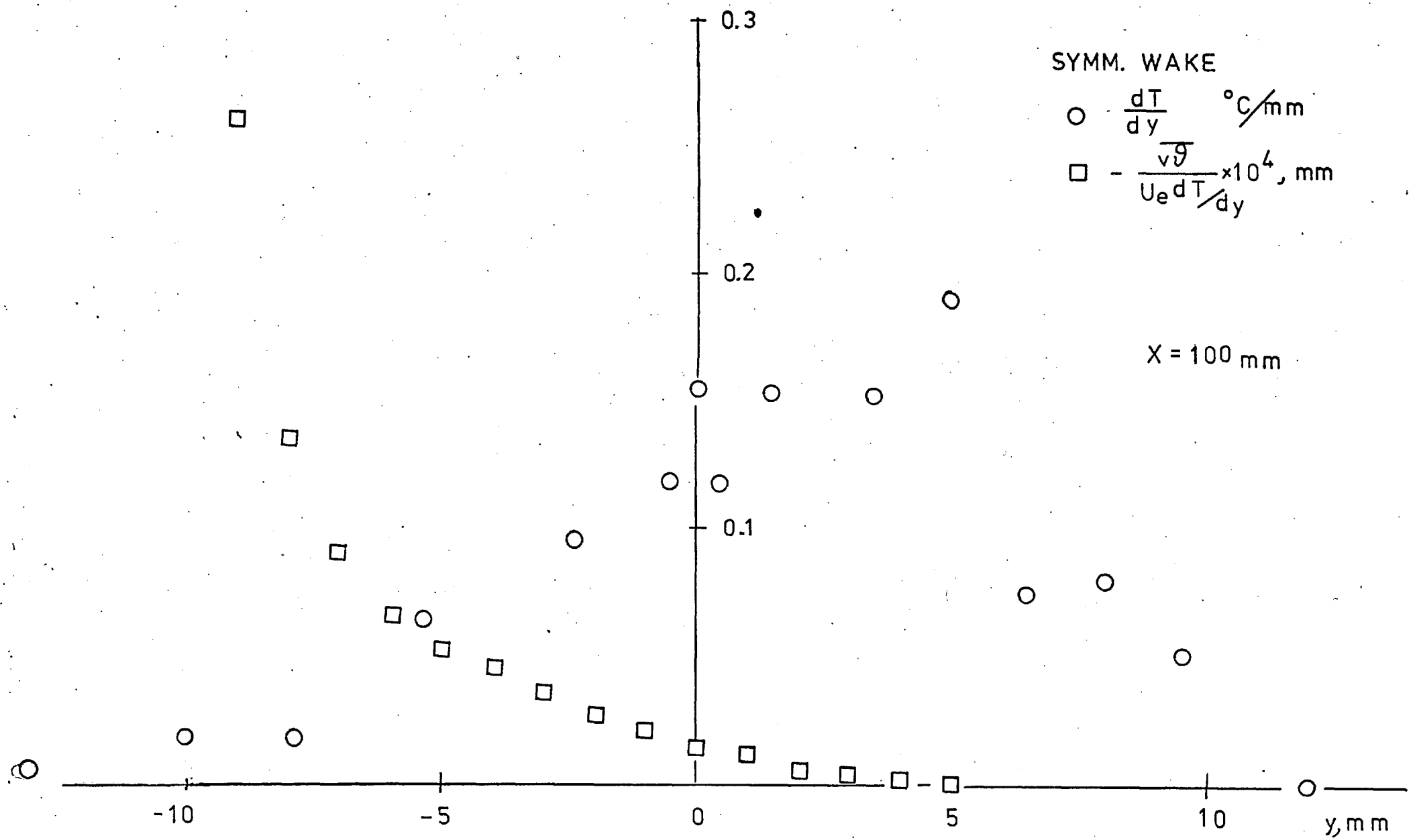

FIG. 6.50 NORMAL TEMPERATURE GRADIENT AND THERMAL EDDY DIFFUSIVITY

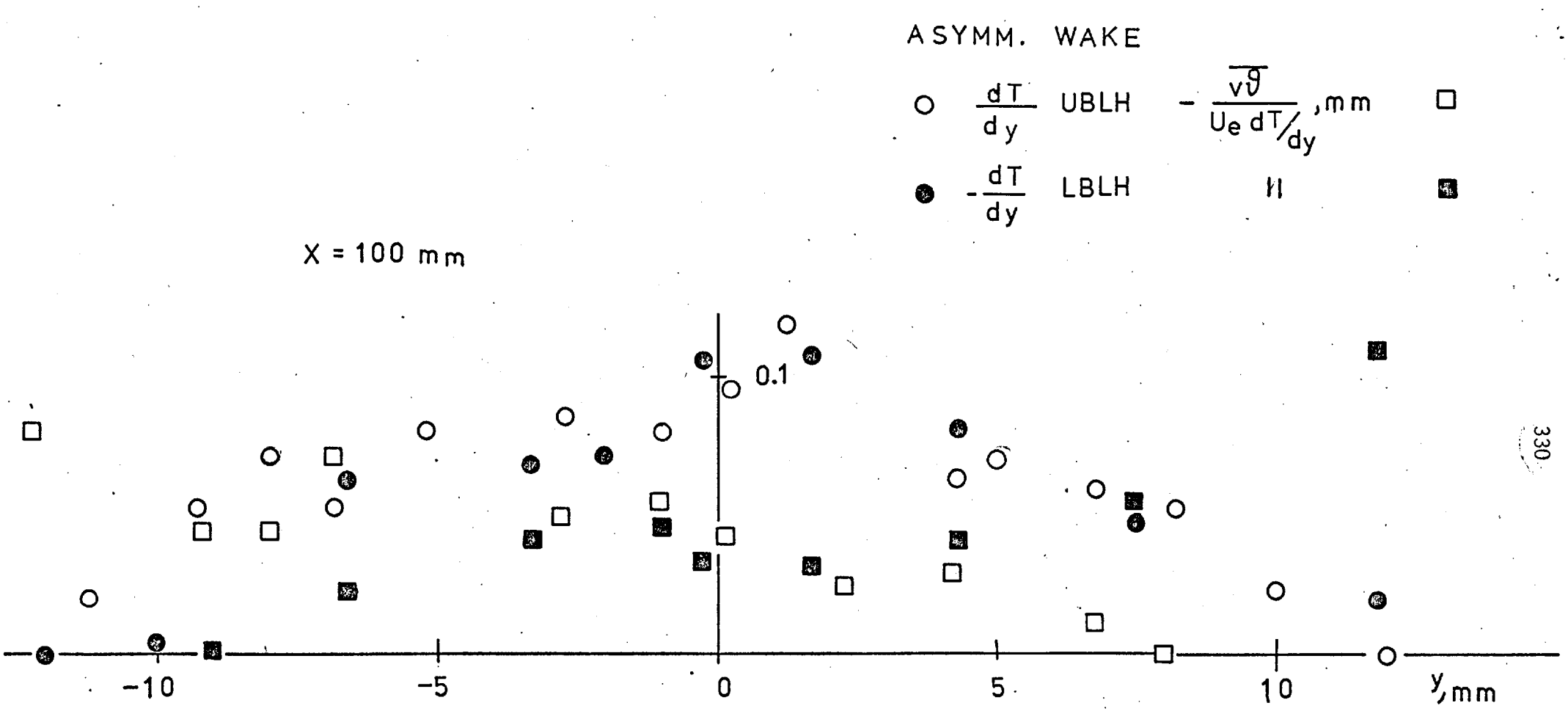

FIG. 6.51 NORMAL TEMPERATURE GRADIENT AND THERMAL EDDY DIFFUSIVITY

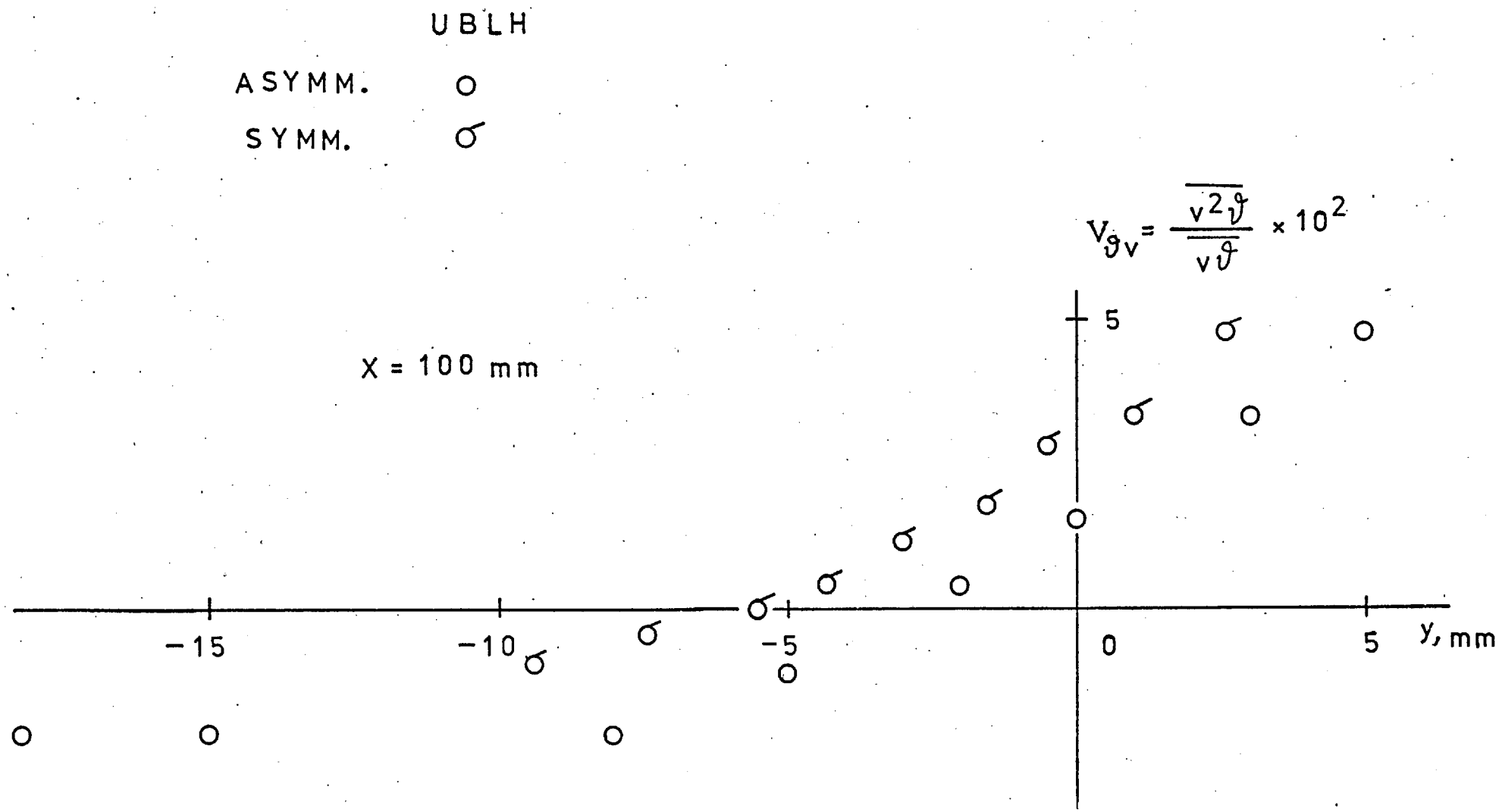

FIG. 6.52 $V_{\theta v}$ TRANSPORT VELOCITY

$$V_\theta = \frac{\overline{v\vartheta^2}}{\overline{\vartheta^2}}$$

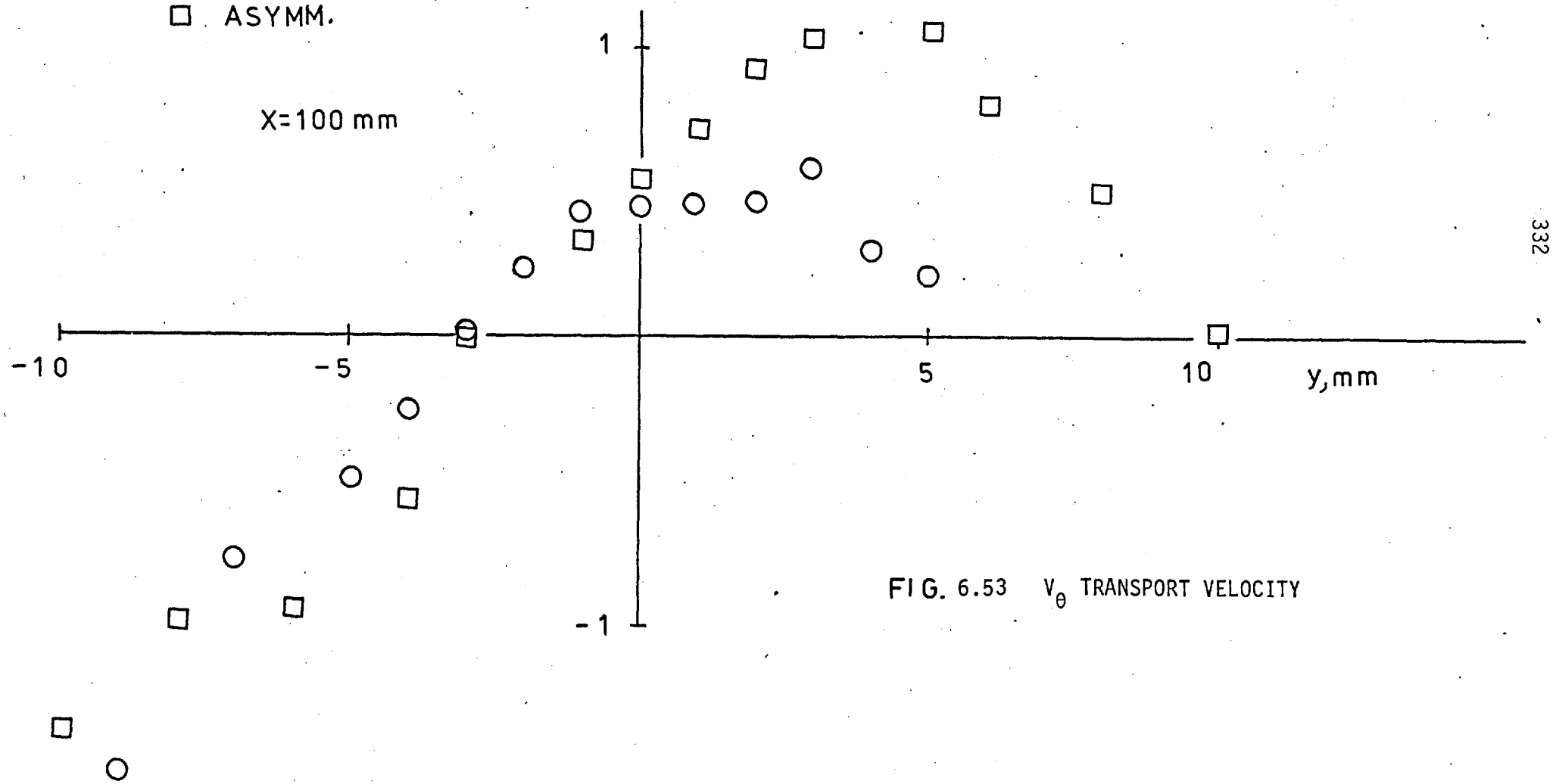

FIG. 6.53 V_θ TRANSPORT VELOCITY

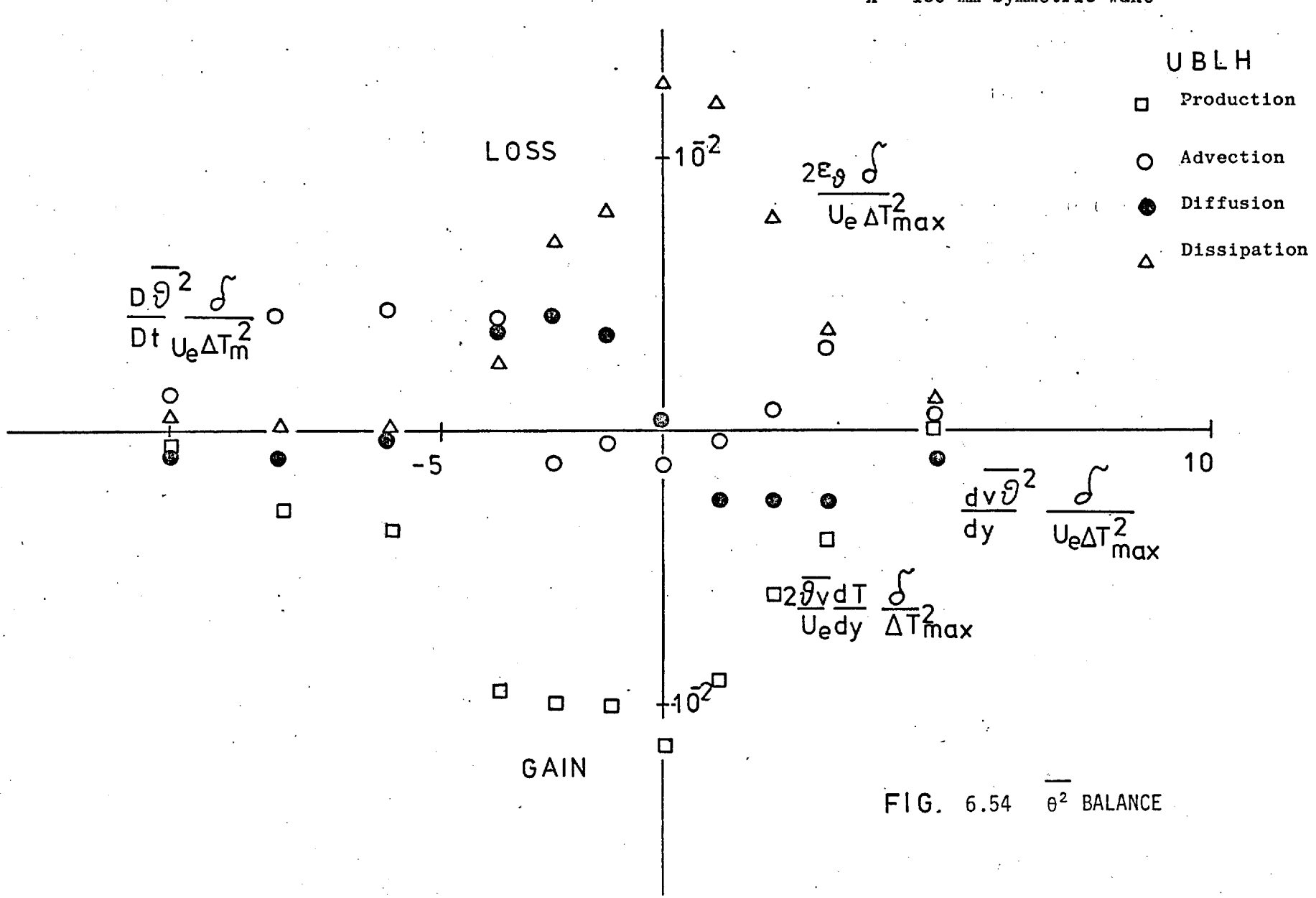

FIG. 6.54 $\overline{\theta^2}$ BALANCE

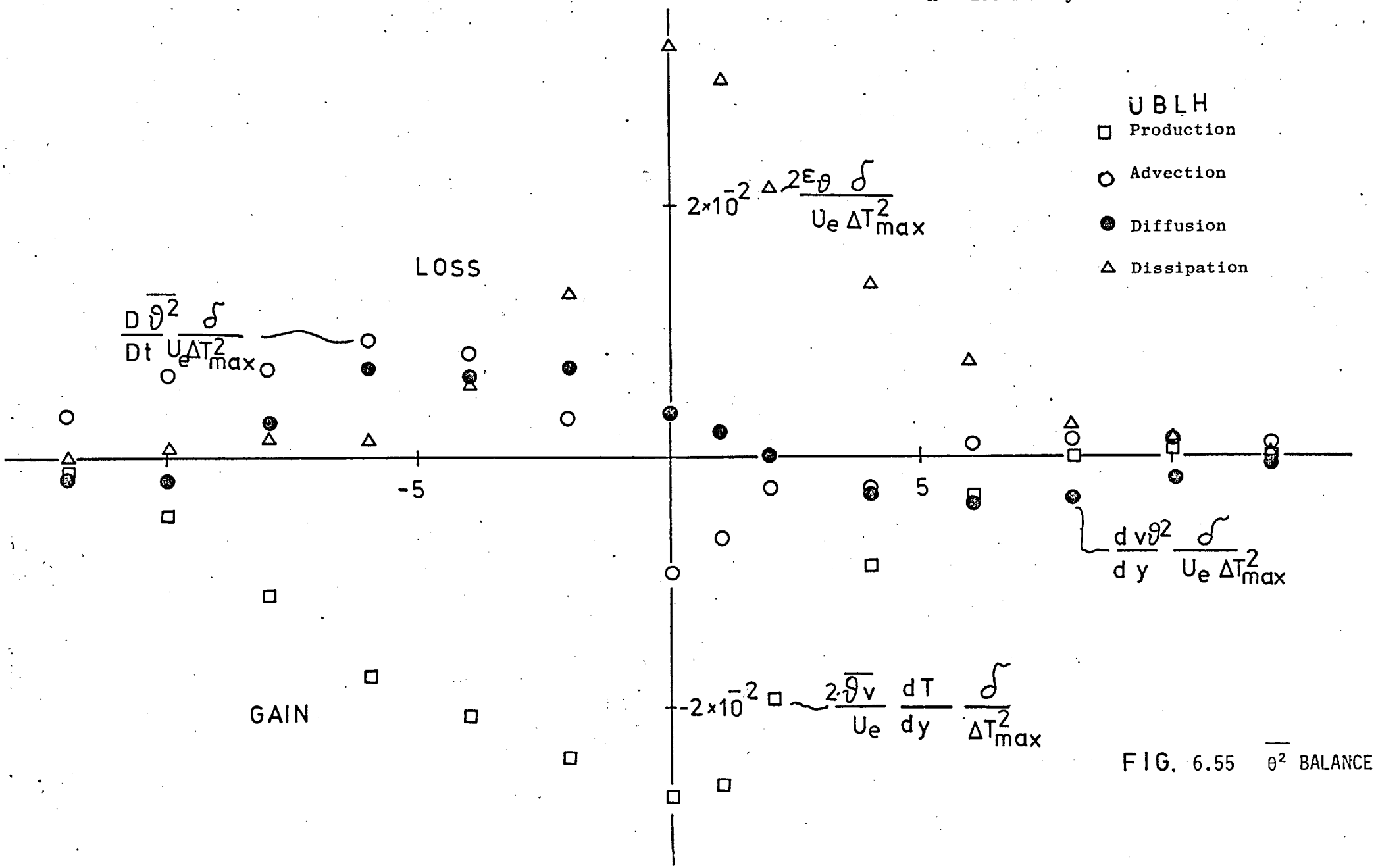

FIG. 6.55 $\overline{\theta^2}$ BALANCE

7. FURTHER RESULTS AND DISCUSSION

In Section 1.1, it was mentioned that the aim of the present experimental investigation was to gain more information about the way the two boundary layers interact after merging to form the near wake. In the last three chapters, most of the results which have been obtained from the present work have been presented and some interesting phenomena have been revealed. In this chapter, some more derived results will be presented and discussed.

7.1 The Inner Wake Behaviour

As mentioned earlier, the results suggest that the wake flow can be divided into the inner wake region and two outer regions (or outer layers), one on either side (Fig. 4.00). In the outer part of the symmetric wake, little change occurs. The mean U velocity at given y is independent of x in the region $x \leqslant 400$; strictly $\partial U/\partial x$ on a given streamline retains the small value it had in the boundary layer upstream. In the asymmetric wake, V is asymmetric so it may be necessary to examine U (strictly total pressure P) on a given streamline rather than at given y.

Similar behaviour characterizes the conventional mean turbulent quantities. In the outer part of the asymmetric wake, some changes start to happen at $x = 400$ mm especially in the lower side since there is a net transport of kinetic energy and shear stress from the upper fluid towards the lower tending to "smooth" the asymmetry between the two layers.

For $x < 400$ mm, the inner wake is the region of the flow which is mainly affected by the interaction of the two boundary layers. The mean edges of this region obtained from various definitions based on perturbations of the mean velocity, shear stress and intermittency

coefficient profiles across the wake compare well with the hypothesis of Bradshaw et al (1967) that any small perturbation near the wall is confined in a region bounded by the outgoing characteristic of their hyperbolic model.

At the edges of the inner wake the turbulent kinetic energy and shear stress reached high values. Generally, as has been shown earlier (Sections 4.2 and 5.2), there is a transport of turbulent kinetic energy and shear stress towards the centre-line, while in the outer part of the wake, the opposite phenomenon takes place. If a transport velocity of kinetic energy, $V_q = (\overline{u^2 v} + \overline{v^3})/(\overline{u^2} + \overline{v^2})$, is defined, it has higher negative values in the upper side indicating direction towards the centre-line (see Fig. 7.1) and a positive value for the lower layer.

The shear stress transport velocity, similarly defined as $V_\tau = \overline{uv^2}/\overline{uv}$, plotted in Fig. 7.2, shows the same trend: inwards transport of shear stress. The $\overline{uv^2}$ does not change sign where $\overline{uv}$ does. Thus, at these points, V_τ reaches indefinite values. It is worth noting that V_τ is almost everywhere higher than V_q.

7.2 Turbulent Kinetic Energy Balance

The various terms in the transport equation for the turbulent kinetic energy, which is described in Appendix G, were estimated as follows. The advection term requires previous knowledge of V. V has been evaluated from the continuity equation as described in Appendix H. Since in the present work no quantities involving the component w have been measured, the approximate relations $\overline{w^2} = \frac{1}{2}(\overline{u^2} + \overline{v^2})$ has been assumed, so that:-

$$\frac{1}{2}\overline{q^2} = \frac{3}{4}(\overline{u^2} + \overline{v^2})$$

A similar assumption was used in calculating the normal diffusion term:-

$$\frac{\partial}{\partial y}\frac{1}{2}\overline{q^2 v} = \frac{3}{4}\frac{\partial}{\partial y}\left(\overline{u^2 v} + \overline{v^3}\right)$$

while the longitudinal $\frac{\partial}{\partial x}\frac{1}{2}\overline{q^2 u}$ found to be much less than the normal and was, therefore, neglected. The diffusion by the pressure fluctuation term is also neglected since it is very difficult to measure and it is likely to be small.

The normal-stress production term, $-\left(\overline{u^2} - \overline{v^2}\right)\frac{\partial U}{\partial x}$ has also been found to be very small in comparison with the $-\overline{uv}\frac{\partial U}{\partial y}$ term and, thus, has been neglected. Similarly for the $-\overline{uv}\frac{\partial V}{\partial x}$ term.

It is worth mentioning that, in determining these derivatives graphically, approximate smooth curves have to be drawn through scattered data points especially in the $\overline{v^3}$ curves. Where any larger-than-usual uncertainty in the slope determination appears, it is mentioned in the discussion below.

The energy balance terms should be symmetric about the centre-line. As the symmetry or antisymmetry of the turbulence factors such as $\overline{uv}$ or $\overline{q^2 v}$ has been demonstrated above, the energy balance has not been explicitly evaluated for $y < 0$.

The dissipation term obtained by difference will include errors or out-of-balance quantities together with the pressure diffusion term.

Figs. 7.3 and 7.4 show the energy balance for the symmetric and asymmetric wake at $x = 100$ mm. All the terms have been non-dimensionalized by δ/U_e^3 where δ is the upper boundary layer thickness at the trailing edge.

The production in the outer part of the wake is small since both $\overline{uv}$ and $\partial U/\partial y$ are small. There is also there a small gain by diffusion and a loss by advection. These are expected to be almost exactly the same as in the outer layer of a boundary layer.

Then at points close to the centre-line, the production increases as well as the dissipation, which, more or less, follows the dissipation of a boundary layer in equilibrium (diffusion and advection negligibly small).

Let us now concentrate on the symmetric wake. The production still increases at positions close to the centre-line, up to a maximum value at about y = 7 mm and then decreases to zero with the shear stress and velocity gradient. Indeed, at y = 0, since $-\overline{uv}\,\frac{\partial U}{\partial y}$ is zero, the production term, $-(\overline{u^2} - \overline{v^2})\,\frac{\partial U}{\partial x}$ must be reconsidered ($\overline{uv}\,\partial V/\partial x = 0$). Its contribution is small but enough to say that there is everywhere positive production even on the centre-line.

In a boundary layer, the production increases rapidly very close to the wall but it is expected to be zero on the wall. From this point of view, there is a similarity between the boundary layer and a wake with the difference that in the latter, the region where the production drops is much thicker than the viscous sublayer.

At further downstream position, the production is expected to be less since $-\overline{uv}$ drops with x and so does $\partial U/\partial y$, as can be seen in Fig. 7.5 (which is a sensitive demonstration that outer-layer conditions do not change).

The advection term is very small in the outer part of the wake. Since no large changes in the streamwise and normal directions occurred, $U\,\frac{\partial\,\frac{1}{2}q^2}{\partial x}$ is small and positive and $V\,\frac{\partial\,\frac{1}{2}q^2}{\partial y}$ is smaller but negative in a way such that the overall advection is positive, i.e. loss of energy from a given control volume. At $y/\delta \simeq 0.6$, $U\,\frac{\partial\,\frac{1}{2}q^2}{\partial x}$ becomes

small and then negative and thus a gain of energy appears, continuing at smaller y down to about the point where the maximum kinetic energy is reached. After that point $\partial\ \overline{\frac{1}{2}q^2}/\partial y$ changes sign and so the overall gain by advection decreases up to the centre-line where $\partial\ \overline{\frac{1}{2}q^2}/\partial y$ is zero but $\partial\ \overline{\frac{1}{2}q^2}/\partial x$ is not. Thus, on the centre-line, the advection is not zero but small anyway while at the edges of the inner wake, it becomes very high.

The diffusion term in the outer part of the wake behaves more or less like that in the boundary layer. At the outer edge, the measurements show that advection $\simeq \frac{\partial}{\partial y}\frac{1}{2}\overline{q^2v}$ and production $\simeq 0$. The dissipation, therefore, is negligible and so is the diffusion by pressure fluctuation.

At the point where the advection changes sign, so does the diffusion. Then there is a further loss for smaller y followed by a change of sign and finally reaching a high value on the centre-line. There are a few points where the graphical determination of the derivative was vague. The uncertainties are mentioned in the plot of diffusion and reflect similar uncertainties in the corresponding points of dissipation.

As has been pointed out by Bradshaw (1966), the diffusion terms should integrate to zero throughout the shear layer (provided, of course, that the longitudinal diffusion is zero or negligibly small so that only $\frac{\partial}{\partial y}\overline{p'v} + \frac{1}{2}\overline{q^2v}$ remains). In the present case, this condition is nearly satisfied.

The dissipation has been evaluated by difference. It indicates loss of energy with maximum value near the centre-line. It is interesting to note that production is equal to dissipation outside the inner wake and not near the edge of the outer layer; this is as expected in an unperturbed boundary layer.

Generally, the outer part of the wake behaves like the outer part of a boundary layer, at zero pressure gradient. The inner wake obviously differs from the inner layer of a boundary layer, although there are no measurements very close to the wall for a complete comparison: advection and diffusion have significantly high values in the inner wake implying that dissipation is not equal to the production. Another difference is that on the centre-line the dissipation is counter-balanced by diffusion mainly, i.e. in general, the inner wake has high production at its edges, low production near the centre-line.

At stations further downstream, it is expected that all terms will fall to lower values. In the asymmetric wake, there are obviously differences originating in the asymmetry between the two boundary layers at the trailing edge.

The production in the outer part on the rough side looks more or less like the symmetric wake. It increases towards the centre-line and then decreases because both $-\overline{uv}$ and $\partial U/\partial y$ decrease and at $y \simeq 4.3$ mm, it changes sign which is retained up to $y = 2.3$ mm where a positive production starts again. In this region $\partial U/\partial y$ and $\overline{uv}$ go to zero at different y, and since anyway $\overline{uv}\,\frac{\partial U}{\partial y}$ is small for better accuracy all production terms have been taken into account:-

$$(\overline{u^2} - \overline{v^2})\,\frac{\partial U}{\partial x} + \overline{uv}\left(\frac{\partial U}{\partial y} + \frac{\partial V}{\partial x}\right)$$

The first term has values always positive there and thus the negative production becomes stronger while $\partial V/\partial x$ is positive and $\overline{uv}\,\frac{\partial V}{\partial x}$ is negative, so it implies a positive production which reduces the effect of the negative production of the other terms but not drastically. Thus there is a negative production in this region meaning that a reversal of kinetic energy from the turbulent to the mean motion happens. This

feature is rather common to all asymmetric flows and it is quite similar to the negative production of temperature fluctuation mentioned in Chapter 6.

Outside this region, the production rises sharply and reaches a maximum value at $y \simeq -5$ mm on the "smooth" side since there $\overline{uv}$ reaches a maximum as $\partial U/\partial y$ does (see Fig. 7.6). The peak in $\partial U/\partial y$ on the "smooth" side ($y < 0$) is much bigger than the peak on the rough, while at the trailing edge it was quite the opposite. At $x = 25$ mm, it is expected that the two peaks will be nearly equal since $\overline{uv}_{max}$ are roughly equal and $\partial U/\partial y$ of the same order, and then at $x = 100$ mm, the high peak is found on the "smooth" side. After the peak, the production drops towards the lower layer edge but with values greater than the symmetric ones.

Advection is also small in the outer part of the asymmetric wake. At the upper edge of the inner layer, it has a maximum value and then reduces continuously, passing through zero at about $y \simeq 3$ mm where $\frac{\partial \frac{1}{2}q^2}{\partial x} \simeq 0$ and $\frac{\partial \frac{1}{2}q^2}{\partial y} \simeq 0$ and then there is a loss of energy by advection at the same region where a big surplus of production exists, mainly because the normal component $V \frac{\partial \frac{1}{2}q^2}{\partial y}$ is high. If the wake was symmetric, a large gain by advection ought to occur. This is the major difference from the symmetric wake and it goes on almost up to the lower wake edge.

The diffusion behaves more or less as in the symmetric case: high losses on the edges of the inner wake, associated with the maximum kinetic energy there, and a maximum gain near the point of minimum kinetic energy.

The energy dissipation ε behaves as expected. It reaches a maximum value near the centre-line and then drops steeply towards the lower wake edge and smoothly towards the upper edges. It is very hard

to find any region where dissipation is equal to the production and, consequently, the dissipation length scale:-

$$L = \frac{(-\overline{uv})^{3/2}}{\varepsilon}$$

is not equal to the mixing length $\ell = (-\overline{uv})^{\frac{1}{2}}/\partial U/\partial y$. Plots of L/δ versus y/δ using values of ε which are found here are in Fig. 7.7. More or less, the L/δ remains the same in the outer part for the symmetric and the asymmetric wake.

In the inner wake, there is an obvious difference due to the fact that the shear stresses do not go to zero at the same point for both the symmetric and asymmetric. The phenomenological agreement of the symmetric case, L, with von Karman's expression for mixing length $\ell = ky$ is rather misleading; production is not equal to dissipation. It may be due to the erratic behaviour of $(\overline{uv})^{3/2}$; L is meaningless for $\overline{uv} = 0$. Indeed, very close to the centre-line, $\overline{uv}$ varies as y and dissipation is roughly constant so $L \sim y^{3/2}$ which is clearly not a linear variation of y.

Since the "dissipation" term (found by difference from the other terms) for both cases, symmetric and asymmetric varies smoothly while the diffusion by velocity fluctuations (triple-products) does not, the "dissipation" term is probably true dissipation without any rapidly-varying pressure diffusion linked to rapidly-varying $\overline{q^2 v}$.

7.3 Shear Stress Balance

The shear stress transport equation is given in Appendix G. The mean transport term:-

$$\left[U \frac{\partial}{\partial x} + V \frac{\partial}{\partial y}\right] (-\overline{uv})$$

was calculated similarly to that for the turbulent kinetic energy balance. As generation, the contribution of two terms have been taken into account:-

$$-\overline{v^2} \frac{\partial U}{\partial y} - \overline{u^2} \frac{\partial V}{\partial x}$$

The turbulent transport of pressure fluctuation terms have been neglected since they should be very small compared to the turbulent transport terms which are both the longitudinal and normal:-

$$-\frac{\partial \overline{u^2 v}}{\partial x} - \frac{\partial \overline{uv^2}}{\partial y}$$

The viscous terms, which represent the destruction of shear stress by viscous forces, $\nu (\overline{u\nabla^2 v} + \overline{v\nabla^2 u})$ have also been neglected since they are very small in high Reynolds number flows except in the viscous sublayer region. At the present case, it is believed that viscous sublayer effects have died out by x = 100 mm. Finally, the pressure-rate of strain term:-

$$\overline{p' \left(\frac{\partial u}{\partial x} + \frac{\partial v}{\partial y}\right)}$$

has been obtained by difference. Thus, it may include two kinds of errors: firstly, the errors due to the presence of neglected terms and, secondly, errors caused by the graphical differentiation of the various terms affected by direct measurement errors.

Typical shear stress balances for symmetric and asymmetric

wake are shown in Figs. 7.8 and 7.9. All terms have been non-dimensionalized by δ/U_e^3 where δ is the upper boundary layer thickness at the trailing edge. All the terms are antisymmetric with respect to the centre-line in the symmetric wake and, consequently, the balance in the lower wake has not been drawn. In the asymmetric wake, there is also an antisymmetric behaviour in shape only.

Shear stress generation takes place by interaction of $\overline{v^2}$ and $\overline{u^2}$ and the mean velocity gradients $\partial U/\partial y$ and $\partial V/\partial x$. However, in the present case, the longitudinal variation of V is very small and the production by $\overline{u^2}\,\frac{\partial V}{\partial x}$ is much smaller than the $\overline{v^2}\,\frac{\partial U}{\partial y}$ except for the regions where the latter goes to zero. Similarly, the longitudinal turbulence transport is smaller than the normal except in the outer part of the layer where both are of the same order of magnitude.

In the symmetric wake, generation peaks near the edges of the inner wake where both $\overline{v^2}$ and $\partial U/\partial y$ reach maximum values. Further inwards, there is a high gain by mean transport. There, the surplus of shear stress is removed by turbulent transport or it is redistributed by pressure fluctuations.

The production in the outer part is very small. In this region, there is a gain by turbulent transport and loss by advection. At about y = 30 mm, these terms change sign and increase in magnitude towards the centre-line where all terms are decreased to cross the centre-line with zero value and change their sign.

Generally, mean and turbulent transport are decreased uniformly as also happens to the generation and pressure-rate of strain terms. All the terms have significant values inside the inner wake, but generation and pressure-rate-of-strain dominate throughout the flow except in the outer part.

In the asymmetric wake, the generation term has two peaks near

the edges with opposite peaks in the pressure-rate of strain term. All terms have generally higher peaks in the lower part of the inner wake since there the generation is high.

In the outer part, the behaviour of all terms is as it is expected with one exception, the turbulent transport in the lower part (smooth side), where it dies out very soon.

7.4 The Use of Heat for Conditional Sampling

The use of heat as a tracer makes the discrimination between fluids from either side of a turbulent - non-turbulent interface much easier. The temperature traces in the outer part of the wake as they have been presented previously in Fig. 3.1a are a good example. There, the "cold" level is constant. Any conductivity effects are small and the only cause of any ambiguity or uncertainty is the presence of some small free stream temperature fluctuations. But the appearance of these was very rare and anyway, their amplitude was believed to be less than the level threshold.

In the "internal" interface, the use of heat for discriminating the two turbulent flows seems to have greater difficulties. But, in any case, it is quite unlikely that the use of any quantity from the velocity field as the basis for conditional sampling will have less problems and will be easier. The classification of "hot", "cold" or "warm" fluid seems to be closer to the reality than a simply "hot" or "cold" discrimination. The reason for that is the fine scale mixing, which is rather intensive around the centre-line.

The present intermittency criteria finds only the newly-entrained "cold" fluid. But it is believed that a large "cold" eddy which is travelling from the trailing edge to a certain point at distance x is subjected to fine scale activities around its boundaries

for a time which is much longer than the travelling time, and thus finally it is not detected as a fully "warm" eddy, i.e. as "hot", but there is still a portion of the original "cold" eddy. Cases like this are expected to be more frequent in the furthest downstream station at x = 400 mm.

A further difficulty arises from the fact that the "hot" fluid is not uniformly heated and thus the plateau which is frequently met on a "hot" burst does not exist. If the free stream on the "hot" side was heated as well but remains irrotational, then we would have a case of uniformly heated flow. However, the present method can cope with that problem since the "cold" fluid is detected correctly and then the heat is changed over to the other layer and, therefore, the truly "hot" fluid can be determined.

Some minor problems are created in the "cold" fluid as well, which is mainly due, unavoidably, to heat from the heated boundary layer "leaking" through the plate and causing some temperature fluctuations on the "cold" fluid: this can be easily treated by increasing the level threshold when appropriate (if their amplitude is not less than the threshold).

It should be noted that in the present analysis, the coincidence of temperature and velocity interfaces, a problem which has been raised earlier in the introduction, does not really matter to the discrimination technique.

7.5 Bursting Phenomena

Previous studies of the turbulent boundary layer structure near the wall in the zone $y^+ < 100$, show that essentially all turbulence production occurs during intermittent "bursting" periods; see, for example, Kim, Kline and Reynolds (1971). Wallace et al (1972) found

that the positive-stress-(- uv)-producing motions ($u < 0$, $v > 0$ and $u > 0$, $v < 0$) have larger time scales than the negative-stress-(uv)-producing motions. Moreover, Lu and Willmarth (1973) found that, on average, bursts ($v > 0$) account for 77% of $\overline{uv}$, while sweeps ($v < 0$) provide 55%, with the excess percentage balanced to other small negative contributions.

The sweeps bring inwards fluid from the outer part while bursts carry fluid to larger y. Various attempts have been made to explain the bursting process in turbulent boundary layers. But since reliable measurements are very difficult to acquire and visualization techniques are sometimes misleading, these attempts are mainly speculations.

In the present experiment, the inner wake can be considered as the continuation of the two inner layers of the two boundary layers after the wall "disappears" at $x = 0$. Turbulence production does not cease to take place in the wake and thus the existence of any sort of bursting phenomenon in the wake is not a surprise. Indeed, the conditional averages (unfactored by γ) confirmed this.

Apparently, "hot"/"cold" contributions are, in general, the result of strong eruptions across the centre-line as is clearly shown by the triple-products, $\overline{u^2v}$, $\overline{v^3}$, $\overline{uv^2}$. If top-side fluid, regardless of being "hot" or "cold", crosses the centre-line it creates "sweeps" on the lower side and similarly bottom fluid crossing the centre-line causes "bursts" on the upper side. Consequently, the bursts or "sweeps" of the "warm" or mixed fluid which constitute the centre-line region, seem to be pushed by the host layer "sweeps" or "bursts" respectively.

Generally, the "bursts" or "sweeps" of "cold" fluid bring inwards turbulent kinetic energy while the "warm" "bursts" or "sweeps" carry kinetic energy outwards except for a small region very close to

the centre-line where there is transfer outwards. Discussions of the transport of kinetic energy and shear stress will be continued in Section 7.6.

7.6 Zone Turbulent Characteristics and Parameters

As was mentioned earlier in Section 3.2, the averages of the "cold" fluid are easier to interpret since "hot" fluid includes the "warm" as well. In this section, some characteristics of the "cold" and "warm" zone will be discussed. A correlation coefficient can be defined as $\overline{uv}_c/\sqrt{\overline{u^2}_c}\ \sqrt{\overline{v^2}_c}$ or $\overline{uv}_w/\sqrt{\overline{u^2}_w}\ \sqrt{\overline{v^2}_w}$. These have been plotted in Fig. 7.10.

The "cold" fluid seems to have a correlation coefficient similar to a shear layer one which means it has not been affected by the interaction of the two boundary layers. The "warm" fluid behaves exactly as the conventional R_{uv}, i.e. it can be treated as an isolated layer.

In Fig. 7.11, the structural parameter $a_1 = \overline{uv}/(\overline{u^2} + \overline{v^2})$ is plotted. The coincidence of both symmetric and asymmetric "cold" fluid values indicates the universality of a_1, which is more or less constant.

In Fig. 7.12, the transport velocity of turbulent kinetic energy is plotted for the "cold" and "warm" fluid. As it is shown, the "warm" transport velocity is much smaller than the "cold", as was expected, since "cold" fluid is mainly occupied by large eddies and "warm" fluid by small scale eddies. Around the centre-line V_{qw} is negligible for both symmetric and asymmetric cases.

Another useful point is that transport velocity of the lower fluid is more or less the same for the symmetric and asymmetric cases. Similar behaviour characterizes the shear stress transport velocity

$V_\tau = \overline{uv^2}/\overline{uv}$ plotted in Fig. 7.13. For the lower fluid, i.e. the "cold" fluid when the upper boundary layer is heated, V_τ is not affected by the upper fluid regardless of the latter being smooth or rough. It is also clear that V_τ reaches an asymptotic value, before it disappears to an indefinite value $\frac{0}{0}$, for both cases: 0.075 for UBLH and 0.15 for LBLH.

As far as the "warm" fluid $V_{\tau w}$ is concerned, as was expected, there are no differences between the symmetric and asymmetric cases, except near the points where $\overline{uv}_w$ goes to zero and, therefore, V_τ tends to infinity as is shown in Fig. 7.14.

7.7 Considerations on a Possible Calculation Method

In any attempt to predict the near wake flow, two phenomena must be represented:-

(a) The effect of interaction on large scale structures.

(b) Fine-grained mixing.

As was seen previously, the structural parameters of the large scale motion (i.e. "cold" average ones) do not change significantly indicating that the effect of the interaction on the large eddies is rather weak.

As for the fine-grained mixing (i.e. the small scale eddies), it is likely that these small eddies are more closely related to the local mean velocity gradient than the large eddies are. Indeed, a "warm-zone" eddy viscosity defined as $\nu_{\tau w} = -\overline{uv}_w/(\partial U/\partial y)$ might express the small scale motion very satisfactorily. In Fig. 7.15, the "warm" eddy viscosity for the symmetric and asymmetric (i.e. "warm-zone") is plotted. There is a constant value of $\nu_{\tau w}$ around the centre-line, a

fact which supports the above argument.

Some more eddy viscosities are plotted in Fig. 7.16 for x = 25 and 400 mm together with those at x = 100 mm for comparison.

The "warm" region eddy viscosity of the asymmetric wake might suffer from the same trauma which a conventional eddy viscosity suffers: $\overline{uv}_w$ and $\partial U/\partial y$ do not go to zero at the same point. However, the present results indicate, within the accuracy of $\overline{uv}_w$ determination, that these two points rather coincide. Since the small-scale (i.e. "warm") motion evidently scales quite well on $\partial U/\partial y$ without explicit effect of the large eddies, and since no large changes of turbulent structure occur in the large eddy motion (i.e. in the "cold" and truly "hot" region), the corresponding two Reynolds stress fields together with the fine scale motion of the "warm" zone could all be superimposed to predict a wake flow. Superposition of two weakly interacting shear layers in a duct has been successfully applied by Bradshaw et al (1973). In the present case, with the concept of three independent zones already well established, a calculation attempt can proceed as follows.

For the "upper" and the "lower" fluid, two independent shear stress transport equations can be employed. The "mixed" fluid shear stress can be derived from the eddy viscosity formula, i.e. from the mean velocity gradient. Any interaction between the three layers is supposed to take place only through the mean velocity profile. If the above ideas are applied to Bradshaw et al's (1967) calculation method as it has been revised by Bradshaw and Unsworth (1974), the proposed equations for solving are:-

Continuity

$$\frac{\partial U}{\partial x} + \frac{\partial V}{\partial y} = 0 \qquad (7.6.1)$$

x-momentum

$$U \frac{\partial U}{\partial x} + V \frac{\partial U}{\partial y} = \frac{1}{\rho} \frac{\partial \tau}{\partial y} - \frac{1}{\rho} \frac{\partial p}{\partial x} \tag{7.6.2}$$

where:-

$$\tau = \tau_H + \tau_C + \tau_W \tag{7.6.3}$$

Shear stress transport equation of the purely "hot" zone

$$\left(U \frac{\partial}{\partial x} + V \frac{\partial}{\partial y}\right) \left(\frac{\tau_H}{2\rho a_1}\right) = \frac{\tau_H}{\rho} \frac{\partial U}{\partial y} - \frac{\partial}{\partial y} \left[G \left(\frac{\tau_H}{\rho}\right) \left(\frac{\tau_{H,MAX}}{\rho}\right)^{\frac{1}{2}}\right] - \frac{\tau_H^{3/2}}{L} \tag{7.6.4.}$$

Shear stress transport equation of the "cold" zone

$$\left(U \frac{\partial}{\partial x} + V \frac{\partial}{\partial y}\right) \left(\frac{\tau_C}{2\rho a_1}\right) = \frac{\tau_C}{\rho} \frac{\partial U}{\partial y} - \frac{\partial}{\partial y} \left[G \left(\frac{\tau_C}{\rho}\right) \left(\frac{\tau_{C,MAX}}{\rho}\right)^{\frac{1}{2}}\right] - \frac{\tau_C^{3/2}}{L} \tag{7.6.5}$$

Shear stress of the "warm" region

$$\tau_W = \rho \nu_{\tau W} \frac{\partial U}{\partial y} \tag{7.6.6}$$

The dissipation length scale L is given from the transport equation:-

$$\left(U \frac{\partial}{\partial x} + V \frac{\partial}{\partial y}\right) L = C\, L \frac{\partial U}{\partial y} - \frac{\partial}{\partial y} (L\, V_L) + f \cdot \tau^{\frac{1}{2}}$$

V_L has the dimensions of velocity and may be specified by a gradient diffusion assumption or algebraic equations. f, C are dimensionless

functions.

The rest of the constants are by definition:-

$a_1 = \dfrac{\hat{\tau}}{\rho \cdot \overline{q^2}}$ with $\overline{q^2}$ being the kinetic energy

$$G \equiv \left(\frac{\overline{p'v}}{\rho} + \frac{1}{2}\overline{q^2 v}\right) \Bigg/ \left(\frac{\hat{\tau}}{\rho}\right)\left(\frac{\tau_{MAX}}{\rho}\right)^{\frac{1}{2}}$$

$L = \left(\dfrac{\hat{\tau}}{\rho}\right)^{3/2} \dfrac{1}{\varepsilon}$ ε: energy dissipation rate

where $\hat{\tau} = \tau_H$ or τ_C as appropriate.

8. CONCLUDING REMARKS

In this chapter, the main points of the results of the present investigation will be recapitulated.

The near-wake is the flow resulting from two boundary layers which meet with their high-turbulence, low-velocity sides opposing each other and mix very rapidly after the trailing edge to compose the inner wake region, with mainly small scale eddies inside since these eddies were the former occupants of the inner layers and viscous sub-layers of the boundary layers. This is a complete contrast to the large-eddy weak interaction in a duct. As a result, the intermittency on the centre-line of the symmetric wake, defined as the percentage of time the fluid is "hot", is not 0.5 as is expected from symmetry considerations but 0.10 only is "hot", 0.10 is "cold" and 0.8, "warm". This does not provide direct evidence against superposition of large eddies since only an intermittency algorithm which is able to resolve fine scale intermittency can give the right answer to that.

It has been shown that the interaction between the two boundary layers is confined inside the inner wake, the width of which at various x positions seems to obey some simple laws while in the outer parts of the wake, the changes which take place are very weak.

"Hot" or "cold" contributions seem to be the result of strong eruptions across the centre-line which transport kinetic energy and shear stress towards the centre-line.

Turbulent kinetic energy production is very high at the edges of the inner wake, where advection and diffusion have also high values, but production and advection go to zero at the centre-line.

Very similar is the shear stress generation and mean transport, the turbulent transport on the centre-line being zero while the kinetic energy diffusion is not.

Similar behaviour again characterizes the temperature-fluctuation production and dissipation, with advection and diffusion of $\overline{\theta^2}$ being quite different.

The zone structural parameters indicated that "cold" or "hot" zones do not affect each other and that any communication between them seems to be through the mean velocity profile only. The eddy viscosity concept was found to work well for the fine scale structure of the "warm" region.

Finally, a calculation method is proposed based on physical arguments previously mentioned.

It is hoped that the data which have been accumulated and the results that have been presented here, together with the various interpretations and discussions of the phenomena appearing in the present investigations, have given more information about the highly interacting complex turbulent flow in the near wake of an aerofoil.

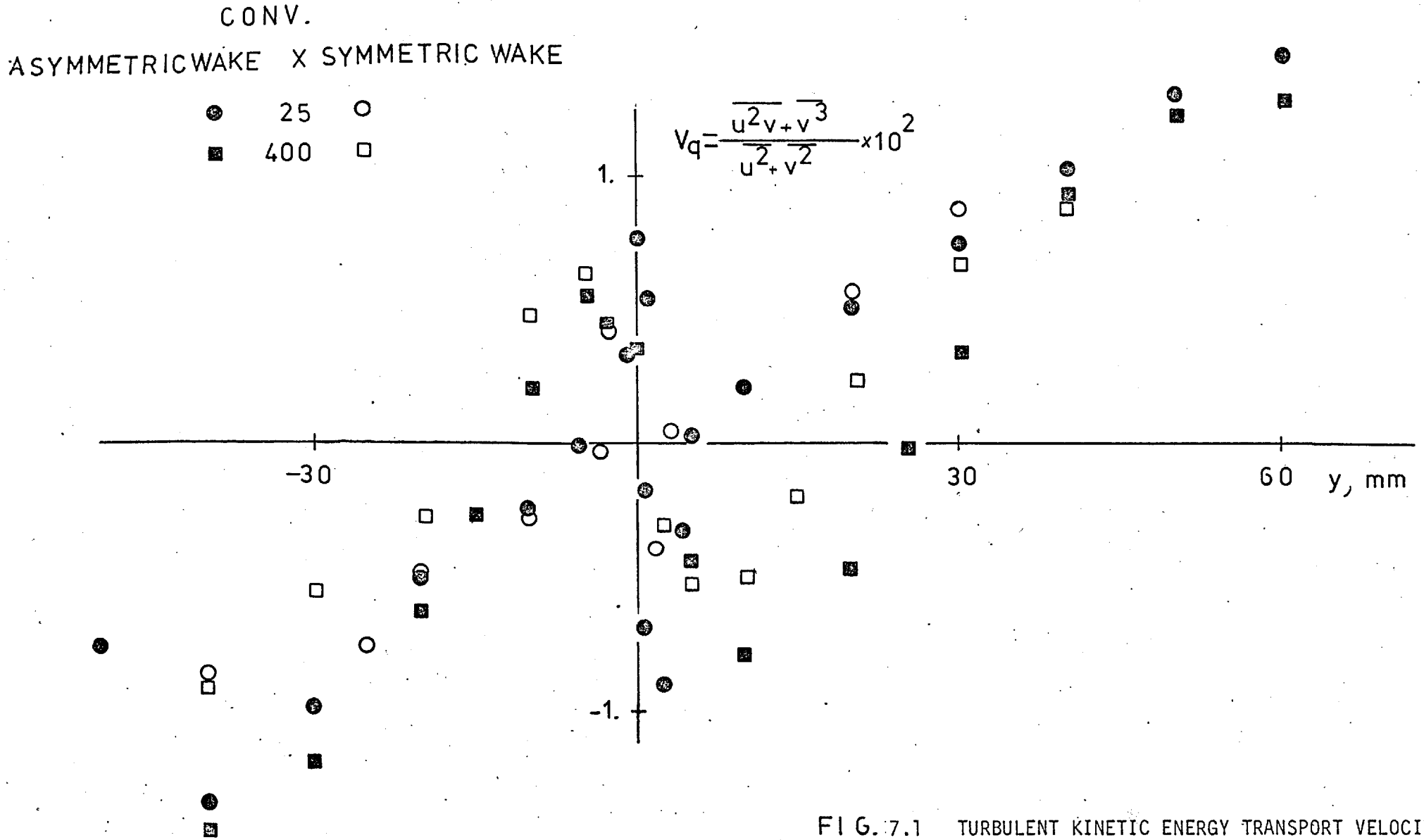

FIG. 7.1 TURBULENT KINETIC ENERGY TRANSPORT VELOCITY V_q

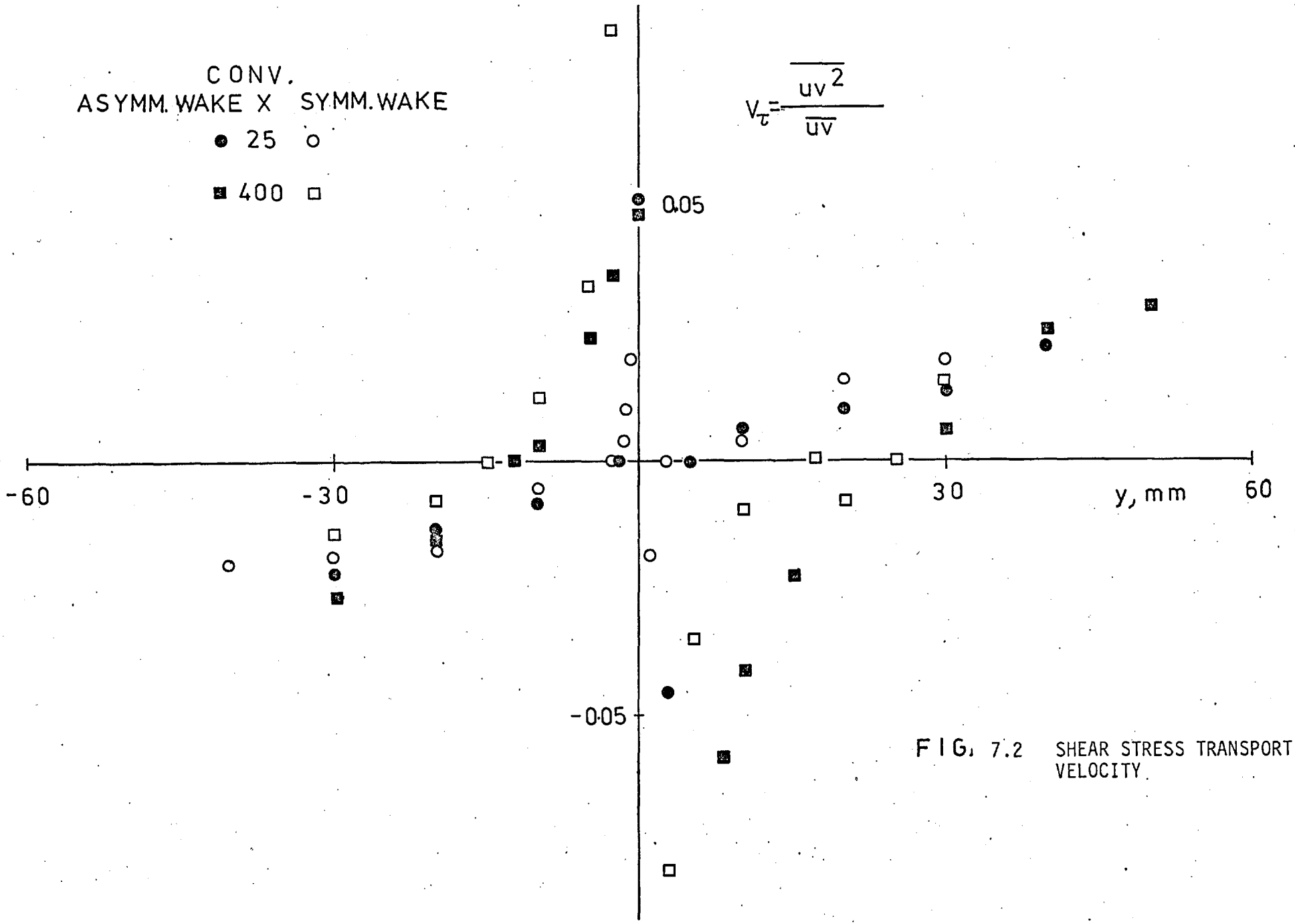

FIG. 7.2 SHEAR STRESS TRANSPORT VELOCITY.

Turbulent Kinetic Energy Balance

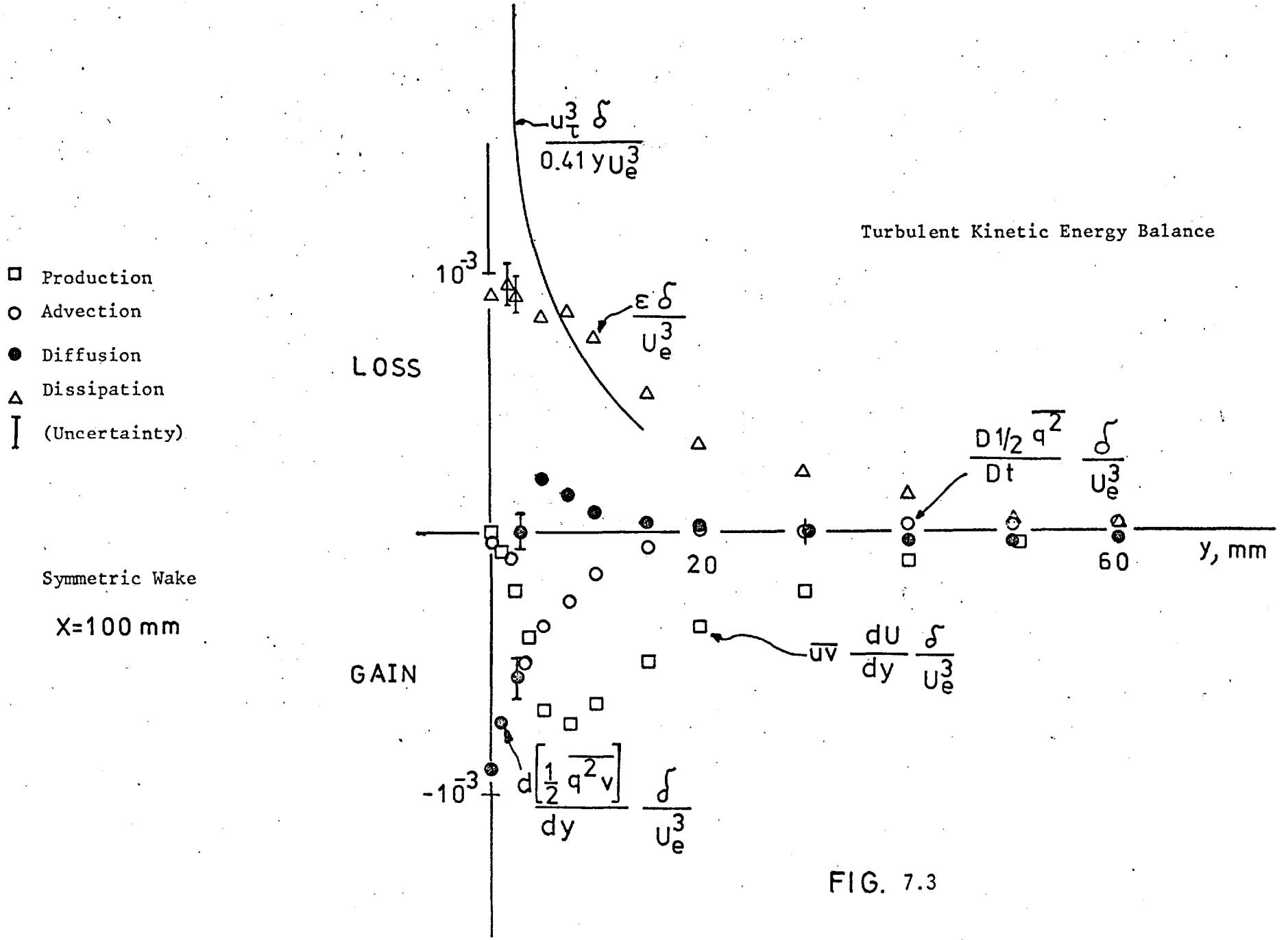

FIG. 7.3

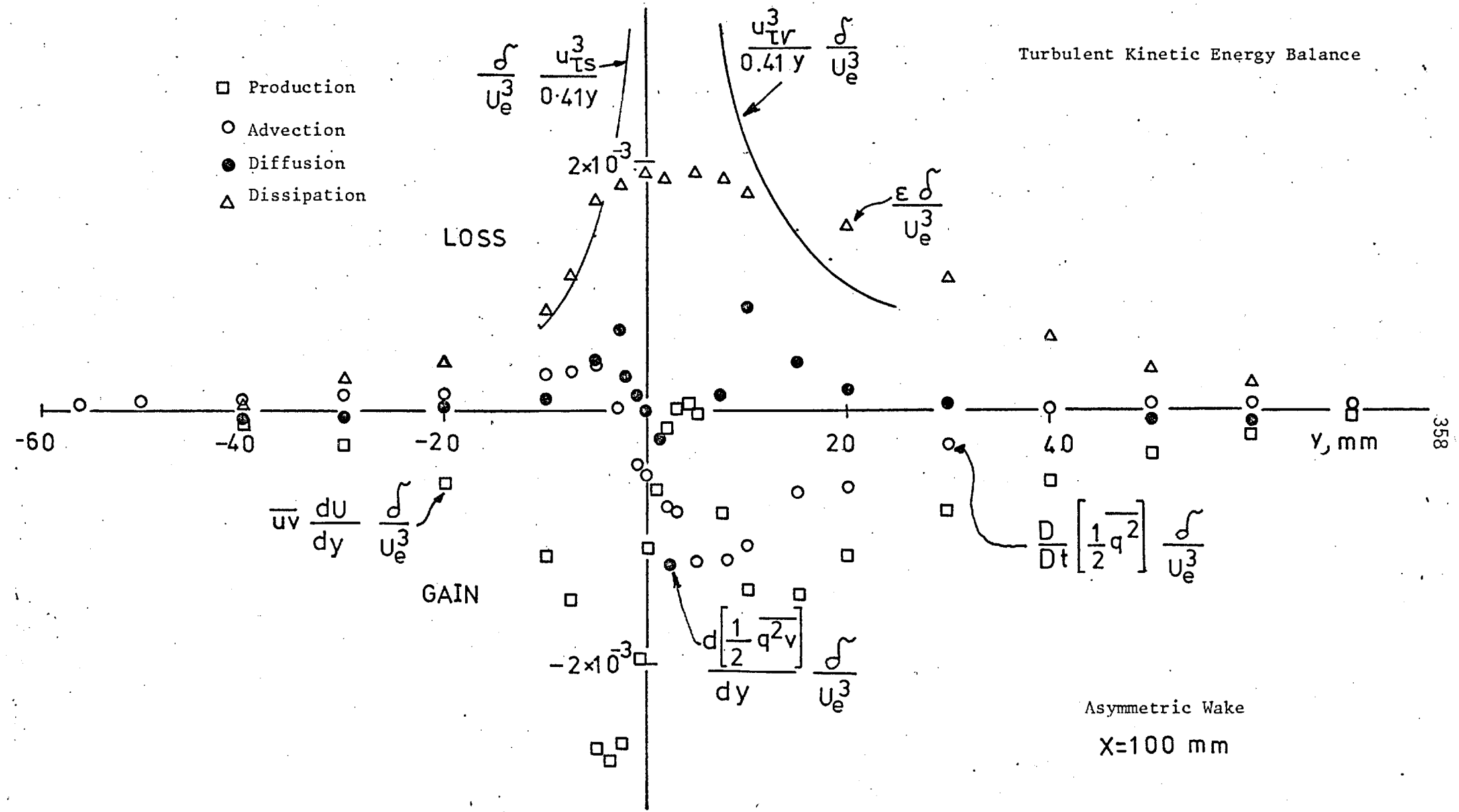
Turbulent Kinetic Energy Balance
Production
Advection
Diffusion
Dissipation
$\frac{\delta}{U_e^3}\frac{u_{ts}^3}{0.41y}$
$\frac{u_{tv}^3}{0.41y}\frac{\delta}{U_e^3}$
2×10^{-3}
LOSS
$\frac{\varepsilon\delta}{U_e^3}$
-60
-40
-20
20
40
y, mm
$\overline{uv}\frac{dU}{dy}\frac{\delta}{U_e^3}$
GAIN
$\frac{D}{Dt}\left[\frac{1}{2}\overline{q^2}\right]\frac{\delta}{U_e^3}$
-2×10^{-3}
$\frac{d\left[\frac{1}{2}\overline{q^2v}\right]}{dy}\frac{\delta}{U_e^3}$
Asymmetric Wake
X=100 mm
358

FIG. 7.4

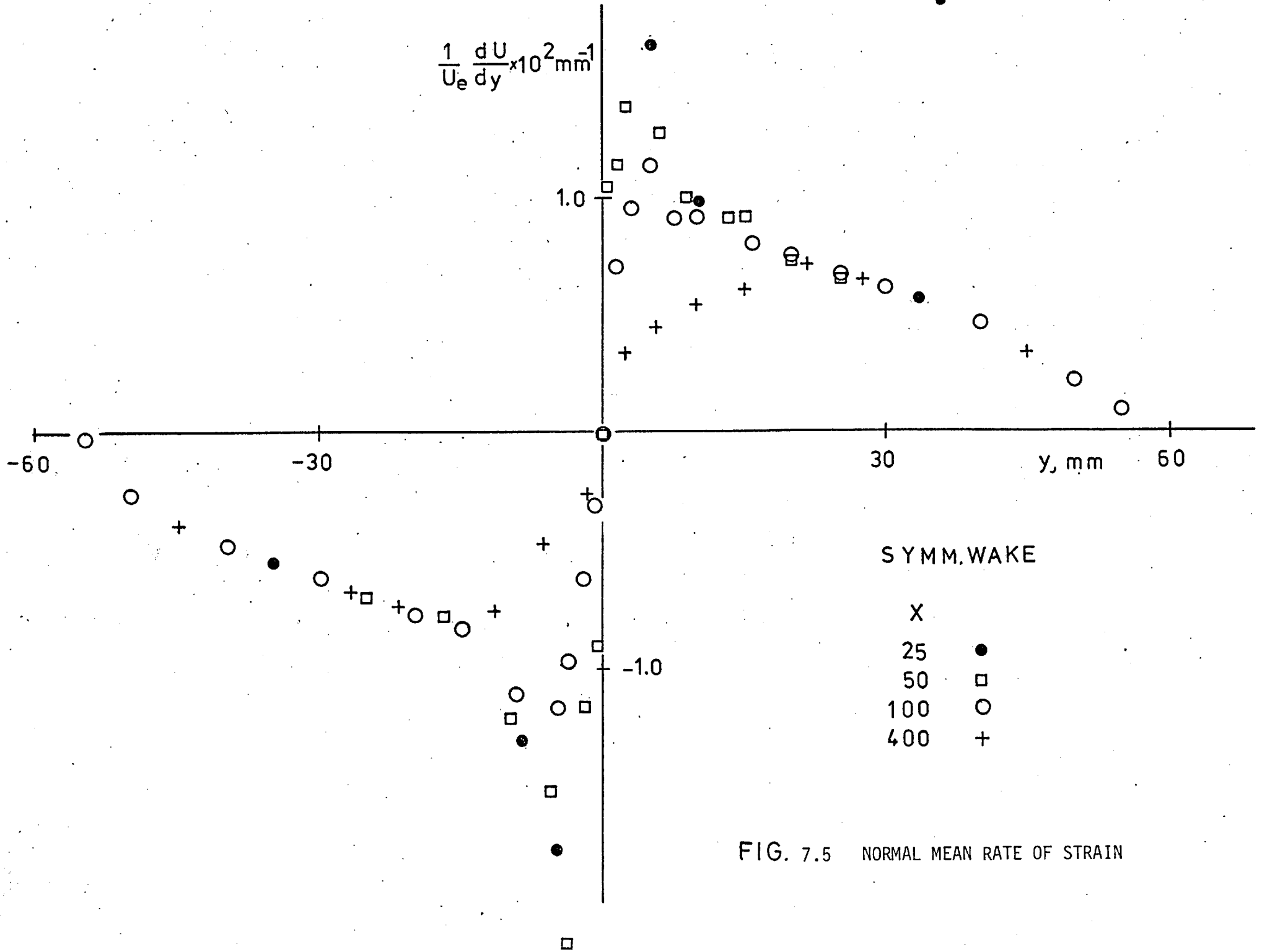

FIG. 7.5 NORMAL MEAN RATE OF STRAIN

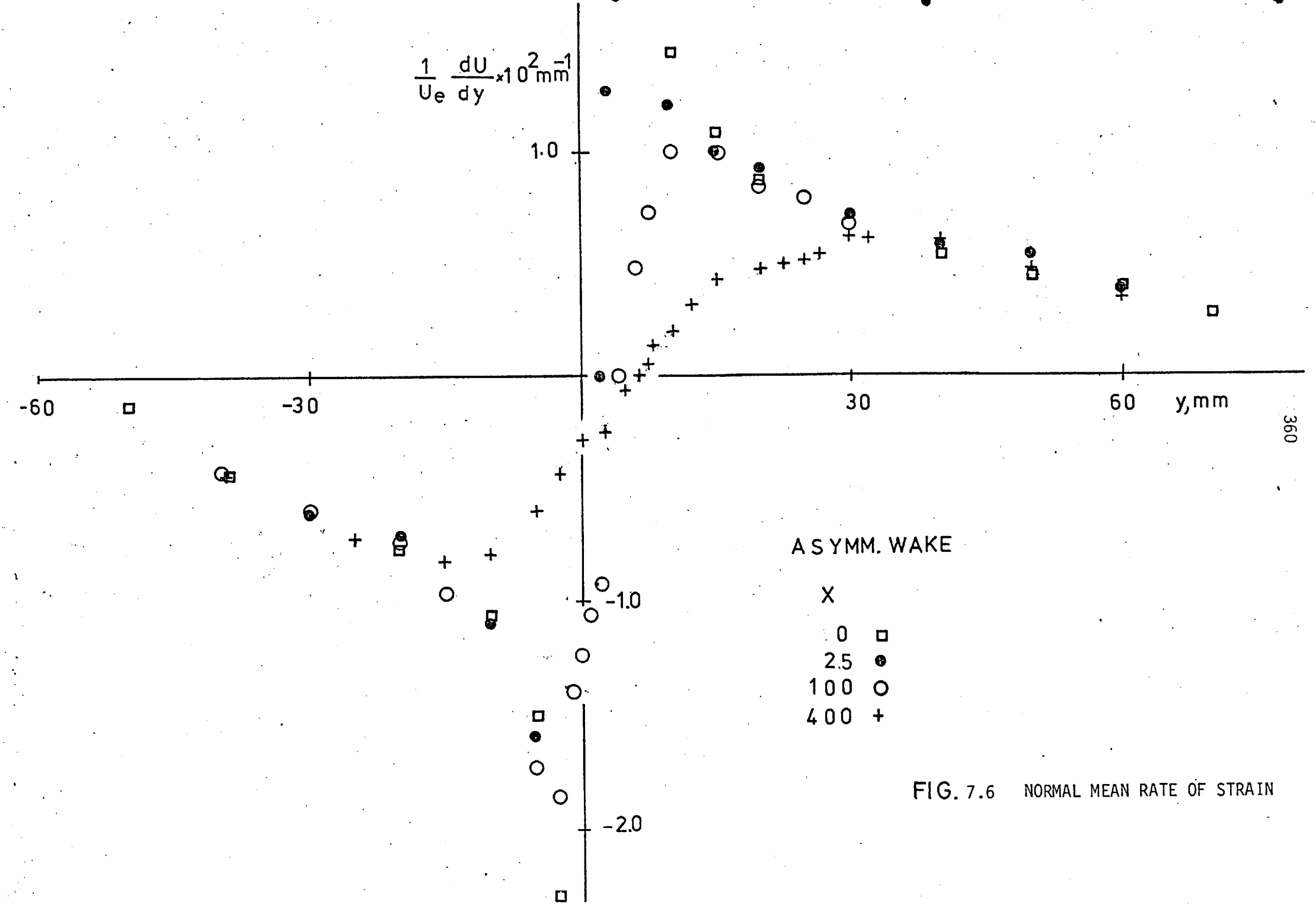

FIG. 7.6 NORMAL MEAN RATE OF STRAIN

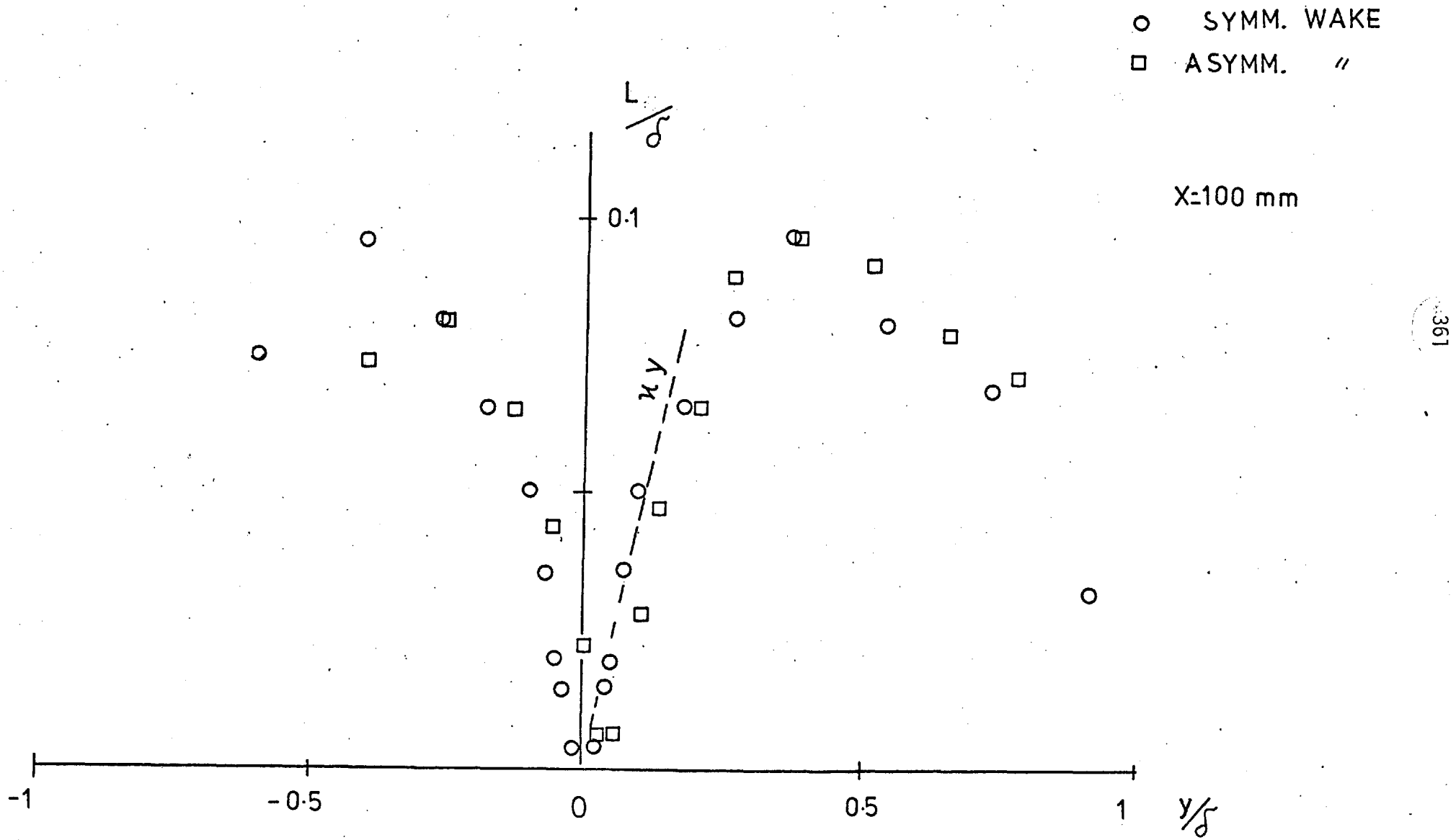

FIG. 7.7 LENGTH SCALE PROFILE

Symmetric Wake

△ Pressure rate of strain

□ Generation

○ Mean transport

● Turbulent transport

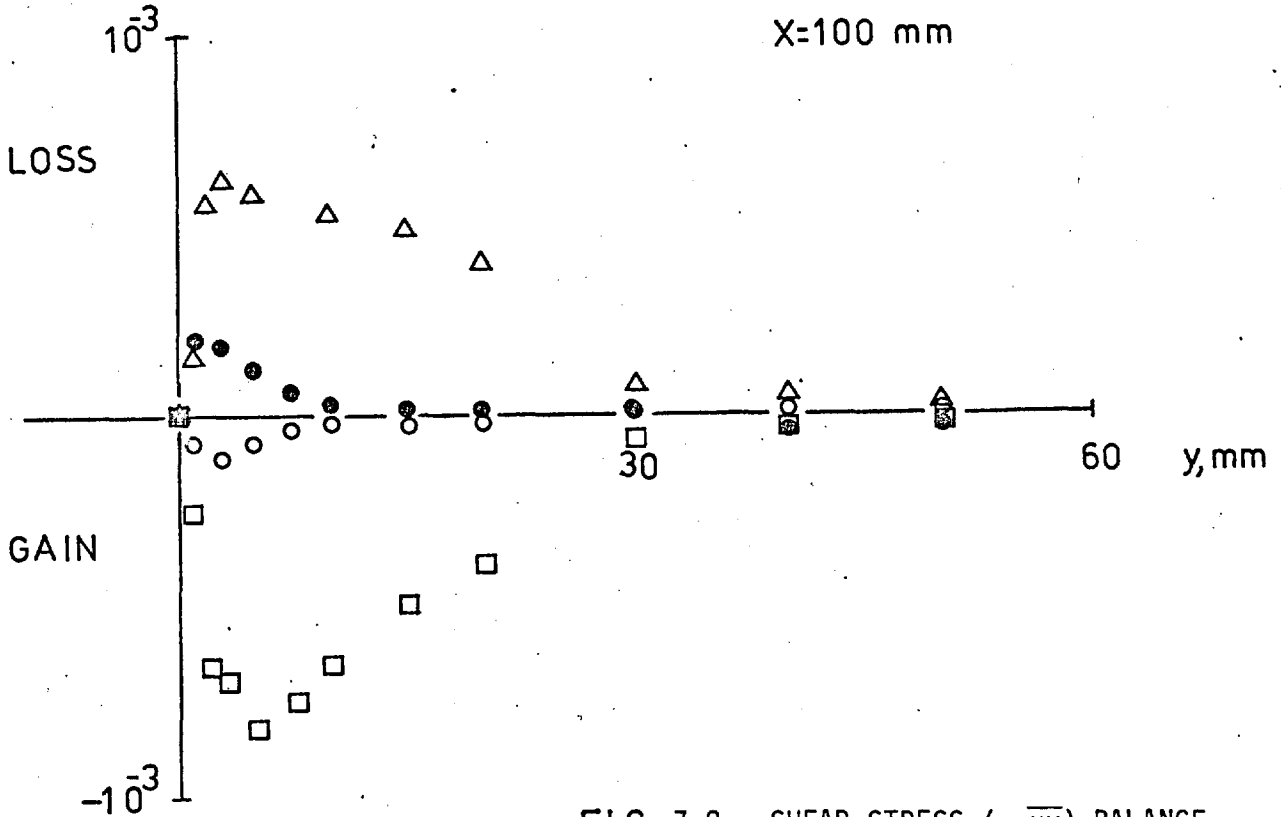

FIG. 7.8 SHEAR STRESS (- $\overline{uv}$) BALANCE

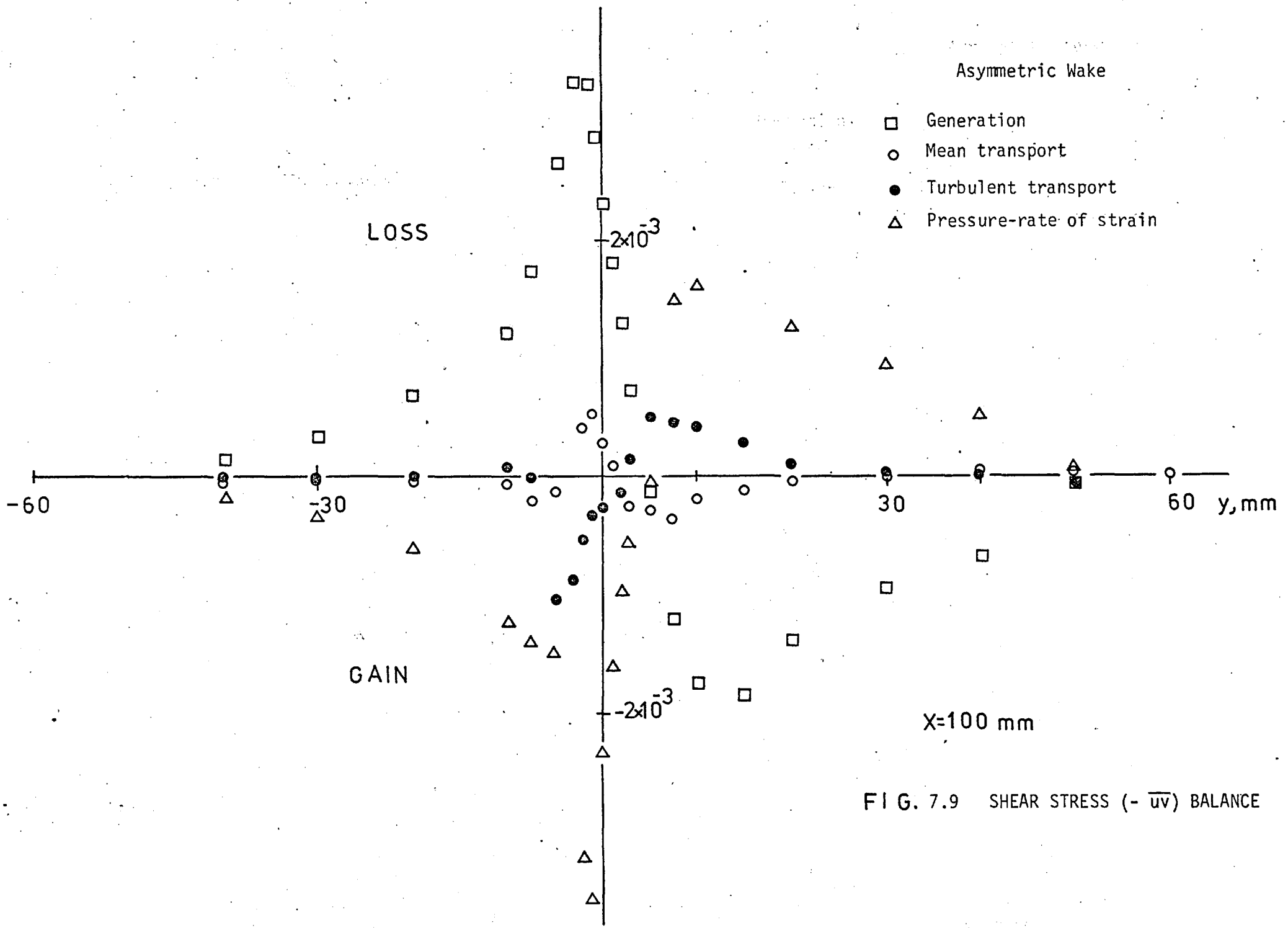

FIG. 7.9 SHEAR STRESS ($-\overline{uv}$) BALANCE

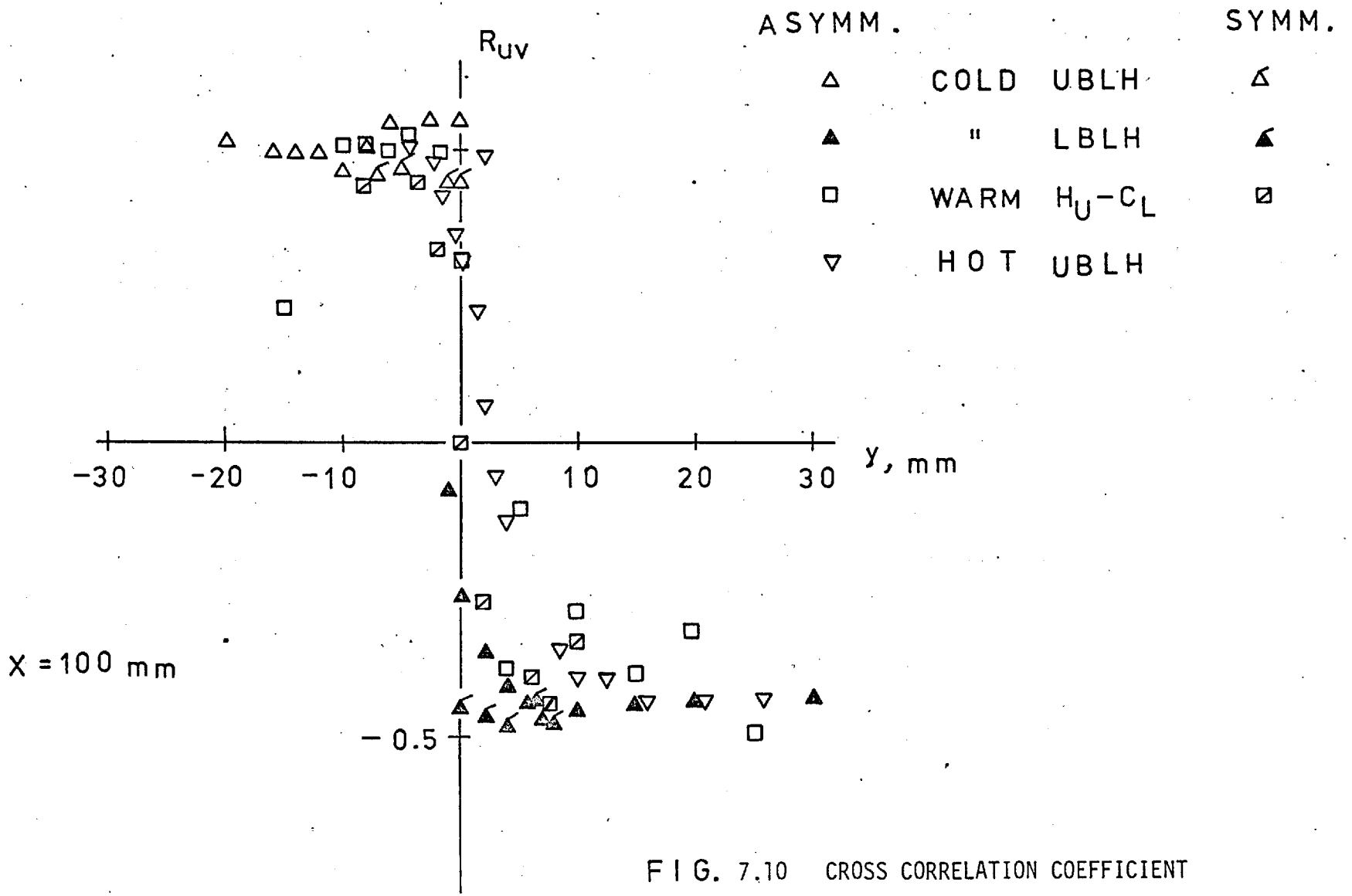

FIG. 7.10 CROSS CORRELATION COEFFICIENT

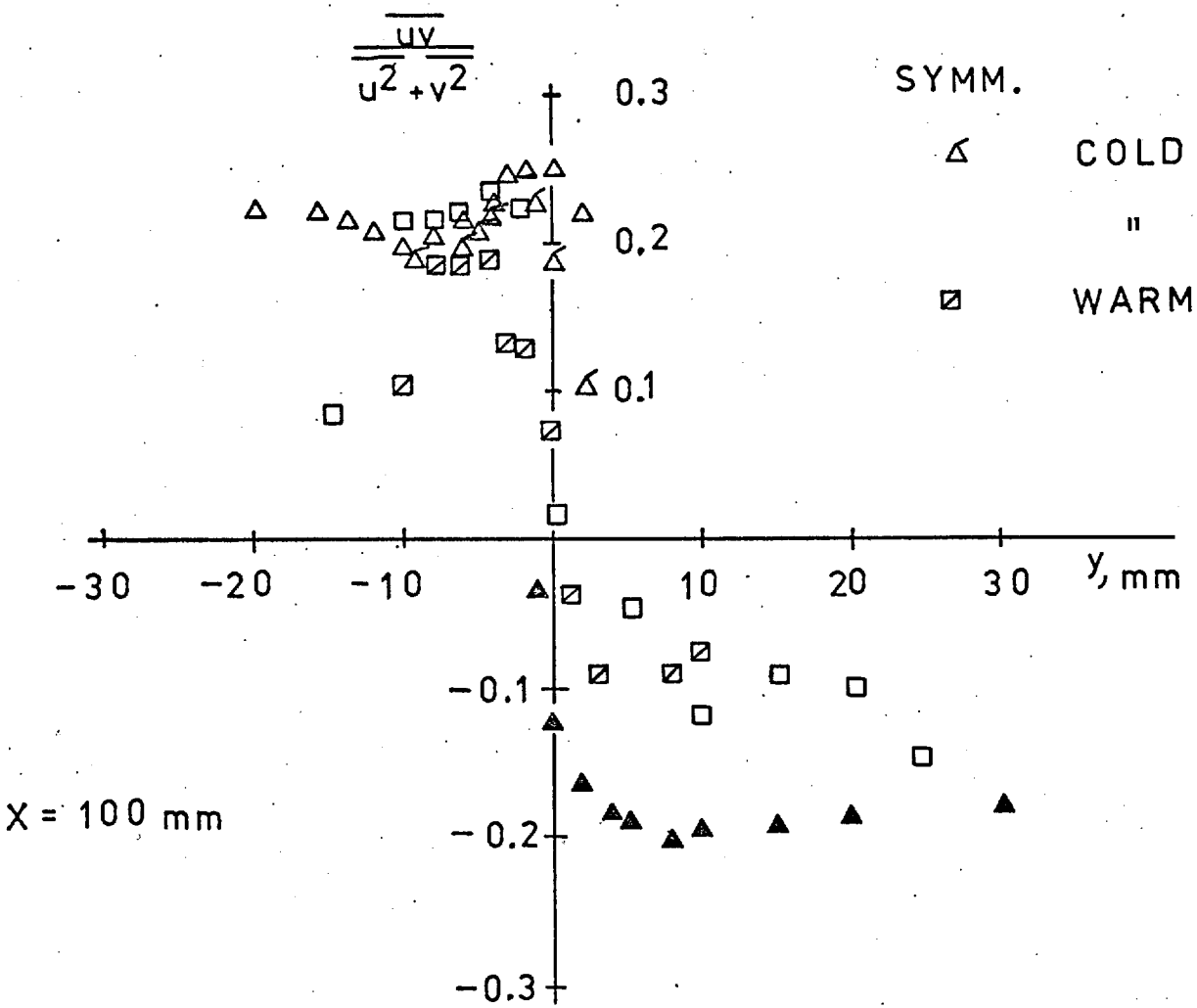

FIG. 7.11 $\frac{\overline{uv}}{\overline{u^2} + \overline{v^2}}$ PROFILE

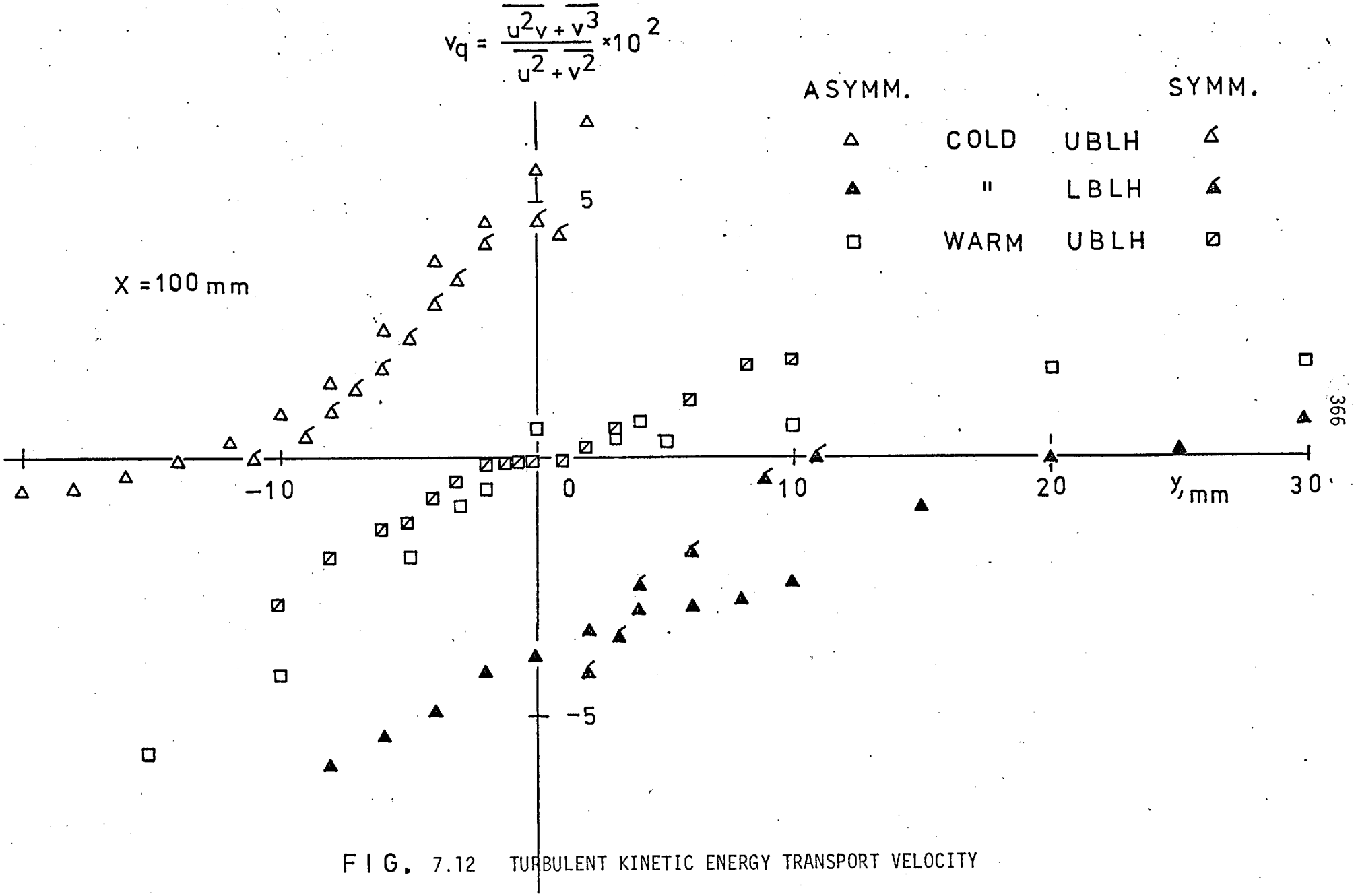

FIG. 7.12 TURBULENT KINETIC ENERGY TRANSPORT VELOCITY

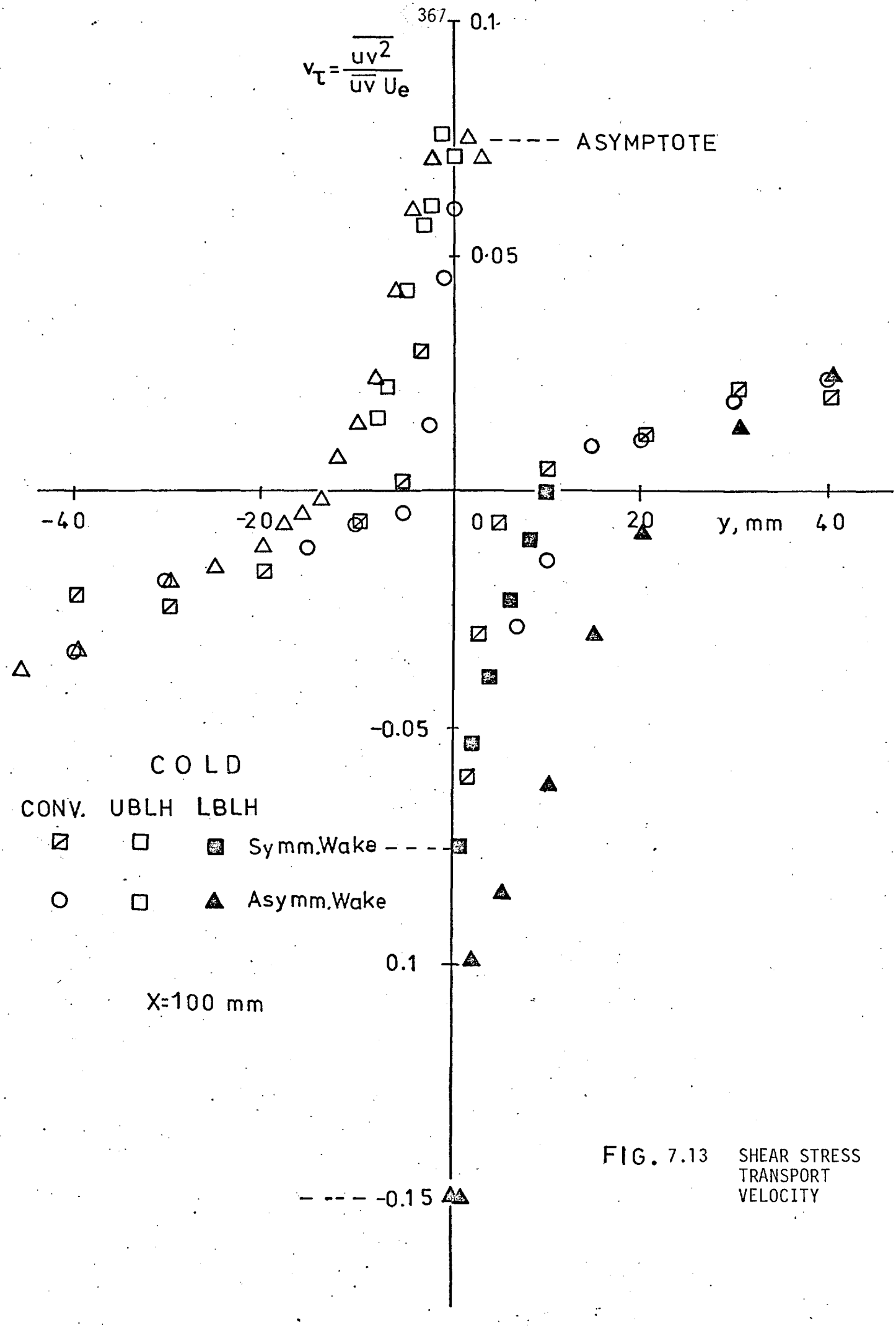

FIG. 7.13 SHEAR STRESS TRANSPORT VELOCITY

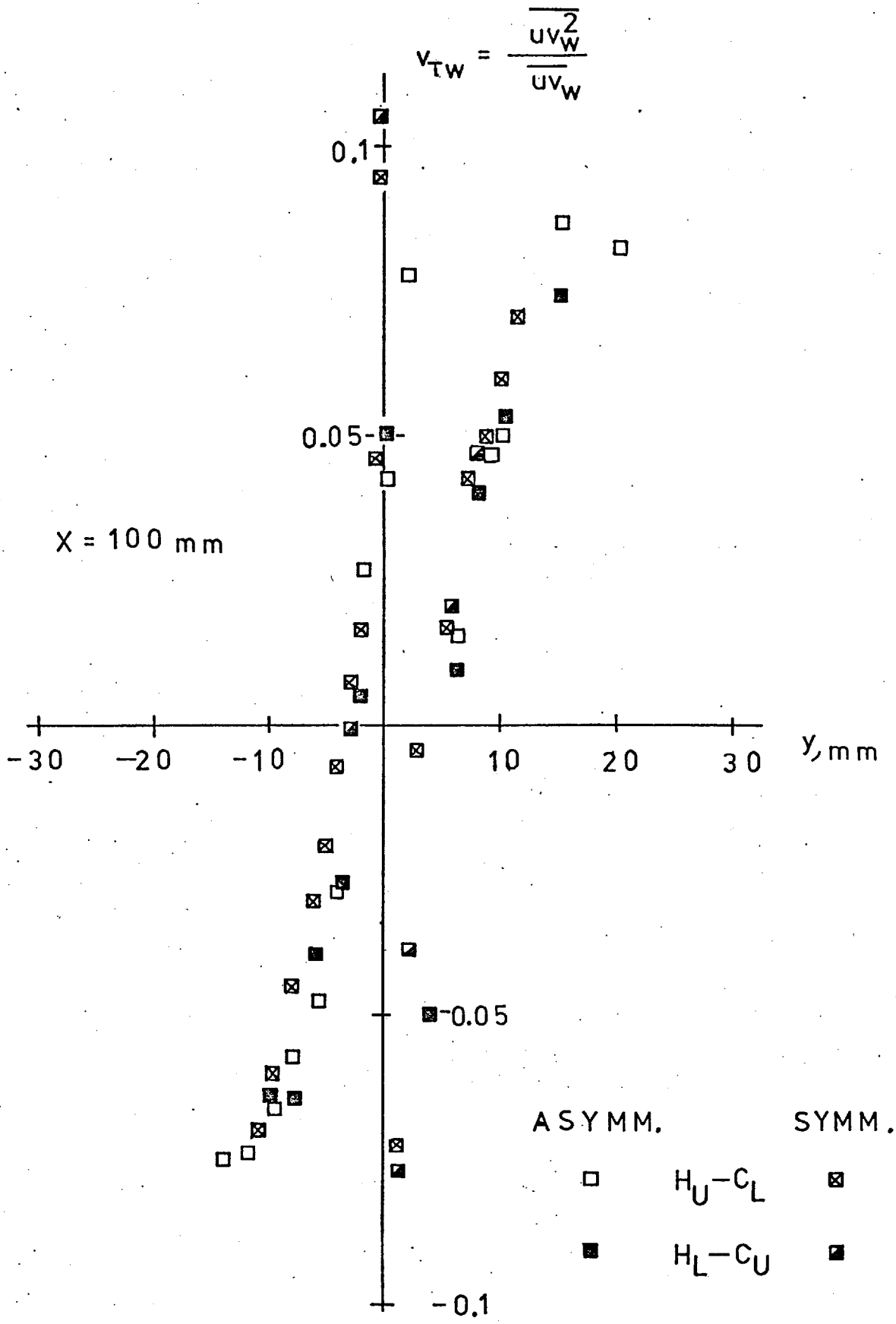

FIG. 7.14 WARM SHEAR STRESS TRANSPORT VELOCITY

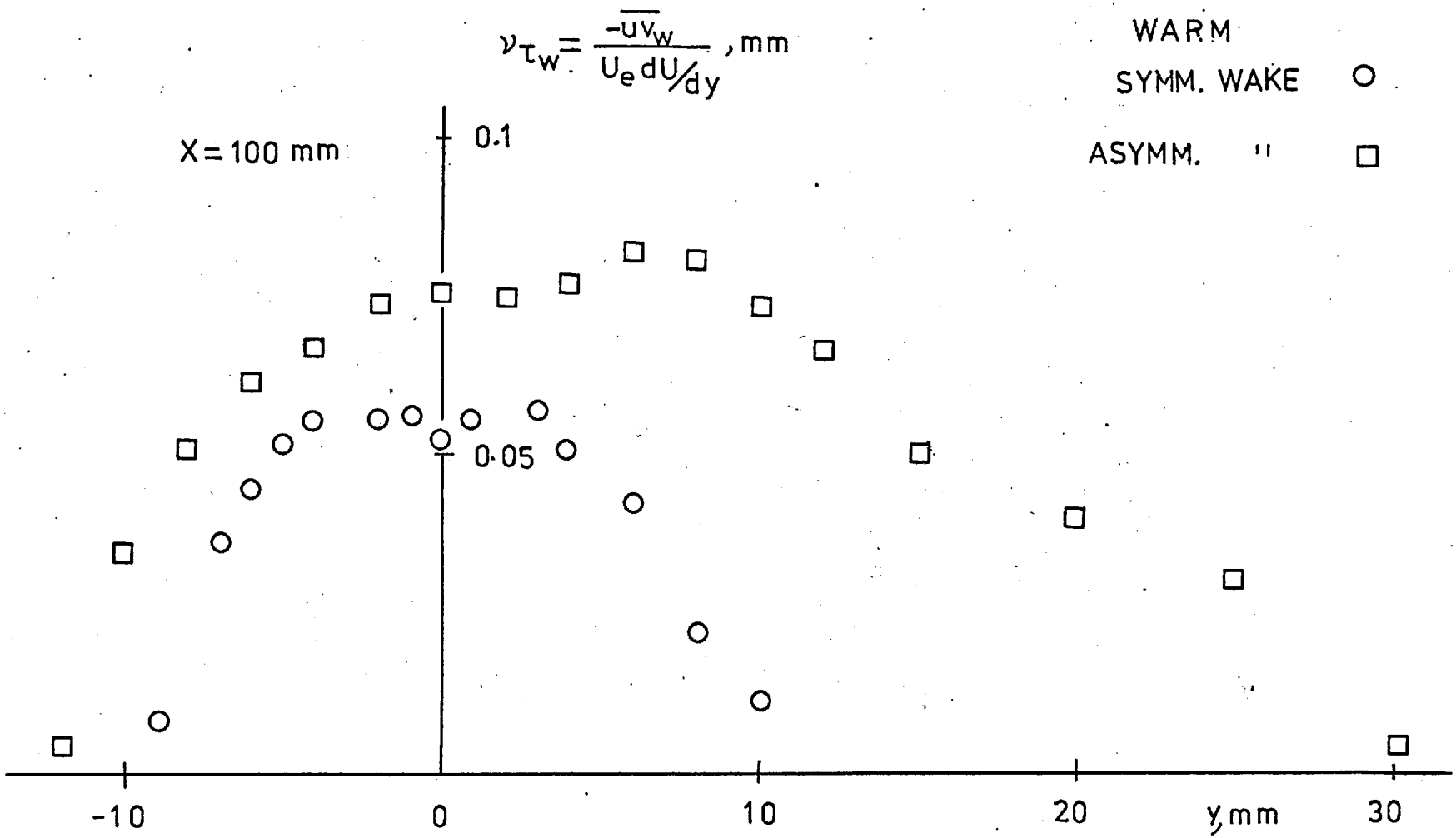

FIG. 7.15 WARM EDDY VISCOSITY

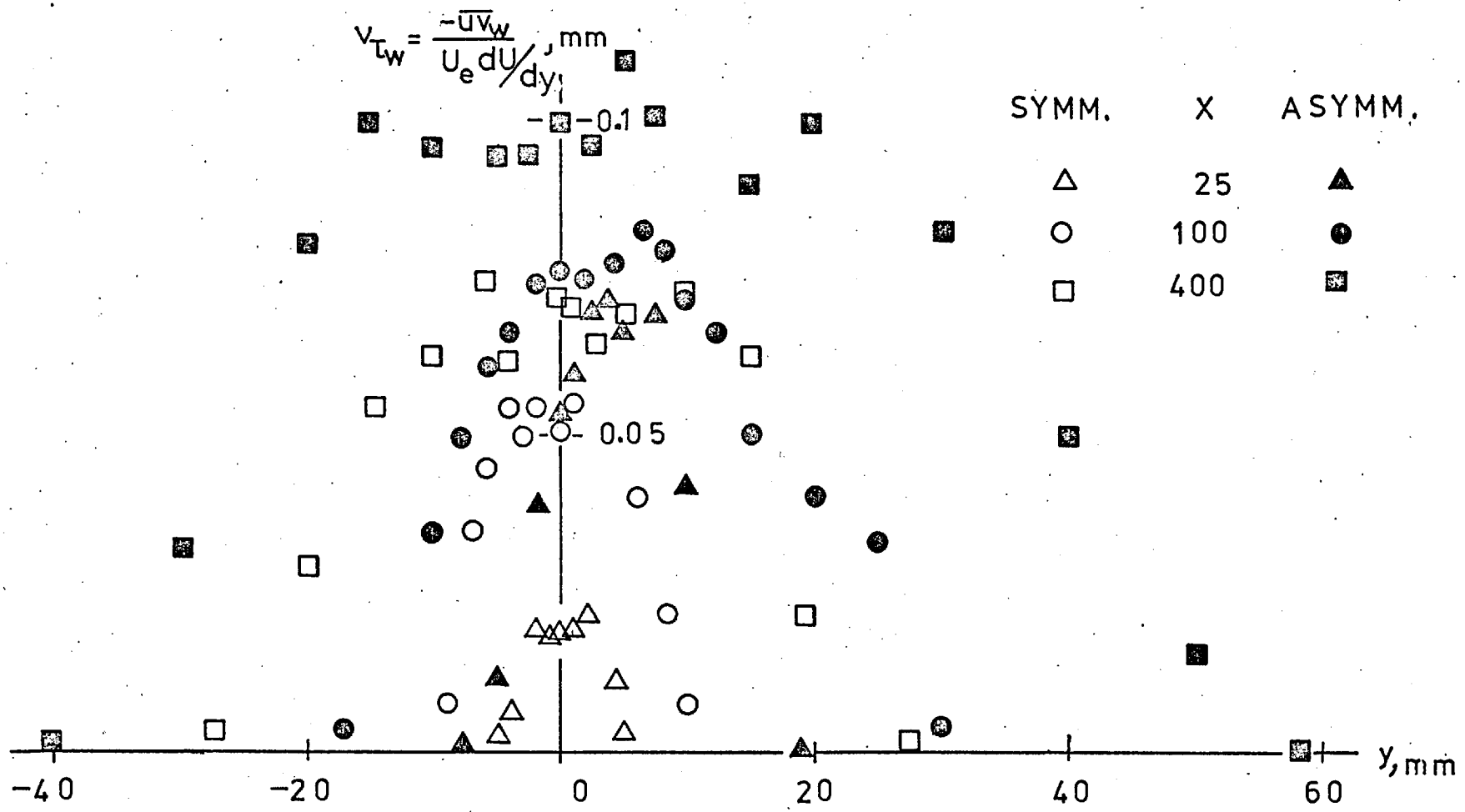

F I G. 7.16 WARM EDDY VISCOSITY

REFERENCES

AGRAWAL, M. L., PANDE, P. K. and PRAKASH, R. (1977)
"Study of the Turbulent Near Wake of a Flat Plate".
AIAA Journal, Vol. 15, No. 5, pp. 740-743.

ALEXOPOULOS, C. C. and KEFFER, J. F. (1968)
"The two dimensional turbulent wake in a stratified contaminant field".
UTME-TP6810 Dept. of Mech. Engng., University of Toronto.

ANTONIA, R. A., PRABHU, A. and STEPHENSON, S. E. (1975)
"Conditionally sampled measurements in a turbulent jet".
J. Fluid Mech., Vol. 72, pp. 455-480.

ANTONIA, R. A. and LUXTON, R. E. (1974)
"Characteristics of turbulence within an internal boundary layer".
Adv. Geoph. 18A, p. 263.

ANTONIA, R. A. (1974)
"The distribution of temperature in the intermittent region of a turbulent shear flow".
Proc. 5th Int. Heat Transfer Conf., Tokyo, Vol. 2, p. 95.

ANTONIA, R. A. and LUXTON, R. E. (1971)
"The response of a turbulent boundary layer to a step change in surface roughness: Part 1 Smooth-to-rough".
J. Fluid Mech., Vol. 48, pp. 721-762.

ANTONIA, R. A. and LUXTON, R. E. (1972)
"The response of a turbulent boundary layer to a step change in surface roughness: Part 2 Rough-to-smooth".
J. Fluid Mech., Vol. 53, pp. 737-757.

ANTONIA, R. A., DAHN, H. Q. and PRABHU, A. (1977)
"Response of a turbulent boundary layer to a step change in surface heat flux".
J. Fluid Mech., Vol. 80, pp. 153-177.

BEARMAN, P. W. (1971)
"Correction for the Effect of Ambient Temperature Drift on Hot-wire Measurements in Incompressible flows".
DISA INFORMATION, No. 11, May, 1971.

BEGUIER, C., FULACHIER, L., KEFFER, J. F. and DUMAS, R. (1975)
Comptes Rendus, B 280, 493.

BEGUIER, C., FULACHIER, L. and KEFFER, J. F. (1976)
J. Phys., 37, C1 - 187.

BRADSHAW, P., FERRISS, D. H. and ATWELL, N. P. (1967)
"Calculation of boundary layer development using the turbulent energy equation".
J. Fluid Mech., Vol. 28, pp. 593-616.

BRADSHAW, P. (1969)
"Calculation of boundary layer development using the turbulent energy equation. V. wakes near a trailing edge".
NPL Aero. Report, 1285.

BRADSHAW, P. (1971)
"An Introduction to Turbulence and its Measurement ".
Pergamon Press.

BRADSHAW, P., DEAN, R. B. and McELIGOT, D. M. (1973)
"Calculation of Interacting Turbulent Shear layers: Duct Flow".
J. Fluids Engng., Trans. ASME, 95, pp. 241-260.

BRADSHAW, P. and MURLIS, J. (1974)
"On the measurement of Intermittency in Turbulent Flow".
Imperial College Aero. Report, No. 74-04.

BRADSHAW, P. and UNSWORTH, K. (1974)
"An improved fortran program for the Bradshaw Ferris-Atwell method of calculating turbulent shear layers".
Imperial College Aero. Report, 74-02.

BRADSHAW, P. (1975)
"The Imperial College Aero. Dept. Digital Magtape Data Logging System".
Imperial College Aero. TN 72-101.

BRADSHAW, P. (1975)
"Review-Complex Turbulent Flows".
J. of Fluid Eng., Vol. 97, 146.

CASTRO, I. P.
"A highly distorted turbulent free shear layer".
Ph.D. Thesis, Imperial College, University of London.

CHAMPAGNE, F. H., SCHLEICHER, C. A. and WEHRMANN, O. H. (1967)
"Turbulence measurements with inclined hot wires".
Parts 1 and 2, J. Fluid Mech., Vol. 28, pp. 153-193.

CHANDRSUDA, C.
"A reattaching turbulent shear layer in incompressible flow".
Ph.D. Thesis, Imperial College, University of London.

CHEVRAY, R. and KOVASZNAY, L. S. G. (1969)
"Turbulent measurements in the wake of a thin flat plate".
TN AIAA Journal, Vol. 7, No. 8, p. 1641.

CHEVRAY, R. and TUTU, N. K. (1972)
"Simultaneous measurements of Temperature and Velocity in heated flows".
Rev. Sci. Instr., Vol. 43, 1417.

CHEVRAY, R. and TUTU, N. K. (1976)
"Kinematic and thermal structures of a round heated jet".
Symposium on Turbulent Shear Flows, Pen. State Conference, April 18 - 20, 1977.

COLEMAN, H. W., MOFFAT, R. T. and KAYS, W. M. (1977)
"The accelerated fully rough turbulent boundary layer".
J. Fluid Mech., Vol. 82, pp. 507-528.

COLES, D. E. (1968)
"Data tabulation in Proc. AFOSR-IFP Stanford Conference on computation of turbulent boundary layers", Thermosci. divn, Stanford Univ.

CORRSIN, S. (1943)
"Investigation of flow in an axially symmetrical heated jet".
NACA Rep. No. W-94.

CORRSIN, S. (1949)
"Extended amplications of the hot wire anemometry".
NACA TN 1864.

CORRSIN, S. and KISTLER, A. L. (1954)
"Free stream boundaries of turbulent flows".
NACA TN 3133.

CORRSIN, S. and UBEROI, M. S. (1949)
"Sectra and diffusion in a round turbulent jet".
NACA TN 2124.

CORRSIN, S. (1952)
"Heat Transfer in Isotropic Turbulence".
J. of Applied Physics, Vol. 23, pp. 113-118.

DEAN, R. B. and BRADSHAW, P. (1976)
"Measurements of interacting shear layers in a duct".
J. Fluid Mech., Vol. 78, pp. 641-676.

FABRIS, G. (1976)
"Turbulent temperature and thermal flux characteristics in the wake of a cylinder".
Symposium on Turbulent Shear Flows, Penn. State Conference, April 18 - 20, 1977.

FIEDLER, H. and HEAD, M. R. (1966)
"Intermittency measurements on the turbulent boundary layer".
J. Fluid Mech., Vol. 25, pp. 719-735.

FRIEHE, F. H. and SCHWARZ, W. H. (1968)
"Deviation from cosine law for yawed cylindrical anemometer sensors".
Trans. ASME, 35E, 655.

FULACHIER, L. and DUMAS, R. (1976)
"Spectral analogy between temperature and velocity fluctuations in a turbulent boundary layer".
J. Fluid Mech., Vol. 77, pp. 257-277.

FULACHIER, L. and BEGUIER, C. (1977)
"Interpretation of negative production of temperature fluctuations by spectral analysis".
Symposium on Turbulent Shear Flows, Penn. State Conference, April 18 - 20, 1977.

GIBSON, M. M. and LAUNDER, B. E. (1976)
"On the Calculation of Horizontal, Turbulent, Free Shear Flows Under Gravitational Influence".
Trans. ASME, 98C, 81.

HANCOCK, P. E. (1978)
"The effects of free stream turbulence on turbulent shear layers".
Ph.D. Thesis, Imperial College, University of London.

HANJALIC, K. and LAUNDER, B. E. (1972a)
"Fully developed asymmetric flow in a plane channel".
J. Fluid Mech., Vol. 51, pp. 301-335.

HANJALIC, K. and LAUNDER, B. E. (1972b)
"A Reynolds stress model of turbulence and its application to thin shear flows".
J. Fluid Mech., Vol. 52, pp. 609-638.

JOHNSON, D. S. (1959)
"Velocity and Turbulence Fluctuation Measurements in a Turbulent Boundary Layer Downstream of a Stepwise Discontinuity in Wall Temperature".
J. of Applied Mechanics, Trans. ASME, Vol. 81, pp. 325-336.

KIM, H. T., KLINE, S. J. and REYNOLDS, W. C. (1971)
"The production of turbulence near a smooth wall in a turbulent boundary layer".
J. Fluid Mech., Vol. 50, pp. 133-160.

KLEBANOFF, P. S. (1955)
"Characteristics of turbulence in a boundary layer with zero pressure gradient".
NACA Rep. N. 1247.

KOVASZNAY, L. S. G. and ALI, F. (1974)
"Structure of the turbulence in the wake of a heated flat plate".
Proceeding of Fifth Int. Heat Transfer Conf., II, 99, Tokyo.

LA RUE, J. C. (1973)
"The Temperature Characteristics in the Turbulent Wake".
Ph.D. Thesis, University of California at San Diego.

LAUNDER, B. E. (1976)
"Heat and Mass Transport".
Topics in Applied Physics, Vol. 12, Editor: P. Bradshaw, Springer-Verlag.

LAUNDER, B. E., REECE, G. J. and RODI, W. (1975)
"Progress in the development of a Reynolds-stress turbulence closure".
J. Fluid Mech., Vol. 67, pp. 537-566.

LAWN, C. J. (1971)
"Turbulent temperature fluctuations in liquid metals".
Int. J. Heat Mass Transfer, Vol. 20, pp. 1035-1044.

LEUCHTER, O. (1976)
"The Effects of Freestream Turbulence and Initial Boundary Layers on the

Development of Turbulent Mixing Layers".
Project SQUID Workshop: Turbulence in internal flows by S. N. B. Murthy, Hemisphere Publishing Corporation.

LU, S. S. and WILLMARTH, W. W. (1973)
"Measurements of the Structure of Reynolds stress in a turbulent boundary layer".
J. Fluid Mech., Vol. 60, pp. 481-511.

MASUDA, S., SASAKI, N., ARIGA, I. and WATANABE, I. (1972)
"Effects of Free Stream Velocity Profile on Turbulent Boundary layer, with some Reference to the Effects of Free Stream Turbulence".
The Second Intern. JSME Symposium Fluid Machinery and Fluidics.

MOREL, T. (1972)
"Calculation of the free turbulent mixing:interaction approach".
Ph.D. Thesis, Illinois Institute of Technology.

NG, B. S. and HUFFMAN, G. D. (1976)
"The Modelling of a Turbulent Near Wake Using the Interactive Hypothesis".
Project SQUID Workshop: Turbulence in internal flows by S. N. B. Murthy, Hemisphere Publishing Corporation.

PALMER, M. D. and KEFFER, J. F. (1972)
"An experimental investigation of an asymmetrical turbulent wake".
J. Fluid Mech., Vol. 53, pp. 593-610.

PERRY, A. E. and JOUBERT, P. N. (1963)
"Rough wall boundary layers in adverse pressure gradients".
J. Fluid Mech., Vol. 17, pp. 193-211.

PIMENTA, M. M. (1975)
Ph.D. Thesis, Mech. Engng. Dept., Stanford University.

REICHARDT, H. (1941)
"Gesetzmässigkeit der freien Turbulenz".
Z. angew. Math. und Mech., 21, pp. 257-264.

SMITS, A. (1974)
"Further developments of hot wire and layer methods in fluid mechanics".
Ph. D. Thesis, University of Melbourne.

TOYODA, K. and HIRAYAMA, N. (1975)
"Turbulent Near Wake of a Flat Plate".
Bulletin of the JSEM, Vol., 18, No. 120, pp. 605-611.

TOWNSEND, A. A. (1976)
"The Structure of Turbulent Shear Flow".
Cambridge University Press.

WALLACE, J. M., ECKELMANN, H. and BRODKEY, R. S. (1972)
"The wall region in turbulent shear flow".
J. Fluid Mech., Vol. 54, pp. 39-48.

WEIR, A. D. (1976)
"Program TUVTER: An Aid to Selecting Intermittency Criterion".
Imperial College Aero. TN76-103, Algorithm.

WEIR, A. D. and BRADSHAW, P. (1974)
"Apparatus and programs for digital analysis of fluctuating quantities in turbulent flow".
Imperial College Aero. Report, 74-09.

WEIR, A., WOOD, D. and BRADSHAW, P. (1978)
"Interacting turbulent shear layers in a plane jet".
To be submitted to J. Fluid Mech.

WYNGAARD, J. C. (1971)
"The effect of velocity sensitivity on temperature derivative statistics in isotropic turbulence".
J. Fluid Mech., Vol. 48, pp. 763-769.

APPENDIX A

HOT WIRE CALIBRATIONS

1. Velocity Calibration

A hot wire, operating at constant temperature mode, usually obeys the King's law:-

$$Nu = A + B' Re^n$$

where:-

$$Nu = \frac{H_f/\ell}{\pi k_f (T_w - T_f)} \qquad Re = \frac{Ud_w}{\nu}$$

to good accuracy over the 2 : 1 velocity range covered by the present measurements.

Since the heat transfer rate is proportional to the electric power input to the wire, we finally obtain:-

$$E^2 = E_o^2 + BU^n$$

A value of $n = 0.45$, adequate for U less than 50 ms^{-1}, was used.

2. Yaw Calibration

When a hot wire is at an angle ψ to the flow and assuming the validity of the "cosine law" to a first approximation, the effective cooling velocity will be:-

$$U_{eff} = U \cos \psi$$

In fact the cosine law is not an adequate approximation as shown by Champagne et al (1967) and Friehe et al (1968), who pointed out that the cooling of the wire by the velocity component parallel to the wire is significant. Also, it is rather difficult to measure wire angles to good accuracy.

In the following method, as described by Bradshaw (1971), these problems are solved by determining an "effective" angle of the wire, not necessarily coinciding with the geometrical angle.

If ψ_1 and ψ_2 are the effective angles of wires 1 and 2 respectively and δ is the yaw angle, then:-

$$E_1^2 = E_{01}^2 + B_1 \left[U \cos (\psi_1 + \delta) \right]^n$$

$$E_2^2 = E_{02}^2 + B_2 \left[U \cos (\psi_2 + \delta) \right]^n$$

Assuming that E_{01} and E_{02} do not change with δ, for $\delta = 0$ we obtain:-

$$E_{1\,\delta=0}^2 = E_{01}^2 + B_1 \left[U \cos \psi_1 \right]^n$$

$$E_{2\,\delta=0}^2 = E_{02}^2 + B_2 \left[U \cos \psi_2 \right]^n$$

and so:-

$$\frac{\cos (\psi_1 + \delta)}{\cos \psi_1} = \left[\frac{E_1^2 - E_{01}^2}{E_{1\,\delta=0}^2 - E_{01}^2} \right]^{\frac{1}{n}}$$

and:-

$$\frac{\cos(\psi_2 - \delta)}{\cos \psi_2} = \left[\frac{E_2^2 - E_{02}^2}{E_{2\,\delta=0}^2 - E_{02}^2}\right]^{\frac{1}{n}}$$

or, finally:-

$$\cos \delta - \left[\frac{E_1^2 - E_{10}^2}{E_{1\,\delta=0}^2 - E_{10}^2}\right]^{\frac{1}{n}} = \tan \psi_1 \sin \delta$$

$$\cos \delta - \left[\frac{E_2^2 - E_{20}^2}{E_{2\,\delta=0}^2 - E_{20}^2}\right]^{\frac{1}{n}} = \tan \psi_2 \sin \delta$$

Thus, knowing E_{01}^2 and E_{02}^2 from the velocity calibration and plotting the left hand side of the last equations against sin δ, for various small values of the angle δ, gives usually a straight line through the origin with slope tan ψ_1 or tan ψ_2. Typical examples of velocity and yaw calibrations are shown in Figs. A1 and A2. All the constants have been derived by a least-square fitting to a straight line.

Useful comments on the limitations and errors of the above technique are given by Castro (1973).

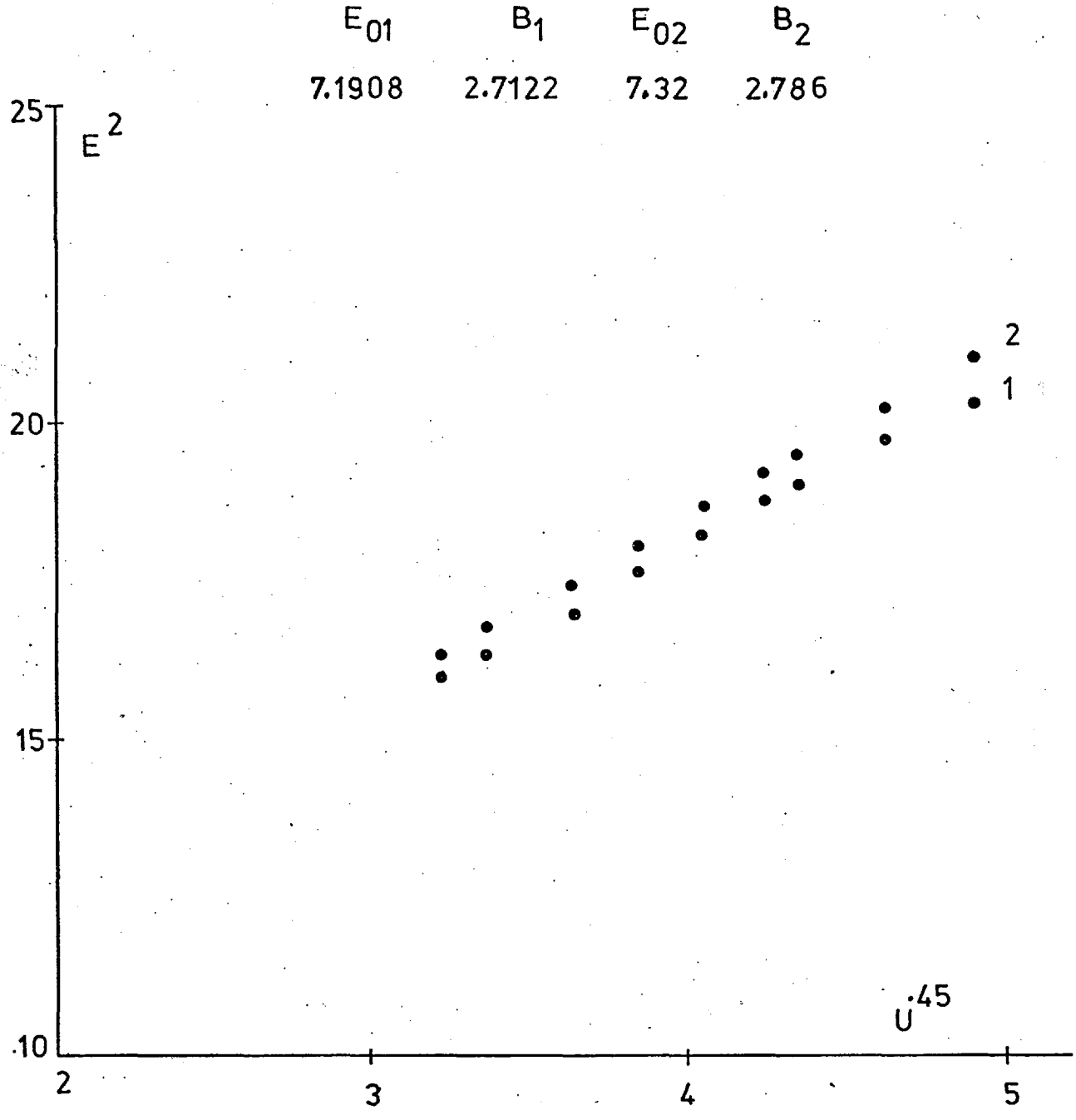

FIG. A.1

TYPICAL VELOCITY CALIBRATION OF x-WIRE

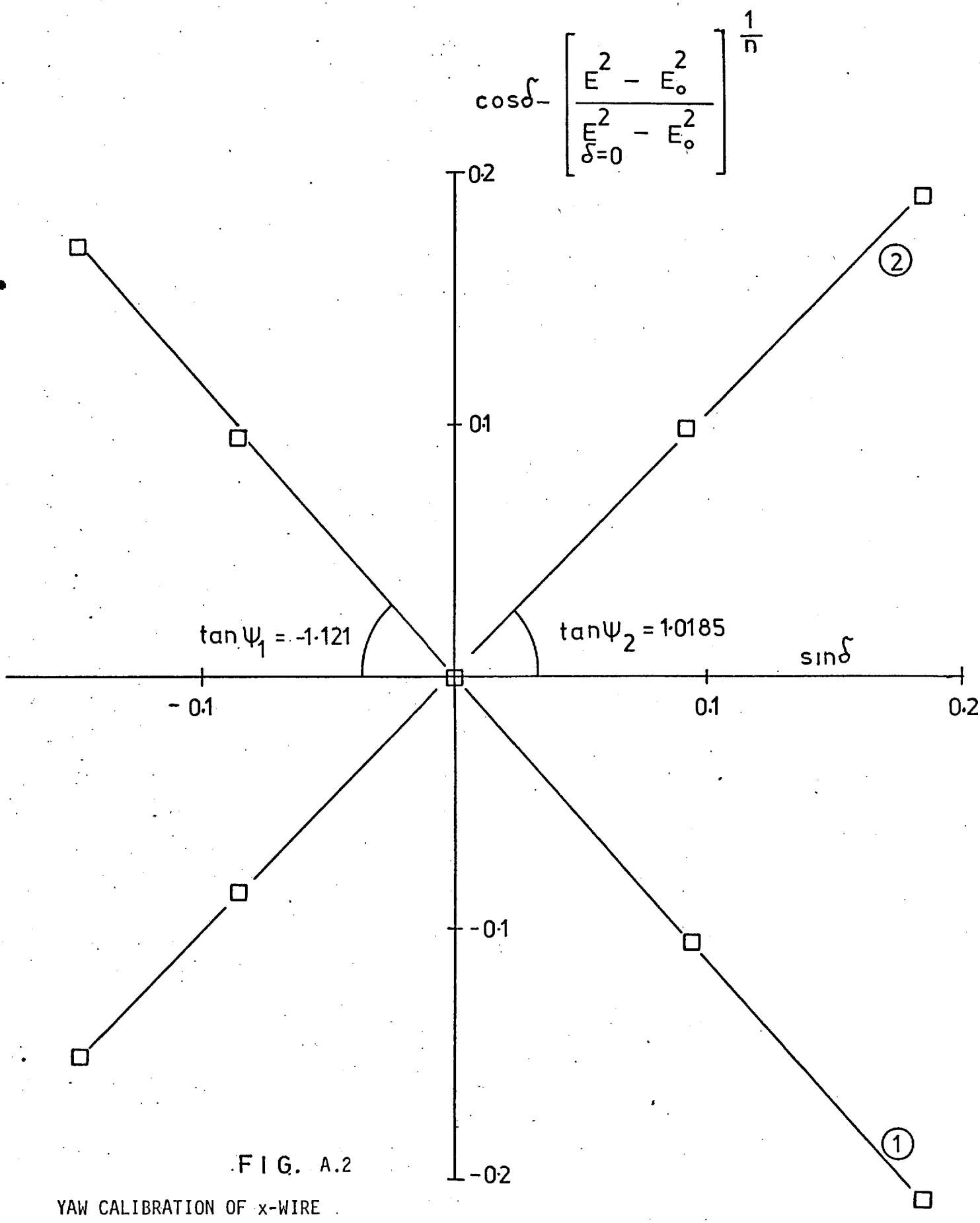

FIG. A.2

YAW CALIBRATION OF x-WIRE

APPENDIX B

TEMPERATURE FLUCTUATIONS

The circuit used is shown in Fig. B.1a. The probe current is $I = E_i/(R + R_w)$, but since $R_w \ll R$, $I \simeq E_i/R$ is independent of R_w. (Typical values of R_w are between 50 and 90 Ω for 1 μm wire of 0.8 - 1 mm length).

The voltage across the "cold" wire operating in constant current mode is:-

$$E = I R_w$$

and so any variation in R_w will cause a small variation in E:-

$$\Delta E = I \Delta R_w$$

If the variations in E are due to variations of the temperature of the wire only, then:-

$$\Delta R_w = - \alpha R_w \Delta T$$

where α is the temperature resistivity of the platinum wire. So:-

$$\Delta E = - I \alpha R_w \Delta T$$

For small ΔT:-

$$e = - I \alpha R_w \theta$$

or:-

$$e = \beta\theta$$

The determination of the constant β can be done either by the calculation $\beta = I\,\alpha R_w$ or by measuring the voltage decrease ΔE due to a temperature increase ΔT. During the present investigation, both methods gave good agreement.

The Problem of Velocity Fluctuation

Corrsin (1949) first expressed the relation:-

$$\Delta E = \frac{\partial E}{\partial T}\Delta T + \frac{\partial E}{\partial U}\Delta U$$

where $\partial E/\partial T$ and $\partial E/\partial U$ are the temperature and the velocity sensitivities of the wire.

If $\partial E/\partial T\ \Delta T >> \partial E/\partial U\ \Delta U$, then the velocity fluctuations do not contribute to the ΔE. In fact here for typical values $R_w = 60\ \Omega$ $I = 1.6$ mA and $\partial R/\partial U = 0.0005\ \Omega/(m/s)$, see Fig. B.1b.

$$\frac{\partial E}{\partial U} = I\,\frac{\partial R}{\partial U} = 0.0008 \text{ mv/m/sec}$$

$$\frac{\partial E}{\partial T} = \alpha I\, R_w = 0.374 \text{ mv/}^{o}\text{C}$$

so:-

$$\frac{\partial T}{\partial U} = \frac{\partial E}{\partial U} \Big/ \frac{\partial E}{\partial T} = 2.13 \times 10^{-3}\ ^{o}\text{C/m/s}$$

and for typical $\Delta U = \sqrt{\overline{u^2}_{max}} = 2.3$ m/sec

$$\Delta T = \sqrt{\overline{\theta^2}_{max}} = 0.45\ ^{o}C$$

the error is 1%.

In the asymmetric wake, the turbulence intensity increased by a factor of $\sqrt{C_{f_r}/C_{f_s}} \simeq \sqrt{2} = 1.4$ and, hence, the wire current was reduced to $\sim$ 1 mA, although some runs with I = 1.6 mA gave closely the same results.

Another estimate of the relative sensitivity can be obtained by using Wyngaard's (1971) formula:-

$$c = \frac{\overline{I}^2\ \overline{R}_w\ (0.25\ Re^{.45})}{\pi\ k_f\ \ell\ \overline{U}_1\ (0.24 + 0.56\ Re^{.45})^2} \qquad \left(\frac{^{o}C}{m/s}\right)$$

where:-

c	is the relative sensitivity $\partial T/\partial U$
Re	is the Reynolds number on wire diameter
ℓ	is the wire's length
k_f	is the thermal conductivity of air $\left(0.025\ \frac{A^2 \times \Omega}{m\ ^{o}C}\right)$
R_w	is the resistance of wire
$\overline{U}_1$	is the mean velocity

The result is about twice the previously measured value and has still negligible effects. The same order of difference is in Wyngaard's comparisons between measured and estimated values. He also pointed out that moments of temperature up to second order are hardly affected by velocity sensitivity.

The mean temperature was obtained by directly measuring the mean voltage across the wire with a digital voltmeter.

All the "grounds" were connected at the same mains earth to eliminate noise due to ground loops. The autotransformers powering the boundary layer heating wires were plugged to the mains quite separately from all the other instruments, since sometimes they produced hum on the velocity and temperature signals of 50 or 100 Hz. The traverse gear system was also earthed. Special arrangements were made to eliminate the spikes on the temperature signal caused by the nearby thyristors in the control cubicle of the tunnel motor. With all these precautions to minimise the effect of noise spikes or hum, it was not necessary to filter the temperature signal after the preamplifier. (A low pass filter with an equivalent real-time cutoff of 20 kHz was used to remove noise from the analogue tape recorder signal when digitizing).

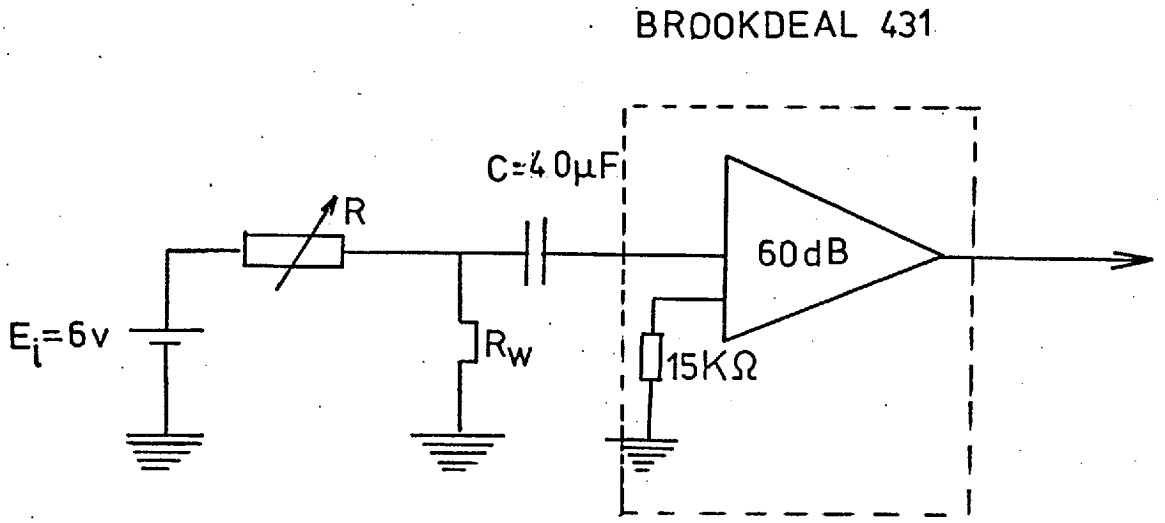

FIG. B.1a CONSTANT CURRENT ANEMOMETER

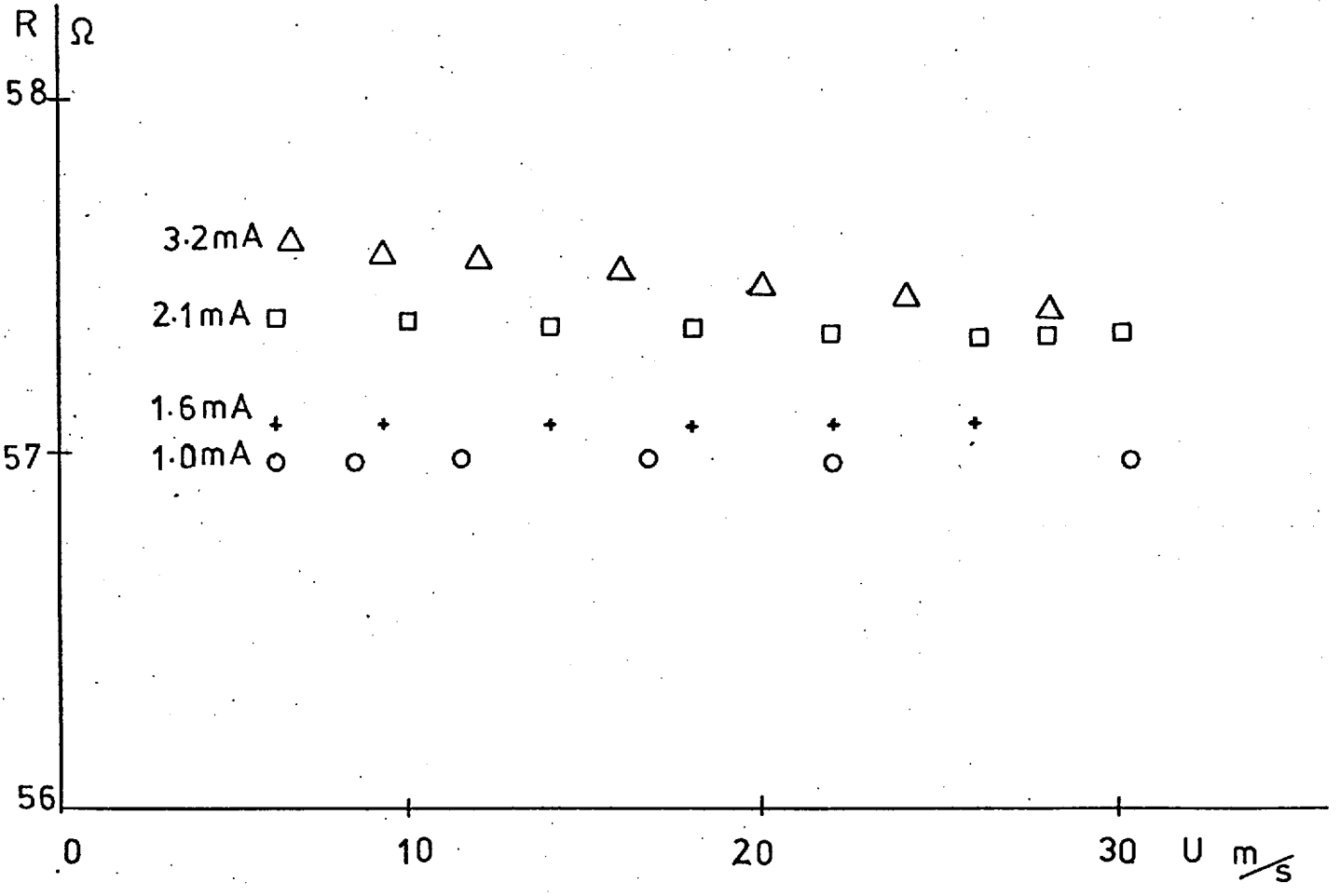

FIG. B.1b

VELOCITY CALIBRATION OF TEMPERATURE WIRE

APPENDIX C

TEMPERATURE CORRECTIONS OF HOT WIRE SIGNALS

The corrections, due to changes of the fluid temperature, are according to Dean and Bradshaw (1976). By using the Nusselt number definition and demanding it not to vary with the fluid temperature T_f, they derived:-

$$\frac{\Delta E}{E} = -\frac{1}{2}\frac{\Delta\theta}{T_w - T_f}$$

where $\Delta\theta$ is the temperature change in the fluid and ΔE, the "error" voltage.

This expression is equivalent to Bearman's (1971) correction:-

$$\frac{\Delta E}{E} = -\frac{\alpha}{2(R-1)}\Delta\theta$$

where R is the overheat ratio and α is the temperature resistivity of the wire.

For $T_w - T_f = \Delta T \simeq 230^{\circ}C$ (overheat ratio 1.8) and approximating E by its mean value $\bar{E}$, we obtain:-

$$e_{true} = e_{meas} - \frac{1}{2}\frac{T_i - T_{ref}}{\Delta T}E$$

where T_i is the instantaneous temperature $= T + \theta$ and T_{ref} is usually the calibration temperature. The amount of correction is very small and is incorporated with the main hot wire relation in the data analysis program D3E.

APPENDIX D

COMPENSATION CIRCUIT

The frequency limit of a 1 μm wire is rather low (∿ 1 kHz). For frequencies above the cut-off frequency, it is necessary to compensate the thermal lag up to the frequencies of interest, or to the amplifier cut-off frequency. In practice, the amplitude response falls as $1/\left[1 + (f/f_0)^2\right]^{\frac{1}{2}}$ and, consequently, the proposed circuit should provide amplification proportional to $\left[1 + (f/f_0)^2\right]^{\frac{1}{2}}$ for frequencies higher than the wire "cut-off" (3dB) frequency f_0. A typical compensation circuit is shown in Fig. D.1a. The capacitor C_2 of value 470 pf (much less than the working range of the compensating capacitor C_1) operates as a low pass filter, and was set to the upper frequency of interest.

The transfer function is:-

$$\frac{e_o}{e_i} = \frac{R_2}{R_1}\left[\frac{1 + jR_1C_1\omega}{1 + jR_2C_2\omega}\right] \quad \text{with } j = \sqrt{-1}$$

In fact, this circuit acts as a high frequency noise amplifier as well and so causes some limitations on the amount of compensation which can be added.

The time constant depends mainly on the thermal lag (inertia) of the wire if the end conduction effects can be eliminated by increasing the ℓ/d ratio. Smits (1974) pointed out that the time constant is mainly a function of velocity and does not vary significantly with small changes of the probe temperature. Therefore, the compensator must be set at each operating point because of the velocity variation across the shear layer. However, Smits estimated that an error of 10% in the mean velocity will cause an error of only 3% in the sensitivity

at high frequencies and the error in broad-band temperature fluctuation measurements will be much less than this. Bearing in mind the last point, the following procedure was adopted for setting up the proper compensation. The temperature wire was placed in the outer part of the wake or boundary layer where the temperature signal was expected to be like a square wave. Then, the capacitor C_1 was adjusted until the output signal had as sharp rise as possible (see Fig. D.1b). With this technique, the frequency response went up to about 8 kHz estimated very roughly from the Calcomp plots.

Special care was taken to avoid any extreme case like over-compensation or undercompensation. In Fig. D.1b, it is clear what actually happens in such cases. A correct compensation ensures a smooth operation of the intermittency subroutine, while an over-compensated signal upsets it.

The time constant so adjusted deteriorated with time due to contamination of the wire by dust and dirt particles and it was possible to observe, even in the inner wake regions, the absence of high frequencies on the temperature signal. Therefore, a re-adjustment of the time constant by the above procedure was necessary. However, when the time constant of the wire became unacceptably high (excessive compensation required and thus noise introduced), the wire was cleaned by immersing it in a bath of methanol.

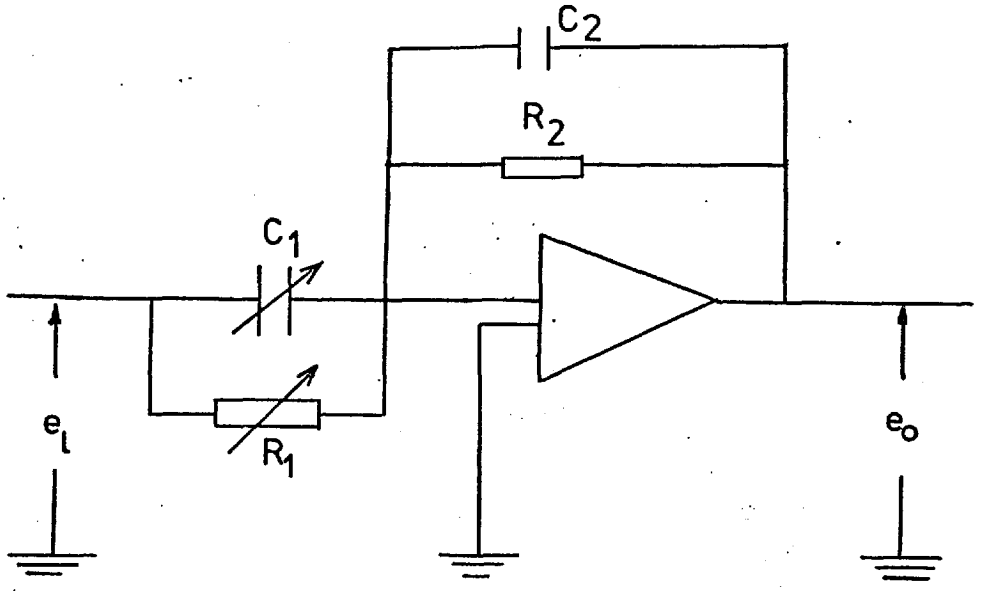

FIG. D.1a COMPENSATION CIRCUIT

Correctly compensated

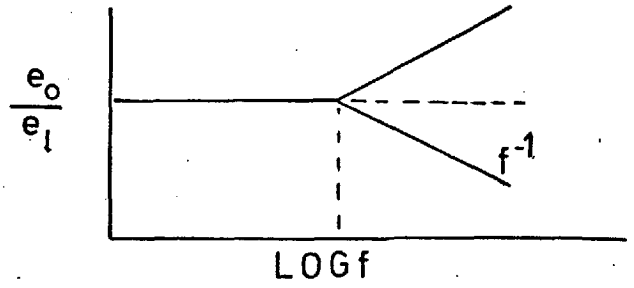

Under-compensated

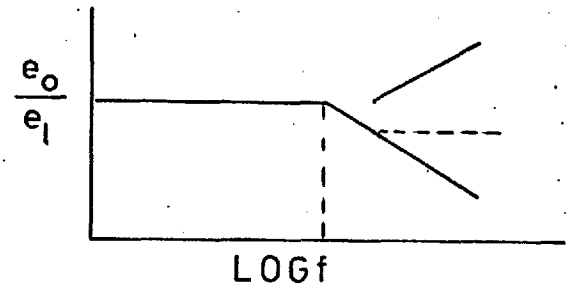

Over-compensated

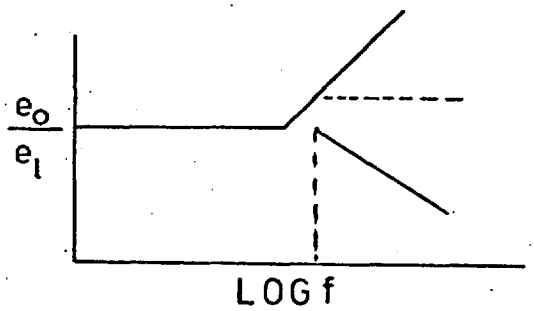

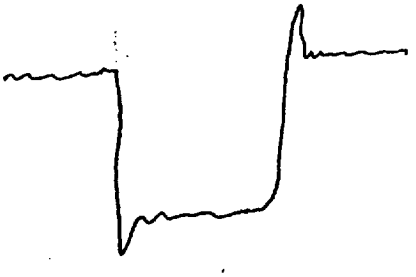

FIG. D.1b

APPENDIX E

DIGITIZATION TECHNIQUES

The three signals recorded on the Ampex FR 1300 were played back at 15 i.p.s. at $\frac{1}{4}$ of the recording speed and fed into sample and hold units (one for each channel) as shown in Fig. E1. These sample values are then held while the multiplexer connects the 10-bit A-to-D converter to each unit in turn and then these values are transmitted to part of the minicomputer core, which acts as a buffer. While one of the two buffers is loaded by the A-D converter, the other is unloaded to the digital tape transport unit. The whole transfer of data from and to the core store is controlled by a preloaded minicomputer program.

The total sampling frequency of the system is 20 kHz (6.7 kHz per channel for three channels) and by reducing the playback speed of the analogue tape recorder, we can increase the effective real-time sampling frequency.

The data transferred from the minicomputer buffer to the digital tape, which is analysed on the Imperial College CDC computer, are in 12-bit words (10-bits of A-D output and two trailing zeros). The computer's hardware assembly ten six-bit bytes into a 60-bit word. The data analysis program must unpack the 60-bit words into the original 12-bit minicomputer words and recover the 10-bit A-D words. For more details, see Weir and Bradshaw (1974).

The D3E program which performs most of the data analysis is composed of the following subroutines:-

BUFFIN Reads input data from the digital mag tape.

UNPACK Unpacks data into meaningful words.

RESOLV Resolves input data into physical data.

TDATA	Reads in calibration constants.
LAGTHR	Sorts out "hot" and "cold" points.
TUVS	Computes conventional and zone averages.
AVOUT	Print averages from TUVS.
CONV	Convergence test.
PLOTS	Plots u, v, T signals.

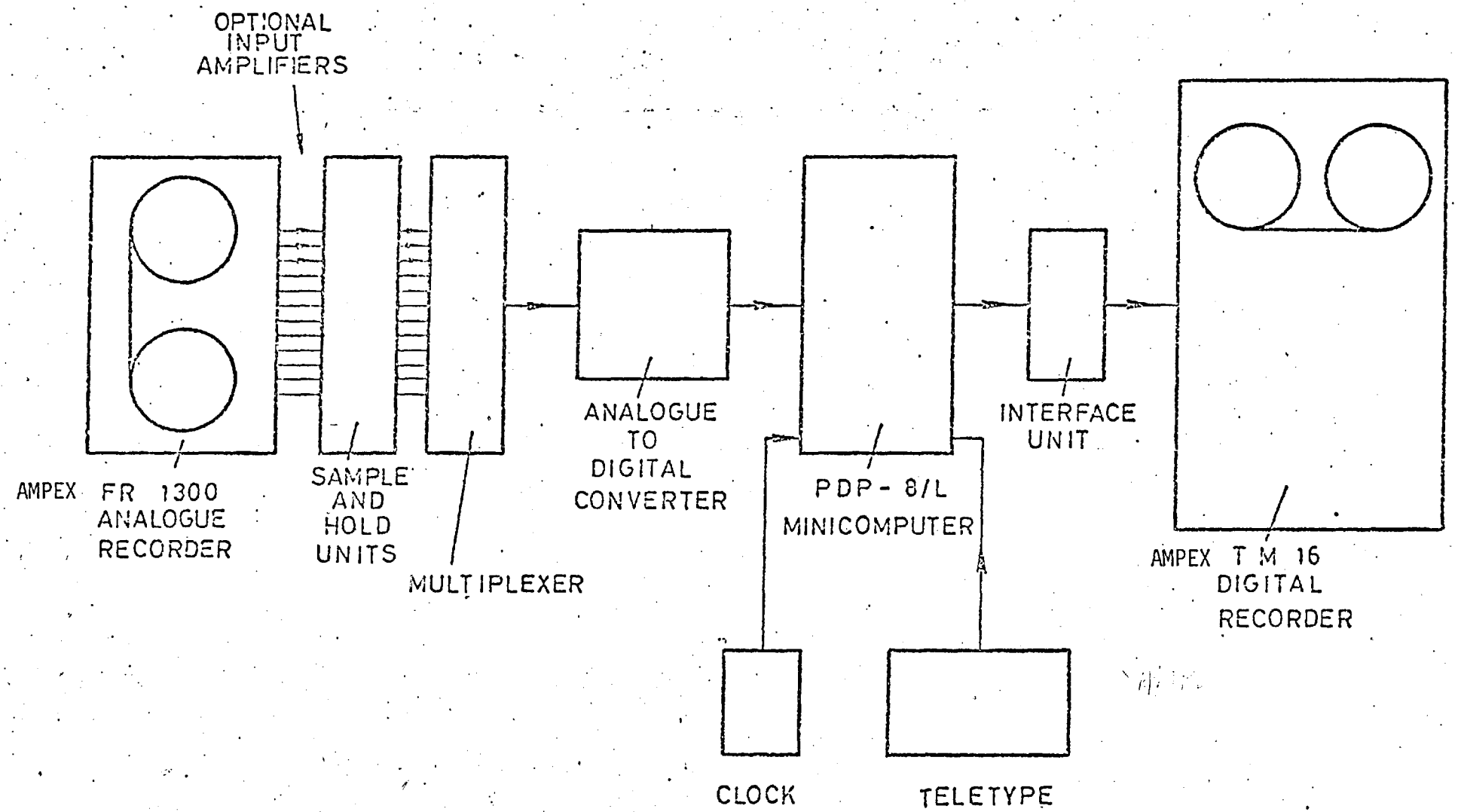

FIG. E.1 BLOCK DIAGRAM OF SYSTEM.

APPENDIX F

INTERMITTENCY SUBROUTINE

T	Instantaneous temperature
Θ_a	$T_{cold} + \Theta_2$
T_{cold}	Temperature of last "cold" point
Θ_2	Threshold level or permitted variation within a "cold" burst
Θ_{3u}	Slope criterion for rises from "cold"
Θ_{3d}	Slope criterion for falls to "cold"
T_{lag}	Temperature at the point J-N_{lag}
N_{lag}	Lag length (number of points)
Θ_b	$T_{bot}^{(5)} + \Theta_4$ = highest "reasonable" "cold" level
Θ_4	Permitted variation of "cold" level over several records (drift)
$T_{bot}^{(5)}$	Minimum temperature over last 5 records
$T_m^{(0)}$	Minimum temperature of current "cold" burst
$T_m^{(1)}$	Minimum temperature in last "cold" burst
$T_m^{(2)}$	Minimum temperature in one before last "cold" burst
ID	Intermittency factor
N_1)	
N_2)	
NP_2)	
NP_3)	
NTH_2)	Counters
NTH_3)	
NTH_4)	
I_1)	
I_2)	
NL	Typical length of "hot" bursts (number of points)

NU Longest expected "hot" burst

The values of the thresholds which were mainly used in the present investigation are:-

Θ_2 0.1 ^{o}C

Θ_{3u} 0.22 ^{o}C

Θ_{3d} 0.75 ^{o}C

Θ_4 0.2 ^{o}C

They were based on constant VARIACS settings, i.e. the same current input at the same mains voltage. The small variations of the value of level criterion from profile to profile may be caused by a variation of the mains voltage.

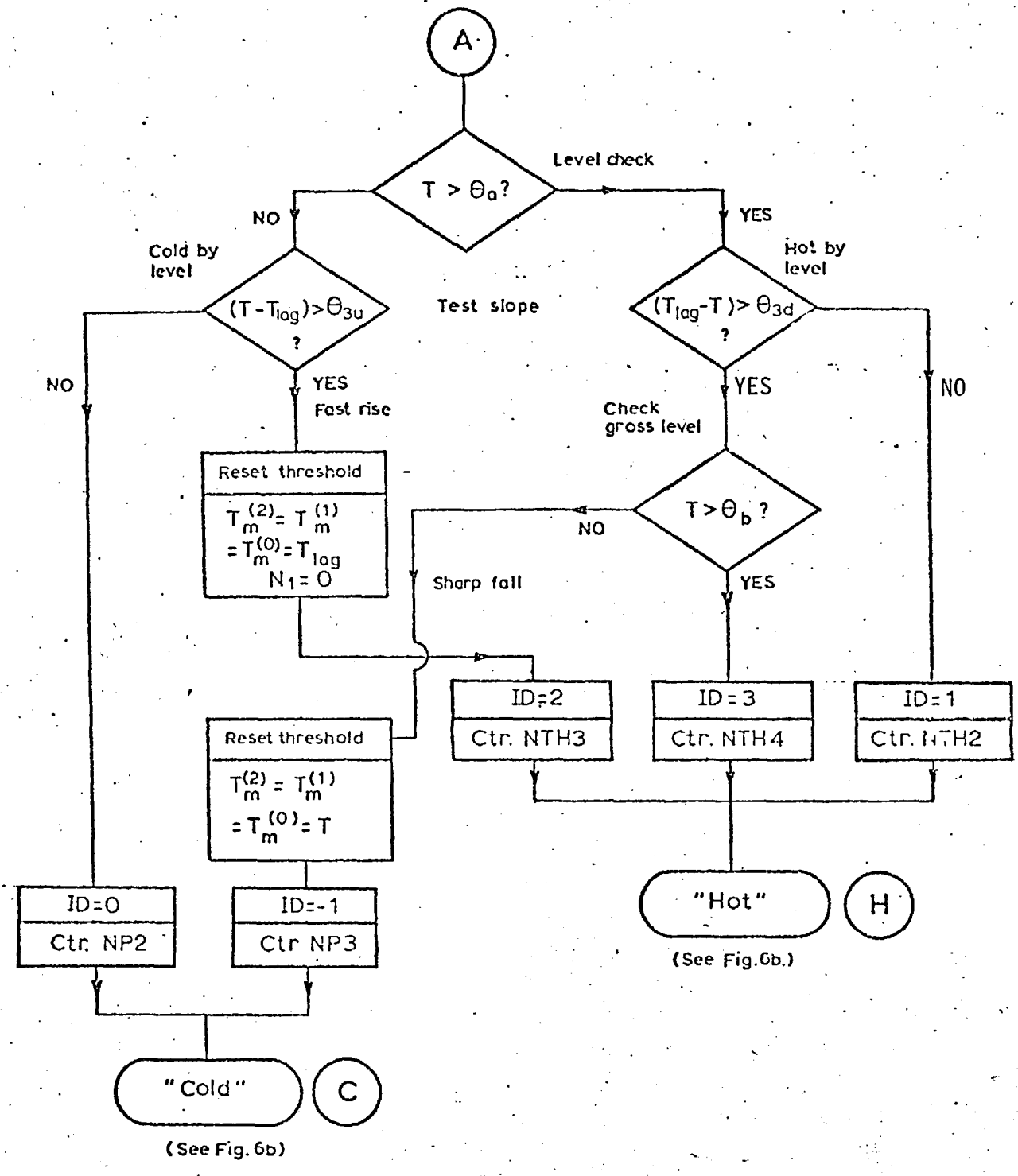

Flow chart of subroutine LAGTHR for finding intermittency from "level then slope" of temperature T.

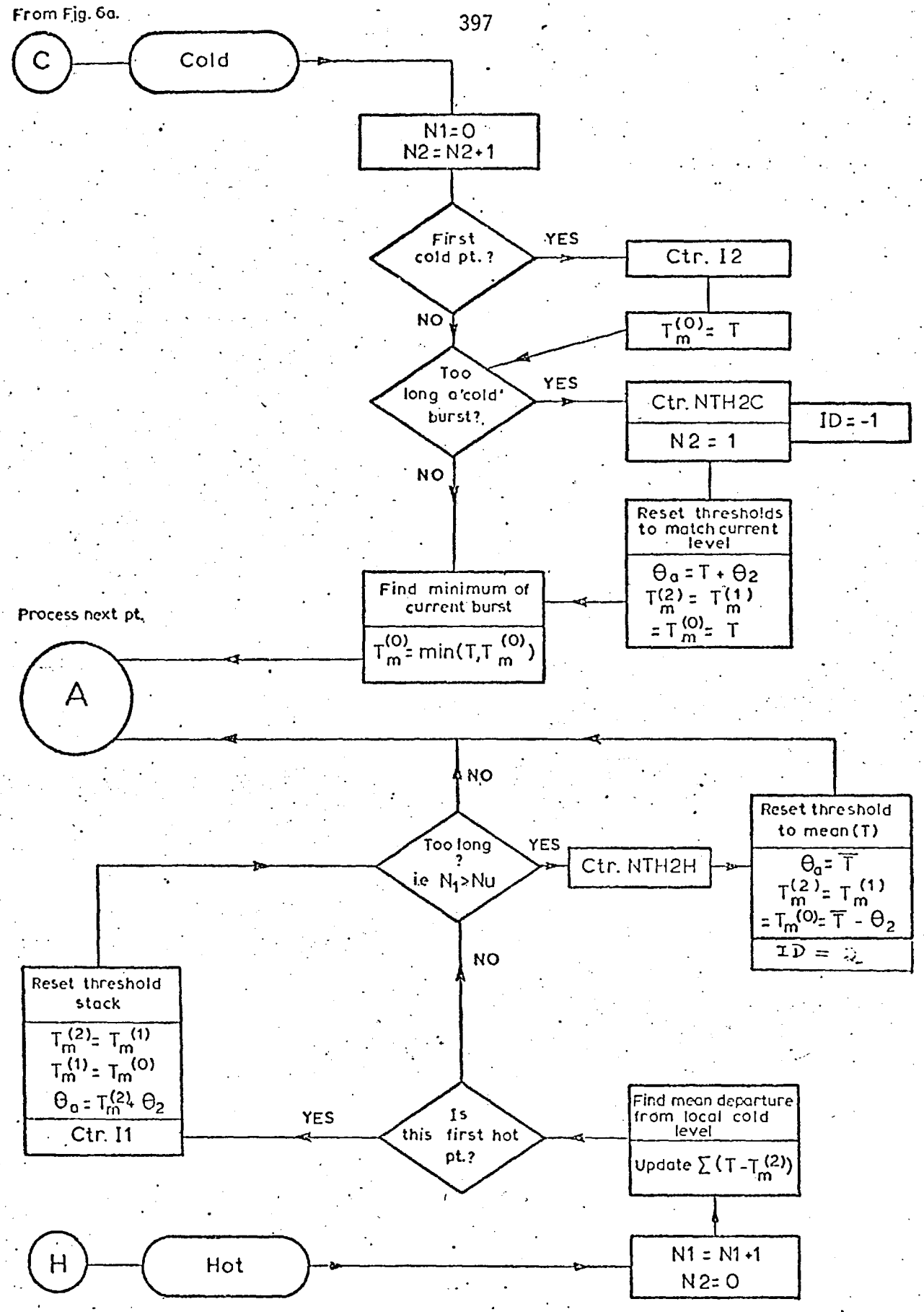

Details of how thresholds may be set in 'hot' and 'cold' bursts in LAGTHR.

APPENDIX G

TRANSPORT EQUATIONS

The mean momentum transport equation for a viscous incompressible turbulent fluid written in Cartesian-tensor notation is as follows (Townsend (1976)):-

$$U_k \frac{\partial U_i}{\partial x_k} = - \frac{1}{\rho} \frac{\partial \overline{P}}{\partial x_i} + \frac{\partial}{\partial x_k} \left(\nu \frac{\partial U_i}{\partial x_k} - \overline{u_k u_i} \right) \tag{G.1}$$

The continuity equation is:-

$$\frac{\partial U_i}{\partial x_i} = 0 \tag{G.2}$$

The exact transport equation for any turbulent stress, again in tensor notation, can be expressed by:-

$$\frac{D\ (+ \overline{u_i u_j})}{Dt} = - \left(\overline{u_i u_k} \frac{\partial U_j}{\partial x_k} + \overline{u_j u_k} \frac{\partial U_i}{\partial x_k} \right) \quad \text{Production term}$$

$$- \frac{\partial}{\partial x_k} (\overline{u_i u_j u_k}) - \frac{1}{\rho} \left(\overline{\frac{\partial p' u_i}{\partial x_j}} + \overline{\frac{\partial p' u_j}{\partial x_i}} \right) \quad \text{Turbulent diffusion term}$$

$$+ \overline{p' \left(\frac{\partial u_i}{\partial x_j} + \frac{\partial u_j}{\partial x_i} \right)} \quad \text{Pressure-rate of strain term}$$

$$+ \nu \overline{\left(u_i \frac{\partial^2 u_j}{\partial x_k^2} + u_j \frac{\partial^2 u_i}{\partial x_k^2} \right)} \quad \text{Viscous term} \tag{G.3}$$

with:-

$$\frac{D}{Dt} = U \frac{\partial}{\partial x} + V \frac{\partial}{\partial y} + W \frac{\partial}{\partial z}$$

In particular, the turbulent kinetic energy transport equation is (putting j = i):-

$$\frac{D \frac{1}{2} \overline{u_i^2}}{Dt} = - \overline{u_i u_k} \frac{\partial U_i}{\partial x_k} - \frac{\partial}{\partial x_k} \left(\overline{p' u_k} + \frac{1}{2} \overline{u_i^2 u_k} \right) + \nu \overline{u_i \frac{\partial^2 u_i}{\partial x_k^2}} \qquad (G.4)$$

where the term on the left hand side is the advection, the first on the right the turbulent energy production, the second is the diffusion by turbulence and pressure fluctuations and the last is the dissipation.

The transport equation of $\overline{\theta^2}$ in a turbulent shear flow is:-

$$\frac{D\overline{\theta^2}}{Dt} = - 2 \overline{\theta u_i} \frac{\partial T}{\partial x_i} - \frac{\partial}{\partial x_i} \overline{u_i \theta^2} + \alpha \frac{\partial^2 \overline{\theta^2}}{\partial x_i^2} - 2\alpha \overline{\left(\frac{\partial \theta}{\partial x_i} \right)^2} \qquad (G.5)$$

with the term on the left being the advection, the first on the right the production, the second the diffusion, the third the molecular dissipation, and the last being the dissipation.

Finally, the transport equation of any temperature-velocity correlation $\overline{u_i \theta}$ is as follows:-

$$\frac{D \overline{u_i \theta}}{Dt} = - \overline{u_i u_k} \frac{\partial T}{\partial x_k} - \overline{u_k \theta} \frac{\partial U_i}{\partial x_k} - \frac{\partial}{\partial x_k} \left(\overline{u_i u_k \theta} \right) - \frac{1}{\rho} \overline{\theta \frac{\partial p'}{\partial x_i}} +$$

$$+ \alpha \overline{u_i \frac{\partial^2 \theta}{\partial^2 x_j}} + \nu \overline{\theta \frac{\partial^2 u_i}{\partial x_j^2}} \qquad (G.6)$$

For a two-dimensional turbulent flow, the above equations are transformed into:-

$$U \frac{\partial U}{\partial x} + V \frac{\partial U}{\partial y} = - \frac{1}{\rho} \frac{\partial \overline{p}}{\partial x} - \frac{\partial \overline{u^2}}{\partial x} - \frac{\partial \overline{uv}}{\partial y} + \nu \nabla^2 U \qquad (G.7)$$

$$U \frac{\partial \overline{uv}}{\partial x} + V \frac{\partial \overline{uv}}{\partial y} = - \overline{u^2} \frac{\partial U}{\partial x} - \overline{v^2} \frac{\partial U}{\partial y} - \frac{\partial}{\partial x} \left(\overline{u^2 v} + \overline{\frac{p' v}{\rho}} \right) - \frac{\partial}{\partial y} \left(\overline{uv^2} + \overline{\frac{p' u}{\rho}} \right) -$$

$$- \overline{p' \left(\frac{\partial u}{\partial x} + \frac{\partial v}{\partial x} \right)} + \nu \overline{u \nabla^2 v} + \nu \overline{v \nabla^2 u} \qquad (G.8)$$

$$U \frac{\partial \frac{1}{2} \overline{q^2}}{\partial x} + V \frac{\partial \frac{1}{2} \overline{q^2}}{\partial y} = - (\overline{u^2} - \overline{v^2}) \frac{\partial U}{\partial x} - \overline{uv} \left[\frac{\partial U}{\partial y} + \frac{\partial V}{\partial x} \right] -$$

$$- \frac{\partial}{\partial x} \left(\overline{p' u} + \frac{1}{2} \overline{q^2 u} \right) - \frac{\partial}{\partial y} \left(\overline{p' v} + \frac{1}{2} \overline{q^2 v} \right) - \varepsilon \qquad (G.9)$$

with:-

$$\varepsilon = - \nu \, u_i \overline{\frac{\partial^2 u_i}{\partial x_k^2}} = - \nu \frac{\partial^2}{\partial x_k^2} \overline{\left(\frac{1}{2} u_i^2 \right)} + \nu \overline{\left(\frac{\partial u_i}{\partial x_j} \right)^2} \simeq \nu \overline{\left(\frac{\partial u_i}{\partial x_j} \right)^2}$$

Similarly, for the temperature fluctuation equation:-

$$U \frac{\partial \overline{\theta^2}}{\partial x} + V \frac{\partial \overline{\theta^2}}{\partial y} = - 2 \overline{\theta u} \frac{\partial T}{\partial x} - 2 \overline{\theta v} \frac{\partial T}{\partial y} - \frac{\partial}{\partial x} (\overline{u \theta^2}) - \frac{\partial}{\partial y} (\overline{v \theta^2}) +$$

$$+ \alpha \frac{\partial^2 \overline{\theta^2}}{\partial x^2} + \alpha \frac{\partial^2 \overline{\theta^2}}{\partial y^2} - 2 \varepsilon_\theta \qquad (G.10)$$

with:-

$$\varepsilon_\theta = \alpha \overline{\left(\frac{\partial\theta}{\partial x}\right)^2}$$

The $\overline{u\theta}$ and $\overline{v\theta}$ transport equations become:-

$$U\frac{\partial\overline{u\theta}}{\partial x} + V\frac{\partial\overline{u\theta}}{\partial y} = -\overline{u\theta}\frac{\partial U}{\partial x} - \overline{v\theta}\frac{\partial U}{\partial y} - \overline{u^2}\frac{\partial T}{\partial x} - \overline{uv}\frac{\partial T}{\partial y} - \frac{\partial}{\partial x}(\overline{u^2\theta}) -$$

$$- \frac{\partial\overline{uv\theta}}{\partial y} - \overline{\theta\frac{\partial p'}{\partial x}} + \alpha\,\overline{u\,\nabla^2\,\theta} + \nu\,\overline{\theta\,\nabla^2\,u} \qquad \text{(G.11)}$$

$$U\frac{\partial\overline{v\theta}}{\partial x} + V\frac{\partial\overline{v\theta}}{\partial y} = -\overline{v\theta}\frac{\partial V}{\partial y} - \overline{u\theta}\frac{\partial V}{\partial x} - \overline{vu}\frac{\partial T}{\partial x} - \overline{v^2}\frac{\partial T}{\partial y} - \frac{\partial\overline{uv\theta}}{\partial x} -$$

$$- \frac{\partial\overline{v^2\theta}}{\partial y} - \frac{1}{\rho}\overline{\theta\frac{\partial p'}{\partial y}} + \alpha\,\overline{v\,\nabla^2\,\theta} + \nu\,\overline{\theta\,\nabla^2\,v} \qquad \text{(G.12)}$$

APPENDIX H

NUMERICAL INTEGRATION TO FIND MEAN V

Mean velocity V is needed for the turbulent kinetic energy or shear stress balance since it is involved in the advection or mean transport terms.

Hot wire measurements of mean velocities may suffer from errors higher than are acceptable in deducing V, so it was decided to calculate V from the mean velocity profiles using the continuity equation:-

$$\frac{\partial U}{\partial y} + \frac{\partial V}{\partial y} = 0 \qquad (H.1)$$

and:-

$$V(y) - V(y') = - \int_{y'}^{y} \frac{\partial U}{\partial x} \, dy \qquad (H.2)$$

where $V(y')$ is the velocity at a reference point y'. For the symmetric wake, y' has been taken on the geometrical centre-line $y = 0$ with $V(y') = 0$, by symmetry arguments. For the asymmetric symmetric wake y' has been taken on the upper boundary layer edge $y = \delta_U$; so $V(y') = V_{eU}$.

V_{eU} has been evaluated from the entrainment equation:-

$$\frac{V_{EU}}{U_e} = \frac{d\delta_U}{dx} - \frac{V_{eU}}{U_e} \qquad (H.3)$$

assuming that V_E remains unchanged with x.

In fact, the same argument applies for the lower boundary

layer entrainment velocity:-

$$\frac{V_{EL}}{U_e} = \frac{d\delta_L}{dx} - \frac{V_{eL}}{U_e} \qquad (H.4)$$

This relation has been used for cross checking the results obtained by (H.3) and (H.2).

Regardless of whether the above argument is correct or not, another method was tried.

The x-momentum equation after the thin shear layer approximation and assuming $dp/dx = 0$ is as follows:-

$$U \frac{\partial U}{\partial x} + V \frac{\partial U}{\partial y} = \frac{\partial \ (- \overline{uv})}{\partial y}$$

In the outer layer is $\partial U/\partial x \simeq 0$; so V can be evaluated from the shear stress and mean U velocity profiles. These results checked those obtained from the continuity equation with rather good agreement for the symmetric and asymmetric wake.